Development of fluorescent ligands for A_1 adenosine receptor and cannabinoid receptors

A dissertation submitted for the degree of
Doctor of Philosophy at the University of Otago, Dunedin, New Zealand

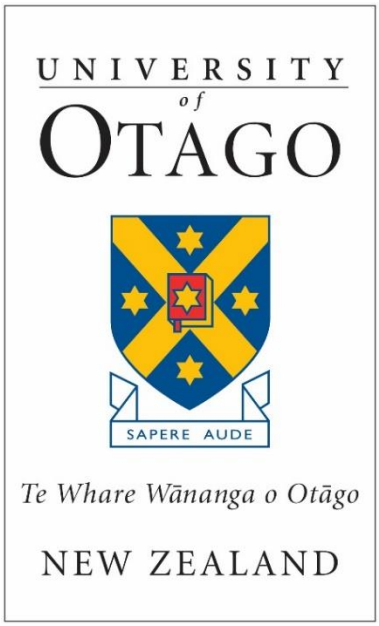

Sameek Singh

July 2018

Abstract

Adenosine A_1 receptor (A_1AR), cannabinoid type 1 receptor (CB_1R) and cannabinoid type 2 receptor (CB_2R) are class A G protein-coupled receptors (GPCRs) and play important roles in human pathophysiological conditions such as cardiovascular, neurological, metabolic and immunological disorders. Fluorescent ligands are powerful tools to investigate processes such as receptor expression, localisation, trafficking and receptor-protein interactions in the native cell environment. Fluorescent ligands can also be used as tracers in pharmacological assays, instead of the commonly used radioligands that carry inherent safety risks. The development of fluorescent ligands with high affinity, selectivity and suitable imaging properties for A_1AR, CB_1R and CB_2R would greatly contribute to an increased understanding of receptor biology and thus facilitate the drug development process. Development of fluorescent ligands with sufficient polarity for cannabinoid receptors (CBRs), which have lipid-based endogenous ligands, is an especially challenging task. This thesis describes the development of small molecule-based fluorescent ligands for A_1AR, CB_1R and CB_2R, via attachment of a linker and fluorophore to a ligand.

(Benzimidazolyl)isoquinolinols, analogues of previously reported high affinity A_1AR (benzimidazolyl)isoquinolines, were explored in chapter 2 for the development of A_1AR fluorescent ligands. A procedure for 2,3-dichloro-5,6-dicyano-1,4-benzoquinone (DDQ) mediated aromatisation of tetrahydroisoquinolines and multistep synthesis for the preparation of (benzimidazolyl)isoquinolinols was developed. Based on the previously reported structure–activity relationship (SAR), linkers (and linker plus fluorophore conjugates) were introduced in the C-6 or C-7 position of (benzimidazolyl)isoquinolinols. Unfortunately, these fluorescent ligands did not exhibit any significant affinity for A_1AR in a bioluminescence resonance energy transfer (BRET) assay using the NanoLuc luciferase and it was concluded that (benzimidazolyl)isoquinolinols might not be a suitable scaffold for the development of A_1AR fluorescent ligands. NMR spectroscopy and reverse phase HPLC studies showed (benzimidazolyl)isoquinolinols exhibit tautomerism.

Chromenopyrazoles, previously reported as high affinity CB_1R ligands, were investigated for development into CB_1R fluorescent ligands in chapter 3. Based on previous SAR,

linkers then fluorophores were introduced at six different chromenopyrazole positions. Disappointingly, fluorescent chromenopyrazoles did not exhibit high affinity for CB_1R in a radioligand binding assay. However, several chromenopyrazoles including a linker conjugate **3.22** and a peptide linker conjugate **3.39** exhibited high affinity for CB_2R that were promising candidates for development of CB_2R fluorescent ligands. All of the chromenopyrazoles that were evaluated in a cyclic adenosine monophosphate (cAMP) functional assay behaved as agonists at CB_2R. Docking studies were carried out using a CB_2R homology model and showed that high affinity CB_2R chromenopyrazoles with linkers attached likely exit via a cavity located between transmembrane helix (TM) 1 and TM7.

In chapter 4, efforts were made to develop high affinity CB_2R fluorescent ligands and more polar CB_2R linker conjugates that built on the results of chapter 3. The highest affinity CB_2R linker conjugate **3.22** (obtained in chapter 3) was conjugated to four different fluorophores (BODIPY-FL, Cy5, TAMRA, BODIPY-630/650) and two high affinity CB_2R fluorescent ligands (**4.01**, **4.02**) were obtained. The highest affinity CB_2R fluorescent ligand **4.02** (K_i = 41.8 ± 4.5 nM at hCB_2R; 5856 ± 1264 nM at hCB_1R) behaved as an inverse agonist (**4.02**, EC_{50} = 142.0 ± 13.1 nM at hCB_2R, 196.7 ± 9.11 % of forskolin response at hCB_2R) in the cAMP functional assay and showed CB_2R-specific-binding in widefield imaging experiments using CB_2R expressing HEK-293 cells. Fluorescent ligand **4.02** exhibited higher affinity for CB_2R than any other reported CB_2R fluorescent ligands and is the first high affinity CB_2R fluorescent ligand for which functional data has been reported (as of July 2018). Fluorescent ligand **4.02** possesses suitable CB_2R imaging properties and will be a useful tool for researchers studying CB_2R biology in techniques such as fluorescence-based assays, widefield microscopy and flow-cytometry and can be used in resonance energy transfer experiments with other fluorescent partners. In addition, three high-moderate affinity peptide linker conjugates (**4.06**, **4.07**, **4.08**) with considerably higher polarity compared to commonly used cannabinoid receptor ligand CP55,940 were obtained, all of which behaved as CB_2R agonists.

Development of high affinity CB_1R ligands based on a reported pyridyl scaffold was explored in chapter 5. Fluorescent ligands were designed using previously reported SAR coupled with results obtained from CB_1R docking using the reported CB_1R crystal

structure. *O*-Linker pyridyl-2-carboxamides and corresponding fluorescent conjugates were prepared via a multistep synthesis. Unfortunately, none of the fluorescent ligands exhibited any significant affinity for CB_1R, however, three moderate affinity CB_1R linker conjugates (**5.33**, **5.34**, **5.35**) were obtained. It was therefore concluded that optimised derivatives of pyridyl-2-carboxamide with different *O*-linkers or with linkers conjugated at different positions of the pyridine could be another strategy for the development of CB_1R fluorescent ligands.

Acknowledgements

First, I would like to say a huge thank you to my primary supervisor Dr Andrea Vernall for her astute guidance, tremendous support and endless patience throughout my PhD. Thank you for providing me the opportunity to work under your supervision, for teaching me a lot of things, and providing guidance with my scientific writing. I would also like to express my sincere gratitude to my co-supervisor Associate Professor Joel Tyndall for his support throughout the PhD and for teaching me the computational studies.

My sincere appreciation goes to the many lovely people in the medicinal chemistry group (now the expanded group), who have been part of this journey. Anna – you have been a great friend. It was awesome to have you as my partner in computational studies, in review writing, and in the fume-hood; I am sure you are going to impress everyone at Heptares. Sara you and I started together and you have been very supportive. Thanks for taking care of the lab and tolerating me. Deji, we have a great chemistry between us, the random talks, and the after hour jokes, which I am going to miss. Siddharth and Sumit, the members of after hour club, it has been a pleasure working with you guys. Jess, you are a fellow pharmacist, and it has been a pleasure seeing you transit into a medicinal chemist. The new members of the group – Daniel, Shivaji (part of the badminton club), Fiona, Jasmine, Lohitha, Yasmin, Dhanya – it was real fun working with you guys. I would also like to thank my good friend – Basanth (especially for cooking those delicious dishes), Sassi, Arnold (for the video gaming sessions) and members of the badminton club.

I am very grateful to the School of Pharmacy, University of Otago for providing scholarship for my studies throughout the PhD and the Otago medical research foundation for the travel grants. I am thankful to members of Professor Stephen hill's research group at the University of Nottingham, United Kingdom for carrying out biological studies for the compounds described in chapter 2. I would like to express my gratitude to Professor Michelle glass at the University of Auckland for providing me the opportunity to learn and carry out radioligand binding assays and functional assays for compounds described in chapter 3, 4, and 5. Special thanks go to Christa MacDonald for providing me with the training in radioligand assays, functional assays, and culturing cells for my functional

studies, and Dr Natasha Grimsey, Caitlin Oyagawa for carrying out widefield imaging experiments.

This journey would have been impossible without the support of my family. My elder sister Anu, my younger sister Tanu (for sending me rakhi throughout my time here in New Zealand); my mum, my dad (for all the sacrifices), Manu bhai, and all the young champions of the family.

Table of contents

Abbreviations

2D	Two dimensional
2-AG	2-Arachidonoylglycerol
2-AGE	2-Arachidonyl glyceryl ether
A_1AR	A_1 adenosine receptor
bA_1AR	Bovine A_1 adenosine receptor
hA_1AR	Human A_1 adenosine receptor
pA_1AR	Porcine A_1 adenosine receptor
rA_1AR	Rat A_1 adenosine receptor
A_{2A}Ar	A_{2A} adenosine receptor
bA_{2A}Ar	Bovine A_{2A} adenosine receptor
hA_{2A}AR	Human A_{2A} adenosine receptor
rA_{2A}AR rat	Rat A_{2A} adenosine receptor
A_{2B}AR	A_{2B} adenosine receptor
hA_{2B}AR	Human A_{2B} adenosine receptor
A_3AR	A_3 adenosine receptor
hA_3AR	Human A_3 adenosine receptor
rA_3AR	Rat A_3 adenosine receptor
ADR	Adrenergic receptor
AEA	*N*-arachidonoylethanolamine (Anandamide)
AIBN	2,2′-Azobis(2-methylpropionitrile)
Ala	Alanine
aq.	Aqueous
Ar	Aromatic
AR	Adenosine receptor
Asn	Asparagine
ATP	Adenosine triphosphate
Boc	*tert*-Butyloxycarbonyl
BODIPY	Borondipyrromethene
BODIPY-630/650	(*E*)-6-(2-(4-(2-(5,5-difluoro-7-(thiophen-2-yl)-5*H*-5λ^4,6λ^4-dipyrrolo[1,2-*c*:2',1'-*f*][1,3,2]diazaborinin-3-yl)vinyl)phenoxy)acetamido)hexanoyl

BODIPY-FL	5-(5,5-Difluoro-7,9-dimethyl-5*H*-5λ^4,6λ^4-dipyrrolo[1,2-c:2',1'-*f*][1,3,2]diazaborinin-3-yl)pentanoyl
BRET	Bioluminescence resonance energy transfer
BSA	Bovine serum albumin
cAMP	Cyclic adenosine monophosphate
CAMYEL	cAMP sensor using YFP-Epac-RLuc
CBN	Cannabinol
CBR	Cannabinoid receptor
CB_1R	Cannabinoid type 1 receptor
cCB_1R	Canine cannabinoid type 1 receptor
hCB_1R	Human cannabinoid type 1 receptor
mCB_1R	Murine cannabinoid type 1 receptor
rCB_1R	Rat cannabinoid type 1 receptor
CB_2R	Cannabinoid type 2 receptor
hCB_2R	Human cannabinoid type 2 receptor
mCB_2R	Murine cannabinoid type 2 receptor
CHO	Chinese hamster ovary
clogP	Calculated logP
CSD	Cambridge Structural Database
Cy5	1-(5-Carboxypentyl)-3,3-dimethyl-2-((1*E*,3*E*)-5-((*E*)-1,3,3-trimethylindolin-2-ylidene)penta-1,3-dien-1-yl)-3*H*-indol-1-ium
DAG	Diacylglycerol
DCM	Dichloromethane
DDQ	2,3-Dichloro-5,6-dicyano-1,4-benzoquinone
DIPEA	*N*,*N*-Diisopropylethylamine
DMF	*N*,*N*-Dimethylformamide
DMSO	Dimethyl sulphoxide
DOPE	Discrete optimised protein energy
DPCPX	Dipropylcyclopentylxanthine
EC_{50}	Concentration that produces half maximal response
EL	Extracellular loop
E_{max}	Maximum response
EPAC1	Exchange protein activated by cAMP 1
ERK	Extracellular signal regulated kinase

FAAH	Fatty acid amide hydrolase
FAF	Fatty acid free
FDA	Food and Drug Administration
Fmoc	Fluorenylmethyloxycarbonyl
FRET	Fluorescence resonance energy transfer
gCOSY	Gradient homonuclear correlation spectroscopy
gHMBC	Gradient heteronuclear multiple bond correlation spectroscopy
gHSQC	Gradient heteronuclear single quantum coherence spectroscopy
GIRK	G protein-coupled inwardly-rectifying potassium channel
GPCR	G protein-coupled receptor
GTP	Guanosine triphosphate
h	Hour(s)
HATU	1-[Bis(dimethylamino)methylene]-1*H*-1,2,3-triazolo[4,5-b]pyridinium 3-oxid hexafluorophosphate
HBTU	*N*,*N*,*N*′,*N*′-Tetramethyl-*O*-(1*H*-benzotriazol-1-yl)uronium hexafluorophosphate
HEK	Human embryonic kidney
HEPES	(4-(2-hydroxyethyl)-1-piperazineethanesulfonic acid)
hGPR55	Human GPR55 receptor
HOBt	1-Hydroxybenzotriazole
RP-HPLC	Reverse phase-high performance liquid chromatography
HRMS	High-resolution electrospray ionisation mass spectra
HTS	High-throughput screening
IL	Intracellular loop
IC_{50}	Concentration that reduces response by half
IP_3	Inositol 1,4,5-trisphosphate
K_d	Dissociation constant
K_i	Inhibitor constant
MAPK	Mitogen-activated protein kinases
MS	Low-resolution mass spectrometry
mid DBT cells	Mouse delayed brain tumour cells
min	Minute(s)
NBD	Nitrobenzoxadiazole
NBS	*N*-Bromosuccinimide

NIR	Near-infrared
NMR	Nuclear magnetic resonance
PDB	Protein Data Bank
PEG	Polyethylene glycol
PIP_2	Phosphatidylinositol 4,5-bisphosphate
PLC	Phospholipase C
PPA	Polyphosphoric acid
ppm	part(s) per million
r	Rat
R_f	Retention factor
RLuc	*Renilla* luciferase
rt	Room temperature
SAR	Structure–activity relationship
SD	Standard deviation
SE	Succinimidyl ester
SEM	Standard error of the mean
Ser	Serine
TAMRA	2-(3,6-bis(dimethylamino)xanthylium-9-yl)-5-carboxybenzoate
THC	(−)-trans-Δ^9-tetrahydrocannabinol
THF	Tetrahydrofuran
TFA	Trifluoroacetic acid
TFFH	Tetramethylfluoroformamidinium Hexafluorophosphate
TLC	Thin-layer chromatography
TM	Transmembrane α-helix
Trt	Trityl
WT	Wild-type
YFP	Yellow fluorescent protein

Single and three letter amino acid codes

A	Ala	Alanine
C	Cys	Cysteine
D	Asp	Aspartic acid
E	Glu	Glutamic acid
F	Phe	Phenylalanine
G	Gly	Glycine
H	His	Histidine
I	Ile	Isoleucine
K	Lys	Lysine
L	Leu	Leucine
M	Met	Methionine
N	Asn	Asparagine
P	Pro	Proline
Q	Gln	Glutamine
R	Arg	Arginine
S	Ser	Serine
T	Thr	Threonine
V	Val	Valine
W	Trp	Tryptophan
Y	Tyr	Tyrosine

Publications

A literature review article and a research article (of work discussed in chapter 2 of this thesis) have been published:

- Cooper, A.; Singh, S.; Hook, S.; Tyndall, J. D. A.; Vernall, A. J., Chemical Tools for Studying Lipid-Binding Class A G Protein–Coupled Receptors. *Pharmacol. Rev.* **2017,** *69* (3), 316-353.

- Singh, S.; Cooper, S. L.; Glenn, J. R.; Beresford, J.; Percival, L. R.; Tyndall, J. D. A.; Hill, S. J.; Kilpatrick, L. E.; Vernall, A. J., Synthesis of novel (benzimidazolyl)isoquinolinols and evaluation as adenosine A1 receptor tools. *RSC Advances* **2018,** *8* (29), 16362-16369.

Research work described in chapter 3, 4 and 5 of this thesis will be published in due course.

Chapter 1 Introduction

1.1 G protein-coupled receptors

G protein-coupled receptors (GPCRs) constitute the largest family of human transmembrane proteins with approximately 800 members.[1] GPCRs play an important regulatory role in numerous physiological processes and are responsible for the signal mediation of various bioactive substances such as peptides, lipids, carbohydrates, proteins, and small organic molecules as well as other stimuli such as light and ions.[1-2] These receptors have been the subject of intense drug discovery effort and approximately 34% of all currently marketed drugs target GPCRs.[1] GPCRs are grouped into five major families: class A rhodopsin-like, class B secretin-like, class C metabotropic glutamate/pheromone, cyclic adenosine monophosphate (cAMP) receptors, vomeronasal receptors (V1R and V3R), and taste receptors T2R.[3] Among these families, class A rhodopsin-like is the most studied and the largest family accounting for 80% of all known GPCRs.[1] Adenosine A_1 receptor (A_1AR)[**] and cannabinoid receptors (CBRs)[††] belong to the family of class A GPCRs.

Structurally, GPCRs consist of an extracellular *N*-terminal and an intracellular *C*-terminal, which are connected by seven transmembrane α-helices (TMs) (Figure 1.1, panel A). An alternate sequence of three intracellular (IL) (IL1, IL2, and IL3) and three extracellular loops (EL) (EL1, EL2, and EL3) connect the seven transmembrane helices. GPCRs exhibit structural similarity in the transmembrane region, however, large structural diversity is observed in the loop regions.

X-ray crystallography is widely used to determine the structure of proteins at the atomic level. However, determination of the X-ray crystal structure of GPCRs has been challenging due to the difficulties encountered in the crystallisation of membrane proteins. These difficulties arise from the instability of GPCRs in detergents, structural heterogeneity (from the presence of receptors in glycosylated, phosphorylated, and palmitoylated forms), and conformational heterogeneity due to the inherent flexible

[**] human (h) adenosine receptors, unless specified, throughout this thesis
[††] human (h) cannabinoid receptors, unless specified, throughout this thesis

nature of GPCRs.[4] Nevertheless, remarkable progress has been made recently and there are now 44 distinct GPCR X-ray crystal structures reported (as of July 2018).[1] However, the static nature of structures obtained from X-ray crystallography coupled with a number of thermostabilising receptor mutations usually incorporated for successful crystallisation has to be taken into account when studying dynamic receptor structure and processes in the native cell environment. In addition to X-ray crystallography, nuclear magnetic resonance (NMR) spectroscopy is also used to study GPCR structures[5] and more recently cryoelectron microscopy has been increasingly used to determine GPCR structures.[6-8]

GPCR signalling is primarily mediated by heterotrimeric G proteins,[9-10] which consist of three subunits: G_{α}, G_{β}, and G_{γ} (Figure 1.1, panel B shows β_2 adrenergic receptor (β_2ADR) bound to heterotrimeric G protein). Close to the submission date of this thesis a cryoelectron microscopy structure of A_1AR complexed with G protein was also reported[8] (not shown in Figure 1.1). Activation of a GPCR, often with an agonist, promotes the exchange of guanosine diphosphate (GDP) by guanosine triphosphate (GTP) in the G_{α} subunit. This G_{α}.GTP complex then dissociates from G_{β} and G_{γ} subunits and modulates downstream pathways.

According to the structure and function of the α subunit, G proteins can be classified into four types: $G_{\alpha s}$, $G_{\alpha i/o}$, $G_{\alpha q/11}$, and $G_{\alpha 12/13}$. Once activated, $G_{\alpha s}$ stimulates enzyme adenyl cyclase which catalyses the production of cyclic adenosine monophosphate (cAMP) from adenosine triphosphate (ATP), whereas $G_{\alpha i/o}$ inhibits the activity of adenyl cyclase. $G_{\alpha q/11}$ activates enzyme phospholipase C (PLC) which then produces inositol 1,4,5-trisphosphate (IP_3) and diacylglycerol (DAG) from hydrolysis of membrane bound phosphatidylinositol 4,5-bisphosphate (PIP_2). The $G_{12/13}$ subunit is involved in the activation of RhoGEF (guanine nucleotide exchange factor).[9-10] All of these messengers then modulate the activity of various other effectors.

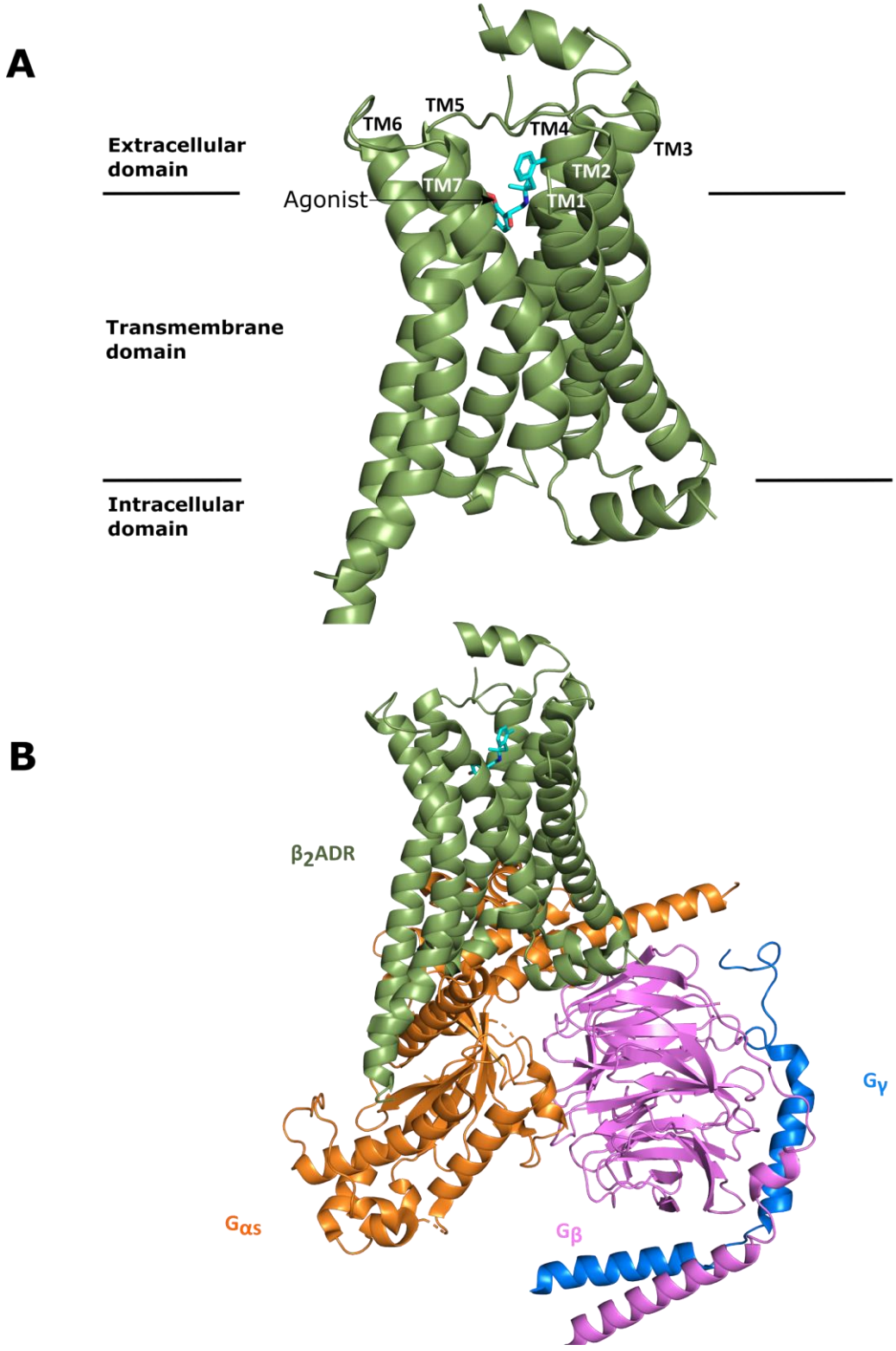

Figure 1.1 Panel (A) Cartoon representation as a forest green ribbon of a β_2ADR (a class A GPCR, Protein Data Bank (PDB) ID: 3P0G) with bound agonist BI-167107 (cyan carbons, red oxygens, blue nitrogen).[11] Heterotrimeric G proteins, T4 lysozyme, and a stabilising nanobody are not shown. TM helices 1-7 labelled. **Panel (B)** Crystal structure of β_2ADR (forest green, PDB ID: 3P0G,[11] also shown in panel (A)) with heterotrimeric G proteins – $G_{\alpha s}$ (orange), G_{β} (magenta), and G_{γ} (blue). T4 lysozyme and stabilising nanobody used to facilitate crystallisation are not shown.

In addition to signalling via heterotrimeric G proteins, GPCRs can also signal by G protein-independent mechanisms. The G protein-independent signalling commences with the phosphorylation of agonist-bound GPCR by G protein-coupled receptor kinases (GRKs). The phosphorylated GPCR subsequently binds to β-arrestin which leads to receptor desensitisation, internalisation, ubiquitination, and initiates G protein-independent signalling (which includes extracellular signal regulated kinase (ERK), c-Jun *N*-terminal kinase (JNK), and SRC proto-oncogene non-receptor tyrosine kinase c-Src).[12-15]

There has been growing interest towards preparing small molecules with biased signalling, that is preference for one signalling pathway over another (for example, β-arrestin signalling over G protein signalling) in order to reduce the associated side effects of an unbiased ligand.[16] For example, a selective μOR (μ-opioid receptor) agonist PZM21 with preference for G protein signalling over β-arrestin signalling was prepared and showed analgesic activity without opioid associated respiratory depression in mouse models.[17] However, in a later study, PZM21 was found to activate both G protein and β-arrestin signalling and depressed respiration in a mouse model.[18] GPCRs have also been shown to signal from both cell membrane as well as intracellular compartments,[19] and a location bias for signalling has been demonstrated.[20] Increasing evidence has indicated that GPCRs signal via oligomers, which can be targeted with a bivalent ligand.[21] Allosteric modulation of GPCR signalling is another key area of research with potential to provide ligands with therapeutic benefits without associated side effects of orthosteric ligands.[22-23] As this thesis is focused on the development of fluorescent ligands as tools to study GPCRs, these concepts will not be covered in more depth.

1.2 Chemical tools to study Class A GPCRs

Considering the central role GPCRs play in human pathophysiology, significant efforts have been invested in understanding the pharmacology of these receptors. Chemical tools are commonly used to study GPCRs in both *in vivo* and *in vitro* experiments and can provide crucial information regarding the role of the GPCRs in pathophysiological conditions.[24] Aside from small molecule ligands, tools can be designed with some traceability or read out – for example radioligands, covalent ligands and fluorescent

ligands. Chemical tools for lipid-binding receptors (for example CBRs) have recently been reviewed by Cooper and Singh *et al.*[25], and are also briefly discussed further in the following sections.

1.2.1 Radioligands

Radioligands used in pharmacological studies are compounds which exhibit high affinity and selectivity for a particular receptor or protein of interest and contain a radioisotope such as ^{3}H, ^{123}I, ^{125}I, ^{35}S, ^{11}C, and ^{18}F. The incorporated radioisotope undergoes nuclear decay to emit β particles, positrons, or γ radiation, which can be detected and consequently the amount of radioligand bound to the receptor can be quantified. The most common radioisotope used is ^{3}H. For a radioligand to be used successfully in GPCR pharmacological studies, it should have a minimal amount of non-specific membrane interactions.

Radioligands are significant tools in the identification of GPCR subtypes and in studying GPCR distribution. The parameters obtained from the study of radioligand-receptor interactions such as dissociation constant (K_d), inhibitor constant (K_i), and receptor density provide a quantitative description of the drug-receptor interaction, which can be used to propose and validate receptor activation models. Radioligands have been used for *in vivo* studies of GPCRs using techniques such as positron emission tomography and single-photon emission computed tomography to identify changes in the receptor expression in healthy and disease conditions, for example [^{18}F]MK-9470[26-28] (a high affinity cannabinoid type 1 receptor (CB_1R) inverse agonist).

Radioligands are extensively used to study GPCRs *in vitro*. One of the most common applications of radioligands is in the determination of the affinity (K_i) of a test compound by displacement of the radioligand in a competition-binding assay. It is particularly challenging to prepare radioligands of adequate polarity for GPCRs whose endogenous ligands are lipid-based compounds, as is the case with CBR. For example, most CBR radioligands are lipophilic compounds with $logD_{7.4}$ in the range of 3.3 - 6.0. Radioligands with high lipophilicity often exhibit a high level of non-specific membrane interactions.[29] Radioligand [^{3}H]-dipropylcyclopentylxanthine (DPCPX) (K_d = 3.86 nM at human A_1

adenosine receptor (hA_1AR))[30] and [^{3}H]-CP55,940 (K_d = 0.54 ± 0.07 nM at human cannabinoid type 1 receptor (hCB_1R)[31], 2.55 ± 0.19 nM at human cannabinoid type 2 receptor (hCB_2R)[32]) are commonly used for *in vitro* studies of A_1AR and CBR respectively (Figure 1.2).

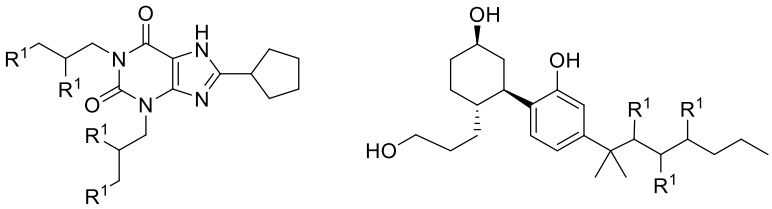

DPCPX, R^1= H
[^{3}H]-DPCPX, R^1 = [^{3}H]

CP55,940, R^1= H
[^{3}H]-CP55,940, R^1 = [^{3}H]

Figure 1.2. Commonly used radioligands [^{3}H]-DPCPX and [^{3}H]-CP55,940 for studying A_1AR and CBRs.

1.2.2 Covalent ligands

A covalent ligand binds with moderate to high affinity to the target receptor and forms a covalent bond with a receptor amino acid residue(s). This binding can be irreversible or reversible depending on the structure of covalent adduct formed. Covalent ligands belong to two main categories – electrophilic ligands and photoactivatable ligands. The electrophilic covalent ligands contain an electrophilic moiety such as isothiocyanates, halomethyl ketones, thiols, Michael acceptors and nitrogen mustards, which react with a nucleophilic residue of the target receptor. Photoactivatable ligands, on the other hand, contain an inert moiety, such as a benzophenone, azide, and diazirine, which, after irradiation with light of suitable wavelength, convert to a reactive moiety such as a carbene or nitrene that undergoes reaction with amino acids of the target receptor.

Use of covalent ligands along with computational and mutagenesis studies is a powerful approach to identify key amino acids involved in ligand-receptor binding and receptor activation.[25] For example, one study with a commonly used CBR covalent ligand AM841 (Figure 1.3) showed the involvement of both central and peripheral mCBR in the anti-inflammatory action of CBR ligands.[33] Recently, a photoactivatable diazirine based covalent ligand LEI121 for studying cannabinoid type 2 receptor (CB_2R) expression and for use in CB_2R isolation was reported.[34] Covalent ligands have also been used to stabilise

GPCRs for structure determination by X-ray crystallography, for example the covalent antagonist DU172 (Figure 1.3) was used to stabilise A_1AR in a report of the A_1AR crystal structure by Glukhova *et al*.[35]

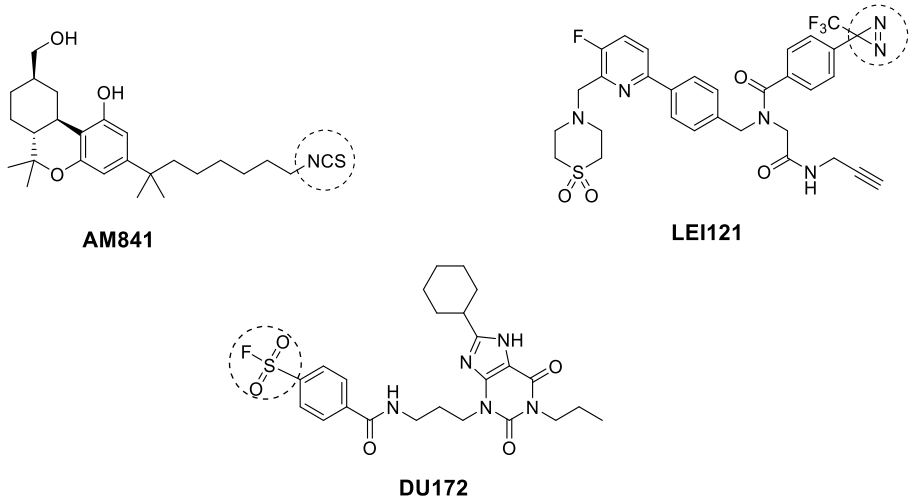

Figure 1.3 CB_1R covalent ligand AM841 CB_2R covalent ligand LE1121 and A_1AR covalent ligand DU172; the reactive functional group is circled.

1.2.3 Fluorescence

Fluorescence is widely used in molecular pharmacology. Absorption of a photon (from irradiated light) by a compound excites an electron from the ground state (S_0) to an excited state (S_1). When the excited electron relaxes, a photon (of emitted light) of lower energy is emitted along with some energy loss, which occurs by a non-radiative relaxation process such as heat. The wavelength of emitted light (E_{em}) is longer than the wavelength of irradiated light (E_{ex}) and the difference between E_{em} and E_{ex} is called the Stokes shift. A large Stokes shift allows for easier separation of excitation light from emission light with optical filters during biological experiments. A crucial parameter directly related to the brightness of the fluorophore (and consequently sensitivity of biological experiments) is determined by quantum yield and is the ratio of the number of photons emitted to the number of photons absorbed by a fluorophore. The loss (or reduction) of the fluorescence of a fluorophore after repetitive excitation is called photobleaching, that can adversely affect sensitivity of the experiment. This loss of fluorescence can occur due to a change in the structure of fluorophore in an excited state by reaction with oxygen.

Use of fluorescence to study GPCRs is wide ranging, for example green fluorescent protein and yellow fluorescent protein (YFP) -tagged receptors have been used to study receptor localisation, trafficking, and oligomerisation.[36-38] Receptor selective antibodies conjugated to fluorophores are also used to study GPCR distribution.[37] However, a number of antibodies developed chiefly for CBRs, were shown to lack receptor specificity.[39-41] Only small molecule-based fluorescent ligands will be discussed further in this chapter.

1.2.3.1 Fluorescent ligands

A fluorescent ligand should exhibit affinity and selectivity for a molecular target (receptors, enzymes, proteins etc.) and emit detectable fluorescent radiation. Some examples of such fluorescent ligands are – small fluorescent molecules,[24] antibody conjugates, and quantum dots.[42]

Small molecule fluorescent ligands with a fluorophore included as a substructure of the core ligand have been reported (for example– NMP6, described in section 1.4.4). Another approach to prepare fluorescent ligands is via *in situ* reaction of the fluorophore and the ligand partners, which have been previously derivatised with a biorthogonal functional groups such as an alkyne or azide, or with biotin or streptavidin (for example 2-arachidonylglycerol ether (2-AGE)-biotin-3b, biotin-HU210-1, and biotin-HU308-3 described in section 1.4.4). More commonly, small molecule-based fluorescent ligands for studying GPCRs have been developed by tethering a high affinity ligand to a fluorophore via a linker as a single chemical entity before using as a tool (Figure 1.4). The selection of the ligand is guided by the previous structure–activity relationship (SAR) data indicative of receptor affinity and subtype selectivity, the ability to accommodate bulky substituents, synthetic feasibility, and desired application of the ligand (agonist or antagonist etc.).

A fluorophore is attached via a linker of sufficient length to a ligand such that the binding of the ligand with the receptor is not affected by the usually large sized fluorophore (compared to ligand). Fluorescent ligands with high affinity for a target GPCR and appreciable polarity are desired to obtain high sensitivity in the imaging studies and

pharmacological assays. Peptide linkers are particularly useful in improving polarity and receptor affinity (by introduction of hydrogen bond donors and acceptors) of the ligand. Peptide linkers can also provide subtype specificity to a particular receptor as has been demonstrated in the case of adenosine receptors (AR).[43] Fluorophores are selected based on the excitation E_{ex} and emission E_{em} profile, quantum yield, stability to photobleaching, chemical structure, and spectral sensitivity to environmental factors such as the pH and polarity of the medium. A number of fluorophores are commercially available with amine-reactive functional groups such as succinimidyl esters (SE), sulfonyl chlorides, isothiocyanates, and tetrafluorophenyl esters for facile preparation of fluorescent ligands; for example borondipyrromethene (BODIPY, structure of a BODIPY derivative – BODIPY-630/650 – shown in Figure 2.2, chapter 2), cyanine (structure of a cyanine fluorophore – Cy5 – shown in Figure 4.2, chapter 4), Alexa Fluor® (structure of an Alexa fluorophore – Alexa488 – shown in Figure 4.2, chapter 4), and rhodamine (structure of TAMRA, a rhodmine derivative shown in Figure 4.2, chapter 4).

Figure 1.4. Schematic representation of a small molecule-based fluorescent ligand consisting of a high affinity ligand conjugated to a fluorophore via a linker.

The development of fluorescent ligands is challenging notably for GPCRs with endogenous lipid-based ligands such as CBRs due to the conflicting requirement of preparing a ligand with sufficient polarity for obtaining a suitable imaging agent.

The functional activity of the fluorescent ligand may be different to the individual parent ligand. Despite this possibility, many reported fluorescent ligands have not been characterised for functional activity (none of the literature reported CBR fluorescent ligands are characterised for functional activity, section 1.4.4). Development of fluorescent ligands for GPCRs is a relatively new field compared to radioligands. Notwithstanding this, there are now many fluorescent ligands reported for studying predominantly Class A GPCRS.[24-25]

1.2.3.2 Applications of fluorescent ligands

Fluorescent ligands are extensively used to study receptor pharmacology.[25] Fluorescent ligands have been used in confocal microscopy to study processes such as receptor expression, localisation, distribution, and internalisation at the single cell level.[24, 44-45] Resonance energy transfer techniques (FRET and BRET) with fluorescent ligands have been used to study processes such as receptor oligomerisation, receptor-fluorescent ligand and receptor-protein interactions.[24, 42, 44-45] Flow cytometry has been used for sorting cells based on the binding of fluorescent ligands to a particular receptor expressed by cells, for example NMP6[46] and HU210-Alexa488[47] (described in section 1.4.4). HTS with fluorescent ligands has been used to identify novel orthosteric and allosteric ligands, for example T1117[48] and NIR-mbc94[49] (described in section 1.4.4). Progress has also been made on the use of near-infrared (NIR) fluorescent ligands for the diagnostic imaging of GPCRs in healthy versus disease conditions (see section 1.4.4). The development of a high affinity fluorescent ligand also provides a robust platform for the preparation of other conjugates/chemical tools such as multivalent ligands, magnetic resonance active ligands, covalent ligands, and theranostic agents.

1.3 Adenosine A_1 receptor

Adenosine receptors (ARs) are class A GPCRs and are classified in four distinct subtypes - A_1AR, A_{2A} adenosine receptor (A_{2A}AR), A_{2B} adenosine receptor (A_{2B}AR) and A_3 adenosine receptor (A_3AR).[50] The endogenous nucleoside adenosine acts as an agonist at all AR subtypes and exhibits high affinity for A_1AR, A_{2A}AR and low affinity for A_{2B}AR, A_3AR.[51] Adenosine is clinically used for the treatment of supraventricular tachycardia. Initial indication for the existence of AR came from an increase in cAMP production by adenosine in guinea pig brain slices.[52] Later, each AR subtype was characterised based on the responses in pharmacological assays with agonists, antagonists and molecular cloning experiments.[53]

Activation of A_1AR and A_3AR inhibits adenyl cyclase via G protein $G_{\alpha i/o}$ and therefore decreases cAMP production. Activation of A_{2A}AR and A_{2B}AR stimulates adenyl cyclase via G protein $G_{\alpha s/o}$ and thus increases cAMP production.[51] Besides cAMP, AR also mediates signalling via modulation of messengers such as PLC, mitogen-activated protein

kinases (MAPK), ERK, and β-arrestin.[54] AR subtypes are expressed by many cells throughout the body with predominant expression in CNS, heart, lung, spleen, thymus, leukocytes, and platelets.[55] ARs are important drug targets for cardiovascular, renal, metabolic, immunological, and neurological disorders.[55] Regadenoson, an A_{2A}AR agonist, is commonly used for the diagnosis of coronary artery disease.[56]

A_1AR is primarily expressed in brain (cortex, hippocampus, cerebellum), spinal cord (dorsal horn), heart, eye, adrenal gland and its amino acid sequence is highly conserved among different species (≥94% sequence identity among six species).[53, 57] A_1AR modulation by synthetic small molecules is being pursued to treat various pathological conditions such as supraventricular tachycardia, angina pectoris, atrial fibrillation, myocardial infarction, congestive heart failure, hypertriglyceridaemia, diabetes, glaucoma, pain, liver fibrosis, Alzheimer's disease, Parkinson's disease, renal and immunological disorders.[58-61] Conversely, many such attempts have not been successfully translated into clinically used medicines. For example, one of the clinical trials conducted for rolofylline (a selective A_1AR antagonist) for the treatment of heart failure failed due to a lack of efficacy and increased occurrences of seizures and stroke compared to placebo.[62]

Adenosine A_1 receptor structure

Two A_1AR crystal structures were published in 2017 by Glukhova *et al.*[35] and Cheng *et al.*[63] (Figure 1.5). Glukhova *et al.* reported a 3.2 Å structure of A_1AR bound to A_1AR selective covalent antagonist DU172 (Figure 1.3) and Cheng *et al.*[63] reported a 3.3 Å structure of A_1AR (Figure 1.5) bound to A_1AR selective antagonist PSB36. Both of these crystal structures were obtained by incorporating a number of thermostabilising mutations in wild-type (WT) A_1AR to aid in the crystallisation process. Overall, the two structures were very similar to each other and both showed a difference in the conformation of EL2 compared to a previously reported A_{2A}AR crystal structure by Segala *et al.*[64] A cryoelectron microscopy structure of A_1AR complexed with a G protein was also reported near the submission date of this thesis.[8]

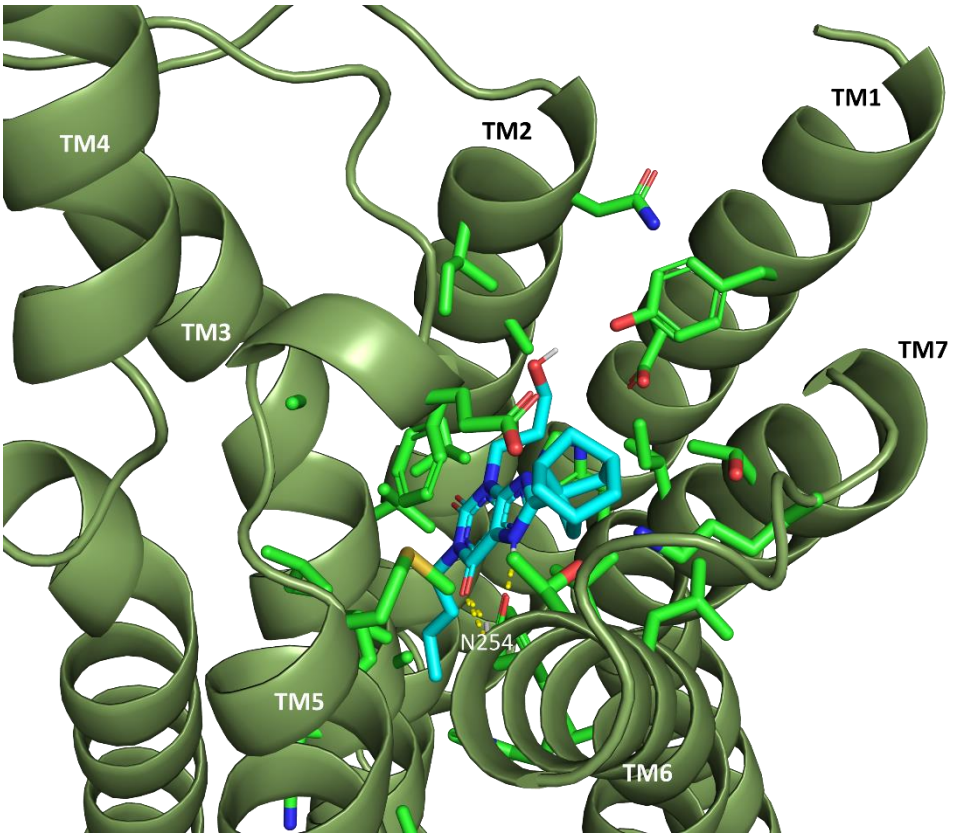

Figure 1.5. Crystal structure of A_1AR-PSB36 complex reported by Cheng *et al.*[63] (PDB ID 5N2S), hydrogen bond between PSB36 (cyan carbons, red oxygens, blue nitrogens) and N254 are shown as yellow lines, A_1AR (forest green ribbon). Side chain residues forming hydrogen bonds or hydrophobic interactions with PSB36 are shown as sticks (leaf green).

1.3.1 Small molecule ligands for Adenosine A_1 receptor

A brief overview of reported small molecule-based A_1AR ligands is provided in the following section. For a comprehensive review of these ligands, refer to reviews by Jacobson *et al.*[65], Müller *et al.*[66], Varani *et al.*[60], Giorgi *et al.*[59], and Dinh *et al.*[58].

Xanthine-based ligands

The discovery of xanthines such as caffeine (Figure 1.6, K_i = 10,700 nM at hA_1AR; 23,400 nM at human A_{2A} adenosine receptor (hA_{2A}AR); 33,800 nM at human A_{2B} adenosine receptor (hA_{2B}AR); 13,300 nM at human A_3 adenosine receptor (hA_3AR))[67-69] as AR antagonists led to intensive exploration of this scaffold for the development of AR ligands. Many reported xanthine-based AR ligands lack subtype selectivity, though A_1AR

selective xanthine analogues have been prepared. The xanthine based A_1AR selective antagonists mostly contain a cycloalkyl moiety at C-8 position, for example C-8 cyclopentyl xanthine DPCPX (Figure 1.2).[66] Some other xanthine-based high affinity and selective A_1AR antagonists (Figure 1.6) are – rolofylline (K_i = 0.72 nM at hA_1AR; 108 nM at hA_{2A}AR; 296 nM at hA_{2B}AR; 4930 nM at hA_3AR),[70-71] naxifylline (K_i = 0.45 nM at hA_1AR; 1100 nM at hA_{2A}AR; 611 nM at hA_{2B}AR; 4810 nM at hA_3AR)[70, 72] and tonapofylline (K_i = 7.4 nM at hA_1AR; 6410 nM at hA_{2A}AR; 90 nM at hA_{2B}AR; 10,000 nM at hA_3AR).[71] Rolofylline, naxifylline, and tonapofylline were investigated for the treatment of congestive heart failure, but failed to show any efficacy in clinical trials.[66, 73]

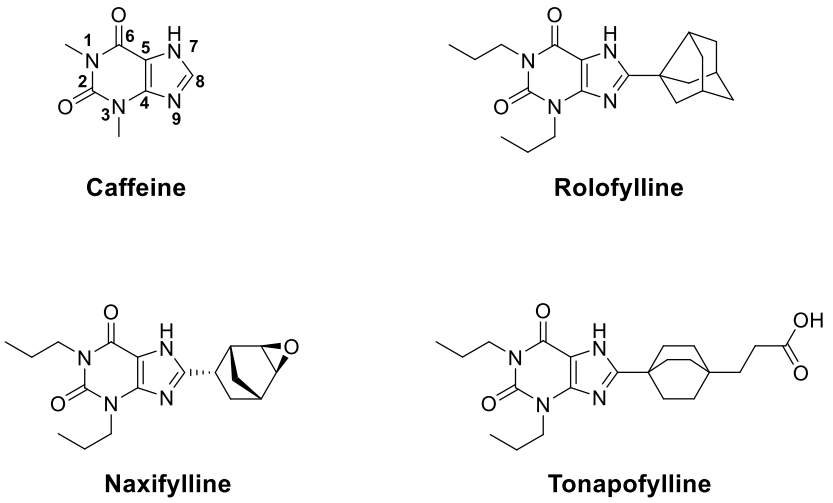

Figure 1.6. Non-selective xanthine AR antagonist caffeine and high affinity, A_1AR selective xanthine antagonists.

Most A_1AR agonists are derivatives of adenosine and contain a ribose moiety, which likely also contributes to the high affinity for A_1AR.[66] Tecadenoson (K_i = 0.45 nM at porcine A_1 adenosine receptor (pA_1AR); 2315 nM at hA_{2A}AR,) and selodenoson (data not reported in the literature) (Figure 1.7) are examples of selective xanthine A_1AR agonists which were investigated in clinical trials for the treatment of atrial fibrillation.[66]

Figure 1.7. A_1AR selective xanthine agonists.

Non-xanthine based ligands

A number of non-xanthine-based A_1AR antagonists have been reported. These include monocyclic pyrazoles, pyrimidines, triazines, thiazoles, fused bicyclic pyrazolopyrimidines, imidazopyridines, benzimidazoles, pyrazolopyridines, pyrrolopyrimidines, and fused tricyclic imidazoquinolines, pyrazoloquinolines.[74] SLV320 (Figure 1.8, K_i = 1.0 nM at hA_1AR; 398 nM at hA_{2A}AR; 3981 nM at hA_{2B}AR; 200 nM at hA_3AR) is a non-xanthine A_1AR antagonist which was investigated for the treatment of congestive heart failure.[75] (Benzimidazolyl)isoquinoline-based selective A_1AR antagonists have been reported,[76] and were investigated for the development into A_1AR fluorescent ligands in this thesis (chapter 2).

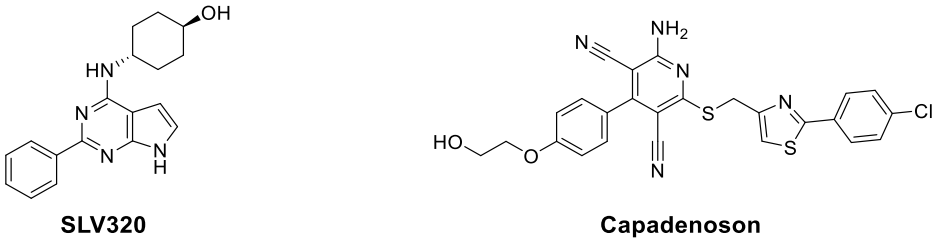

Figure 1.8. Non-xanthine A_1AR selective antagonist SLV320, and A_1AR, and A_{2B}AR selective agonist Capadenoson.

There are few reported non-adenosine-based A_1AR agonists.[77-78] Capadenoson[79] (Figure 1.8, EC_{50} = 0.1 nM at hA_1AR; >900 fold selectivity over hA_{2A}AR and hA_{2B}AR[61]), the first non-xanthine A_1AR agonist, was in clinical trials in patients suffering from atrial fibrillation but failed to show efficacy.[78] Although initially reported as a selective A_1AR agonist, capadenoson in a later report was shown to be an A_1AR and A_{2B}AR agonist.[80]

1.3.2 Fluorescent ligands of the adenosine A_1 receptor

As discussed in section 1.3, ARs are valuable drug targets and efforts have been made to develop fluorescent ligands for studying these receptors. Since the first report of an AR fluorescent ligand by Jacobson *et al.*[81], a number of AR fluorescent ligands based on adenosine, xanthine, and other fused ring heterocycles have been reported.[81-85 86-88] Most of the xanthine-based fluorescent ligands lack selectivity for AR subtypes.[83, 89] AR fluorescent ligands have been used to study various receptor processes such as receptor internalisation, and as tracers in fluorescence-based assays.[84, 90-91]

CA200645 (Figure 9; K_b = 3.98 nM at hA_1AR; 2.95 nM at hA_3AR) has been reported as a non-AR-subtype-selective fluorescent ligand and was used in chapter 2 of this thesis for determining AR affinity of the (benzimidazolyl)isoquinoline-based ligands.[92] Fluorescent ligands with high affinity and selectivity for $hA_{2A}AR$, $hA_{2B}AR$, and hA_3AR have been reported.[43, 82, 86, 93] Some examples of such fluorescent ligands include hA_3AR selective AV039 (K_d = 0.43 nM at hA_3AR; 275 nM at hA_1AR; >1000 nM at $hA_{2B}AR$);[54] $hA_{2A}AR$ selective BODIPY-650/665 derivative-14 (K_i = 15.1 ± 1.8 nM at $hA_{2A}AR$; 58 ± 4% inhibition at hA_1AR; 28 ± 3% inhibition at hA_3AR),[93] and $A_{2B}AR$ selective PSB-12105 (K_i = 1.83 ± 0.76 nM at $hA_{2B}AR$; >10,000 nM at $hA_{2A}AR$; >10,000 nM at hA_1AR; >10,000 nM at hA_3AR).[88]

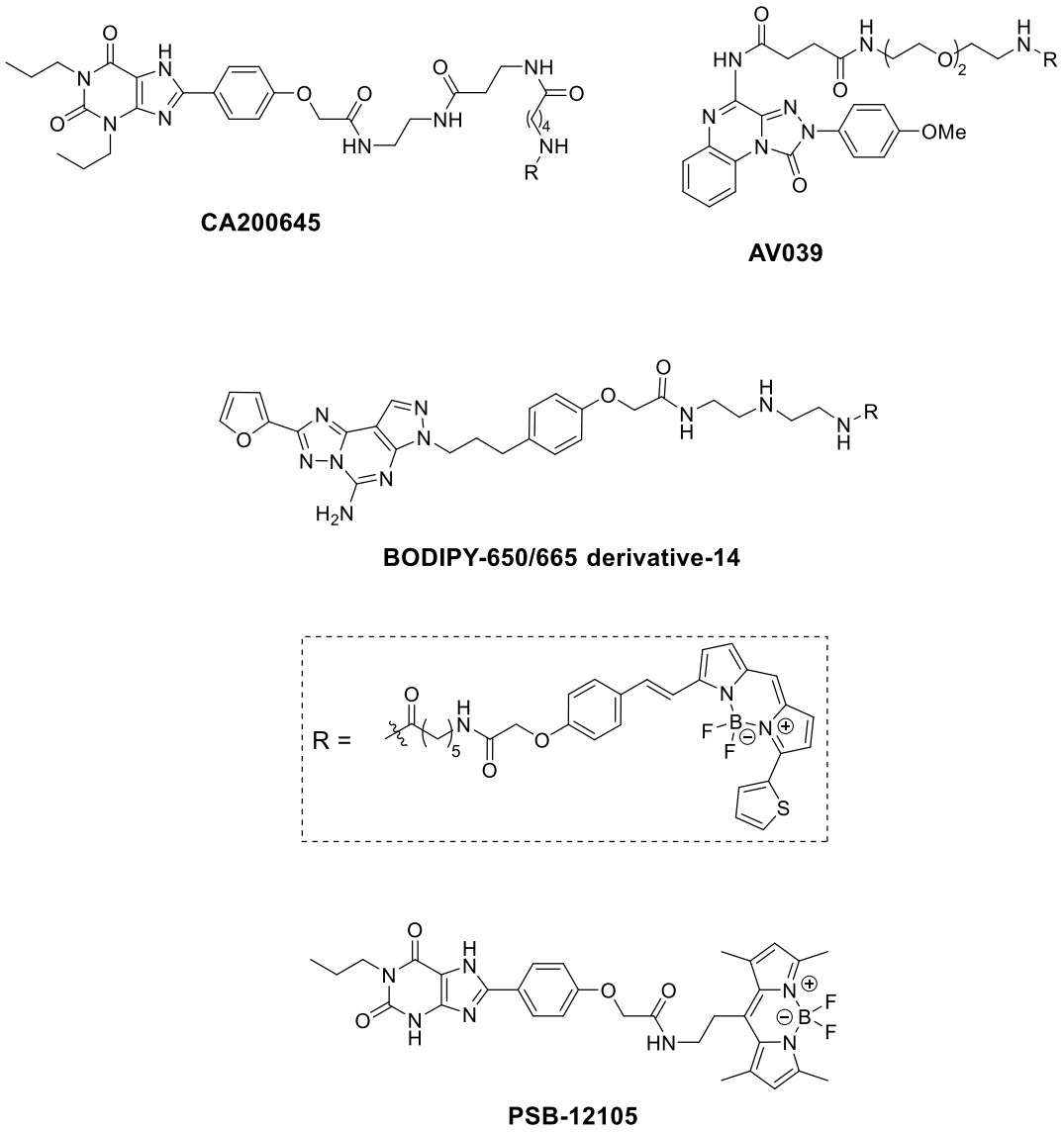

Figure 1.9. Reported high affinity AR fluorescent ligands CA200645, AV039, BODIPY-650/665 analogue-14, and PSB-12105.

There is a lack of a high affinity and selective A_1AR fluorescent ligands. Macchia *et al.*[94] reported rat A_1 adenosine receptor (rA_1AR) selective fluorescent ligands by modification of a non-selective AR agonist NECA (*N*-ethylcarboxamidoadenosine). Alkyl linkers of varying length were conjugated to NECA and the dansyl fluorophore (E_{ex} = 340 nM; E_{em} = 520 nm) was attached at the other end of the linker. Among the fluorescent ligands reported by Macchia *et al.*[94], dansyl derivative-1c (Figure 1.10, K_i = 27 ± 3 nM at rA_1AR; 4300 ± 400 nM at rat A_{2A} adenosine receptor (rA_{2A}AR); 3600 ± 260 nM at rat A_3 adenosine receptor (rA_3AR)) displayed the highest affinity for rA_1AR and selectivity over other AR subtypes. Fluorescent ligand dansyl derivative-1c was used for imaging rA_1AR in rat cerebral cortex. This dansyl fluorophore present in fluorescent ligand dansyl-1c

exhibits short excitation/emission wavelengths, which limit the application in imaging experiments. Macchia *et al.*[95] then developed a second series of fluorescent ligands by substituting the dansyl fluorophore of dansyl derivative-1c with nitrobenzoxadiazole (NBD) (E_{ex} = 465 nM; E_{em} = 535 nm). Nonetheless, the newly prepared fluorescent ligands did not exhibit significant affinity for A_1AR but exhibited high affinity for A_3AR. The highest affinity A_3AR fluorescent ligand of this series was NBD derivative-2d (Figure 1.10, K_i = 7.44 ± 2.38 nM at hA_3AR; 3476 ± 521 nM at hA_1AR; 5096 ± 764 nM at hA_{2A}AR).

Macchia *et al.*[96] subsequently prepared dansyl conjugates of a selective A_1AR antagonist naphthyridine. The naphthyridine-based dansyl derivative-3 (Figure 1.10) showed high affinity and selectivity at bovine A_1 adenosine receptor (bA_1AR) (K_i = 13 ± 2 nM) over bovine A_{2A} adenosine receptor (bA_{2A}AR) (K_i = 1430 ± 40 nM) and A_3AR (K_i = 1560 ± 36 nM at hA_3AR). Affinity data of the dansyl derivative-3 at A_1AR was not reported.

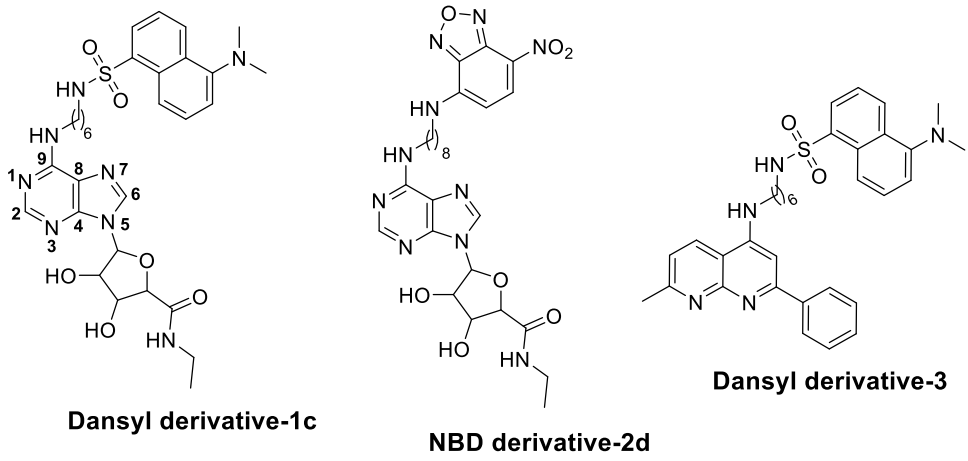

Figure 1.10. Previous attempts on the development of A_1AR selective fluorescent ligands.

In addition to these reports, other high affinity A_1AR fluorescent ligands that are non-AR-subtype-selective (or for which data at other AR subtypes is not reported) have been described in the literature.[81, 86, 89, 97-98 43, 88]

1.4 Cannabinoid receptors

Cannabinoid receptors (CBRs) are class A GPCRs and there are two subtypes – CB_1R and CB_2R. These receptors, along with endogenous CBR ligands such as anandamide (AEA; Figure 1.12) and regulatory proteins including enzymes and transporters, constitutes the endocannabinoid system.[99-100]

Two CBR agonists are in clinical use in New Zealand – nabilone (a derivative of (−)-trans-Δ^9-tetrahydrocannabinol (Figure 1.13; THC) derivative) for neuropathic pain and dronabinol (THC) for chemotherapy-associated vomiting.

1.4.1 Cannabinoid type 1 receptor

Initial evidence for the existence of CBR was provided by specific binding of the CBR radioligand [^{3}H]-CP55,940 to rat brain membrane,[101] and CB_1R was cloned in 1990.[102] CB_1R is one of the most highly expressed GPCRs in the CNS with the highest expression in substantia nigra, basal ganglia, globus pallidus, cerebellum, hippocampus and low expression in peripheral organs.[103-105] CB_1R primarily signals via coupling to G protein $G_{\alpha i/o}$, though recently signalling via coupling to $G_{\alpha s}$ and/or $G_{\alpha q}$ has also been reported.[106] Activation of CB_1R results in inhibition of adenyl cyclase and reduction in the production of cAMP in CB_1R expressing cells.[106] CB_1R also mediates signals via modulation of other messengers such as PLC, MAPK, ERK, calcium, and potassium channels.[106-107] CB_1R, located in the presynaptic terminal of the neurons, participates in the retrograde signalling by inhibition of release of excitatory and inhibitory neurotransmitters.[107] Further, CB_1R is known to signal via β-arrestin[108] and a study[109] conducted with β-arrestin 2 knockout mice suggested that CB_1R ligands showing preference for G protein signalling over β-arrestin-2 signalling might show analgesic activity with reduced side effects associated with CBR ligands.

CB_1R is involved in the regulation of a variety of pathological processes including obesity, pain, multiple sclerosis, Parkinson's disease, Alzheimer's disease, Huntington's disease, myocardial infarction, heart failure, atherosclerosis, stroke, liver cirrhosis, pancreatitis, anxiety, schizophrenia, rheumatoid arthritis, and cancer.[99, 110] SR141716A

(Rimonabant; Figure 1.14), a selective CB_1R inverse agonist, was approved by the European Medicines Agency for the treatment of obesity but was withdrawn due to associated psychiatric disorders including suicide.[25]

Cannabinoid type 1 receptor structure

The first three crystal structures of CB_1R were published in 2016 and 2017. Shao *et al.*[111] reported a 2.6 Å structure of CB_1R complexed to CB_1R selective inverse agonist taranabant. Hua *et al.*[112] reported a 2.8 Å structure of CB_1R complexed to CB_1R antagonist AM6538 and subsequently a 2.8 Å structure of CB_1R complexed to CB_1R agonist AM11542[113] (Figure 1.11). The inverse agonist taranabant complex and antagonist AM6538 bound structure showed overall similarity. Significant structural differences were observed in the agonist AM11542-CB_1R structure compared to the inverse agonist and antagonist-CB_1R structures, including major conformational changes in the TM1, TM2, and TM6. In agreement with the crystal structure of the active state β_2ADR (bound to $G_{\alpha s}$),[114] the agonist AM11542-CB_1R structure showed outward movement of cytoplasmic part of TM6. Notably, a large reduction in the volume of the ligand-binding pocket in the agonist AM11542-CB_1R structure compared to antagonist AM6538-CB_1R structure was observed.

The differences observed in the agonist-CB_1R and antagonist-CB_1R structures emphasise the importance of choosing a suitable agonist/antagonist structure for docking studies of CBR ligands. The CB_1R crystal structure (PDB ID: 5XRA) reported by Hua *et al.*[113] was used for the docking studies of ligands in chapter 5 (section 5.1) of this thesis.

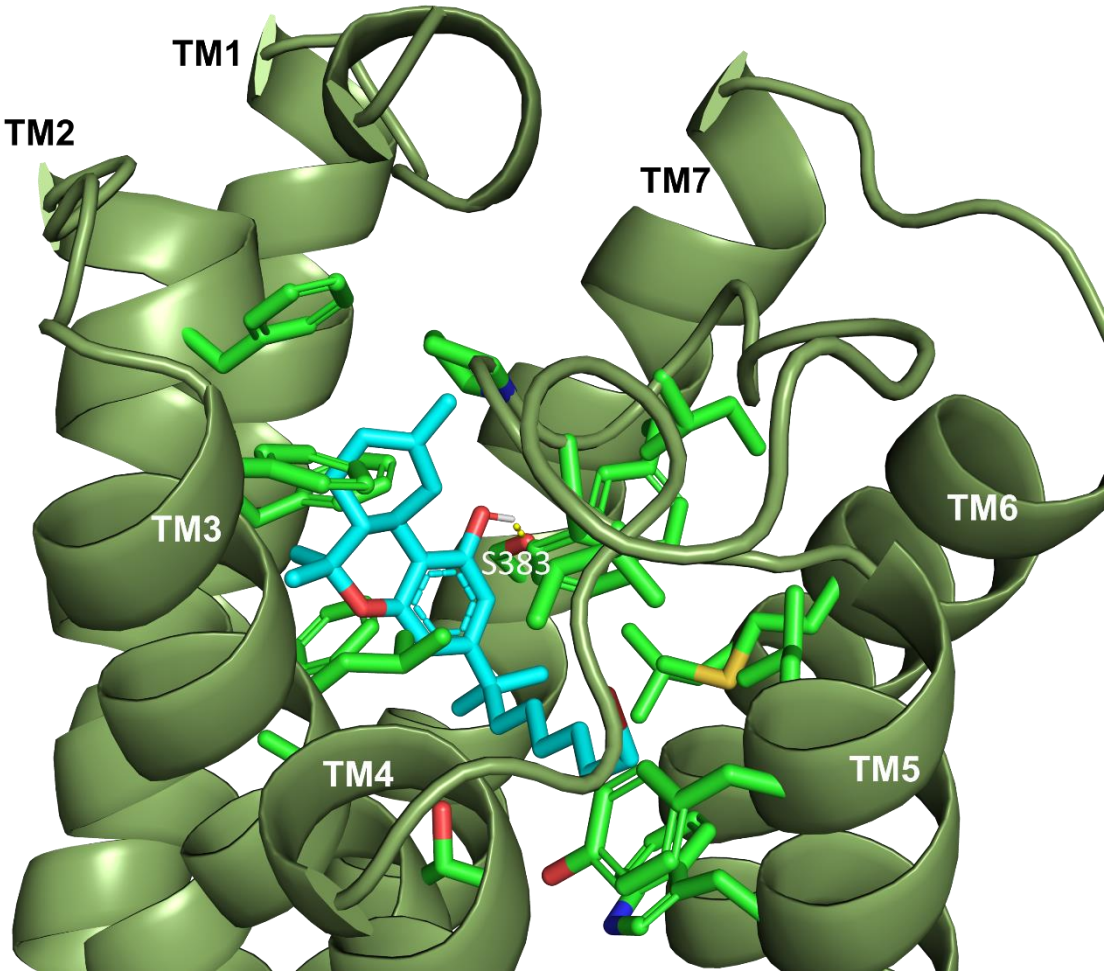

Figure 1.11. Crystal structure of CB_1R-AM11542 complex (PDB ID: 5XRA) reported by Hua *et al.*[113], the hydrogen bond between AM11542 (cyan carbons, red oxygens, blue nitrogens) and S383 is shown as a yellow line, CB_1R (forest green ribbon). Side chain residues forming hydrogen bonds or hydrophobic interactions with AM11542 are shown as sticks (leaf green).

1.4.2 Cannabinoid type 2 receptor

The CB_2R was cloned in 1990[102] and is primarily expressed in immune cells, spleen, tonsils,[115] with low expression in CNS.[116] Similar to CB_1R, CB_2R primarily signals via coupling to G protein $G_{\alpha i/o}$ and modulates messengers such as adenyl cyclase, MAPK, ERK, potassium, and calcium channels.[117] CB_2R is also recognised to signal via β-arrestin pathway.[118-119]

CB_2R plays an important role in a number of pathological processes including inflammation, pain, atherosclerosis, multiple sclerosis, HIV-induced encephalitis, cancer, Parkinson's disease, Alzheimer's disease, Huntington's disease, myocardial infarction,

heart failure, atherosclerosis, stroke, liver cirrhosis, pancreatitis, and rheumatoid arthritis.[99, 110, 117, 120] In contrast to CB_1R, agonists targeting CB_2R are thought to exhibit reduced or no psychoactive side effects due to the low abundance of CB_2R in the brain.[117] A number of CB_2R agonists are being investigated in clinical trials for analgesic activity.[121]

At the time of writing this thesis, the crystal structure of CB_2R was not reported. CB_1R and CB_2R have 44% overall sequence identity and 68% sequence identity in the TM region,[122] and a number of ligands activate both CB_1R and CB_2R including the endogenous ligands AEA and 2-arachidonylglycerol (2-AG; Figure 1.12.). Hence, it is likely that these receptors share substantial structural similarity and possess a similar orthosteric ligand-binding pocket. Homology modelling is commonly used to generate a structure of a protein based on the structure of a closely related protein. In chapter 3 (section 3.4) of this thesis, a homology model of CB_2R was built using CB_1R crystal structure (PDB ID: 5XRA) reported by Hua *et al.*[113] and was used for ligand docking studies.

1.4.3 Small molecule ligands for cannabinoid receptors

Small molecule CBR ligands have been comprehensively covered in reviews by Pertwee *et al.*[107], Ganesh *et al.*[123], Tabrizi *et al.*[124], and only a brief overview of small molecule CBR ligands is provided here.

Endogenous cannabinoid receptor ligands

The most studied endogenous CBR ligands are arachidonic acid derivatives – AEA (K_i = 70 ± 30 nM at hCB_1R; 180 ± 20 nM at hCB_2R)[125], 2-AG (K_i = 480 ± 12 nM at hCB_1R; 1300 ± 215 nM at hCB_2R)[125] (Figure 1.12) and both act as agonists at CBRs. Most of the endogenous CBR ligands show modest selectivity for CB_1R over CB_2R and contain a hydrophobic chain joined to a polar head group.[121] In contrast to the typical neurotransmitters (such as serotonin, epinephrine, dopamine, and histamine), these endogenous CBR ligands are not stored in vesicles but are synthesised on demand by specific enzymes from membrane phospholipids, and after participating in signalling via

interaction with CBRs are degraded by regulatory enzymes.[126] Inhibitors of regulatory enzymes such as fatty acid amide hydrolase (FAAH) and monoacylglycerol lipase are being developed as therapeutic agents for CBR associated diseases.[127] One such FAAH inhibitor BIA 10-2474 produced mild to severe neurotoxicity in some volunteers in a phase 1 clinical trial.[128] In a later study[129], BIA 10-2474 was shown to inhibit many other serine hydrolases besides FAAH and this lack of selectivity might have contributed to the neurotoxicity of BIA 10-2474.

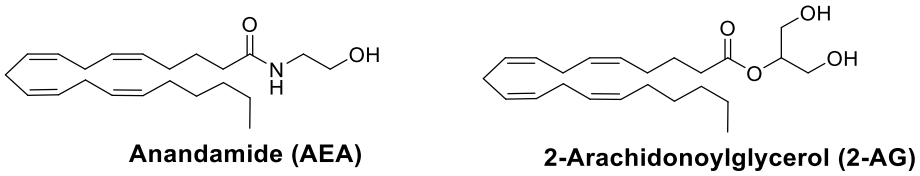

Figure 1.12. Endogenous CBR ligands anandamide and 2-arachidonylglycerol.

Cannabis-derived cannabinoid receptor ligands

THC (Figure 1.13, K_i = 40.7 ± 1.70 nM at hCB_1R; 36.4 ± 10.0 nM at hCB_2R),[130] a non-selective CBR agonist, was identified as the primary psychoactive constituent of *Cannabis sativa* in 1964 by Gaoni *et al.*[131] Since then a number of structural derivatives of THC have been synthesised and comprehensive SAR data is available.[132] Among the THC analogues, a side chain of seven carbons is observed to be optimal for CBR binding.[132] Most of the THC analogues are non-selective CBR ligands, however, CB_2R selective compounds have been prepared by removal of the C-1 hydroxyl.[121, 132]

Most of the CBR ligands exhibit high lipophilicity and a water-soluble prodrug of a THC derivative – O-1057 (Figure 1.13), has been reported.[121, 133] A bicyclic analogue of THC – CP55,940 (Figure 1.2; K_i = 0.55 nM at hCB_1R; 3.63 nM at hCB_2R)[119] exhibits high affinity for both CBRs and the ^3H labelled analogue [^3H]-CP55,940 (Figure 1.2) is a commonly used tracer in the pharmacological experiments. Cannabidiol (Figure 1.13, K_i = 4350 ± 390 nM at hCB_1R; 2860 ± 1230 nM at hCB_2R)[121] is a major constituent of cannabis extract, which exhibits weak affinity and high potency antagonism at CBRs.[134-135] Cannabidiol is currently being investigated in clinical trials for the treatment of a number of inflammatory diseases[136] and was recently recommended by the Food and

Drug Administration (FDA) for investigation in the treatment of Lennox-Gastaut syndrome and Dravet syndrome. Chromenopyrazole CBR ligands,[137] which are structural derivatives of cannabinol (CBN; Figure 1.13, K_i = 211.2 ± 35.0 nM at rat cannabinoid type 1 receptor (rCB_1R); 126.4 ± 26.0 nM at hCB_2R)[138] were explored in this thesis for the development of CBR fluorescent ligands (chapters 3 and 4).

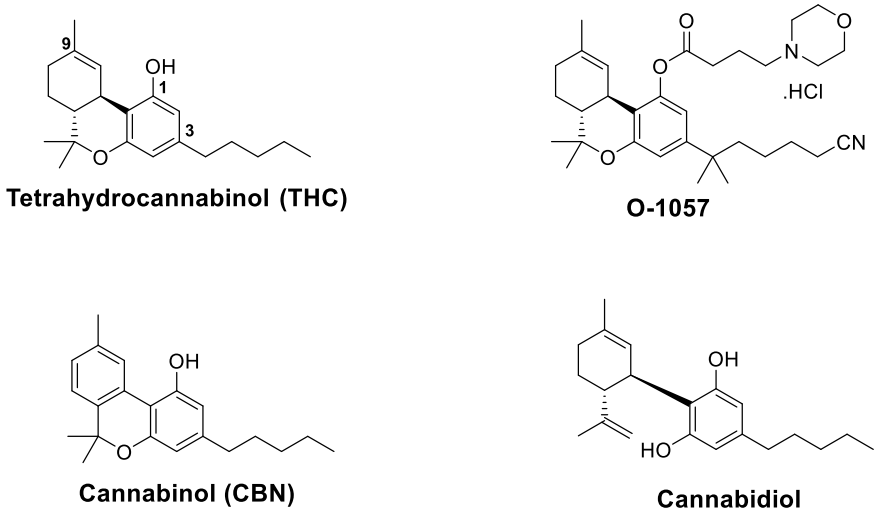

Figure 1.13. Representative examples of plant-derived CBR ligands – THC, cannabidiol, and prodrug O-1057.

Synthetic cannabinoid receptor ligands

The development of ligands antagonising CB_1R has undergone a significant change in direction since the associated psychiatric side-effects of CB_1R antagonists became known with the clinical trial results of SR141716A. Since then, most of the medicinal chemistry efforts targeting CBR have focused on the development of CB_2R agonists, biased CB_1R agonists, and peripherally-restricted CB_1R agonists.[117, 139-140] A number of heterocyclic derivatives exhibiting excellent selectivity and affinity for CB_1R or CB_2R are reported in the literature.[107, 124, 141] The most studied of these CBR ligands contain pyrazole or indole heterocycles.

Most of the pyrazole CBR ligands contain aryl groups at N-1 and C-5 positions and a carboxamide moiety at the C-3 position (Figure 1.14). Notable pyrazole CBR ligands are SR141716A (Figure 1.14, K_i = 25.0 ± 15 nM at hCB_1R; 1580 ± 150 nM at hCB_2R)[142] and

SR144528 (Figure 1.14, K_i = 437 ± 33 nM at hCB_1R; 0.60 ± 0.13 at hCB_2R)[143] developed by Sanofi. SR141716A is a high affinity, selective CB_1R inverse agonist which inhibits many *in vitro* and *in vivo* effects produced by CB_1R activation and along with its tritiated form [^{3}H]-SR141716A (Figure 1.14, K_d = 1.05 ± 0.19 nM at hCB_1R)[144] is frequently used in pharmacological experiments.[141] SR144528 is a selective CB_2R antagonist which counters many of the *in vitro* effects produced by CB_2R activation and is also commonly used in pharmacological experiments.[141]

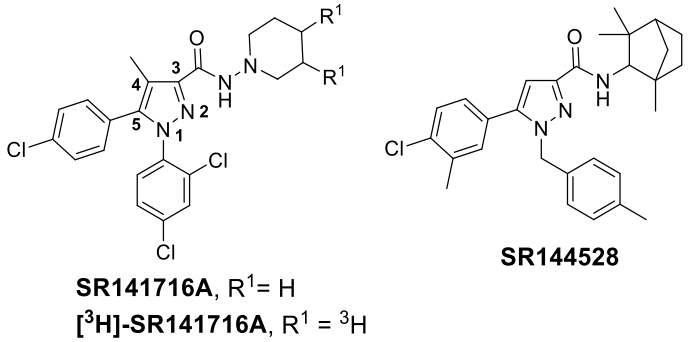

Figure 1.14. Representative examples of pyrazole cannabinoid receptor ligands – SR141716A, [^{3}H]-SR141716A, and SR144528.

Most of the indole-based CBR ligands contain a carboxamide moiety at the C-3 position and an alkyl chain at the N-1 position (Figure 1.15). A notable CBR indole-based ligand is *R*-(+)-WIN55212 (Figure 1.15, K_i = 40.9 ± 1.7 nM at hCB_1R; 2.9 ± 0.3 nM at hCB_2R),[145] which along with its tritiated form [^{3}H]-WIN55212 (racemic mixture, K_d = 11.9 ± 1.9 nM at hCB_1R[146]; 2.1 ± 0.2 nM at hCB_2R[147]) are commonly used as CBR agonists in pharmacological studies. A number of analogues of the indole scaffold have also been prepared as CBR 'designer drugs' or better known in New Zealand as 'legal highs' (although now illegal), for example, AB-FUBICA (Figure 1.15, EC_{50} = 21 nM at hCB_1R; 15 nM at hCB_2R).[148]

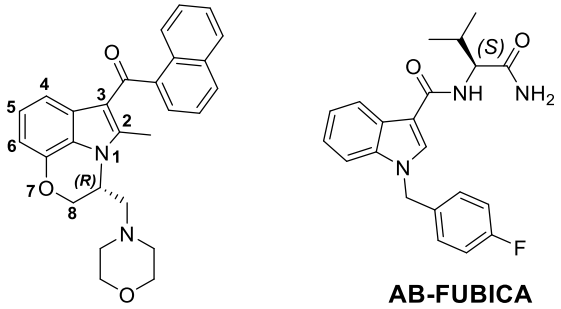

Figure 1.15. Representative examples of indole cannabinoid receptor ligands – *R*-(+)-WIN55212 and AB-FUBICA.

In addition to the small molecule CBR radioligands shown in this chapter that are used primarily in *in vitro* studies, a number of highly selective CBR radioligands for *in vivo* imaging have been reported. For example [^{11}C]OMAR (K_i = 11 ± 7 nM at hCB$_1$R),[149] [^{18}F]MK-9470 (IC_{50} = 0.7 nM at hCB$_1$R; 44 nM at hCB$_2$R)[150] and [^{11}C]NE40 (K_i > 1000 nM at hCB$_1$R; 9.6 nM at hCB$_2$R).[151]

1.4.4 Fluorescent ligands for cannabinoid receptors

Fluorescent ligands for *in vitro* experiments

Earliest reports of CBR ligands-based fluorescent compounds detailed the preparation of dansyl derivatives of THC[152] in 1971 and benzoxadiazole derivatives of AEA[153] in 1995. Both of these reports prepared fluorescent ligands as tools to study the bio-distribution of AEA and chromatographic studies of AEA and THC.

The first development of fluorescent ligands for specifically studying CBR was of NBD derivatives of CB$_2$R agonist JWH-015 by Yates *et al.*[154] in 2005. This NBD derivative was designed using *de novo* drug design and the position of linker attachment to JWH-015 was identified with docking studies using a CB$_2$R homology model. Unfortunately, the NBD-JWH-015 derivative did not exhibit significant CB$_2$R affinity (for example only 25% displacement of [^{3}H]-CP55,940 from hCB$_2$R at 10 μM of one NBD derivative) and in confocal microscopy experiments showed non-specific accumulation in the cytosol.[154] Cooper *et al.*[155] also reported indole-based CB$_2$R fluorescent ligands. Among the different indole positions explored for linker attachment, a C-7 *O*-propyl linker derivative

(K_i = 504.6 ± 148.2 at hCB_1R; 5.7 ± 1.4 nM at hCB_2R) exhibited the highest affinity for CB_2R out of the various derivatives reported. Interestingly, a positional dependence of functional activity was observed with C-5 indole derivatives being agonists and C-7 indole derivatives being inverse agonists in a cAMP BRET assay. Unfortunately, none of the indole-linker-BODIPY630/650 derivatives exhibited any significant affinity for CB_2R.[155]

Petrov *et al.*[46] reported a derivative of the CBR ligand isatin acylhydrazone where the morpholine group was substituted with a NBD fluorophore to provide a CB_2R selective fluorescent ligand NMP6 (Figure 1.16, K_i = 387 nM at hCB_2R; <40% displacement of [^{3}H]-CP55,940 at hCB_1R at 10 μM). This substitution was based on the assumption that the lipophilic CB_2R cavity, believed to interact with the morpholine moiety of the parent ligand, would accommodate the NBD fluorophore. Confocal imaging with NMP6 showed specific binding of NMP6 to CB_2R expressing $CD4^+$ T-cells, which was abolished by preincubation with selective CB_2R agonist GW842166X. NMP6 was also shown to be useful in flow cytometry experiments to study CB_2R expression in mouse lung mononuclear B cells.[46] The functional activity of NMP6 at CBRs was not reported.[46] The NBD (E_{ex} = 465 nM; E_{em} = 535 nm) fluorophore in NMP6 shows short excitation/emission wavelengths, which limit its use in other imaging experiments.

T1117 (tocrifluor 1117, Figure 1.16) is a commercially available fluorescent ligand, and can be prepared by conjugation of a AM251 derivative to a 2-(3,6-bis(dimethylamino)xanthylium-9-yl)-5-carboxybenzoate (TAMRA) fluorophore. Contradictory pharmacological results have been reported for T1117. Daly *et al.*[156] reported T1117 to exhibit only weak affinity for CB_1R with binding at GPR55 (indicated by the increased Ca^{2+} response in GPR55 expressing human embryonic kidney (HEK)-293 cells). However, in a subsequent study, T1117 (K_d = 460 ± 80 nM at rCB_1R) was reported to exhibit a moderate affinity for CB_1R.[48] T1117 was used as a tracer in a fluorescence-based HTS at CB_1R to identify orthosteric ligands AEA, AM251 (with obtained IC_{50} values in agreement with those reported in the literature) and allosteric CBR ligand ORG27569.[48] However, T1117 showed non-specific membrane binding which limits its use in studying CB_1R in native cell environments.[48]

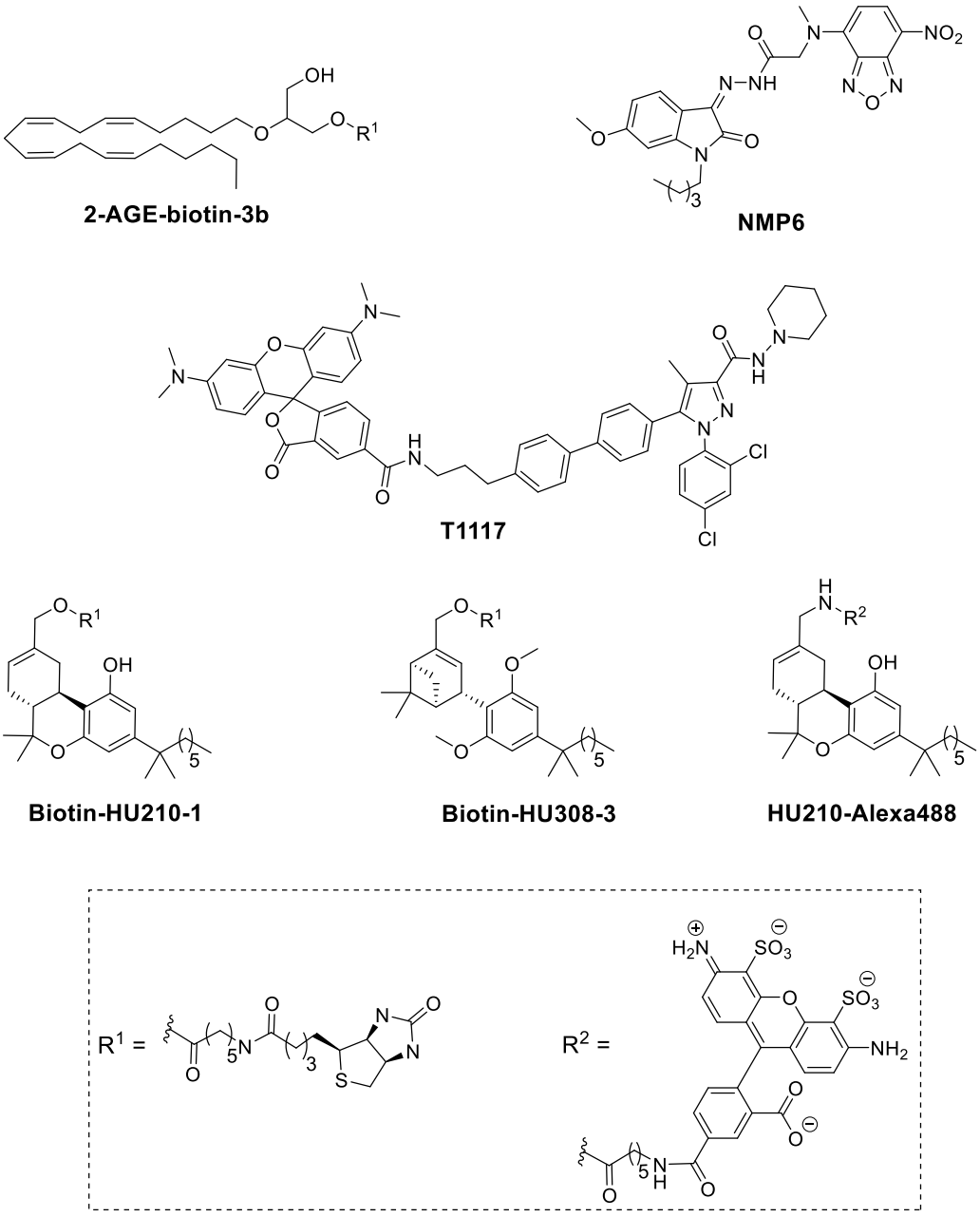

Figure 1.16. Fluorescent CBR ligands for *in vitro* imaging reported in the literature.

Martín-Couce *et al.*[157] reported biotin or alkyne derivatives of endocannabinoids AEA, 2-AG, and 2-AGE for the subsequent *in situ* labelling with a streptavidin-fluorophore or a 'click' reaction partner. The alkyne derivative of 2-AGE (K_i = 84.7 ± 0.8 nM at hCB_1R; 84.9 ± 0.6 nM at hCB_2R) exhibited the highest affinity but lacked subtype selectivity whereas biotin derivative 2-AGE-biotin-3b (Figure 1.16, K_i = 221 ± 8 nM at hCB_1R; 450±11 nM at hCB_2R) showed some subtype selectivity. Imaging studies were carried out with 2-AGE-biotin-3b and streptavidin-Alexa488 fluorophore in CB_1R expressing mouse hippocampal cells. However, some background fluorescence in control

experiments with non-transfected mouse hippocampal cells or on co-treatment with unlabelled CBR agonist HU210 was observed. As endocannabinoids such as 2-AGE are lipid derivatives, high non-specific membrane binding is likely and emphasises the advantages of using non-lipid-based ligands as the basis for the development of fluorescent ligands.

In further work, Martín-Couce *et al.* described biotin derivatives of high affinity CBR ligands HU210 and HU308 for subsequent *in situ* conjugation with a streptavidin-fluorophore conjugate.[158] Biotin-HU210-1 (Figure 1.16, K_i = 2.4 ± 0.4 nM at hCB_1R; = 1.6 ± 0.4 nM at hCB_2R) exhibited high affinity for CBR but lacked subtype selectivity whereas biotin-HU308-3 (Figure 1.16, K_i = 44 ± 4 nM at hCB_2R; >5000 nM at hCB_1R) showed high CB_2R selectivity. Biotin-HU210-1 and biotin-HU308-3 together with *in situ* reaction partner streptavidin-Alexa488 fluorophore were used to study CBR expression in neurons and microglia and specific binding was established by treatment with unlabelled HU210.[158] In a subsequent report by the same research group, biotin-HU210-1 along with an *in situ* reaction partner streptavidin-Alexa488 fluorophore were used to show high CB_1R expression in B,T, and dendritic cells of donors suffering from rhinitis, atopic dermatitis or food allergies.[159]

The same group of researchers subsequently reported a high affinity and CB_1R selective fluorescent ligand HU210-Alexa488 (Figure 1.16, K_i = 27 ± 4 nM at hCB_1R; 800 ± 200 nM at hCB_2R), prepared by conjugation of HU210 with fluorophore Alexa488.[47] HU210-Alexa488 was used to study CB_1R expression in immune cells by flow cytometry and confocal microscopy. A change in membrane CB_1R expression following prolonged stimulation with a CBR agonist was also studied using HU210-Alexa488. Mononuclear cells were treated with CBR agonist HU210 or WIN55212 for 18 h and subsequent analysis by flow cytometry using HU210-Alexa488 showed a decrease in the percentage of mononuclear cells expressing CB_1R.[47] The functional activity of HU210-Alexa488 at CBRs was not reported.[47] The Alexa488 (E_{ex} = 490 nM; E_{em} = 525 nm) fluorophore present in HU210-Alexa488 displays short excitation/emission wavelengths, which might limit its use in some imaging experiments.

Fluorescent ligands with near-infrared wavelength fluorophores

A number of NIR fluorescent ligands amenable to *in vivo* imaging of CB_2R have been reported. NIR fluorophores with fluorescence in the NIR region (700-900 nm) or NIR-II region (1,000-1,700 nm) are attractive for *in vivo* imaging as can be detected at a tissue depth of 5-7 mm.

Bai *et al.*[160] prepared mbc94 (Figure 1.17, K_i = 15 nM at murine cannabinoid type 2 receptor (mCB_2R)) by conjugation of a linker to SR144528 (a selective CB_2R inverse agonist, Figure 1.14). Conjugation of mbc94 to IRDye 800CW provided fluorescent ligand NIR-mbc94 (Figure 1.17, K_i = 260 nM at mCB_2R) with some loss in CB_2R affinity compared to mbc94.[49] A HTS assay was developed to identify CB_2R ligands using NIR-mbc94 and CB_2R-mid DBT cells (mouse delayed brain tumour cells transfected with CB_2R). However, imaging experiments with NIR-mbc94 at mouse microglia cells that natively expressed CB_2R showed a high degree of non-specific binding.[49]

The same team of researchers subsequently reported NIR760-mbc94 (Figure 1.17, K_d = 26.9 ± 3.7 nM at mCB_2R), prepared by the conjugation of previously reported mbc94 with a NIR760 fluorophore.[161] Experiments were carried out to determine specific binding of NIR760-mbc94 by incubation with CB_2R-mid DBT cells in the presence and absence of non-fluorescent SR144528. CB_2R-mid DBT cells preincubated with SR144528 showed 40% reduction in fluorescence compared to CB_2R-mid DBT cells incubated with only NIR760-mbc94. The residual fluorescence indicated non-specific binding and according to authors arose from non-specific protein binding of negatively charged NIR760-mbc94. As CB_2R plays important role in inflammation, NIR760-mbc94 was used by Zhang *et al.*[162] for *in vivo* imaging of mCB_2R expression in Freund's adjuvant-induced inflammation mouse model, however high non-specific binding of NIR760-mbc94 as indicated by appearance of fluorescence all over the mouse body was observed.

The same research group reported NIR760-Q (Figure 1.17, K_d = 75.51 ± 27.97 nM at hCB_2R), prepared by conjugation of a quinolone ligand with a NIR760 fluorophore.[163] Imaging experiments with NIR760-Q in Jurkat cells that naturally express CB_2R showed non-specific binding of NIR760-Q, which the authors attribute to the negative charge of

NIR760-Q. The same researchers then reported zwitterionic NIR-fluorophore-derivative ZW760-mbc94 (Figure 1.17, K_d = 53.9 ± 13.0 nM at mCB_2R). *In vitro* experiments by incubating CB_2R-mid DBT cells with ZW760-mbc94 in the presence or absence of unlabelled CB_2R ligand 4Q3C (a non-fluorescent, high affinity, selective CB_2R agonist) showed some CB_2R-specific binding. *In vivo* imaging experiments in a mouse cancer model (mouse injected with CB_2R-mid DBT cells in right flank) showed low CB_2R specific binding with high fluorescence in the liver and throughout the whole body.[163]

The same team of researchers then conjugated a pyrazolopyrimidine ligand to a NIR760 fluorophore to give NIR760-XLP6 (Figure 1.17, K_d = 169.1 ± 66.09 nM at mCB_2R; > 10,000 nM at murine cannabinoid type 1 receptor (mCB_1R)).[164] *In vivo* imaging experiments to determine CB_2R specific binding were carried out and showed 40% higher fluorescence in mice with CB_2R-mid DBT tumours compared to mice with CB_1R-mid DBT tumours (mice injected with hCB_1R transfected mid DBT cells) indicating non-specific binding of NIR760-XLP6.

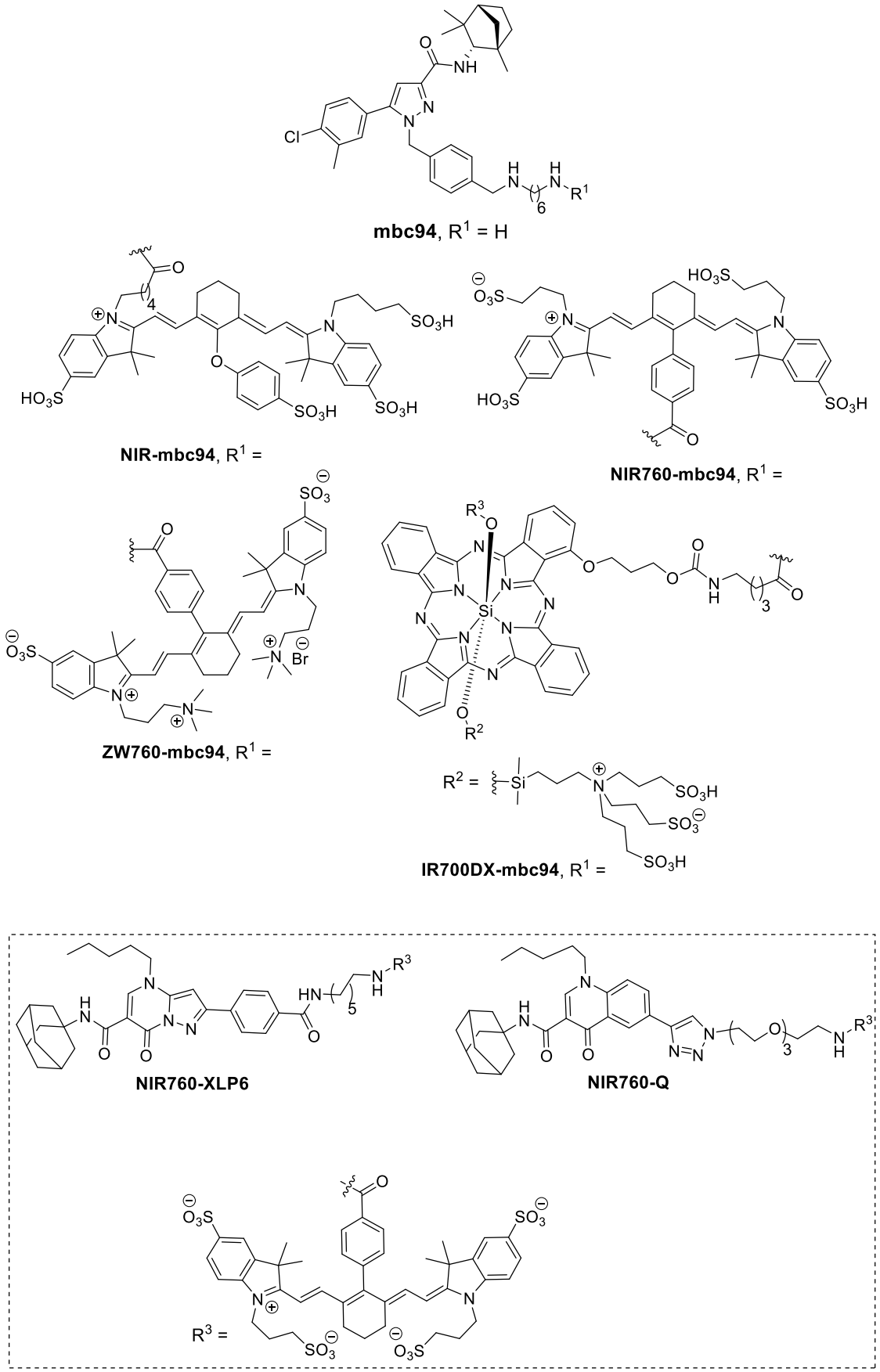

Figure 1.17. Fluorescent CB_2R ligands amenable to *in vivo* imaging reported in the literature.

In photodynamic therapy, photosensitisers (compounds that absorb light of a particular wavelength to produce cytotoxic oxygen reactive species) are used for the treatment of a number of diseases including cancer. Zhang *et al.*[165], part of the same research group as Bai *et al.*, have described a CB_2R photosensitiser – IR700DX-mbc94 (Figure 1.17, K_d = 42.0 ± 19.6 nM at mCB_2R) by conjugating fluorophore IR700DX to mcb94. Irradiation with light (wavelength 670-710 nm) in photosensitiser IR700DX-mbc94 injected mice inhibited the growth of CB_2R-mid DBT tumours and not that of the CB_2R negative-tumours. The same group of researchers has also reported SR144528 derivatives conjugated to an IRDye800CW fluorophore, a topoisomerase inhibitor (such as etoposide), and a gadolinium chelate in a patent report.[166]

As described in this section, progress has been made in the development of CBR fluorescent ligands. However, most of the reported CBR fluorescent ligands either lack high affinity and selectivity at CBR subtypes, exhibit high non-receptor-specific binding in imaging studies, and/or contain short wavelength fluorophores (for example NBD and Alexa488, with fluorescence spectra susceptible to interference from the fluorescence of cellular components), and thus have drawbacks in imaging studies and in studying CBR in native cell environments.

1.5 Biological evaluation of ligands described in this thesis

Biological evaluation of the compounds synthesised as potential A_1AR ligands (chapter 2) was carried out by members of Professor Stephen Hill's research group at the University of Nottingham, United Kingdom. Therefore these pharmacological assays are not described herein (for details refer to the published manuscript of this work[167]). Biological evaluation of CBR ligands synthesised in this thesis (chapters 3-5) was carried by myself with the training and assistance of collaborators at the University of Auckland. Hence an overview of the CBR pharmacological assays is provided below.

1.5.1 Radioligand binding assays for cannabinoid receptors

A competition radioligand binding assay with radioligand [^{3}H]-CP55,940 and CB_1R or CB_2R expressing HEK-293 cells was used for determining the binding affinity of novel ligands (refer to chapter 7, experimental section 7.1.2 for experimental details). A fixed concentration of radioligand and membrane preparation expressing CB_1R or CB_2R are treated with an increasing concentration of a test compound. The membrane preparation bound radioligand is separated from the free radioligand and the radioactivity of the membrane preparation is measured. A high affinity test compound would better compete with radioligand for the receptor binding site and hence a lower radioactivity for the membrane preparation (compared to a weak affinity test compound) would be measured.

The affinity (K_i) of the test compound is then calculated by non-linear regression using the amount of radioactivity retained in the membrane preparation and by using a previously measured K_d for the radioligand. Competition radioligand binding assay data of some high affinity compounds are presented in the form of a sigmoid curve by plotting bound radioligand (radioactivity count) against the logarithm of test ligand concentration.

1.5.2 Functional assays for cannabinoid receptors

Radioligand binding assays provide information about the affinity of a ligand to a receptor, but do not provide information about the functional nature of a ligand, that is agonist, antagonist, or inverse agonist. There are a number of CBR signalling pathways (described in section 1.4.1 and 1.4.2), and there are a range of reported assays that can be used to measure the activity of a CBR ligand in each pathway. Some of the commonly used assays used to determine functional activity of CBR ligands are by measurement of cAMP production, GTPγS binding, β-arrestin recruitment, G protein-coupled inwardly-rectifying potassium channels (GIRK), and phosphorylation of ERK activation.[32, 117, 119, 168]

The function of CBR ligands described in chapters 3-5 was evaluated using a cAMP BRET assay as described previously by Cawson *et al*.[169] and Jiang *et al.*[170] As mentioned previously in sections 1.4.1 and 1.4.2, both CB_1R and CB_2R are $G_{\alpha i}$ coupled receptors,

which upon activation by an agonist, inhibit adenyl cyclase and consequently decreases the production of cAMP.

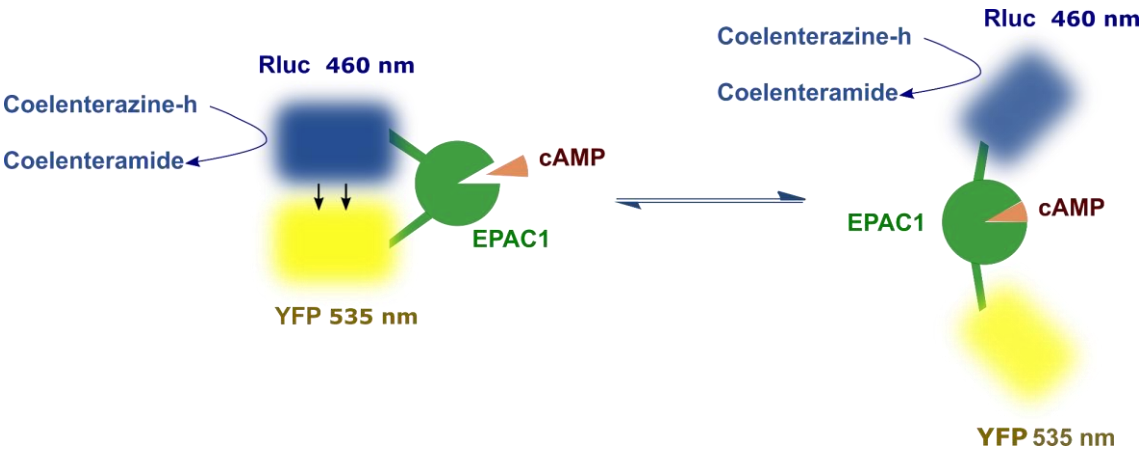

Figure 1.18. Schematic representation of BRET CAMYEL sensor for real-time cAMP measurement reported by Cawson *et al.*[169] and Jiang *et al.*[170]

The cAMP BRET assay reported by Cawson *et al.*[169] and Jiang *et al.*[170] probes the function of CBR ligands by measuring the change in intracellular cAMP concentration upon incubation of CBR expressing cells with the test ligand. Cawson *et al.*[169] and Jiang *et al.*[170] used a cAMP sensor (YFP-Epac-RLuc (CAMYEL)) for measuring the change in the cAMP concentration. The CAMYEL sensor contains a cAMP binding domain – Epac1 (exchange factor directly activated by cAMP 1) that separates BRET pairs of YFP and RLuc (Figure 1.18; Renilla luciferase). cAMP binding to Epac1 induces a conformational change in CAMYEL, increasing the distance between YFP and RLuc and thus interrupting energy transfer between these two BRET pairs (Figure 1.18). Therefore, with increasing intracellular cAMP concentration the 'inverse BRET ratio' (ratio of Rluc (energy donor) signal at 460 nm to YFP (energy acceptor) signal at 535 nm) also increases. Accordingly, a CBR agonist will decrease cAMP production and a corresponding decrease in the inverse BRET ratio will be observed, whereas the reverse will be true for an inverse agonist. A neutral antagonist would not change forskolin-stimulated cAMP production and consequently no change in BRET ratio would be observed. The raw data obtained from a cAMP functional assay can be analysed by non-linear regression to calculate of EC_{50}/IC_{50} and E_{max}.

1.6 Aims and objectives of this PhD thesis

This PhD thesis aimed to:

a) **Develop fluorescent ligands for adenosine A_1 receptor**
b) **Develop fluorescent ligands for cannabinoid receptors**

These aims were to be achieved by:

1) A literature review to identify high affinity A_1AR and CBR ligands with suitable properties, including SAR that indicates positions on the selected ligands amenable for conjugation of linkers and fluorophores.
2) Design of new A_1AR and CBR ligands based on the literature SAR with or without the aid of computational studies.
3) Synthesis of newly designed A_1AR and CBR ligands (including linker and linker-fluorophore conjugates).
4) Measurement and evaluation of the binding affinity and functional activity of the newly synthesised CBR ligands, and evaluation of the A_1AR biological data.
5) Design and synthesis of a follow up series of A_1AR and/or CBR ligands as appropriate based on the SAR obtained from the first series of compounds.

Chapter 2 Synthesis of (benzimidazolyl)-isoquinolinols as potential fluorescent ligands for Adenosine A_1 receptor

2.1 Design rationale for (benzimidazolyl)isoquinolinol-based fluorescent ligands

Xanthine-based adenosine receptor (AR) ligands (for example high affinity and selective A_1AR ligand DPCPX; shown in chapter 1, Figure 1.2) are attractive lead compounds for the development of A_1AR fluorescent ligands because of the availability of a large amount of SAR data[171] (AR xanthine ligands described in chapter 1, section 1.3.1). However, xanthine amine congener-fluorescent conjugates were previously reported as either non-AR subtype selective or A_3AR[43] selective and accordingly were not considered for the development of A_1AR selective fluorescent ligands in this thesis.

Novellino *et al.*[172] reported a series of (benzimidazolyl)quinoxalines (representative compounds **2.1**-**2.2** shown in Table 2.1) as AR antagonists, which were identified by the pharmacophore substructure search in the Cambridge Structural Database (CSD)[173] of previously reported selective A_1AR and A_3AR antagonists. In a subsequent study, Cosimelli *et al.*[76] (part of the same research group as Novellino *et al.*[172]) published 1- and 3-(benzimidazolyl)isoquinolines (representative compounds **2.3**-**2.8** shown in Table 2.1) as high affinity AR antagonists (including selective A_1AR antagonists **2.5**-**2.8**, Table 2.1). The (benzimidazolyl)quinoxaline **2.2** and 3-(benzimidazolyl)isoquinoline **2.5** were evaluated in a functional assay carried out at smooth muscle preparations of human colon and behaved as antagonists.[76] Based on the high affinity for A_1AR and selectivity over other ARs, the 1- and 3-(benzimidazolyl)isoquinolines (**2.5**-**2.8**) were selected as lead compounds for the development of A_1AR fluorescent ligands.

The 1- and 3-(benzimidazolyl)isoquinolines reported by Cosimelli *et al.*[76] (including **2.3**-**2.8**, Table 2.1) contained only small lipophilic substituents on the benzamidazole (methyl, ethylthiol, and chlorine) and lacked a bulky substituent (which would indicate a position tolerant of accommodating a bulky linker). Based on the high A_1AR affinity of 1- and 3-(benzimidazolyl)isoquinolines[76] (including **2.3**-**2.8**, Table 2.1) containing these small

lipophilic substituents, it was thought that the benzimidazole moiety might be interacting with an A_1AR lipophilic cavity. Linkers were also not appended from 1- ,3- and 4-position of isoquinoline as 1,3-substituted isoquinoline analogue VUF5455[174] and 2,4-substituted quinoline analogue LUF6096[175] were previously reported as allosteric A_3AR ligands. Hence, it was decided to conjugate linkers at the C-6 – C-7 position of the benzene ring of the isoquinoline moiety.

Table 2.1. Previously reported (benzimidazolyl)quinoxalines and 1- and 3-(benzimidazolyl)isoquinolines AR antagonists in literature[76, 172]

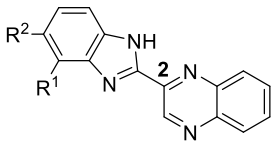

2.1-2.2

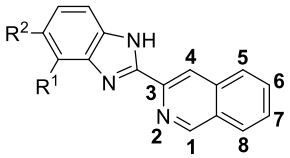

2.3-2.5

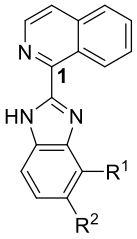

2.6-2.8

	R^1	R^2	K_i hA_1AR(nM ± SEM)*	K_i $hA_{2A}AR$(nM ± SEM)*	K_i hA_3AR(nM ± SEM)*	*Ref*
2.1	H	H	50.0 ± 15.0	561.0 ± 17.0	763.0 ± 13.0	172
2.2	SC_2H_5	H	0.50 ± 0.01	3440.0 ± 980.0	955.0 ± 215.0	172
2.3	H	H	3.2 ± 0.2	3750.0 ± 245.0	156.0 ± 13.4	76
2.4	H	CH_3	3.5 ± 0.3	>10000	264.7 ± 23.0	76
2.5	SC_2H_5	H	1.4 ± 0.1	>10000	>1000	76
2.6	H	H	14.1 ± 1.6	>10000	>1000	76
2.7	H	Cl	6.3 ± 0.4	>10000	>1000	76
2.8	H	CH_3	6.6 ± 0.5	>10000	>1000	76

*Binding affinity (K_i) obtained by competition binding assay performed on membranes obtained from chinese hamster ovary (CHO) cells expressing hA_1AR (using [^{3}H]-DPCPX as radioligand) or CHO cells expressing $hA_{2A}AR$ (using [^{3}H]-NECA as radioligand) or CHO cells expressing hA_3AR (using [^{125}I]-ABMECA as radioligand).

The benzene ring of isoquinoline in compounds such as **2.8** lacks a reactive substituent for the conjugation of a linker and subsequent fluorophore. Therefore hydroxyl derivatives of 1- and 3-(benzimidazolyl)isoquinolines (1- and 3-(benzimidazolyl)-isoquinolinols) were designed (Figure 2.1). The hydroxyl group offers a good handle to introduce linkers, for example by an ether bond that is non-ionised at physiological pH.

It was decided to prepare alkyl, polyethylene glycol (PEG) and peptide linker derivatives of (benzimidazolyl)isoquinolinols (Figure 2.1) to evaluate the effect of variations in the chemical structure and physicochemical properties on A_1AR biological activity. Only a selected subset of (benzimidazolyl)isoquinolinols (as shown in Figure 2.1) would be prepared due to limitations of the purchase of commercial fluorophores and limitations of an appropriate number of compounds that could be biologically evaluated by collaborators.

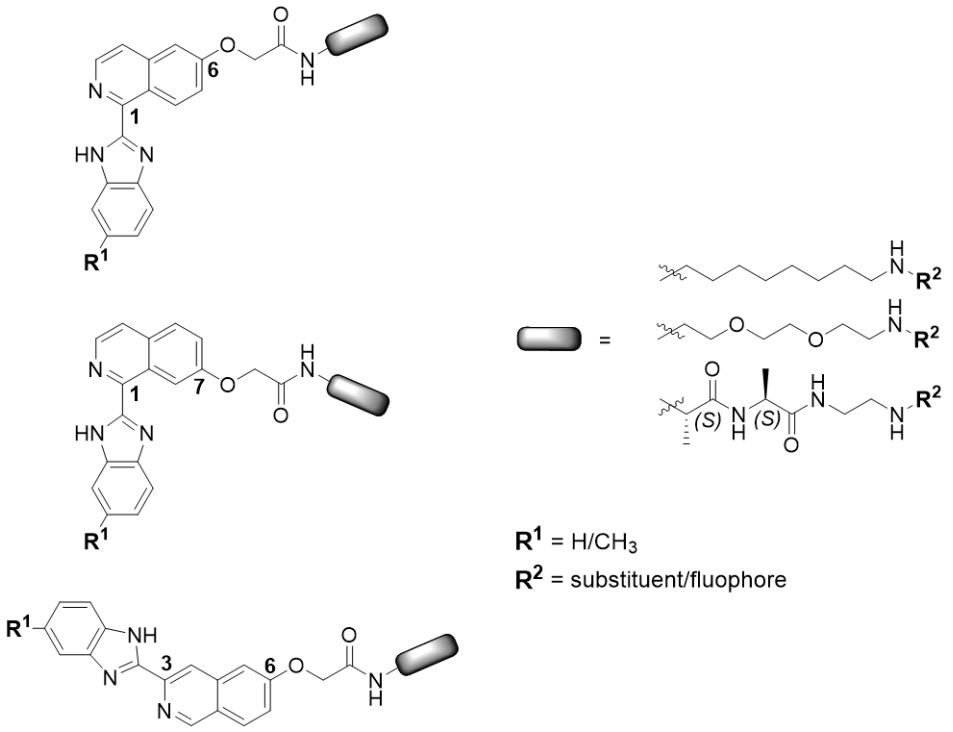

Figure 2.1. Design of (benzimidazolyl)isoquinolinols as potential A_1AR ligands.

It was decided that the (benzimidazolyl)isoquinolinol-based fluorescent ligands would be prepared by reaction of (benzimidazolyl)isoquinolinol-linker conjugates with the (*E*)-6-(2-(4-(2-(5,5-difluoro-7-(thiophen-2-yl)-5*H*-5λ^4,6λ^4-dipyrrolo[1,2-*c*:2',1'-*f*][1,3,2]-diazaborinin-3-yl)vinyl)phenoxy)acetamido)hexanoyl-succinimidyl ester- (BODIPY-630/650-SE) fluorophore (Figure 2.2). BODIPY-630/650 was selected because of its success as fluorophore in previously reported fluorescent ligands for GPCRs[24, 87, 176] and its suitable spectroscopic properties as an acceptor in a previously reported bioluminescence resonance energy transfer (NanoBRET) assay using the luciferase NanoLuc (NLuc; Promega Corporation, USA) to directly measure A_1AR activity.[90] The (benzimidazolyl)isoquinolinol-linker conjugates would be synthesised by reaction of

corresponding short linker-(benzimidazolyl)isoquinolinols with different linker derivatives. The (benzimidazolyl)isoquinolinols would be prepared by condensation reaction of phenylenediamine with isoquinoline carboxylic acids, which would be prepared from the aromatisation reactions of hydroxytetrahydroisoquinoline carboxylic acids (Figure 2.2).

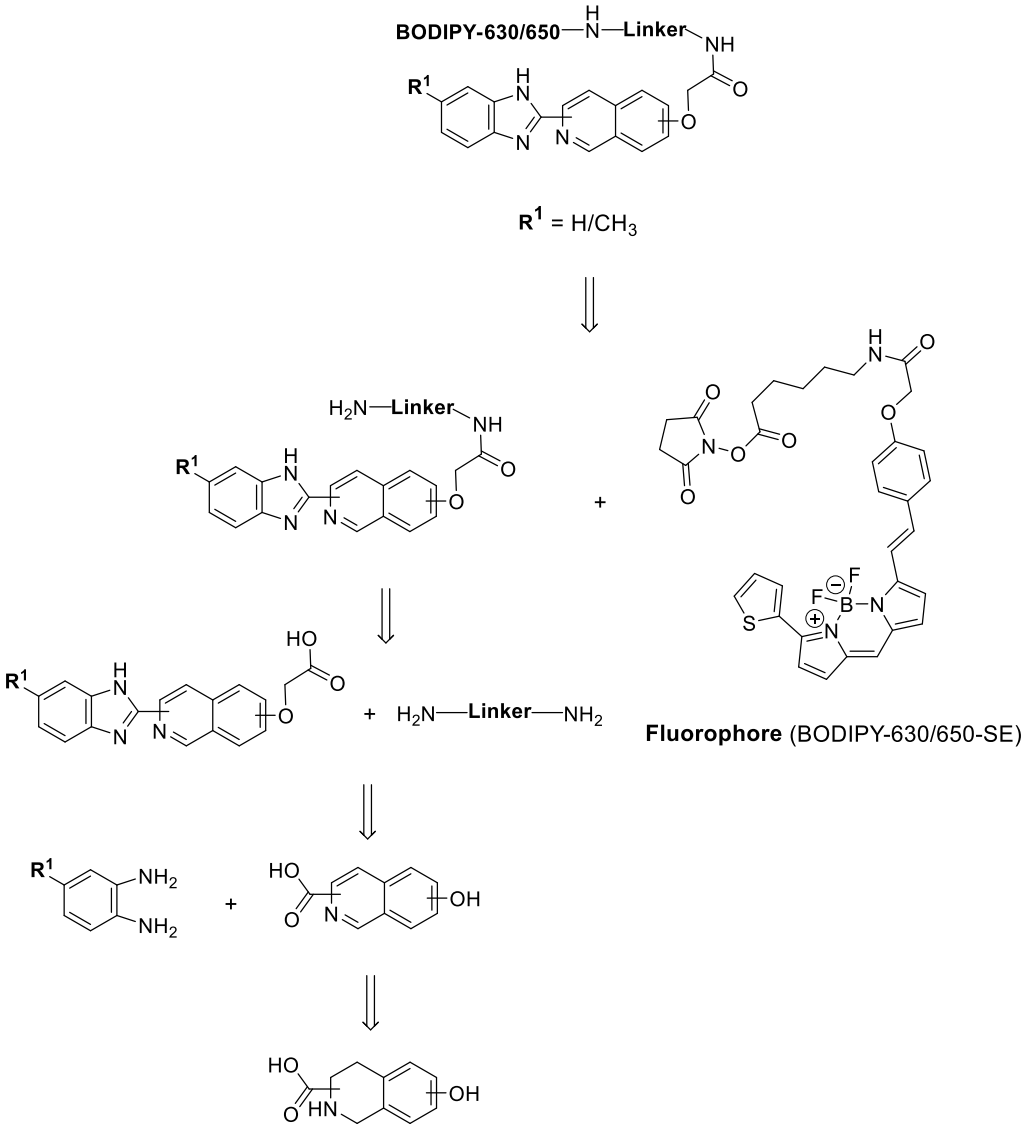

Figure 2.2. Retrosynthetic scheme of fluorescent (benzimidazolyl)isoquinolinols.

2.2 Synthesis and structural characterisation

2.2.1 Synthesis of linkers

The synthesis of alkyl linker **2.10** (Scheme 2.1), PEG linker **2.12** (Scheme 2.2) and peptide Alanine-Alanine (Ala-Ala) linker **2.18** (Scheme 2.3), used in the synthesis of (benzimidazolyl)isoquinolinol linker conjugates (synthesis described in section 2.2.2, 2.2.3 and 2.2.4 respectively), is described in this section.

The *N*-Boc protected linker **2.10** was prepared by reaction of commercially available alkyl diamine **2.9** with $(Boc)_2O$ according to a previously reported synthesis[177] (Scheme 2.1). Selective mono *N*-Boc protection was achieved by a slow, controlled addition of a solution of $(Boc)_2O$ in dioxane to a solution of amine **2.9** in dioxane with vigorous stirring.

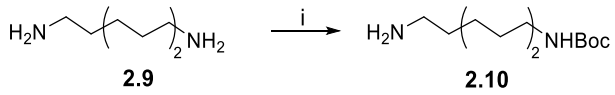

Scheme 2.1. (i) $(Boc)_2O$, 1,4-dioxane, 75%.

Boc-protection of commercially available PEG amine **2.11** with $(Boc)_2O$, according to a previously reported literature synthesis,[178] provided **2.12** (Scheme 2.2). Similar to **2.10**, mono *N*-Boc protected product **2.12** was prepared by a controlled addition of a solution of $(Boc)_2O$ in DCM to a solution of amine **2.11** in DCM.

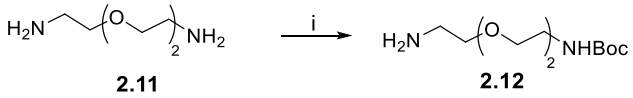

Scheme 2.2. (i) $(Boc)_2O$, DCM, 89%.

The synthesis of peptide (Ala-Ala) linker **2.18** was carried out using solution phase peptide synthesis (Scheme 2.3). The commercially available Fmoc-Ala-OH **2.13** was coupled with *N*-Boc-ethylenediamine **2.14** using HBTU, HOBt.H_2O and DIPEA to give **2.15**. Fmoc deprotection of **2.15** with diethylamine gave amine **2.16**, which was not purified and reacted with Fmoc-Ala-OH **2.13** using coupling reagents HBTU, HOBt.H_2O, and DIPEA as a base to provide **2.17**. Fmoc deprotection of **2.17** with diethylamine gave

peptide (Ala-Ala) linker amine **2.18**, which was not purified and used as such in the next reaction.

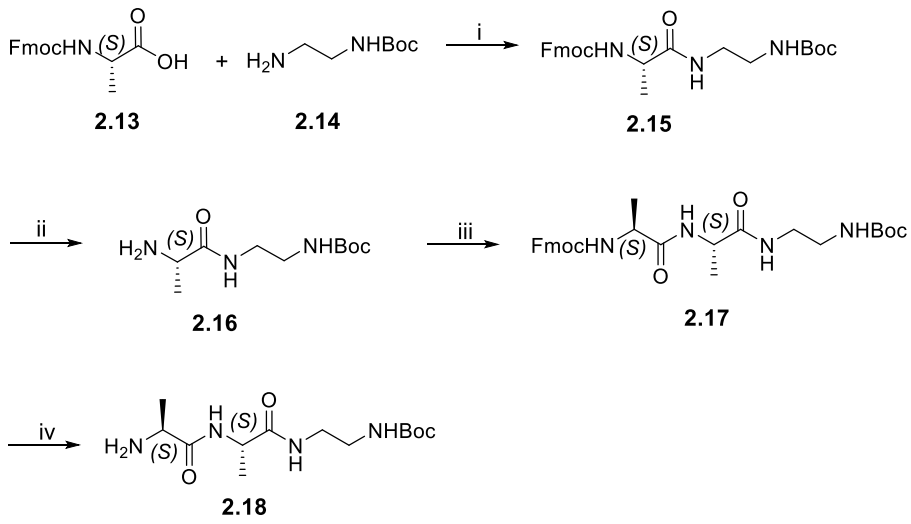

Scheme 2.3. (i) HBTU, HOBt.H_2O, DIPEA, DMF, 86%. (ii) Diethylamine, DCM. (iii) **2.13**, HBTU, HOBt.H_2O, DIPEA, DMF, 82%. (iv) Diethylamine, DCM, MeOH.

2.2.2 Synthesis of 1-(benzimidazolyl)isoquinoline-6-ol derivatives

According to a previously reported procedure,[179] demethylation of the commercially available **2.19** with aqueous HBr solution (48% *w*/*w*) provided amine salt **2.20**, which was not purified (Scheme 2.4). Initial attempts to carry out a Pictet–Spengler reaction of 3-(2-aminoethyl)phenol hydrobromide **2.20** with glyoxylic acid monohydrate following a previously reported synthesis of **2.21** by Li *et al.*,[179] were unsuccessful and starting material **2.20** was recovered as such. Pleasingly, **2.21** was obtained in good yield by instead following the synthesis reported by Maillard *et al.*.[180] In contrast to the procedure reported by Li *et al.*,[179] the Maillard *et al.*[180] procedure reported addition of Et_3N to the amine hydrobromide salt before the addition of glyoxylic acid monohydrate. It seems likely that the higher amount of free amine generated from the neutralisation of amine salt **2.20** with Et_3N reacts with glyoxylic acid monohydrate to form the corresponding imine (mechanism shown in the rectangle box drawn in scheme 2.4), which drives the Pictet–Spengler reaction to completion.

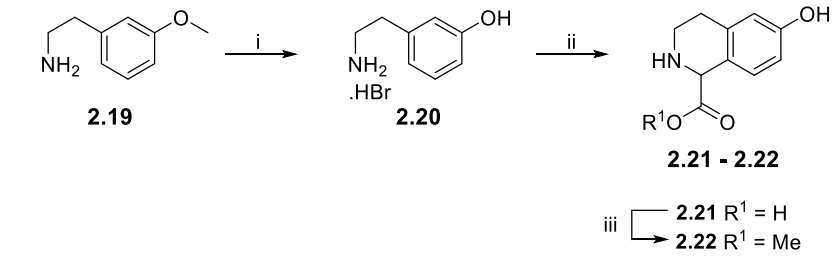

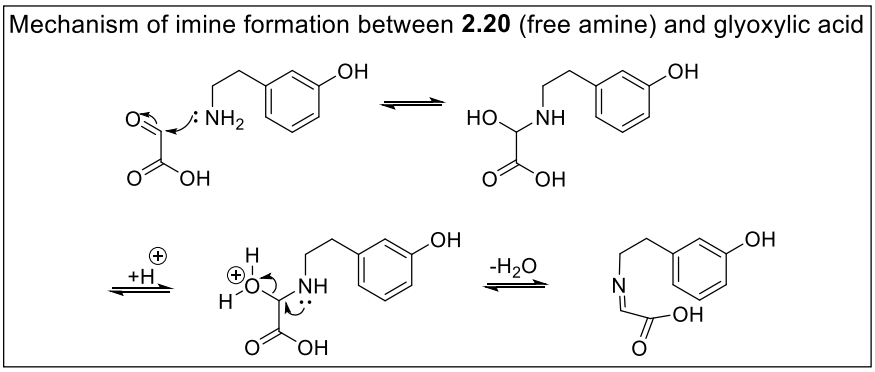

Scheme 2.4. (i) Aqueous (Aq.) HBr solution (48% *w/w*), 100 °C. (ii) Et_3N, glyoxylic acid monohydrate, EtOH, 71%. (iii) $SOCl_2$, MeOH, 65 °C, quantitative. Imine fomation between **2.20** (free amine) and glyoxic acid likely occurs by the mechanism shown in rectangle.

Attempts to aromatise carboxylic acid **2.21** with MnO_2 or 2,3-dichloro-5,6-dicyano-1,4-benzoquinone (DDQ) (with optimised conditions later discussed and used for the preparation of **2.24**, synthesis shown in Scheme 2.5) were unsuccessful. The aromatisation of carboxylic acid **2.21** was not pursued further because of the difficulties encountered in analysing the polar reactant and likely polar product(s) in the reaction mixture. Therefore carboxylic acid **2.21** was esterified to give methyl ester **2.22** (synthesis of **2.22** was previously reported by Ma *et al.*[181] but no spectroscopic data was reported).

Initial attempts to carry out aromatisation of hydroxytetrahydroisoquinoline **2.22** with DDQ following a procedure described for the DDQ-mediated aromatisation of **2.53**[182] (synthesis shown in Scheme 2.9 and described later in section 2.2.4) proved futile. Attempts were made to change the reaction solvents (THF or 1,4-dioxane or toluene) or temperature (rt, 45 °C or 100 °C) or to carry out reactions under either a N_2 atmosphere or in a closed reaction vessel. However, all of these failed to produce the aromatised product. In one attempt, heating a solution of **2.22** and DDQ in THF and 1,4-dioxane at 110 °C under N_2 atmosphere provided the partially oxidised dihydroisoquinoline **2.23** as the major product (Scheme 2.5). Reaction of **2.22** with DDQ at moderate temperature and with vigorous stirring in a flask open to the atmosphere was instead carried out, which

gave desired product **2.24** in moderate yield. The reasons for the moderate yield of DDQ-air mediated aromatisation of **2.22** is not known but may be due to low solubility of **2.24** in organic solvents and the susceptibility to ester hydrolysis during basic work up. The isoquinoline **2.24** has only been reported once before in the literature in a Japanese patent[183] without any spectroscopic data.

As the aromatisation of hydroxytetrahydroisoquinoline **2.22** did not occur in the absence of atmospheric air, it is likely that dihydroisoquinoline **2.23** (formed from reaction with DDQ) is formed in this reaction as an intermediate and then aromatised by oxygen to give isoquinoline **2.24**. Oxygen has been used previously as an oxidant in aromatisation reactions reported in literature.[184-185] In one such study, Dong *et al.*[186] used oxygen with a base in DMSO to convert *N*-tosyltetrahydroisoquinolines into isoquinolines. Analogous to the partially oxidised imine **2.23** isolated in this thesis with the exclusion of air, Dong *et al.*[186] also obtained an imine under an argon atmosphere instead of the aromatised isoquinoline product. In a previous literature report of DDQ-based cross-dehydrogenative coupling reactions of tetrahydroisoquinolines, an iminium ion (analogous to 3,4-dihydroisoquinoline) was observed as an intermediate.[187]

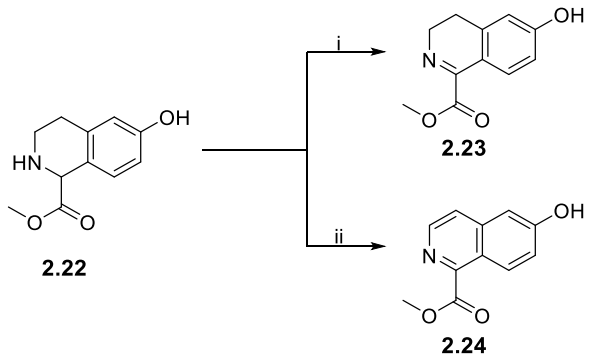

Scheme 2.5. (i) DDQ, 1,4-dioxane, THF, 110 °C, 32%, reaction carried out under N_2 atmosphere. (ii) DDQ, 1,4-dioxane, THF, 45 °C, atmospheric oxygen, 49%.

Hydrolysis of ester **2.24** with aqueous LiOH provided carboxylic acid **2.25**, which was condensed with commercially available diamines (*o*-phenylenediamine or 3,4-diaminotoluene) using hot polyphosphoric acid (PPA) to provide 1-(benzimidazolyl)isoquinolinols (**2.26** and **2.27**) in low yield (Scheme 2.6). The low yields of PPA mediated condensation reactions are likely due to a number of factors, including

poor dehydration yield and a difficult isolation of the polar 1-(benzimidazolyl)isoquinolinols (**2.26** and **2.27**) from the viscous reaction mixture.

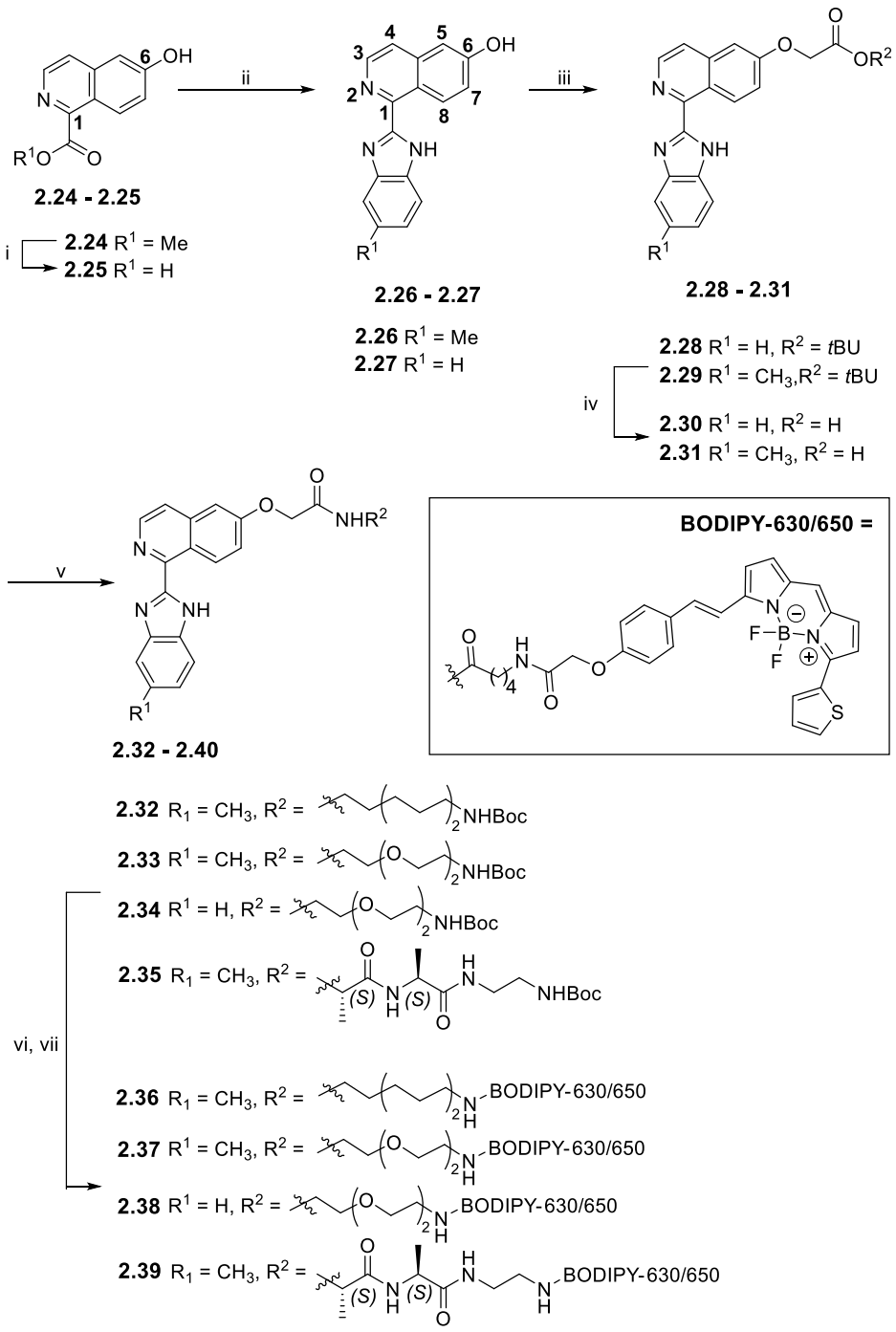

Scheme 2.6. (i) LiOH, THF, H_2O, 96%. (ii) 3,4-Diaminotoluene or *o*-phenylenediamine, PPA, 250 °C, 18-21%. (iii) *tert*-Butyl bromoacetate, K_2CO_3, THF, 60 °C, 93-96%. (iv) TFA, DCM, 64% - quantitative. (v) **2.10** or **2.12** or **2.18,** HATU, DIPEA, DMF, 29-69%. (vi) TFA, DCM, quantitative (vii) BODIPY-630/650-SE, DIPEA, DMF, 33-84%.

The yield of the condensation reaction for the preparation of (benzimidazolyl)isoquinolinols was slightly improved by using a mixture of phosphorus pentoxide and PPA. For example, reaction of **2.45** (Scheme 2.8) with 3,4-diaminotoluene and a mixture of phosphorus pentoxide and PPA (~20% *w*/*w*) provided **2.46** (Scheme 2.8) in 37% yield, whereas reaction with PPA alone provided **2.46** in 24% yield). The (benzimidazolyl)isoquinolinols (**2.26** and **2.27**) were reacted with *tert*-butyl bromoacetate using K_2CO_3 as a base to afford corresponding *tert*-butyl esters (**2.28** and **2.29**), which were reacted with TFA to give carboxylic acids (**2.30** and **2.31**; Scheme 2.6). The reaction of carboxylic acid **2.30** with PEG linker **2.12** (Scheme 2.2) using HATU as a coupling reagent and DIPEA as base gave (benzimidazolyl)isoquinolinol-linker conjugate **2.34**. Similarly, the coupling of **2.31** with linkers (**2.10**, **2.12** and **2.18**) gave (benzimidazolyl)isoquinolinol-linker conjugates **2.32**, **2.33** and **2.35**. The (benzimidazolyl)isoquinolinol-linker conjugates (**2.32**-**2.35**) were reacted with TFA to give the Boc-deprotected **2.32**-**2.35** as amino trifluoroacetate salts, which were purified by semi-preparative reverse phase-high performance liquid chromatography (RP-HPLC) and the purified amino salts reacted with BODIPY-630/650-SE to afford fluorescent ligands (**2.36**-**2.39**; Scheme 2.6). All of the fluorescent ligands prepared in this thesis were purified by semi-preparative RP-HPLC.

The fluorescence spectra of (benzimidazolyl)isoquinolinol-based fluorescent ligands were measured by collaborators at the University of Nottingham to check if these fluorescent ligands exhibit similar absorption and emission maxima as the 'free' BODIPY630/650 fluorophore. The fluorescence spectra of compounds **2.36–2.39** (Scheme 2.6)**, 2.50** (Scheme 2.8), **2.61** and **2.62** (Scheme 2.9) showed excitation maxima at 624 nm and emission maxima at either 641 or 642 nm (detailed in experimental chapter 7, section 7.2.1), similar to that of 'free' BODIPY-630/650.

2.2.3 Synthesis of 1-(benzimidazolyl)isoquinoline-7-ol-derivatives

Attempts to prepare the tetrahydroisoquinoline **2.41** (Scheme 2.7) from commercially available tyramine **2.40** and glyoxylic acid monohydrate using a similar procedure as described for the preparation of **2.21** (section 2.2.2; except without using Et_3N as amine **2.40** was not a salt) were unsuccessful and starting material **2.40** was recovered. Failure

of this condensation reaction is likely due to the lack of an activating group in tyramine **2.40**, compared to the presence of an activating *para* hydroxyl relative to the point of condensation for **2.20** (Scheme 2.4).

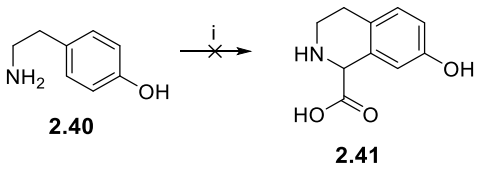

2.40 **2.41**

Scheme 2.7. (i) Glyoxylic acid monohydrate, EtOH.

Instead, 1-(benzimidazolyl)isoquinoline-7-ol- derivatives were prepared using a synthetic route reported for the synthesis of *N*-Fmoc protected **2.41** by Maillard *et al.*[180] Thus, Fmoc protection of commercially available tyramine **2.40** gave **2.42** (Scheme 2.8). Reaction of **2.42** with glyoxylic acid monohydrate gave *N*-Fmoc protected **2.41** (not shown in Scheme 2.8, reported by Maillard *et al.*[180]), which was esterified to give **2.43** in low yield over two steps (Scheme 2.8). The NMR spectra of ester **2.43** showed a mixture of isomers that were elucidated to be rotamers rather than regioisomers via variable temperature NMR experiments (described in experimental chapter 7, section 7.2.1).

The Fmoc-protected ester **2.43** was initially reacted with diethylamine for Fmoc deprotection, however subsequent reaction of Fmoc-deprotected **2.43** (compound not purified) with DDQ provided poor yield of **2.44**, most likely due to the residual diethylamine. Fmoc deprotection of **2.43** was observed in high temperature NMR spectra in DMSO-d_6 that was carried out to study rotamers, and indeed there is literature precedent that Fmoc cleavage can be conducted in neat DMSO at high temperature.[188] Hence, Fmoc deprotection of **2.43** in DMSO, followed by reaction with DDQ (using the optimised procedure described for the preparation of **2.24** (Scheme 2.5, section 2.2.2)) provided **2.44** (Scheme 2.8).

Subsequent synthesis of (benzimidazolyl)isoquinolinol-linker conjugate **2.49** and BODIPY-630/650 conjugate **2.50** was carried out using a similar methodology as described in section 2.2.2. Hydrolysis of **2.44** with aqueous LiOH gave carboxylic acid **2.45**, which was reacted with 3,4-diaminotoluene to give (benzimidazolyl)isoquinolinol **2.46** (Scheme 2.8). Alkylation of **2.46** with *tert*-butyl bromoacetate gave **2.47**, which was

reacted with TFA to give **2.48**. Reaction of the carboxylic acid **2.48** with PEG linker **2.12** (Scheme 2.2, section 2.2.1) using HATU as a coupling reagent and DIPEA as a base provided **2.49**. (Benzimidazolyl)isoquinolinol-linker conjugate **2.49** was reacted with TFA to give Boc-deprotected **2.49** as an amino trifluoroacetate salt, which was purified by semi-preparative RP-HPLC and the purified amino salt reacted with BODIPY-630/650-SE to afford fluorescent ligand **2.50**.

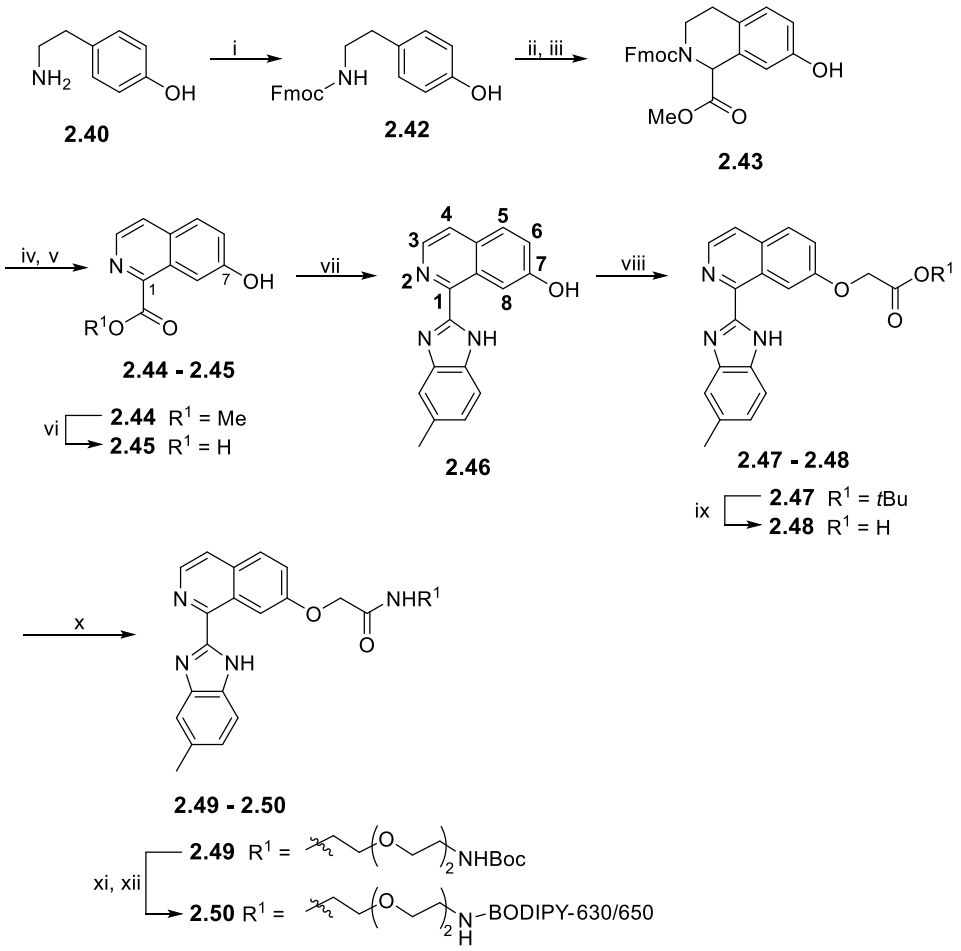

Scheme 2.8. (i) Fmoc-Cl, DIPEA, DCM, 82%. (ii) Glyoxylic acid monohydrate, H_2SO_4, CH_3CO_2H. (vii) $SOCl_2$, MeOH, 18% over two steps. (iv) DMSO, MeOH, 60 °C. (v) DDQ, THF, 1,4 dioxane, 45 °C, 61% over two steps from **2.43**. (vi) LiOH, THF, H_2O, 70%. (vii) 3,4-Diaminotoluene, PPA, 250 °C, 24%, (37% with a mixture of P_2O_5 and PPA (~20% *w*/*w*)) (viii) *tert*-Butyl bromoacetate, K_2CO_3, THF, 60 °C, 66%. (ix) TFA, DCM. (x) **2.12**, HATU, DIPEA, DMF, 43%. (xi) TFA, DCM, quantitative. (xii) BODIPY-630/650-SE, DIPEA, DMF, 49%.

2.2.4 Synthesis of 3-(benzimidazolyl)isoquinoline-6-ol-derivatives

Synthesis of 3-(benzimidazolyl)isoquinoline-6-ols was carried out following similar synthetic methodology as described for the preparation of 1-(benzimidazolyl)isoquinoline-6-ols (section 2.2.2). Reaction of the commercially available (+/-)-*m*-tyrosine **2.51** with formaldehyde, according to a literature synthesis,[189] gave **2.52**. The carboxylic acid **2.52** was esterified to give **2.53** and then aromatised with DDQ to provide **2.54** (using optimised reaction conditions described for the preparation of **2.24**, section 2.2.2; Scheme 2.5). The synthesis of methyl ester **2.54** from **2.53** has previously been reported in iterature[182, 190-193] including in a patent report[13]. Attempts at aromatisation of **2.53** and **2.22** (section 2.2.2) following the method described in this patent report[13] were unsuccessful. None of these reported syntheses include spectroscopic data for **2.54**.

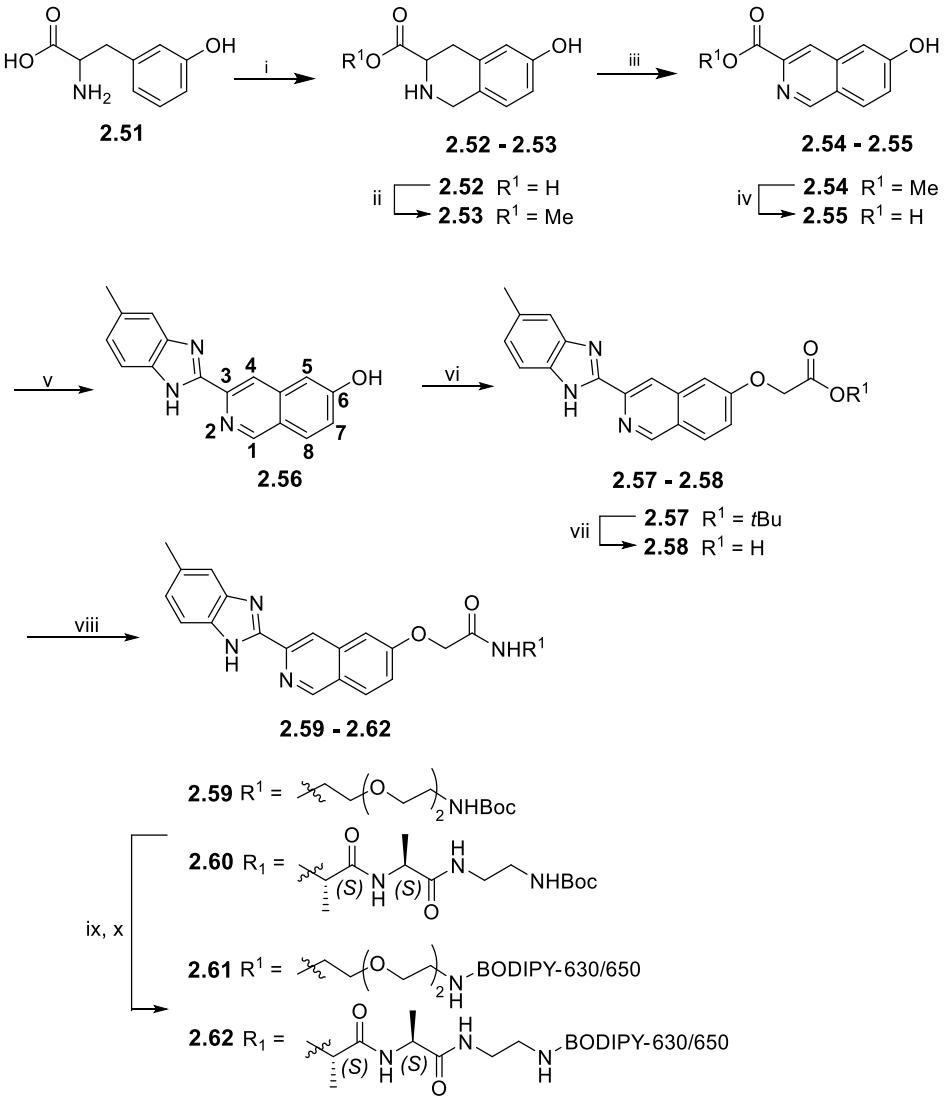

Scheme 2.9. (i) HCl (0.05 M, aqueous solution), formaldehyde (37 wt. % in H_2O), 90 °C, 48%. (ii) H_2SO_4, MeOH, 96%. (iii) DDQ, THF, 1,4 dioxane, 45 °C, 52%. (iv) LiOH, THF, H_2O, 90%. (v) 3,4-Diaminotoluene, PPA, 250 °C, 26%. (vi) *tert*-Butyl bromoacetate, K_2CO_3, THF, 60 °C, 94%. (vii) TFA, DCM. (viii) **2.12** or **2.18**, HATU, DIPEA, DMF, 37-39%. (ix) TFA. (x) BODIPY-630/650-SE, DIPEA, DMF, 73-86%.

Alkaline hydrolysis of ester **2.54** gave carboxylic acid **2.55**, which was condensed with 3,4-diaminotoluene to give (benzimidazolyl)isoquinolinol **2.56** (Scheme 2.9). Alkylation of **2.56** with *tert*-butyl bromoacetate gave **2.57**, which was reacted with TFA to give **2.58**. The coupling of carboxylic acid **2.58** with PEG linker **2.12** (synthesis described in section 2.2.1) or peptide linker **2.18** (synthesis described in section 2.2.1) using HATU as a coupling reagent yielded linker conjugates **2.59** or **2.60** respectively. Reaction of the linker conjugates (**2.59** and **2.60**) with TFA gave Boc-deprotected **2.59** and **2.60** as amino trifluoroacetate salts, which were purified by semi-preparative RP-HPLC and the purified

amino salts reacted with BODIPY-630/650-SE to afford fluorescent ligands **2.61** and **2.62** (Scheme 2.9).

2.2.5 Synthesis of 1-*(1H*-1,3-benzodiazol-2-yl)isoquinoline

(Benzimidazolyl)isoquinoline **2.6** (K_i = 14.1 ± 1.6 nM at hA_1AR, Table 2.1), a high-affinity A_1AR antagonist previously reported by Cosimelli *et al.*[76], is not commercially available so was synthesised for use as a literature control in pharmacological experiments (section 2.3). According to a previous synthesis,[76] literature compound **2.6** was prepared by condensation of commercially available isoquinoline-1-carboxylic acid **2.63** with commercially available *o*-phenylenediamine using PPA (Scheme 2.10).

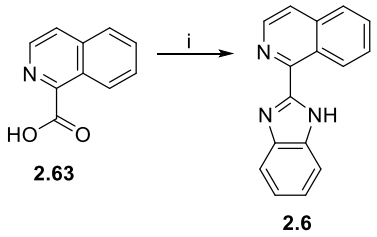

Scheme 2.10. (i) *o*-Phenylenediamine, PPA, 250 °C, 38%.

2.2.6 Conformers of 1-(benzimidazolyl)isoquinoline-6-ol (2.26)

This section describes the investigation of the NMR spectra and RP-HPLC spectra of novel (benzimidazolyl)isoquinolinols.

The NMR spectra of (benzimidazolyl)isoquinolinols (**2.26**, **2.27**, **2.46** and **2.56**, synthesis described in section 2.2.2, section 2.2.3 and section 2.2.4) showed broadened peaks (^{1}H NMR spectra, solvent MeOD-d_4) or multiple sets of peaks (^{1}H and ^{13}C NMR spectra, solvent DMSO-d_6). These peculiar NMR spectra peaks were investigated using **2.26** as a model compound. The peculiar NMR spectra peaks of **2.26** could arise from either the presence of discrete chemical entities (for example regioisomers or chemical impurities) or from conformational isomers (tautomers and/or rotamers). The chemical exchange of protons between N-9 and N-11 (usually with the participation of solvent molecules) in **2.26** would give rise to tautomers of **2.26** (Figure 2.3 (A)). On the other hand, the restricted rotation around the C-1–C-10 bond of **2.26** (the bond connecting the benzimidazole and isoquinoline heterocycles) would give rise to rotamers of **2.26** (Figure 2.3 (B)).

The rate of interconversion of conformers is dependent on factors such as solvent type (different hydrogen bond acceptor or donor ability), change in temperature and concentration of the compound. Consequently, if peak appearance and multiplicity in NMR and RP-HPLC spectra are sensitive to factors such as solvent, temperature and concentration of compound, it would indicate the presence of conformers (tautomers or rotamers) rather than discrete chemical entities (regioisomers or chemical impurities).

The most non-equivalent NMR signals should be observed between the atoms which are exposed to different spatial surrounding in the conformers. Therefore, a number of NMR spectroscopy and RP-HPLC experiments were carried out using **2.26** as a model (benzimidazolyl)isoquinolinol to evaluate whether interconvertible conformers (tautomers or rotamers) or discrete chemical entities were present.

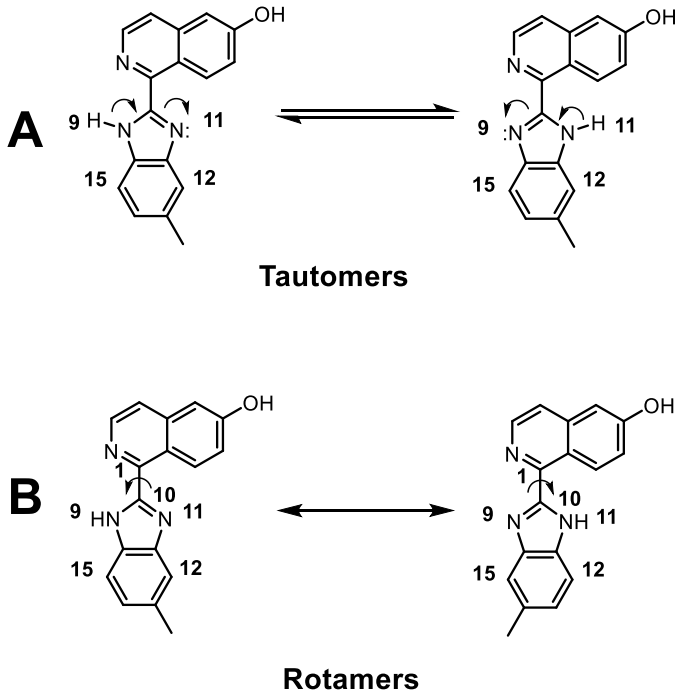

Figure 2.3. Interconversion of possible (A) tautomers or (B) rotamers of **2.26**.

2.2.6.1 NMR spectroscopic studies

The ^{1}H NMR spectrum of **2.26** in MeOD-*d*$_4$ (Figure 2.4, section 2.2.6.4) showed sharp peaks for the isoquinoline protons but broadened peaks for the benzimidazole protons. Similarly, the ^{13}C NMR spectrum of **2.26** in MeOD-*d*$_4$ (Figure 2.5, section 2.2.6.4) showed sharp peaks for the isoquinoline carbons but weak intensity peaks or no peaks for the benzimidazole carbons (refer to experimental chapter 7, section 7.2.1 for peak lists in MeOD-*d*$_4$). Interestingly, more signals were seen in the ^{1}H NMR spectrum (Figure 2.6) and ^{13}C NMR spectrum (Figure 2.7) of **2.26** in DMSO-*d*$_6$ than observed in the corresponding NMR spectra in MeOD-*d*$_4$.

^{1}H and ^{13}C NMR spectra signals of **2.26** were assigned using spectra obtained from gradient homonuclear correlation spectroscopy gCOSY, gradient heteronuclear single quantum coherence spectroscopy (gHSQC) and gradient heteronuclear multiple bond correlation spectroscopy (gHMBC) (Appendix, Figure A.2-A.7). The atom numbering of **2.26** used in assigning NMR signals in the following paragraphs is shown in Figure 2.4.

2.26 ^{1}H NMR (400 MHz, DMSO-d_6) δ 2.45 (s, 2.84H, 16-H), 7.07 (d, 0.62H, *J* = 7.6 Hz, 14-H), 7.12 (d, 0.41H, *J* = 8.0 Hz, 14-H), 7.21 (d, 1H, *J* = 2.4 Hz, 5-H), 7.33 – 7.40 (m, 1.53H, 7-H and 12-H), 7.47 (d, 0.41H, *J* = 8.3 Hz, 15-H), 7.60 (s, 0.41H, 12-H), 7.68 (d, 0.60H, *J* = 8.3 Hz, 15-H), 7.74 (d, 0.96H, *J* = 5.6 Hz, 4-H), 8.49 (d, 1.0H, *J* = 5.6 Hz, 3-H), 9.90 – 9.99 (m, 1.02H, 8-H), 10.53 (s, 1.53H, 17-H), 12.98 (s, 0.63H, 9-H), 12.99 (s, 0.40H, 9-H). (Additional ^{1}H NMR signals than were expected by magnetic equivalence for one chemical structure of **2.26**, are due to the presence of another conformer)

2.26 ^{13}C NMR (101 MHz, DMSO-d_6) δ 21.33 (16-C), 21.48 (16-C), 107.63 (5-C), 111.52 (15-C), 111.59 (12-C), 119.18 (12-C and 15-C), 120.78 (4-C), 121.07 (7-C), 123.54 (14-C), 125.02 (14-C), 130.12 (8-C), 130.78 (13-C), 132.01 (11a-C or 15a-C), 132.86 (13-C), 134.21 (11a-C or 15a-C), 139.16 (8a-C or 4a-C), 141.68 (3-C), 142.24 (11a-C or 15a-C), 144.40 (11a-C or 15a-C), 146.19 (8a-C or 4a-C), 150.97 (10-C), 151.31 (1-C), 158.93 (6-C). (Additional ^{13}C NMR signals then were expected by magnetic equivalence for one chemical structure of **2.26**, are due to the presence of another conformer).

Twenty-three aromatic carbon signals were observed in the ^{13}C NMR spectrum of **2.26** in DMSO-d_6, however only seventeen carbons are present in **2.26**. Twelve C-H correlations were observed in the gHSCQ spectrum of **2.26** (Appendix, Figure A.6), however **2.26** has only nine carbons with at least one hydrogen attached. The gHSQC correlations with data from gCOSY and gHMBC spectra revealed that an additional three C-H correlations in gHSQC spectrum and additional carbon signals in ^{13}C NMR spectrum were from atoms belonging to the benzimidazole moiety (gCOSY and gHMBC spectra reported in Appendix, Figure A.5, A.7). The identification of atoms belonging to benzimidazole moiety was primarily based on the gHSQC and gHMBC correlations to the clearly identifiable H-16 protons.

Variable temperature ^{1}H NMR spectra

The rate of interconversion of conformers is dependent on temperature. Therefore, a complex NMR spectrum of two conformers should simplify (or start to simplify) at a higher temperature as the rate of conversion of conformers increases and reaches beyond that observable on NMR timescale. ^{1}H NMR spectra of **2.26** carried out in DMSO-d_6 at three different temperatures (Figure 2.8) showed coalescence of proton signals as

temperature increased, supporting the presence of conformers rather than discrete non-interchangeable chemical entities.

Addition of D_2O

It was thought that the strong hydrogen bond accepting property of DMSO-d_6 compared to MeOD-d_4 might be responsible for the complex NMR spectra of **2.26** in DMSO-d_6. Accordingly, the addition of D_2O to a solution of **2.26** in DMSO-d_6 should weaken a hydrogen bond thought to exist between NH of benzimidazole and DMSO-d_6. The weakening of this hydrogen bond should increase the rate of interconversion of conformers and a less complex NMR spectra should be observed. In agreement with this hypothesis, less complex signals were observed in both ^1H and ^{13}C NMR spectra of **2.26** in DMSO-d_6 spiked with D_2O (Figure 2.9, Figure 2.10).

Tautomer or rotamer?

It seemed likely that **2.26** exhibited tautomerism as the NMR spectra showed that only the benzimidazole atoms were affected by the change in NMR solvent and temperature. If rotamers of **2.26** were predominantly present, then the isoquinoline atoms would also be affected (Figure 2.3 (B)). Presumably, exchange of hydrogen between N-9 and N-11 in MeOD-d_4 exposes neighbouring atoms: 11a, 12, 13, 14, 15 and 15a to a fluctuating local chemical environment resulting in either broadening or absence of $^1H/^{13}C$ NMR spectra signals of their corresponding atoms (Figures 2.4 and 2.5).

It seems likely that a strong hydrogen bond exists between the benzimidazole NH of **2.26** and DMSO-d_6, which slows down the rate of exchange of hydrogen between N-9 and N-11 and consequently the rate of interconversion of tautomers, hence leading to the observation of both tautomers in the NMR time scale (Figures 2.6, 2.7).

2.2.6.2 RP-HPLC studies

The peak shape in the analytical RP-HPLC chromatogram of (benzimidazolyl)isoquinolinols (**2.26**, **2.27**, **2.46** and **2.56**) (synthesis described in section 2.2.2, section 2.2.3 and section 2.2.4) was observed to be concentration dependent. This

was investigated using **2.26** as the model compound, which at higher concentration showed an elongated, square shoulder peak (Figure 2.11).

It was thought that the peculiar RP-HPLC spectra peak shape might be due to the presence of conformers (rotamers or tautomers), peak tailing, or the presence of discrete chemical entities (for example regioisomers or chemical impurities).

Analytical RP-HPLC chromatograms from of **2.26**, **2.27**, **2.46** and **2.56** revealed that peak shape was concentration dependent. Again using **2.26** as the model compound, at higher concentrations, an elongated, square shoulder peak was observed (Figure 2.11). Further RP-HPLC experiments were carried out to exclude the presence of discrete chemical entities (regioisomers or chemical impurities). Semi-preparative RP-HPLC of **2.26** was carried out and the peak containing **2.26** (Figure 2.12) was fractionated into ten separately timed fractions. An analytical RP-HPLC spectrum of each fraction was run (Figure 2.13 (A), which revealed broad peaks for fractions with high concentration and sharp peaks for fractions with low concentration. Analysis of the dilute solution prepared by combination of aliquots from each fraction by analytical RP-HPLC showed a single peak (Figure 2.13 (B)), which made the presence of discrete chemical entities (regioisomers or chemical impurities) unlikely. Variable temperature RP-HPLC experiments (at 25 - 40 °C) were also carried out to investigate the effect of temperature on the more concentrated analytical RP-HPLC chromatogram of **2.26** (Figure 2.11). However, a significant change in chromatogram peak shape was not observed in this temperature range. It seems likely that a much higher temperature would be required to see a significant change in the chromatogram of **2.26**, in accordance with ^{1}H NMR spectra results that showed little change from 25 °C to 45 °C but a much larger change at 60 °C. Variable temperature RP-HPLC experiments at higher temperature (> 40 °C) were not carried due to incompatibility of solvent and column with higher temperatures.

2.2.6.3 Summary of NMR spectroscopy and RP-HPLC studies

The NMR spectroscopy and RP-HPLC experiments suggest that **2.26** is a mixture of interconvertible tautomers. The synthetic route used for the preparation of (benzimidazolyl)isoquinolinols made it unlikely that regioisomers would be present and

this was supported by the high-temperature NMR spectroscopy and RP-HPLC experiments. As the high-resolution electrospray ionisation mass spectra (HRMS) spectrum of **2.26** matched the expected molecular formula mass and no other major peaks were observed, the presence of an impurity with different molecular formula is unlikely (this is also supported by RP-HPLC experiments). It can be concluded that the peculiar NMR and RP-HPLC spectra observed for (benzimidazolyl)isoquinolinol **2.26** arose from the presence of tautomers. This conclusion is supported by the fact that benzimidazole moiety present in (benzimidazolyl)isoquinolinols is well known for exhibiting tautomerism.[194-199]

2.2.6.4 NMR Spectra and RP-HPLC chromatograms

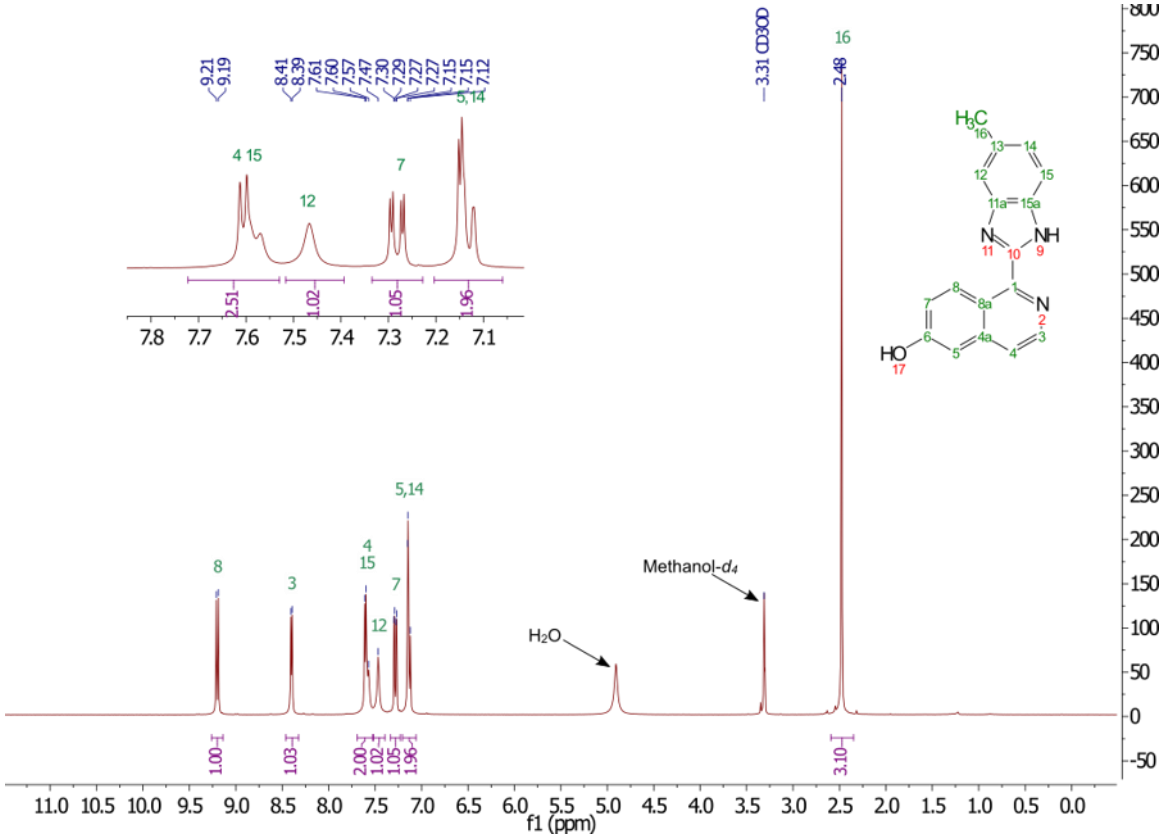

Figure 2.4. [1]H NMR spectra (inset shows aromatic region) of **2.26** in MeOD-d_4 at 25 °C.

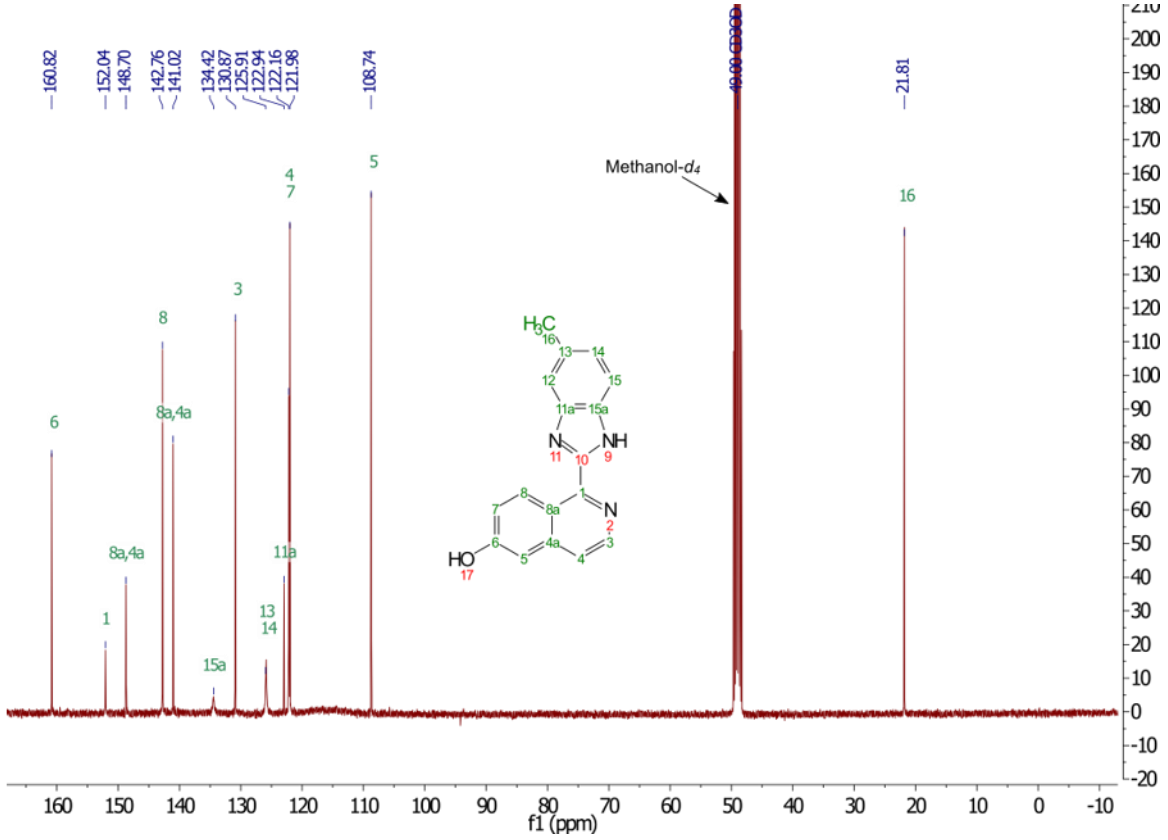

Figure 2.5. ^{13}C NMR spectra of **2.26** in MeOD-d_4 at 25 °C.

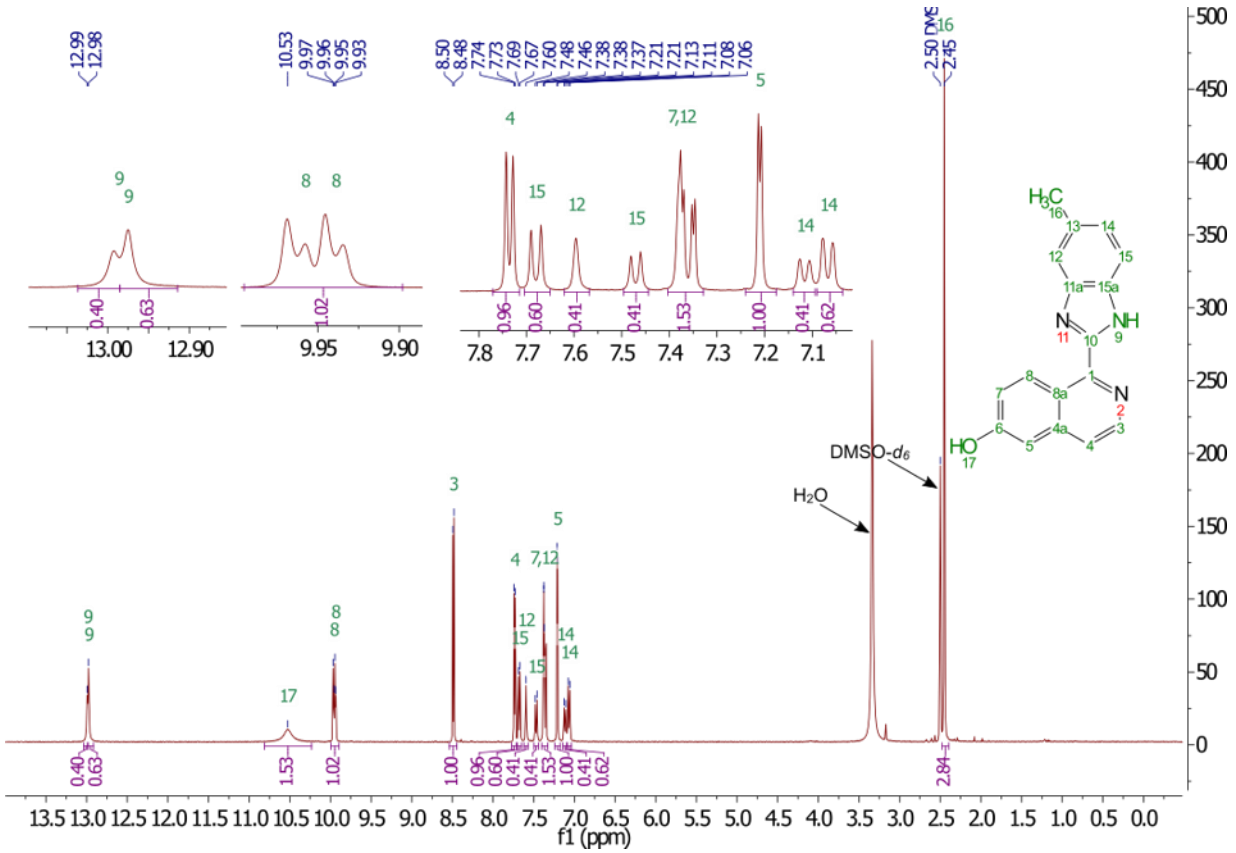

Figure 2.6. ^{1}H NMR spectra (inset shows aromatic region) of **2.26** in DMSO-d_6 at 25 °C.

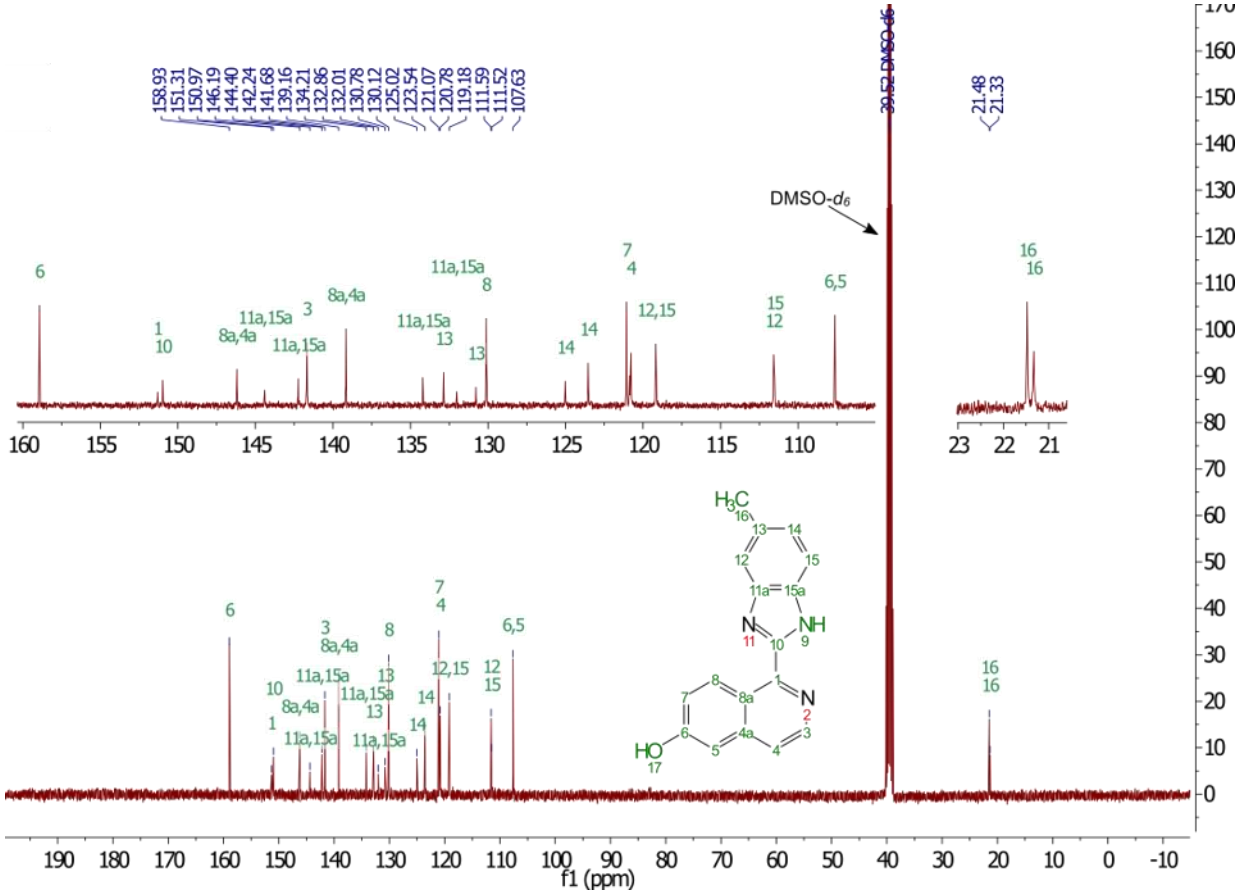

Figure 2.7. ^{13}C NMR spectra (inset shows aromatic region) of **2.26** in DMSO-d_6 at 25 °C.

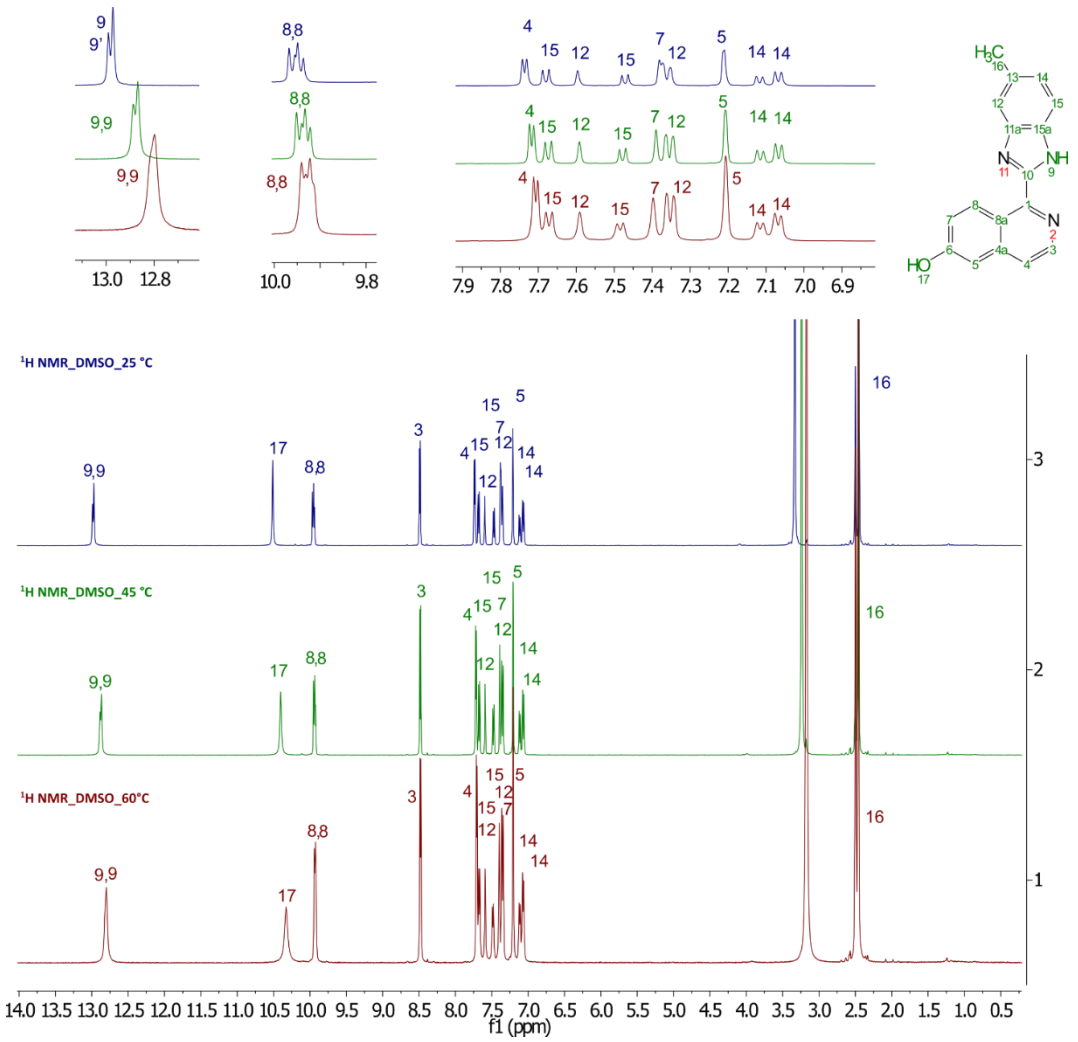

Figure 2.8. [1]H NMR experiments of **2.26** in DMSO-d_6 were carried at three different temperatures: Top (25 °C in blue), middle (45 ˚C in green), bottom (60 ˚C in red), the inset shows aromatic region.

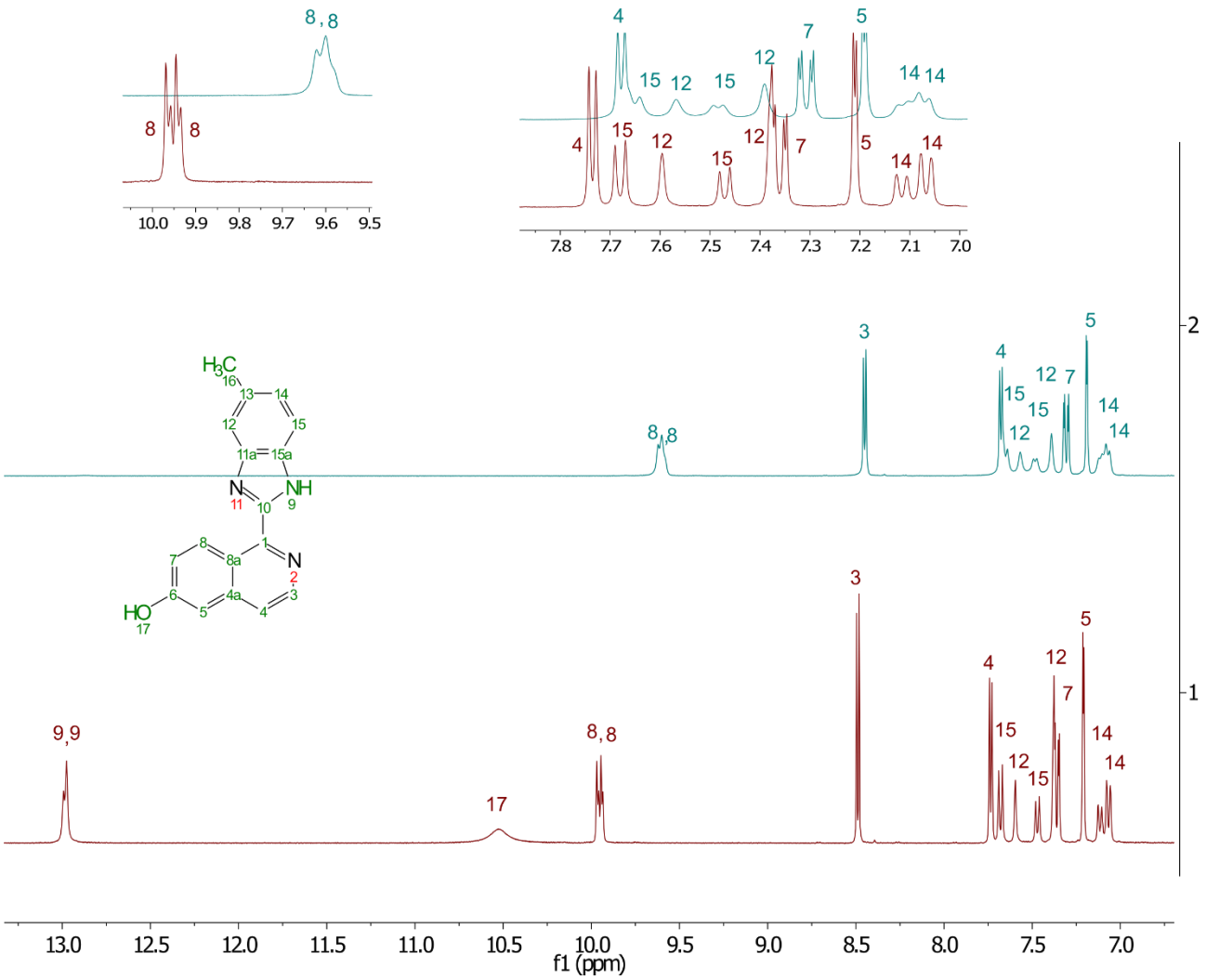

Figure 2.9. ^{1}H NMR spectrum of **2.26** in DMSO-d_6 (0.7 mL) at 25 °C (bottom), and after addition of 0.1 mL D_2O (Top).

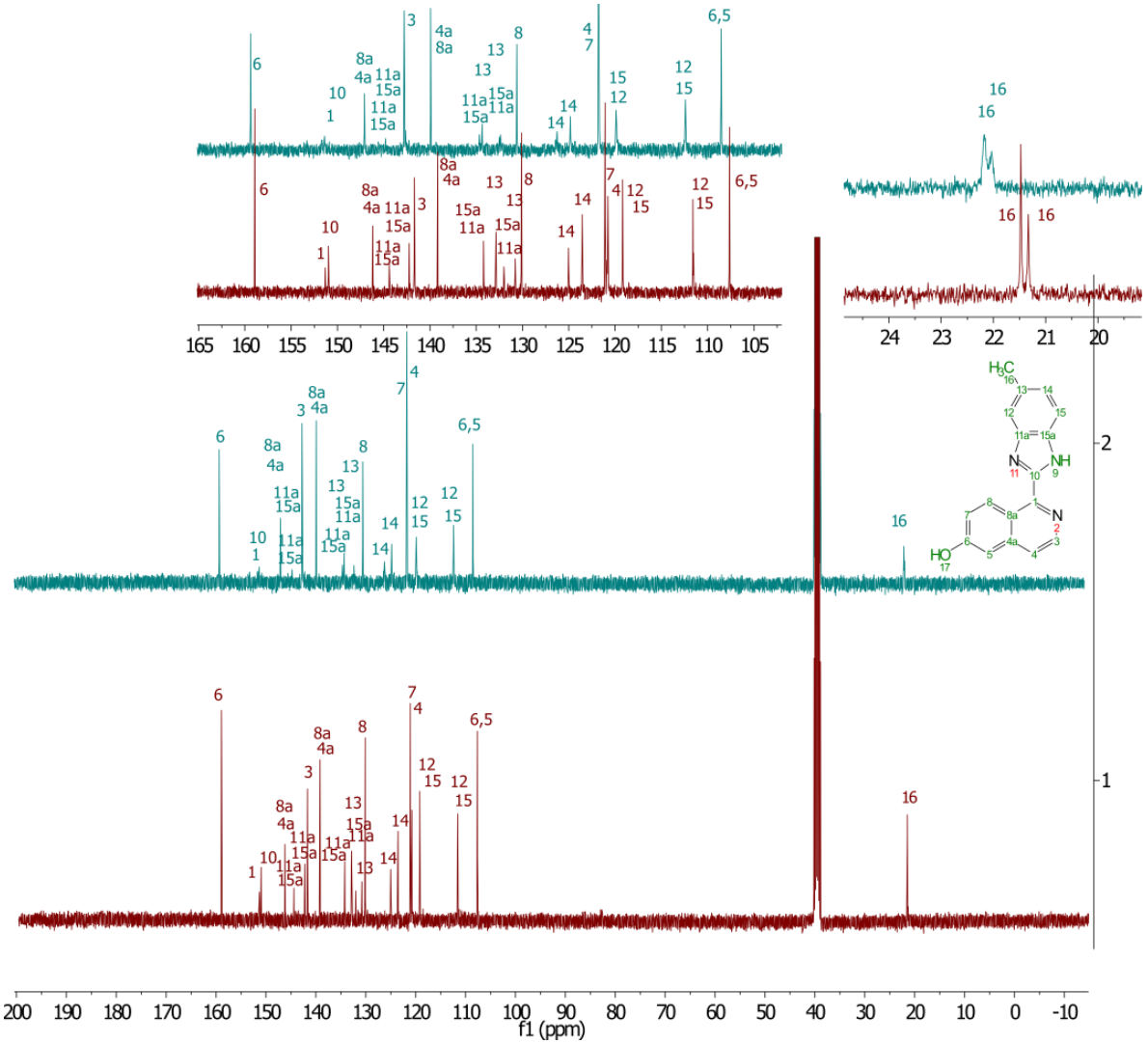

Figure 2.10. ^{13}C NMR spectrum of **2.26** in DMSO-d_6 (0.7 mL) at 25 °C (bottom), ^{13}C NMR spectrum after addition of 0.1 mL D_2O (Top).

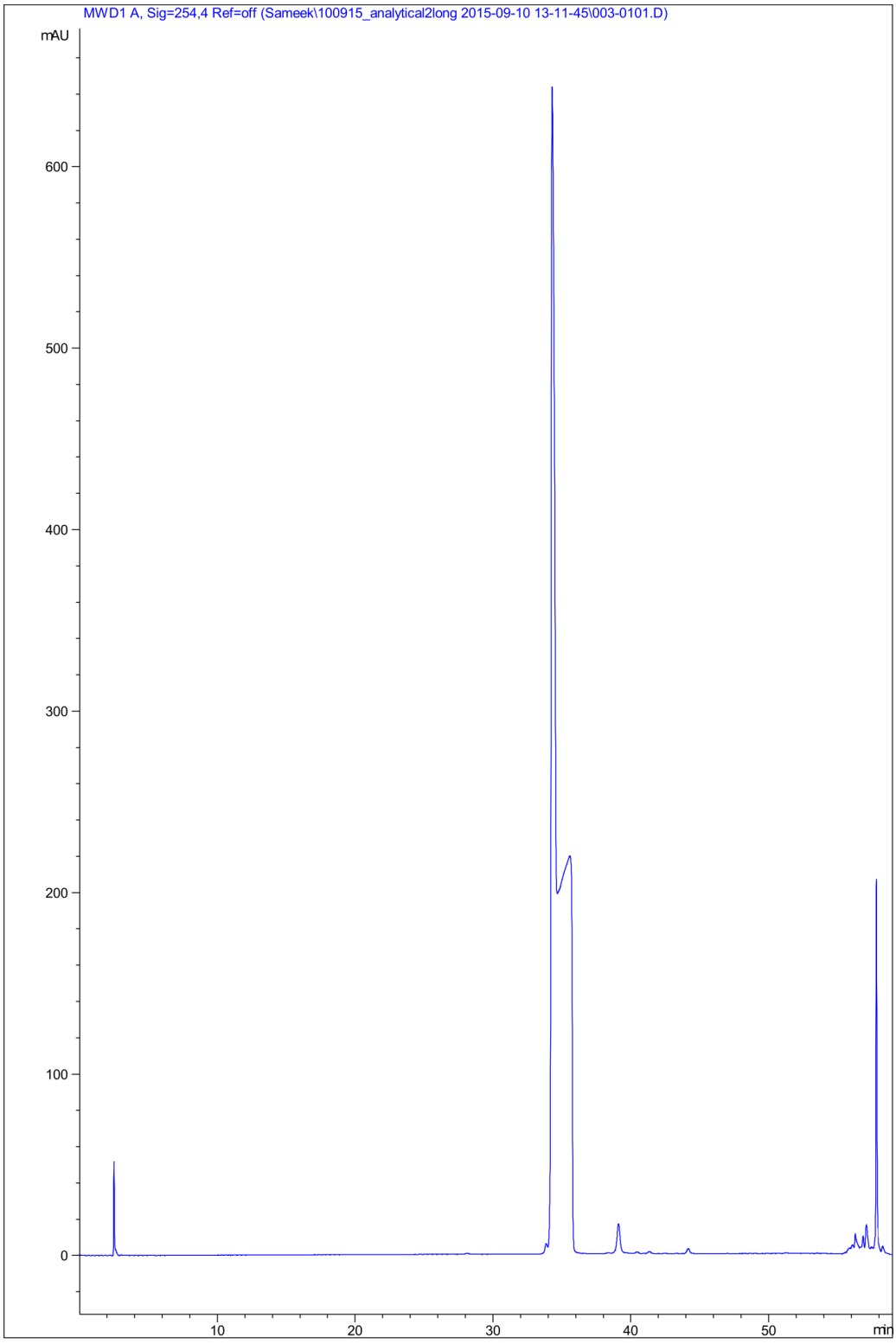

Figure 2.11. Analytical RP-HPLC chromatogram of **2.26** at high concentration showed a shoulder peak. The following Analytical RP-HPLC method was used for obtaining analytical RP-HPLC chromatograms reported in Figure 2.11 and Figure 2.13 (A), (B) - 5% solvent B 1 min, gradient of 5-20% solvent B 1-51 min, 95% solvent B 52-53 min, gradient of 95-5% solvent B 53-55 min, 5% solvent B 55-59 min.

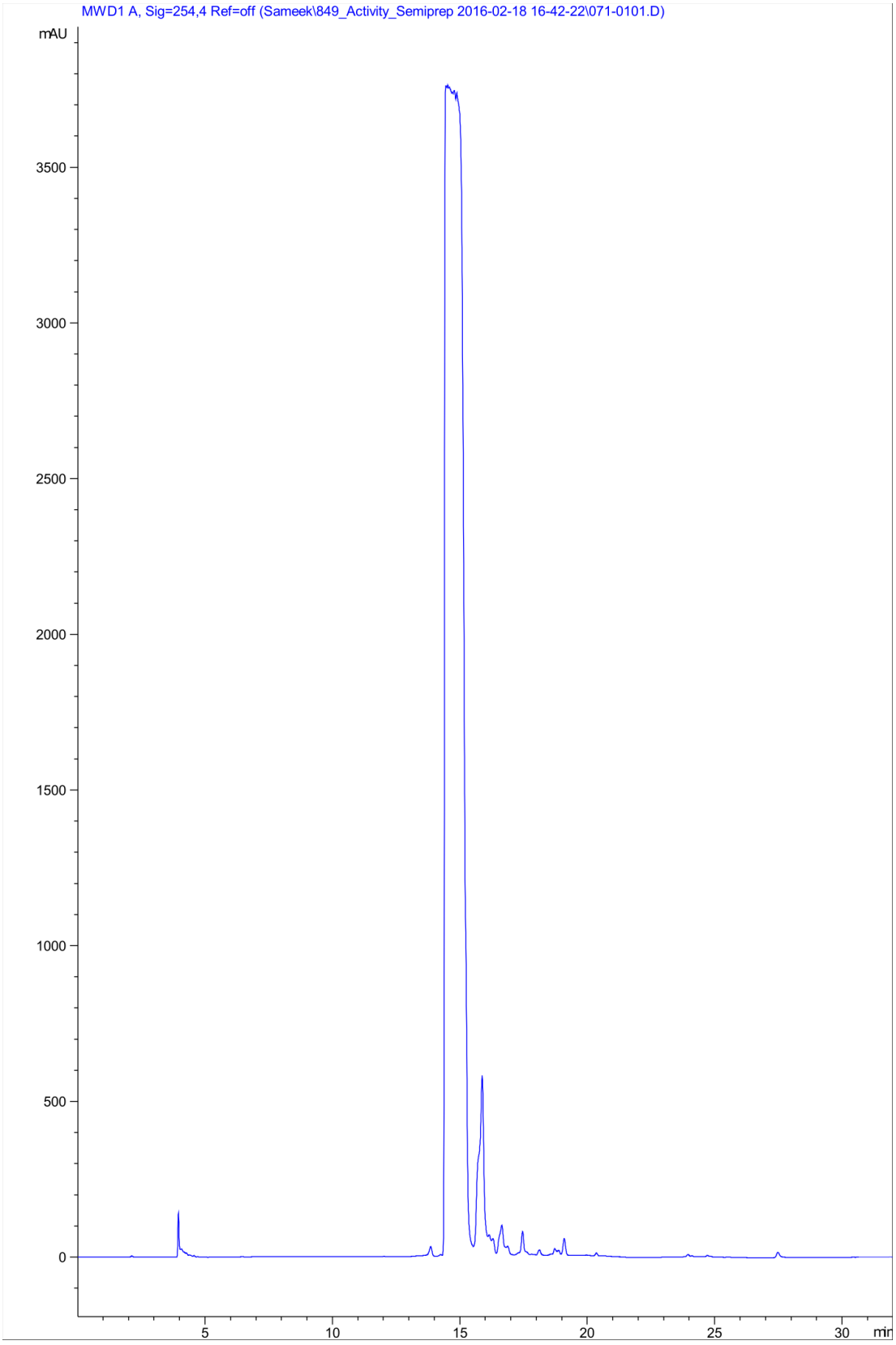

Figure 2.12. Semi-preparative RP-HPLC chromatogram of **2.26**.

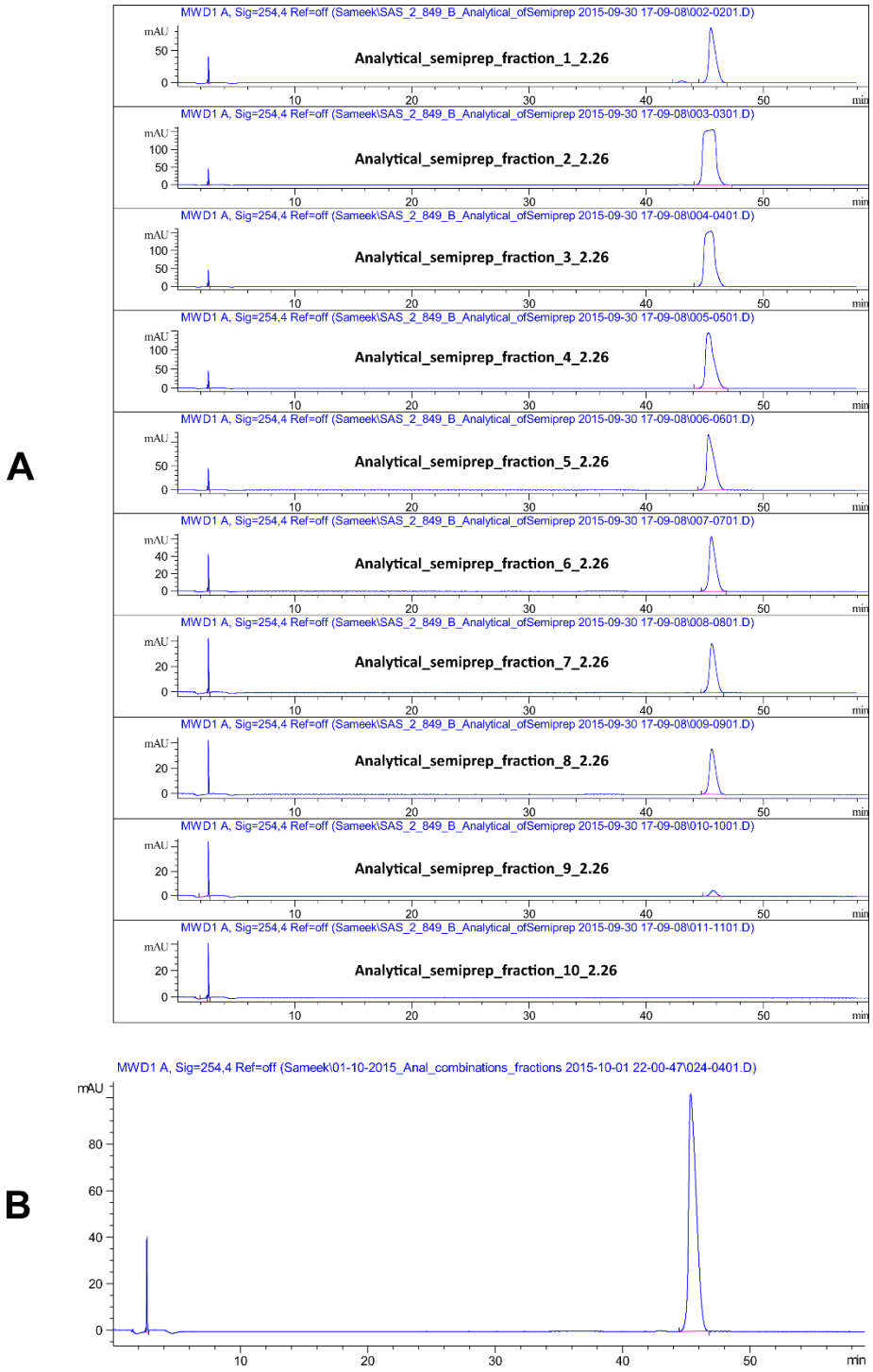

Figure 2.13. (A) Analytical RP-HPLC chromatogram of 10 separate fractions collected from peak corresponding to **2.26** (14.5 to 15.5 min) in the semi-preparative RP-HPLC chromatogram (Figure 2.12). **(B)** Analytical RP-HPLC chromatogram of combined fractions.

2.3 Biological studies

All biological experiments of (benzimidazolyl)isoquinolinols (synthesis described in section 2.2) were carried out by members of Professor Stephen Hill's group at the University of Nottingham, Nottingham, United Kingdom. Detailed experimental methods are described in the published research article reporting these novel compounds and their biological activity (Singh *et* al. 2018[167]).

A previously reported NanoBRET assay using the luciferase NanoLuc (NLuc; Promega Corporation, USA) was used for determining the A_1AR affinity of BODIPY-630/650 analogues of (benzimidazolyl)isoquinolinols **2.36**-**2.39**, **2.50**, **2.61** and **2.62** (section 2.2.2, 2.2.3 and 2.2.4).[90] The NanoBRET assay is a bioluminescence resonance energy transfer-based binding assay, which uses NanoLuc luciferase instead of the more commonly used Firefly and *Renilla* luciferases. NanoLuc luciferase is smaller and exhibits greater stability and brightness compared to firefly and *Renilla* luciferases.[200] The NanoBRET assay offers a direct measurement of the interaction of a fluorescent ligand with the receptor without depending on the indirect displacement of the radioligand by a test ligand. In this NanoBRET assay, HEK-293 cells expressing *N*-terminal NanoLuc labelled A_1AR were treated with increasing concentrations of the (benzimidazolyl)isoquinolinol fluorescent ligands (**2.36**-**2.39**, **2.50**, **2.61** and **2.62**). Non-specific binding was determined by incubation with DPCPX (a high affinity, non-fluorescent, selective A_1AR antagonist).

Unfortunately, none of the tested fluorescent ligands (**2.36**-**2.39**, **2.50**, **2.61** and **2.62**) showed significant binding at NanoLuc-A_1AR. For example, data is shown for **2.37** and **2.38** (Figures 2.14 (a-b)). As some of the structurally analogous compounds (for example **2.1**-**2.4**, Table 2.1) were reported as A_3AR antagonists, it was decided to evaluate some fluorescent ligands (**2.36**-**2.39**) at NanoLuc-A_3AR in a similar NanoBRET assay. Non-specific binding of the new fluorescent ligands was accessed by incubation with MRS1220 (a high affinity, non-fluorescent, selective A_3AR antagonist). A small degree of binding to NanoLuc-A_3AR was observed for (benzimidazolyl)isoquinolinol **2.38** and to a lesser extent for **2.37** (Figures 2.12 (c-d)). A small window of specific binding was observed and there was a large error in the calculated K_d values (**2.37** K_d = 534 ± 254 nM

at A_3AR; **2.38** K_d = 162 ± 65.5 nM at A_3AR). The (benzimidazolyl)isoquinolinols **2.36** and **2.39** did not show any specific binding to NanoLuc-A_3AR (data in appendix, Figure A.9).

The non-specific binding for fluorescent ligands (**2.36**-**2.39**) at NanoLuc-A_1AR expressing HEK-293 cells or NanoLuc-A_3AR expressing HEK-293 cells in the NanoBRET assay was determined by measuring BRET in the presence of non-fluorescent ligands DPCPX or MRS1220 respectively. This non-specific binding is a measure of the ability of the non-fluorescent ligand to prevent the binding of a fluorescent ligand by interacting with the same or an overlapping area of the receptor ligand-binding pocket. The non-specific binding component (obtained in the presence of DPCPX) for NanoLuc-A_1AR is linear (Figure 2.14 (a-b)). However, for NanoLuc-A_3AR, it can be seen from Figure 2.14 (c-d) that the non-specific binding component (obtained in the presence of MRS1220) is not linear and is better fitted to a saturable binding curve. Hence, a possibility remains (along with non-specific membrane binding) that an A_3AR ligand-binding pocket for (benzimidazolyl)isoquinolinol **2.37** and **2.38** is different from the ligand-binding pocket of MRS1220 at A_3AR.

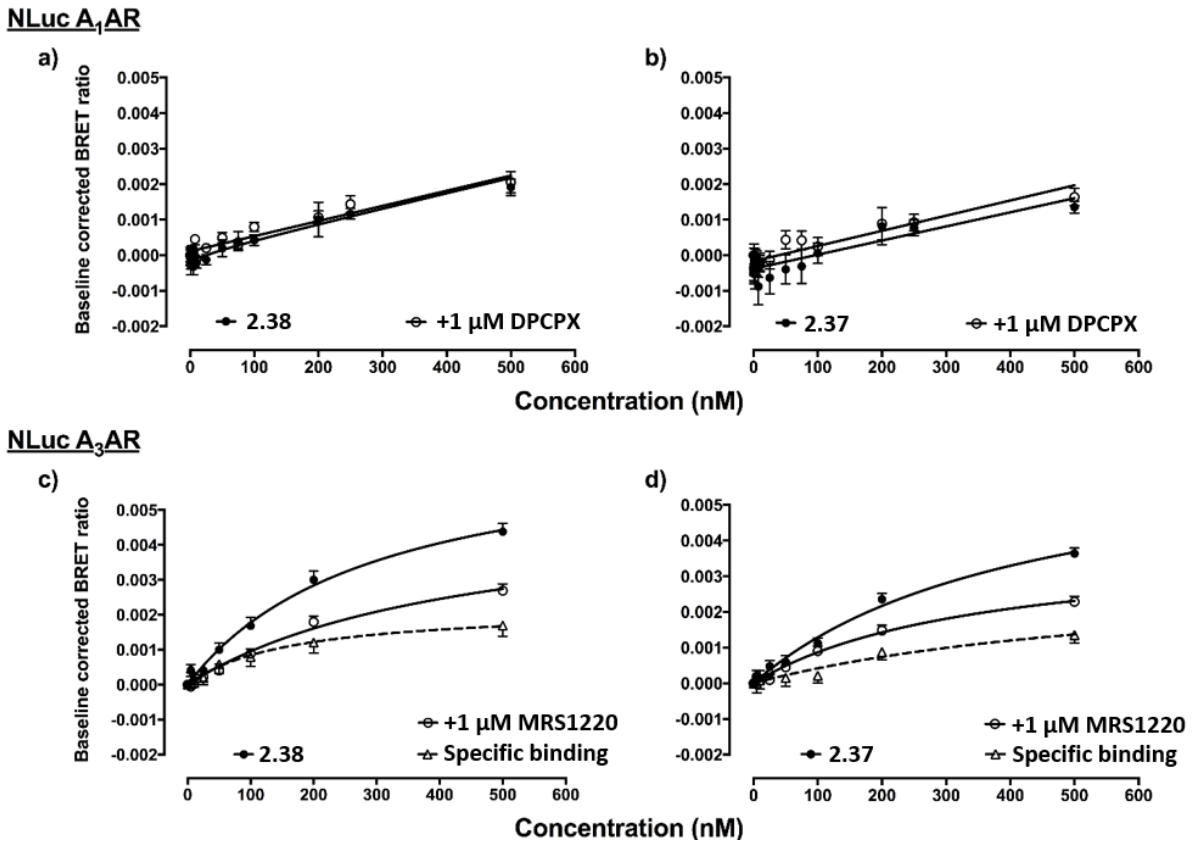

Figure 2.14. HEK-293 cells expressing *N*-terminally NanoLuc-tagged hA_1AR or hA_3AR were treated with increasing concentrations of fluorescent ligand (**2.38** or **2.37**) and the BRET ratio measured after addition of the NanoLuc substrate furimazine (10µM).[90] Non-specific binding was assessed in the absence and presence of 1µM DPCPX (NanoLuc-hA_1AR) or 1µM MRS1220 (NanoLuc-hA_3AR). Pooled data of raw BRET ratios was baseline corrected (minus vehicle + furimazine BRET ratios) so that data is expressed as fold increase in BRET ratios over basal. (a) NanoLuc-hA_1AR and **2.38**, (b) NabnoLuc-hA_1AR and **2.37**, (c) NanoLuc-hA_3AR and **2.38** and (d) NanoLuc-hA_3AR and **2.37**. Data represents four - seven independent experiments (in triplicate) and is expressed as mean ± SEM. Data is generated by members of Professor Stephen Hill's group at the University of Nottingham.

There is a possibility that lack of NanoLuc-A_1AR binding of fluorescent ligands (**2.36**-**2.39**, **2.50**, **2.61** and **2.62**) might be due to the steric hindrance arising from the presence of the *N*-terminal NanoLuc tag. This possibility was explored by collaborators, who carried out the NanoBRET assay with a known fluorescent non-selective AR ligand CA200645 (structure shown in chapter 1, Figure 1.9) at NanoLuc-A_1AR. In the NanoBRET assay, CA200645 showed specific binding with a large observation window (Figure 2.15 (A); K_d = 110 nM ± 18.46 at hA_1AR), which is in accordance with previously reported high affinity for CA200645 at NanoLuc-A_1AR (K_d = 7.5 ± 2.4 nM at hA_1AR).[90] These results indicate that the NanoLuc tag does not hinder binding of CA200645 to the receptor, hence it seems unlikely that NanoLuc tag is responsible for the poor affinity of fluorescent ligands **2.36**-**2.39**, **2.50**, **2.61** and **2.62**.

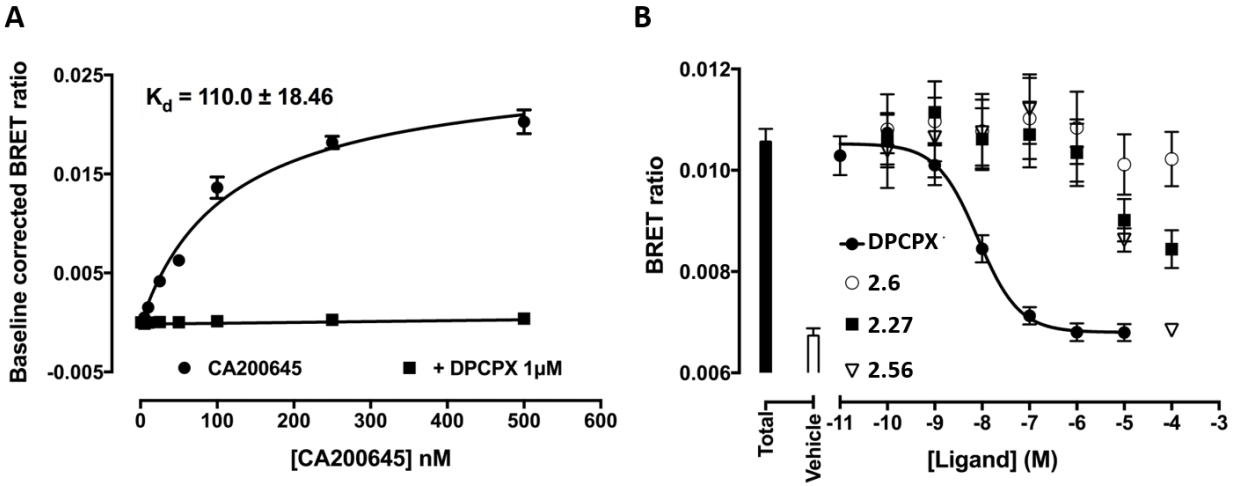

Figure 2.15. HEK-293 cells stably expressing *N*-terminal NanoLuc tagged hA_1AR were treated with increasing concentrations of CA200645 (5-500nM; 1 hr at 37°C; **A**). Non-specific binding was defined using 1 μM DPCPX, an A_1AR selective antagonist. The NanoLuc substrate furimazine was added (10 μM), with luminescence and fluorescence emissions recorded using a Pherastar FS. Data was pooled from independent experiments (n=5) and baseline corrected (minus vehicle + furimazine BRET ratios) so that data is expressed as fold increase in BRET ratios over basal and where appropriate fit using one site saturation binding (mean ± SEM). For competition experiments (**B**), NanoLuc-hA_1AR were co-incubated with a fixed concentration of CA200645 and increasing concentrations of unlabelled ligand (**2.6** or **2.27** or **2.56**; 1 hr at 37°C). Total CA200645 binding and vehicle are shown by the black and white bars respectively. Data was pooled from five independent experiments and is expressed as mean ± S.E.M. All data generated by members of Professor Stephen Hill's group at the University of Nottingham.

As significant binding was not observed for the fluorescent ligands (**2.36**-**2.39**, **2.50**, **2.61** and **2.62**) at NanoLuc-A_1AR, it was decided to test a subset of (benzimidazolyl)isoquinolinols (**2.26**, **2.27**, **2.33**, **2.46**, **2.49**, **2.56** and **2.59**, described in sections 2.2.2, 2.2.3, and 2.2.4, and literature (benzimidazolyl)isoquinoline **2.6**, Table 2.1) in the NanoBRET assay. Since the (benzimidazolyl)isoquinolinols (**2.26**, **2.27**, **2.33**, **2.46**, **2.49**, **2.56** and **2.59**) do not contain a fluorophore capable of interacting with NanoLuc tag via BRET, instead the competitive displacement of fluorescent ligand CA200645 by the (benzimidazolyl)isoquinolinols was measured by collaborators at the University of Nottingham. DPCPX was used as a positive control. Displacement of CA200645 was only observed when the concentration of benzimidazolyl)isoquinolinol (**2.26**, **2.27**, **2.33**, **2.46**, **2.49**, **2.56** or **2.59**) was greater than 10^{-6} M (Figure 2.15 (B); **2.6** and representative (benzimidazolyl)isoquinolinols **2.27** and **2.56** shown; data for **2.26**, **2.33**, **2.46**, **2.49** and **2.59** shown in Appendix, Figure A.10). Except for DPCPX (pK_i; 8.82 ± 0.16 nM, at hA_1AR), collaborators could not calculate the pK_i for any of the test compounds. Surprisingly, displacement of CA200645 with literature (benzimidazolyl)isoquinoline **2.6** was not observed. The (benzimidazolyl)-isoquinoline **2.6** was previously reported as a selective and high affinity A_1AR antagonist (K_i = 14.1 ± 1.6 nM at hA_1AR, Table 2.1) in a competition radioligand binding assay using CHO cells overexpressing A_1AR, using [^{3}H]DPCPX as the radioligand.[76] Interestingly, better binding to NanoLuc-A_1AR (although still limited) was observed for 1-(1H-1,3-benzodiazol-2-yl)isoquinolin-6-ol **2.27** and 3-(6-methyl-1H-1,3-benzodiazol-2-yl)isoquinolin-6-ol **2.56** compared to the literature (benzimidazolyl)isoquinoline **2.6** (Figure 2.15 (B)). The reasons for low A_1AR binding affinity of literature (benzimidazolyl)isoquinoline **2.6** obtained in this thesis are not known.

2.4 Conclusions

Novel (benzimidazolyl)isoquinolinols along with linker (alkyl, PEG, and peptide (Ala-Ala)) conjugates and BODIPY-630/650 conjugates (section 2.2) were synthesised with the aim of developing a high affinity, selective A_1AR fluorescent ligands. Synthesis of isoquinolinols from tetrahydroisoquinolinols involved the development of a procedure using DDQ and atmospheric air mediated aromatisation. As there are only two previous reports[182, 201] (with unclear experimental details and poor product characterisation) of metal-free aromatisation reaction of unprotected tetrahydroisoquinolinols to isoquinolinols, the mild aromatisation method reported here will be useful in the preparation of pharmacologically interesting isoquinolines and isoquinolinols. The NMR spectra peak multiplicity and peak broadening of novel (benzimidazolyl)isoquinolinols was investigated for a representative compound (**2.26**) via NMR spectroscopy and RP-HPLC studies and was concluded to arise from the tautomerism of the benzimidazole moiety.

The aim of developing new A_1AR selective fluorescent ligands was not achieved in this thesis and the biological data indicates that conjugation of a fluorophore to the (benzimidazolyl)isoquinolinol scaffold via the C-6 or C-7 position of the isoquinoline is unlikely to attain this goal. There remains a possibility of developing an A_1AR selective fluorescent ligand via exploring other positions of the (benzimidazolyl)isoquinoline scaffold (such as the benzimidazole) for linker attachment. However, as the literature (benzimidazolyl)isoquinoline **2.6** did not exhibit any significant A_1AR affinity, it seems logical to explore other ligand classes for the development of A_1AR fluorescent ligands.

Chapter 3 Development of chromenopyrazoles as fluorescent ligands for cannabinoid type 1 receptor

3.1 Design rationale for chromenopyrazole-based fluorescent ligands

The availability of rich SAR data[132] for cannabis-derived CBR ligands (for example THC, described in chapter 1, section 1.4.3) along with the high affinity and potency for CBRs make these ligands attractive leads for development of the fluorescent ligands. However, structural variations of cannabis-derived CBR ligands such as THC and CBN have generally not been very successful in attaining CBR subtype selectivity.[132]

Cumella *et al.*[137] reported chromenopyrazole derivatives as CBR agonists, obtained by replacing the phenyl ring of CBN (Figure 3.1) with a pyrazole (Table 3.1). Representative examples of these chromenopyrazoles,[137] including those with *N*-aryl and *N*-alkyl substituents on which the fluorescent ligand design rationale was based, are shown in Table 3.1. Chromenopyrazoles with an n-pentyl side chain (for example **3.6**-**3.9**) showed weak or no affinity for CBRs while those with a dimethylheptyl side chain showed high affinity for CBRs. These results are consistent with those of Rhee *et al.*,[138] who reported derivatives of CBN and THC with a dimethylheptyl side chain that showed higher affinity and potency at both CBRs compared to n-pentyl side chain analogues. Prior to the report of CBR chromenopyrazoles by Cumella *et al.*[137], chromenopyrazoles were also reported by Chiodini *et al.*[202] and Press *et al.*[203] which were inactive in pharmacological tests carried out to study CNS effects of chromenopyrazoles (data was not reported by the authors).

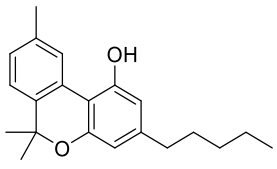

Cannabinol (CBN)

Figure 3.1. Cannabinoid receptor ligand cannabinol.

Among the dimethylheptyl chromenopyrazoles reported by Cumella *et al.*[137] was **3.4** (Table 3.1) with a *N*1-2,4-dichlorophenyl moiety, which exhibited high affinity for CB_1R and good selectivity over CB_2R. The high affinity of **3.4** at CB_1R was in contrast to the structurally similar regioisomer **3.3** (Table 3.1) with a *N*1-3,4-dichlorophenyl moiety, which showed moderate affinity for both CBRs. Chromenopyrazoles **3.1**, **3.2** and **3.5** inhibited electrically induced contraction of mouse vas deferens (a tissue commonly used to evaluate CB_1R function of CBR ligands[204]) and therefore behaved as mCB_1R agonists. It was envisioned that a CB_1R selective (over CB_2R) fluorescent agonist could be developed by maintaining a dimethylheptyl side chain and careful substitution of the atoms near *N*1 pyrazole position.

Table 3.1. Previously reported chromenopyrazole and chromenoisoxazole CBR ligands in literature[137, 202-203, 205]

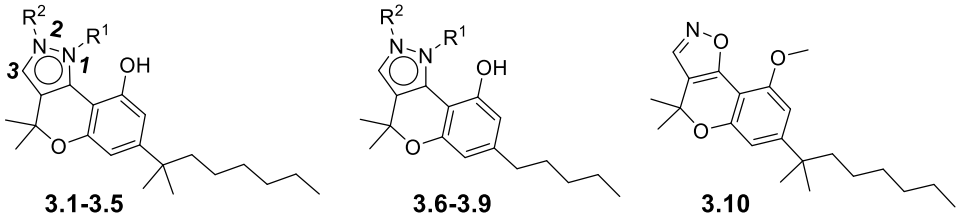

	R^1	R^2	K_i hCB_1R (nM ± SEM)*	K_i hCB_2R (nM ± SEM)*	Ref
3.1	H	H	28.5 ± 23.7	>40000	*137*
3.2	Ethyl	H	4.5 ± 0.6	>40000	*137*
3.3	3,4-Dichlorophenyl	H	514 ± 205	270	*137*
3.4	2,4-Dichlorophenyl	H	5.2 ± 4.3	>40000	*137*
3.5	H	Ethyl	18.6 ± 4.1	>40000	*137*
3.6	H	H	4100 ± 800	2010 ± 500	*137, 202*
3.7	Ethyl	H	9610	>40000	*137*
3.8	3,4-Dichlorophenyl	H	607 ± 151	>40000	*137*
3.9	H	Methyl	22100 ± 1410	>40000	203,*137*
3.10	-	-	>40000	12.8 ± 2.4	*205*

*Binding affinity (K_i) obtained by competition binding assay performed on membranes obtained from HEK-293 cells expressing either hCB_1R or hCB_2R with [^{3}H]-CP55,940 as radioligand.

While this PhD thesis was underway, Morales *et al.*[205], part of the same research group as Cumella *et al.*[137], reported a revised series of chromenopyrazoles and new

chromenoisoxazoles with high affinity and selectivity for CB_2R. Some of the *N*-alkylated chromenopyrazoles and chromenoisoxazoles (for example **3.10**) described by Morales *et al.*[205] behaved as CB_2R agonists in a cAMP BRET assay.[205] The same group of researchers also reported chromenopyrazolediones as CBR ligands (Figure 3.2), which exhibited *in vivo* antitumor activity against human prostate cancer[206] and human triple-negative breast cancer tumours[207] generated in mice. One of these, chromenopyrazoledione **3.11** (K_i > 40000 nM at hCB_1R; 529 ± 26 nM at hCB_2R, Figure 3.2) was shown to exhibit its antitumor activity by induction of apoptosis through CB_2R activation and oxidative stress (by formation of reactive oxygen species). Morales *et al.*[208] also reported chromenopyrazoles lacking phenolic hydroxyl and the dimethylheptyl side chain as GPR55 (a GPCR) antagonists and partial agonists (for example **3.12**, EC_{50} = 1.28 nM at human GPR55 (hGPR55)).

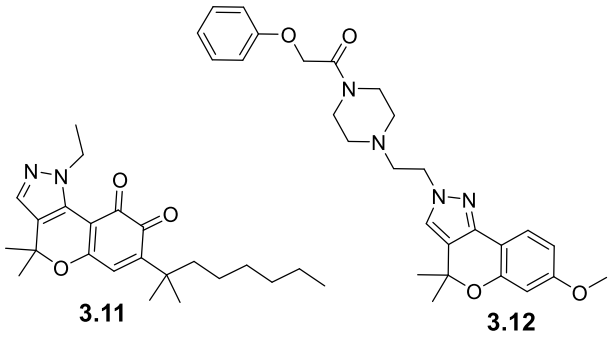

Figure 3.2. Chromenopyrazoledione **3.11**[207] exhibited *in vivo* antitumor activity against human triple-negative breast cancer tumours generated in mice. Chromenopyrazole **3.12**[208] is a selective GPR55 agonist.

As has been discussed in chapter 1 (section 1.2.3.1), small molecule based fluorescent ligands consist of a high affinity ligand tethered to a fluorophore via a suitable length linker. At the time when this project commenced, the crystal structure of CB_1R was not reported. SAR data available for the chromenopyrazoles indicated that the best position to introduce a linker would likely be around the pyrazole nucleus. Accordingly, the primary aim was to identify a robust position around the pyrazole nucleus for the conjugation of linkers to the chromenopyrazole scaffold.

It was decided to prepare chromenopyrazole-linker conjugates with aryl or alkyl linkers attached to atoms belonging to pyrazole nucleus. Further, an *O*-alkylated chromenopyrazole was also designed as a potential CB_1R chromenopyrazole-linker

conjugate. Five *N*-phenyl-chromenopyrazoles with a functional group attached at the para, meta and ortho position were designed to determine which position on the phenyl ring could tolerate attachment of substituents including that of long linkers (Figure 3.3). This was particularly important considering the difference in CBR binding affinity of *N*-(meta, para-dichlorophenyl)-chromenopyrazole **3.3** and *N*-(ortho,para-dichlorophenyl)-chromenopyrazole **3.4**.

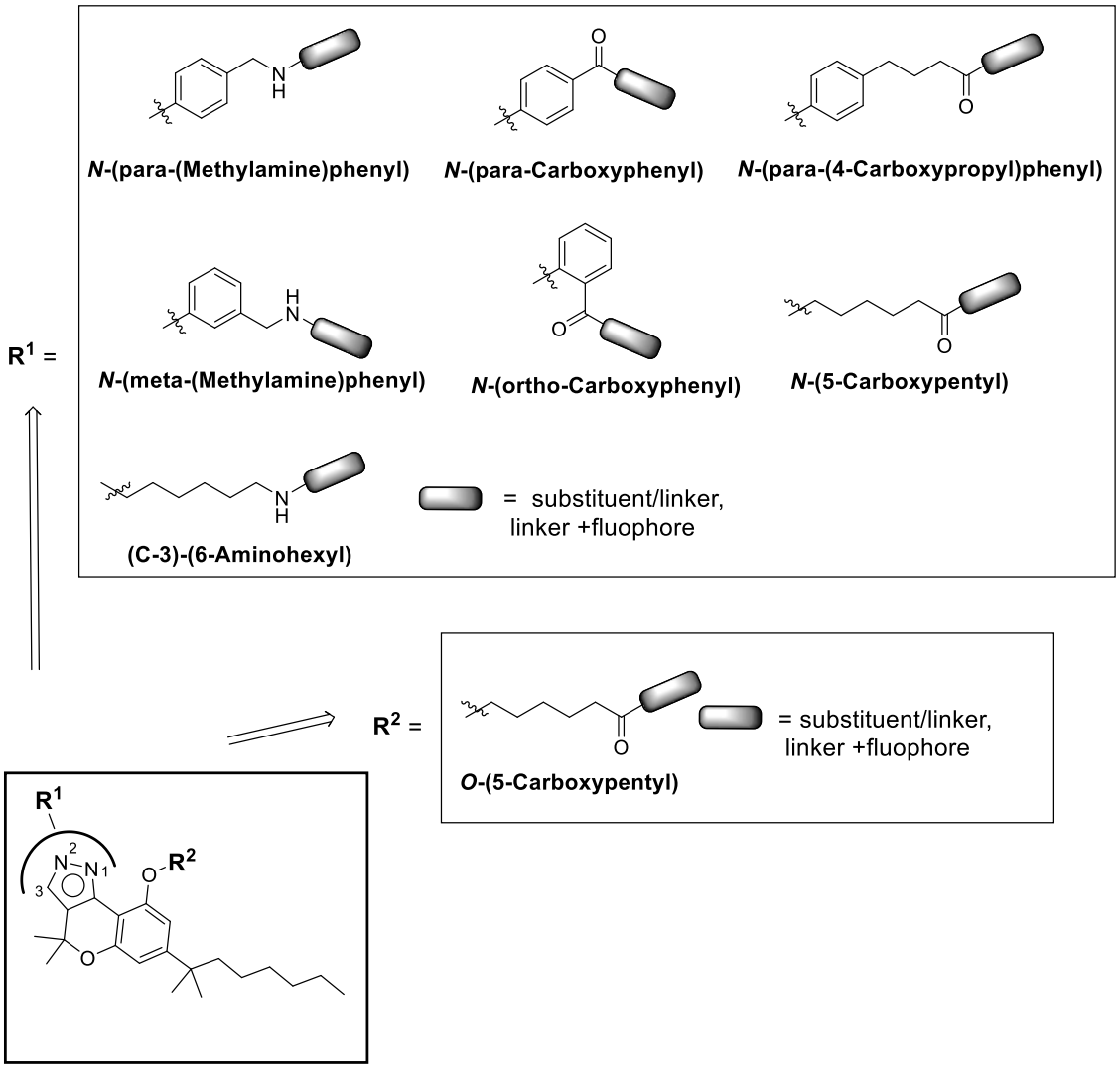

Figure 3.3. New chromenopyrazoles designed as potential CB_1R agonists.

Among the *N*-phenyl-chromenopyrazoles designed were *N*-(para-(methylamine)-phenyl)-chromenopyrazoles and *N*-(para-carboxyphenyl)-chromenopyrazoles. *N*-(para-(methylamine)phenyl)-chromenopyrazoles have an amine-substituent/linker bonded with phenyl ring via a methylene sp^3 carbon whereas *N*-(para-carboxyphenyl)-chromenopyrazoles have an sp^2 carbonyl carbon bonded carboxyl-substituent/linker with

a phenyl ring. The sp^3 carbon in *N*-(para-(methylamine)phenyl)-chromenopyrazoles provides a greater degree of rotational freedom to the amine-substituent (or amine-linker) compared to the carboxy-substituent in *N*-(para-carboxyphenyl)-chromenopyrazoles. It was reasoned that this greater flexibility might be important for tolerance to a long linker-chromenopyrazole in the CB_1R binding site.

As the ligand-binding pocket of CBRs is lipophilic, a series of *N*-(para-(4-carboxypropyl)phenyl)-chromenopyrazoles with a short lipophilic alkyl chain separating the chromenopyrazole pharmacophore from longer linkers (PEG, peptide and alkyl) were designed (Figure 3.3). It was thought that this alkyl chain might also minimise any detrimental effect of bulky linkers on the CB_1R binding affinity of the chromenopyrazoles.

Two other *N*-phenyl-chromenopyrazoles were designed – *N*-(meta-(methylamine)-phenyl)-chromenopyrazoles and *N*-(ortho-carboxyphenyl)-chromenopyrazoles (Figure 3.3). Comparison of the binding affinity of *N*-(meta-(methylamine)phenyl)-chromenopyrazoles and *N*-(para-(methylamine)phenyl)-chromenopyrazoles would be useful in determining the suitability of meta or para position for introduction of the longer linkers.

N-(5-Carboxypentyl)-chromenopyrazoles and (C-3)-(6-aminohexyl)-chromenopyrazoles (linker attached at the third pyrazole position, Figure 3.3) were also designed. In the case of *N*-(5-carboxypentyl)-chromenopyrazoles, alkyl linkers would be attached from both *N*1 and *N*2 positions of the chromenopyrazole. (C-3)-Alkyl-chromenopyrazoles were designed on the basis of spatial closeness of C-3 carbon to the previously substituted *N*1 and *N*2 of pyrazole (*N*-substituted **3.2**, **3.3**, **3.4**, and **3.5** are high affinity CB_1R agonists (Table 3.1)).

It was planned that the final fluorescent ligands would be synthesised using a reliable amide coupling reaction between a pharmacophore-linker-amine and a fluorophore (for example BODIPY-630/650-SE; Figure 3.4). Initially, fluorescent ligands were only made with the BODIPY-630/650 fluorophore due to its previous success in developing other class A GPCR ligands,[43, 86] high fluorescence quantum yield and emission in the red spectral region, thus allowing imaging studies with minimal interference from molecules

present in cells. If a high affinity CB_1R chromenopyrazole-linker was developed, it could then be conjugated with different fluorophores (such as 1-(5-carboxypentyl)-3,3-dimethyl-2-((1*E*,3*E*)-5-((*E*)-1,3,3-trimethylindolin-2-ylidene)penta-1,3-dien-1-yl)-3*H*-indol-1-ium (Cy5), 5-(5,5-difluoro-7,9-dimethyl-5*H*-5λ^4,6λ^4-dipyrrolo[1,2-c:2',1'-*f*][1,3,2]diazaborinin-3-yl)pentanoyl (BODIPY-FL), and TAMRA) to investigate the pharmacological and spectral properties of the resulting fluorescent ligands. Considering the time available for synthesis and biological evaluation, it was decided to prepare only a subset of compounds possible from a combination of different chromenopyrazole pharmacophores and linkers described in previous paragraphs, which depending on biological results could be refined to prepare a second generation of chromenopyrazoles.

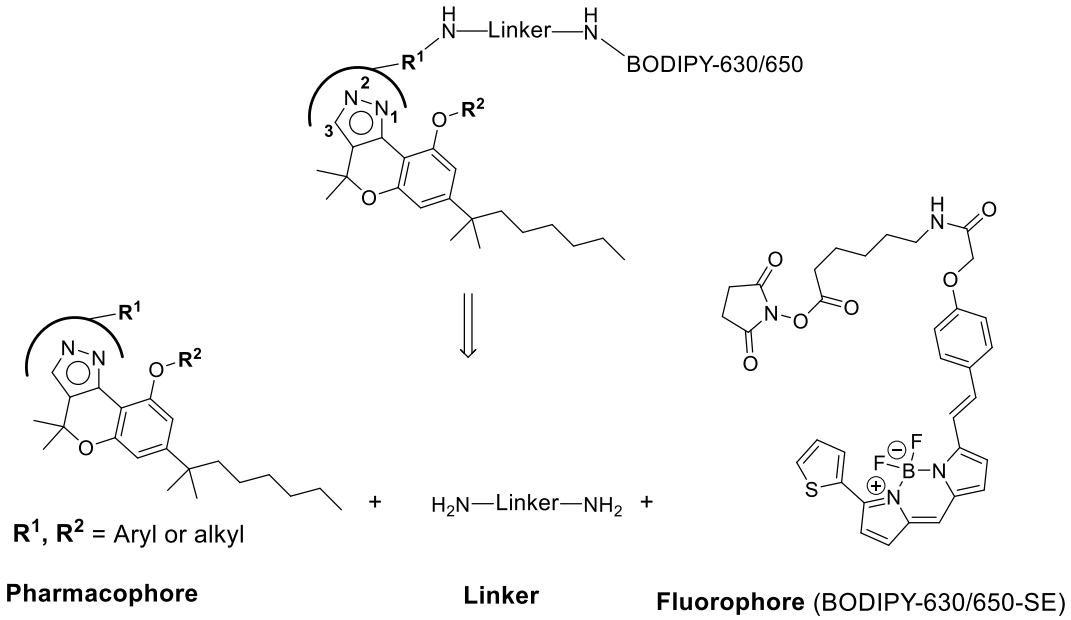

Figure 3.4. Retrosynthetic scheme of fluorescent chromenopyrazole agonists designed in this chapter.

3.2 Synthesis and structural characterisation

3.2.1 Synthesis of *N*-Phenyl-chromenopyrazoles

3.2.1.1 Synthesis of *N*-(para-(methylamine)phenyl)-chromeno-pyrazoles

Following a literature procedure, condensation of mono-Boc-protected amine **2.12** (synthesis described in chapter 2, section 2.2.1) with succinic anhydride gave the carboxylic acid linker **3.13**[86] (Scheme 3.1).

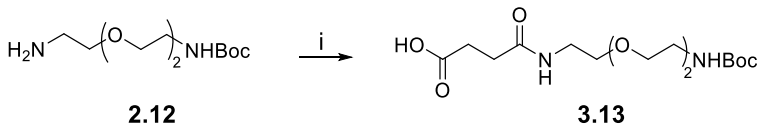

2.12 **3.13**

Scheme 3.1. (i) Succinic anhydride, $CHCl_3$, 65%.

The commercially available diol **3.14** was reacted with 3,3-dimethylacrylic acid, methanesulfonic acid, and phosphorous pentoxide as described in a literature procedure[137] to provide **3.15** (Scheme 3.2). The first step of this reaction occurs via Friedel–Crafts acylation mechanism to provide an ortho-acylated diol,[209] which then undergoes oxa-Michael addition of the aromatic hydroxyl to acrylate to provide chromene **3.15**.

α–Formylation of **3.15** with ethyl formate using excess sodium hydride as a base afforded β-ketoaldehyde **3.16**. This reaction was carried out according to a literature procedure[137] but used conventional heating instead of the reported microwave irradiation. An excess of sodium hydride was used to compensate for some of the base consumed in the deprotonation of the aromatic hydroxyl group of **3.15**. β-Ketoaldehyde **3.16** is a key compound in this thesis and is used in subsequent synthetic schemes in chapters 3 and 4. Initial attempts to directly synthesise acid **3.19** by heating a mixture of **3.16** with commercially available 4-hydrazinobenzoic acid at 90 °C for 20 h provided a mixture of the reaction intermediate enehydrazinone **3.17** and cyclised acid **3.19** as determined by low-resolution mass spectrometry (MS). Protic acids such as H_2SO_4 have been previously used in the preparation of pyrazoles.[210] Accordingly, it was decided to use H_2SO_4 to facilitate the formation of the pyrazole, that at the same time would esterify the carboxylic acid to give methyl ester **3.18**, which would be easier to purify than a carboxylic acid.

Condensation of **3.16** with 4-hydrazinobenzoic acid in methanol with H_2SO_4 still gave a mixture of the reaction intermediate enehydrazinone **3.17** and cyclised acid **3.19** (determined by MS) after 4 h of heating at 75 °C, but increasing the reaction time to 8 h provided ester **3.18** as the sole product (Scheme 3.2).

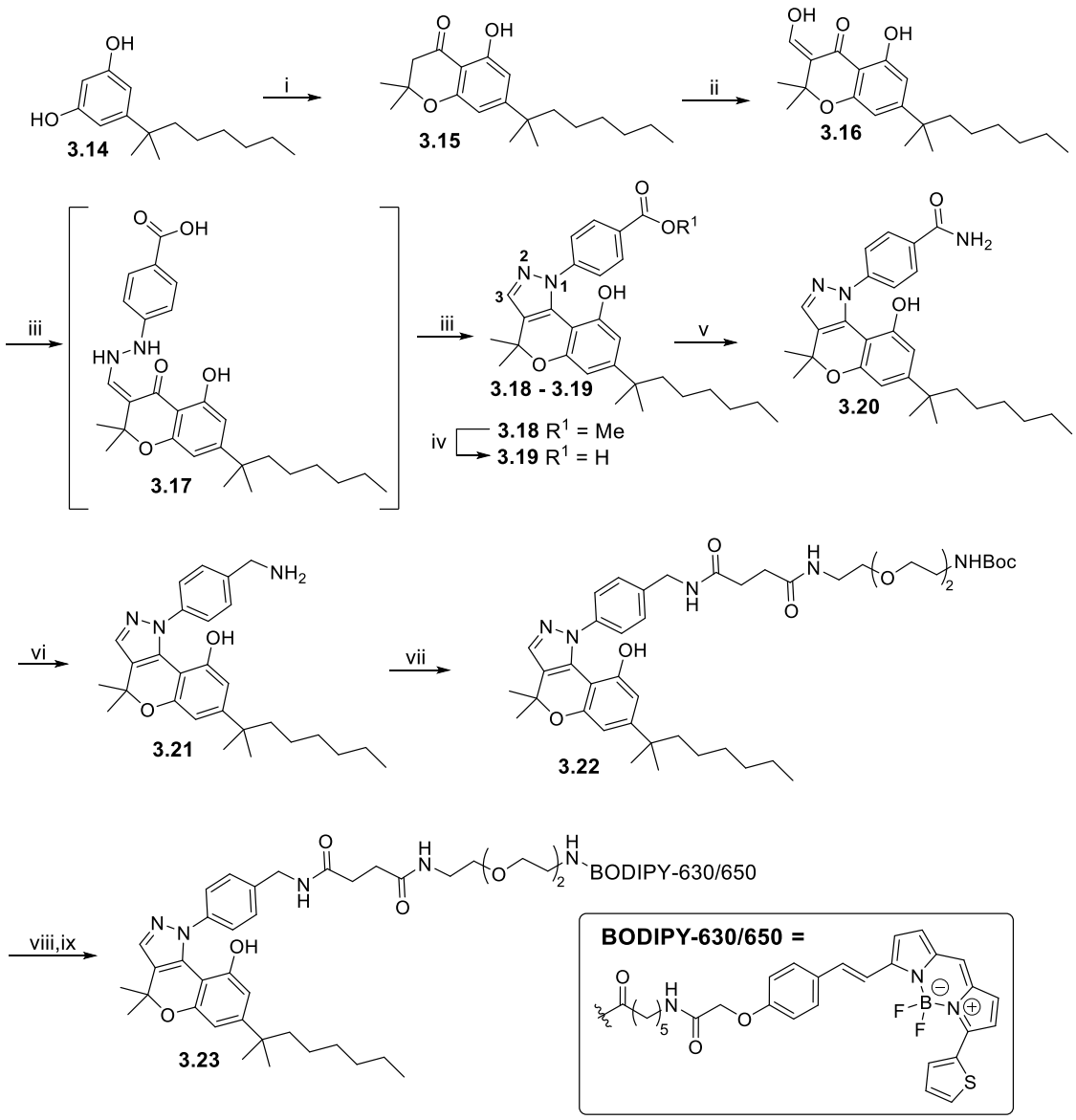

Scheme 3.2. (i) 3,3-Dimethylacrylic acid, methanesulfonic acid, P_2O_5, 70 °C, 69%. (ii) Ethyl formate, NaH, 45 °C then 65 °C, 70%. (iii) 4-Hydrazinobenzoic acid, H_2SO_4, MeOH, 75 °C, 61%. (iv) aq. LiOH, THF:H_2O, quantitative. (v) NH_4Cl, HBTU, DIPEA, DMF, 81%. (vi) $LiAlH_4$, THF, 70 °C. (vii) **3.13**, HBTU, DIPEA, DMF, 34%. (viii) TFA, DCM, quantitative. (ix) BODIPY-630/650-SE, DIPEA, DMF, quantitative.

Conversion of **3.16** to give **3.18** is an example of the Knorr pyrazole synthesis, which first involved condensation of the primary amine of 4-hydrazinobenzoic acid and the aldehyde

of **3.16** to give enehydrazinone **3.17**, followed by condensation of the secondary amine and ketone to yield **3.18** (Scheme 3.2). Although two regioisomers can be formed via condensation of an unsymmetrical hydrazine with β-ketoaldehyde **3.16** (Figure 3.5), only the *N*1 regioisomer was isolated upon condensation of 4-hydrazinobenzoic acid with **3.16**. Analysis via RP-HPLC of the optimised crude reaction mixture and subsequent analysis of RP-HPLC fractions by MS indicated formation of only one compound with a molecular weight corresponding to **3.18** (Scheme 3.2), however this does not reveal information regarding the identity of regioisomer.

Investigation of the potentially regioisomeric nature of **3.18** by 2D (two dimensional) NMR techniques such as gHMBC was inconclusive. Comparison of ^{1}H and ^{13}C NMR chemical shifts of **3.18** with reported chromenopyrazoles (**3.2, 3.3, 3.4, 3.5, 3.7** and **3.8**) supported the structure of **3.18** as the *N*1 regioisomer. In particular, this assignment was based on NMR data reported by Cumella *et al.*[137], which revealed that ^{1}H and ^{13}C chemical shifts of H-3 and C-3 nuclei of *N*1 chromenopyrazoles are upfield by at least 0.2 parts per million (ppm) and 9.0 ppm respectively, as compared to the *N*2 isomers. Chemical shifts of atoms of pyrazole ring (especially H-3 (7.45 ppm) and C-3 (^{13}C = 134.90 ppm)) of **3.18** were closer to *N*1 chromenopyrazole regioisomers than *N*2 isomers reported by Cumella *et al.*[137] In subsequent syntheses (Schemes 3.5, 3.7 and 3.8), only the *N*1 regioisomer (assigned using chemical shift comparison with chromenopyrazole regioisomers reported by Cumella *et al.*[137]) was isolated on condensation of **3.16** with aryl hydrazines (for example **3.29** in Scheme 3.5, **3.41** in Scheme 3.7, and **3.48** in Scheme 3.8) or with 6-hydrazinylhexanoic acid (6-hydrazinylhexanoic acid was used in Scheme 3.11 to prepare **3.51**). Later, *N*2-alkyl-chromenopyrazole **3.59** (Scheme 3.12) was also prepared. The structure of **3.51** as the *N*1 regioisomer and **3.59** as the *N*2 regioisomer were supported by 2D NMR techniques (described in detail in section 3.2.2.1 and section 3.2.2.2).

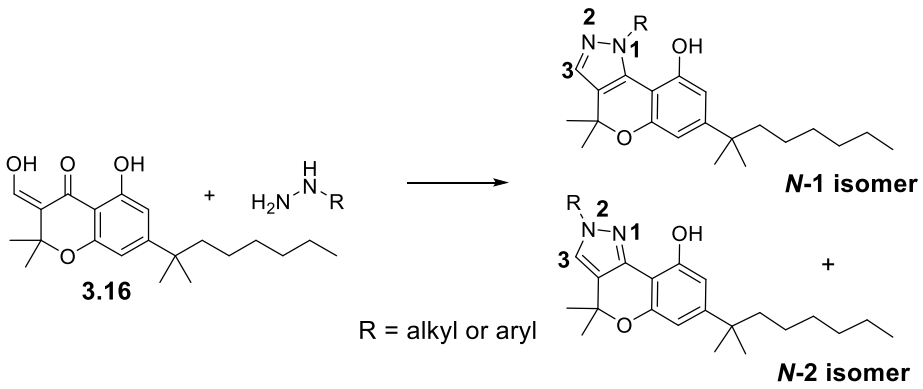

Figure 3.5. Two possible regioisomeric pyrazoles that can form from condensation of **3.16** with hydrazine derivatives via the Knorr pyrazole synthesis.

Formation of the *N*1 instead of the *N*2 regioisomer is likely due to the steric hindrance of the secondary amine compared to the primary amine in the case of arylhydrazines and long alkyl chain hydrazine **3.51** (synthesis shown in Scheme 3.11). In the case of arylhydrazines, the secondary amine is also less nucleophilic compared to the primary amine hence disfavouring the formation of the *N*2 regioisomer. Formation of only the *N*1 regioisomer with aryl hydrazines and cyclohexylhydrazine was also reported by Cumella *et al.*[137], while they obtained both *N*1 and *N*2 regioisomers upon reaction of methyl and ethyl hydrazine with **3.16**. In this PhD thesis, 6-hydrazinylhexanoic acid (as used in Scheme 3.11 to prepare **3.51**) is a bulkier alkyl hydrazine similar to cyclohexylhydrazine used by Cumella *et al.*[137] and favoured the formation of only the *N*1 regioisomer.

The synthesis continued with hydrolysis of the methyl ester **3.18** with aq. LiOH, which provided the carboxylic acid **3.19** (Scheme 3.2). This was then reacted with ammonia, using HBTU as a coupling reagent and NH_4Cl as a source of ammonia in the presence of DIPEA to prepare benzamide **3.20**. Reduction of **3.20** with $LiAlH_4$ in refluxing THF provided benzylamine **3.21**, which was not purified and used as such in the next reaction. Benzylamine **3.21** was coupled with carboxylic acid linker **3.13** using HBTU as coupling reagent and DIPEA as base to provide chromenopyrazole **3.22**. The lower yield obtained in the synthesis of **3.22** and subsequent linker conjugates (**3.32** (Scheme 3.5), **3.45** (Scheme 3.7), **3.53** (Scheme 3.11)) is likely due to the loss of the polar product during silica gel column chromatography.

Boc-deprotection of **3.22** with TFA, followed by semi-preparative RP-HPLC purification of the amino trifluoroacetate salt then reaction with the commercially available fluorophore BODIPY-630/650-SE using DIPEA as a base provided the fluorescent ligand **3.23** in a quantitative yield.

The calculated yield for the reaction of commercially available BODIPY-630/650-SE with amine linker conjugates to give fluorescent ligands was more than quantitative in some cases. It is believed that this is due to the commercial supply of BODIPY-630/650-SE in slightly higher amounts than that specified on the container (the amount of fluorophore specified on the container was used in the calculation of yield). BODIPY-630/650-SE is moisture and light sensitive so was not weighed accurately but instead DMF was added to the commercial bottle and used directly in the coupling reactions. Other members of the Vernall research group have observed greater than quantitative yields of the coupling reactions with the same commercially available fluorophore and pack size. Lower yield of the coupling reaction observed for the preparation of fluorescent ligand **3.46** (Scheme 3.7) and fluorescent ligand **3.54** (Scheme 3.11) is likely due to the loss of the compound during semi-preparative RP-HPLC purification.

It was reasoned that pharmacological comparison of a short linker conjugate such as **3.25** (Scheme 3.3) with long linker conjugate **3.22** (Scheme 3.2) would provide useful information regarding the effect of linker length on the affinity of chromenopyrazole-linker conjugates for CBRs. So, preparation of **3.25** commenced with reaction of **3.21** with acetic anhydride, which provided *N*,*O*-diacetylated product **3.24** and *N*-acetylated product **3.25**, as determined by MS and ^{1}H NMR spectroscopy. The ratio of *N*,*O*-diacetylated product **3.24** to *N*-acetylated product **3.25** was approximately 3:1 (determined by ^{1}H NMR spectra analysis of the crude mixture). The mixture of **3.24** and **3.25** was then subjected to alkaline hydrolysis conditions to give **3.25** (Scheme 3.3). Chemoselective hydrolysis of the ester functional group in **3.24** and the presence of an amide in **3.25** is supported by combined MS and NMR experiments (gHMBC correlation between benzylic protons and acetyl carbonyl carbon (Figure 3.6)). Formation of the *N*-acetylated product **3.25** and *N*,*O*-diacetylated product **3.24** is in contrast to formation of only *N*-acylated product in the case of **3.23** (section 3.2.1.1). This is likely due to lower electrophilicity of HBTU-activated carboxylic acid **3.13** compared to acetic anhydride

and due to a lower amount of **3.13** (1 equivalent) than acetic anhydride (3 equivalents), used in the reaction with amine **3.21**.

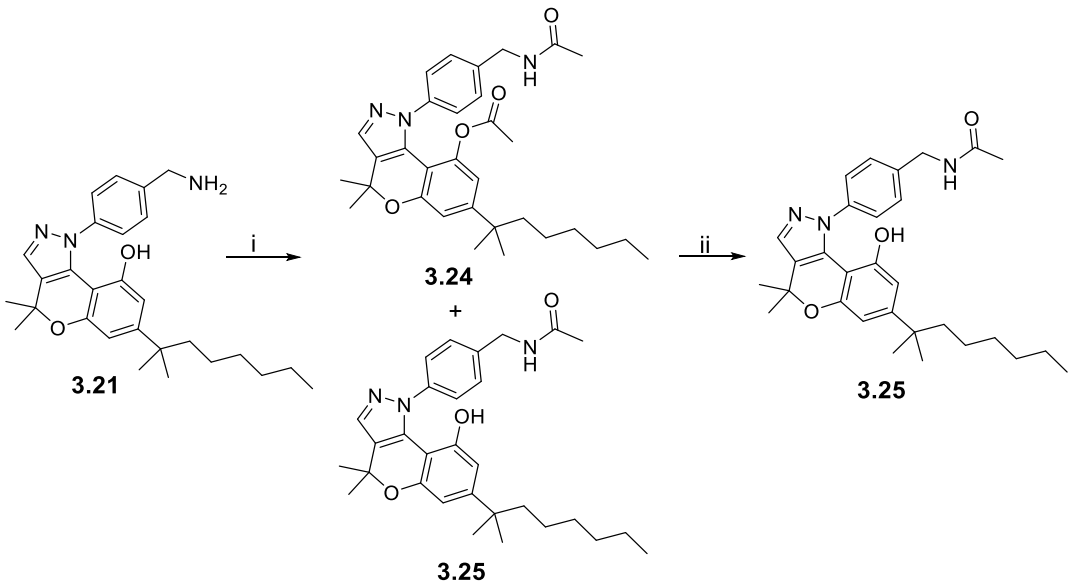

Scheme 3.3. (i) Ac_2O, Et_3N, DCM. (ii) NaOH, MeOH, 42% over 2 steps.

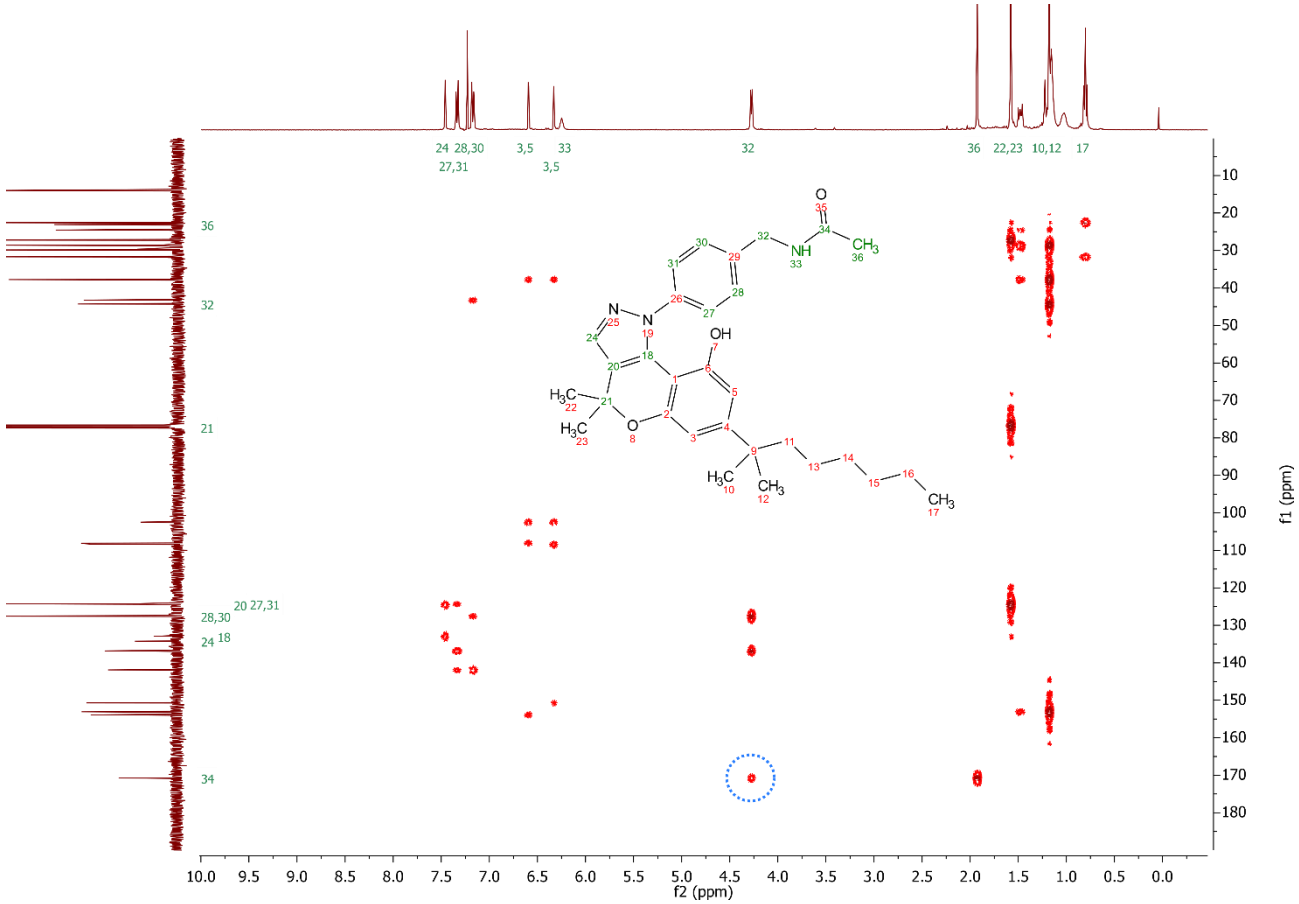

Figure 3.6. Evidence for **3.25** as an *N*-acetylated product - gHMBC spectrum of **3.25** in $CDCl_3$, correlation between H-32 and C-34 is circled.

3.2.1.2 Synthesis of *tert*-butyl *N*-(2-{2-[2-({4-[9-hydroxy-4,4-dimethyl-7-(2-methyloctan-2-yl)-1H,4H-chromeno[4,3-c]pyrazol-1-yl] phenyl}formamido) ethoxy]ethoxy}ethyl) carbamate

As discussed in section 3.1, comparison of CB_1R binding affinity of **3.22** and **3.26** will provide information about the effect of flexibility at the point of linker attachment. **3.26** was prepared by coupling **3.19** with linker **2.12** (synthesis described in chapter 2, section 2.2.1) using HATU as coupling reagent and DIPEA as a base (Scheme 3.4).

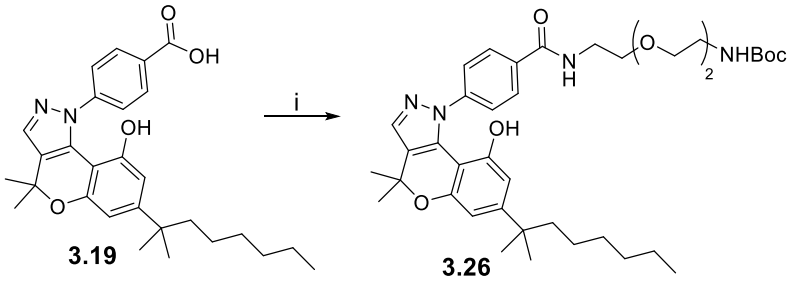

Scheme 3.4. (i) **2.12**, HATU, DIPEA, DMF, 60%.

3.2.1.3 Synthesis of *N*-(para-(4-carboxypropyl)phenyl)-chromenopyrazoles

Synthesis of this series began with reaction of commercially available **3.27** with sodium nitrite and hydrochloric acid to generate a diazo compound, which was reduced *in situ* with tin(II) chloride dihydrate to provide the hydrazine hydrochloride salt **3.28** (Scheme 3.5).

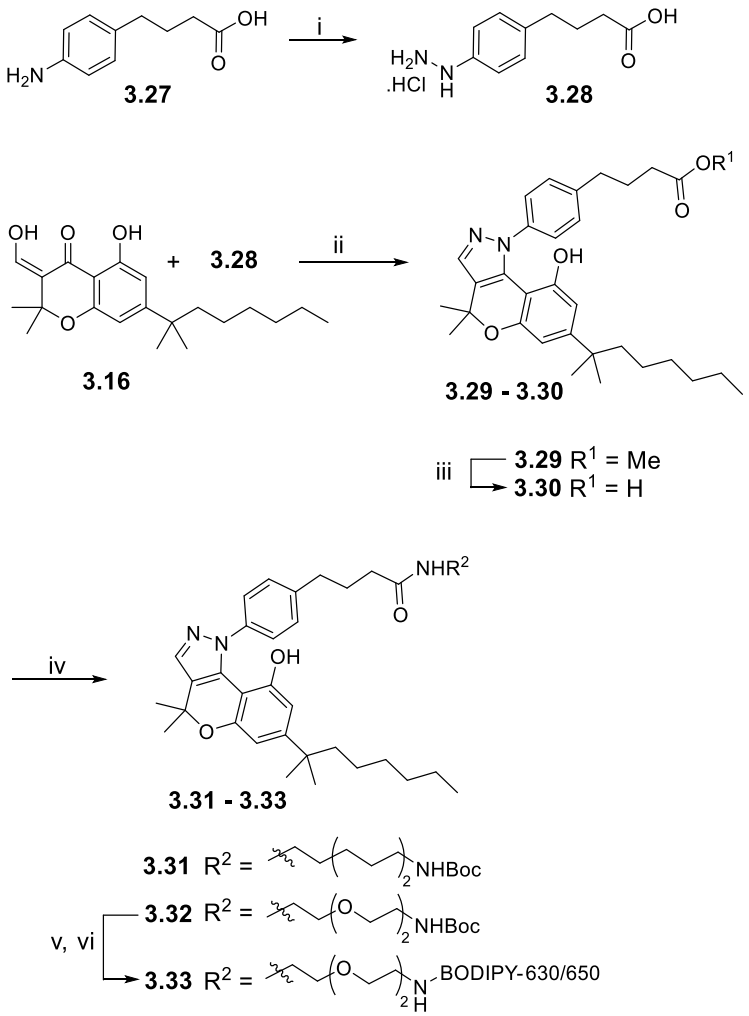

Scheme 3.5. (i) HCl aq., $NaNO_2$, $SnCl_2.2H_2O$, 120 °C to -5 °C to -20 °C, 50%. (ii) H_2SO_4, MeOH, 75 °C, 43%. (iii) LiOH, THF, H_2O, 91%. (iv) **2.10** or **2.12**, HBTU, DIPEA, DMF, 53-72%. (v) TFA, DCM, quantitative. (vi) BODIPY-630/650-SE, DIPEA, DMF, 88%.

Condensation of **3.28** with **3.16** using conditions optimised for the synthesis of **3.18** (Scheme 3.2) gave chromenopyrazole ester **3.29** as the *N*1 regioisomer, which on hydrolysis with aqueous LiOH provided carboxylic acid **3.30**. Reaction of **3.30** with mono-Boc-protected **2.10** or **2.12** (synthesis described in chapter 2, section 2.2.1) gave PEG or alkyl chromenopyrazole-linker conjugates **3.31** and **3.32** respectively. Boc-protected **3.32** was treated with TFA to give the Boc-deprotected **3.32**, which after semi-preparative RP-HPLC purification was reacted with BODIPY-630/650-SE to provide fluorescent ligand **3.33**.

Fmoc solid-phase peptide synthesis was used to synthesise peptide-linked **3.38**, which is an analogue of **3.31** and **3.32** (Scheme 3.5). Reaction of 1,2-diaminoethane trityl resin **3.34** with Fmoc-Ala-OH, HBTU and DIPEA gave resin-bound **3.35** (Scheme 3.6).

Coupling of Fmoc-Ala-OH with 1,2-diaminoethane trityl resin **3.34** was repeated to maximise resin loading. The resin was then capped by reacting any unreacted resin-primary-amine sites with Ac_2O in DMF. The amount of Fmoc-Ala bound to the resin was determined by an Fmoc loading test (details in chapter 7, section 7.3.1) and was found to be 0.78 mmol/g. Fmoc deprotection of resin-bound **3.35** with a solution of piperidine in DMF (20% *v*/*v*), followed by reaction with Fmoc-Ala-OH, HBTU and DIPEA gave resin-bound **3.36**. Resin-bound **3.36** was again subjected to Fmoc deprotection using a solution of piperidine in DMF (20% *v*/*v*) and then the free primary amine was coupled with carboxylic acid **3.30** (Scheme 3.5) using HATU and DIPEA to give resin bound **3.37**. Cleavage from the trityl resin was performed by treating resin-bound **3.37** with TFA. Peptide linker conjugate **3.38** thus obtained was purified using semi-preparative RP-HPLC and then reacted with acetic anhydride or BODIPY-630/650-SE in separate reactions to give **3.39** and **3.40** respectively.

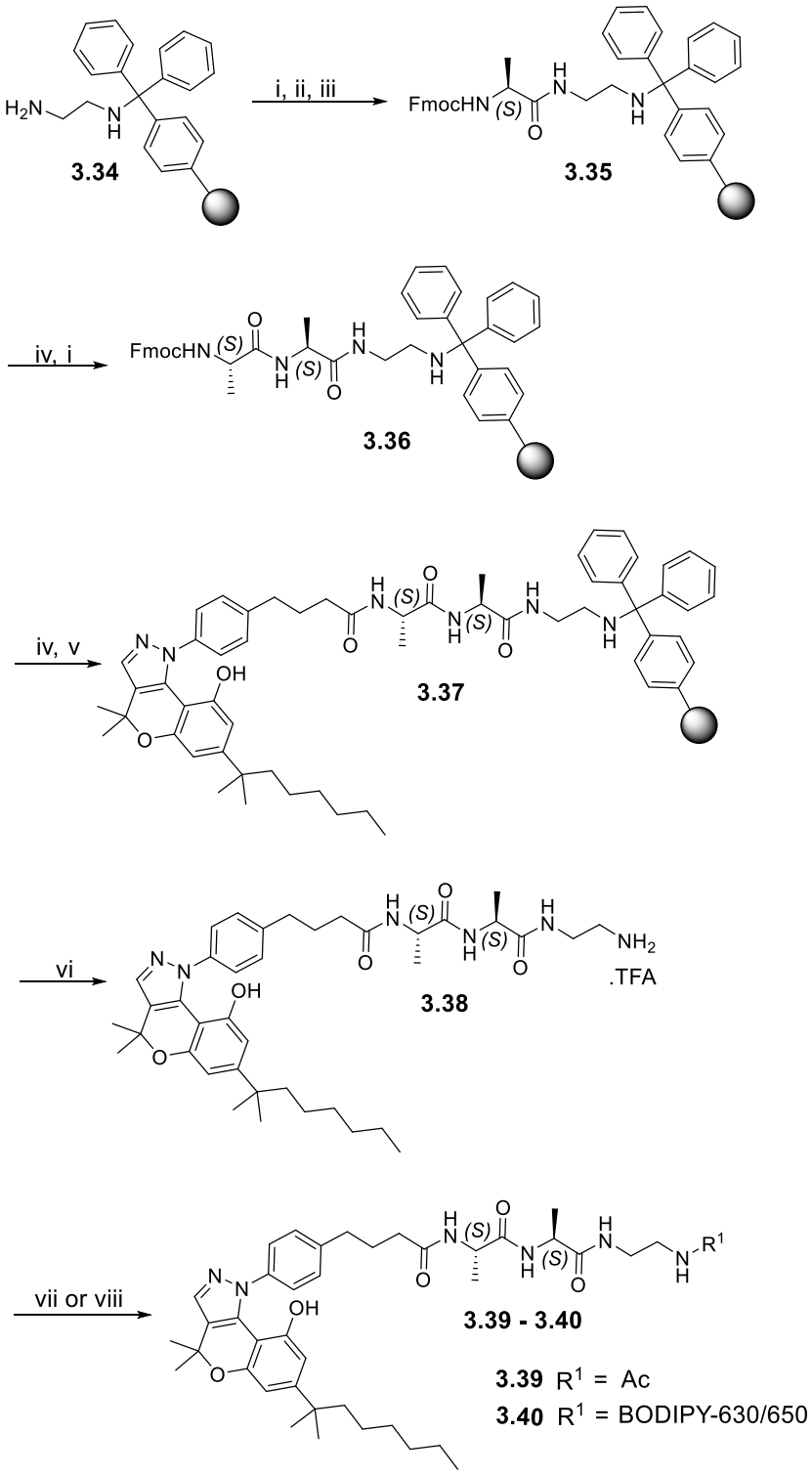

Scheme 3.6. (i) Fmoc-Ala-OH, HBTU, DIPEA, DMF. (ii) Fmoc-Ala-OH, HBTU, DIPEA, DMF (double coupling). (iii) Ac_2O, DIPEA DMF. (iv) Piperidine, DMF. (v) **3.30**, HATU, DIPEA, DMF. (vi) TFA, DCM. (vii) Ac_2O, Et_3N, DCM, 94%. (viii) BODIPY-630/650-SE, DIPEA, DMF, 49%.

3.2.1.4 Synthesis of *N*-(meta-(methylamine)phenyl)-chromeno-pyrazoles

Synthesis of this series of compounds, including **3.47** and fluorescent ligand **3.46** (Scheme 3.7), was carried out using similar methodology as described in section 3.2.1.1. Condensation of **3.16** with 3-hydrazinobenzoic acid hydrochloride provided **3.41** as the *N*1 regioisomer. Hydrolysis of **3.41** with aqueous LiOH gave carboxylic acid **3.42**, which was reacted with NH_4Cl to give benzamide **3.43**. Reduction of benzamide **3.43** with $LiAlH_4$ gave benzylamine **3.44** (compound not purified), which on coupling with carboxylic acid **3.13** gave chromenopyrazole **3.45**. Boc-deprotection of **3.45** with TFA, followed by reaction of the semi-preparative RP-HPLC purified amino trifluoroacetate salt with BODIPY-630/650-SE gave fluorescent ligand **3.46**. As observed for **3.21** (Scheme 3.3), acetylation of benzylamine **3.44** with Ac_2O gave a mixture of *N*,*O*-diacetylated product and *N*-acetylated product, which on alkaline hydrolysis with aqueous NaOH gave **3.47**.

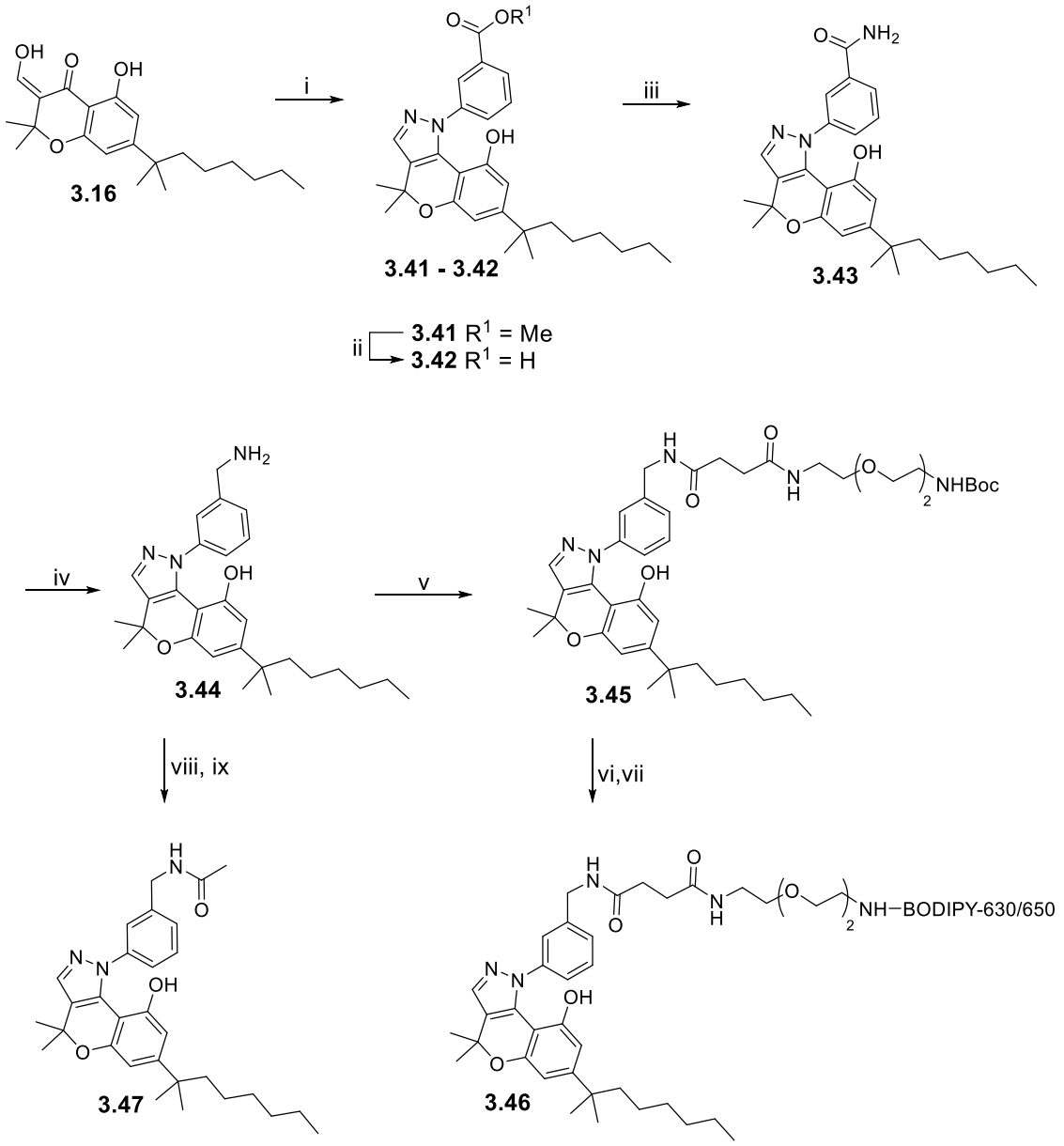

Scheme 3.7. (i) 3-Hydrazinobenzoic acid hydrochloride, H_2SO_4, MeOH, 75 °C, 49%. (ii) LiOH, THF:H_2O, 93%. (iii) NH_4Cl, HBTU, DIPEA, DMF, 78%. (iv) $LiAlH_4$, THF, 70 °C. (v) **3.13**, HBTU, DIPEA, DMF, 37%. (vi) TFA, DCM, quantitative. (vii) BODIPY-630/650-SE, DIPEA, DMF, 14%. (viii) Ac_2O, Et_3N, DCM. (ix) NaOH, MeOH, 36% over two steps.

3.2.1.5 Synthesis of *N*-(ortho-carboxyphenyl)-chromenopyrazoles

It was decided that only one compound (**3.48,** Scheme 3.8) would be made for this series and depending on the biological results, further **3.48**-linker conjugates could be prepared as a second generation of compounds. The *N*-(ortho-carboxyphenyl)-chromenopyrazole **3.48** was prepared by condensation of β-ketoaldehyde **3.16** with commercially available

2-hydrazinobenzoic acid. This reaction was carried out according to the optimised procedure for **3.18** (Scheme 3.2). As in the case of **3.18** (Scheme 3.2), chromenopyrazole **3.48** was obtained as an *N*1 regioisomer.

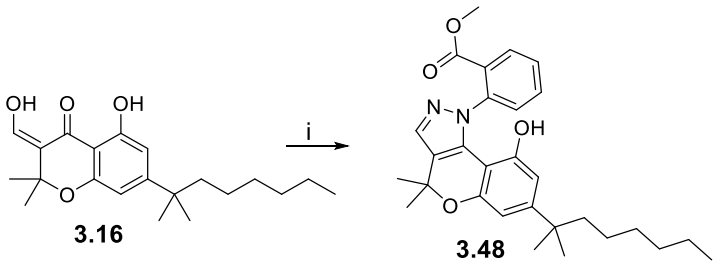

Scheme 3.8. (i) 2-Hydrazinobenzoic acid, H_2SO_4, MeOH, 75 °C, 41%.

3.2.1.6 Synthesis of 1-(2,4-dichlorophenyl)-4,4-dimethyl-7-(2-methyloctan-2-yl)-1,4-dihydrochromeno[4,3-c]pyrazol-9-ol (3.4)

Chromenopyrazole **3.4** is a high affinity chromenopyrazole CB_1R agonist previously reported in the literature by Cumella *et. al*.[137] Chromenopyrazole **3.4** was synthesised to use as a literature control in pharmacological experiments (section 3.3.1). It was synthesised by condensing **3.16** with commercially available (3,4-dichlorophenyl)hydrazine (Scheme 3.9) according to the procedure optimised for **3.18** (Scheme 3.2).

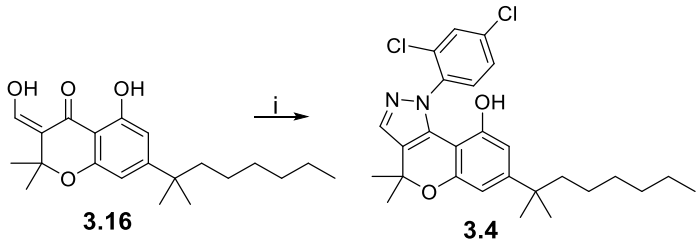

Scheme 3.9. (i) (3,4-Dichlorophenyl)hydrazine.HCl, MeOH, 75 °C, 72%.

3.2.2 Synthesis of *N- and O-* alkyl-chromenopyrazoles

3.2.2.1 Synthesis of *N*-(5-carboxypentyl)-chromenopyrazoles

Synthesis of these compounds began with preparation of hydrazine acid **3.50** (Scheme 3.10). Initially, Et_3N or $Ba(OH)_2.8H_2O$ were used as bases in the substitution reaction of bromo carboxylic acid **3.49** with hydrazine hydrochloride due to the ease of removal from the reaction mixture. However, the reaction was likely unsuccessful due to the weak basicity of Et_3N or low solubility of $Ba(OH)_2.8H_2O$ in water. Compound **3.50** was instead synthesised from reaction of **3.49** and hydrazine hydrochloride using NaOH as the base. Hydrazine acid **3.50** is an amphoteric compound with high water solubility and low solubility in non-polar solvents. Removal of excess hydrazine hydrochloride from crude **3.50** present in the reaction mixture proved difficult and attempts to use crude **3.50** contaminated with hydrazine hydrochloride in the condensation reaction with **3.16** resulted in the formation of **3.57** (condensation product of **3.16** and hydrazine, synthesis shown in Scheme 3.12) as the sole product. Finally, hydrazine was removed from crude **3.50** by repeated co-evaporation of the alkaline reaction mixture with water, acidification of the residual mixture to pH 2.0-3.0 and extraction of **3.50** with a mixture of EtOH:EtOAc (25% *v*/*v*).

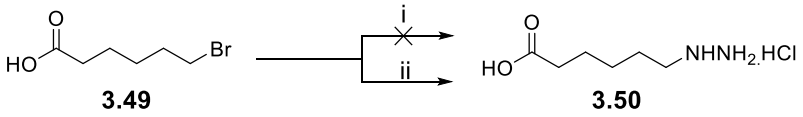

3.49 **3.50**

Scheme 3.10. (i) $NH_2NH_2.HCl$, Et_3N, dioxane, H_2O, 90 °C or $NH_2NH_2.HCl$, $Ba(OH)_2.8H_2O$, THF, H_2O, 90 °C. (ii) $NH_2NH_2.HCl$, NaOH, dioxane, water, 90 °C, HCl(aq.), 61%.

Condensation of hydrazine acid **3.50** with **3.16** provided hydrazine ester **3.51** (Scheme 3.11). Although a compound corresponding to molecular weight of **3.51** was the only major compound isolated, as discussed previously for **3.18** (section 3.2.1.1), it could be either the *N*1 or *N*2 regioisomer. Consequently, the structure of hydrazine ester **3.51** was investigated by 2D-NMR spectroscopy. gHMBC spectrum showed a correlation between H-17 and C-10 of **3.51** thus supporting that **3.51** was the *N*1 regioisomer (Figure 3.7). In addition, a gHMBC correlation was not observed between H-17 and C-13, which would have supported the structure of **3.51** as *N*2 regioisomer. The *N*2 regioisomer of **3.51** was also synthesised later (section 3.2.2.2).

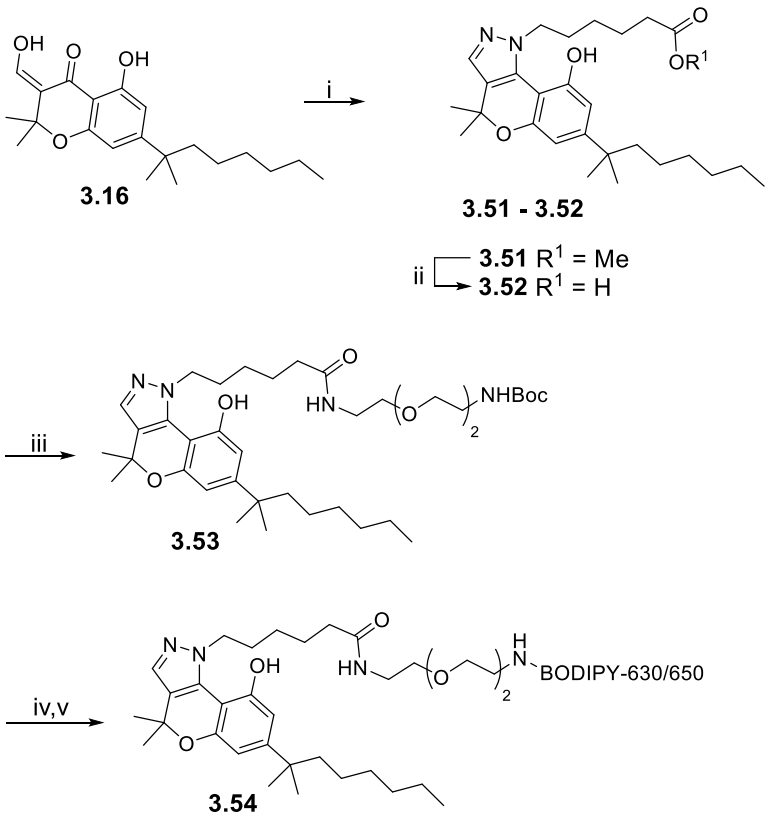

Scheme 3.11. (ii) **3.50**, H_2SO_4, MeOH, 75 °C, 42%. (ii) LiOH, THF:H_2O, 81%. (iii) **2.12**, HATU, DIPEA, DMF, 39%. (iv) TFA, DCM, quantitative. (v) BODIPY-630/650-SE, DIPEA, DMF, 37%.

Basic hydrolysis of hydrazine ester **3.51** with aq. LiOH provided carboxylic acid **3.52**. An amide coupling of **3.52** with **2.12** using HATU as coupling reagent yielded linker conjugate **3.53**. Boc-deprotection of **3.53** with TFA and coupling reaction of the resulting semi-preparative RP-HPLC purified amine trifluoroacetate salt with BODIPY-630/650-SE yielded fluorescent ligand **3.54**.

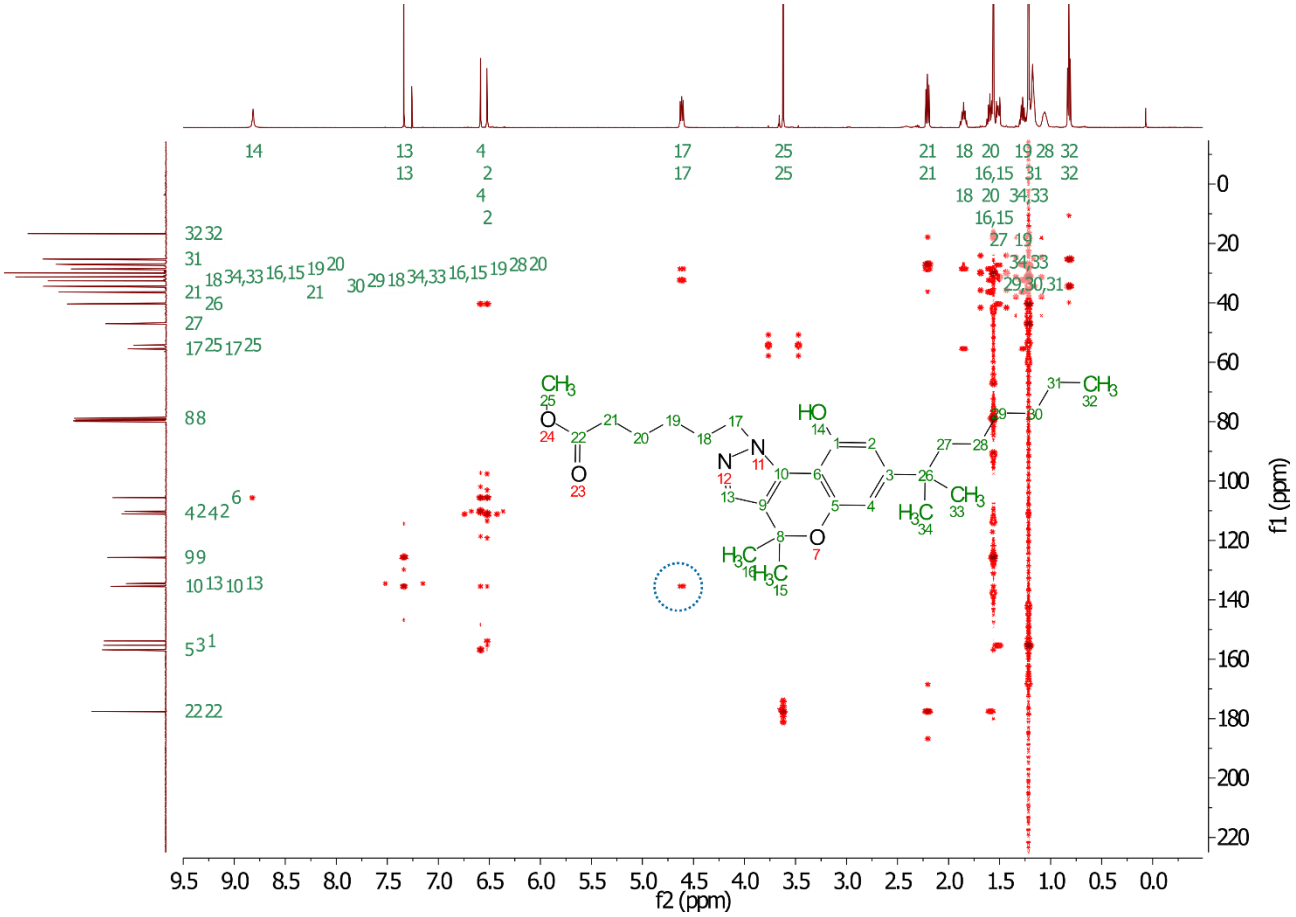

Figure 3.7. Evidence of *N*1-alkylation alkyl product **3.51** - gHMBC spectrum of **3.51** in $CDCl_3$, correlation between H-17 and C-10 is circled.

3.2.2.2 Synthesis of *O*-(5-carboxypentyl)-chromenopyrazoles

It was planned that alkylation of the aromatic hydroxyl of **3.57** (Scheme 3.12) with bromo ester **3.56** would provide *O*-alkyl-chromenopyrazoles **3.58**. It was decided to initially just synthesise and test *O*-linked chromenopyrazole **3.58** and depending on the biological data a fluorescent derivative could then be made. Some issues of chemoselectivity were expected from this strategy as chromenopyrazole **3.57** can undergo either *N*- or *O*-alkylation by substitution of bromide or react with the ester of **3.56.** Nevertheless, alkylated products can be easily identified from ester reacted products by MS owing to different molecular masses.

Bromo ester linker **3.56** was prepared by esterification of commercially available **3.55**. Condensation of **3.16** with hydrazine hydrochloride gave chromenopyrazole **3.57**. An initial attempt to alkylate **3.57** with linker **3.56** using NaH as a base proved fruitless as thin-layer chromatography (TLC) and MS indicated the presence of mostly unreacted **3.57** along with formation of a small amount of new compound with molecular mass corresponding to hydrolysed esters of **3.58** or **3.59**. This is most likely due to basic hydrolysis of **3.58** or **3.59** by reaction with NaOH, formed by reaction of NaH with trace moisture or during the aq. work up.

Next, alkylation of **3.57** with methyl 6-bromohexanoate **3.56** using caesium carbonate was attempted. TLC analysis of the reaction mixture showed formation of a higher TLC retention factor (R_f) spot and a lower TLC R_f spot compared to TLC R_f of starting material **3.16**. Column purification to isolate each spot, followed by MS indicated both compounds possessed a mass corresponding to an alkylated product. NMR experiments were carried out to determine the structure of these compounds, which indicated the higher TLC R_f compound to be *N*2-alkylated **3.59** and the lower TLC R_f compound to be *O*-alkylated **3.58**. This conclusion was based on the gHMBC correlation of H-17 and C-13 of *N*2-alkylated **3.59** (Figure 3.8), versus the gHMBC correlation between H-17 and C-1 in case of O-alkylated **3.58** (Figure 3.9).

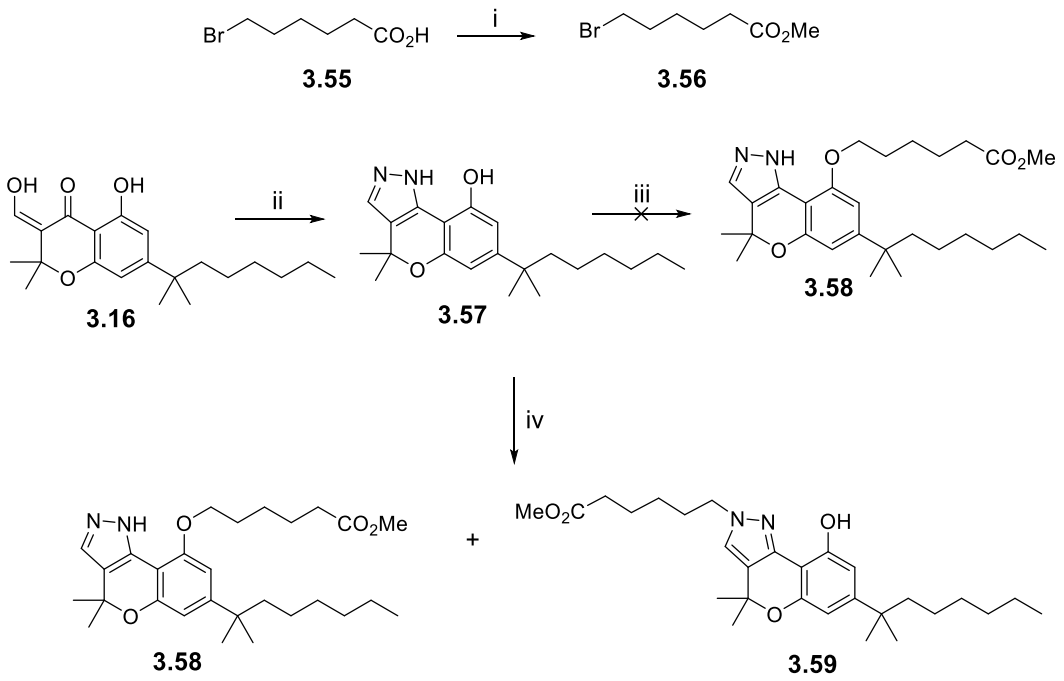

Scheme 3.12. (i) H_2SO_4, MeOH, 70 °C, 63%. (ii) NH_2NH_2.HCl, H_2SO_4, MeOH, 75 °C, 83%. (iii) **3.56**, NaH, THF, 70 °C. (iv) **3.56**, Cs_2CO_3, THF, 75 °C, 40% for **3.59** and 50% for **3.58**.

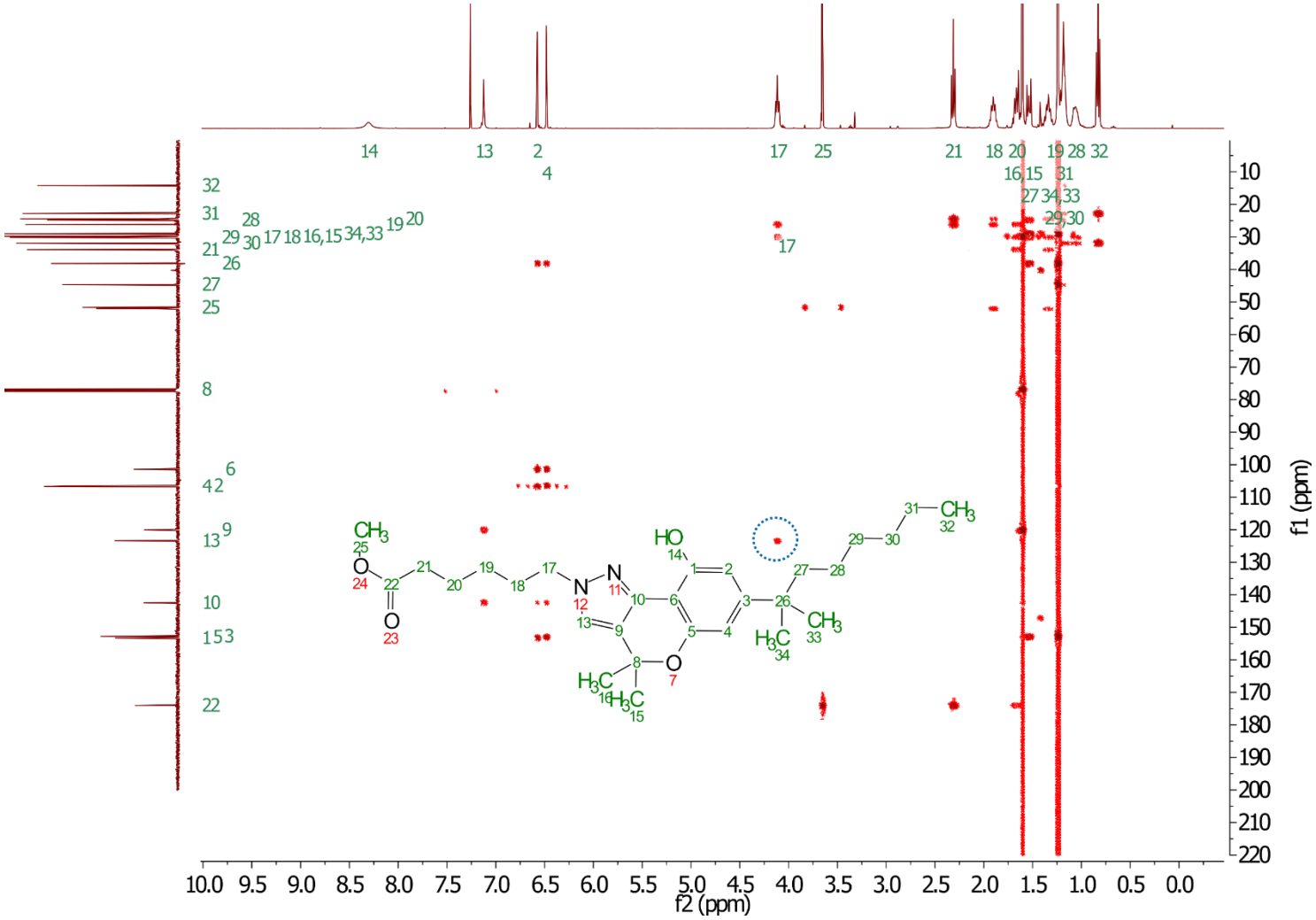

Figure 3.8. Evidence for *N*- alkylation. gHMBC spectrum of **3.59**, correlation between H-17and C-13 circled.

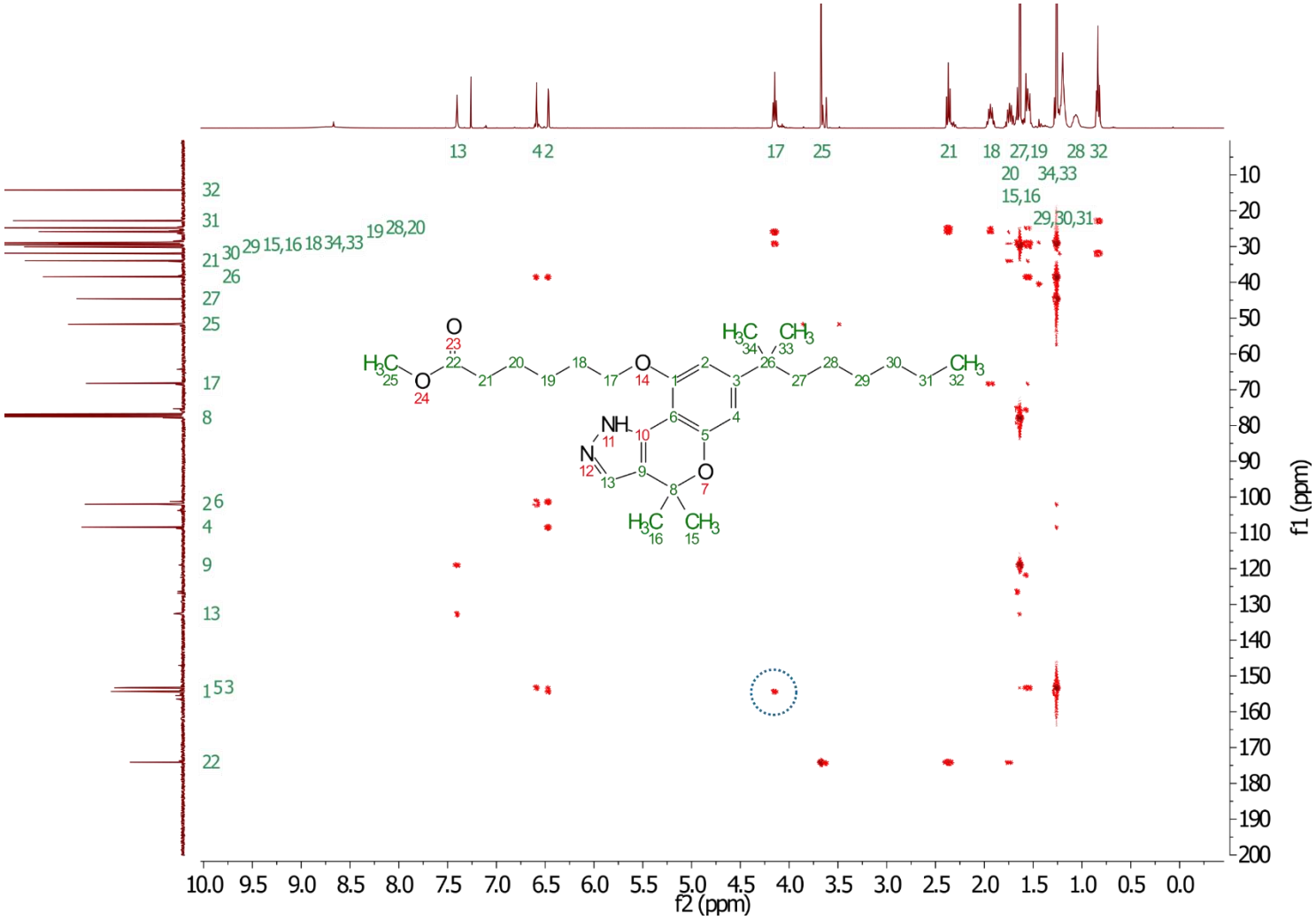

Figure 3.9. Evidence for *O*- alkylation gHMBC spectrum of **3.58**, correlation between H-17 and C-1 is circled.

3.2.2.3 Attempted synthesis of (C-3)-(6-aminohexyl)-chromenopyrazoles

It was envisaged that α-acylation of ketone **3.15** with an acylating reagent (for example Weinreb amide **3.62**) would provide diketone chromenopyrazole **3.63**, which could be reacted with hydrazine to provide (C-3)-(6-aminohexyl)-chromenopyrazole **3.64** (Scheme 3.13). Although the aromatic hydroxyl of **3.15** might react with acylating agents, previously successful formylation of **3.15** despite an unprotected hydroxyl (Scheme 3.2) indicated that acylation without protecting the hydroxyl of **3.15** might be possible.

Hence, Boc-protection of amino heptanoic acid **3.60** gave **3.61**, which was reacted with *N*,*O*-dimethylhydroxylamine hydrochloride using HBTU to provide the Weinreb amide **3.62** (Scheme 3.13). Attempts to acylate **3.15** with **3.62** using NaH or *n*-BuLi as the base were unsuccessful and starting compound **3.15** was recovered. It was thought that failure of this reaction might be due to low reactivity of Weinreb amide **3.62**. Therefore, alternate acylating reagent succinimidyl ester **3.65** was prepared by reaction of **3.61** with *N*-hydroxysuccinimide. Unfortunately, acylation of **3.15** with **3.65** using NaH or *n*-BuLi as base didn't succeed either and starting compound **3.15** was recovered. Another alternative acylating reagent was synthesised by reaction of **3.61** with TFFH and Et_3N to provide the in situ generated acid fluoride of **3.61** (not shown in Scheme 3.13), which was neither purified nor characterized by spectroscopic techniques. However, reaction of **3.15** with the acid fluoride of **3.61** using NaH as base (not shown in Scheme 3.13) provided a new compound which was determined by ^{1}H NMR spectroscopy and MS to be a compound other than the desired product **3.63**. The structure of this new compound could not be determined. Failure of the acylation reaction of **3.15** with **3.62**, **3.65**, and the acid fluoride of **3.61** might be due to the low electrophilicity of the acylating reagents, or due to side reactions of these acylating reagents with the hydroxyl of **3.15** or with the bases employed. *O*-Protection of **3.15** (for example by a benzyl group) might be more successful in these acylation reactions, however this was not carried out.

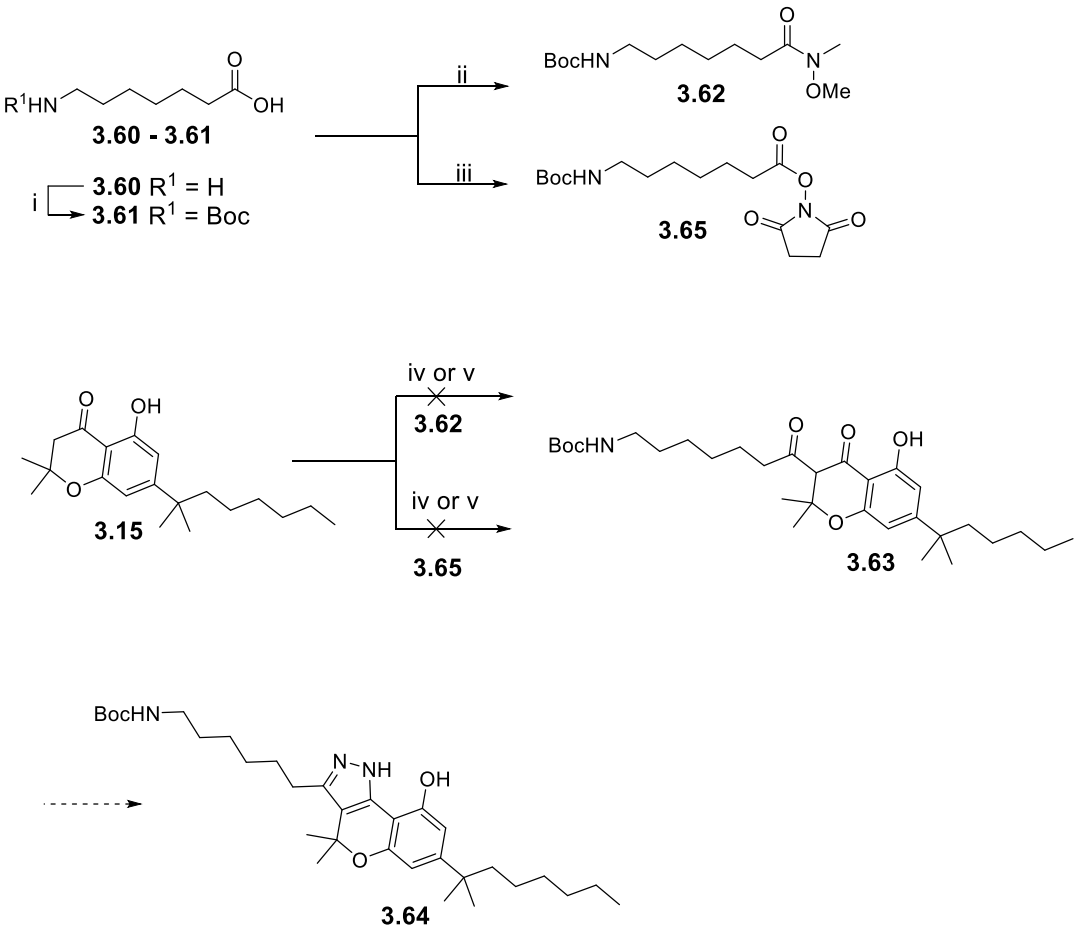

Scheme 3.13. (i) $(Boc)_2O$, NaOH, Dioxane, water, 98%. (ii) *N,O*-Dimethylhydroxylamine hydrochloride, HBTU, DIPEA, THF, 85%. (iii) *N*-Hydroxysuccinimide, HBTU, DIPEA, DMF, 91%. (iv) NaH, THF, 60 °C (v) *n*-BuLi, THF, -78 °C.

Another approach to synthesise C-3-linker-chromenopyrazoles could involve coupling of linkers with a 3-amino-chromenopyrazole (likely obtainable by reaction of α-cyano derivative of ketone **3.15** with hydrazine; a similar method was reported for the synthesis of some aminothiazoles[211]). However, based on the biological results of newly synthesised chromenopyrazoles (section 3.3.1), synthesis of this series of compounds was not further pursued.

3.3 Biological studies

3.3.1 Radioligand binding assays

Due to the time constraint of being able to visit the collaborator's laboratory for only a few weeks over summer, it was decided to evaluate a planned subset of the chromenopyrazoles described in section 3.2 for determining the binding affinity and functional activity at CBRs. Selection of these chromenopyrazoles was done with the aim of obtaining meaningful SAR data which could be used in the design of a second generation of high affinity chromenopyrazoles.

A commonly used CBR radioligand, [^{3}H]-CP55,940 (described in chapter 1, section 1.2.1), was used to determine the affinity of synthesised chromenopyrazoles at membrane preparations derived from HEK-293 cells transfected with either CB_1R or CB_2R according to a previously described method.[169, 212] An initial screen of chromenopyrazoles (**3.4**, **3.18**, **3.19**, **3.22**, **3.23**, **3.25**, **3.26**, **3.29**, **3.31**, **3.32**, **3.33**, **3.39**, **3.40**, **3.41**, **3.45**, **3.46**, **3.47**, **3.48**, **3.51**, **3.53**, **3.54**, **3.58** and **3.59**) at 10 µM was carried out to determine the percentage displacement of [^{3}H]-CP55,940 from CBRs (Figure 3.10, panels A and B) in a competition radioligand binding assay. Compounds that displaced [^{3}H]-CP55,940 from both CBRs by more than 50% at a 10 µM concentration were then analysed in a concentration-dependent way to determine concentration response curves and calculate binding affinity (K_i). When there was no significant difference between displacement of [^{3}H]-CP55,940 by a test compound (at concentration of 10 µM) compared to vehicle, a compound K_i was reported as no binding (Table 3.2, Figure 3.10, panel A and B). Some compounds exhibiting weak affinity for CBRs were reported as having K_i >5000 nM, which was calculated as described in the following paragraph.

The radioligand [^{3}H]-CP55,940 with a K_d (equilibrium dissociation constant) of 3 nM at CB_1R was used at 2.5 nM concentration in the radioligand assay carried out for CB_1R. The K_i of the test compounds (with IC_{50} of 10 µM for the compounds displacing 50% of total [^{3}H]-CP55,940 at CB_1R at 10 µM) was calculated according to the Cheng–Prusoff equation:

$$K_i = \frac{IC_{50}}{1 + [\text{radioligand concentration}]/K_d} = \frac{10}{1 + [2.5]/3} = 5.45\ \mu M$$

So, for the test compounds which displaced less than 50% of total [^{3}H]-CP55,940 at 10 µM at CB_1R, K_i was reported as >5000 nM (K_i value rounded off to account for the experimental errors) (Table 3.2). Similarly, for the test compounds which displaced less than 50% of total [^{3}H]-CP55,940 at 10 µM at CB_2R, K_i was reported as >5000 nM (calculated for [^{3}H]-CP55,940 used at a concentration of 1 nM and with K_d of 1.7 nM for CB_2R).

It was unexpected that the high reported affinity of CB_1R selective literature compound **3.4** (K_i = 5.2 ± 6 nM at hCB_1R; >40000 nM at hCB_2R)[137] could not be reproduced in this study (Table 3.2, last entry). In this PhD thesis, **3.4** (K_i = 499.9 ± 40 nM at hCB_1R; 162.5 ± 68 nM at hCB_2R) exhibited higher affinity for CB_2R over CB_1R. As membrane preparations obtained from HEK-293 cells expressing CB_1R or CB_2R and [^{3}H]-CP55,940 was used as radioligand both in this thesis and by Cumella *et al.*[137], the reason for this difference in the binding affinity of **3.4** is not known.

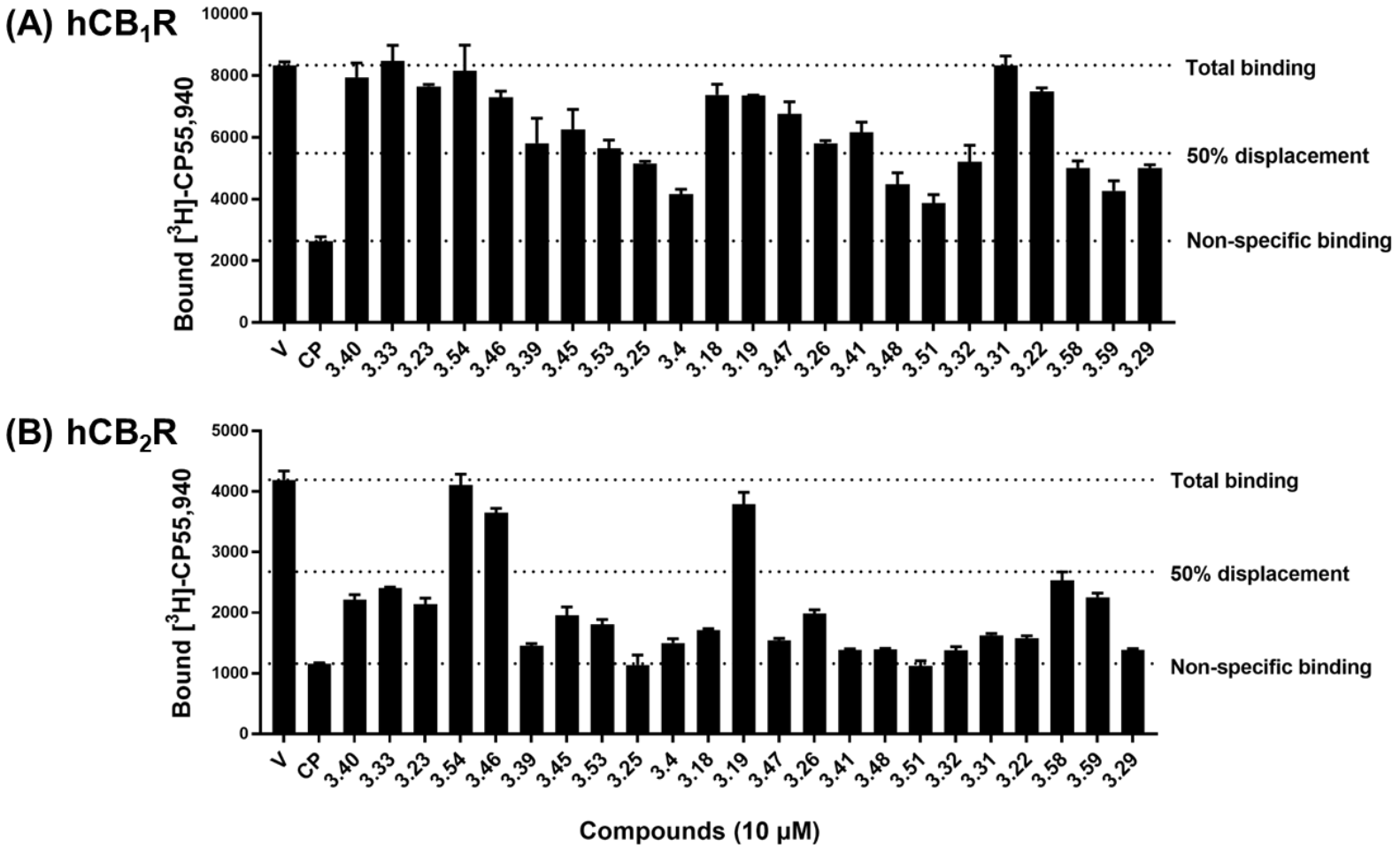

Figure 3.10. Radioligand binding assay: Screen of synthesised chromenopyrazoles at 10 μM at HEK-293 cells expressing hCB_1R (panel **A**) or hCB_2R (panel **B**), with [^{3}H]-CP55,940 as the radioligand. Data represented is from a single experiment carried out in triplicate and is expressed as mean ± SEM. V (vehicle), CP (CP55,940).

Table 3.2. Radioligand binding affinity data for synthesised chromenopyrazoles

Compound	Structure		hCB_1R K_i (nM ± SEM)*	hCB_2R K_i (nM ± SEM)*	hCB_2R selectivity
3.25	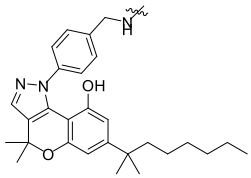		> 1000	13.2 ± 3.4	>75
3.22		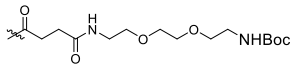	> 5000	71.1 ± 6.7	>70
3.23		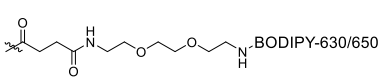	> 5000	2312 ± 298	-
3.29	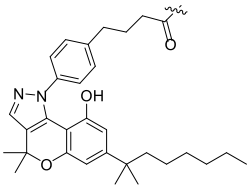		2220 ± 316[a]	251.5 ± 21	8
3.31		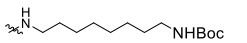	> 5000	148.9 ± 15.5	>33
3.32		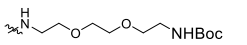	3716 ± 1202	104.6 ± 39.9	35
3.33		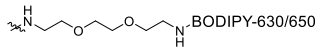	No binding	3996 ± 612	-
3.39		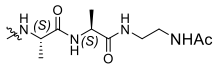	> 5000	138.4 ± 6.75	>36
3.40		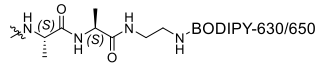	No binding	2693 ± 302	-
3.47	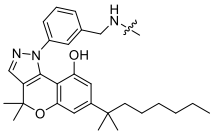		> 5000	397.3 ± 40.5	>12
3.45		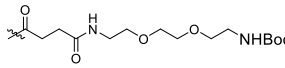	> 5000	1277 ± 94.3	>4
3.46		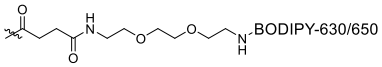	> 5000	> 5000	-
3.51	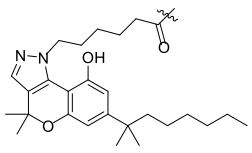		964 ± 372	101 ± 13	9
3.53		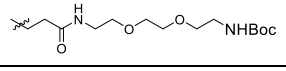	> 5000	1291 ± 303.6	>3
3.54		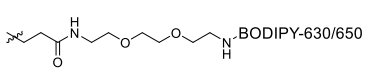	No binding	No binding	-

Table 3.2 continued

Compound	Structure	hCB_1R K_i (nM ± SEM)*	hCB_2R K_i (nM ± SEM)*	hCB_2R selectivity
3.26	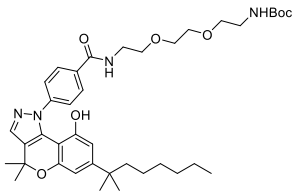	> 5000	1434 ± 370.2	>3
3.59	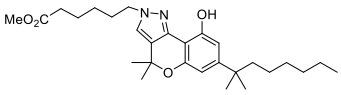	4200 ± 594	1016 ± 173	4
3.58	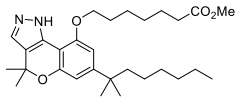	1371 ± 309	2031 ± 582	0.6
3.18	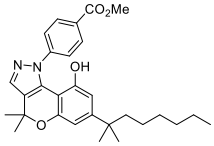	> 5000	435.6 ± 63.1	>11
3.19	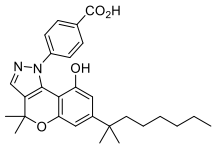	> 5000	> 5000	-
3.41	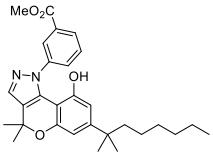	> 5000	274.5 ± 42.7	>18
3.48	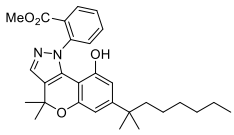	2343 ± 906	304.5 ± 44.8	7
3.4	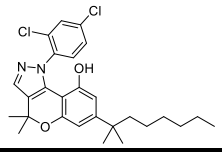	499 ± 40	162.5 ± 68	3

*Binding affinity (K_i) obtained by competition binding assay performed on membranes obtained from HEK-293 cells expressing either hCB_2R or hCB_1R with [^{3}H]-CP55,940 (K_d = 1.7 nM for hCB_2R and 3.0 nM for hCB_1R). All data is from at least three individual experiments performed in triplicate, except [a] which is two individual experiments performed in triplicate.

3.3.2 SAR discussion of cannabinoid type 2 receptor binding affinity data of chromenopyrazoles

None of the chromenopyrazoles other than the literature chromenopyrazole **3.4** (K_i = 499 ± 40 nM at hCB_1R) tested in this chapter exhibited appreciable affinity for CB_1R (Table 3.2). Widely used CBR ligand CP55,940 (K_i = 4.53 ± 0.22 nM at hCB_1R; K_i = 1.66 ± 0.31 nM at hCB_2R) was used as a positive control in this study. CP55,940 exhibited affinity for CBR in agreement with a recent literature report (pK_i = 9.26 ± 0.12 nM at hCB_1R, (K_i = 0.55 nM)) and (pK_i = 8.44 ± 0.18 nM at hCB_2R (K_i = 3.63 nM)).[119] As the majority of these chromenopyrazoles revealed high affinity and selectivity for CB_2R over CB_1R, the following SAR discussion will primarily be derived from the comparison of the CB_2R affinities.

N-(para-(Methylamine)phenyl)-chromenopyrazole **3.25** (K_i = 13.2 ± 3.4 nM at hCB_2R; > 1000 nM at hCB_1R) exhibited the highest affinity and selectivity for CB_2R over CB_1R among all the tested chromenopyrazoles (Table 3.2; competition binding curve for **3.25** shown in Figure 3.11). The analogue of **3.25** with a PEG linker, **3.22** (K_i = 71.1 ± 6.7 nM at hCB_2R; >5000 nM at hCB_1R; competition binding curve for **3.22** shown in Figure 3.11) exhibited the highest affinity and selectivity (CB_2R:CB_1R selectivity of 70) for CB_2R among the chromenopyrazole-linker conjugates tested in this chapter. This tolerance of the long PEG linker in **3.22** was an exciting result and provided a promising lead compound to prepare high affinity CB_2R fluorescent ligands. However disappointingly, the BODIPY-630/650 analogue **3.23** (K_i = 2312 ± 298 nM at hCB_2R) provided only a moderate affinity fluorescent ligand, which showed approximately 32-fold reduced CB_2R binding affinity compared to **3.22**. Although the reasons for this reduction in the CB_2R binding affinity are not known, it is likely due to the steric clashes of the bulky BODIPY-630/650 of **3.23** with the CB_2R amino acid residues. The fluorescent ligand **3.23** did not exhibit any significant binding at CB_1R.

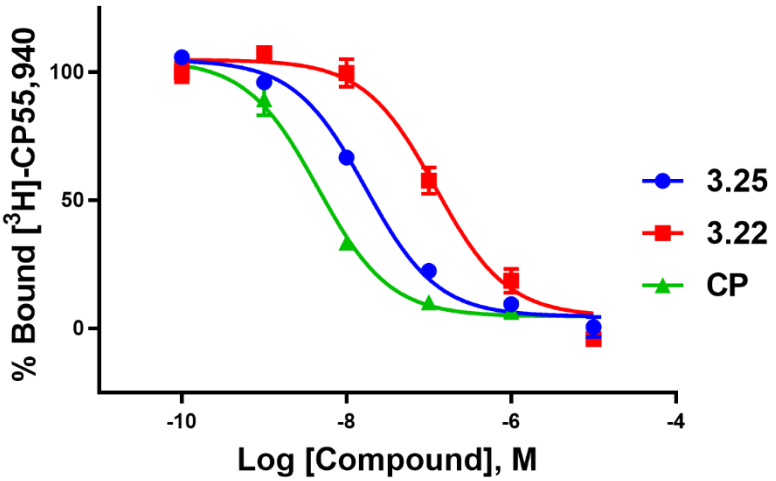

Figure 3.11. Competition binding curves for the highest affinity CB_2R chromenopyrazole **3.25**, the highest affinity CB_2R chromenopyrazole-linker conjugate **3.22** and CP (CP55,940) using radioligand [^{3}H]-CP55,940 (K_d = 1.7 nM for hCB_2R) at HEK-293 cells expressing hCB_2R. Data represented is from a single experiment carried in triplicate and is expressed as mean ± SEM.

N-(para-(4-Carboxypropyl)phenyl)-chromenopyrazole **3.29** (K_i = 251.5 ± 21 nM at hCB_2R; 2220 ± 316 nM at hCB_1R) exhibited high affinity for CB_2R and moderate affinity for CB_1R. The three different linker (alkyl, PEG and Ala-Ala peptide) conjugates of **3.29** provided high affinity and selective CB_2R ligands **3.31** (K_i = 148.9 ± 15.5 nM at hCB_2R; >5000 nM at hCB_1R), **3.32** (K_i = 104.6 ± 39.9 nM at hCB_2R; 3716 ± 1202 nM at hCB_1R) and **3.39** (K_i = 138.4 ± 6.75 nM at hCB_2R; >5000 nM at hCB_1R) respectively. Remarkably, **3.31**, **3.32** and **3.39** contain three different types of linkers but still exhibited similar high affinities at CB_2R. Although the specific reasons for this similar high affinity for CB_2R of the **3.29**-linker conjugates (**3.31**, **3.32** and **3.39**) are not known, it might be due to the presence of the long linkers extended from **3.29** in the extracellular space, out of the ligand-binding pocket of CB_2R (refer to section 3.4 for computational studies). The high affinities at CB_2R of **3.29**-linker conjugates (**3.31**, **3.32** and **3.39**) and the tolerance of the linker to change make these ligands highly promising leads for developing the CB_2R fluorescent ligands. The BODIPY-630/650 conjugates of **3.39** and **3.32** gave moderate affinity fluorescent ligands **3.40** (K_i = 2693 ± 302 nM at hCB_2R) and **3.33** (K_i = 3996 ± 612 nM at hCB_2R) respectively. Similar to **3.23**, decreased binding affinity of **3.39** and **3.32** is likely due to steric clashes of BODIPY-630/650 with CB_2R amino acid residues. Fluorescent ligands **3.40** and **3.33** did not exhibit any significant binding at CB_1R.

N-(meta-(Methylamine)phenyl)-chromenopyrazole **3.47** (K_i = 397.3 ± 40.5 nM at hCB_2R) exhibited moderate to high affinity for CB_2R. Extension of PEG linker from **3.47** provided **3.45** (K_i = 1277 ± 94.3 nM at hCB_2R), a moderate affinity CB_2R ligand with three times reduced CB_2R affinity compared to **3.47**. This decrease in CB_2R affinity upon attachment of PEG linker to parent chromenopyrazole was also observed in case of **3.22**. Fluorescent ligand **3.46**, a BODIPY-630/650 conjugate of **3.45**, did not exhibit any significant binding at either CBR.

*N*1-Alkyl-chromenopyrazole **3.51** (K_i = 101 ± 13 nM at hCB_2R; 964 ± 372 nM at hCB_1R) exhibited high affinity for CB_2R and moderate affinity for CB_1R. The **3.51** PEG linker conjugate **3.53** (K_i = 1291 ± 303.6 nM at hCB_2R) exhibited reduced binding affinity for CB_2R by approximately 12-fold compared to **3.51**. This decrease in CB_2R affinity upon attachment of long linker was also observed in case of **3.22** and **3.45**. The **3.53** BODIPY-630/650 conjugate **3.54** did not exhibit any significant binding at CBRs likely due to steric clashes of BODIPY-630/650 with CB_2R amino acid residues in line with other fluorescent ligand trends.

N-(para-Carboxyphenyl)-chromenopyrazole **3.26** (K_i = 1434 ± 370.2 nM at hCB_2R) showed moderate affinity for CB_2R, which was 20-fold less than the binding affinity of the highest overall chromenopyrazole-linker conjugate **3.22**. Reasons for this difference could be that the linker of **3.26** is bonded to the chromenopyrazole pharmacophore by a sp^2 carbon atom whereas **3.22** contains a sp^3 carbon atom linking directly to the pharmacophore. This difference in attachment by different carbon types provides a higher flexibility to the attached linker in case of **3.22** compared to **3.26**. Another difference is the linker length and chemical functionality – the PEG linker of **3.26** is five atoms shorter and contains one less amide functional group than **3.22**. These differences provide a longer linker and additional hydrogen bonding atoms in case of **3.22** which might also be responsible for the higher binding affinity of **3.22** compared to **3.26**.

*N*2-Alkyl-chromenopyrazole **3.59** (K_i = 1016 ± 173 nM at hCB_2R) exhibited 10-fold reduced affinity for CB_2R compared to *N*1-alkyl-chromenopyrazole **3.51** (K_i = 101 ± 13 nM at hCB_2R). Reasons for this difference in the CB_2R affinity is not known but might be due to the steric clashes of linker attached in **3.59** with the CB_2R amino acid residues. *O*-Alkyl chromenopyrazole **3.58** (K_i = 1371 ± 309 nM at hCB_1R; 2031 ± 582 nM at

hCB$_2$R) displayed moderate affinity for CB$_1$R and CB$_2$R. Although *N*- and *O*- alkyl chromenopyrazole–linker conjugates (such as **3.2**, **3.5**, **3.9**, and **3.10**; Table 3.1) with short linkers have been reported in literature,[137, 205] none of the reported compounds contain linkers of six atoms or longer as described in this chapter. These CB$_2$R affinity data indicated that *N*- and *O*- alkyl chromenopyrazole–linker conjugates are not suitable leads for developing CB$_2$R fluorescent ligands.

Among the *N*-(methoxycarbonylphenyl)-chromenopyrazoles (**3.18**, **3.41** and **3.48**), **3.41** (K_i = 274.5 ± 42.7 nM at hCB$_2$R) exhibited the highest affinity for CB$_2$R, and none of the three compounds exhibited high affinity for CB$_1$R. Chromenopyrazole **3.19**, a carboxylic acid derivative of **3.18**, did not exhibit any significant binding at CB$_1$R or CB$_2$R. Chromenopyrazole **3.19** would exist predominantly in an ionised form (RCO_2^-) at physiological pH and thus this charge would likely disrupt binding at the lipophilic binding pocket of CBRs, which might explain low affinity of **3.19** compared to **3.18**.

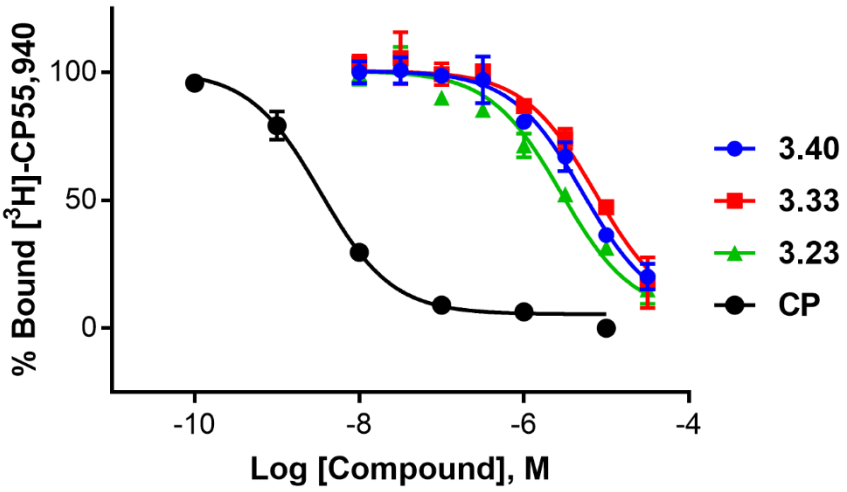

Figure 3.12. Competition binding curve for fluorescent ligands **3.40**, **3.33**, **3.23**, and literature CBR agonist CP (CP55,940) using [^{3}H]-CP55,940 (K_d = 1.7 nM for hCB$_2$R) at HEK-293 cells expressing hCB$_2$R. Data represented is from a single experiment carried in triplicate and is expressed as mean ± SEM.

Chromenopyrazole **3.51** showed the highest affinity for CB$_1$R whereas **3.25** exhibited highest affinity for CB$_2$R among all the novel chromenopyrazoles synthesised. None of the fluorescent ligands synthesised by conjugation of chromenopyraozle-linker-conjugates with BODIPY-630/650 exhibited any significant binding at CB$_1$R however

3.23, **3.33**, and **3.40** exhibited moderate affinity for CB_2R (Figure 3.12). Among the moderate affinity fluorescent ligands, **3.23**, a **3.22**-BODIPY-630/650 conjugate displayed the highest affinity (although still only moderate).

Comparison of **3.25** with **3.18**, **3.22** with **3.26** and **3.47** with **3.41** indicated that atoms near the pyrazole-*N*-phenyl substituent play an essential role in determining the binding affinity of the ligand. Among the *N*-(methoxycarbonylphenyl)-chromenopyrazoles, meta-substituted **3.41** displayed higher binding affinity than para-substituted **3.18**. Notwithstanding this result, the binding affinity comparison of **3.25** with **3.47**, **3.22** with **3.45** and **3.23** with **3.46** showed that the *N*-(para-(methylamine)phenyl)-chromenopyrazole series exhibited greater tolerance to bulky substituents than *N*-(meta-(methylamine)phenyl)-chromenopyrazole series at CB_2R binding site.

3.3.3 cAMP Functional assays

Due to the time constraints as mentioned previously, the functional activity of only selected high affinity CB_2R *N*-phenyl-chromenopyrazoles (**3.22**, **3.25**, **3.29**, **3.31**, **3.39**, and **3.47**) that exhibited robust tolerance of substituents/linkers was determined. Functional activity of these chromenopyrazoles was determined by a cAMP BRET assay[169] (described in chapter 1, section 1.5.2). Despite the fact that these chromenopyrazoles were designed as CB_1R agonists, their functional nature at CB_1R was not determined due to their poor binding affinity for CB_1R.

As described in chapter 1 (section 1.5.2), CBR agonists decrease the 'inverse BRET ratio' (obtained from cAMP BRET assay), inverse agonists increase it and neutral antagonists don't produce a change. For example, the high affinity CB_2R chromenopyrazole **3.25** behaved as an agonist at CB_2R since in the initial screen at 10 µM, **3.25** decreased the inverse BRET ratio compared to forskolin alone (Figure 3.13). The literature CBR agonist CP55,940 was used as a positive control in the 10 µM screen and also decreased the inverse BRET ratio compared to forskolin alone (Figure 3.13). None of the chromenopyrazoles tested in the cAMP assay in this chapter showed any activity at 10 µM concentration in the cAMP BRET assay at WT HEK-293 cells and thus did not

exhibit CB_2R independent effects on cAMP levels (Table 3.4; Figure 3.14 shows cAMP screen of the highest affinity chromenopyrazole **3.25** at WT HEK-293 cells).

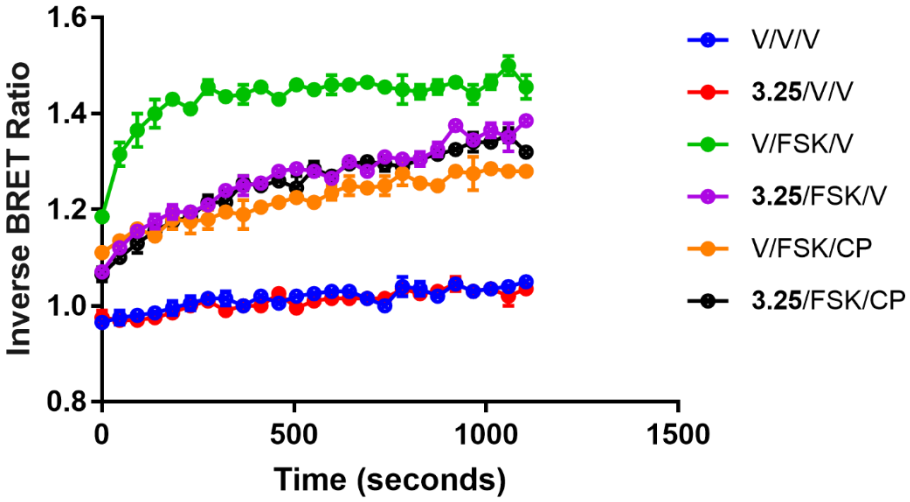

Figure 3.13. The highest CB_2R binding affinity chromenopyrazole **3.25** (10 µM) screened in a cAMP BRET assay using HEK-293 cells expressing hCB_2R. Data is representative of a single experiment carried in duplicate and is expressed as mean ± SEM. Literature agonist CP (CP55, 940), FSK (Forskolin), V (vehicle).

Area under the curve analysis was used to calculate the potency (EC_{50}) and efficacy (E_{max}) of the chromenopyrazoles (Table 3.3) from raw cAMP functional assay data. Literature control CP55, 940 (EC_{50} = 1.7 ± 0.23 nM at hCB_2R; E_{max} = 43 ± 0.75 % of forskolin response at hCB_2R) exhibited potency and efficacy in agreement with those reported in a recent literature report (EC_{50} = 5.6 ± 2.3 nM; E_{max} = 41 ± 1.4 % of forskolin response at hCB_2R).[155]

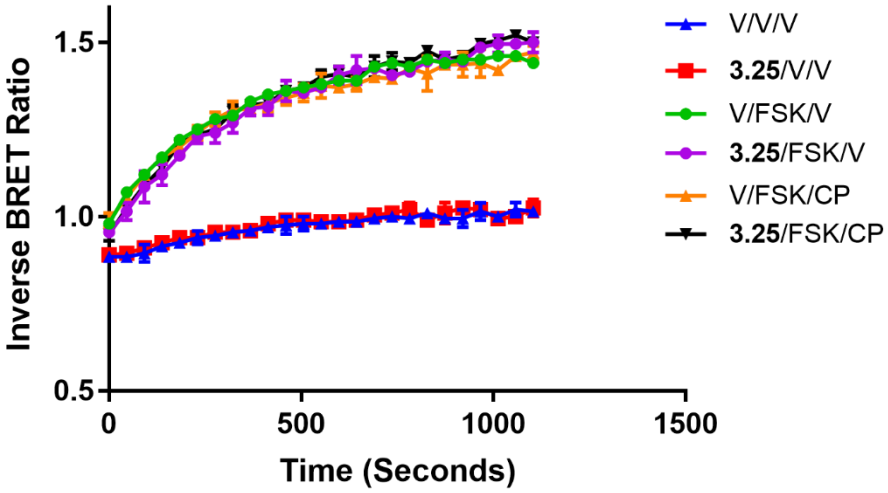

Figure 3.14. Screen of the highest affinity chromenopyrazole **3.25** tested at 10 µM at WT HEK-293 cells by a cAMP BRET assay. Data is representative of a single experiment carried in duplicate and is expressed as mean ± SEM. Literature agonist CP (CP55, 940), FSK (Forskolin), V (vehicle).

Table 3.3. Functional data for selected chromenopyrazoles obtained from cAMP BRET assay.

Compound	EC_{50} (nM± SEM) *	E_{max} (%FSK response ± SEM)#	Functional activity
3.25	12.5 ± 2.3	59.9 ± 2.04	Agonist
3.22	338.2 ± 20.2	49.91 ± 3.94	Agonist
3.29	152.5 ± 21.6	54.31 ± 3.09	Agonist
3.31	511.2 ± 56.0	53.75 ± 2.32	Agonist
3.39	17.3 ± 5.3	61.2 ± 1.53	Agonist
3.47	181.3 ± 13.3	70.36 ± 2.67	Agonist
CP	1.7 ± 0.23	43.33 ± 0.75	Agonist

*Potency (EC_{50}) and #efficacy (E_{max}) data for selected chromenopyrazoles, CP (CP55,940) obtained from cAMP BRET assay using HEK-293 cells expressing hCB_2R. All data is from at least three individual experiments performed, raw data is normalised to forskolin (100 %) and vehicle (0 %).

The highest CB_2R affinity (highest affinity among the novel chromenopyrazoles tested) chromenopyrazole **3.25** (EC_{50} = 12.5 ± 2.3 nM at hCB_2R) also displayed the highest potency for CB_2R out of the novel chromenopyrazoles tested (Table 3.3 and Figure 3.15). Chromenopyrazole-linker conjugate **3.22** (E_{max} = 49.91 ± 3.94 % of forskolin response at hCB_2R) showed the highest efficacy and was only slightly less efficacious than the literature control CP55,940 (E_{max} = 43.33 ± 0.75 % of forskolin response at hCB_2R; Table 3.3; Figure 3.15). It was a good result as it indicated that the linker in **3.22** improved the efficacy of **3.22** compared to **3.25** and revealed **3.22** as a promising lead in developing

agonist-based CB_2R fluorescent ligands. Remarkably, all of the chromenopyrazoles tested in the cAMP assay including linker conjugates of **3.25** and **3.29** behaved as agonists (Table 3.3). Previously, Cumella *et al.*[137] had also shown chromenopyrazoles **3.1, 3.2** and **3.5** (Table 3.1) as mCB_1R agonists by inhibition of contraction of mouse vas deferens.[137]

Another important result was the agonist functional nature and high potency of a chromenopyrazole-peptide linker conjugate **3.39** (EC_{50} = 17.3 ± 5.3 nM at hCB_2R). Most of the reported cannabinoid receptor agonists are highly lipophilic in nature, and hence peptide linker conjugates such as **3.39** provide a crucial lead for the development of polar cannabinoid receptor agonists. These polar cannabinoid receptor agonists would be useful as chemical tools to investigate CB_2R trafficking studies (GPCRs are known to signal from intracellular vesicles, also discussed in chapter 1, section 1.1). A cAMP BRET assay was used to determine the functional nature of the novel chromenopyrazoles (**3.22**, **3.25**, **3.29**, **3.31**, **3.39** and **3.47**) in this chapter; it would be interesting to investigate the functional nature of these ligands in other CBR signalling pathways such as activation of ERK, GIRKs, and recruitment of β-arrestin.

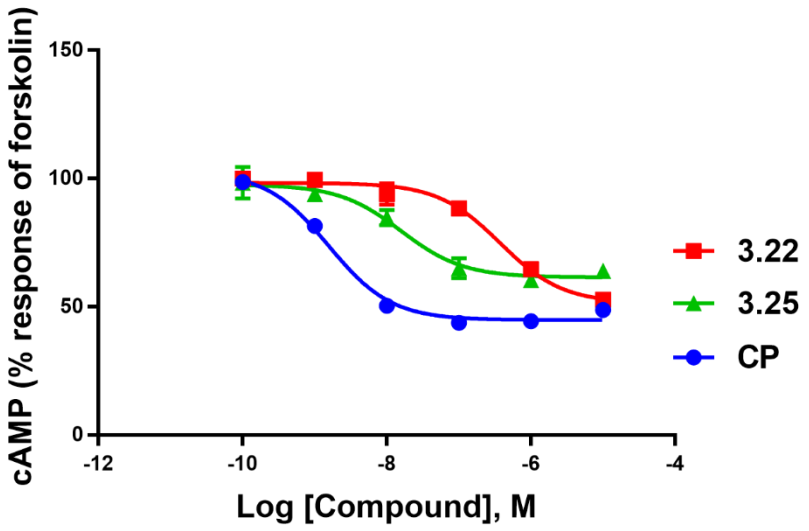

Figure 3.15. Concentration-response curve for highest affinity CB_2R chromenopyrazole **3.25**, highest affinity CB_2R chromenopyrazole-linker conjugate **3.22** (highest affinity among chromenopyrazoles tested in this chapter) and literature CBR agonist CP (CP55,940) using cAMP BRET assay with HEK-293 cells expressing hCB_2R. All data is from at least three individual experiments performed and is expressed as mean ± SEM. Raw data is normalised to forskolin (100 %) and vehicle (0 %).

Table 3.4 % Response in cAMP BRET assay at wild type HEK-293 cells.

Compound	%FSK Response ± SEM*
3.39	104.51 ± 1.068
3.25	100.15 ± 2.76
3.47	106.46 ± 1.92
3.31	98.28 ± 1.64
3.22	100.89 ± 4.71
3.29	102.40 ± 4.05

*cAMP BRET assay for the test compounds (10 μM) was carried out at WT HEK-293 cells. All data is from at least two individual experiments performed in duplicate, raw data is normalised to forskolin response (100 %) and vehicle response (0 %). A one-sample t-test was used to determine whether the % cAMP response of test compounds was significantly different from the forskolin only response.

3.4 Molecular modelling and docking studies

Computational studies were carried out to rationalise some key SAR results obtained from biological evaluation of the chromenopyrazoles (section 3.3). These key SARs included the greater tolerance of the long linkers in the *N*-(para-(methylamine)phenyl)-chromenopyrazoles compared to the *N*-(meta-(methylamine)phenyl)-chromeno-pyrazoles and similar high affinities at CB_2R of **3.29**-long linker conjugates (**3.31**, **3.32**, and **3.39**).

At the time of writing this thesis the crystal structure of CB_2R was not published, however three crystal structures of CB_1R (two with inverse agonists[111-112] and one with an agonist[113]) were published. As all of the novel chromenopyrazoles tested in the cAMP functional assay in this chapter behaved as agonists, it was decided to build a homology model of CB_2R based on the higher resolution active state structure of CB_1R (PDB ID: 5XRA) published by Hua *et al.*[113] The CB_1R structure (PDB ID: 5XRA) (CB_1R structure described in chapter 1, section 1.4.1) was crystallised with ligand AM11542 (shown in Figure 3.16), which shares good structural similarity with the novel chromenopyrazoles synthesised in this thesis.

Previously, computational studies for the literature chromenopyrazoles and the chromenoisoxazoles (Table 3.1) was carried out by Hurst *et al.*[137] with a homology model of CB_2R built using the bovine rhodopsin as the template. Results obtained from the

computational studies carried out by Hurst *et al.*[137] will not be compared with those obtained in this chapter due to the use of different homology models obtained from different template structures.

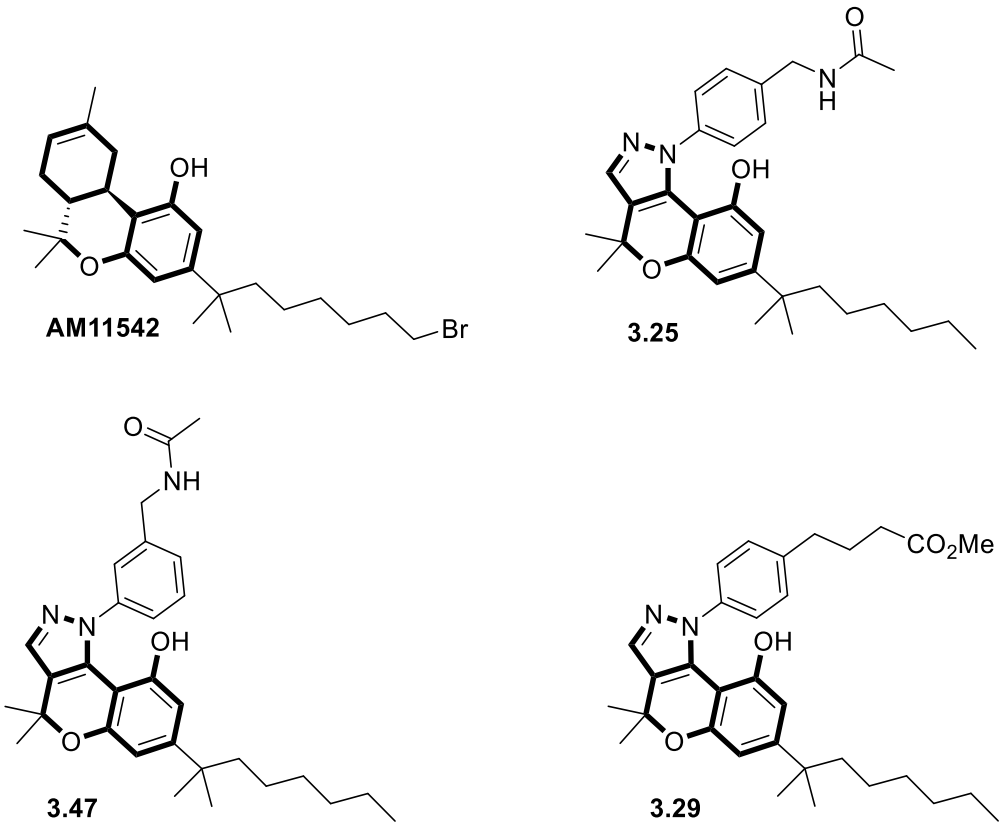

Figure 3.16. The scaffold constraint was applied in docking studies to match the location of the chromenopyrazolol moiety (structure fragment with bold bonds of **3.25**, **3.47**, and **3.29**) in the CB_2R homology model-binding site to the dibenzopyranol moiety (structure fragment with bold bonds) of AM11542.

The alignment of the CB_1R sequence (Uniprot id – P21554) against the CB_2R sequence (Uniprot id - P34972) was carried out using a multiple sequence alignment web server T-coffee[213] (Figure 3.17). Modeller[214] was used for building the active state homology model of CB_2R using the CB_1R active state crystal structure (PDB ID: 5XRA) published by Hua *et al.*[113] In total, 25 models were built and the model with the lowest DOPE (Discrete Optimized Protein Energy) score[215] was used for the docking studies.

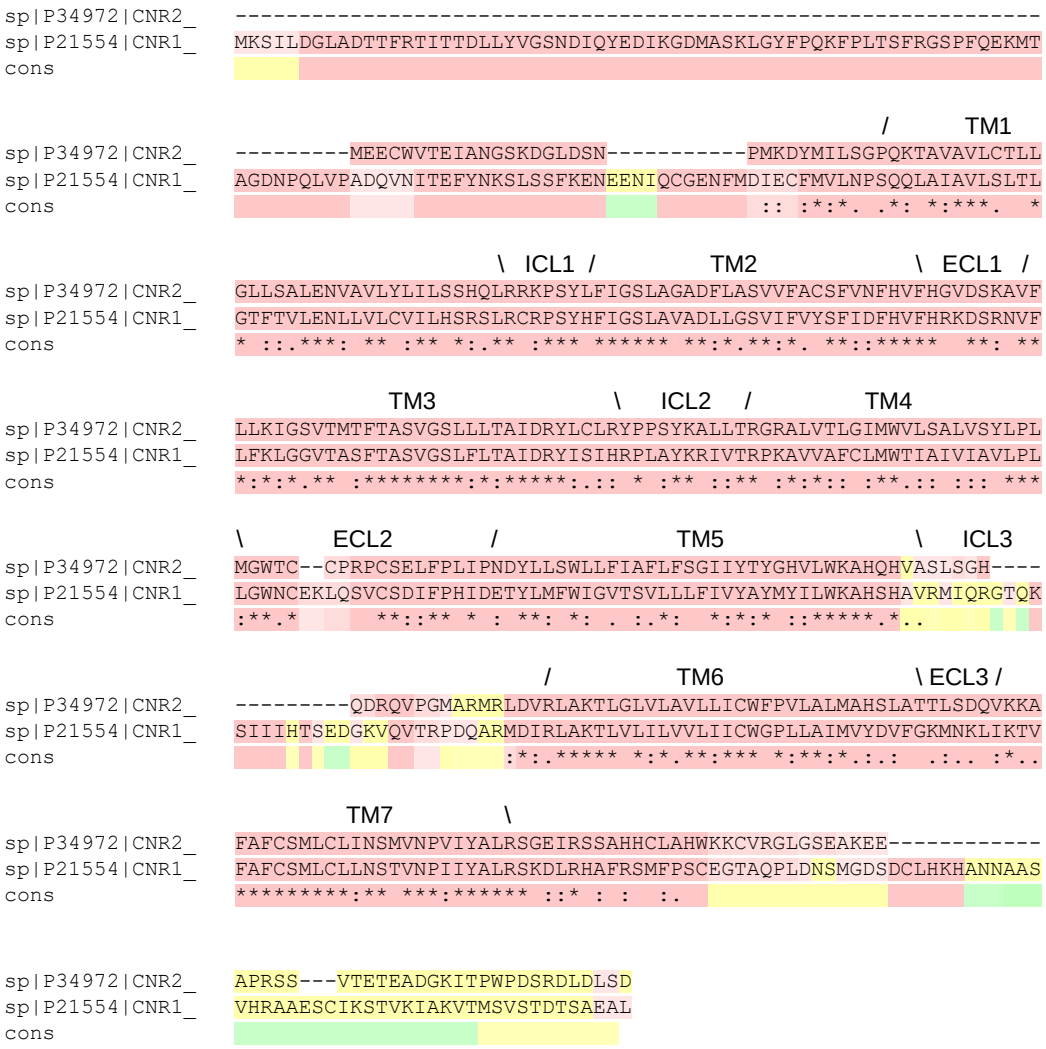

Figure 3.17. Sequence alignment of hCB$_1$R sequence (Uniprot id – P21554) against the hCB$_2$R sequence (Uniprot id - P34972) was carried out with web server T-coffee[213] and manually improved. The alignment is colour coded for agreement with the library used by T-coffee – pink colour (good), yellow (average), and green (bad).

The ligands were drawn in Avogadro[216] and the structures optimised by energy minimisation using the Merck Molecular ForceField (MMFF94). GOLD[217], a docking programme, was used for docking studies with the CB$_2$R binding site of the ligands defined as 20 Å region around the CB$_1$R co-crystallised ligand AM11542 (PDB ID: 5XRA). The scaffold constraint was applied to match the location of the chromenopyrazolol moiety of the ligands (**3.25**, **3.47**, and **3.29**; Figure 3.16) to the dibenzopyranol moiety of AM11542 in the CB$_2$R homology model-binding site. The docking studies were carried out only with three small-linker/substituent *N*-phenyl-chromenopyrazole conjugates – **3.25** (*N*-(para-(methylamine)phenyl)-chromenopyrazole), **3.47** (*N*-(meta-(methyl-amine)phenyl)-chromenopyrazole, and **3.29**

(*N*-(5-carboxypentyl)-chromenopyrazoles) that showed high CB_2R affinity. The docking studies of the chromenopyrazole-long linker or (long linker-fluorophore) conjugates were not carried out due to the large degree of freedom of the linker atoms, which usually produces varied binding poses. Docking poses of the ligands were visualised with PyMOL.

The docking studies indicated a hydrogen bond between aromatic hydroxyl of **3.25** and S285 (Figure 3.18). In a previous study, S285 was shown to play an essential role in the binding of CB_2R agonists such as HU243.[218] A hydrogen bond was also observed between the amine of **3.25** and the carboxyl group of K278. In this docking pose, the methylamine linker exits out of the binding pocket from the cavity located between TM1 and TM7. Thus, the long PEG linker extended from **3.25** (PEG linker in **3.22**) will likely reside in the extracellular environment and might explain the high CB_2R binding affinity of **3.22** (section 3.3.2). In a previous literature report, it has been suggested using molecular dynamics simulations, that cannabinoid ligands enter the CBR via the lipid membrane[219] and THC enters CB_1R via the cavity located between helices TM1 and TM7[220]. Shao *et al.*[111], who reported the CB_1R crystal structure with inverse agonist taranabant, have also suggested that lipophilic ligands enter CB_1R orthosteric binding site via the cavity between helices TM1 and TM7. Aromatic interactions were observed between the aromatic rings of **3.25** and F106, F183, F281, F87, F94, F91 and H95. van der Waals interactions were observed between dimethyl side chain of **3.25** and residues M265, V261, T114, F117 and W194.

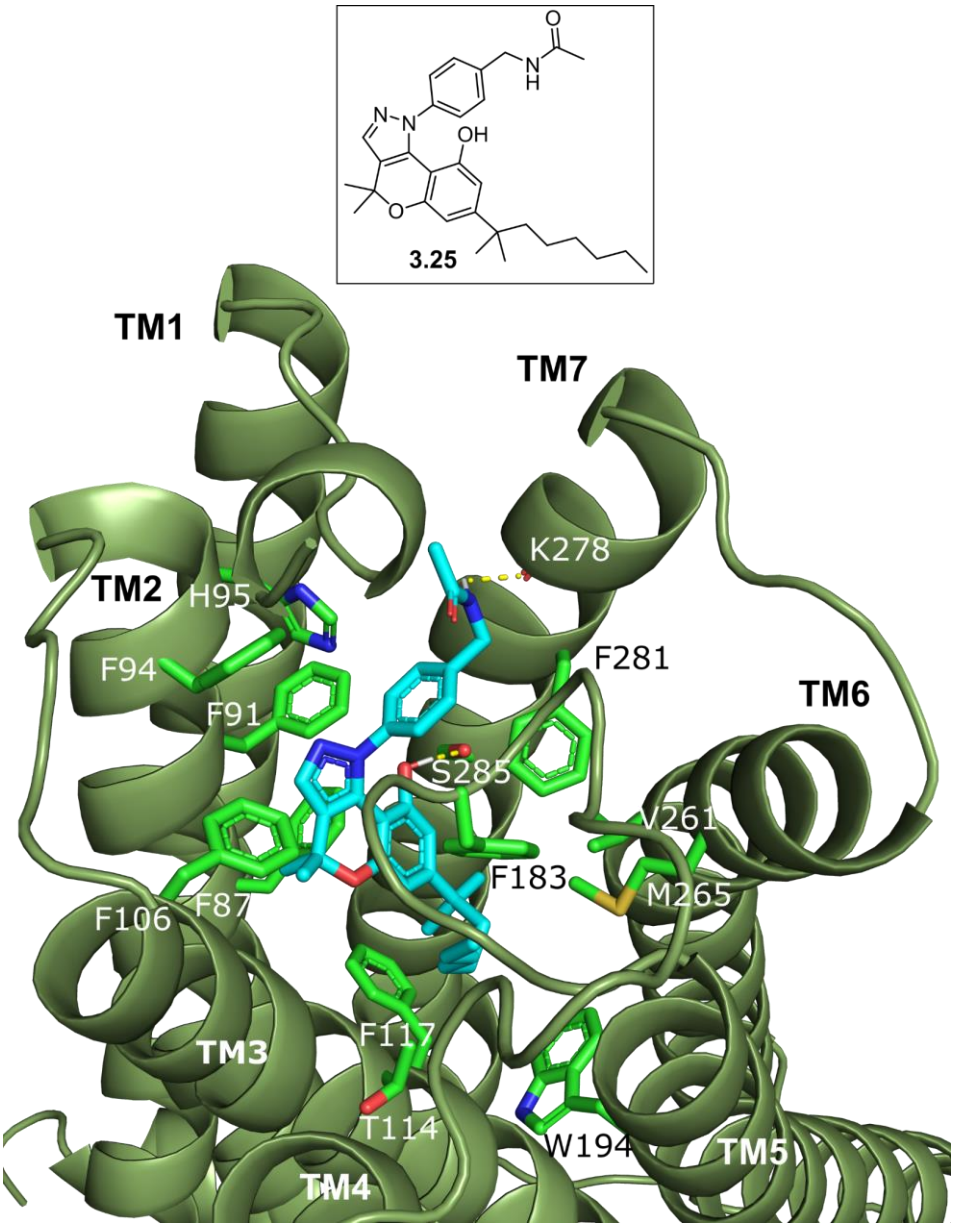

Figure 3.18. Docking pose of **3.25** (cyan carbons, red oxygens, blue nitrogens, white hydrogens) in CB_2R homology model (forest green ribbon). Side chain residues forming hydrogen bonds or hydrophobic interaction with **3.25** are shown as sticks (leaf green). Hydrogen bonds are shown as yellow lines.

The docking studies of **3.47** (Figure 3.19) showed a hydrogen bond between the aromatic hydroxyl of **3.47** and S285, and between the carboxyl group of Y25 and the amine of **3.47**. Although **3.47** bound in a similar docking pose to **3.25**, extension of a longer linker from **3.47** likely introduces steric clashes leading to decreased CB_2R binding affinity of **3.47**-linker conjugate **3.45** (section 3.3.2). Similar to **3.25**, aromatic interactions between aromatic rings of **3.47** with F106, F183, F281, F87, F94, F91, H95 and van der Waals interactions between the dimethyl side chain of **3.47** with M265, V113, T114, F117, W194, W285, Leu191 were observed.

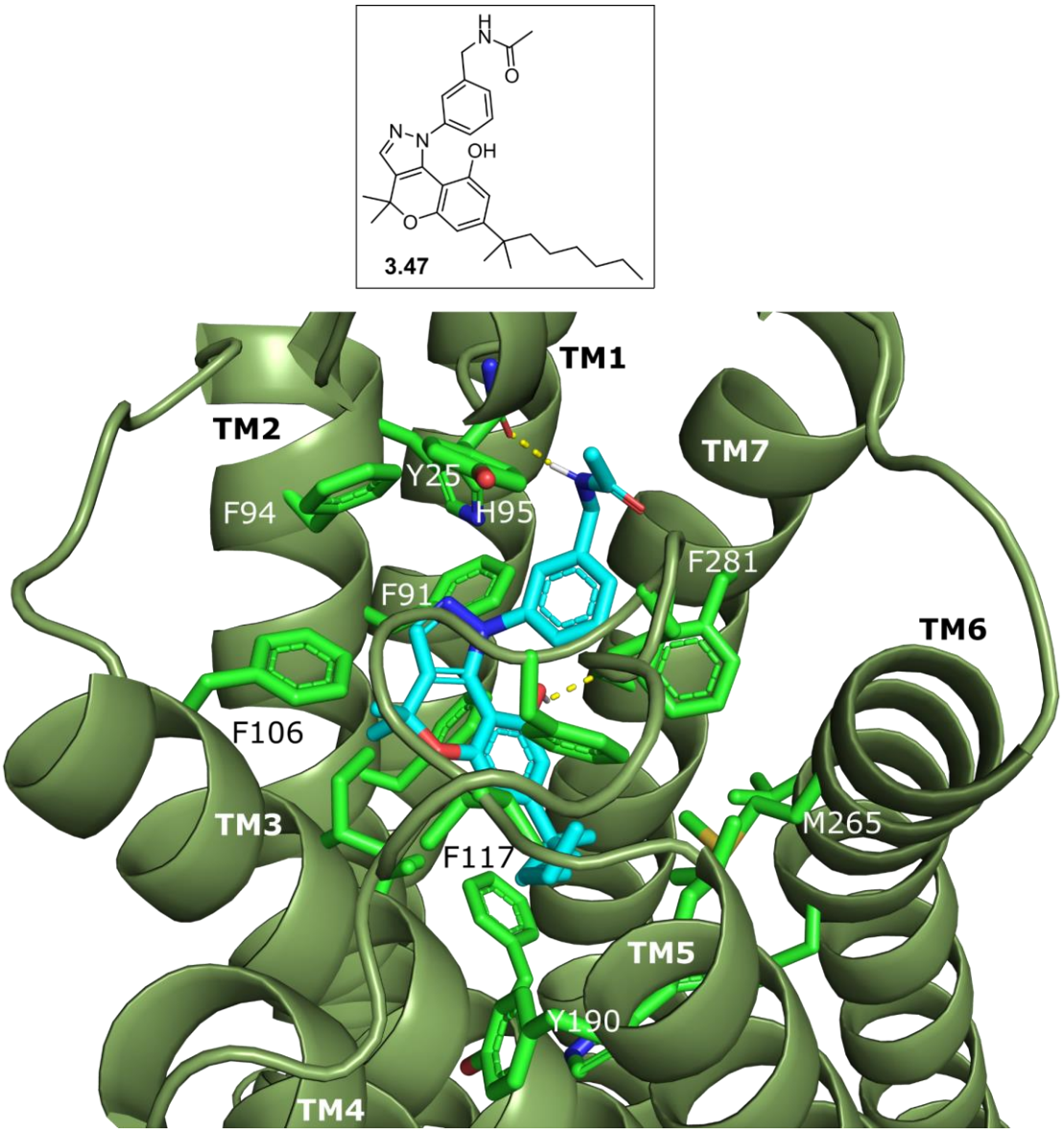

Figure 3.19. Docking pose of **3.47** (cyan carbons, red oxygens, blue nitrogens, white hydrogens) in CB_2R homology model (forest green ribbon). Side chain residues forming hydrogen bonds or hydrophobic interaction with **3.47** are shown as sticks (leaf green). Hydrogen bonds are shown as yellow lines.

Similar to **3.25** and **3.47**, docking studies of **3.29** showed a hydrogen bond between aromatic hydroxyl of **3.29** and S285 (Figure 3.20). The long linkers (alkyl, PEG and peptide) extended from **3.29** likely exit the CB_2R binding pocket through the cavity located between TM1, TM7 and resides in the extracellular cavity, which might explain the similar high binding affinity of **3.29**-linker conjugates (**3.31**, **3.32** and **3.39**) (section 3.3.2). Similar to **3.25** and **3.47**, aromatic interactions between aromatic rings of **3.29** with M265, V261, T114, F117, W194 and van der Waals interactions between the dimethyl side chain of **3.29** with W194 T114, M265 V113 were observed.

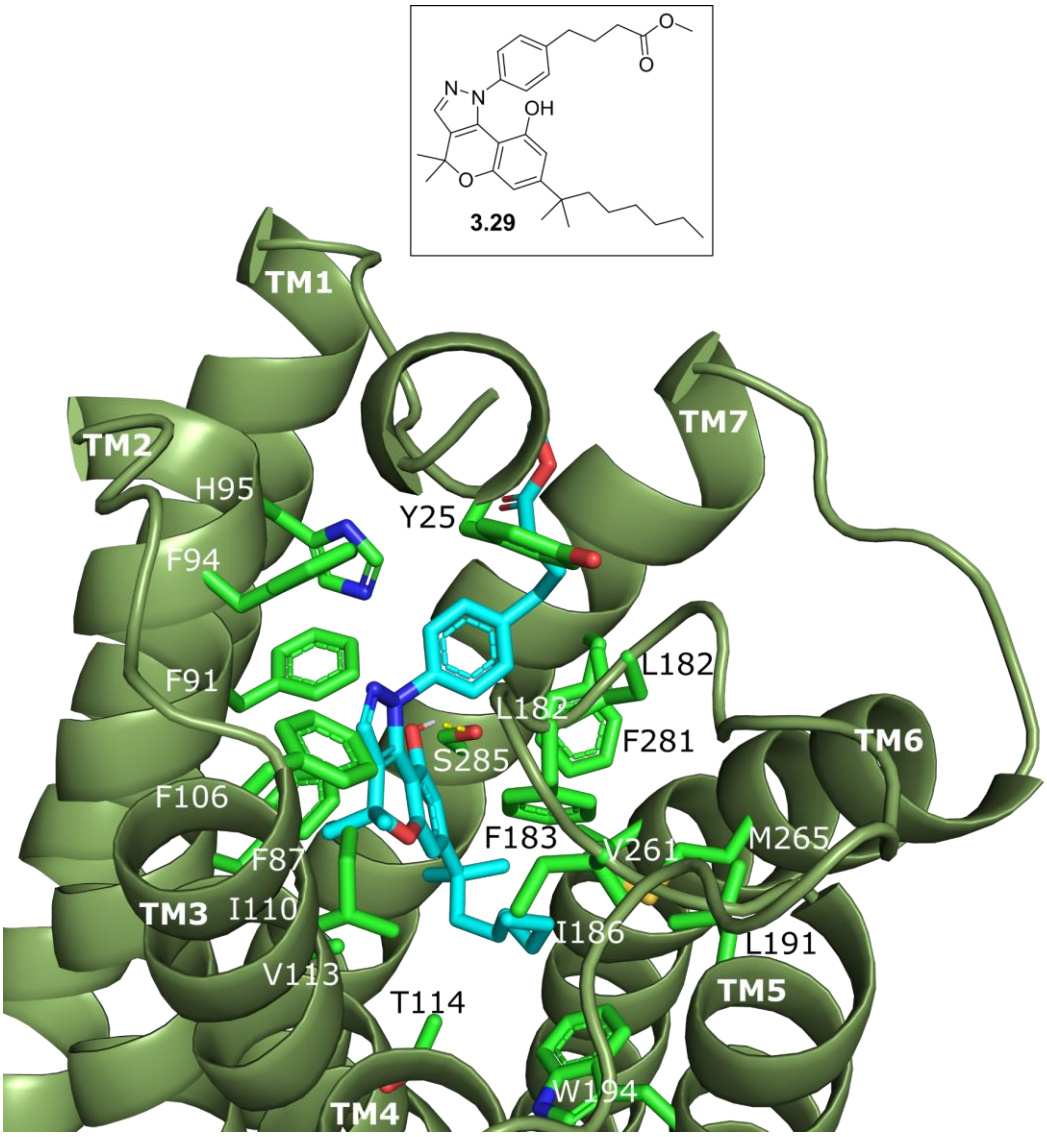

Figure 3.20. Docking pose of **3.29** (cyan carbons, red oxygens, blue nitrogens, white hydrogens) in CB_2R homology model (forest green ribbon). Side chain residues forming hydrogen bond or hydrophobic interaction with **3.25** are shown as sticks (leaf green). Hydrogen bonds are shown as yellow lines.

The docking studies of chromenopyrazole-long linker plus fluorophore conjugates were not carried out due to the difficulty in obtaining accurate binding poses of these compounds containing a number of rotatable bonds with a CB_2R homology model. It is likely that the decrease in CB_2R binding affinity upon attachment of fluorophore to the linker conjugates could be due to steric clashes of the fluorophore with the CB_2R amino acid residues present in the TM helices or EL(s).

A previous report suggests that the CBR ligands enter the CBR ligand binding site via the lipid membrane.[219] It is therefore likely that polarity, charge and molecular size of the

chromenopyrazoles (listed in Table 3.2) might affect the ability of these ligands to enter via the lipid membrane and hence influence CBR affinity through this mechanism too.

3.5 Summary and conclusions

With the aim of developing a high affinity CB_1R fluorescent agonist, chromenopyrazole derivatives with the linkers conjugated at six different positions of the chromenopyrazole core (section 3.2) were prepared. These derivatives were synthesised from reaction of the β-ketoaldehyde **3.16** with different hydrazines. The steric/electronic factors led to the formation of only the *N*1 isomer from the reactions of aryl hydrazines and long chain alkyl hydrazine with **3.16**. Three different types of linkers (alkyl, PEG and peptide) were conjugated to the synthesised chromenopyrazoles. The fluorophore BODIPY-630/650 was also conjugated to a set of the chromenopyrazole-linker derivatives to provide the fluorescent ligands **3.23**, **3.33**, **3.40**, **3.46**, and **3.54**.

Disappointingly, most of the synthesised chromenopyrazoles, including fluorescent ligands, did not exhibit high binding affinity for CB_1R in the radioligand binding assay (Table 3.2). Nonetheless, the majority of the chromenopyrazoles showed higher affinity for CB_2R as well selectivity over CB_1R. The chromenopyrazole **3.25** (K_i = 13.2 ± 3.4 nM at hCB_2R) displayed the highest overall affinity and also the best selectivity (greater than 75 fold) for CB_2R over CB_1R. The long linkers were best tolerated at the para-substituted *N*-phenyl-chromenopyrazoles than the meta-substituted *N*-phenyl-chromenopyrazoles. Among chromenopyrazole-linker conjugates, **3.22** (K_i = 71.1 ± 6.7 nM at hCB_2R) exhibited highest affinity for CB_2R and selectivity (greater than 70 fold) over CB_1R. Three moderate affinity CB_2R fluorescent ligands **3.23**, **3.33** and **3.40** were also obtained.

The highest affinity CB_2R chromenopyrazoles (**3.29**, **3.31**, **3.22**, **3.25**, **3.39**, and **3.47**) were tested in a cAMP functional assay to investigate the functional activity of these chromenopyrazoles (Table 3.3). The chromenopyrazole-linker conjugate **3.22** (E_{max} = 49.91 ± 3.94 % of forskolin response at hCB_2R) exhibited the highest efficacy and **3.25** (EC_{50} = 12.5 ± 2.3 nM at hCB_2R) exhibited highest potency.

The CB_2R binding affinity of **3.25** and **3.29** (Table 3.2) were also preserved/improved in their linker conjugates (**3.22**, **3.31**, **3.32**, and **3.39**). Taken together, these functional and

binding affinity results indicated that the linker conjugates of **3.25** and **3.29** would be promising leads for the development of CB_2R fluorescent ligands.

Docking studies of **3.25**, **3.47**, and **3.29** using the homology model of CB_2R revealed that the short linkers exit the CB_2R binding pocket through cavity located between TM1 and TM7 (section 3.4). Although the initial aim of developing a high affinity CB_1R fluorescent ligand was not achieved, several chromenopyrazoles exhibiting high affinity for CB_2R and selectivity over CB_1R were obtained. Importantly, in contrast to the typically lipophilic cannabinoids, a high affinity polar peptide linker containing conjugate **3.39** along with several other high affinity chromenopyrazole-linker conjugates (**3.22**, **3.31**, **3.32** and, **3.39**) were successfully developed. With these lead CB_2R chromenopyrazoles in hand, efforts were then directed towards development of selective CB_2R fluorescent ligands (described in chapter 4). A new series of pyridyl-based ligands were instead explored for development of CB_1R fluorescent ligands (described in chapter 5).

Chapter 4 Optimisation of chromenopyrazoles as high affinity fluorescent ligands for cannabinoid type 2 receptor

4.1 Design rationale for optimisation of chromenopyrazole-based fluorescent ligands

The chromenopyrazoles **3.22** (linker analogue of **3.25**) and **3.31**, **3.32**, **3.39** (linker analogues of **3.29**, Figure 4.1) described in chapter 3, showed high affinity and selectivity for CB_2R over CB_1R. Disappointingly, the BODIPY-630/650 analogues of **3.22**, **3.32**, and **3.39** provided only moderate affinity CB_2R ligands. High affinity for the target receptor along with favourable polarity (to reduce non-specific membrane binding) are two essential criteria a fluorescent ligand should possess for being used as an imaging tool (refer to chapter 1, section 1.2.3.1). So, the second-generation of chromenopyrazole-based fluorescent ligands was developed with the aim of improving the CB_2R affinity by refining fluorophore and linkers around the chromenopyrazole ligand core. A second-generation of chromenopyrazole peptide-linker conjugates were also developed in an effort to make more polar compounds while maintaining high affinity for CB_2R.

The BODIPY-630/650 derivatives (**3.40**, **3.33**, and **3.23**) of high affinity chromenopyrazole-linker conjugates (**3.39**, **3.32**, and **3.22**) showed poor CB_2R affinity. One way to test the effect the fluorophore has on CB_2R affinity would be to substitute BODIPY-630/650 with a range of different fluorophores such as BODIPY-FL, TAMRA and Cy5. As the chromenopyrazole-linker conjugate **3.22** (Figure 4.1; K_i = 71.1 ± 6.7 nM at hCB_2R; Table 3.2, chapter 3) displayed the highest affinity for CB_2R, it was decided to append the fluorophores (BODIPY-FL, TAMRA and Cy5) to **3.22** (**4.01 - 4.03**; Figure 4.2). All of these fluorescent ligands (**4.01** – **4.03**) were designed with PEG linkers of equal length so that the trend in CB_2R affinity could be directly correlated to the type of fluorophore present.

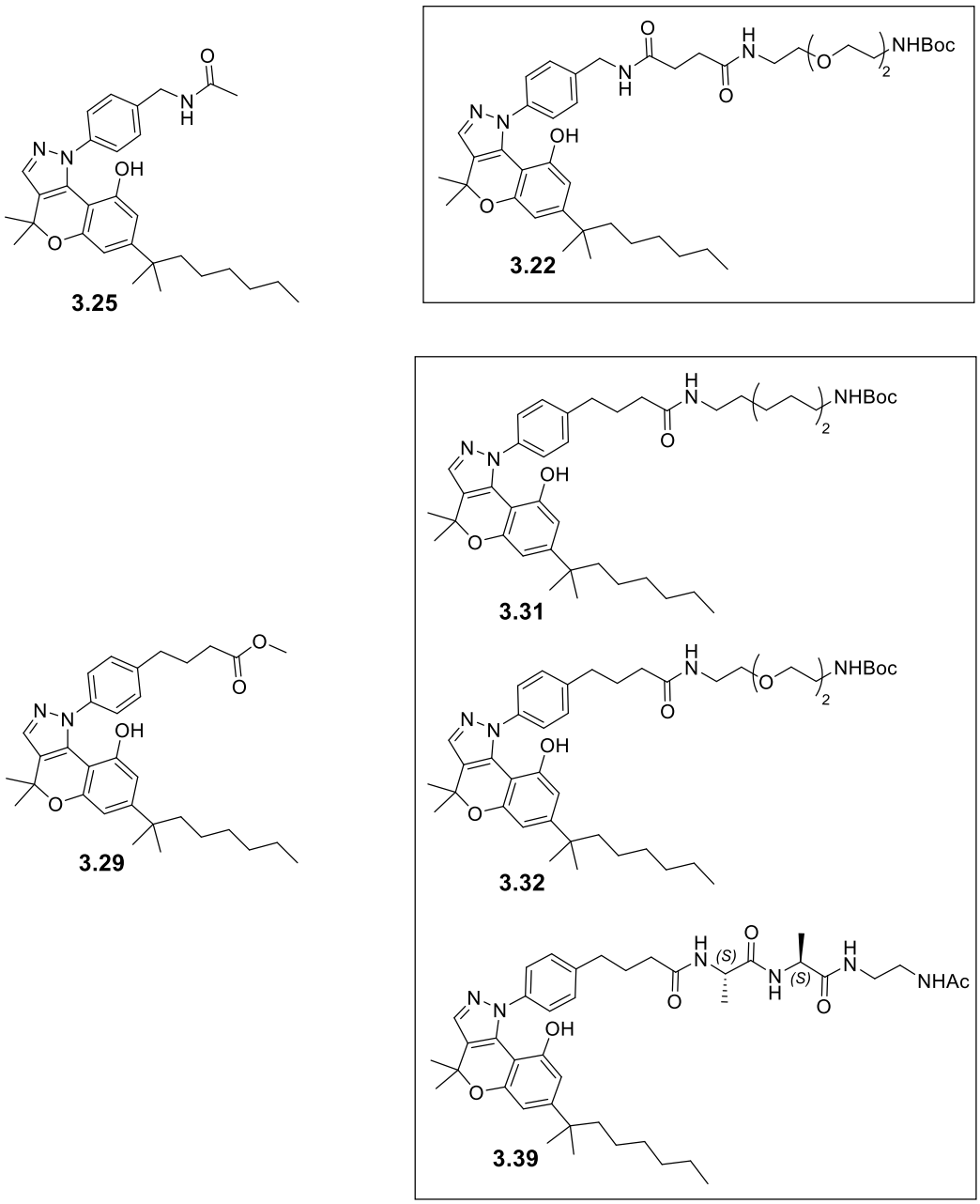

Figure 4.1. The high affinity CB_2R chromenopyrazoles **3.25**, **3.29** and the linker conjugates **3.22**, **3.31, 3.32** and **3.39** prepared in chapter 3.

The fluorophore BODIPY-FL (excitation 505 nM, emission 513 nM) was selected, as it is structurally similar but smaller compared to BODIPY-630/650. It was hoped that the smaller-sized BODIPY-FL-based fluorescent ligand **4.01** (Figure 4.2) might exhibit higher affinity for CB_2R compared to the BODIPY-630/650 based fluorescent ligand **3.23** (K_i = 2312 ± 298nM at hCB_2R, Table 3.2, chapter 3) due to the reduced steric clashes with the CB_2R amino acid residues. The red-emitting fluorophore Cy5 (excitation 646 nM, emission 662 nM) consists of two indoline moieties separated by a pentamethine

spacer. Replacement of the BODIPY-630/650 of fluorescent ligand **3.23** with Cy5 to give fluorescent ligand **4.02** will preserve the red fluorescence but the variation in structure might improve the CB_2R affinity. The rhodamine-based fluorophore TAMRA (excitation 565 nM, emission 580 nM) lacks a short linker present in other fluorophores (BODIPY-630/650, BODIPY-FL and Cy5). As the aim was to maintain the similar linker length of **3.23** while changing the fluorophore, it was decided to prepare a new chromenopyrazole-based linker conjugate **4.13** (synthesis described in section 4.2.1.3) for preparing TAMRA based fluorescent ligand **4.03** (Figure 4.2).

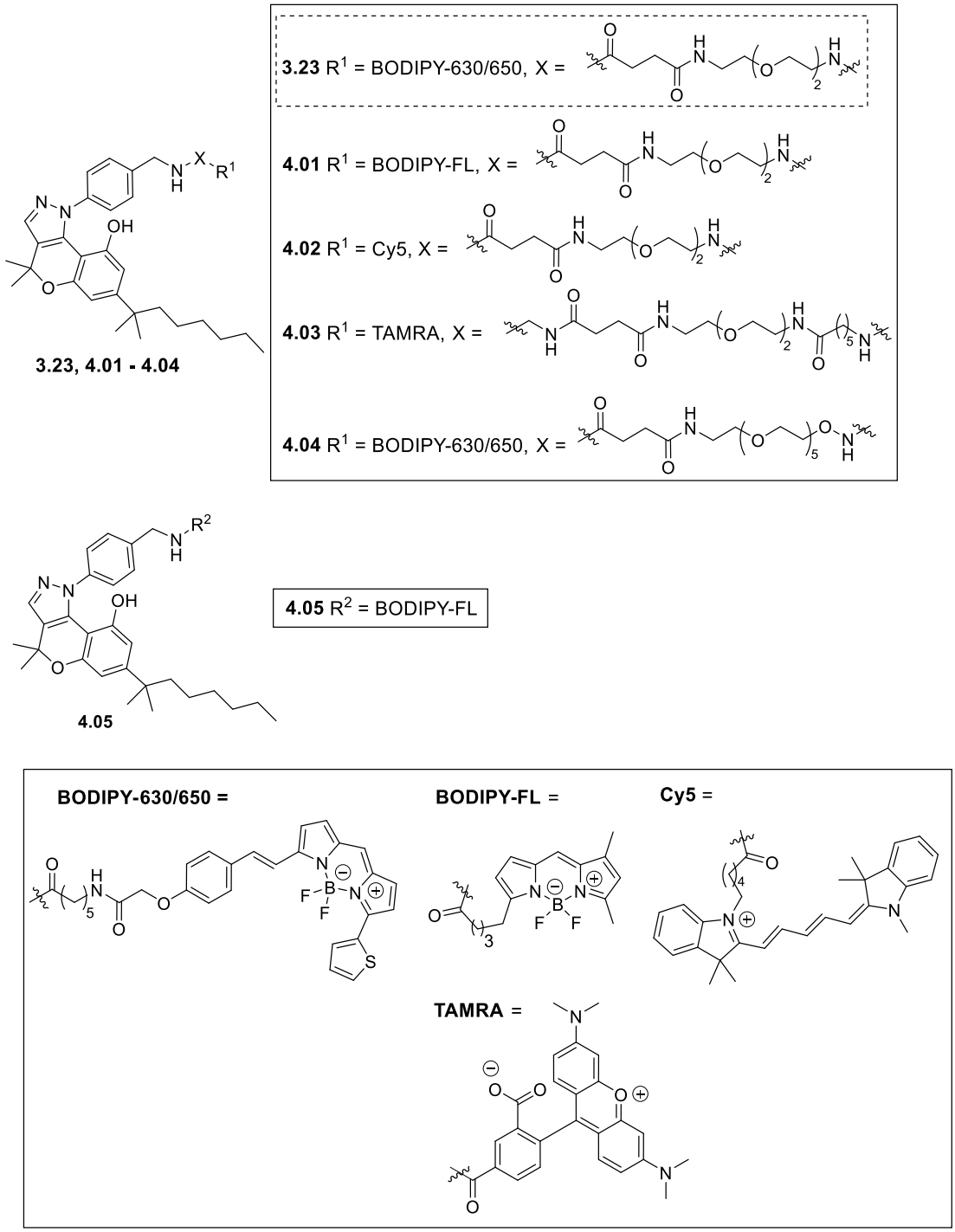

Figure 4.2. Lead chromenopyrazole CB_2R fluorescent ligand **3.23** (developed in chapter 3) and second-generation fluorescent ligands (**4.01** – **4.05**) designed as potential CB_2R ligands.

Fluorescent ligands **4.04** (a long linker analogue of **3.23**) and **4.05** (a short linker analogue of **4.01**) were also designed to assess the influence of PEG linker length on the CB_2R affinity (Figure 4.2). It was hoped that fluorophore BODIPY-630/650 of **4.04** might suffer reduced steric clashes with the CB_2R amino acid residues compared to BODIPY-630/650 of **3.23** due to the greater separation of fluorophore and pharmacophore by a longer PEG

linker. The fluorescent ligand **4.05** was designed to investigate whether the fluorophore BODIPY-FL could be tolerated in close proximity to the pharmacophore to make a high affinity CB_2R fluorescent ligand.

A polar, high affinity fluorescent ligand is desired as it usually displays lower non-specific membrane binding compared to a non-polar fluorescent ligand and is especially challenging to make for a lipid receptor such as CB_2R (chapter 1, section 1.2.3.1). Among the chromenopyrazole-linker conjugates described in chapter 3, **3.39** (Figure 4.3, K_i = 138.4 ± 6.75 at hCB_2R; Table 3.2, chapter 3) was particularly promising as despite containing a peptide linker (Ala-Ala), it displayed high affinity and functional activity (agonist, EC_{50} = 17.3 ± 5.3 nM; Emax = 61.2 ± 1.53% of forskolin response at hCB_2R) at CB_2R. A second-generation of polar peptide linker-chromenopyrazole conjugates (**4.06 - 4.08**) containing serine and asparagine amino acids was designed (Figure 4.3). The amino acids serine and asparagine were selected as these contain more hydrophilic (but non-ionised at physiological pH) side chain residues compared to Ala, which might make hydrogen bonds with the CB_2R amino acid residues.

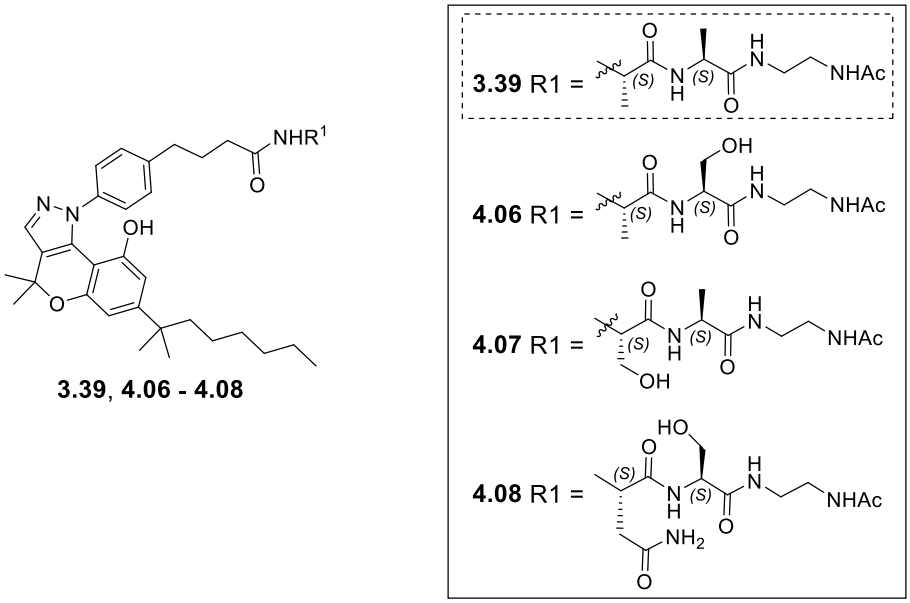

Figure 4.3. Lead chromenopyrazole CB_2R peptide-linker conjugate **3.39** (developed in chapter 3) and second-generation peptide linker-conjugates (**4.06** – **4.08**) designed as potential CB_2R polar ligands.

Based on the comparison of CB_2R affinity of chromenopyrazoles (**3.25**, **3.18**), (**3.22** (Figure 4.3), **3.26**) and (**3.41**, **3.47**), it was concluded in chapter 3 (section 3.3.2) that the

atoms near the pyrazole-*N*-phenyl substituent of the chromenopyrazole might play a crucial role in CB_2R binding. It was thought that a modification near the benzylic position might improve the CB_2R affinity of chromenopyrazole-linker conjugates. Accordingly, a new heterocyclic analogue **4.09** of **3.22** was designed by substituting the phenyl ring of **3.22** with a pyridyl ring (Figure 4.4). The presence of a pyridine in **4.09** would also increase the polarity of the linker conjugate and may reduce the non-specific membrane interactions of the **4.09**-based fluorescent ligands. Due to the time constraints of pharmacological testing, only one compound **4.09** was to be tested for pharmacological activities and depending on the pharmacological results additional derivatives of **4.09** including fluorescent ligands would be prepared.

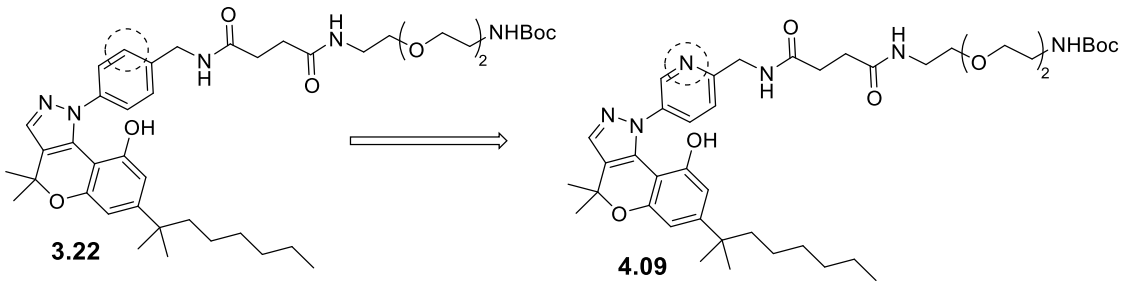

Figure 4.4. Pyridyl chromenopyrazole **4.09** designed by substitution of phenyl carbon atom (circled) of **3.22** with a nitrogen atom (circled).

4.2 Synthesis and structural characterisation

4.2.1 Synthesis of second-generation fluorescent conjugates of chromenopyrazole (3.22)

4.2.1.1 Synthesis of BODIPY-FL-based fluorescent ligands

The benzylamine **3.21** (synthesis described in chapter 3, section 3.2.1.1) was used in crude form in the amide coupling reactions to prepare chromenopyrazole linker conjugates in chapter 3. However, it was decided to purify the crude benzylamine **3.21** before reacting with the commercially available fluorophore BODIPY-FL-SE. For the ease of purification on suitable scale, benzylamine **3.21** was reacted with Boc anhydride to give **4.10**, which was then purified by silica gel column chromatography (Scheme 4.1). The low yield of Boc protection is likely due to crude benzylamine **3.21** used.

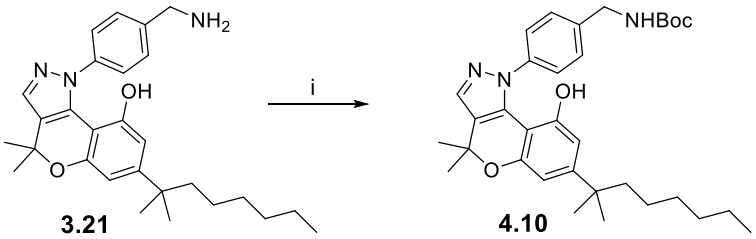

3.21 **4.10**

Scheme 4.1. (i) $(Boc)_2O$, Et_3N, DCM, 35%.

Boc deprotection of **4.10** with TFA and reaction of the semi-preparative RP-HPLC purified trifluoroacetate salt with BODIPY-FL-SE using DIPEA as a base provided fluorescent ligand **4.05** (Scheme 4.2). Similarly, fluorescent ligand **4.01** was prepared by reaction of Boc-deprotected **3.22** (synthesis described in chapter 3, section 3.2.1.1) with BODIPY-FL-SE.

As also noted in chapter 3 (section 3.2.1.1), calculated yields of reactions of commercially available fluorophore succinimidyl esters to give fluorescent ligands (**4.01**-**4.05**) (Scheme 4.2, 4.3, 4.4 and 4.5) with chromenopyrazoles were greater than quantitative. This was assumed to be because the commercially available fluorophore succinimidyl esters are supplied in higher amounts than that specified on the container. The amount of fluorophore specified on the container was used in the calculation of yield.

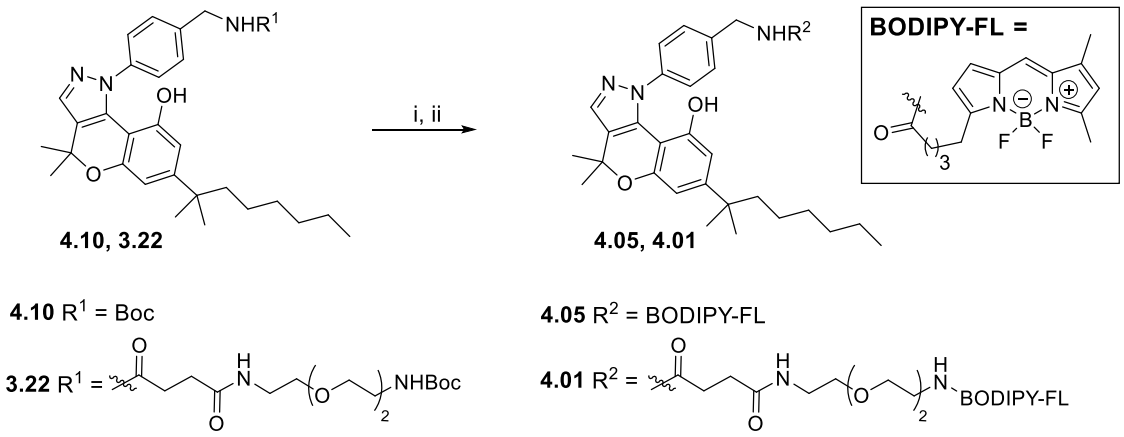

Scheme 4.2. (i) TFA, DCM, quantitative. (ii) BODIPY-FL-SE, DIPEA, DMF, quantitative.

4.2.1.2 Synthesis of a Cy5-based fluorescent ligand

The fluorescent ligand **4.02**, which is the Cy5 analogue of **3.23**, was synthesised by reaction of Boc-deprotected chromenopyrazole **3.22** (RP-HPLC purified) with commercially available fluorophore Cy5-SE using DIPEA as a base.

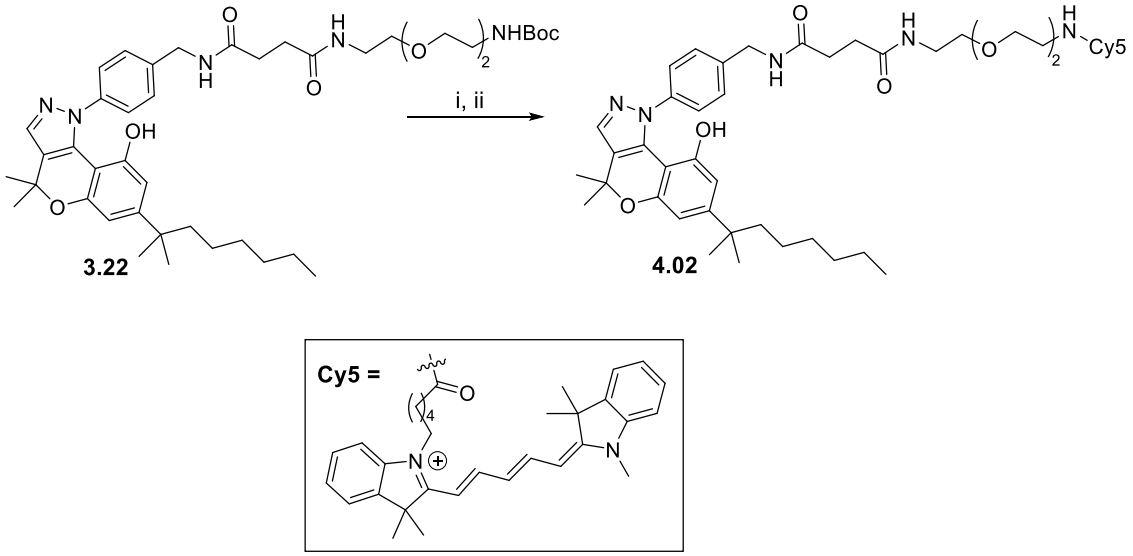

Scheme 4.3. (i) TFA, DCM, quantitative. (ii) Cy5-SE, DIPEA, DMF, quantitative.

4.2.1.3 Synthesis of a TAMRA-based fluorescent ligand

A new chromenopyrazole-based linker conjugate **4.13** was prepared for reaction with TAMRA-SE so that the resulting TAMRA fluorescent ligand **4.03** would have a linker length similar to other fluorescent ligands (**3.23**, **4.01**, **4.02**, and **4.04**). Synthesis of fluorescent ligand **4.03** began with Boc protection of commercially available 6-aminohexanoic acid **4.11** according to a previously reported literature synthesis[221] to give **4.12** (Scheme 4.4). The reaction of **4.12** with Boc-deprotected **3.22** using TFFH as a coupling reagent and Et_3N as a base gave **4.13**. The low yield obtained for **4.13** is attributed to the loss of the polar compound during silica gel column purification. Chromenopyrazole-linker conjugate **4.13** was reacted with TFA and the resulting Boc-deprotected **4.13** was then reacted with commercially available TAMRA-SE using DIPEA as a base to provide fluorescent ligand **4.03** (Scheme 4.4).

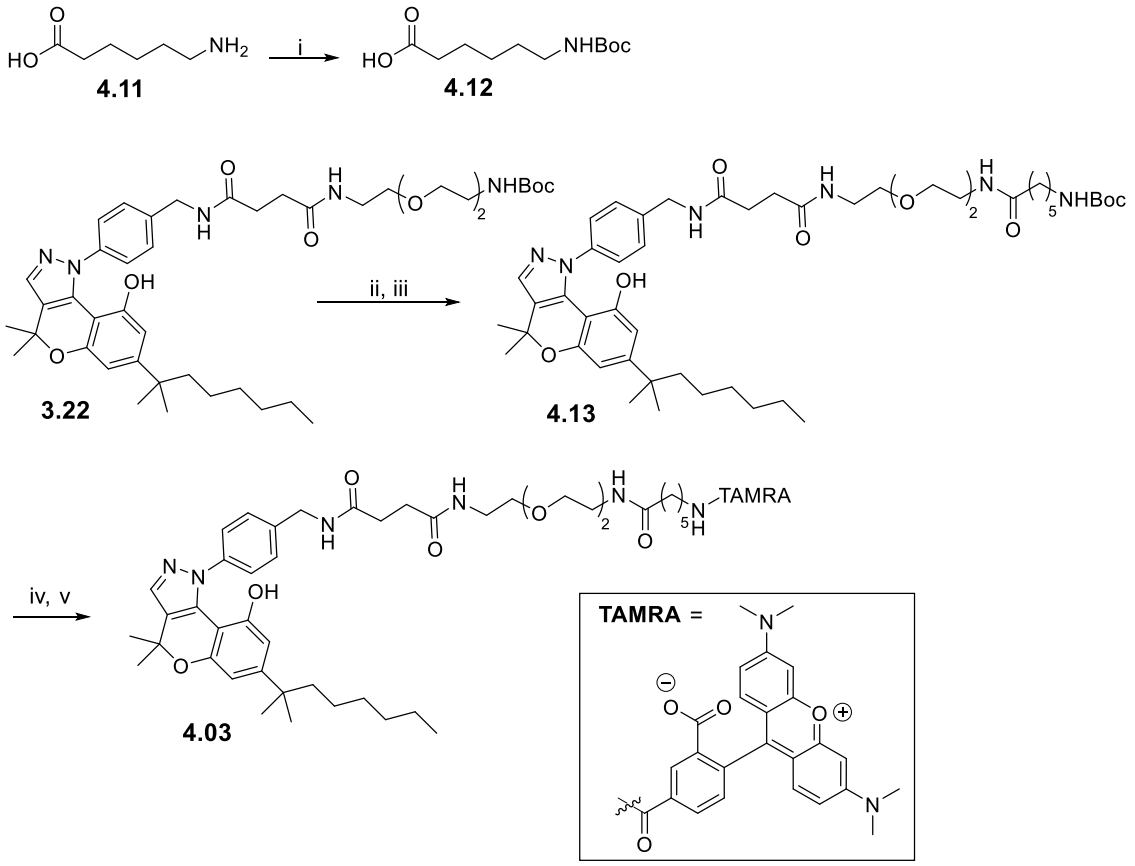

Scheme 4.4. (i) $(Boc)_2O$, NaOH, 1,4-dioxane, H_2O, 71%. (ii) TFA, DCM, quantitative. (iii) **4.12**, TFFH, Et_3N, DCM, 34%. (iv) TFA, DCM, quantitative. (v) TAMRA-SE, DIPEA, DMF, quantitative.

4.2.1.4 Synthesis of chromenopyrazole-long linker-BODIPY-630/650 fluorescent ligand analogue of 3.23

Preparation of the fluorescent ligand **4.04** commenced with the reaction of commercially available PEG linker **4.14** with succinic anhydride to yield carboxylic acid **4.15**. The coupling of **4.15** with Boc-deprotected **4.10** using TFFH as a coupling reagent gave **4.16**. As in the case of **4.13**, the low yield obtained for **4.16** is likely due to the loss of polar compound during silica gel column purification. Chromenopyrazole linker conjugate **4.16** was then reacted with TFA and the resulting Boc-deprotected **4.16** was subsequently reacted with BODIPY-630/650-SE using DIPEA as a base to give fluorescent ligand **4.04**.

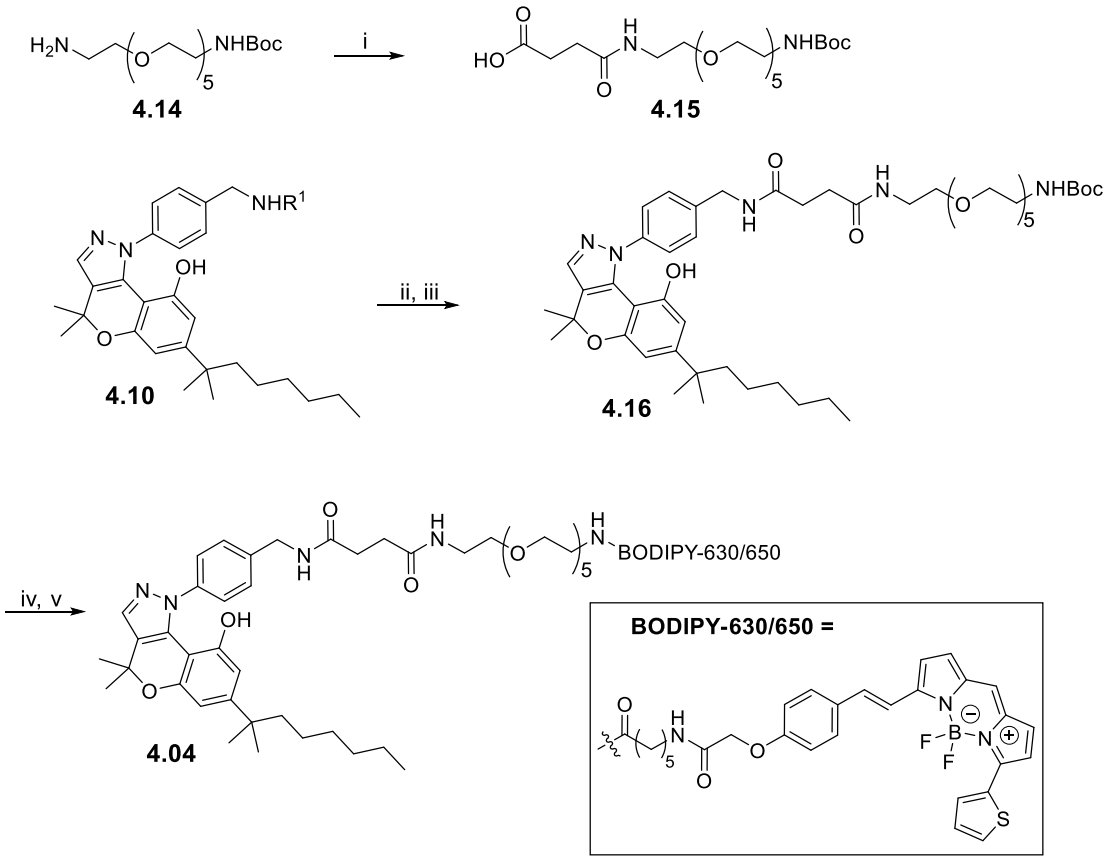

Scheme 4.5. (i) Succinic anhydride, $CHCl_3$. (ii) TFA, DCM, quantitative. (iii) **4.15**, TFFH, Et_3N, DCM. 25%. (iv) TFA, DCM, quantitative. (v) BODIPY-630/650-SE, DIPEA, DMF, quantitative.

4.2.2 Synthesis of second-generation chromenopyrazole peptide linker conjugates

Fmoc solid-phase peptide synthesis was used for the preparation of new chromenopyrazole peptide linker conjugates (**4.25**-**4.27**; Scheme 4.6). Coupling of 1,2-diaminoethane trityl resin **3.35** with Fmoc-Ser(tBu)-OH or Fmoc-Ala-OH using HBTU and DIPEA gave **4.17** and **4.18**. The resins were then capped by reacting any unreacted resin-amine sites with Ac_2O in DMF. The Fmoc deprotection of resin-bound (**4.17**-**4.18**) with a solution of piperidine in DMF (20% *v*/*v*), followed by reaction with Fmoc-Ala-OH or Fmoc-Ser(tBu)-OH or Fmoc-Asn(Trt)-OH, HBTU, and DIPEA gave resin-bound **4.19**-**4.21** respectively. Fmoc deprotection of resin-bound **4.19**-**4.21** with a solution of piperidine in DMF (20% *v*/*v*) and then coupling of the free primary amines with carboxylic acid **3.30** (synthesis described in chapter 3, section 3.2.1.3) using HATU and DIPEA gave resin-bound **4.22**-**4.24** respectively. Compounds were cleaved from the trityl resins by treating resin-bound **4.22**-**4.24** with TFA. Peptide linker conjugates **4.25**-**4.27**

thus obtained were purified using semi-preparative RP-HPLC and then reacted with acetic anhydride in separate reactions to give, Ala-Ser conjugate **4.06**, Ser-Ala conjugate **4.07** and, Asn-Ser conjugate **4.08** respectively.

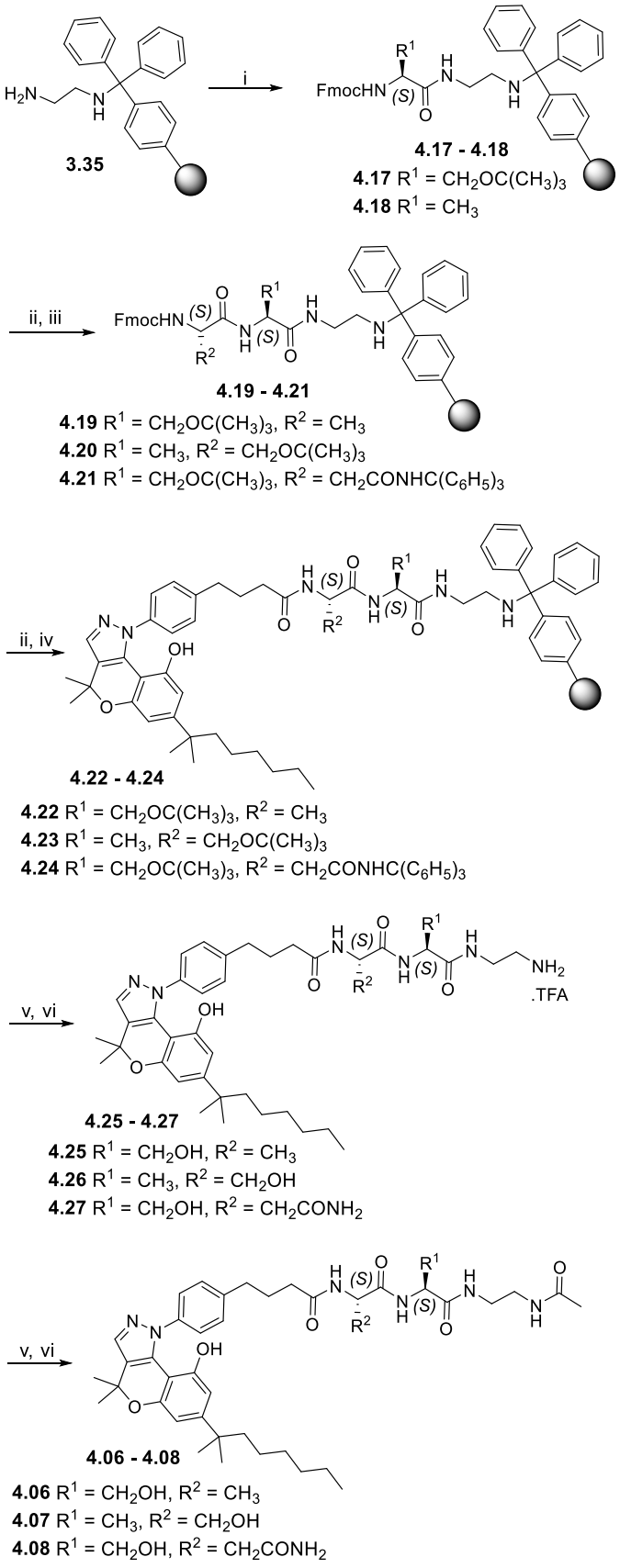

3.35

4.17 - 4.18

4.17 $R^1 = CH_2OC(CH_3)_3$

4.18 $R^1 = CH_3$

4.19 - 4.21

4.19 $R^1 = CH_2OC(CH_3)_3$, $R^2 = CH_3$

4.20 $R^1 = CH_3$, $R^2 = CH_2OC(CH_3)_3$

4.21 $R^1 = CH_2OC(CH_3)_3$, $R^2 = CH_2CONHC(C_6H_5)_3$

4.22 - 4.24

4.22 $R^1 = CH_2OC(CH_3)_3$, $R^2 = CH_3$

4.23 $R^1 = CH_3$, $R^2 = CH_2OC(CH_3)_3$

4.24 $R^1 = CH_2OC(CH_3)_3$, $R^2 = CH_2CONHC(C_6H_5)_3$

4.25 - 4.27

4.25 $R^1 = CH_2OH$, $R^2 = CH_3$

4.26 $R^1 = CH_3$, $R^2 = CH_2OH$

4.27 $R^1 = CH_2OH$, $R^2 = CH_2CONH_2$

4.06 - 4.08

4.06 $R^1 = CH_2OH$, $R^2 = CH_3$

4.07 $R^1 = CH_3$, $R^2 = CH_2OH$

4.08 $R^1 = CH_2OH$, $R^2 = CH_2CONH_2$

Scheme 4.6. (i) Fmoc-Ser(tBu)-OH or Fmoc-Ala-OH, HBTU, DIPEA, DMF (ii) Piperidine, DMF (iii) Fmoc-Ala-OH or Fmoc-Ser(tBu)-OH or Fmoc-Asn(Trt)-OH, HBTU, DIPEA, DMF (iv) **3.29**, HATU, DIPEA, DMF (v) TFA, DCM (vi) Ac_2O, Et_3N, $CHCl_3$, 30 - 67%.

4.2.3 Synthesis of pyridyl analogue of (3.22)

Synthesis of chromenopyrazole-linker conjugate **4.09** commenced with the preparation of hydrazine **4.29**, by reaction of commercially available aminopyridine **4.28** with $NaNO_2$, HCl (6 M aqueous solution) and $SnCl_2.2H_2O$ according to a previously reported literature synthesis[222] to give **4.29** (Scheme 4.7). Attempts to purify **4.29** from the crude reaction mixture (identified as present in the crude reaction mixture by ^{1}H NMR spectroscopy and HRMS) by acid-base work up or crystallisation proved futile. It was soon learnt that hydrazine **4.29** slowly degraded to a less polar compound (observed as a higher TLC R_f spot relative to **4.28**). The structure of this non-polar impurity could not be determined from the ^{1}H NMR spectrum and MS of the crude mixture also containing **4.29** and **4.28**. Therefore, the crude reaction mixture of **4.29** was condensed with β-ketoaldehyde **3.16** (synthesis described in chapter 3, section 3.2.1.1) to give nitrile **4.30**, which was reduced by $LiAlH_4$ to give benzylamine **4.31**. Reaction of **4.31** with carboxylic acid **3.13** (synthesis described in chapter 3, section 3.2.1.1) using HBTU as a coupling reagent and DIPEA as a base provided chromenopyrazole-linker conjugate **4.09** (Scheme 4.7).

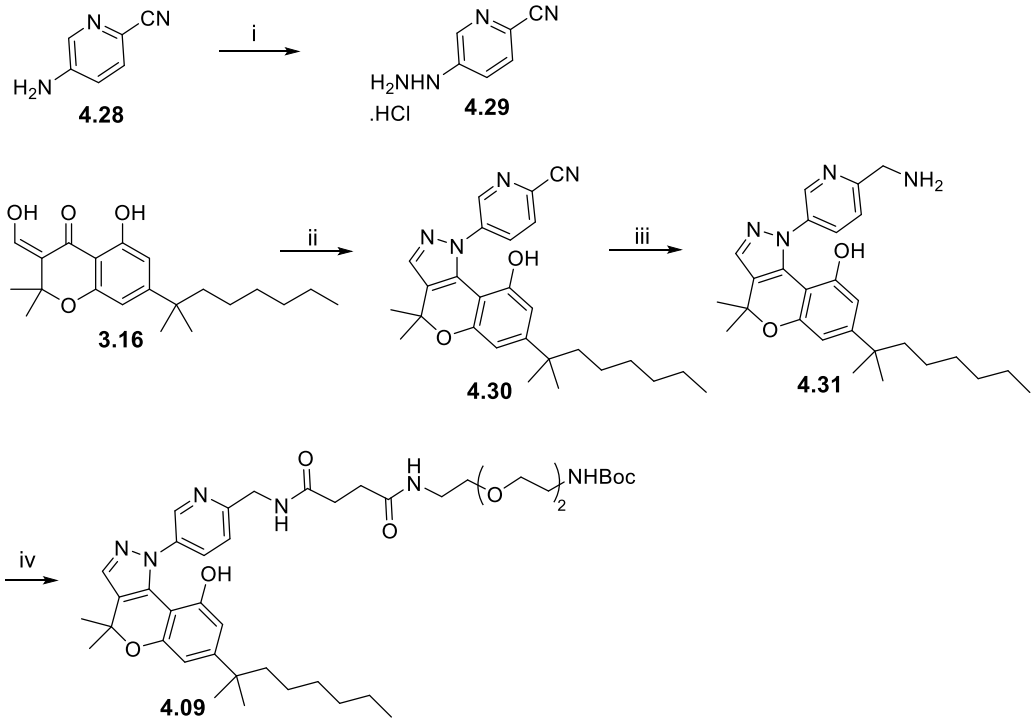

Scheme 4.7. (i) HCl, $NaNO_2$, $SnCl_2.2H_2O$, -10 °C to rt. (ii) **4.29**, MeOH, H_2SO_4, 70 °C, 86%. (iii) $LiAlH_4$, THF, 0°C to rt. (iv) **3.13**, **4.31**, HBTU, DIPEA, DMF, 46%.

4.3 Biological studies

4.3.1 Radioligand binding assays

The CB_2R affinity of second-generation chromenopyrazoles was determined using radioligand binding assays (as described in chapter 3, section 3.3.1) with the commonly used CBR radioligand [^{3}H]-CP55,940 and membrane preparations derived from HEK-293 cells transfected with either CB_1R or CB_2R according to a previously described method.[169, 212] Chromenopyrazoles (**4.01**-**4.09**) were initially screened in the competition radioligand binding assay at 10 µM to determine the percentage displacement of [^{3}H]-CP55,940 from CBRs (Figure 4.5, panels A and B). The chromenopyrazoles (**4.01**-**4.09**) which displaced [^{3}H]-CP55,940 from CBRs by more than 50% were then analysed in a concentration-dependent way to determine concentration response curves and calculate affinity (K_i).

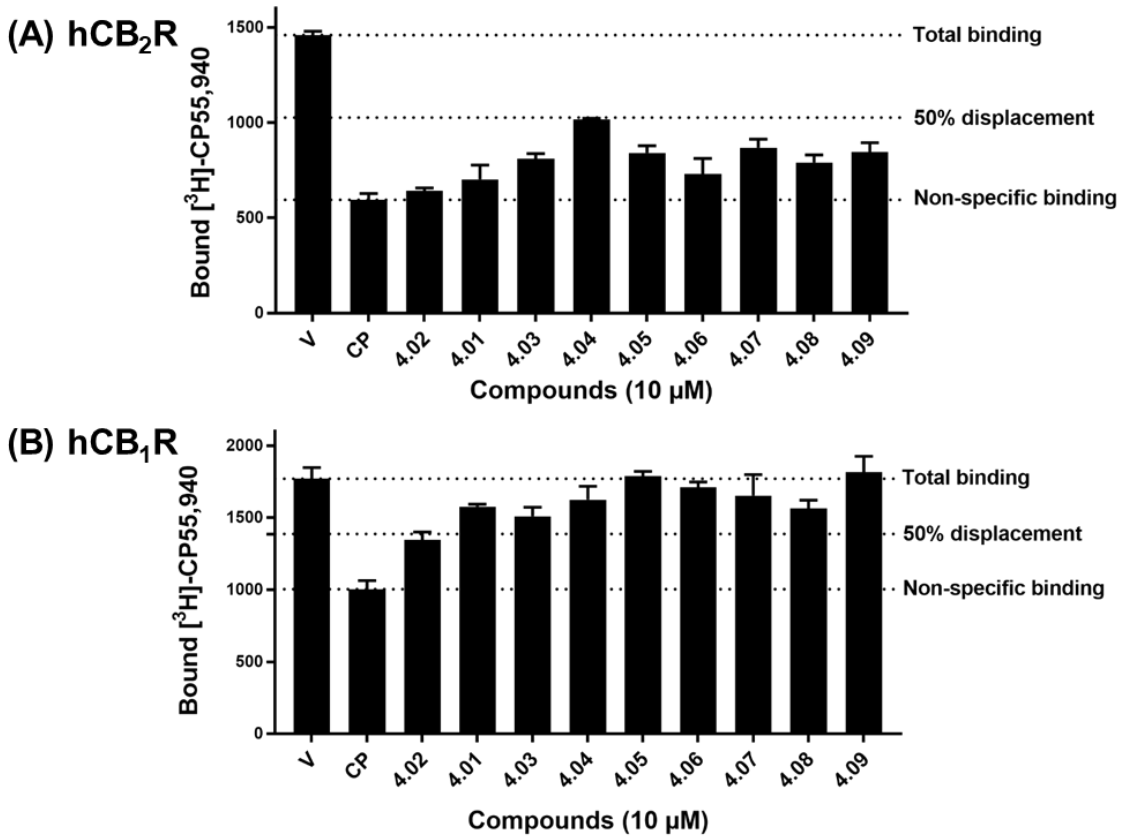

Figure 4.5. Radioligand binding assay: Screen of novel chromenopyrazoles at 10 µM at HEK-293 cells expressing hCB_2R (panel **A**) or hCB_1R (panel **B**), with [^{3}H]-CP55,940 as the radioligand. Data represented is from a single experiment carried out in triplicate and is expressed as mean ± SEM. V (vehicle), CP (CP55,940).

Pleasingly, BODIPY-FL-based fluorescent ligand **4.01** (K_i = 145.5 ± 11.8 nM at hCB_2R; Table 4.1) exhibited high affinity for CB_2R, which was fifteen-fold higher than analogous BODIPY-630/650 based fluorescent ligand **3.23** (K_i = 2312 ± 298nM at hCB_2R; Table 3.2, chapter 3).

Table 4.1. Radioligand binding affinity data for second-generation chromenopyrazoles

Compound	Structure		hCB_2R K_i (nM ± SEM)*	hCB_1R K_i (nM ± SEM)*	hCB_2R selectivity
4.01	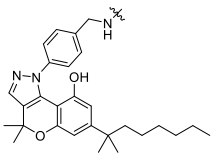	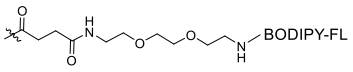	145.5 ± 11.8	> 1000	>6
4.02		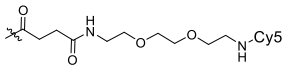	41.8 ± 4.5	5856 ± 1264	>140
4.03		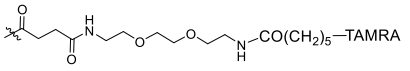	938.7 ± 127.9	> 1000	-
4.04		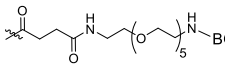	1730 ± 377.3	> 5000	>2
4.05			661.7 ± 59.1	> 5000	>7
4.06	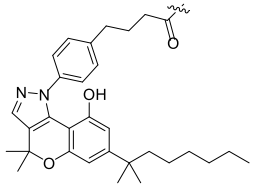	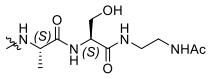	184 ± 37.8	> 1000	>5
4.07		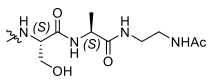	317.06 ± 55.9	> 1000	>3
4.08		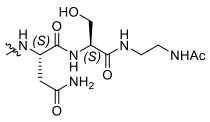	461.8 ± 18.5	> 1000	>2
4.09	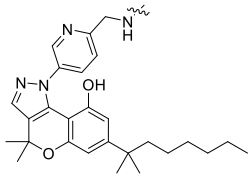	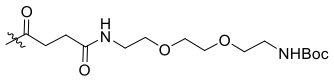	1600 ± 466.6	> 5000	>3

*Binding affinity (K_i) obtained by competition binding assay performed on membranes obtained from HEK-293 cells expressing hCB_2R or hCB_1R with [^{3}H]-CP55,940 as radioligand (K_d = 1.7 nM for hCB_2R and 3.0 nM for hCB_1R). All data is from at least three individual experiments performed in triplicate.

As both fluorescent ligands **4.01** and **3.23** contain similar chromenopyrazole-linker structures, the observed difference in the CB_2R affinities is likely due to the presence of different fluorophores. One possible reason for the higher CB_2R affinity of **4.01** compared to **3.23** might be the relatively smaller size of **4.01**. The fluorescent ligand **4.01**, owing to its smaller size, might be free from the steric clashes suffered by **3.23** with the CB_2R amino acid residues. Other possible reasons for the difference in the CB_2R affinities might

include the different CB_2R binding conformation of **4.01** compared to **3.23** or due to some favourable interactions of BODIPY-FL fluorophore with the CB_2R amino acids.

The Cy5 conjugate **4.02** (K_i = 41.8 ± 4.5 nM at hCB_2R; 5856 ± 1264 nM at hCB_1R) exhibited the highest affinity and selectivity for CB_2R over CB_1R among all the second-generation chromenopyrazoles (Figure 4.6, Table 4.1). This was an excellent result as **4.02**, despite containing a bulky fluorophore as in analogous BODIPY-630/650-based fluorescent ligand **3.23**, exhibited fifty-five fold higher affinity for CB_2R than **3.23**. The fluorescent ligand **4.02** also exhibited higher affinity and selectivity at CB_2R than any reported CB_2R fluorescent ligand (as of July 2018).[25, 155] Although both fluorescent ligands **4.02** and **3.23** contain bulky fluorophores, the higher affinity for CB_2R of **4.02** might be due to the different CB_2R binding conformation of Cy5-based fluorescent ligand **4.02**, free from steric clashes suffered by **3.23** conformation. However, similar to **4.01**, the high CB_2R affinity of **4.02** could also be a result of other possibilities such as favourable interactions of the Cy5 fluorophore with the CB_2R amino acid residues.

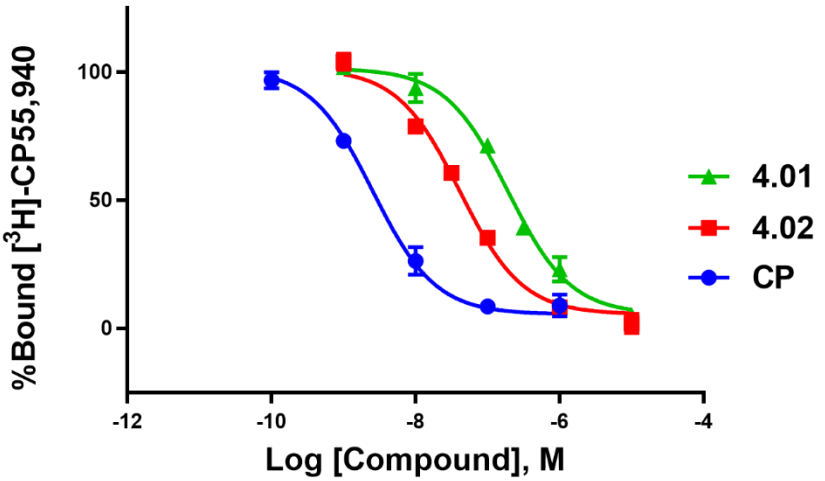

Figure 4.6. Competition binding curves for the highest affinity CB_2R fluorescent ligand **4.01**, **4.02**, and **CP** using radioligand [^{3}H]-CP55,940 (K_d = 1.7 nM for hCB_2R) at HEK-293 cells expressing hCB_2R. Data represented is from a single experiment carried in triplicate and is expressed as mean ± SEM.

The fluorophore Cy5 carries a net positive charge. The positive nitrogen could engage in specific ionic interactions with the acidic/anionic CB_2R amino acids (such as E2, E3, E8, D18, D24) likely to be present in the vicinity of methylamine linker as indicated by the

docking pose of structurally related chromenopyrazole **3.25** (chapter 3, section 3.4), which might contribute to the high affinity for CB_2R of **4.02**.

TAMRA-based fluorescent ligand **4.03** (K_i = 938.7 ± 127.9 nM at hCB_2R; Table 4.1) had moderate affinity for CB_2R, which was two times better than BODIPY-630/650-derivative **3.23**. This improvement in CB_2R affinity might be ascribed to the similar reasons described for **4.02** and **4.01**, that is due to the difference in the CB_2R binding conformation of **4.03** compared to **3.23** or due to some favourable interactions of TAMRA fluorophore with the CB_2R amino acid residues.

The fluorescent ligands, **4.04** and **4.05**, were prepared to evaluate the effect of the linker length (or more broadly the distance between fluorophore and ligand) on the CB_2R affinity of **3.23**. The BODIPY-630/650 derivative **4.04** (K_i = 1730 ± 377.3 nM at hCB_2R), a long linker analogue of **3.23**, exhibited a similar CB_2R affinity to **3.23**, revealing that increasing the **3.23** linker length did not improve CB_2R affinity.The short linker BODIPY-FL derivative **4.05** (K_i = 661.7 ± 59.1 nM at hCB_2R; Table 4.1) exhibited moderate affinity for CB_2R. The reduced CB_2R affinity of **4.05** compared to the longer-linker BODIPY-FL derivative **4.01** is likely due to the steric clashes of the **4.05**-BODIPY-FL fluorophore with the CB_2R amino acid residues. This result revealed that the linker present in **4.05** is not of sufficient length to provide enough separation between the BODIPY-FL fluorophore and the chromenopyrazole pharmacophore.

The new polar peptide linker conjugates (**4.06**, **4.07**, and **4.08**) exhibited high to moderate affinity for CB_2R (Table 4.1). The Ala-Ser linker conjugate **4.06** (K_i = 184 ± 37.8 nM at hCB_2R) exhibited higher affinity for CB_2R than Ser-Ala linker conjugate **4.07** (K_i = 317.06 ± 55.9 nM at hCB_2R) and Asn-Ser linker conjugate **4.08** (K_i = 461.8 ± 18.5 nM at hCB2R). The lower affinity for CB_2R of the new peptide linker conjugates (**4.06**, **4.07** and **4.08**) compared to lead Ala-Ala peptide linker conjugate **3.39** (K_i = 138.4 ± 6.75 nM at hCB_2R, Table 3.2, chapter 3) might be due to the presence of bulkier amino acid side chain residues on the ligand which may suffer from steric clashes with the CB_2R amino acid residues. These polar peptide linker conjugates (**4.06** (calculated logP (clogP) = 3.42)[‡], **4.07** (clogP = 3.42), and **4.08** (clogP = 1.94)) exhibit significantly higher polarity

[‡] cLogP was calculated using MarvinSketch (version 16.10) with ChemAxon calculation method using default settings.

compared to the commonly used literature CBR ligands, which are highly lipophilic, for example CP55,940 (clogP = 5.57), and therefore would be useful as chemical tools in CB_2R studies requiring a polar ligand.

The pyridyl chromenopyrazole **4.09** (K_i = 1600 ± 466.6 nM at hCB_2R, Table 4.1), designed to access the effect of a heteroatom near the pyrazole-*N*-phenyl substituent on CB_2R affinity, displayed twenty-two fold reduced affinity for CB_2R compared to the benzene analogue **3.22** (K_i = 71.1 ± 6.7 nM at hCB_2R, Table 3.2, chapter 3). This result showed that atoms near the pyrazole-*N*-phenyl substituent likely participate in important interactions with the CB_2R amino acid residues.

The docking studies of the second-generation fluorescent ligands (**4.01**-**4.05**) and the chromenopyrazole-linker conjugates (**4.06**-**4.09**) at CB_2R were not carried out. The presence of long linkers having multiple rotatable bonds coupled with difficulty in homology modelling of loop region amino acids (which likely play an extensive role in CB_2R binding with a large molecule such as a fluorescent ligand) make prediction of the CB_2R binding poses of these ligands challenging and not particularly accurate. It is likely that these fluorescent ligands and linker conjugates would occupy similar CB_2R binding pockets and bind in similar docking-poses as the ligand docking poses generated for chromenopyrazoles **3.25** and **3.29** respectively (chapter 3, section 3.4).

It was suggested in a previous literature report that the cannabinoid receptor ligands enter CBR via the lipid membrane.[219] It is likely that the ability of these chromenopyrazoles (shown in Table 4.1) to enter the lipid membrane would be affected by their polarity, charge, and molecular size and hence, these factors might also be important determinants of the chromenopyrazoles' CB_2R affinity of the.

4.3.2 cAMP Functional assays

The functional nature of second-generation chromenopyrazoles (**4.01**-**4.08**) at CB_2R was determined by cAMP BRET assay as described in chapter 1 (section 1.5.2) and chapter 3 (section 3.3.3), where the change in intracellular cAMP concentration was determined indirectly by a change in inverse BRET ratio (ratio of Rluc signal at 460 nm to YFP signal

at 535 nm). The functional nature of these chromenopyrazoles (**4.01**-**4.08**) was not determined at CB_1R due to the low affinity for CB_1R (Table 4.1).

Functional determination of the fluorescent ligands (**4.01**-**4.05**) proved challenging as the fluorescence of these ligands changed the inverse BRET ratio of the cAMP BRET assay components including that of the vehicle (used as a negative control) (fluorescence interference in the cAMP assay conduced at WT HEK-293 cells shown in Appendix, Figure A.11). The initial screen of (**4.01**-**4.05**) was carried out at 10 µM concentration at CB_2R expressing HEK-293 cells or at WT HEK-293 cells. It was hoped that for the high affinity CB_2R fluorescent ligands (**4.01** and **4.02**), a lower concentration (1 or 3 µM) would not interfere with the inverse BRET ratio but would be sufficient to produce a significant response in the cAMP BRET assay.

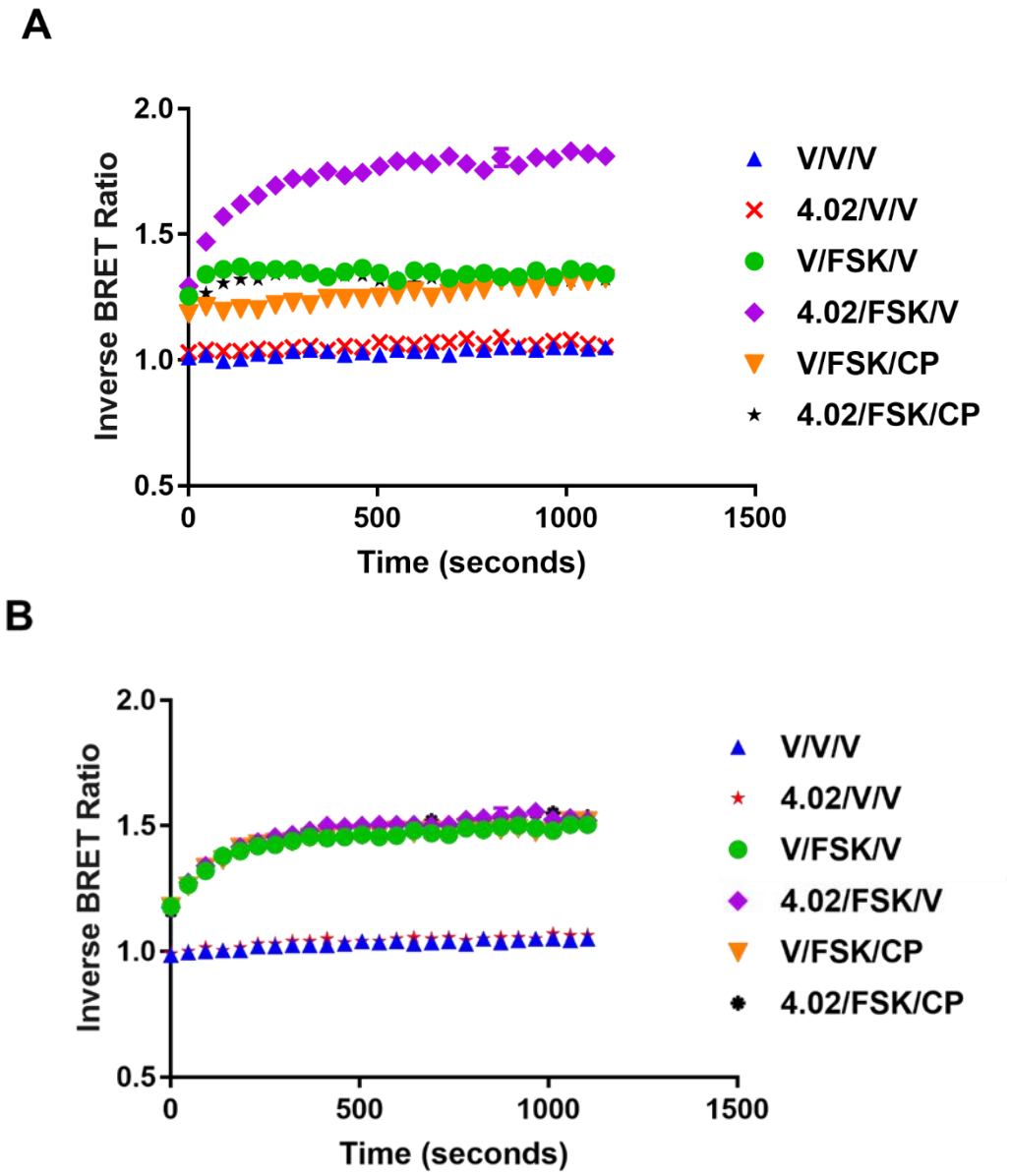

Figure 4.7. The highest affinity CB_2R fluorescent ligand **4.02** (1 µM) screened in a cAMP BRET assay: (**A**) cAMP BRET assay of **4.02** at HEK-293 cells stably expressing hCB_2R. (**B**) cAMP BRET assay of **4.02** at WT HEK-293 cells. Data is representative of a single experiment carried in duplicate and is expressed as mean ± SEM. Literature agonist CP (CP55,940), FSK (Forskolin), V (vehicle).

The fluorescent ligand **4.02** at 1 µM (Figure 4.7, panel A and B, Table 4.3) did not change the inverse BRET ratio of either the vehicle controls or any other cAMP BRET assay reaction components while a minimal change was observed when **4.02** was tested at 3 µM concentration (Figure 4.8 panel, A and B). The fluorescent ligand **4.02** (1 µM or 3 µM) increased the intracellular cAMP concentration at CB_2R expressing HEK-293 cells thus showing that **4.02** behaves as an inverse agonist (Figures 4.7 and Figure 4.8). The fluorescent inverse agonist **4.02** exhibited higher potency and efficacy (IC_{50} = 142.0 ±

13.1 nM; Emax = 196.7 ± 9.11 % of forskolin response at hCB_2R, Table 4.2) than the commonly used selective CB_2R inverse agonist SR144528 (IC_{50} = 536.1 ± 72.4 nM; Emax = 148.3 ± 14.17 % of forskolin response at hCB_2R - values obtained in this thesis and in agreement with a recent literature report[155]). The fluorescent ligand **4.02** is the first high affinity CB_2R fluorescent ligand for which functional data has been reported (as of July 2018).[25, 155]

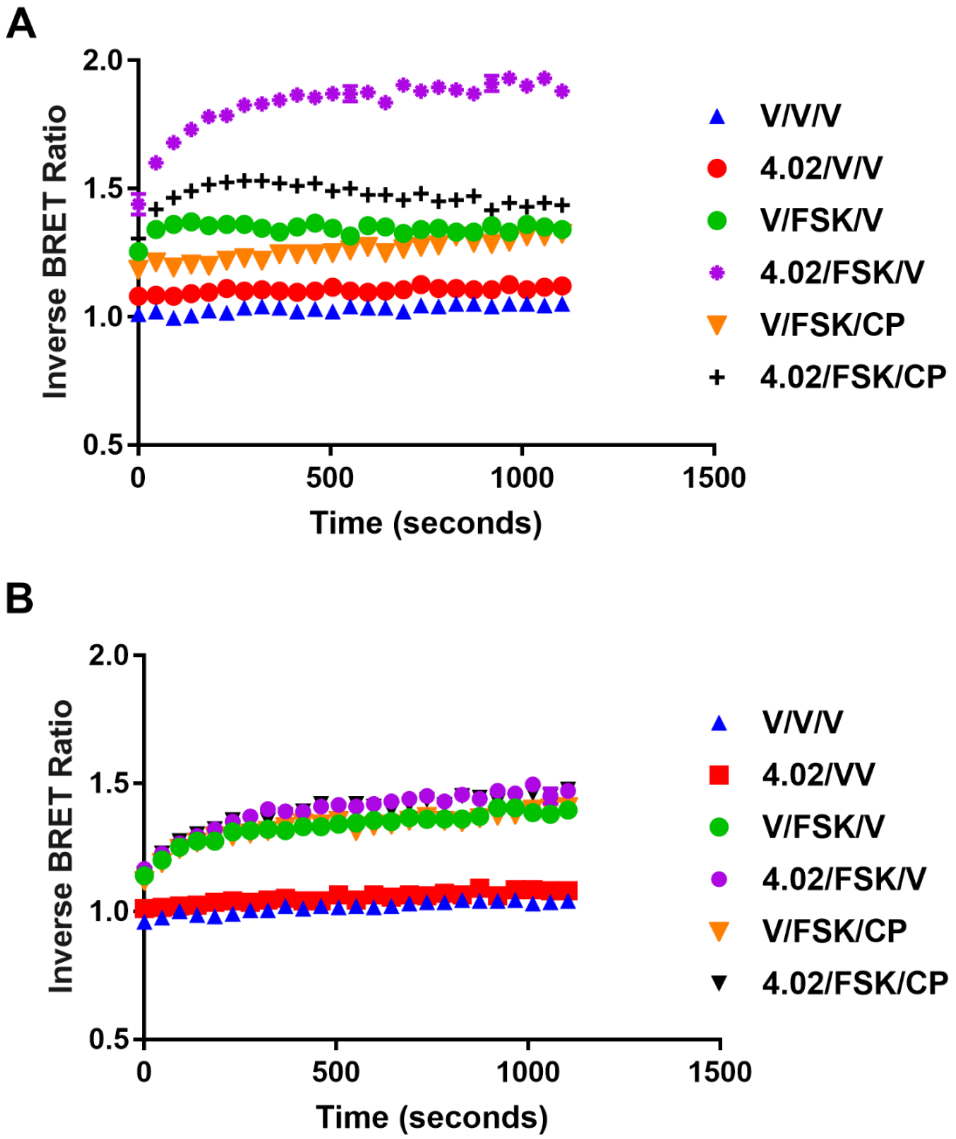

Figure 4.8. The highest affinity CB_2R fluorescent ligand **4.02** (3 μM) screened in a cAMP BRET assay: (**A**) cAMP BRET assay of **4.02** at HEK-293 cells stably expressing hCB_2R. (**B**) cAMP BRET assay of **4.02** at WT HEK-293 cells. Data is representative of a single experiment carried in duplicate and is expressed as mean ± SEM. A minimal change was observed in the inverse BRET ratio of the cAMP BRET assay reaction components. CP (CP55,940), FSK (Forskolin), V (vehicle).

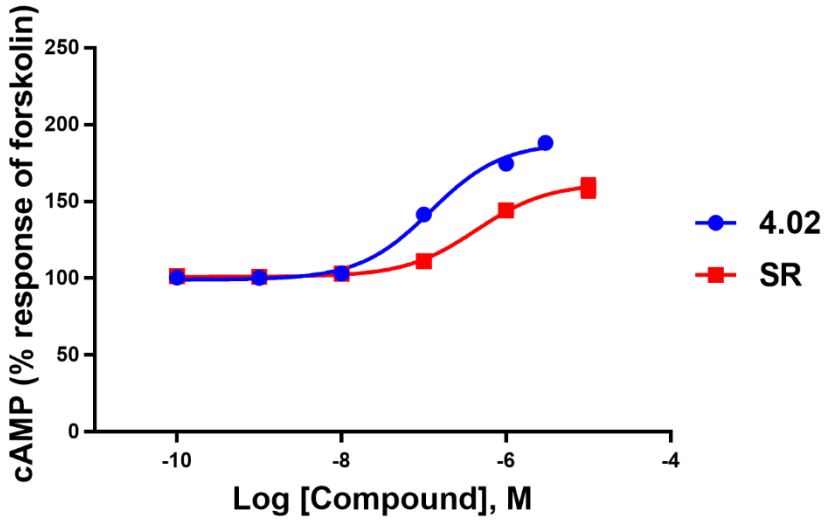

Figure 4.9. Concentration-response curve for the highest affinity CB_2R fluorescent ligand **4.02** and literature CBR inverse agonist SR (SR144528) using HEK-293 cells stably expressing hCB_2R. All data is from at least three individual experiments performed and is expressed as mean ± SEM. Raw data is normalised to forskolin response (100 %) and vehicle response (0 %).

Unfortunately, the fluorescent ligand **4.01** at 1 µM did not produce any significant response in the cAMP BRET assay and at 3 µM, a significant change in the inverse BRET ratio of the cAMP BRET assay reaction components due to the fluorescence of **4.01** was observed (data for cAMP BERT assay carried out for **4.01** (1 µM and 3 µM) shown in Appendix, Figure A.12). Consequently, the functional nature of **4.01** could not be determined by this cAMP BRET assay. The fluorescent ligand **4.01** produces a large change in the inverse BRET ratio in the cAMP BRET assay as BODIPY-FL excitation and emission (excitation 460 nM, emission 535 nM) falls in the same range as the BRET signal (Rluc signal at 460 nm and YFP signal at 535 nm) in the cAMP assay. Interestingly, the BRET assay data for another BODIPY-FL fluorescent ligand **4.05** does not show significant change in the BRET ratio of cAMP BRET assay reaction components (shown in Appendix, Figure A.11, panel E). However, considering the large interference observed for **4.01** and the fact that BODIPY-FL fluorescence spectra falls in the cAMP BRET assay signal range, it is likely that the magnitude of the fluorescence interference produced by **4.05** is reduced by some unclear mechanisms.

Fluorescent ligand **4.03** (excitation 565 nM, emission 580 nM) also has excitation and emission in a similar range as to cAMP assay signal, and again interference was observed in the cAMP BRET assay. In contrast, fluorescent ligands **4.02** (excitation 646 nM,

emission 662 nM) and **4.04** (excitation 630 nM, emission 650 nM) do not exhibit excitation and emission in the cAMP BRET assay signal range (Figure A.11, panel C). Nevertheless, a significant fluorescence interference was observed in the cAMP assay with **4.02** and **4.04** at 10 μM (shown in Appendix, Figure A.11, panel B and panel D). In future studies, the functional nature of **4.01** and **4.03** - **4.05** could be determined by non-fluorescence based functional assays such as a [^{35}S]GTPγS assay.

All of the newly synthesised polar peptide chromenopyrazole conjugates (**4.06**-**4.08**) behaved as agonists at CB_2R. None of the peptide conjugates (**4.06**-**4.08**, at 10 μM) showed a response significantly different from forskolin in the cAMP BRET assay at WT HEK-293 cells (Table 4.3) and thus did not exhibit CB_2R independent cAMP effects. The Asn-Ser peptide linker conjugate **4.08** (EC_{50} = 44.1 ± 5.0 nM; E_{max} = 73.27 ± 1.21 % of forskolin response at hCB_2R) exhibited lower potency and efficacy than Ala-Ser peptide linker conjugate **4.06** (EC_{50} = 32.7 ± 2.9 nM; E_{max} = 55.96 ± 1.07 % of forskolin response at hCB_2R) and Ser-Ala peptide linker conjugate **4.07** (EC_{50} = 23.7 ± 3.2 nM; E_{max} = 61.55 ± 3.51 % of forskolin response at hCB_2R; Table 4.2). Although all three new peptide linker conjugates (**4.06**-**4.08**) were less potent than Ala-Ala-conjugate **3.39** (EC_{50} = 17.3 ± 5.3 nM at hCB_2R; chapter 3, Table 3.3), the Ala-Ser peptide linker conjugate **4.06** (E_{max} = 55.96 ± 1.07 % of forskolin response at hCB_2R) showed higher efficacy than **3.39** (E_{max} = 61.2 ± 1.53 nM % of forskolin response at hCB_2R; chapter 3, Table 3.3).

It is difficult to rationalise the complex role of conformational changes, lipophilicity, steric bulk, and hydrogen bonding to explain the trends in the CB_2R potency and efficacy of the peptide linker conjugates (**3.39**, **4.06**-**4.08**). In the cAMP BRET assay carried out in this thesis, all of the tested novel chromenopyrazoles (**3.22**, **3.25**, **3.29**, **3.31**, **3.47** including peptide conjugates **3.39**, **4.06**-**4.08**) described in this chapter or chapter 3 behaved as CB_2R agonists, however, the highest affinity CB_2R fluorescent ligand **4.02** behaved as an inverse agonist. Perhaps an appreciable increase in the molecular size of a small sized agonist (for example **3.25** to **4.02**) might be partly responsible for the change in the functional nature of the ligand from agonist to inverse agonist.

Table 4.2. CB_2R functional data of the second-generation chromenopyrazoles

Compound	EC_{50} (nM± SEM)*	E_{max} (%FSK response ± SEM)#	Functional activity
4.02	142.0 ± 13.1[b]	196.7 ± 9.11	Inverse Agonist
4.06	32.7 ± 2.9[a]	55.96 ± 1.07	Agonist
4.07	23.7 ± 3.2[a]	61.55 ± 3.51	Agonist
4.08	44.1 ± 5.0[a]	73.27 ± 1.21	Agonist

*Potency (EC_{50}) and #efficacy (E_{max}) data for the chromenopyrazoles, obtained from cAMP BRET assay using HEK-293 cells expressing hCB_2R. All data is from at least three individual experiments performed, raw data is normalised to forskolin response (100 %) and vehicle response (0 %). [a] EC_{50} for agonists. [b] IC_{50} for inverse agonists.

The functional nature of novel chromenopyrazoles (**3.25**, **3.22**, **3.29**, **3.31**, **3.39**, **3.47**, **4.02**, **4.06**-**4.08**) in this thesis was determined by a cAMP BRET assay, other CBR signalling pathways such as activation of ERK, GIRK and recruitment of β-arrestin are yet to be investigated.

Table 4.3. % Response in cAMP BRET assay at wild type HEK-293 cells.

Compound	% FSK Response ± SEM*
4.02	102.99 ± 3.56
4.06	101.70 ± 1.77
4.07	105.86 ± 7.29
4.08	98.33 ± 3.73

*All compounds tested at (10 μM) in the cAMP BRET assay at WT HEK-293 cells except for **4.02** (tested at 1 μM). All data is from at least two individual experiments performed in duplicate, raw data is normalised to forskolin response (100 %) and vehicle response (0 %). A one-sample t-test was used to determine whether the % cAMP response of test compounds was significantly different from the forskolin only response.

4.3.3 Imaging studies

Widefield imaging experiments were carried out by collaborators at the University of Auckland to determine the suitability of highest affinity CB_2R fluorescent ligand **4.02** to visualise CB_2R at a single cell level in the CB_2R expressing HEK-293 cells. Pleasingly, the fluorescent ligand **4.02** exhibited clear cell surface labelling with no intracellular accumulation (Figure 4.10 – panel (A) and panel (D)). Yellow colour at the cell surface seen in panel (A) arises from colocalisation of **4.02** (red) and mouse anti-HA primary

antibody, Alexa 488-conjugated goat anti-mouse secondary antibody (green). CB_2R specific binding was evident since there was only a very low amount of **4.02** binding when the cells were co-incubated with SR144528 (30 µM, a selective CB_2R inverse agonist) (Figure 4.10 – panel (B) and panel (E)). Further CB_2R specific binding was shown by the very low **4.02** binding on incubation with HEK-293 cells transfected with an empty vector (Figure 4.10 – panel (C) and panel (F)). These studies show that **4.02** possess suitable properties for the imaging of CB_2R at the single cell level.

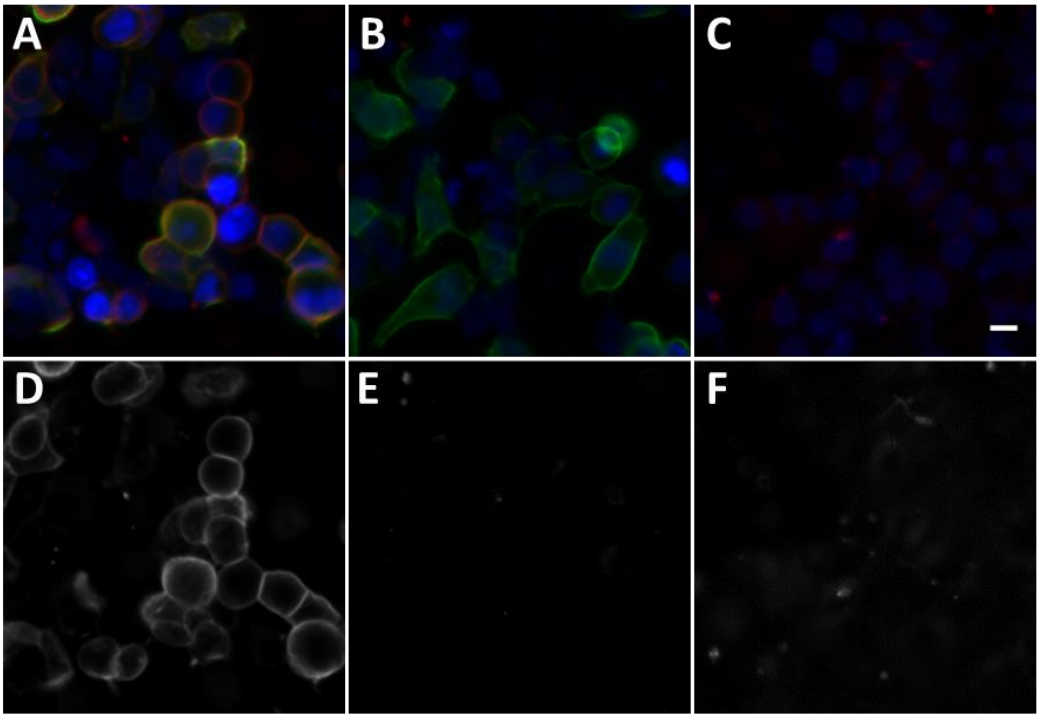

Figure 4.10. Widefield fluorescence microscopy imaging of **4.02** at HEK-293 cells expressing hCB_2R. (A) HEK-Flp cells transfected with pplss-HA-hCB_2R incubated for 2 min at rt with 1 µM of **4.02** (red). Mouse anti-HA primary antibody and Alexa 488-conjugated goat anti-mouse secondary antibody (green) were used to visualise hCB_2R, and Hoechst 33258 (blue) was used to visualise nucleus respectively. (B) – similar experiment as (A) except that cells were also co-incubated with 30 µM of SR144528 (a non-fluorescent, selective CB_2R inverse agonist. (C) – similar experiment as in (A) except that HEK-Flp WT cells transfected with an empty vector. (D), (E) and (F) are similar experiments as shown in (A), (B) and (C) respectively except that cells were incubated for 2 min at rt with 1 µM of **4.02** and no Hoechst 33258 stain or antibodies were used and images shown in black/white colour. Data was generated by the collaborators at the University of Auckland. Scale bar 10 µm.

4.4 Summary and conclusions

The second-generation fluorescent ligands (**4.01**-**4.05**, Table 4.1), based on the previously developed lead fluorescent ligand **3.23** (Table 3.2, chapter 3), were prepared with the aim of improving CB_2R affinity. The new fluorescent ligands were designed to contain similar chromenopyrazole-linker structures so that the CB_2R affinity of different fluorescent ligands could be directly correlated with the different fluorophores. Three new polar peptide linker analogues containing polar amino acids serine and asparagine (**4.06**-**4.08**, Table 4.1), following on from peptide linker conjugate **3.39** (Table 3.2, chapter 3), were also prepared. A pyridyl derivative **4.09** (Table 4.1) of **3.22** was also prepared with the aim of interrogating the importance of atoms near the pyrazole-*N*-phenyl substituent in CB_2R binding.

All of the new chromenopyrazoles were then evaluated for CBR affinity using a radioligand competition-binding assay. Similar to the CBR affinity trends observed in chapter 3 (section 3.3.2, chapter 3), most of the chromenopyrazoles (**4.01**-**4.09**, Table 4.1) displayed higher affinity for CB_2R and selectivity over CB_1R (Table 4.1). Delightfully, the Cy5-based fluorescent ligand **4.02** (K_i = 41.8 ± 4.5 nM at hCB_2R; 5856 ± 1264 nM at hCB_1R, Table 4.1) and BODIPY-FL-based fluorescent ligand **4.01** (K_i = 145.5 ± 11.8 nM at hCB_2R; > 1000 nM at hCB_1R, Table 4.1) displayed high affinity for CB_2R and selectivity over CB_1R. Three moderate affinity CB_2R fluorescent ligands (**4.03**, **4.04, 4.05**; Table 4.1) were also prepared. New polar peptide linker conjugates (**4.06**-**4.08**, Table 4.1) showed high to moderate affinity for CB_2R and selectivity over CB_1R. Chromenopyrazole **4.09** (Table 4.1), pyridyl analogue of **3.22**, showed twenty two-fold reduced CB_2R affinity compared to **3.22**.

The highest affinity CB_2R fluorescent ligand **4.02** (EC_{50} = 142.0 ± 13.1 nM; E_{max} = 196.7 ± 9.11 % of forskolin response at hCB_2R) behaved as an inverse agonist in the cAMP functional assay (Table 4.2). Importantly, all of the new polar peptide linker conjugates (**4.06**, **4.07**, and **4.08**; Table 4.1) behaved as agonists in the cAMP BRET assay. These polar peptide linker agonists would be useful in CB_2R studies requiring a polar ligand, for example in receptor trafficking studies. The peptide linker conjugate **4.06** (E_{max} =

55.96 ± 1.07) exhibited the highest efficacy and peptide linker conjugate **4.07** (EC_{50} = 23.7 ± 3.2 nM) exhibited the highest potency.

The highest affinity CB_2R fluorescent ligand **4.02** (Table 4.1) was evaluated in widefield imaging experiments by collaborators and showed CB_2R specific binding (Figure 4.10). The aim of developing a high affinity CB_2R fluorescent ligand with suitable properties for imaging CB_2R was therefore achieved.

4.5 Future directions

The highest affinity CB_2R fluorescent ligand **4.02** is currently being used for studying CB_2R pharmacology via widefield imaging experiments. Another high affinity CB_2R fluorescent ligand **4.01** containing different fluorophore and with different molecular charge compared to **4.02** will be evaluated in various imaging and pharmacological assays.

Fluorescent ligand **4.02** behaved as an inverse agonist at CB_2R in the cAMP assay, however, the functional nature of the other fluorescent ligands (**4.01**, **4.03**-**4.05**) could not be determined due to the fluorescence interference. Determination of the functional nature of the fluorescent ligands (**4.01**-**4.05**) ideally via a non-fluorescence based assay and in various CB_2R signalling pathways (for example activation of ERK, GIRK, and recruitment of β-arrestin) could be carried out. CB_2R chromenopyrazole agonists (**3.22**, **3.25**, **3.29**, **3.31**, **3.39**, **3.47**) are promising leads for developing a fluorescent CB_2R agonist.

As can be seen from the CB_2R affinities of the fluorescent ligands reported in this chapter (Table 4.1), fluorophores exert a huge influence on the CB_2R affinity. Hence, preparation of new fluorophore conjugates including a sulphonic acid derivative of Cy5 would be an attractive strategy to improve the polarity of the fluorescent ligand.

Synthesis of the chromenopyrazole-linker conjugates containing linkers of different length and new peptide-linker conjugates can be made to improve the polarity and CB_2R affinity. The peptide linker analogues of only high CB_2R affinity chromenopyrazole **3.29**

(chapter 3, Table 3.2) were prepared in this thesis, however, the peptide analogues of the highest CB_2R affinity chromenopyrazole-linker conjugate **3.22** (chapter 3, Table 3.2) remain to be explored. A polar peptide chromenopyrazole-linker conjugate would be useful tool to study CB_2R trafficking. The polar peptide chromenopyrazoles could also be conjugated with different fluorophores for the development of CB_2R fluorescent ligands.

Chapter 5 Development of pyridyl derivatives as fluorescent ligands for cannabinoid type 1 receptor

5.1 Design rationale for pyridyl-2-carboxamide-based fluorescent ligands

Most of the chromenopyrazoles designed as CB_1R agonists in chapter 3 of this thesis did not exhibit high affinity for CB_1R. In this chapter, pyridyl derivatives were investigated as a new series for development into CB_1R fluorescent agonists.

Researchers at AstraZeneca reported pyridyl derivatives as high affinity CB_1R agonists.[223-224] Representative examples of these pyridyl derivatives, including those on which the design rationale was based, are shown in Table 5.1. The lead compound **5.1** of this pyridyl series was identified by screening a GPCR compound library. Efforts to improve the CB_1R affinity by substitution of the 'core' phenyl ring of **5.1** with a pyridyl ring led to pyridyl-2-carboxamide **5.2** with high affinity for CB_1R and reduced lipophilicity.

Further optimisation of **5.2** was carried out by the researchers at AstraZeneca to identify a number of high affinity CB_1R agonists.[223-224] The SAR studies of these pyridyl-2-carboxamides (including **5.3**-**5.7**) revealed that aromatic moieties including naphthalene with a polar triazoline group or quinoline at the C-3 position of the pyridine were well tolerated at CB_1R (Table 5.1). These pyridyl-2-carboxamides (**5.3**-**5.7**) with cyclic aliphatic moieties such as cyclobutylmethyl at the C-2 position of the pyridine exhibited high affinity for CB_1R (Table 5.1). Importantly, these pyridyl-2-carboxamides tolerated bulky/long substituents at the C-6 position of the pyridine, for example compound **5.4** and **5.7**, indicating potential for the tolerance of a bulky/long linker in this position (Table 5.1). The high affinity for CB_1R (and selectivity over CB_2R) of these pyridyl-2-carboxamides, tolerance of the bulky/long substituents, favourable polarity, and presence of aromatic hydroxyl, amide functional groups (for the introduction of linkers) made these ligands attractive scaffolds for the development of CB_1R fluorescent ligands.

Table 5.1. Previously reported phenyl/pyridyl carboxamide CBR ligands[137, 202-203, 205]

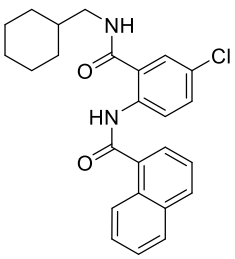

5.1

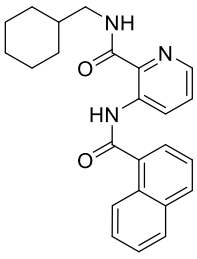

5.2

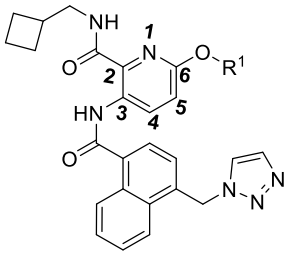

5.3-5.4

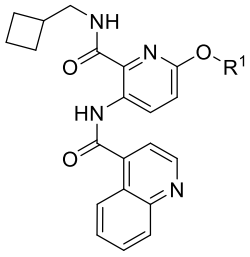

5.5-5.7

	R^1	IC_{50} or K_i hCB_1R (nM)*	IC_{50} or K_i hCB_2R (nM)*	*Ref*
5.1	-	160[a]	1800[a]	223
5.2	-	10[a]	110[a]	223
5.3	CH_3	0.97[a]	ND[a]	223
5.4	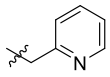	3.2[b]	Not reported	224
5.5	H	28[a]	82[a]	223
5.6	CH_3	15[a]	100[a]	223
5.7	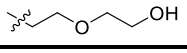	10[a]	1200[a]	223

*Binding affinity (K_i or IC_{50}) obtained by competition binding assay performed on membranes obtained from HEK-293 cells expressing hCB_1R or Sf9 cells expressing hCB_2R with [^{3}H]-CP55,940 as radioligand. [a]IC_{50}, [b]K_i

Computational studies were used to further evaluate the suitability of the C-6 position for the introduction of long linkers to the pyridyl-2-carboxamides in this thesis. As the pyridyl-2-carboxamides (**5.2-5.7**) were reported as CB_1R agonists (determined by a [^{35}S]GTPγS assay at HEK-293 cells expressing canine cannabinoid type 1 receptor (cCB_1R)[223]), the active state structure of CB_1R (PDB ID: 5XRA) published by Hua *et al.*[113] was used for the ligand docking studies.

The pyridyl-2-carboxamides (including **5.2-5.7**) contain a flexible 'core' of pyridine with 2-carboxamide and 3-aminocarbonyl substituents. It was reported previously that these pyridyl-2-carboxamides (including **5.2-5.7** in Table 5.1) likely bind to CB_1R in a planar conformation, which exists due to the presence of an intramolecular hydrogen bond between NH of the 2-carboxamide moiety and nitrogen of the pyridine.[223] This assumption was based on a marked higher affinity for CB_1R of **5.2-5.7** relative to **5.1** and other pyridyl or pyrazinyl isomers[223] (structures not shown) which lacked the heteroaromatic nitrogen α to the 2-carboxamide moiety (necessary for the formation of

the intramolecular hydrogen bond to obtain the planar conformation). A hydrogen bond was observed in this thesis (discussed in section 5.2.2) between NH of 3-aminocarbonyl moiety and oxygen of 2-carboxamide moiety in the new pyridyl-2-carboxamides (**5.3**, **5.30**-**5.35**, **5.37**-**5.39**, **5.49**-**5.52** and **5.54**; synthesis described in section 5.2.2, 5.2.3, 5.2.4, 5.2.5 and 5.2.6).

So, before commencing CB_1R docking studies, a conformational search for the highest affinity CB_1R literature pyridyl-2-carboxamide **5.3** (used as a model compound for the CB_1R docking studies of pyridyl-2-carboxamides) was performed in MarvinSketch. [225] [224] [224] [224] The lowest energy conformation of **5.3** (a planar conformation) showed intramolecular hydrogen bonds between the pyridine nitrogen and NH of 2-carboxamide moiety and another between NH of 3-aminocarbonyl moiety, oxygen of the 2-carboxamide moiety (Figure 5.1 (A)).

Further, a search of three-dimensional structures similar to **5.3** with a pyridine substructure query (shown in Figure 5.2 (A)) was carried out using the Cambridge Structural Database[173] (searched using ConQuest), but did not provide any results. Another search with a benzene substructure query (shown in Figure 5.2 (B)) provided three compounds (CSD ID – ALUCAN,[226] CUCYAC,[227] and MUDKUT[228]), all of which showed an intramolecular hydrogen bond between NH of aminocarbonyl and oxygen of carboxamide moieties. However, in contrast to the lowest energy conformation obtained from MarvinSketch (Figure 5.1 (A)), the carboxamide and aminocarbonyl moieties were not planar in these known compounds. These differences might be because the compounds were benzene derivatives and not pyridine derivatives, as was **5.3 (**there is a hydrogen present in the benzene ring where the pyridyl nitrogen would be and thus causing a potential clash with the carboxamide NH). Based on the results obtained from MarvinSketch, CSD, and the previous report[223] of the pyridyl-2-carboxamides, it was decided to use the lowest energy conformation of **5.3** with selected rotatable bonds (bold bonds in Figure 5.1 (B)) restricted from the rotation in the CB_1R docking studies.

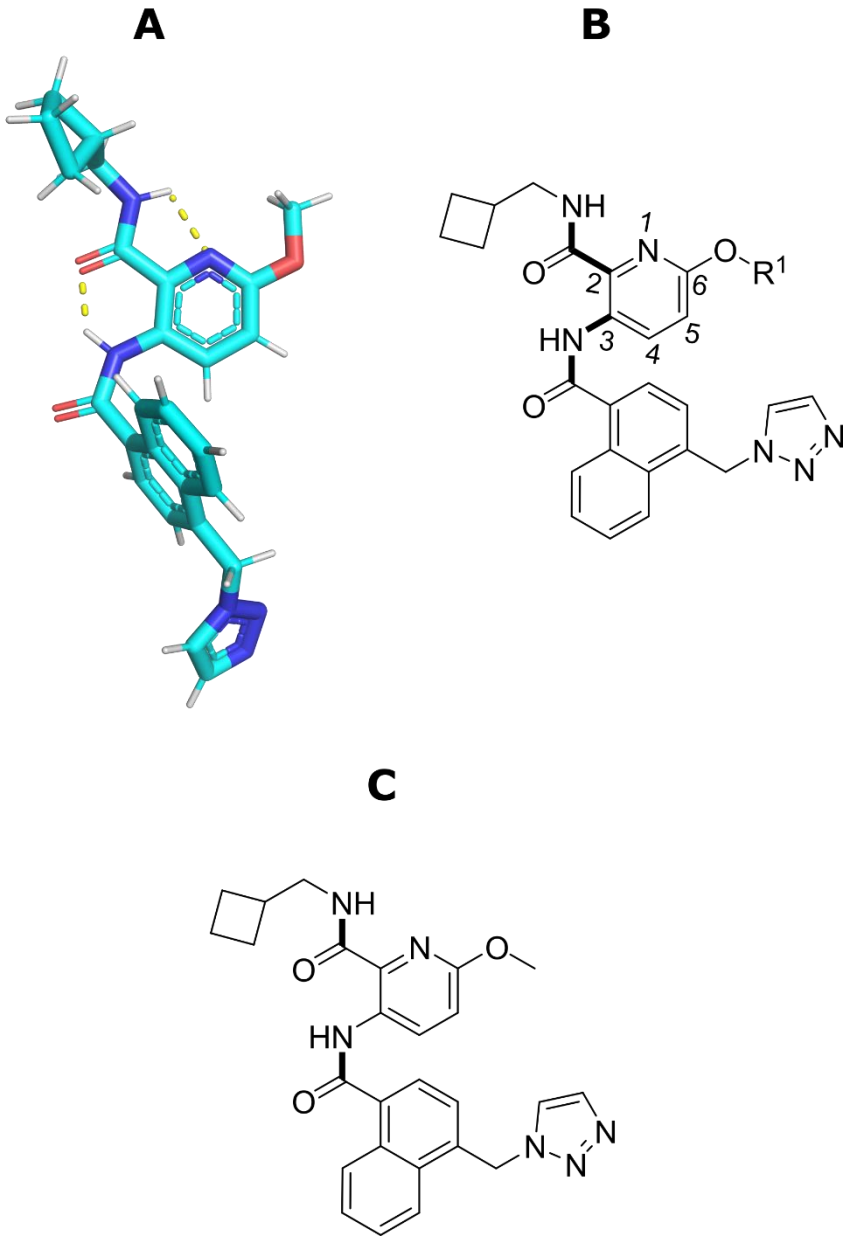

Figure 5.1. (**A**) The lowest energy conformation of **5.3** (obtained by a conformational search using MarvinSketch, [225 224 224 224] (cyan carbons, red oxygens, blue nitrogens, white hydrogens)). Hydrogen bonds are shown as yellow lines. (**B**) The selected bonds (bold) of **5.3** were fixed from the rotation in one of the CB_1R docking studies – shown in Figure 5.3. (**C**) Only amide bonds (bold) of **5.3** were fixed from the rotation in a second CB_1R docking study – shown in Figure 5.5.

GOLD[217] was used for the docking studies with the CB_1R binding site of the **5.3** defined as a 15 Å region around the CB_1R co-crystallised ligand AM11542 (PDB ID: 5XRA). The docking studies were carried out only with **5.3** as other designed analogous pyridyl-2-carboxamides (shown in Figure 5.6) were believed to bind CB_1R in similar docking poses. The docking poses of **5.3** were visualised with PyMOL.

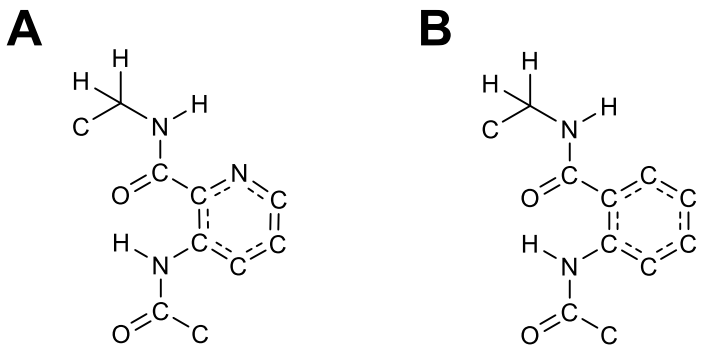

Figure 5.2. (A) Pyridine and **(B)** benzene – substructures queries used for search of compounds similar to pyridyl-2-carboxamide **5.3** in CSD with ConQuest.

The docking studies (carried out with rotation-restricted bonds of the lowest energy conformation of **5.3**; Figure 5.1 (B)) showed **5.3** to occupy a similar region in the CB_1R binding pocket (Figure 5.3) as was previously observed for AM11542 in the CB_1R crystal structure (PDB ID: 5XRA). A hydrogen bond was observed between AM11542 and S383 in the CB_1R crystal structure (PDB ID: 5XRA), however, no hydrogen bond(s) was observed between **5.3** and CB_1R amino acids in the docking studies carried out in this thesis. Previously, another CB_1R ligand AM6538 (PDB ID: 5TGZ) was observed to interact with CB_1R amino acids primarily by a number of aromatic and van der Waals interactions and a hydrogen bond interaction was not observed. In the docking studies of **5.3**, the aromatic interactions were observed between aromatic rings of **5.3** and F268, F379, W279, Y275, F200, F170, F174, F177, H178. van der Waals interactions were also observed between **5.3** and residues S173, K192, I267, I271, P269, L193, L359, M363, T275, L276, and V196 (Figure 5.3). The docking pose of **5.3** showed that the methoxy moiety was pointing towards a small cavity located between TM1 and TM7, near the extracellular *N*-terminal of CB_1R (Figure 5.3). The cyclobutylmethanamine moiety and triazoloylmethylnaphthalene moiety were buried in the TM region and appeared unsuitable for the introduction of linkers.

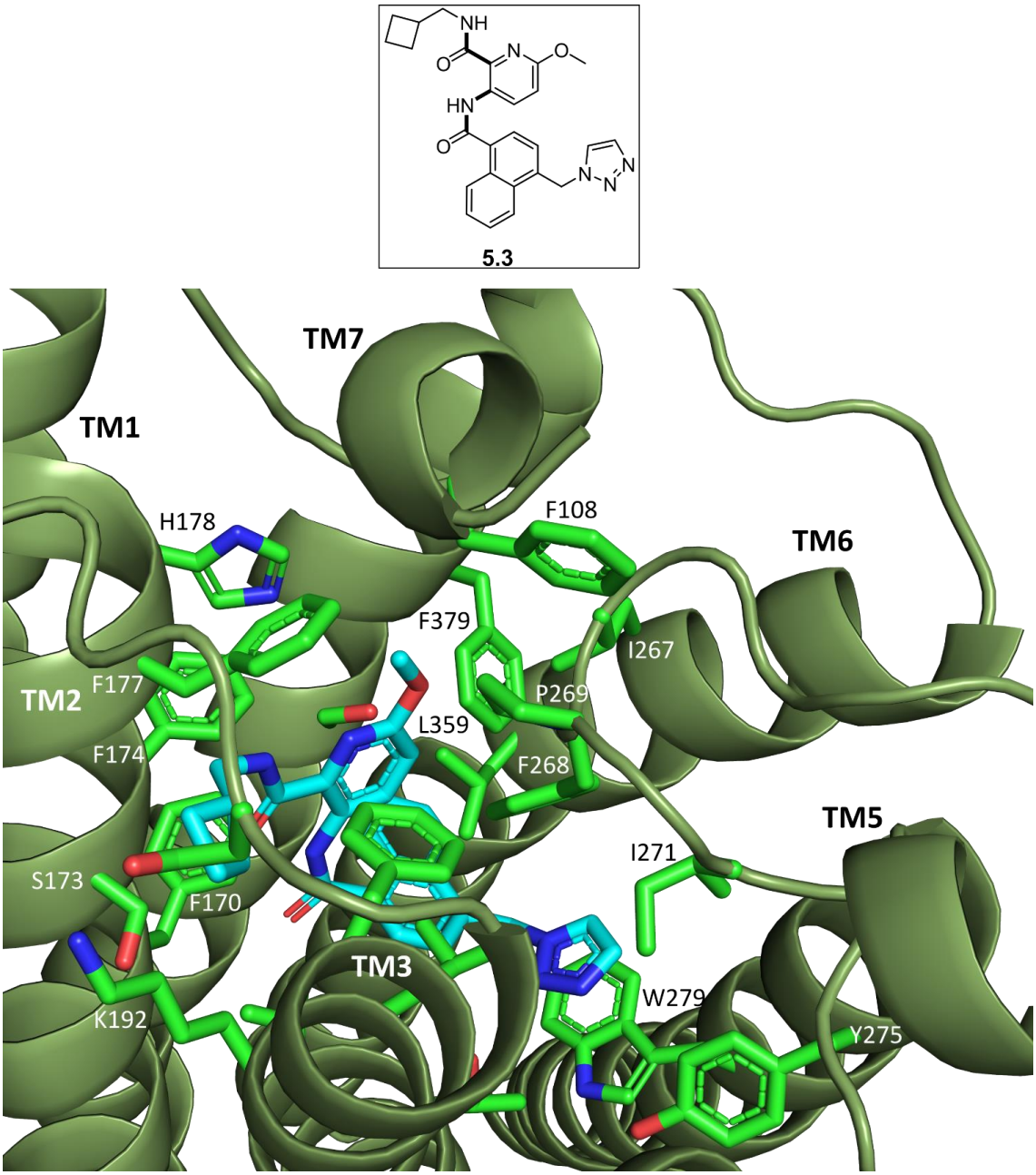

Figure 5.3. Docking pose of **5.3** (cyan carbons, red oxygens, blue nitrogens) in the CB_1R crystal structure (PDB ID: 5XRA; forest green ribbon). Side chain residues forming hydrophobic interactions with **5.3** are shown as sticks (leaf green). Docking carried out with restricting rotation of the selected bonds of the lowest energy conformation of **5.3** (bold bonds in structure shown in rectangle)

Docking studies were also carried out without restricting rotation of the bonds of **5.3** (lowest energy conformation; Figure 5.1 (A)) and showed the triazoloylmethylnaphthalene moiety (particularly the unsubstituted naphthyl ring atoms) as the most promising position for the introduction of linkers (Figure 5.4). In these docking studies carried out without rotation-restricting the bonds of **5.3** (lowest energy

conformation; Figure 5.1 (A)), GOLD changed the conformation of the amide bond (the amide bond between naphthyl moiety and C-3 pyridine; Figure 5.1(A)) of **5.3** from *cis* to *trans* during the ligand initialisation stage, before commencing the actual docking run.

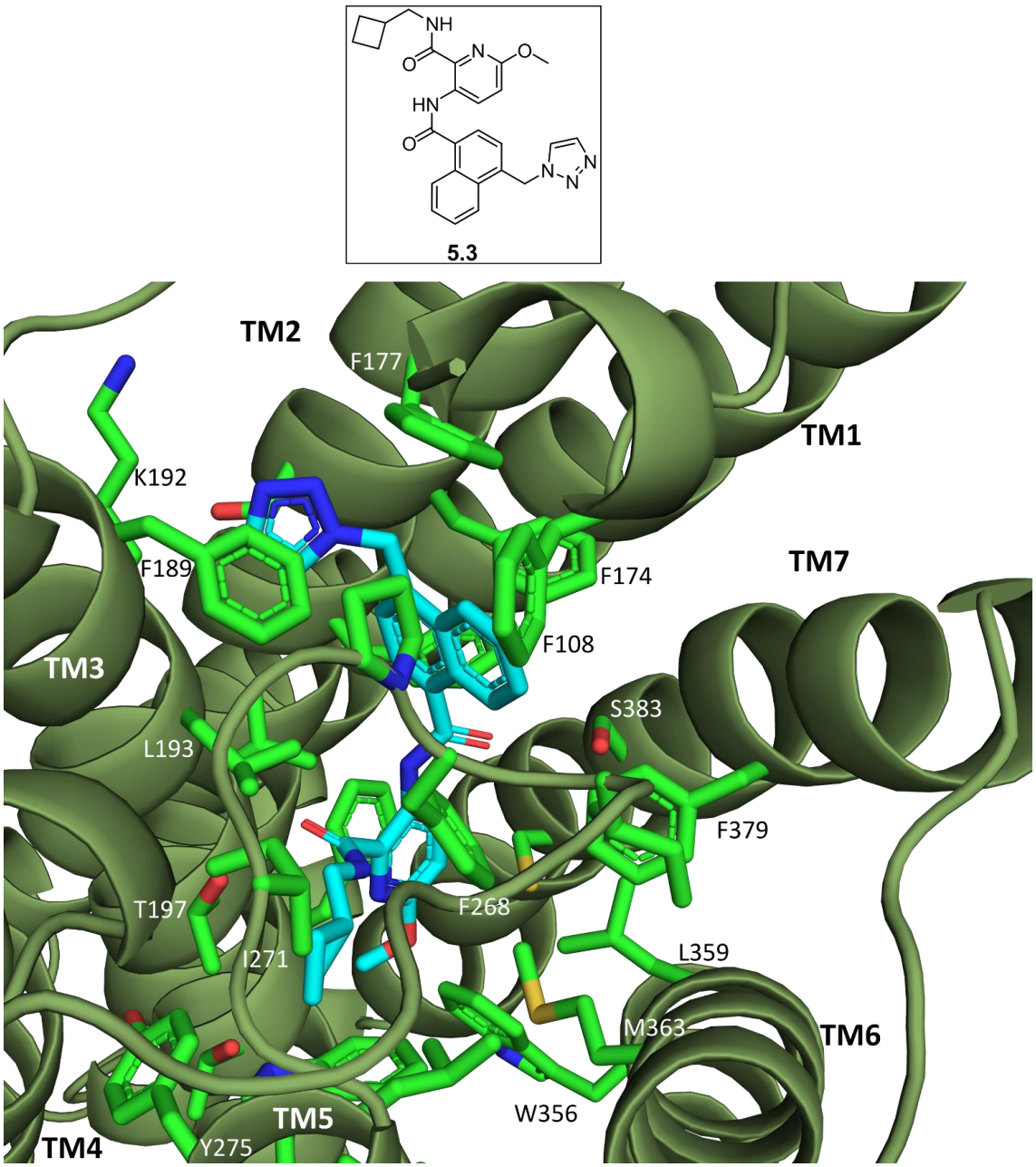

Figure 5.4. Docking pose of **5.3** (cyan carbons, red oxygens, blue nitrogens) in the CB_1R crystal structure (PDB ID: 5XRA; forest green ribbon). Side chain residues forming hydrophobic interactions with **5.3** are shown as sticks (leaf green). Docking study was carried out without restricting rotation of the amide bonds of the lowest energy conformation of **5.3** (structure shown in Figure 5.1 (A); structure also shown in rectangle). The amide bond between naphthyl moiety and C-3 pyridine of **5.3** was flipped from *cis* to *trans* during the ligand initialisation stage.

It was decided to carry out another docking study with the conformation of amide bonds preserved (by restricting rotation of only amide bonds (bold bonds) shown in Figure 5.1 (C)) (docking pose shown in Figure 5.5). Docking studies carried out with restricted-rotation of only amide bonds, rotation of the single bond connecting C-2 and the 2-carboxamide carbon caused the movement of 2-carboxamide moiety such that the intramolecular hydrogen bonds observed in the lowest energy conformation of **5.3** (Figure 5.1 (A)) were not feasible. These docking studies with restricted-rotation of only amide bonds showed the methoxy moiety as the most promising position for the introduction of linkers (Figure 5.5; as was also observed for docking studies shown in Figure 5.3).

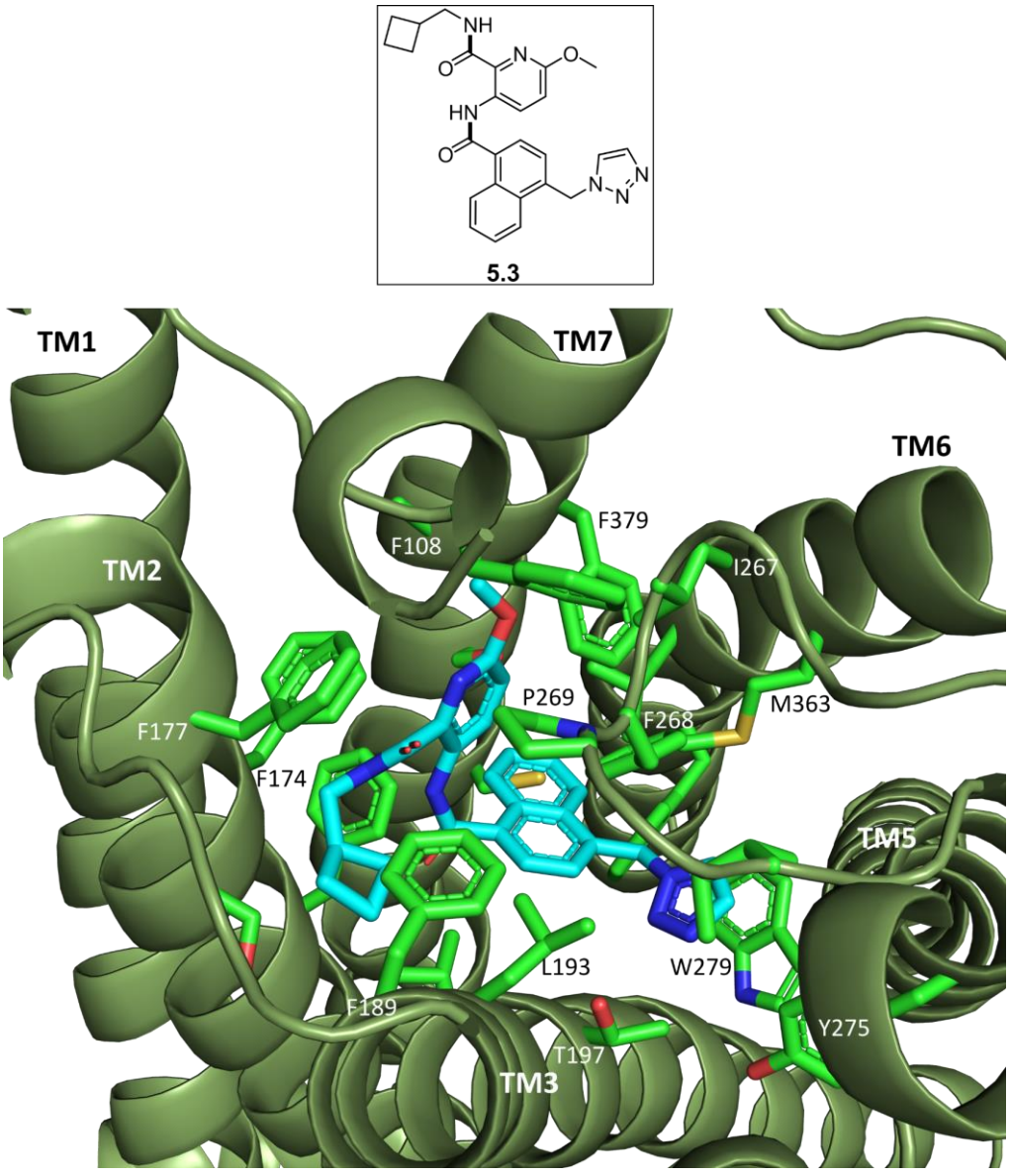

Figure 5.5. Docking pose of **5.3** (cyan carbons, red oxygens, blue nitrogens) in the CB_1R crystal structure (PDB ID: 5XRA; forest green ribbon). Side chain residues forming hydrophobic interactions with **5.3** are

shown as sticks (leaf green). Docking study carried out with restricting only amide bonds from rotation of the lowest energy conformation of **5.3** (bold bonds in structure shown in rectangle).

Overall, the docking studies (carried out with or without rotation restricting the bonds of lowest energy conformation of **5.3**) showed that the most suitable positions for conjugation of long linkers would be either the triazoloylmethylnaphthalene moiety or the methoxy moiety (bonded to the C-6 atom).

Based on the docking studies but with emphasis on the previously reported pyridyl-2-carboxamides SAR[223-224] (for example **5.4** and **5.7** in Table 5.1), it was concluded that the C-6 position of the pyridyl-2-carboxamides would be most suitable for the conjugation of bulky/long linkers. It was decided to prepare two series of (C-6)-linkers-pyridyl-2-carboxamides – one with triazoloylmethylnaphthalene moiety and another with a quinoline moiety at the C-3 position of the pyridyl-2-carboxamides.

New triazoloylmethylnaphthalene-pyridyl-2-carboxamides containing PEG linkers, alkyl-PEG linkers, and peptide linkers were designed (Figure 5.6) to build knowledge regarding the influence of different linkers on CB_1R affinity. The alkyl-PEG linker derivative with a short lipophilic alkyl chain separating the pharmacophore from the hydrophilic PEG linker was designed. The short alkyl chain would hopefully contribute to the tolerance of the hydrophilic linker in the lipophilic CB_1R binding pocket. Further, a pyridyl-PEG-linker derivative of triazoloylmethylnaphthalene-pyridyl-2-carboxamides was designed as a similar pyridyl moiety was previously well tolerated, for example **5.4** (Table 5.1). It was envisioned that if an extended linker derivative of **5.4** with moderate affinity for CB_1R was identified, linker-regioisomers of **5.4** could be synthesised to probe the chemical space around the short pyridyl linker.

It was decided to prepare only PEG linker conjugates of quinoline-pyridyl-2-carboxamides series, which could be compared with analogous triazoloylmethyl-naphthalene-pyridyl-2-carboxamides (Figure 5.6). It was hoped that PEG linker derivatives of the quinoline-pyridyl-2-carboxamide series would retain high affinity for CB_1R as a similar PEG derivative, **5.7** was reported as a high affinity CB_1R agonist (Table 5.1).

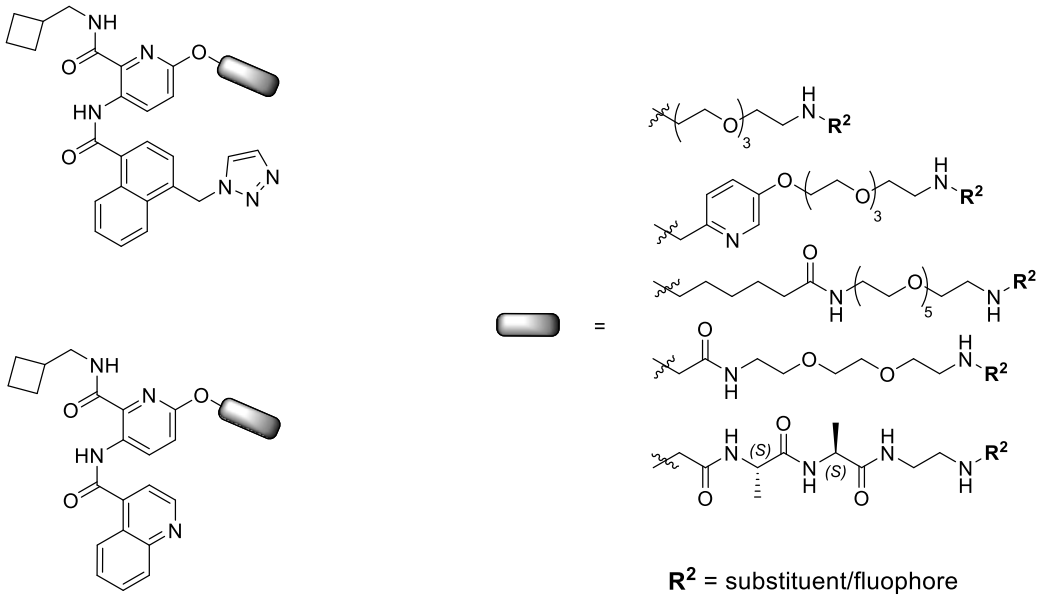

Figure 5.6. New pyridyl-2-carboxamides designed as potential CB_1R agonists.

The new pyridyl-2-carboxamide-based fluorescent ligands would be prepared by facile reaction of pyridyl-2-carboxamide-linker conjugates with a fluorophore (BODIPY-630/650-SE; Figure 5.7). The pyridyl-2-carboxamide-linker conjugates would be synthesised by reaction of corresponding hydroxypyridines with the linker derivatives. The hydroxypyridines would be prepared from the key intermediate **5.8** using an analogous synthetic route as reported previously for the synthesis of pyridyl-2-carboxamides by researchers at AstraZeneca.[223] It was thought that the key intermediate **5.8** could be prepared from the commercially available pyridine **5.9** by the nucleophilic aromatic substitution, reduction and hydrolysis reactions (Figure 5.7).

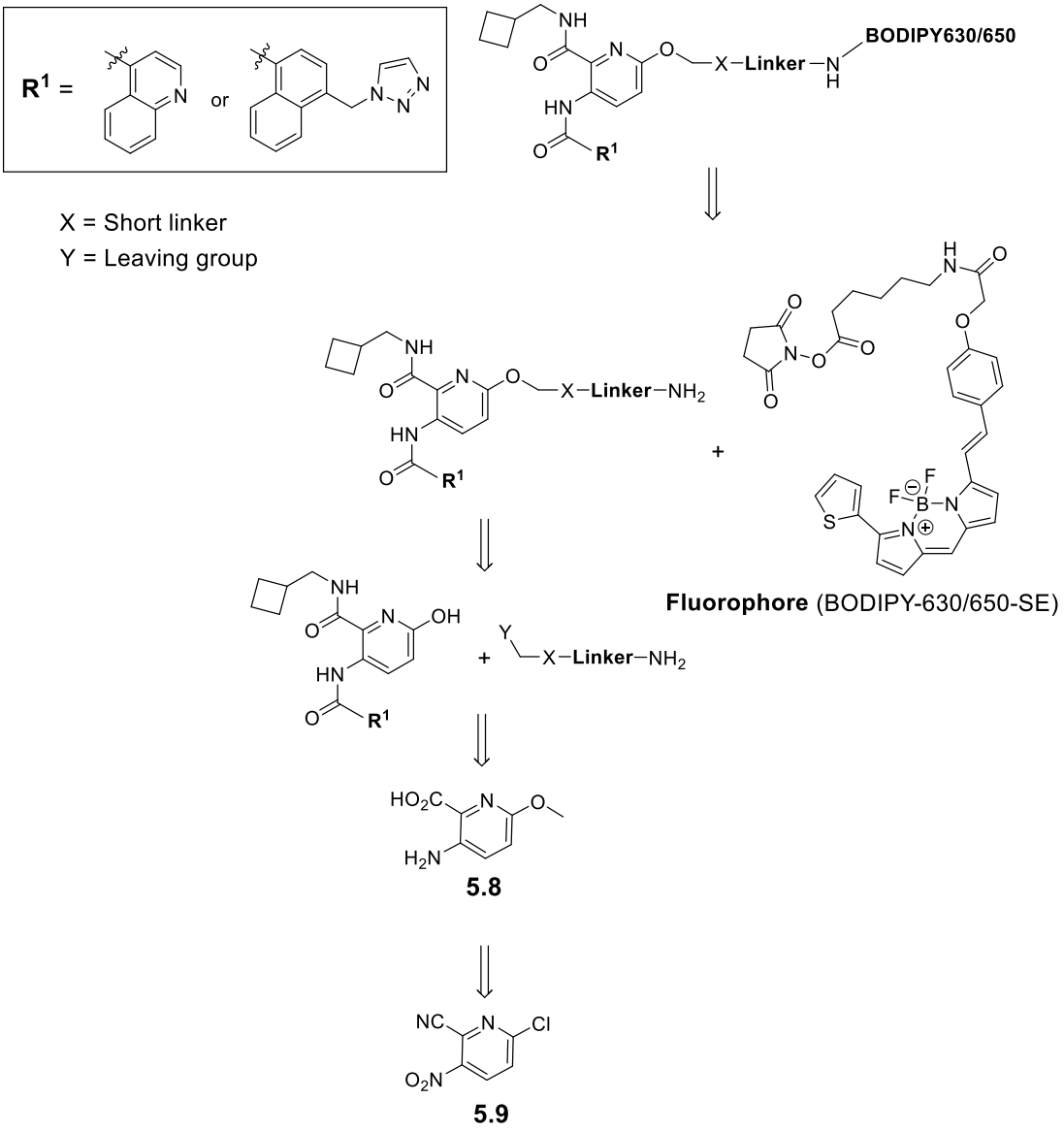

Figure 5.7. Retrosynthesis of fluorescent pyridyl-2-carboxamides designed in this chapter.

Only a subset of the designed pyridyl-2-carboxamides were synthesised (described in Figure 5.6) due to the limited number of compounds that could be pharmacologically evaluated during this PhD timeframe in the collaborator's laboratory. The fluorophore BODIPY-630/650 was selected because of the superior spectroscopic properties including high quantum yield and emission in the red spectral region and previous use in developing GPCR fluorescent ligands. [43, 86] Depending on the initial biological results, a revised series of high affinity pyridyl-2-carboxamide-based linker and fluorophore conjugates (for example with BODIPY-FL, Cy5, TAMRA) could be developed.

5.2 Synthesis and structural characterisation

5.2.1 Synthesis of linkers

Four types of linkers were used in the synthesis of pyridyl-2-carboxamide-linker-conjugates described in this chapter. Synthesis of the PEG linker **5.12**, pyridyl-PEG linker **5.17**, and alkyl-PEG linker **5.18** are described in this section and synthesis of pyridyl-2-carboxamide peptide linker conjugates (**5.45** and **5.46**) are described in section 5.2.5.

Boc-protection of the commercially available amine **5.10** gave **5.11**, which was reacted with methanesulfonyl chloride to give the PEG linker mesylate **5.12** (Scheme 5.1).

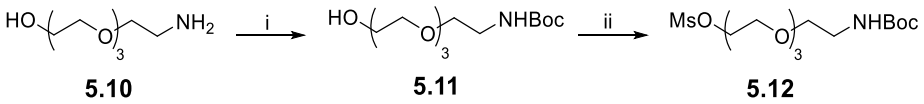

5.10 **5.11** **5.12**

Scheme 5.1. (i) $(Boc)_2O$, EtOH. (ii) $MeSO_2Cl$, Et_3N, DCM, 0 °C to rt, 96% over two steps from **5.10**.

Synthesis of the pyridyl-PEG linker **5.17** began with esterification of the commercially available carboxylic acid **5.13** to give **5.14** (compound not purified). Alkylation of the hydroxypyridine **5.14** with the PEG linker **5.12** using K_2CO_3 as a base gave ester **5.15**, which was reduced with $LiAlH_4$ to give **5.16** (compound not purified). The pyridyl alcohol **5.16** was reacted with methanesulfonyl chloride to afford mesylate **5.17** (compound not purified).

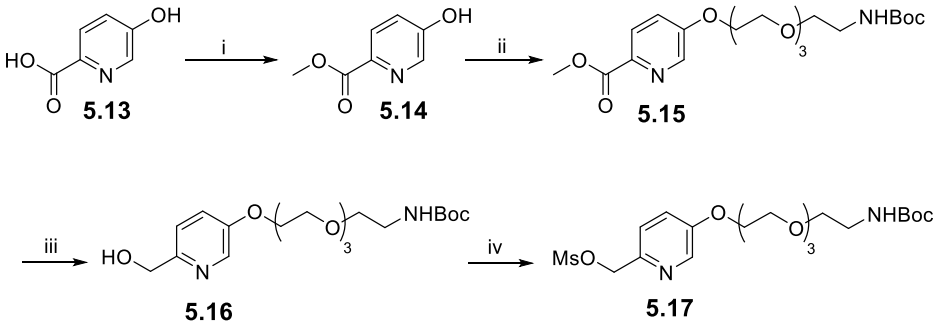

5.13 **5.14** **5.15** **5.16** **5.17**

Scheme 5.2. (i) $SOCl_2$, MeOH, 75 °C. (ii) **5.12**, K_2CO_3, DMF, 60 °C, 64% over two steps from **5.14**. (iii) $LiAlH_4$, THF, 0 °C to r.t. (iv) $MeSO_2Cl$, Et_3N, DCM, 0 °C to rt.

The alkyl-PEG linker **5.18** was prepared by coupling the commercially available bromo acid **3.49** with the commercially available alcohol **4.16** using TFFH as a coupling reagent and Et_3N as a base.

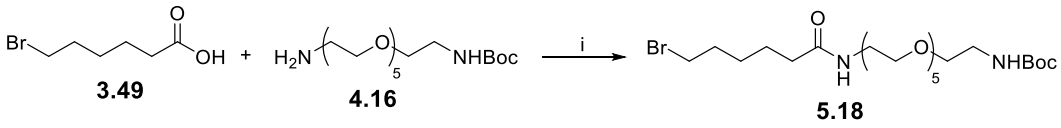

Scheme 5.3. (i) TFFH, Et_3N, DCM, 84%.

5.2.2 Synthesis of PEG linker analogues of *N*-(cyclobutylmethyl)-6-hydroxy-3-{4-[(1*H*-1,2,3-triazol-1-yl)methyl]naphthalene-1-amido}pyridine-2-carboxamide (5.32)

Wohl–Ziegler bromination of the commercially available carboxylic acid **5.19** with *N*-Bromosuccinimide (NBS) and 2,2′-Azobis(2-methylpropionitrile) (AIBN) following a literature procedure[229] gave **5.20** (compound not purified; Scheme 5.4). The naphthylmethyl bromide **5.20** was reacted with 1,2,3-triazoline according to a reported synthesis[230] to provide **5.21**. The carboxylic acid **5.21** was reacted with $SOCl_2$ to provide acid chloride **5.22** (compound not purified).

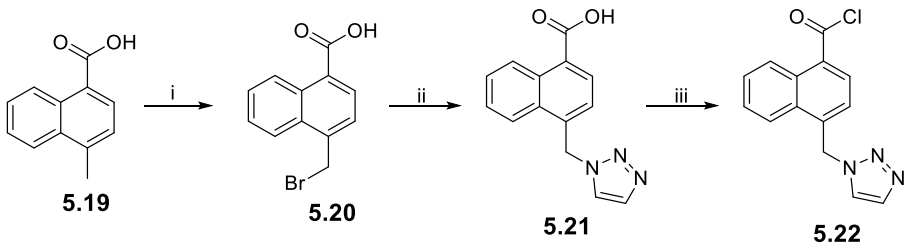

Scheme 5.4. (i) NBS, AIBN, CCl_4, 80 °C. (ii) 1,2,3-Triazoline, DMF, 50 °C, 91% over two steps from **5.19**. (iii) $SOCl_2$, 80 °C.

Synthesis of pyridine **5.8** (a key intermediate in the synthesis of pyridyl-2-carboxamides, Figure 5.7) commenced with the nucleophilic aromatic substitution of the commercially available pyridine **5.9** with NaOMe in an attempt to obtain **5.23** (Scheme 5.5). Disappointingly, initial reactions of the pyridine **5.9** with NaOMe provided **5.24** or a mixture of **5.23** and **5.25**. After several experiments, it was observed that predominantly one product (**5.23** or **5.24** or **5.25**) could be obtained by amending the equivalents of

NaOMe used and the time interval between addition of each equivalent in the substitution reaction (optimised reaction conditions summarised in Table 5.2).

The desired pyridine **5.23** was obtained as the major product upon the reaction of only one equivalent of NaOMe (<15 % *w*/*v* NaOMe solution in MeOH) with **5.9** (Table 5.2). This was not obvious from the outset since **5.23** and starting pyridine **5.9** had a very similar TLC R_f (TLC was used for monitoring the progress of the substitution reaction, the structure of **5.23** was confirmed by NMR spectroscopy and HRMS experiments). Therefore, a TLC spot at the same R_f was incorrectly interpreted as an incomplete reaction and more equivalents of NaOMe were added, leading to the formation of **5.25**.

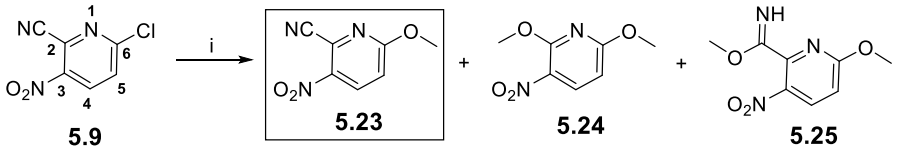

Scheme 5.5. (i) NaOMe, MeOH, 0 °C. Attempts to prepare pyridine **5.23** resulted in the formation of **5.24** and **5.25.** Reaction conditions for the preparation of a particularly substituted pyridine (**5.23** or **5.24** or **5.25**) are summarised in Table 5.2.

Table 5.2. Optimised reaction conditions for the preparation of **5.23** from **5.9**.

Equivalent(s) of NaOMe	**Reaction Conditions**	**Major product formed**
1.0	<15 % *w*/*v* NaOMe solution in MeOH added to the reaction mixture; <5 % *w*/*v* concentration of NaOMe in the reaction mixture.	**5.23**
2.0 or more	20 % *w*/*v* NaOMe solution in MeOH added to the reaction mixture.	**5.24**
2.0 or more	Reaction with one equivalent of NaOMe, followed by reaction with another equivalent of NaOMe after a delay of 10 min. NaOMe used as <15 % *w*/*v* solution in MeOH.	**5.25**

The pyridine **5.24** was obtained as the sole product upon reaction of two or more equivalents of NaOMe (20 % *w*/*v* NaOMe solution in MeOH) with the pyridine **5.9** (Table 5.2). On the other hand, pyridine **5.25** was obtained as the major product from the reaction of **5.9** with one equivalent of NaOMe (<15 % *w*/*v* NaOMe solution in MeOH), followed

by a time interval of 10 minutes and then reaction with another equivalent of NaOMe (Table 5.2).

These observations could be explained by the fact that reaction of **5.9** with one equivalent of NaOMe forms **5.23**, in which the influence of the +R (resonance) electron donating OMe group decreases the reactivity of the pyridine ring towards further nucleophilic substitution and so additional equivalents of NaOMe results in additional reaction at the electrophilic nitrile carbon to form **5.25**. The reasons for the formation of the dimethoxy pyridine **5.24** are less clear but likely involve nucleophilic aromatic substitution at C-2 of **5.9**, followed by substitution at C-6 of **5.9** with NaOMe. The dimethoxy pyridine **5.24** does not form via **5.23** as an intermediate because pyridine **5.25** was the only major product isolated (yield 95%) upon reaction of additional equivalents (two or more) of NaOMe with **5.23**.

Efforts were then focused on synthesising pyridyl-2-carboxamide **5.3** (Scheme 5.6). The nitropyridine **5.23** was reduced with $SnCl_2.2H_2O$ to provide **5.26**. The cyanopyridine **5.26,** upon alkaline hydrolysis using aqueous KOH, gave **5.8**. Reaction of carboxylic acid **5.8** with cyclobutylmethanamine using HATU as a coupling reagent provided **5.27** and cyclobutylmethanamine to give **5.27**

Coupling was then attempted between **5.27** and carboxylic acid **5.21** (synthesis shown in Scheme 5.4) using HATU or TFFH as the coupling reagent, however both attempts were unsuccessful. This failure of the coupling reaction is attributed to the low nucleophilicity of the amino group of **5.27** due to the presence of the electron withdrawing α-carboxamide moiety and the pyridine ring. Instead, following a literature procedure for the synthesis of analogous pyridyl-2-carboxamides,[223] **5.3** was successfully obtained by the reaction of **5.27** with acid chloride **5.22** (synthesis shown in Scheme 5.4) (Scheme 5.6).

The ^{1}H NMR spectrum of pyridyl-2-carboxamide **5.3** indicated that the NH of 3-aminocarbonyl participates in a hydrogen bond. The participation of 3-aminocarbonyl NH in hydrogen bonding was suggested by the upfield chemical shift of 3-aminocarbonyl NH (12.64 ppm) and presence of 3-aminocarbonyl NH as a sharp peak (likely due to the slow chemical exchange). It is likely that NH of the 3-aminocarbonyl participates in an intramolecular hydrogen bond with the oxygen of the neighbouring 2-carboxamide, as

observed in the lowest energy conformation of **5.3** (section 5.1, Figure 5.1 (A) and the compounds (CSD ID – ALUCAN,[226] CUCYAC,[227] and MUDKUT[228]) obtained from the CSD search, section 5.1). Subsequently synthesised pyridyl-2-carboxamides (**5.3**, **5.30**-**5.35**, **5.37**-**5.39**, **5.49**-**5.52** and **5.54**; synthesis described in section 5.2.2, 5.2.3, 5.2.4, 5.2.5 and 5.2.6) also indicated the presence of 3-aminocarbonyl NH hydrogen bond. These observations support the assumption that **5.3** and other pyridyl-2-carboxamides likely exist in a conformation with intramolecular hydrogen bond(s) (section 5.1).

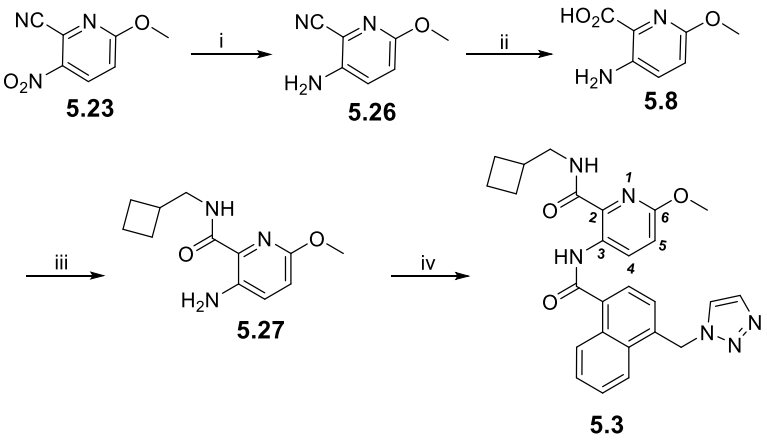

Scheme 5.6. (i) $SnCl_2.2H_2O$, EtOH, 62%. (ii) Aqueous KOH, MeOH, 80 °C, 59%. (iii) 1-Cyclobutylmethanamine hydrochloride, HATU, DIPEA, DMF, 68%. (iv) **5.22**, DIPEA, $CHCl_3$, 80 °C, 92%.

Although pyridyl-2-carboxamide **5.3** was first obtained by following the synthetic route shown in Scheme 5.6, attempts to prepare pyridine **5.23** in larger scale (>500 mg) for preparing other analogues in accordance with conditions optimised in Table 5.2 resulted in the significant formation of **5.25** along with **5.23** (for example reaction of **5.9** (4.0 g) with NaOMe provided **5.23** (62%) and **5.25** (33%)). In addition, the carboxylic acid **5.8** in Scheme 5.6 was difficult to purify. Therefore, a revised synthetic scheme for the preparation of pyridyl-2-carboxamide **5.3** was developed (Scheme 5.7).

In the revised synthesis (Scheme 5.7), commercially available pyridine **5.9** was converted to imidate **5.25** (using optimised reaction conditions shown in Table 5.2), which was not isolated and reacted with methanol under acidic conditions to give **5.28** in a one pot reaction. Conversion of the nitrile of **5.9** to the ester of **5.28** is an example of the Pinner reaction. The nitropyridine **5.28** was then reduced with $SnCl_2.2H_2O$ to give **5.29**.

Aminopyridine **5.29** was reacted with acid chloride **5.22** (Scheme 5.4) using DIPEA as a base to give **5.30**. Hydrolysis of the ester **5.30** with aqueous KOH gave **5.31**, which was coupled with cyclobutylmethanamine using HATU as a coupling reagent and DIPEA as a base to give the pyridyl-2-carboxamide **5.3** (Scheme 5.7).

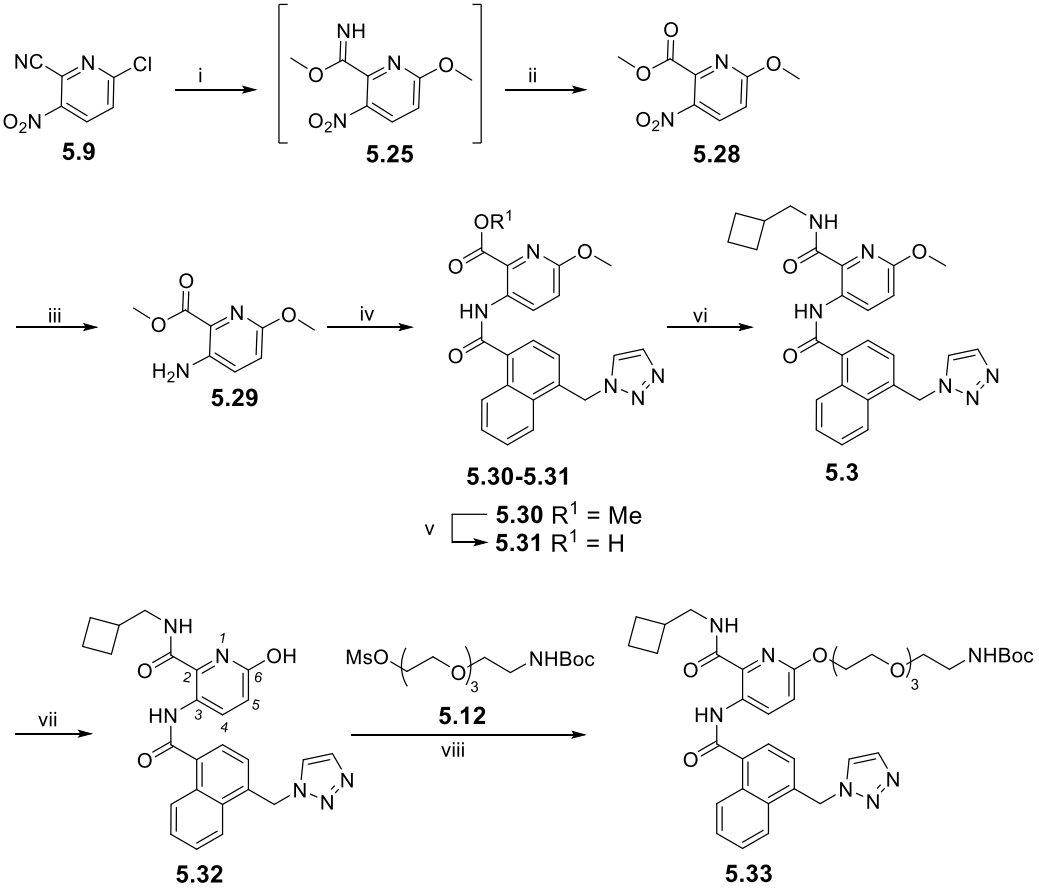

Scheme 5.7. (i) NaOMe, MeOH, 0 °C. (ii) H_2SO_4, H_2O, MeOH, 70%. (iii) $SnCl_2.2H_2O$, MeOH, 72%. (iv) **5.22**, DIPEA, $CHCl_3$, 80 °C, 69%. (v) aq. KOH, THF:H_2O, 87% (vi) 1-Cyclobutylmethanamine hydrochloride, HATU, DIPEA, DMF, 85%. (vii) Pyridine hydrochloride, 180 °C, 51%. (viii) NaI, Ag_2CO_3, DMF, 90 °C, 25%.

Following a reported synthesis[223] of **5.32**, demethylation of **5.3** with pyridine hydrochloride provided **5.32** (Scheme 5.7). Pyridine **5.32** can exist in two tautomeric forms – 2-hydroxypyridine and 2-pyridone. A literature reported stated **5.32** as the 2-hydroxypyridine tautomer.[223] NMR spectra of **5.32** in this study revealed only one isomer therefore it was assumed to be the 2-hydroxypyridine. Pyridine **5.32** is a key intermediate in the triazoloylmethylnaphthalene-pyridyl-2-carboxamide series and will be used in the subsequent synthetic schemes (Scheme 5.8, 5.9, 5.10) to obtain various *O*-alkylated pyridyl-2-carboxamides. It is important to note here that base deprotonated 2-

hydroxypyridine **5.32** is an ambident anion and can undergo alkylation at either *N*-1 or OH of **5.32**. It is well known that silver salts of 2-hydroxypyridines undergo regioselective *O*-alkylation[231] and indeed Ag_2CO_3 was used for the preparation of *O*-alkylated pyridyl-2-carboxamides by the researchers at AstraZeneca.[223]

Initial attempts to alkylate **5.32** with PEG methanesulphonate **5.12** (synthesis shown in Scheme 5.1) using Ag_2CO_3 as a base proved unsuccessful. The failure of these alkylation reactions were attributed to the use of alkyl methanesulphonate instead of alkyl halides as reported previously for the preparation of *O*-alkylated pyridyl-2-carboxamides.[223] Therefore, it was decided to carry out alkylation of **5.32** with a halide analogue of **5.12**. Pleasingly, the reaction of **5.32** with NaI, Ag_2CO_3 and **5.12** successfully provided pyridyl-2-carboxamide **5.33**. It is thought that **5.12** reacts with NaI to generate *tert*-butyl *N*-(2-{2-[2-(2-iodoethoxy)ethoxy]ethoxy}ethyl) carbamate,[232] which then undergoes an alkylation reaction with **5.32**. The success of Ag_2CO_3 mediated alkylation reaction of **5.32** with alkyl halides but not with alkyl methanesulphonate is attributed to the halophilic nature of silver. The low yield of the reaction obtained for the preparation of **5.33** is due to the difficult separation of **5.33** from **5.12** in the column purification.

5.2.3 Synthesis of pyridyl-PEG linker derivatives of *N*-(cyclobutylmethyl)-6-hydroxy-3-{4-[(1*H*-1,2,3-triazol-1-yl)methyl] naphthalene-1-amido}pyridine-2-carboxamide (5.32)

The pyridyl-PEG linker conjugate **5.34** was synthesised by alkylation of the hydroxypyridine **5.32** with mesylate **5.17** (synthesis shown in Scheme 5.2) (Scheme 5.8). The alkylation reaction was carried out with NaI and Ag_2CO_3, using the optimised reaction conditions as described for the preparation of **5.33** (section 5.2.2).

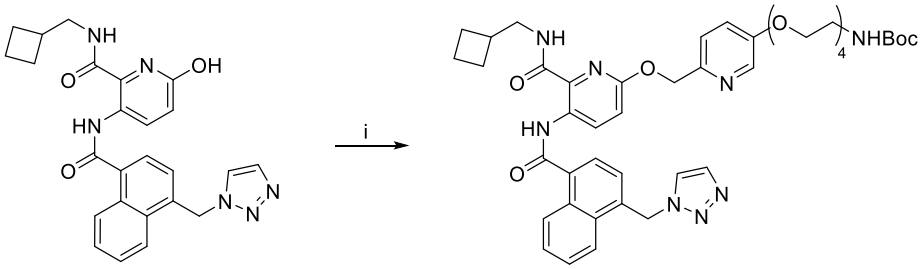

5.32 5.34

Scheme 5.8. (i) **5.17**, NaI, Ag_2CO_3, DMF, 90 °C, 64%.

5.2.4 Synthesis of alkyl-PEG derivatives of *N*-(cyclobutylmethyl)-6-hydroxy-3-{4-[(1*H*-1,2,3-triazol-1-yl)methyl]naphthalene-1-amido}- pyridine-2-carboxamide (5.32)

Synthesis of the fluorescent ligand **5.36** began with alkylation of the hydroxypyridine **5.32** with **5.18** (synthesis shown in Scheme 5.3, section 5.2.1) using Ag_2CO_3 as a base to provide **5.35**. Boc-deprotection of **5.35** with TFA gave a primary amine (TFA salt), which was purified by semi-preparative RP-HPLC and then reacted with BODIPY-630/650-SE to give fluorescent ligand **5.36** (Scheme 5.9).

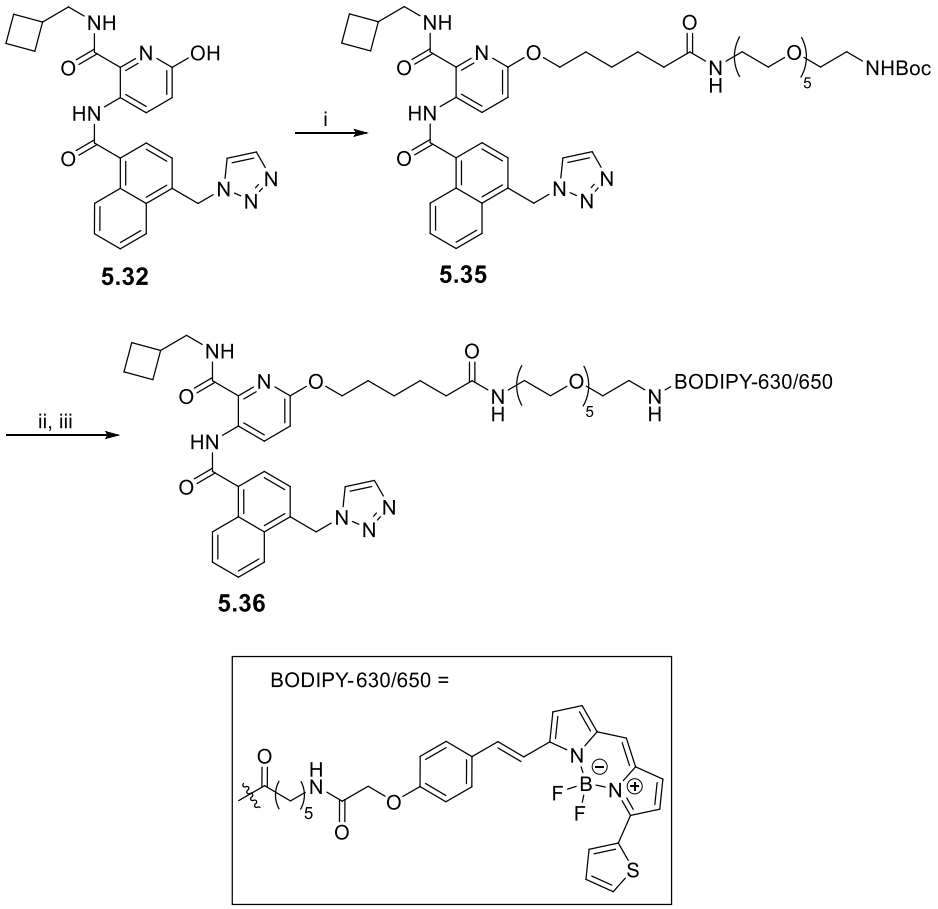

Scheme 5.9. (i) **5.18**, NaI, Ag_2CO_3, DMF, 90 °C, 56%. (ii) TFA, DCM, quantitative. (iii) BODIPY-630/650-SE, DIPEA, DMF, 58%.

5.2.5 Synthesis of PEG or peptide linker derivatives of 2-({6-[(cyclobutylmethyl)carbamoyl]-5-{4-[(1*H*-1,2,3-triazol-1-yl)methyl] naphthalene-1-amido}pyridin-2-yl}oxy)acetic acid (5.38)

The hydroxypyridine **5.32** was alkylated with *tert*-butyl bromoacetate to give **5.37**, which on reaction with TFA gave carboxylic acid **5.38** (Scheme 5.10). The coupling reaction of the carboxylic acid **5.38** with linker **2.12** (synthesis described in chapter 2, section 2.2.1) using HBTU and DIPEA gave **5.39**. The PEG linker conjugate **5.39** was reacted with TFA to give the Boc-deprotected **5.39**, which after semi-preparative RP-HPLC purification was reacted with BODIPY-630/650-SE to provide the fluorescent ligand **5.40** (Scheme 5.10).

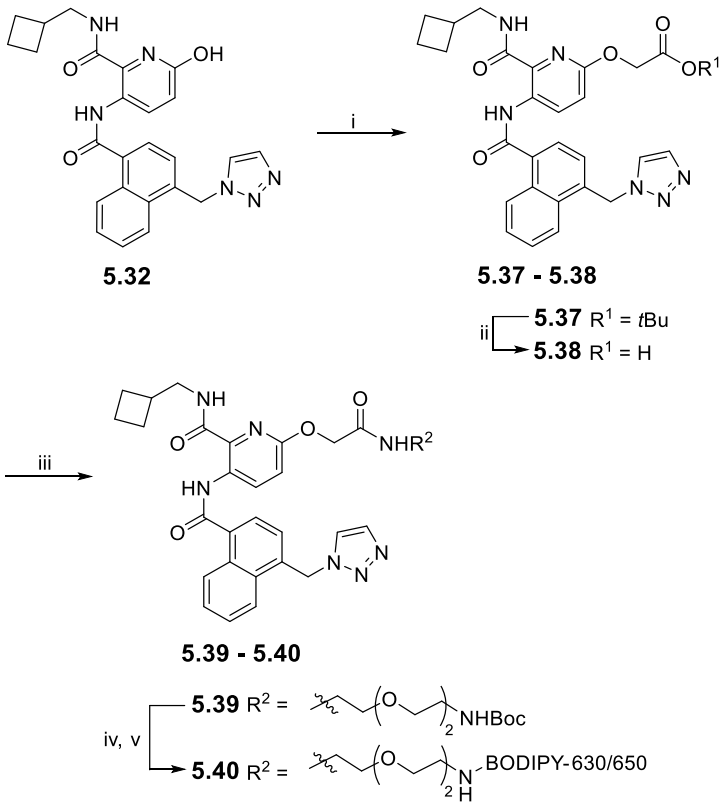

Scheme 5.10. (i) *tert*-Butyl bromoacetate, Ag_2CO_3, DMF, 90 °C, 94%. (ii) TFA, DCM, 95%. (iii) **2.12**, HBTU, DIPEA, DMF, 59%. (iv) TFA, DCM, quantitative. (v) BODIPY-630/650-SE, DIPEA, DMF, 98%.

The peptide linker analogues of pyridyl-2-carboxamides were synthesised by Fmoc solid-phase peptide synthesis (Scheme 5.11). The amino acid Fmoc-Ala-OH was double coupled with 1,2-diaminoethane trityl resin **3.34** using HBTU and DIPEA to give resin-bound **5.41**. Capping of any unreacted resin-primary-amine sites on **5.41** with Ac_2O was carried out. The resin-bound **5.41** was reacted with a solution of piperidine in DMF (20% *v*/*v*) and the resulting Fmoc—deprotected resin-bound **5.41** was reacted with Fmoc-Ala-OH, HBTU, and DIPEA to give resin-bound **5.42**. Fmoc deprotection of resin-bound **5.42** was repeated and the Fmoc-deprotected resin-bound **5.42** was reacted with carboxylic acid **5.38** (synthesis shown in Scheme 5.10, section 5.2.5) using HATU and DIPEA to provide resin bound **5.43**. The resin-bound **5.43** was treated with TFA to undergo resin cleavage and give peptide linker conjugate **5.44**. The peptide-conjugate **5.44** was purified using semi-preparative RP-HPLC and subsequently reacted with Boc anhydride or BODIPY-630/650-SE in separate reactions to give **5.45** or **5.46** respectively. The low yield obtained for **5.46** is due to the poor solubility of **5.46** in a DMSO-water solution, which made purification by semi-preparative RP-HPLC challenging.

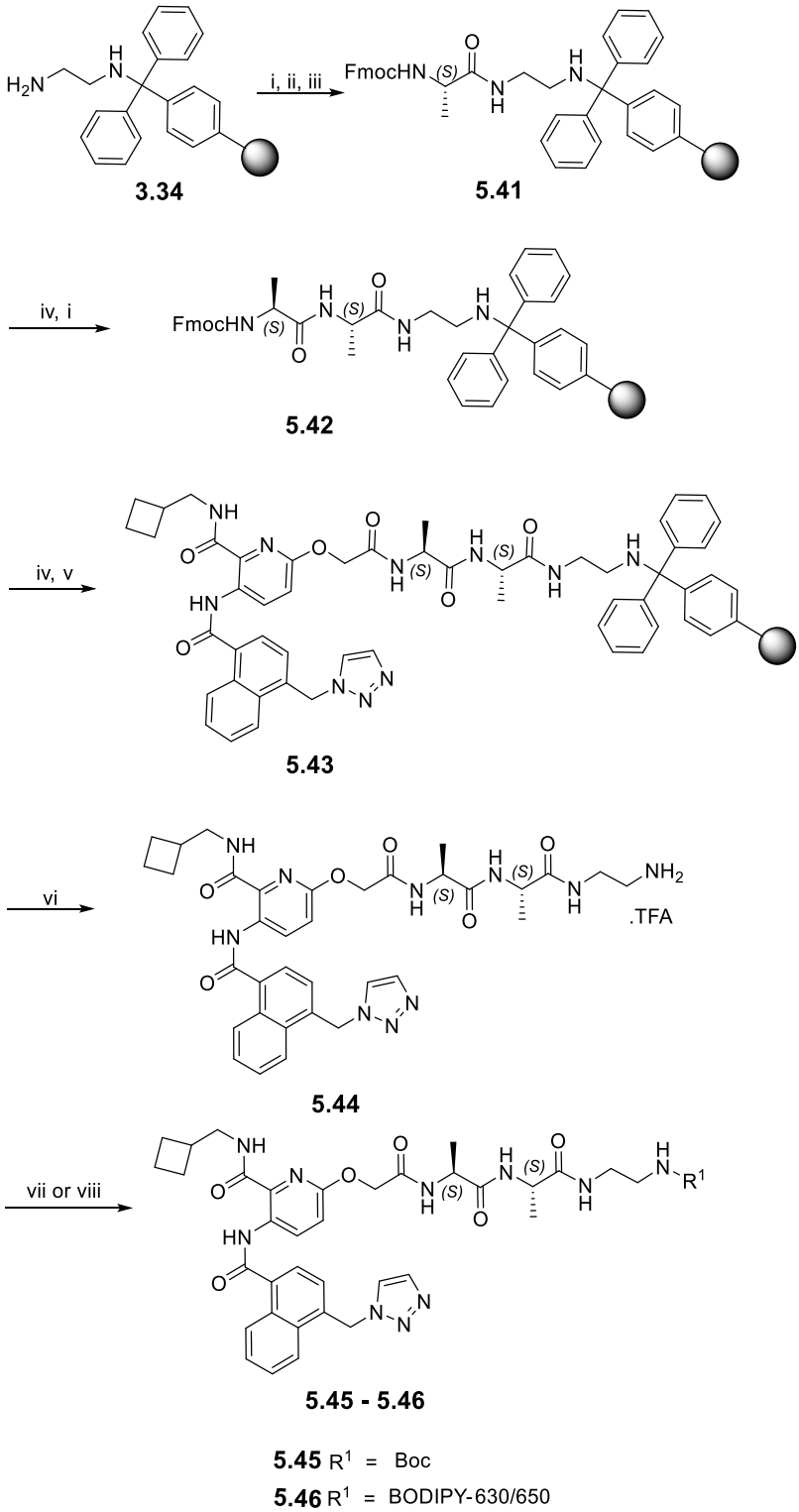

Scheme 5.11. (i) Fmoc-Ala-OH, HBTU, DIPEA, DMF. (ii) Fmoc-Ala-OH, HBTU, DIPEA, DMF (double coupling was done). (iii) Ac_2O, DIPEA DMF. (iv) Piperidine, DMF. (v) **5.38**, HATU, DIPEA, DMF (vi) TFA, DCM. (vii) $(Boc)_2O$, Et_3N, DMF, 38%. (viii) BODIPY-630/650-SE, DIPEA, DMF, 13%.

5.2.6 Synthesis of PEG linker derivatives of 2-({6-[(cyclobutylmethyl)carbamoyl]-5-(quinoline-4-amido)pyridin-2-yl} oxy)acetic acid (5.53)

Synthesis of quinoline-pyridyl-2-carboxamides commenced with reaction of quinoline-4-carboxylic acid **5.47** with $SOCl_2$ to provide acid chloride **5.48** (compound not purified; Sscheme 5.12).

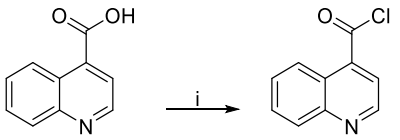

5.47 **5.48**

Scheme 5.12. (i) $SOCl_2$, 80 °C.

Pyridyl-2-carboxamides of this series were synthesised (Scheme 5.13) using a similar synthetic strategy as described in Scheme 5.7. The coupling reaction of aminopyridine **5.29** (synthesis shown in Scheme 5.7, section 5.2.2) with **5.48** provided **5.49**. Hydrolysis of **5.49** with aqueous KOH gave carboxylic acid **5.50**, which on coupling with cyclobutylmethanamine gave **5.6**. Demethylation of **5.6** with pyridine hydrochloride gave **5.51**. Alkylation of the hydroxypyridine **5.51** with *tert*-butyl bromoacetate using conditions optimised for the preparation of **5.33** (synthesis shown in Scheme 5.7) provided **5.52**, which was reacted with TFA to give **5.53**. Coupling of the carboxylic acid **5.53** with **2.12** gave linker conjugate **5.54**. Boc-protected **5.54** was reacted with TFA, purified using semi-preparative RP-HPLC to give Boc-deprotected **5.54** and subsequently reacted with BODIPY-630/650-SE to give fluorescent ligand **5.55** (Scheme 5.13).

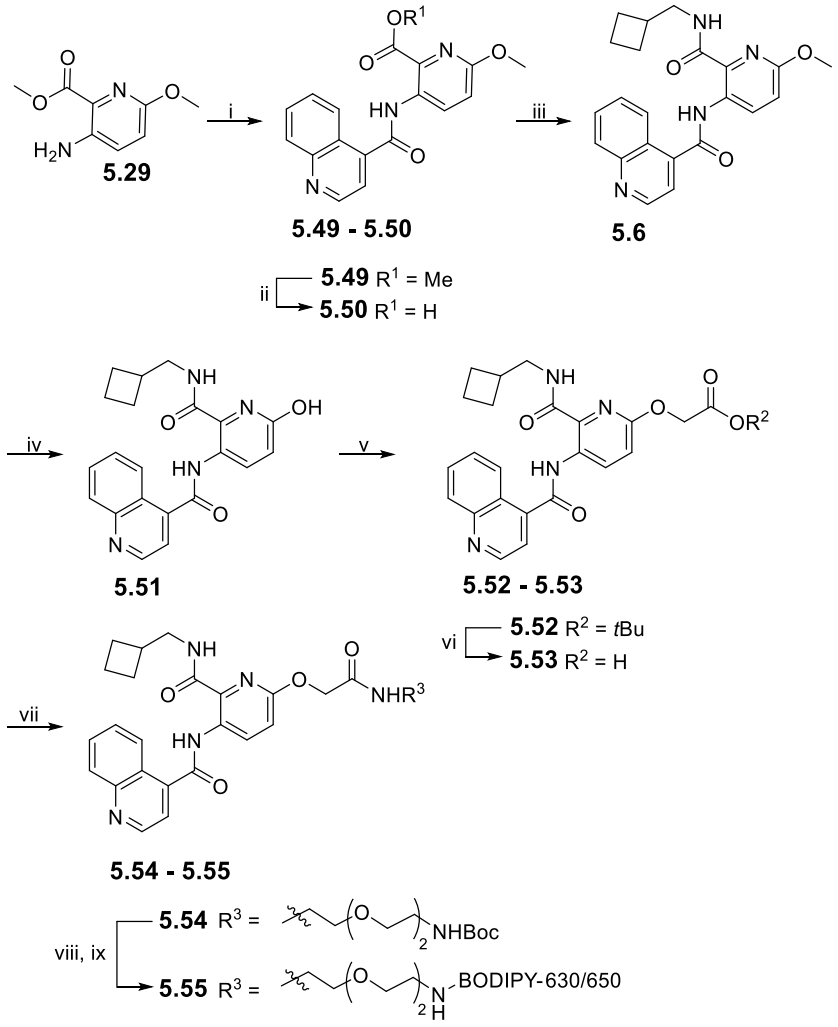

Scheme 5.13. (i) **5.48**, DIPEA, $CHCl_3$, 80 °C, 82%. (ii) KOH, THF:H_2O, quantitative (iii) 1-Cyclobutylmethanamine hydrochloride, HATU, DIPEA, DMF, 93%. (iv) Pyridine hydrochloride, 180 °C, 63%. (v) *tert*-Butyl bromoacetate, NaI, Ag_2CO_3, DMF, 90 °C, 94%. (vi) TFA, DCM (vii) **2.12**, HBTU, DIPEA, DMF, 62%. (viii) TFA, DCM, quantitative. (ix) BODIPY-630/650-SE, DIPEA, DMF, quantitative.

5.3 Biological studies

5.3.1 Radioligand binding assays

A subset of pyridyl-2-carboxamides (synthesised in section 5.2) were analysed for affinity at CBR, due to the availability of only limited time for carrying out biological studies in the collaborator's laboratory. Pharmacological evaluation of these compounds would build knowledge of the effect of different *O*-substituents on CBR affinity and help design a revised series of high affinity CB_1R pyridyl-2-carboxamides.

A radioligand binding assay was used to determine CBR affinity of synthesised pyridyl-2-carboxamides using CBR radioligand [^{3}H]-CP55,940 and membrane preparations derived from HEK-293 cells transfected with either CB_1R or CB_2R according to a previously described method[169, 212] (assay described previously in chapter 3, section 3.3.1; experiments details described in the chapter 7, section 7.1.2). Pyridyl-2-carboxamides (**5.3**, **5.6**, **5.33**, **5.34**, **5.35**, **5.37**, and **5.39**) displaced [^{3}H]-CP55,940 from CB_1R or CB_2R by more than 50% in the initial screen at 10 μM (displacement of [^{3}H]-CP55,940 in initial screen shown in Figure 5.8). Accordingly, these compounds were then analysed in a concentration-dependent way to determine the concentration binding curves and calculate the binding affinity (K_i).

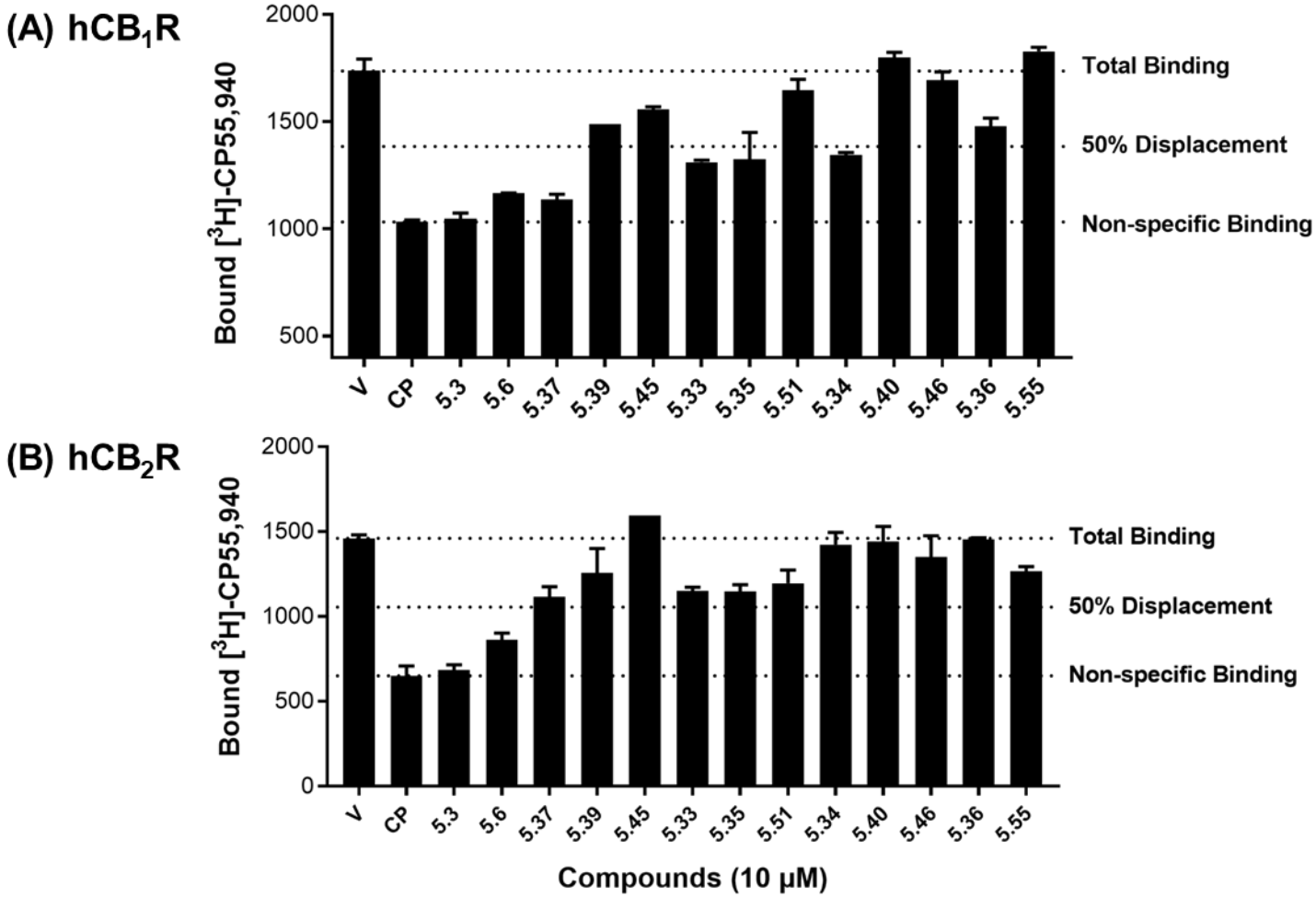

Figure 5.8. Radioligand binding assay: Screen of synthesised chromenopyrazoles at 10 µM at HEK-293 cells expressing hCB_1R (panel **A**) or hCB_2R (panel **B**) with [^{3}H]-CP55,940 as the radioligand. Data represented are from a single experiment carried out in triplicate and is expressed as mean ± SEM. V (vehicle), CP (CP55,940).

The literature compound **5.3** (K_i = 0.81 ± 0.16 nM at hCB$_1$R; 108.6 ± 1.46 nM at hCB$_2$R; Table 5.3, Figure 5.9) showed high affinity for CB$_1$R and selectivity over CB$_2$R, consistent with previous literature reports (**5.3** IC_{50} = 0.97 nM at hCB$_1$R; K_i at CB$_1$R or CB$_2$R not reported)[223-224]. The other literature compound **5.6** also showed high affinity for CB$_1$R (K_i = 77.1 ± 10.4 nM at hCB$_1$R; 559.8 ± 40.4 nM at hCB$_2$R; Table 5.3) and moderate affinity for CB$_2$R, which is similar to the previously reported CBR affinities (**5.6** IC_{50} = 15 nM at hCB$_1$R; IC_{50} = 100 nM at hCB$_1$R)[223]. The positive control CP55,940 (K_i = 4.53 ± 0.22 nM at hCB$_1$R; K_i = 1.66 ± 0.31 nM at hCB$_2$R) showed the CBR affinities consistent with those reported recently – (CP55,940 pK_i = 9.26 ± 0.12 nM at hCB$_1$R, (K_i = 0.55 nM) and (CP55,940 pK_i = 8.44 ± 0.18 nM at hCB$_2$R (K_i = 3.63 nM))[119]. None of the newly synthesised pyridyl-2-carboxamides exhibited significant CB$_2$R affinity, therefore the following SAR discussion primarily analyses the CB$_1$R affinities of the new compounds.

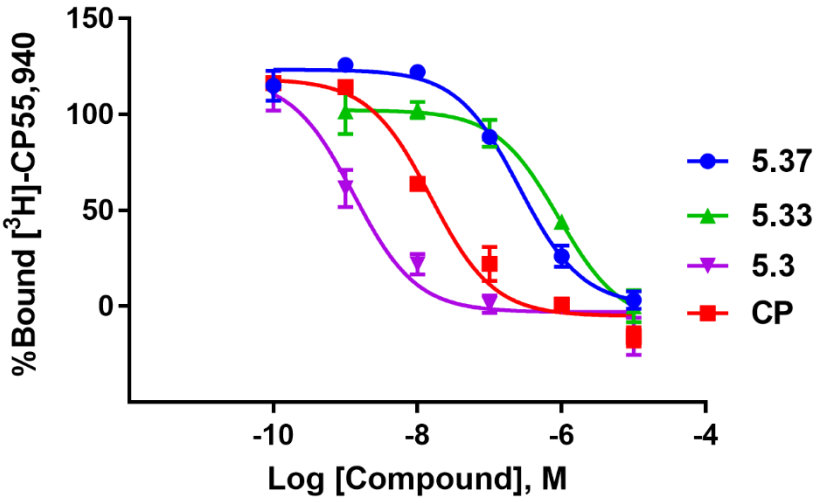

Figure 5.9. Competition binding curves for CB$_1$R pyridyl-2-carboxamide **5.37**, **5.33**, literature compound **5.3**, and CP (CP55,940) using radioligand [^{3}H]-CP55,940 (K_d = 3.0 nM for hCB$_1$R) at HEK-293 cells expressing hCB$_1$R. Data represented are from a single experiment carried in triplicate and is expressed as mean ± SEM.

The short linker conjugate **5.37** (K_i = 245.6 ± 36.4 nM at hCB$_1$R; > 5000 nM at hCB$_2$R; Table 5.3; Figure 5.9) exhibited the highest affinity for CB$_1$R and selectivity over CB$_2$R of the novel compounds tested. Nonetheless, the CB$_1$R affinity of short linker-conjugate **5.37** was reduced 300-fold compared to methyl analogue **5.3** (literature compound).

Table 5.3. Radioligand binding affinity data for synthesised pyridyl-2-carboxamides.

Com-pound	Structure		hCB_1R K_i (nM ± SEM)*	hCB_2R K_i (nM ± SEM)*	hCB_1R selecti-vity
5.3	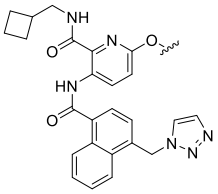	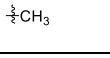	0.81 ± 0.16	108.6 ± 1.46	134
5.37		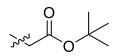	245 ± 36.4	> 5000	> 20
5.33		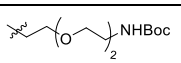	1217 ± 253.6	> 5000	> 4
5.34		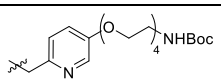	2728 ± 625.2	> 5000	-
5.35		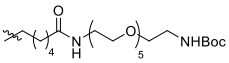	1959 ± 740.4	> 5000	>2
5.36		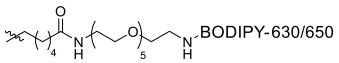	> 5000	> 10000	-
5.39		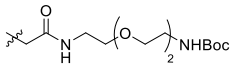	4099 ± 752.2	> 10000	-
5.40		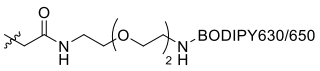	> 10000	> 10000	-
5.45		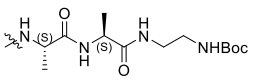	> 10000	> 10000	-
5.46		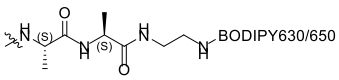	> 10000	> 10000	-
5.6	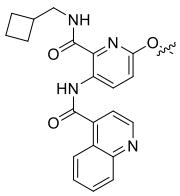		77.1 ± 10.4[a]	559.8 ± 40.3	>7
5.54		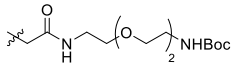	> 10000	> 10000	-
5.55		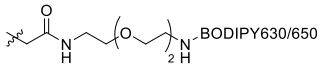	> 10000	> 10000	-

*Binding affinity (K_i) obtained by competition binding assay performed on membranes obtained from HEK-293 cells expressing either hCB_2R or hCB_1R with [^{3}H]-CP55,940 as radioligand (K_d = 1.7 nM for hCB_2R and 3.0 nM for hCB_1R). All data is from at least three individual experiments performed in triplicate, except [a] which is two individual experiments performed in triplicate.

The triazoloylmethylnaphthalene-pyridyl-2-carboxamide linker conjugates **5.33**, **5.34**, and **5.35** exhibited moderate affinity for CB_1R. The CB_1R affinity of **5.33** (K_i = 1217 ± 253.6 nM at hCB_1R; Figure 5.9) was noticeably reduced compared to the previously

reported short PEG-linker conjugate **5.7** (IC_{50} = 10 nM at hCB_1R, Table 5.1)[223-224]. Similarly, the pyridyl-PEG linker **5.34** (K_i = 2728 ± 625.2 nM at hCB_1R) exhibited markedly reduced CB_1R affinity compared to the previously reported pyridyl moiety containing **5.4** (IC_{50} = 3.2 nM at hCB_1R)[223]. The fluorescent ligand **5.36**, a BODIPY-630/650 analogue of **5.35** did not exhibit any significant affinity for CB_1R. The moderate affinity for CB_1R of 29 atoms long linker conjugate **5.35** indicates tolerance of *O*-long linkers in the triazoloylmethylnaphthalene-pyridyl-2-carboxamide series.

The PEG-linker conjugate **5.39** (K_i = 4099 ± 752.2 nM at hCB_1R, which contains a carboxamide moiety in the linker) exhibited decreased CB_1R affinity compared to the PEG-linker conjugate **5.33** (Table 5.3). The fluorescent ligand **5.40** (BODIPY-630/650 analogue of **5.39**), the peptide-linker conjugate **5.45** and fluorescent ligand **5.46** (BODIPY-630/650 analogue of **5.45**) did not exhibit any significant CB_1R affinity (Table 5.3).

In the quinoline-pyridyl-2-carboxamide series, linker conjugates **5.54** and **5.55** (BODIPY-630/650 analogue of **5.54**) did not exhibit any significant CB_1R affinity (Table 5.3). The lack of CB_1R affinity of **5.54** was slightly surprising considering it is a carboxamide-PEG linker analogue of literature pyridyl-2-carboxamide **5.7** (IC_{50} = 10 nM at hCB_1R; Table 5.1), that was reported as a high affinity CB_1R ligand[223].

In summary, the newly synthesised pyridyl-2-carboxamide **5.37** showed the highest affinity for CB_1R of all the novel compounds tested (Table 5.3). The PEG-linker conjugate **5.33** exhibited the best affinity for CB_1R among the newly synthesised pyridyl-2-carboxamide-linker conjugates. None of the BODIPY-630/650 derivatives of pyridyl-2-carboxamide exhibited any significant affinity for CB_1R. A reason for the reduced affinity at CB_1R of the pyridyl-2-carboxamides might be the steric clashes of the linkers with the CB_1R amino acid residues. In the docking studies (section 5.1, Figure 5.3 and 5.5), the methoxy moiety of pyridyl-2-carboxamide **5.3** was pointing towards the extracellular *N*-terminal of CB_1R, indicating linker attachment in this position may be tolerated. However, the reduced CB_1R binding affinities of linker conjugates (Table 5.3) indicate that there might not be a large enough cavity in the *N*-terminal of CB_1R (between TM1 and TM7) for the long *O*-linkers to exit through, or alternatively the *O*-linker conformation is not suitable to exit through the cavity.

5.3.2 cAMP Functional assays

The newly synthesised pyridyl-2-carboxamides (**5.33**, **5.34**, **5.35**, and **5.37**) that exhibited appreciable affinity for CB_1R were evaluated using the cAMP BRET assay as previously described in chapter 3 (section 3.3.3). Due to the low affinity for CB_2R, the functional activities of pyridyl-2-carboxamides (**5.33**, **5.34**, **5.35**, and **5.37**) at CB_2R were not determined.

The newly synthesised pyridyl-2-carboxamides (**5.33**, **5.34**, **5.35**, and **5.37**) were tested at 10 μM at CB_1R expressing HEK-293 cells and at WT HEK-293 cells. All of the pyridyl-2-carboxamides (**5.33**, **5.34**, **5.35**, and **5.37**) behaved as agonists at 10 μM. Incubation of the pyridyl-2-carboxamide (**5.33** or **5.34** or **5.35**, at 10 μM) with WT HEK-293 cells and forskolin increased the inverse BRET ratio compared to forskolin alone (Appendix, Figure A.13 panel B, D, and C), indicating an effect independent of CB_1R cAMP signalling. The observation of a CB_1R independent effect by pyridyl-2-carboxamides **5.33**, **5.34**, and **5.35** led to evaluation of the literature pyridyl-2-carboxamide **5.3** (10 μM) at WT HEK-293 cells and indeed a similar effect independent of CB_1R cAMP signalling was observed (Appendix, Figure A.13 panel A). It should be emphasised here that a CB_1R independent effect of the pyridyl-2-carboxamides (**5.3**, **5.33**, **5.34**, and **5.35**) in the cAMP BRET assay at WT HEK-293 cells does not necessarily translate to the promiscuous nature of these ligands, provided these can be used at a concentration lower than 10 μM (and that this lower concentration does not mediate CB_1R cAMP independent effects). In contrast to the observations for the pyridyl-2-carboxamides (**5.3**, **5.33**, **5.34**, and **5.35**), high affinity CB_1R ligand **5.37** (K_i = 245.6 ± 36.4 nM at hCB_1R) at 10 μM exhibited a cAMP response, which was not significantly different from forskolin alone in the cAMP assay at the WT HEK-293 cells, and hence did not show a CB_1R cAMP independent effect (Table 5.5) (Appendix, Figure A.13 panel E).

The moderate affinity CB_1R pyridyl-2-carboxamide **5.33** (K_i = 1217 ± 253.6 nM at hCB_1R) was then evaluated at 1 μM to determine function at CB_1R (only the highest affinity pyridyl-2-carboxamide-linker conjugate **5.33** was further evaluated due to the

time constraints). It was hoped that at 1 μM, pyridyl-2-carboxamide **5.33** would produce a response in the cAMP BRET assay (at HEK-293 cells expressing CB_1R) sufficient enough to determine function without producing any significant effects in the WT HEK-293 cells (in an independent experiment).

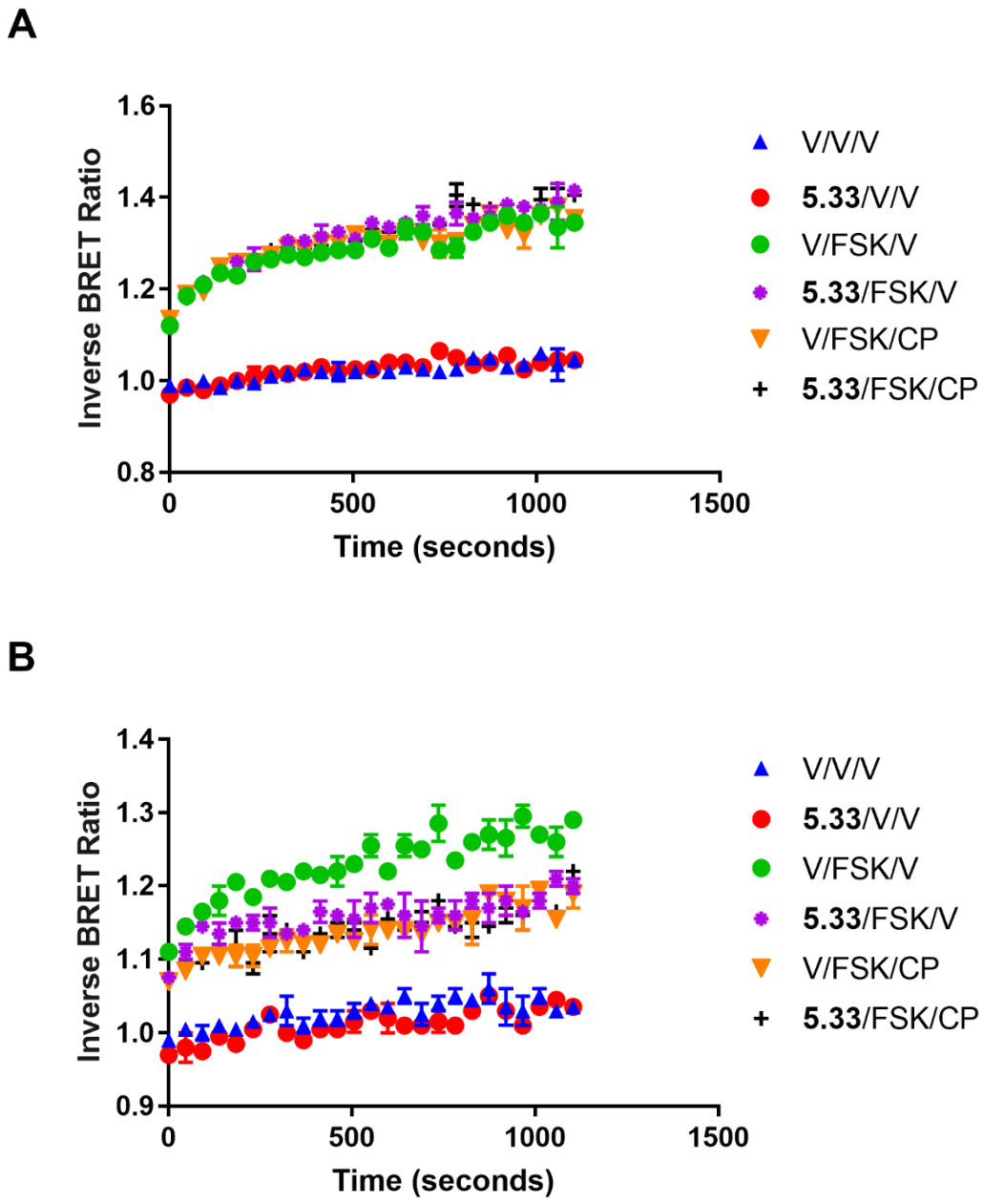

Figure 5.10. The moderate affinity CB_1R linker conjugate **5.33** (1 μM) screened in a cAMP BRET assay: (**A**) cAMP BRET assay of **5.33** at WT HEK-293 cells. (**B**) cAMP BRET assay of **5.33** at HEK-293 cells stably expressing hCB_1R. Data is representative of a single experiment carried in duplicate and is expressed as mean ± SEM. CP (CP55,940), FSK (Forskolin), V (vehicle).

The pyridyl-2-carboxamide **5.33** (at 1 µM) and forskolin, when incubated with WT HEK-293 cells, did not increase the inverse BRET ratio compared to forskolin alone (Figure 5.10 panel A; Table 5.5), thus did not show a CB_1R independent effect in the cAMP BRET assay. Incubation of the pyridyl-2-carboxamide **5.33** (at 1 µM) and forskolin with CB_1R expressing HEK-293 cells decreased the intracellular cAMP concentration compared to forskolin alone, therefore showing that **5.33** behaved as an agonist (Figure 5.10 panel B).

Table 5.4. CB_2R functional data of the pyridyl-2-carboxamides **5.37** and **5.33**.

Compound	EC_{50} (nM± SEM)*	E_{max} (%FSK response ± SEM)#	Functional activity
5.37	135.5 ± 7.6	52.21 ± 0.10	Agonist
5.33	222.7 ± 40.4	66.35 ± 3.21	Agonist

*Potency and #efficacy data for the chromenopyrazoles, obtained from cAMP BRET assay using HEK-293 cells expressing hCB_1R. All data is from at least three individual experiments performed, raw data is normalised to forskolin (100 %) and vehicle (0 %).

Due to time constraints, only newly synthesised pyridyl-2-carboxamides (**5.37** (K_i = 245.6 ± 36.4 nM) and **5.33** (K_i = 1217 ± 253.6 nM at hCB_1R)), which exhibited high to moderate affinity for CB_1R were further evaluated in a concentration-dependent manner to determine the EC_{50} at CB_1R (Figure 5.11, Table 5.4).

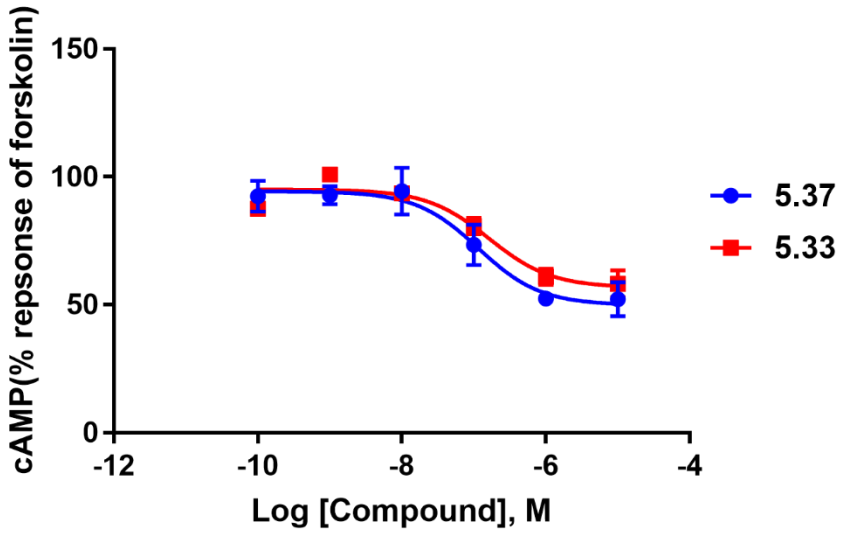

Figure 5.11. Concentration-response curves for pyridyl-2-carboxamides **5.37** and **5.33** using HEK-293 cells stably expressing hCB_1R. All data is from at least three individual experiments performed and is expressed as mean ± SEM, raw data is normalised to forskolin (100 %) and vehicle (0 %).

Pyridyl-2-carboxamide **5.37** (EC_{50} = 135.5 ± 7.6 nM, Emax = 52.21 ± 0.10 % of forskolin response at hCB_1R) exhibited higher potency and efficacy than **5.33** (EC_{50} = 222.7 ± 40.4 nM; Emax = 66.35 ± 3.21 % of forskolin response at hCB_1R). Previously, literature pyridyl-2-carboxamides (**5.2**-**5.7**, Table 5.1) were also reported as CB_1R agonists in a [^{35}S]GTPγS assay using HEK-293 cells expressing cCB_1R.[223]

Table 5.5. % Response of the pyridyl-2-carboxamide **5.37** or **5.33** in the cAMP BRET assay at wild type HEK-293 cells.

Compound	%FSK response ± SEM*
5.37	114.48 ± 4.0
5.33	106.098 ± 4.55

*cAMP BRET carried out at WT HEK-293 cells. **5.37** tested at (10 μM) and **5.33** tested at (1 μM). All data is from at least two individual experiments performed in duplicate, raw data is normalised to forskolin response (100 %) and vehicle response (0 %). A one-sample t-test was used to determine whether the % cAMP response of test compounds was significantly different from the forskolin only response.

5.4 Summary and conclusions

Two series (triazoloylmethylnaphthalene-pyridyl-2-carboxamide and quinoline-pyridyl-2-carboxamide) of *O*-linker conjugates of pyridyl-2-carboxamides were prepared with the aim of developing high affinity CB_1R fluorescent agonists (section 5.2). An efficient synthetic route for the preparation of pyridyl-2-carboxamides from the readily available pyridine derivative **5.9** was developed. A set of alkyl, PEG, peptide linker derivatives and BODIPY-630/650 derivatives of pyridyl-2-carboxamides were also prepared.

The BODIPY-630/650-containing pyridyl-2-carboxamides (**5.36**, **5.40**, **5.46**, and **5.55**) did not exhibit any significant affinity for either CB_1R or CB_2R. The novel pyridyl-2-carboxamide linker conjugates (**5.33** (K_i = 1217 ± 253.6 nM at hCB_1R), **5.34** (K_i = 2728 ± 625.2 nM at hCB_1R), **5.35** (K_i = 1959 ± 740.4 nM at hCB_1R), and **5.39** (K_i = 4099 ± 752.2 nM at hCB_1R)) exhibited moderate to low affinity for CB_1R and selectivity over CB_2R (Table 5.3). The short linker conjugate **5.37** (K_i = 245 ± 36.4 nM at hCB_1R) exhibited high affinity for CB_1R and selectivity over CB_2R. The pyridyl-2-carboxamides **5.37** (EC_{50} = 135.5 ± 7.6 nM; Emax = 52.21 ± 0.10 % of forskolin response at hCB_1R) and **5.33** (EC_{50} = 222.7 ± 40.4 nM; Emax = 66.35 ± 3.21 % of forskolin response at hCB_2R) behaved as CB_1R agonists at hCB_1R, consistent with the agonist behaviour previously reported at cCB_1R.[223]

In this chapter, a high affinity CB_1R pyridyl-2-carboxamide based linker conjugate was not obtained. Nevertheless, the literature compound **5.3** exhibited subnanomolar CB_1R affinity; also, the new linker conjugates (**5.37**, **5.33**, **5.34** and **5.35**) displayed high CB_1R selectivity as well as high to moderate CB_1R affinity. Therefore, the optimised pyridyl-2-carboxamide derivatives could be developed into high affinity CB_1R fluorescent ligands.

5.5 Future directions

Introduction of the long *O*-linkers to subnanomolar CB_1R affinity pyridyl-2-carboxamide **5.3** was tolerated albeit with a reduction in the CB_1R affinity. Accordingly, efforts might be directed to prepare derivatives of **5.3** with different *O*-linkers or with linkers conjugated at different positions of the **5.3** core. To this end, synthesis and biological

evaluation of the pyridyl-2-carboxamides with linkers introduced at C-3 naphthyl moiety could be an attractive strategy to develop CB_1R fluorescent ligands.

Chapter 6 Executive conclusions

The primary aims of this thesis were the development of fluorescent ligands for A_1AR and CBRs. Chapter 2 of this thesis described the development of (benzimidazolyl)isoquinolinols as potential A_1AR fluorescent ligands. A multistep synthesis for the preparation of (benzimidazolyl)isoquinolinols along with a procedure for the DDQ and air mediated aromatisation of (benzimidazolyl)tetrahydroisoquinolinols was developed. Investigation for the conformational isomerism of (benzimidazolyl)isoquinolinols by NMR spectroscopy and RP-HPLC studies indicated tautomerism. Unfortunately, none of the fluorescent (benzimidazolyl)isoquinolinols exhibited any significant binding at the A_1AR and it was concluded that (benzimidazolyl)isoquinolinols might not be a suitable pharmacophore for developing A_1AR fluorescent ligands.

In chapter 3, the chromenopyrazole-based ligands with linkers introduced at six different positions were explored for the development of CB_1R fluorescent agonists. Unfortunately, these chromenopyrazoles only had low affinity for CB_1R however did have high affinity for CB_2R. The chromenopyrazole-linker-conjugate with the highest CB_2R affinity was **3.22** *(*Figure 6.1, K_i = 71.1 ± 6.7 nM at hCB_2R; >5000 nM at hCB_1R). Three moderate CB_2R affinity BODIPY-630/650 conjugates (**3.23**, **3.33** and **3.40**) and a high-affinity CB_2R peptide linker conjugate **3.39** were also obtained. The high affinity chromenopyrazoles behaved as agonists at CB_2R in a cAMP functional assay. Docking studies with a homology model of CB_2R showed that linkers conjugated to the high CB_2R affinity chromenopyrazoles likely exit through a cavity located between TM1 and TM7.

Chapter 4 described new peptide-linker analogues of **3.39** and derivatives of the highest CB_2R affinity linker conjugate **3.22** with three different fluorophores (BODIPY-FL, Cy5, TAMRA, BODIPY-630/650). The newly synthesised polar peptide linker conjugates (**4.06**-**4.08**) also exhibited high to moderate CB_2R affinity. Two high affinity, selective CB_2R fluorescent ligands were obtained, the best being **4.02** (Figure 6.1, K_i = 41.8 ± 4.5 nM at hCB_2R; 5856 ± 1264 nM at CB_1R). Fluorescent ligand **4.02** behaved as an inverse agonist in the cAMP BRET assay and was successfully used to visualise CB_2R in HEK-293 cells stably expressing CB_2R in widefield imaging experiments. Fluorescent ligand

4.02 exhibited the higher CB_2R affinity than any reported CB_2R fluorescent ligands in the literature and is also the only reported high affinity CB_2R fluorescent ligand for which functional data has been reported (as of July 2018). Fluorescent ligand **4.02** possesses suitable properties for imaging CB_2R in live cells and can be used as a fluorescent tool by other researchers, for example in fluorescence-based assays, confocal microscopy, flow-cytometry and in resonance energy transfer experiments with other fluorescent partners for studying CB_2R biology.

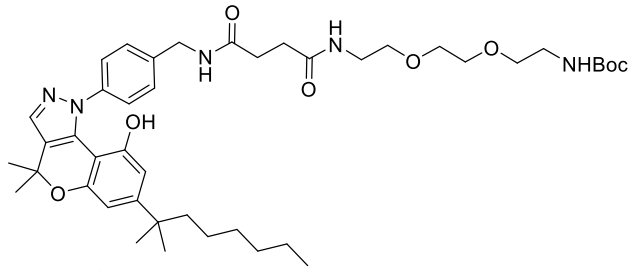

3.22

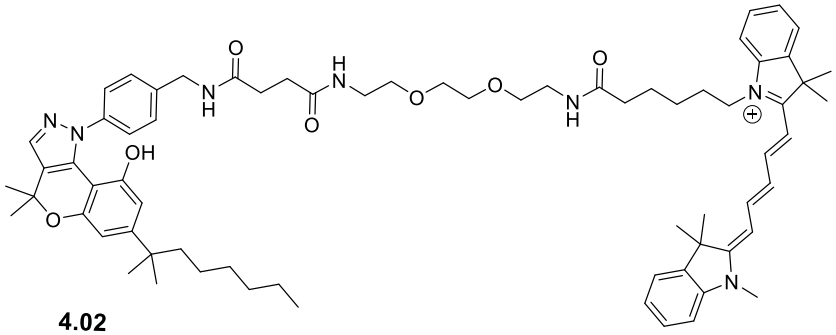

4.02

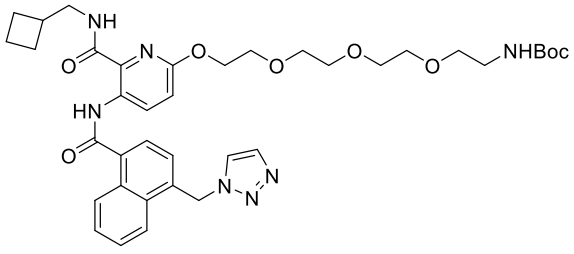

5.33

Figure 6.1. Chromenopyrazole-linker conjugate **3.22**, chromenopyrazole-based-Cy5 conjugate **4.02** and pyridyl-2-carboxamide-linker conjugate **5.33**.

In Chapter 5 previously reported pyridyl derivatives were investigated for the development of CB_1R fluorescent ligands. A multistep synthesis for the preparation of *O*-linker pyridyl-2-carboxamides was developed. Two series of naphthyl and isoquinoline derivatives based on the pyridyl-2-carboxamide scaffold and conjugated to different linkers and BODIY-630/650 were prepared. Although a high CB_1R affinity fluorescent ligand was not obtained, moderate affinity *O*-linker pyridyl-2-carboxamides (for example **5.33**, Figure 6.1, K_i = 1217 ± 253.6 nM at hCB_1R; >5000 nM at hCB_2R) were obtained. It was concluded that pyridyl-2-carboxamide remains a potential scaffold for the development of CB_1R fluorescent ligands and a new series with different *O*-linker-fluorophore or linker-fluorophore introduced at a different position, for example naphthyl, could be explored.

Availability of a high affinity, selective fluorescent ligand with suitable imaging properties will advance the understanding of GPCR biology by enabling use of many fluorescent techniques. These techniques such as confocal microscopy would enable investigation of these receptors in spatiotemporal manner at a single cell level, which has previously not been possible with traditional radioligand assays. One particular application of fluorescent ligand such as **4.02** developed in this thesis could be in determining the expression level of CB_2R in CNS tissue samples using *ex vivo* experiments, which could provide valuable information regarding the role of CB_2R in various neurological disorders and thus guide the development of CB_2R ligands targeted towards CNS disorders. Another important application of **4.02** could be in improving our understanding of the role of CB_2R in various disease conditions such as cancer, a lack of which has likely contributed in the failure of many CB_2R ligands in the clinical trials.

As was described earlier in section 1.2.3.2 of chapter 1, selective fluorescent ligand such as **4.02** could be potentiallly useful as a partner in resonance energy transfer techniques (FRET and BRET) for use in *in vitro* imaging. A derivative of **4.02** containing NIR fluorophore would be potentially useful as an *in vivo* imaging tool in the animal model of disorders implicating CB_2R. Fluorescent ligand **4.02** could also serve as a lead compound for the development of CB_2R selective magnetic resonance active ligands, multivalent ligands, fluorescent covalent ligands, and theranostic agents.

Chapter 7 Experimental

7.1 General methods and experimental procedures

7.1.1 Chemical studies

All chemicals were purchased from Sigma Aldrich, Merck, A K Scientific, or Ark Pharm Inc. BODIPY-630/650-SE and BODIPY-FL-SE were purchased from Life Technologies. Cy5-SE and TAMRA-SE were purchased from Abcam. Reactions were carried out at room temperature (rt) unless otherwise stated. Thin layer chromatography (TLC) for monitoring reactions was performed on commercially available Merck 0.2 mm aluminium-backed silica gel plates 60 F_{254} and visualised under UV light at $\lambda = 254$ and 365 nM, and with ninhydrin, and/or $KMnO_4$ dip. Flash silica gel column chromatography was performed using 40-63 µm silica. An Agilent 1260 Infinity system was used for reverse phase high-performance liquid chromatography (RP-HPLC), with a YMC C8 5 µm (150 × 10 mm) semi-preparative or YMC C8 5 µm (150 × 4.6 mm) analytical column. RP-HPLC solvents were A: H_2O (0.05% TFA) and B: 9:1 MeCN:H_2O (0.05% TFA). For compounds synthesised in chapter 2 (section 7.2.1) analytical RP-HPLC retention times for biologically tested compounds are reported using the method A - 5% solvent B 1 min, gradient of 5-95% solvent B 1-27 min, 95% solvent B 27-28 min, gradient of 95-5% solvent B 28-30 min, 5% solvent B 30-34 min. For compounds synthesised in chapter 3, 4, and 5 (section 7.3.1, 7.4.1, and 7.5.1) analytical RP-HPLC retention times for biologically tested compounds are reported using the method B - 5% solvent B 1 min, gradient of 5-95% solvent B 1-22 min, 95% solvent B 22-28 min, gradient of 95-5% solvent B 28-30 min, 5% solvent B 30-34 min. TFA salts of RP-HPLC purified compounds described in chapter 2 (section 7.2.1) were neutralised using an Amberlyst A21 ion exchange resin before biological testing. Analytical RP-HPLC was used to confirm purity (> 95%) at 254 and 380 nm for all compounds biologically tested. All of the fluorescent ligands were purified by semi-preparative RP-HPLC. High-resolution electrospray ionisation mass spectra (HRMS) was recorded on a Bruker microTOF mass spectrometer. Low-resolution mass spectrometry (MS) was carried out on a Sciex API 3200 quadrupole mass spectrometer. NMR spectroscopy was carried out on a Varian 400-MR or Varian 500 MHz AR Premium Shielded spectrometer. Chemical shifts are listed in ppm (δ), calibrated using residual non-deuterated solvent as the internal standard, and coupling constants (*J*) are recorded in hertz (Hz). Note - not all magnetically non-

equivalent carbons were observed in ^{13}C NMR spectrum for all compounds. In some cases, the calculated yield of the coupling reaction of commercially available fluorophore succinimidyl esters with amine linker conjugates to give fluorescent ligands (obtained in chapters 2, 3, 4, and 5) was greater than quantitative. The proposed reason for this is that the commercially available fluorophore succinimidyl esters are supplied in a higher amount than that specified on the container (usually 1 or 5 mg pack size; the amount of fluorophore specified on the container was used in the calculation of yield). These fluorophores are moisture, light sensitive and were not weighed accurately but instead DMF was added to the whole contents of the container and this DMF solution of the fluorophore was used for the coupling reaction. Other members of the Vernall research group have observed similar high calculated yields of coupling reactions with commercially available fluorophores. ^{1}H and ^{13}C NMR spectra were not obtained for some of the compounds prepared at or near the end of a multistep synthesis (including fluorescent ligands). This was because these compounds were prepared in very small quantities and/or had poor solubility (thereby requiring the use of DMSO-d_6). HRMS was obtained for all of these compounds and these were >95% pure as determined by analytical RP-HPLC. Precursors to these compounds were thoroughly characterised by NMR spectroscopy.

7.1.2 Pharmacological studies

Radioligand binding assays

Competition binding assays were performed with radioligand [^{3}H]-CP55,940 at membrane preparations derived from HEK-293 cells. Preparation of HEK-293 cells stably transfected with either CB_1R or CB_2R was carried out according to a previously described method[169, 212] and protein concentrations determined using the DC Protein Assay Kit (Bio-Rad, Hercules, CA) as previously described.[233] Different concentrations of test compounds and dilutions of [^{3}H]-CP55,940 (PerkinElmer), HEK-293 membrane preparations were prepared in binding buffer (50 mM HEPES (4-(2-hydroxyethyl)-1-piperazineethanesulfonic acid)), 1 mM $MgCl_2$, 1 mM $CaCl_2$, 0.2% [w/v] fatty acid free bovine serum albumin [FAF BSA; MP Biomedicals, Auckland, New Zealand], pH 7.4). All compounds (including radioligand [^{3}H]-CP55,940 and positive control CP55,940) were prepared four times the required concentration in assay. 1 μL of test

compounds (10 mM stock in DMSO) were diluted with binding buffer containing EtOH (249 μL) to give 250 μL solutions, 50 μL of these solutions were added to designated wells of a v-bottom 96-well plate. The concentration of [^{3}H]-CP55,940 used in the radioligand binding assay carried out for chromenopyrazoles and pyridyl-2-carboxamides is described in section 7.3.3, section 7.4.2, and section 7.5.3. CP55,940 was diluted with binding buffer containing DMSO and 50 μL added to a specific well of a v-bottom 96-well plate. HEK-293 membrane preparations were resuspended in binding buffer to give the final assay concentration (protein concentration for determining CBR affinity of chromenopyrazoles and pyridyl-2-carboxamides is described in section 7.3.3, section 7.4.2, and section 7.5.3). The amount of EtOH and DMSO in the vehicle control, test compound dilution, [^{3}H]-CP55,940 dilution and CP55,940 dilution was added such as to maintain consistent solvent levels throughout the dilution series. The final reaction volume of each well was 200 μL including [^{3}H]-CP55,940 and membrane. A solution (50 μL) of binding buffer containing EtOH and DMSO was used in place of test compound or CP55,940 as vehicle controls. The v-bottom 96-well plates containing HEK-293 membrane preparations expressing CB_1R or CB_2R, radioligand [^{3}H]-CP55,940 and test compound (or positive control CP55,940 or vehicle control) were sealed and incubated at 30 °C for 1 h.

During the incubation the GF/C 96-well harvest plate (PerkinElmer) was soaked in 50 μL/well of 0.1% polyethylenimine for 1 h to block the 1.2 μm pore fibreglass filters. At the end of incubation, the harvest plates were washed with 200 μL of ice-cold wash buffer solution (50 mM HEPES pH 7.4, 500 mM NaCl, 0.1% FAF BSA). The 200 μL reaction mixture of the v-bottom plates was transferred into the harvest plates (under vacuum). The v-bottom plates were washed once more with ice-cold wash buffer (200 μL/well) and the contents transferred into the harvest plates. The harvest plates were immediately washed three more times with 200 μL/well of ice-cold wash buffer. The harvest plates were dried overnight at 24 °C, the underside was sealed, and scintillation fluid (50 μL/well) (IRGASAFE PLUS, PerkinElmer) was dispensed. The harvest plates were incubated for 30 min in darkness and scintillation count was read for 2 min/well in a MicroBeta TriLux (PerkinElmer). All of the binding experiments were performed at least three times in triplicate. Data was analysed by nonlinear regression as provided in GraphPad Prism 7 (GraphPad Software, Inc., San Diego, CA, USA).

cAMP functional assays

The functional nature of the test compounds was determined by a commercially available cAMP BRET assay as described previously by Cawson *et al.*[169] and Jiang *et al.*[170] HEK 3HA-CB1 pEF4A or HEK-Flp pcDNA5/FRT HA-3TCS-CB2 63Q (preparation described previously[169, 212]) were seeded in 10 cm tissue culture dishes, one or two days prior to transfection. The next day, 5 μg of pcDNA3L-HIS-CAMYEL plasmid (ATCC, Manassas, VA, USA) that encodes for a cAMP sensor consisting of YFP-Epac-RLuc was transfected into HEK-293 cells using 30 μg of linear PEI (polyethylenimine, molecular weight 25 kDa; Polysciences, Warrington, PA, USA) in 150 mM NaCl. After approximately 24 h, cells were plated in poly-D-lysine (Sigma Aldrich) coated white 96-well Solid White Flat Bottom Polystyrene TC-Treated Microplates (Corning) at a density of 88,000–1,120,000 cells/well in Dulbecco's Modified Eagle's medium (DMEM) containing 10% fetal bovine serum (FBS). After another 24 h, cells were serum-starved for 30 min in Hank's balanced salt solution (pH 7.4) supplemented with 1.0 mg/mL fatty acid free BSA. Cells were treated with luciferase substrate coelenterazine-h (5.0 μM, Nanolight Technology) for 5 min and test compound or vehicle in Hank's balanced salt solution containing 1.0 mg/mL FAF BSA and forskolin (5.0 μM, Tocris, Bristol, UK). Fluorescence emission was immediately measured at 460/25 nM (Renilla luciferase, RLuc) and 535/25 nM (yellow fluorescent protein, YFP) following test compound addition at 37 °C. HEK-293 WT cells matched to the background of the CB_1R or CB_2R expressing cell lines were used as negative controls. Raw data is presented as ratio of fluorescence emission at 460/535 nm (inverse BRET ratio) such that an increase in ratio correlates to an increase in intracellular cAMP concentration. All of the assays were carried out at least three times in duplicate unless stated otherwise.

Data was analysed by nonlinear regression as provided in GraphPad Prism (GraphPad Software, Inc., San Diego, CA, USA). For the area under the curve analysis, raw data (inverse BRET ratio) was normalised to forskolin (100 %) and vehicle (0 %) were normalised to the vehicle (0%) or forskolin (100%) values for individual experiments. The E_{max} value of a test compound was determined as the percentage of normalised forskolin values.

7.2 Experimental procedure and data for compounds as described in chapter 2

7.2.1 Chemical studies

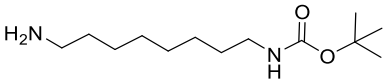

***tert*-Butyl *N*-(8-aminooctyl)carbamate (2.10)**

The compound was synthesised according to a previously reported literature synthesis of **2.10**.[177] To a solution of commercially available 1,8-diaminooctane **2.9** (4.0 g, 27.73 mmol) in 1,4-dioxane (100 mL) was added dropwise a solution of $(Boc)_2O$ (1.27 mL, 5.55 mmol) in 1,4-dioxane (50 mL) at 0 °C. The reaction mixture was warmed to rt and stirred for 12 h. The solvent was removed under reduced pressure and the residue was dissolved in DCM (100 mL). The DCM layer was then carefully washed with warm water (15 × 100 mL, ~35 °C), brine solution, dried over $MgSO_4.H_2O$ and concentrated under reduced pressure to provide **2.10** as a clear oil (1.02 g, 4.17 mmol, 75%). The liquid **2.10** slowly turned into a colourless semisolid upon standing at rt. ^{1}H NMR (400 MHz, $CDCl_3$) δ 1.19 – 1.49 (m, 23H, C(C**H**$_3$)$_3$, 6 × C**H**$_2$ and NH_2), 2.64 (t, 2H, J = 6.8 Hz, CH_2), 2.97 – 3.16 (m, 2H, CH_2), 4.58 (br s, 1H, NH). ^{13}C NMR (101 MHz, $CDCl_3$) δ 26.66, 26.71, 26.76, 28.40, 29.13, 29.22, 29.35, 30.02, 33.72, 40.55, 42.15, 78.90, 155.96. HRMS calculated for $C_{13}H_{29}N_2O_2$ $[M + H]^+$, 245.2218; found, 245.2224.

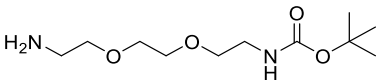

***tert*-Butyl *N*-{2-[2-(2-aminoethoxy)ethoxy]ethyl}carbamate (2.12)**

The compound was synthesised according to a previously reported literature synthesis of **2.12**.[178] To a solution of commercially available diamino-3,6-dioxaoctane **2.11** (5.0 g, 33.73 mmol) in DCM (50 mL) was added dropwise a solution of $(Boc)_2O$ (1.5 mL, 6.75 mmol) in DCM (100 mL) at 0 °C. The reaction mixture was warmed to rt and stirred for 3 h. The DCM solution was washed with water, $NaHCO_3$ solution, brine solution, dried over $MgSO_4.H_2O$ and concentrated under reduced pressure to provide **2.12** (1.50 g, 6.04 mmol, 89%) as a clear oil. ^{1}H NMR (400 MHz, $CDCl_3$) δ 1.41 (s, 9H, C(C**H**$_3$)$_3$), 1.44 (br s, 2H, N**H**$_2$) 2.85 (t, 2H, J = 5.2 Hz, CH_2), 3.23 – 3.33 (m, 2H, CH_2), 3.45 – 3.55 (m, 4H,

2 × C**H**$_2$), 3.59 (s, 4H, 2 × C**H**$_2$), 5.15 (br s, 1H, NH). ^{13}C NMR (101 MHz, $CDCl_3$) δ 28.37, 40.29, 41.69, 70.16, 73.38, 79.09, 155.97. HRMS calculated for $C_{11}H_{25}N_2O_4$ [M + H]$^+$, 249.1809; found, 249.1818.

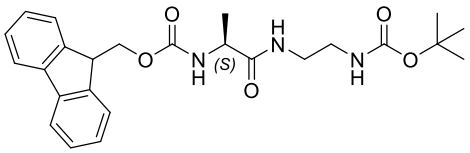

(9*H*-Fluoren-9-yl)methyl *N*-[(1*S*)-1-[(2-{[(*tert*-butoxy)carbonyl]amino}ethyl)-carbamoyl]ethyl] carbamate (2.15)

To a solution of commercially available Fmoc-Ala-OH **2.13** (0.5 g, 1.61 mmol) in DMF (20 mL) was added HBTU (0.61 g, 1.61 mmol), HOBt.H_2O (0.24 g, 1.77 mmol) and DIPEA (0.6 mL, 3.44 mmol) under N_2 atmosphere and the reaction stirred at 0 °C for 10 min. Commercially available *N*-Boc-ethylenediamine **2.14** (0.26 mL, 1.62 mmol) was added to the reaction mixture and reaction stirred at rt for 6 h. The reaction mixture was diluted with EtOAc. The EtOAc solution was washed with water, saturated solution of NH_4Cl, brine, dried over $MgSO_4.H_2O$, concentrated under reduced pressure and the residue purified by silica gel column chromatography (eluting with 70% EtOAc/hexane to 5% MeOH/EtOAc) to provide **2.15** (0.63 g, 1.39 mmol, 86%) as a colourless solid. ^{1}H NMR (400 MHz, $CDCl_3$) δ 1.23 – 1.58 (m, 12H, C**H**$_3$ and C(C**H**$_3$)$_3$), 3.16 – 3.31 (m, 2H, NHC**H**$_2$), 3.29 – 3.47 (m, 2H, NHC**H**$_2$), 4.14 – 4.29 (m, 2H, NHC**H**CH_3, CH Fmoc), 4.31 – 4.50 (m, 2H, OCH_2 Fmoc), 5.11 (br s, 1H, NH), 5.68 (br s, 1H, NH), 6.93 (br s, 1H, NH), 7.24 – 7.34 (m, 2H, Aromatic hydrogen (ArH)), 7.34 – 7.43 (m, 2H, ArH), 7.53 – 7.62 (m, 2H, ArH), 7.68 – 7.82 (m, 2H, ArH). ^{13}C NMR (101 MHz, $CDCl_3$) δ 19.01, 28.46, 40.20, 40.82, 47.23, 50.77, 67.15, 67.18, 79.85, 120.09, 125.18, 127.17, 127.83, 141.39, 143.87, 143.88, 156.11, 157.00, 173.17. HRMS calculated for $C_{25}H_{31}N_3NaO_5$ [M + Na]$^+$, 476.2156; found, 476.2125.

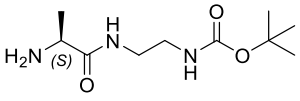

***tert*-Butyl *N*-{2-[(2*S*)-2-aminopropanamido]ethyl}carbamate (2.16)**

To a solution of **2.15** (0.62 g, 1.38 mmol) in DCM (10 mL) was added diethylamine (7.0 mL) at 0°C. The reaction mixture was warmed to rt and stirred for 12 h. The solvent was removed under reduced pressure and the residue was co-evaporated with $CHCl_3$ and

toluene to give **2.16** (0.64 g) as a colourless solid, which was not further purified and used as such for the next reaction.

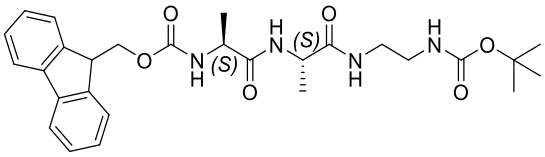

(9*H*-Fluoren-9-yl)methyl *N*-[(1*S*)-1-{[(1*S*)-1-[(2-{[(*tert*-butoxy)carbonyl]amino}ethyl)-carbamoyl] ethyl]carbamoyl}ethyl]carbamate (2.17)

According to the procedure described for **2.15**, Fmoc-Ala-OH (0.43 g, 1.38 mmol) was reacted with **2.16** (0.32 g, 1.38 mmol), HBTU (0.52 g, 1.37 mmol), HOBt.H_2O (0.2 g, 1.37 mmol) and DIPEA (0.5 mL, 2.75 mmol). Purification of the crude compound by silica gel column chromatography (eluting with 20% EtOAc/hexane to 5% MeOH/EtOAc) gave **2.17** (0.59 g, 1.13 mmol, 82%) as a colourless solid. ^{1}H NMR (400 MHz, DMSO-d_6) δ 1.09 – 1.29 (m, 6H, 2 × C**H**$_3$), 1.37 (s, 9H, C(C**H**$_3$)$_3$), 2.88 – 3.02 (m, 2H, NHC**H**$_2$), 3.02 – 3.19 (m, 2H, NHC**H**$_2$), 3.99 – 4.12 (m, 1H, NHC**H**CH$_3$), 4.13 – 4.37 (m, 4H, NHC**H**CH$_3$, CH Fmoc, OCH$_2$ Fmoc), 6.75 (t, 1H, *J* = 5.8 Hz, NH), 7.27 – 7.38 (m, 2H, ArH), 7.38 – 7.47 (m, 2H, ArH), 7.50 – 7.58 (m, 1H, NH), 7.66 – 7.79 (m, 2H, ArH), 7.85 (t, 1H, *J* = 6.0 Hz, NH), 7.87 – 7.97 (m, 3H, NH and ArH). ^{13}C NMR (101 MHz, DMSO-d_6) δ 18.08, 18.39, 28.21, 38.70*, 39.52*, 46.64, 48.15, 50.02, 65.61, 77.65, 120.09, 125.28, 127.07, 127.62, 140.70, 143.78, 143.86, 155.57, 155.75, 172.03, 172.13. (*underneath DMSO-d_6 peaks, identified through gHSQC spectroscopy). HRMS calculated for $C_{28}H_{36}N_4NaO_6$ $[M + Na]^+$, 547.2527; found, 547.2489.

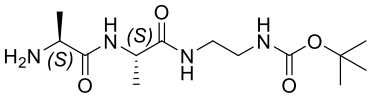

***tert*-Butyl *N*-{2-[(2*S*)-2-[(2*S*)-2-aminopropanamido]propanamido]ethyl}carbamate (2.18)**

The compound was prepared following the procedure used for the preparation of **2.16**, using **2.17** (0.47 g, 0.90 mmol), diethylamine (4.0 mL), DCM (3.0 mL) and MeOH (2.0 mL). Compound **2.18** (0.48 g) was obtained as a colourless solid and used for the next reaction without further purification.

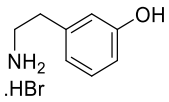

3-(2-Aminoethyl)phenol hydrobromide salt (2.20)

The compound was synthesised according to a previously reported literature synthesis of **2.20**.[179] A solution of commercially available 2-(3-methoxyphenyl)ethan-1-amine **2.19** (5.0 mL, 34.32 mmol) in aq. HBr (30 mL, 48% *w/w*) was stirred for 7 h at 100 °C. The reaction mixture was cooled to rt and the solvent was evaporated under reduced pressure to give a whitish-pink solid. The solid was triturated and co-evaporated with toluene to give **2.20** (8.0 g, 36.86 mmol, quantitative) as a whitish-pink solid, which was used in the next reaction without further purification. ^{1}H NMR (400 MHz, DMSO-d_6) δ 2.74 – 2.81 (m, 2H, CH_2), 2.95 – 3.04 (m, 2H, CH_2), 6.60 – 6.75 (m, 3H, ArH), 7.03 – 7.17 (m, 1H, ArH), 7.80 (m, 3H, NH_2 and OH). HRMS calculated for $C_8H_{12}NO$ $[M + H]^+$, 138.0913; found, 138.0907.

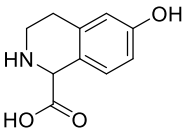

6-Hydroxy-1,2,3,4-tetrahydroisoquinoline-1-carboxylic acid (2.21)

The compound was synthesised according to a previously reported literature synthesis of **2.21**.[180] To a solution of **2.20** (1.0 g, 4.58 mmol) in EtOH (22.0 mL) was added Et_3N (0.7 mL, 5.04 mmol) and the reaction stirred for 10 min. The reaction mixture was cooled to 4 °C and a solution of glyoxylic acid (0.42 g, 4.58 mmol) in EtOH (5.0 mL) was added dropwise and the reaction was stirred for 1 h and then at rt for another 1 h. The resulting solid was filtered and washed with EtOH to give the **2.21** (0.63 g, 3.23 mmol, 71%) as a colourless solid. ^{1}H NMR (400 MHz, DMSO-d_6) δ 2.66 – 2.79 (m, 1H, C**H***HCH$_2$), 2.79 – 2.93 (m, 1H, CH**H***CH$_2$), 3.01 – 3.14 (m, 1H, CH$_2$C**H***H), 3.26 – 3.34 (m, 1H, CH$_2$CH**H***), 4.33 (s, 1H, C**H**CO$_2$H), 6.49 (d, 1H, *J* = 2.5 Hz, ArH), 6.56 – 6.63 (m, 1H, ArH), 7.50 (d, 1H, *J* = 8.5 Hz, ArH), 8.80 (br m, 2H, NH, OH), 9.37 (br s, 1H, CO_2H). (* designates diastereotopic protons). ^{13}C NMR (101 MHz, DMSO-d_6) δ 25.25, 57.82, 113.57, 113.91, 121.19, 129.06, 132.69, 155.88, 167.15. HRMS calculated for $C_{10}H_{10}NO_3$ $[M – H]^-$, 192.0652; found, 192.0666.

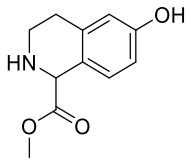

Methyl 6-hydroxy-1,2,3,4-tetrahydroisoquinoline-1-carboxylate (2.22)

To a suspension of **2.21** (6.63 g, 34.32 mmol) in MeOH (150 mL) at 0 °C was added dropwise $SOCl_2$ (7.5 mL, 102.95 mmol) under N_2 atmosphere. The reaction mixture was warmed to rt and stirred for 15 h. The solvent was removed under reduced pressure and the resulting solid was dissolved in THF (30 mL) and neutralised with Et_3N (15 mL). The mixture was filtered to remove $Et_3N.HCl$ and the filtrate evaporated under reduced pressure to give **2.22** (7.11 g, 34.31 mmol, quantitative) as a yellow solid. ^{1}H NMR (400 MHz, MeOD-d_4) δ 2.66 – 2.79 (m, 2H, C**H$_2$***CH$_2$), 2.93 – 3.02 (m, 1H, CH$_2$C**H***H), 3.21 – 3.30 (m, 1H, CH$_2$CH**H***), 3.74 (s, 3H, OCH$_3$), 4.60 (s, 1H, C**H**CO$_2$CH$_3$), 6.54 (d, 1H, *J* = 2.6 Hz, ArH), 6.60 (dd, 1H, *J* = 2.6, 8.4 Hz, ArH), 7.13 (d, *J* = 8.46 Hz, 1H, ArH). (* designates diastereotopic protons). ^{13}C NMR (101 MHz, MeOD-d_4) δ 29.49, 41.18, 52.65, 58.98, 114.60, 116.22, 123.45, 129.77, 137.57, 157.64, 174.89. HRMS calculated for $C_{11}H_{14}NO_3$ $[M + H]^+$, 208.0973; found, 208.0975. The synthesis of **2.22** has previously been reported by Ma *et al.*[181] but without spectroscopic data of **2.22**.

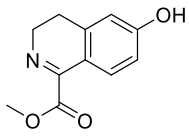

Example of an <u>unoptimised</u> DDQ aromatisation reaction – formation of methyl 6-hydroxy-3,4-dihydroisoquinoline-1-carboxylate (2.23)

Tetrahydroquninoline **2.22** (0.11 g, 0.57 mmol) was reacted with DDQ (0.26 g, 1.13 mmol) in a solvent mixture of THF (3 mL) and 1,4-dioxane (10 mL) at 110 °C under N_2 atmosphere for 6 h. The solvent was removed under reduced pressure and the residue was diluted with EtOAc and washed three times with saturated aq. $NaHCO_3$ solution. The organic washings were combined, washed once with water, brine solution, then dried over $MgSO_4.H_2O$, concentrated under reduced pressure and purified by silica gel column chromatography (30% EtOAc/hexane to 60% EtOAc/hexane) to provide **2.23** (0.03 g, 0.18 mmol, 32%) as a pale yellow solid was isolated. ^{1}H NMR (400 MHz, $CDCl_3$) δ 2.70 – 2.80 (m, 2H, CH_2), 3.77 – 3.88 (m, 2H, CH_2), 3.91 (s, 3H, CH_3), 6.71 (d, 1H, *J* = 2.4 Hz, ArH), 6.75 – 6.83 (m, 1H, ArH), 7.66 (d, 1H, *J* = 8.6 Hz, ArH). HRMS calculated for $C_{11}H_{12}NO_3$ $[M + H]^+$, 206.0812; found, 206.0806.

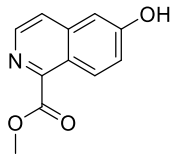

<u>Optimised</u> DDQ aromatisation reaction - preparation of methyl 6-hydroxyisoquinoline-1-carboxylate (2.24)

To a solution of **2.22** (0.17 g, 0.83 mmol) in 1,4-dioxane:THF (10mL 1:1, *v*:*v*) at 45 °C was added DDQ (0.38 g, 1.67 mmol) and the reaction was stirred vigorously at 45 °C for 5 h with the mouth of the flask open to the atmosphere to allow mixing of air. 1,4-Dioxane (10 mL) was added and the reaction mixture filtered, the filtrate was diluted with EtOAc and washed three times with saturated aq. $NaHCO_3$ solution. The organic washings were combined, washed once with water, brine solution, then dried over $MgSO_4.H_2O$, concentrated under reduced pressure and purified by silica gel column chromatography (30% EtOAc/hexane to 50% EtOAc/hexane) to provide **2.24** (84 mg, 0.413 mmol, 49 %) as an off-white solid. ^{1}H NMR (400 MHz, MeOD-d_4) δ 4.04 (s, 3H, OCH_3), 7.16 (d, *J* = 2.5 Hz, 1H, ArH), 7.28 (dd, 1H, *J* = 2.5, 9.3 Hz, ArH), 7.73 (d, 1H, *J* = 5.7 Hz, ArH), 8.30 (d, 1H, *J* = 5.7 Hz, ArH), 8.52 (d, 1H, *J* = 9.3 Hz, ArH). ^{13}C NMR (101 MHz, MeOD-d_4) δ 53.24, 108.72, 122.70, 122.89, 124.25, 129.49, 141.07, 141.83, 149.28, 161.18, 167.61. HRMS calculated for $C_{11}H_{10}NO_3$ $[M + H]^+$, 204.0655; found, 204.0647. The isoquinoline **2.24** has been reported once before in the literature in a Japanese patent[183] but no spectroscopic data was provided.

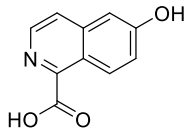

6-Hydroxyisoquinoline-1-carboxylic acid (2.25)

To a solution of **2.24** (2.6g, 12.79 mmol) in THF (20 mL) at 0°C was added a solution of LiOH (0.92 g, 38.38 mmol) in water (15 mL). The reaction mixture was warmed to rt and stirred for another 12 h. The solvent was evaporated under reduced pressure and the residue was acidified (pH 2.0-3.0) with 2.0 N aq. HCl. A yellow precipitate formed that was collected by filtration, washed with 5.0 N aq. HCl (50 mL) and dried to give **2.25** (2.3 g, 12.15 mmol, 96%) as a yellow solid. ^{1}H NMR (400 MHz, DMSO-d_6) δ 7.24 (d, 1H, *J* = 2.5 Hz, ArH), 7.33 (dd, 1H, *J* = 2.5, 9.2 Hz, ArH), 7.85 (dd, 1H, *J* = 0.8, 6.0 Hz, ArH), 8.33 (d, *J* = 5.8 Hz,1H, ArH), 8.65 (d, 1H, *J* = 9.2 Hz, ArH), 10.78 (br s, 1H, CO_2H). ^{13}C NMR (101 MHz, DMSO-d_6) δ 107.77, 120.06, 121.75, 122.26, 129.11,

139.05, 139.42, 149.60, 159.96, 165.99. HRMS calculated for $C_{10}H_7NNaO_3$ $[M + Na]^+$, 212.0318; found, 212.0323.

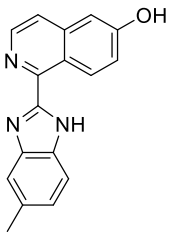

1-(5-Methyl-1*H*-1,3-benzodiazol-2-yl)isoquinolin-6-ol (2.26)

According to a modified literature procedure for the PPA mediated synthesis of (benzimidazolyl)isoquinoline,[76] a mixture of **2.25** (0.1 g, 0.49 mmol), 3,4-diaminotoluene (0.07g, 0.59 mmol) and PPA (polyphosphoric acid, ≥83% phosphate as P_2O_5 basis) (~5 g) were heated at 250 °C for 6 h. The resulting viscous black liquid was slowly basified (pH = 8.0 - 10.0) with KOH at 0 °C (caution:exothermic) and extracted with EtOAc. The EtOAc layer was washed with saturated aq. $NaHCO_3$ solution, water, brine solution, dried over $MgSO_4.H_2O$ and the residue was purified by silica gel column chromatography (10% EtOAc/hexane to 50% EtOAc/hexane) to give **2.26** (24 mg, 0.08 mmol, 18%) as an off-white solid. ^{1}H NMR (400 MHz, MeOD-d_4) δ 2.48 (s, 3H, CH_3), 7.06 – 7.20 (m, 2H, ArH isoquinoline and ArH benzimidazole), 7.24 – 7.32 (m, 1H, ArH isoquinoline), 7.47 (br s, 1H, ArH benzimidazole), 7.53 – 7.69 (m, 2H, ArH isoquinoline and ArH benzimidazole), 8.40 (d, 1H, J = 5.7 Hz, ArH isoquinoline), 9.20 (d, 1H, J = 9.3 Hz, ArH isoquinoline). ^{13}C NMR (101 MHz, MeOD-d_4) δ 21.81, 108.74, 121.98, 122.16, 122.94, 125.91, 130.87, 134.42, 141.02, 142.76, 148.70, 152.04, 160.82. HRMS calculated for $C_{17}H_{14}N_3O$ $[M + H]^+$, 276.1131; found, 276.1118. Analytical RP-HPLC R_t = 13.26 min; determined with HPLC method A.

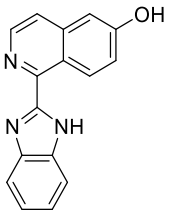

1-(1*H*-1,3-Benzodiazol-2-yl)isoquinolin-6-ol (2.27)

According to the procedure described for **2.26**, a mixture of **2.25** (0.2 g, 1.05 mmol) and *o*-phenylenediamine (0.08 g, 0.74 mmol) were reacted to give **2.27** (27 mg, 0.10 mmol, 21%) as an off-white solid. ^{1}H NMR (400 MHz, MeOD-d_4) δ 7.19 (d, 1H, J = 2.5 Hz,

ArH isoquinoline), 7.27 – 7.38 (m, 3H, ArH isoquinoline, benzimidazole), 7.55 – 7.88 (m, 3H, ArH isoquinoline, benzimidazole), 8.46 (d, 1H, *J* = 5.8 Hz, ArH isoquinoline), 9.25 (d, 1H, *J* = 9.3 Hz, ArH isoquinoline). ^{13}C NMR (101 MHz, MeOD-d_4) δ 101.42, 108.77, 122.12, 122.31, 123.03, 130.86, 141.11, 142.86, 148.67, 152.44, 160.97. HRMS calculated for $C_{16}H_{12}N_3O$ $[M + H]^+$, 262.0975; found, 262.0967. Analytical RP-HPLC R_t = 11.61 min; determined with HPLC method A.

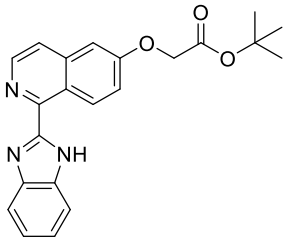

***tert*-Butyl 2-{[1-(1*H*-1,3-benzodiazol-2-yl)isoquinolin-6-yl]oxy}acetate (2.28)**

A mixture of (benzimidazolyl)isoquinolinol **2.27** (45 mg, 0.172 mmol) and K_2CO_3 (48 mg, 0.0.34 mmol) in anhydrous THF (5 mL) were stirred at 60 °C for 20 min under N_2 atmosphere, followed by addition of a solution of *tert*-butyl bromoacetate (40 µL, 0.26 mmol) in anhydrous THF (1 mL). The reaction was stirred at 60 °C for 12 h. The solvent was removed under reduced pressure and the residue was partitioned between EtOAc and saturated aq. NH_4Cl, the EtOAc layer was washed further with brine solution, dried over $MgSO_4.H_2O$ and concentrated under reduced pressure. The residue was purified by silica gel column chromatography (20% EtOAc/hexane to 30% EtOAc/hexane) to give **2.28** (60 mg, 0.16 mmol, 93%) as an off-white solid. ^{1}H NMR (400 MHz, $CDCl_3$) δ 1.51 (s, 9H, C(C**H**$_3$)$_3$), 4.69 (s, 2H, CH_2), 7.03 (d, 1H, *J* = 2.6 Hz, ArH benzimidazole), 7.28 – 7.34 (m, 2H, ArH isoquinoline and ArH benzimidazole), 7.37 – 7.54 (m, 2H, ArH isoquinoline and ArH benzimidazole), 7.58 (d, 1H, *J* = 5.6 Hz, ArH isoquinoline), 7.94 (br s, 1H, ArH benzimidazole), 8.47 (d, 1H, *J* = 5.6 Hz, ArH isoquinoline), 10.17 (d, 1H, *J* = 9.5 Hz, ArH isoquinoline), 11.48 (br s, 1H, NH). ^{13}C NMR (101 MHz, $CDCl_3$) δ 28.20, 65.77, 82.98, 105.71, 111.28, 120.68, 121.41, 121.82, 122.63, 122.95, 124.24, 131.02, 133.35, 139.31, 141.95, 144.95, 146.40, 151.48, 159.28, 167.46. HRMS calculated for $C_{22}H_{22}N_3O_3$ $[M + H]^+$, 376.1656; found, 376.1628.

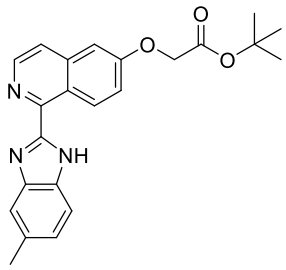

***tert*-Butyl 2-{[1-(5-methyl-1*H*-1,3-benzodiazol-2-yl)isoquinolin-6-yl]oxy}acetate (2.29)**

According to the procedure described for **2.28**, a mixture of **2.26** (150 mg, 0.54 mmol), K_2CO_3 (151 mg, 1.09 mmol) and *tert*-butyl bromoacetate (0.12 mL, 0.82 mmol) were reacted to give **2.29** (203 mg, 0.521 mmol, 96%) as an off-white solid. ^{1}H NMR (400 MHz, $CDCl_3$) δ 1.51 (s, 9H, C(C**H**$_3$)$_3$), 2.50 (s, 3H, CH_3), 4.69 (s, 2H, CH_2), 7.03 (d, 1H, *J* = 2.7 Hz, ArH isoquinoline), 7.10 – 7.17 (m, 1H, ArH benzimidazole), 7.32 (br s, 1H, ArH benzimidazole), 7.48 (dd, 1H, *J* = 2.7, 9.5 Hz, ArH isoquinoline), 7.57 (d, 1H, *J* = 5.6 Hz, ArH isoquinoline), 7.64 – 7.89 (br s, 1H, ArH benzimidazole), 8.45 (d, 1H, *J* = 5.6 Hz, ArH isoquinoline), 10.16 (d, 1H, *J* = 9.5 Hz, ArH isoquinoline), 11.24 (br s, 1H, NH). ^{13}C NMR (101 MHz, $CDCl_3$) δ 21.94, 28.20, 65.78, 82.96, 105.71, 111.19, 120.20, 121.33, 121.63, 122.88, 124.56, 131.09, 133.85, 139.30, 141.89, 146.47, 151.14, 159.27, 167.47. HRMS calculated for $C_{23}H_{24}N_3O_3$ $[M + Na]^+$, 390.1812; found, 390.1783.

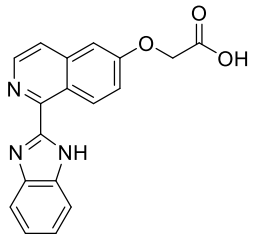

2-{[1-(1*H*-1,3-Benzodiazol-2-yl)isoquinolin-6-yl]oxy}acetic acid (2.30)

To a solution of **2.28** (50 mg, 0.13 mmol) in DCM (5 mL) at 0 °C was added TFA (1 mL, 13.32 mmol) and the mixture stirred for 5 h. The DCM and TFA were removed under reduced pressure to provide an oil, which solidified to a yellow solid upon co-evaporation with $CHCl_3$/hexane. This solid was washed with cold MeOH to give **2.30** (27 mg, 0.08 mmol, 64%) as a yellow solid. ^{1}H NMR (400 MHz, DMSO-d_6) δ 4.91 (s, 2H, CH_2), 7.19 – 7.35 (m, 2H, ArH benzimidazole), 7.42 (d, 1H, *J* = 2.7 Hz, ArH isoquinoline), 7.52 (dd, 1H, *J* = 2.7, 9.5 Hz, ArH isoquinoline), 7.61 (d, 1H, *J* = 7.8 Hz, ArH benzimidazole), 7.83 (d, 1H, *J* = 8.0 Hz, ArH benzimidazole), 7.87 (d, 1H, *J* = 5.6 Hz, ArH isoquinoline), 8.59 (d, 1H, *J* = 5.6 Hz, ArH isoquinoline), 10.04 (d, 1H, *J* = 9.5 Hz, ArH isoquinoline),

13.17 (br m, 2H, NH and CO_2H). ^{13}C NMR (101 MHz, DMSO-d_6) δ 64.64, 105.98, 112.05, 119.66, 121.12, 121.59, 121.82, 121.93, 123.57, 129.87, 133.99, 138.90, 142.21, 144.02, 146.10, 151.25, 158.74, 169.65. HRMS calculated for $C_{18}H_{14}N_3O_3$ $[M + H]^+$, 320.10297; found, 320.1008.

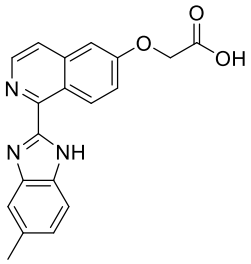

2-{[1-(5-Methyl-1*H*-1,3-benzodiazol-2-yl)isoquinolin-6-yl]oxy}acetic acid (2.31)

According to the procedure described for **2.30**, a mixture of **2.29** (196 mg, 0.503 mmol) and TFA gave **2.31** (172 mg, 0.51 mmol, quantitative) as a yellow solid. ^1H NMR (400 MHz, MeOD-d_4) δ 2.53 (s, 3H, CH_3), 4.90 (s, 2H, CH_2), 7.21 – 7.32 (m, 1H, ArH benzimidazole), 7.35 (d, 1H, *J* = 2.6 Hz, ArH isoquinoline or ArH benzimidazole), 7.48 (dd, 1H, *J* = 2.6, 9.4 Hz, ArH isoquinoline), 7.56 (s, 1H, ArH benzimidazole), 7.66 (d, 1H, *J* = 8.3 Hz, ArH isoquinoline or ArH benzimidazole), 7.85 (d, 1H, *J* = 5.6 Hz, ArH isoquinoline), 8.56 (d, 1H, *J* = 5.7 Hz, ArH isoquinoline), 9.00 (d, 1H, *J* = 9.4 Hz, ArH isoquinoline). ^{13}C NMR (101 MHz, MeOD-d_4) δ 21.79, 65.95, 107.39, 115.10, 115.56, 123.63, 123.70, 124.56, 128.61, 128.81, 133.62, 135.34, 137.94, 140.84, 143.65, 144.56, 149.01, 161.33, 171.68. HRMS calculated for $C_{19}H_{15}N_3NaO_3$ $[M + Na]^+$, 356.1006; found, 356.0997. Analytical RP-HPLC R_t = 13.00 min; determined with HPLC method A.

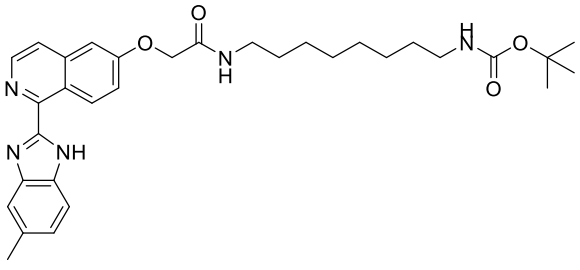

***tert*-Butyl *N*-[8-(2-{[1-(5-methyl-1*H*-1,3-benzodiazol-2-yl)isoquinolin-6-yl]oxy} acetamido)octyl]-carbamate (2.32)**

To a solution of **2.31** (32 mg, 0.09 mmol) and HATU (38 mg, 0.10 mmol) in anhydrous DMF (1 mL) was added DIPEA (30 µL, 0.19 mmol) and the mixture was stirred for 15

min. A solution of **2.10** (70 mg, 0.29 mmol) in DMF (1 mL) was then added and the mixture stirred for 4 h. The solvent was removed under reduced pressure and the resulting residue partitioned between EtOAc and water. The EtOAc layer was washed three times with NH_4Cl solution, once with water and brine solution, dried over $MgSO_4.H_2O$ and the solvent evaporated. The residue was purified by silica gel column chromatography (20% EtOAc/hexane to 50% EtOAc/hexane) to give **2.32** (37 mg, 0.06 mmol, 69%) as a clear oil. ^{1}H NMR (400 MHz, $CDCl_3$) δ 1.08 – 1.32 (m, 8H, 4 × C**H**$_2$), 1.44 (s, 13H, 2 × C**H**$_2$ and C(C**H**$_3$)$_3$), 2.50 (s, 3H, CH_3), 3.05 (q, 2H, *J* = 6.8 Hz, CONHC**H**$_2$ or C**H**$_2$NHBoc), 3.35 (q, 2H, *J* = 6.8 Hz, CONHC**H**$_2$ or C**H**$_2$NHBoc), 4.53 (t, 1H, *J* = 6.0 Hz, NH), 4.66 (s, 2H, OCH_2CO), 6.59 (t, 1H, *J* = 6.0 Hz, NH), 7.09 (d, 1H, *J* = 2.7 Hz, ArH isoquinoline), 7.11 – 7.18 (m, 1H, ArH benzimidazole), 7.43 (dd, 1H, *J* = 2.6, 9.5 Hz, ArH isoquinoline), 7.50 – 7.75 (m, 3H, ArH isoquinoline and ArH benzimidazole), 8.48 (d, 1H, *J* = 5.6 Hz, ArH isoquinoline), 10.18 (d, 1H, *J* = 9.4 Hz, ArH isoquinoline), 11.16 (b s, 1H, NH). ^{13}C NMR (101 MHz, $CDCl_3$) δ 21.94, 26.79, 26.88, 28.58, 29.25, 29.27, 29.63, 30.11, 39.26, 40.68, 67.39, 79.15, 105.92, 120.96, 121.68, 122.97, 124.79, 131.38, 139.28, 142.27, 146.49, 151.01, 156.14, 158.33, 167.41. HRMS calculated for $C_{32}H_{42}N_5O_4$ $[M + H]^+$, 560.3231; found, 560.3196.

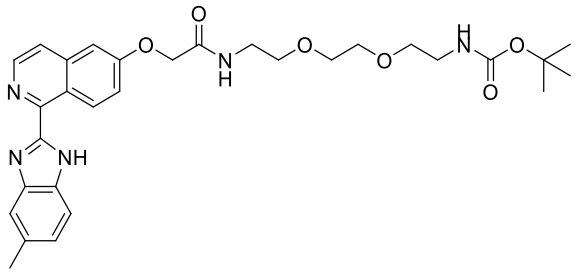

***tert*-Butyl *N*-(2-{2-[2-(2-{[1-(5-methyl-1*H*-1,3-benzodiazol-2-yl)isoquinolin-6-l]oxy} acetamido)ethoxy]-ethoxy}ethyl)carbamate (2.33)**

According to the procedure described for **2.32**, a mixture of **2.31** (60 mg, 0.18 mmol), **2.12** (134 mg, 0.54 mmol), HATU (72 mg, 0.19 mmol) and DIPEA (70 µL, 0.36 mmol) gave a residue that was purified by silica gel column chromatography (50% EtOAc/hexane to 4% MeOH/EtOAc) to give **2.33** (52 mg, 0.09 mmol, 52%) as a colourless solid. ^{1}H NMR (400 MHz, $CDCl_3$) δ 1.42 (s, 9H, C(C**H**$_3$)$_3$), 2.48 (s, 3H, CH_3), 3.25 – 3.32 (m, 2H, CONHC**H**$_2$ or C**H**$_2$NHBoc), 3.45 – 3.63 (m, 10H, 5 × C**H**$_2$), 4.65 (s, 2H, OCH_2CO), 5.06 (br s, 1H, NH), 6.97 – 7.18 (m, 3H, NH, ArH benzimidazole, ArH isoquinoline), 7.28 – 7.79 (m, 4H, ArH benzimidazole, ArH isoquinoline), 8.46 (d, 1H, *J*

= 5.6 Hz, ArH isoquinoline), 10.15 (d, 1H, *J* = 9.4 Hz, ArH isoquinoline), 11.32 (br s, 1H, NH). ^{13}C NMR (101 MHz, $CDCl_3$) δ 21.90, 28.51, 39.03, 40.39, 67.34, 69.78, 70.19, 70.30, 70.35, 79.40, 105.90, 120.92, 121.63, 122.93, 124.96, 131.31, 133.71, 139.23, 142.18, 146.56, 151.00, 156.08, 158.33, 167.61. HRMS calculated for $C_{30}H_{38}N_5O_6$ $[M + H]^+$, 564.2817; found, 564.2798. Analytical RP-HPLC R_t = 16.42 min; determined with HPLC method A.

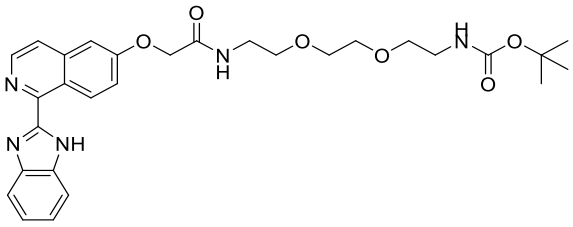

***tert*-Butyl *N*-(2-{2-[2-(2-{[1-(1*H*-1,3-benzodiazol-2-yl)isoquinolin-6-yl]oxy}acetamido) ethoxy]ethoxy}-ethyl)carbamate (2.34)**

According to the procedure described for **2.32**, a mixture of **2.30** (25 mg, 0.08 mmol), **2.12** (40 mg, 0.16 mmol), HATU (31 mg, 0.08 mmol) and DIPEA (30 μL, 0.19 mmol) gave a residue that was purified by silica gel column chromatography (50% EtOAc/hexane to 2% MeOH/EtOAc) to provide **2.34** (23 mg, 0.04 mmol, 55%) as pale yellow oil. ^{1}H NMR (500 MHz, $CDCl_3$) δ 1.41 (s, 9H, C(C**H**$_3$)$_3$), 3.28 (q, 2H, *J* = 5.4 Hz, CONHC**H**$_2$ or C**H**$_2$NHBoc), 3.44 – 3.70 (m, 10H, 5 × C**H**$_2$), 4.61 (s, 2H, OCH_2CO), 5.06 (s, 1H, NH), 7.05 (s, 1H, ArH isoquinoline), 7.12 (s, 1H, NH), 7.29 – 7.44 (m, 3H, ArH isoquinoline or ArH benzimidazole), 7.62 (d, 1H, *J* = 5.6 Hz, ArH isoquinoline), 7.73 – 7.83 (m, 2H, ArH isoquinoline or ArH benzimidazole), 8.36 – 8.49 (m, 1H, ArH isoquinoline), 9.77 (d, 1H, *J* = 9.2 Hz, ArH isoquinoline). ^{13}C NMR (126 MHz, $CDCl_3$) δ 28.54, 29.83, 39.15, 40.44, 67.30, 69.70, 70.24, 70.29, 70.38, 79.53, 106.11, 115.86, 121.64, 122.46, 122.70, 124.41, 130.57, 139.46, 141.55, 145.01, 149.70, 156.20, 158.78, 167.71. HRMS calculated for $C_{29}H_{35}N_5NaO_6$ $[M + Na]^+$, 572.2480; found, 572.2456.

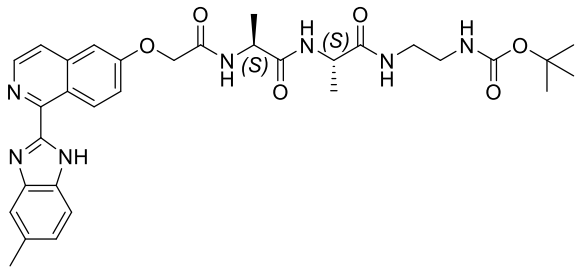

***tert*-Butyl *N*-{2-[(2*S*)-2-[(2*S*)-2-(2-{[1-(5-methyl-1*H*-1,3-benzodiazol-2-yl)-isoquinolin-6-yl]oxy}acetamido)propanamido]propanamido]ethyl}carbamate (2.35)**

According to the procedure described for **2.32**, a mixture of **2.31** (45 mg, 0.13 mmol), **2.18** (122 mg), HATU (54 mg, 0.14 mmol), DIPEA (50 µL, 0.27 mmol) gave a residue that was purified by silica gel column chromatography (70% EtOAc/hexane to 4% MeOH/EtOAc) to give **2.35** (24 mg, 0.04 mmol, 29%) as a pale yellow solid. ^{1}H NMR (500 MHz, MeOD-d_4) δ 1.29 – 1.48 (m, 15H, 2 × C**H**$_3$ alanine and C(C**H**$_3$)$_3$), 2.50 (s, 3H, CH_3 benzimidazole), 3.10 – 3.18 (m, 2H, C**H**$_2$$CH_2$NHBoc or CH_2C**H**$_2$NHBoc), 3.20 – 3.28 (m, 2H, C**H**$_2$$CH_2$NHBoc or CH_2C**H**$_2$NHBoc), 4.25 – 4.35 (m, 1H, C**H**CONH), 4.48 (q, 1H, *J* = 7.1 Hz, C**H**CONH), 4.78 (d, 2H, *J* = 3.0 Hz, OCH_2CO), 7.16 (d, 1H, *J* = 8.4 Hz, ArH benzimidazole), 7.32 – 7.36 (m, 1H, ArH isoquinoline), 7.46 – 7.54 (m, 2H, ArH benzimidazole, ArH isoquinoline), 7.60 (br s, 1H, ArH benzimidazole), 7.78 (d, 1H, *J* = 5.69 Hz ArH isoquinoline), 8.52 (d, 1H, *J* = 5.6 Hz, ArH isoquinoline), 9.42 (d, 1H, *J* = 9.4 Hz, ArH isoquinoline). ^{13}C NMR (126 MHz, MeOD-d_4) δ 18.00, 21.83, 28.75, 40.65, 40.79, 50.51, 50.67, 68.05, 80.14, 107.21, 107.22, 122.18, 122.21, 122.83, 123.91, 125.75, 130.91, 131.05, 140.70, 143.45, 148.59, 152.01, 158.49, 160.39, 170.43, 174.47, 175.07. HRMS calculated for $C_{32}H_{40}N_7O_6$ $[M + H]^+$, 618.3035; found, 618.3078.

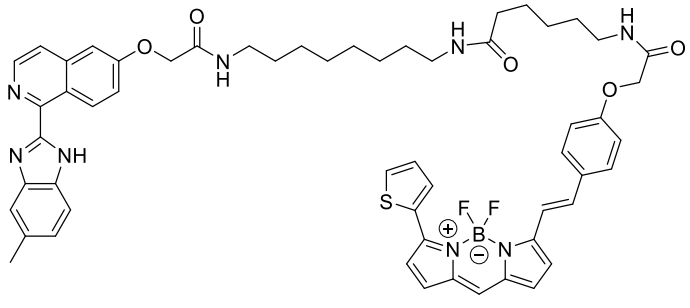

2-Fluoraniumyl-2-fluorescent-4-[(*E*)-2-(4-{[(5-{[8-(2-{[1-(5-methyl-1*H*-1,3-benzodiazol-2-yl)isoquinolin-6-yl]oxy}33acetamido)octyl]carbamoyl}pentyl) carbamoyl]methoxy}-phenyl)ethenyl]-12-(thiophen-2-yl)-1λ^4,3-diaza-2-boratricyclo[7.3.0.0^{3,7}]dodeca-1(12),4,6,8,10-pentaen-2-uide (2.36)

To a solution of **2.32** (6 mg, 0.01 mmol) in DCM (2.0 mL) at 0 °C was added TFA (0.5 mL). The reaction mixture was warmed to rt and stirred for 2 h, volatiles were removed under reduced pressure to provide *N*-(8-aminooctyl)-2-{[1-(5-methyl-1*H*-1,3-benzodiazol-2-yl)isoquinolin-6-yl]oxy}acetamide trifluoroacetate in assumed quantitative yield as a yellow solid. This trifluoroacetate salt was purified using semi-preparative RP-HPLC. To a solution of this semi-preparative RP-HPLC purified trifluoroacetate salt (3.9 mg, 6.79 µmol) in DMF (200 µL), was added a solution of DIPEA (6.42 µL, 36.90 µmol) in DMF (100 µL), followed by addition of solution of BOPIPY630/650-SE (1.7 mg, 2.52 µmol) in DMF (700 µL). The reaction was stirred for 12 h with the exclusion of light then concentrated under reduced pressure and purified by RP-HPLC, freeze-dried, neutralised with Amberlyst A21 ion exchange resin to give **2.36** (0.8 mg, 0.83 µmol, 44%) as a dark blue solid. HRMS calculated for $C_{56}H_{59}BF_2N_8NaO_5S$ [M + Na] $^+$, 1027.4292; found, 1027.4322. Analytical RP-HPLC R_t = 22.85 min; determined with HPLC method A.

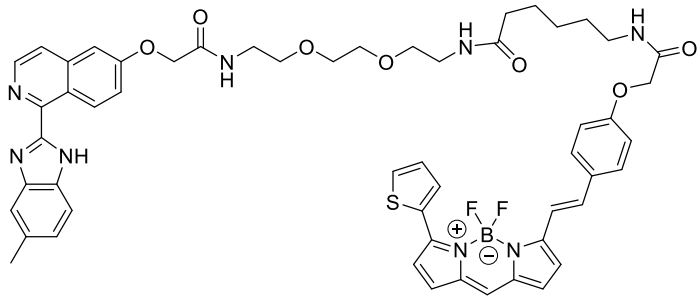

[12-(2-{4-[({5-[(2-{2-[2-(2-{[1-(5-Methyl-1*H*-1,3-benzodiazol-2-yl)isoquinolin-6-yl]oxy}acetamido)ethoxy]ethoxy}ethyl)carbamoyl]pentyl}carbamoyl)methoxy]phenyl}ethenyl)-4-(thiophen-2-yl)-2-(λ²-fluoranidyl)-1λ⁴-aza-3λ⁴-aza-2λ¹-boratricyclo[7.3.0.0³,⁷]dodeca-3,5,7,9,11-pentaene-2,2,2-triium-1-id-2-yl]-λ²-fluoranide (2.37)

According to the procedure for **2.36**, **2.33** (10 mg, 0.02 mmol) was treated with TFA to give *N*-{2-[2-(2-aminoethoxy)ethoxy]ethyl}-2-{[1-(5-methyl-1H-1,3-benzodiazol-2-yl)isoquinolin-6-yl]oxy}acetamide trifluoroacetate salt in assumed quantitative yield as a yellow solid. The trifluoroacetate salt was purified using semi-preparative RP-HPLC. This purified trifluoroacetate salt (5.1 mg, 8.83 µmol) on reaction with BOPIPY630/650-SE (1.2 mg, 1.9 µmol) provided **2.37** (1.0 mg, 0.99 µmol, 54%) as a dark blue solid. HRMS calculated for $C_{54}H_{55}BF_2N_8NaO_7S$ [M + Na]$^+$, 1031.3877; found, 1031.3959. Analytical RP-HPLC R_t = 21.63 min; determined with HPLC method A.

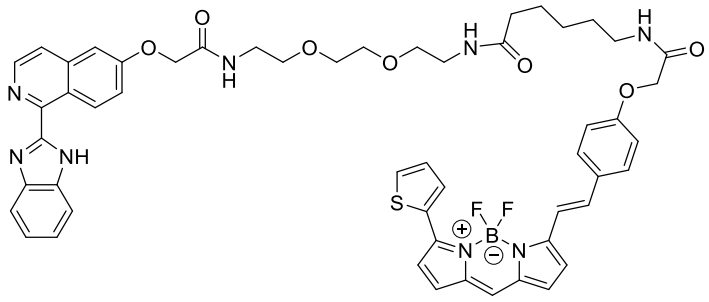

4-[(*E*)-2-{4-[({5-[(2-{2-[2-(2-{[1-(1*H*-1,3-Benzodiazol-2-yl)isoquinolin-6-yl]oxy}acetamido)ethoxy]ethoxy}ethyl)carbamoyl]pentyl}carbamoyl)methoxy]phenyl}ethenyl]-2,2-difluoro-12-(thiophen-2-yl)-1λ^5,3-diaza-2-boratricyclo[7.3.0.0^{3,7}]dodeca-1(12),4,6,8,10-pentaen-1-ylium-2-uid (2.38)

According to the procedure for **2.36**, **2.34** (10 mg, 0.02 mmol) was treated with TFA to give *N*-{2-[2-(2-aminoethoxy)ethoxy]ethyl}-2-{[1-(1*H*-1,3-benzodiazol-2-yl)isoquinolin-6-yl]oxy}acetamide trifluoroacetate salt in assumed quantitative yield as a yellow solid. The trifluoroacetate salt was purified using semi-preparative RP-HPLC. This purified trifluoroacetate salt (5.2 mg, 9.22 µmol) on reaction with BOPIPY630/650-SE (1.2 mg, 1.9 µmol) provided **2.38** (2.1 mg, 2.11 µmol, 84%) as a dark blue solid. HRMS calculated for $C_{53}H_{53}BF_2N_8NaO_7S$ $[M + Na]^+$, 1017.3720; found, 1017.3773. Analytical RP-HPLC R_t = 21.44 min; determined with HPLC method A.

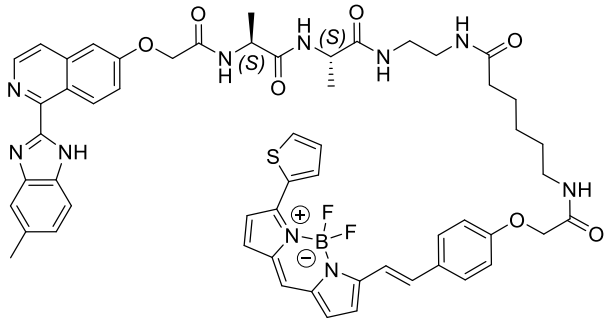

(12-{2-[4-({[5-({2-[(2*S*)-2-[(2*S*)-2-(2-{[1-(5-Methyl-1*H*-1,3-benzodiazol-2-yl)isoquinolin-6-yl]oxy}acetamido)propanamido]propanamido]ethyl}carbamoyl)pentyl]carbamoyl}methoxy)phenyl]ethenyl}-4-(thiophen-2-yl)-2-(λ²-fluoranidyl)-1λ⁴-aza-3λ⁴-aza-2λ¹-boratricyclo[7.3.0.0³,⁷]dodeca-3,5,7,9,11-pentaene-2,2,2-triium-1-id-2-yl)-λ²-fluoranide (2.39)

According to the procedure for **2.36, 2.35** (15 mg, 0.02 mmol) was treated with TFA to give (2*S*)-*N*-[(1S)-1-[(2-aminoethyl)carbamoyl]ethyl]-2-(2-{[1-(5-methyl-1*H*-1,3-benzodiazol-2-yl)isoquinolin-6-yl]oxy}acetamido)propanamide trifluoroacetate salt in assumed quantitative yield as a yellow solid. The trifluoroacetate salt was purified using

semi-preparative RP-HPLC. This purified trifluoroacetate salt (5.5 mg, 8.7 µmol) on reaction with BOPIPY630/650-SE (1.2 mg, 1.9 µmol) provided **2.39** (0.63 mg, 0.59 µmol, 33%) as dark blue solid. HRMS calculated for $C_{56}H_{57}BF_2N_{10}NaO_7S$ $[M + Na]^+$, 1085.4095; found, 1085.4162. Analytical RP-HPLC Rt = 21.05 min; determined with HPLC method A.

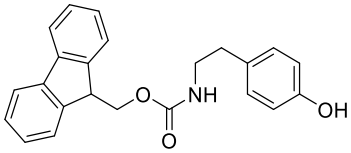

(9*H*-Fluoren-9-yl)methyl *N*-[2-(4-hydroxyphenyl)ethyl]carbamate (2.42)

The compound was synthesised according to a previously reported literature synthesis of **2.42**.[180] To a solution of tyramine **2.40** (10 g, 72.95 mmol) and DIPEA (38.1 mL, 218.8 mmol) in DCM (120 mL) at 0 °C was added a solution of Fmoc-Cl (18.8 g, 72.6 mmol) in DCM (90 mL). The reaction mixture was stirred at 0 °C for 15 min and then warmed to rt and stirred for 20 h. The reaction mixture was diluted with DCM. The DCM solution was washed with saturated solution of $NaHCO_3$ and brine solutions. The DCM layer was dried over dried over $MgSO_4.H_2O$, concentrated under reduced pressure and the residue purified by silica gel column chromatography (30% EtOAc/hexane to 20% Acetone/hexane) to provide **2.42** (21.5 g, 59.82 mmol, 82%) as a colourless solid. ^{1}H NMR (400 MHz, Methanol-d_4) δ 2.67 (t, 2H, J = 7.3 Hz, $NHCH_2C\mathbf{H_2}$), 3.27 (t, 2H, J = 7.3 Hz, $NHC\mathbf{H_2}CH_2$), 4.18 (t, 1H, J = 6.8 Hz, CH Fmoc), 4.32 (d, 2H, J = 6.9 Hz, CH_2 Fmoc), 6.63 – 6.73 (m, 2H, ArH), 7.00 (d, 2H, J = 8.1 Hz, ArH), 7.25 – 7.35 (m, 2H, ArH Fmoc), 7.35 – 7.44 (m, 2H, ArH Fmoc), 7.62 (d, 2H, J = 7.5 Hz, ArH Fmoc), 7.79 (d, 2H, J = 7.5 Hz, ArH Fmoc). HRMS calculated for $C_{23}H_{21}NNaO_3$ $[M + Na]^+$, 382.1414; found, 382.1387.

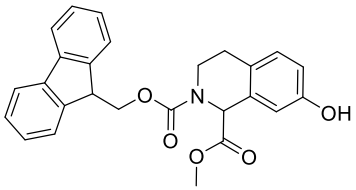

2-(9*H*-Fluoren-9-yl)methyl 1-methyl 7-hydroxy-1,2,3,4-tetrahydroisoquinoline-1,2-dicarboxylate (2.43)

To a solution of **2.42** (19.7 g, 54.85 mmol) in $AcOH/H_2SO_4$ (200 mL, 3:1 *v*:*v*) was added a solution of glyoxylic acid monohydrate (5.5 g, 92.1 mmol) and stirred for 24 h. The

reaction mixture was poured slowly into ice/water (caution: exothermic reaction) and the precipitate formed was separated and dried under vacuum oven (60°C, 300 mbar) for 12 h to give a pinky white solid. This solid was dissolved in DCM and washed with water, brine, dried over $MgSO_4.H_2O$ and solvent evaporated under reduced pressure to give 2-{[(*9H*-fluoren-9-yl)methoxy]carbonyl}-7-hydroxy-1,2,3,4-tetrahydroisoquinoline-1-carboxylic acid (previously reported by Maillard *et al.*[180]) as a pinky white solid (18.4 g) which was used in the next reaction without further purification. To a solution of 2-{[(*9H*-fluoren-9-yl)methoxy]carbonyl}-7-hydroxy-1,2,3,4-tetrahydroisoquinoline-1-carboxylic acid (18.2 g, 43.81 mmol) in MeOH (200 mL) at 0 °C was added dropwise $SOCl_2$ (6.4 mL, 87.62 mmol). The reaction mixture was then heated to 60 °C and stirred for 12 h. The reaction mixture was cooled to rt then concentrated under reduced pressure to give a syrupy residue. This residue was dissolved in EtOAc, washed with saturated aq. $NaHCO_3$ solution, brine solution, dried over $MgSO_4.H_2O$ and purified by silica gel column chromatography (30% EtOAc/hexane to 40% EtOAc/hexane) to give **2.43** (4.3 g, 10.01 mmol, 18% from **2.42**) as a colourless foamy solid. Rt and high temperature NMR spectra revealed the presence of two rotamers in a 2:3 ratio (labelled rotamer A and B). ^{1}H NMR (400 MHz, DMSO-d_6) δ 2.56 – 2.79 (m, 2H, C**H**$_2$CH$_2$NFmoc rotamer A and B), 3.45 – 3.72 (m, 4H, OCH_3, C**H**CO_2CH_3 rotamer A and B), 4.23 – 4.51 (m, 4H, CH_2C**H**$_2$NFmoc and CH_2 Fmoc, rotamer A and B), 5.13 – 5.45 (m, 1H, CHFmoc rotamer A and B) 6.61 – 6.71 (m, 1H, ArH rotamer A and B), 6.81 (dd, *J* = 2.5, 37.4 Hz, 1H, ArH rotamer A and B), 7.00 (t, *J* = 8.5, 8.5 Hz, 1H, ArH rotamer A and B), 7.26 – 7.38 (m, 2H, ArH rotamer A and B), 7.38 – 7.48 (m, 2H, ArH rotamer A and B), 7.57 – 7.71 (m, 2H, ArH rotamer A and B), 7.85 – 7.95 (m, 2H, ArH rotamer A and B), 9.39 – 9.46 (m, 1H, OH rotamer A and B). HRMS calculated for $C_{26}H_{23}NNaO_5$ $[M + Na]^+$, 452.1468; found, 452.1443.

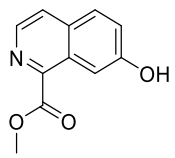

Methyl 7-hydroxyisoquinoline-1-carboxylate (2.44)

According to a modified literature procedure,[188] tetrahydroisoquinoline **2.43** (4.1 g, 9.55 mmol), DMSO (20 mL) and MeOH (20 mL) were stirred at 60 °C for 12 h, diluted with EtOAc, filtered, the filtrate washed with water and dried over $MgSO_4.H_2O$. The solvent was evaporated under reduced pressure to give the Fmoc-deprotected product methyl 7-hydroxy-1,2,3,4-tetrahydroisoquinoline-1-carboxylate, which was then aromatised

according to the procedure for **2.24**, using DDQ (4.4 g, 19.09 mmol) and 1,4-dioxane:THF (1:1 *v*:*v*, 100 mL). The crude compound was purified by silica gel column chromatography (30% EtOAc/hexane to 50% EtOAc/hexane) to provide **2.44** (1.2 g, 5.90 mmol, 61%) as an off-white solid. ^{1}H NMR (500 MHz, MeOD-d_4) δ 4.03 (s, 3H, OCH_3), 7.39 (dd, 1H, *J* = 2.4, 8.9 Hz, ArH), 7.84 – 7.90 (m, 2H, ArH), 8.01 – 8.06 (m, 1H, ArH), 8.31 (d, 1H, *J* = 5.5 Hz, ArH). ^{13}C NMR (126 MHz, MeOD-d_4) δ 53.11, 107.81, 125.21, 125.86, 129.76, 130.23, 133.68, 139.16, 147.02, 159.46, 167.59. HRMS calculated for $C_{11}H_9NNaO_3$ $[M + Na]^+$, 226.0475; found, 226.0481.

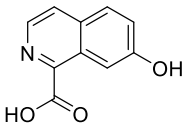

7-Hydroxyisoquinoline-1-carboxylic acid (2.45)

According to the procedure for **2.25**, a solution of **2.44** (1.0 g, 4.92 mmol) and LiOH (0.235 g, 9.84 mmol) gave **2.45** (0.65 g, 3.43 mmol, 70%) as yellowish solid. ^{1}H NMR (500 MHz, D_2O) δ 7.24 – 7.28 (m, 1H, ArH), 7.33 (dd, 1H, *J* = 2.4, 8.9 Hz, ArH), 7.68 (d, 1H, *J* = 5.8 Hz, ArH), 7.80 (d, 1H, *J* = 9.0 Hz, ArH), 8.09 (d, 1H, *J* = 5.7 Hz, ArH). ^{13}C NMR (126 MHz, D_2O) δ 110.27, 123.79, 128.39, 128.88, 131.25, 133.19, 139.13, 158.22, 163.05, 177.87. HRMS calculated for $C_{10}H_8NO_3$ $[M + H]^+$, 190.0499; found, 190.0494.

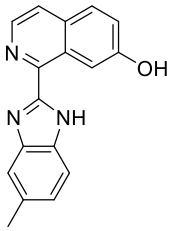

1-(5-Methyl-1*H*-1,3-benzodiazol-2-yl)isoquinolin-7-ol (2.46)

According to the procedure described for **2.26**, a mixture of **2.45** (200 mg, 1.05 mmol) and 3,4-diaminotoluene (130 mg, 1.05 mmol) were reacted to give **2.46** (72 mg, 0.26 mmol, 24%) as an off-white solid. ^{1}H NMR (500 MHz, MeOD-d_4) δ 2.51 (s, 3H, CH_3), 7.16 (d, 1H, *J* = 8.2 Hz, ArH benzimidazole), 7.40 (dd, 1H, *J* = 2.4, 8.9 Hz, ArH isoquinoline), 7.49 (br s, 1H, ArH benzimidazole), 7.60 (br s, 1H, ArH benzimidazole), 7.78 (d, 1H, *J* = 5.5 Hz, ArH isoquinoline), 7.88 (d, 1H, *J* = 8.9 Hz, ArH isoquinoline), 8.44 (d, 1H, *J* = 5.5 Hz, ArH isoquinoline), 8.74 (d, 1H, *J* = 2.4 Hz, ArH isoquinoline). ^{13}C NMR (126 MHz, MeOD-d_4) δ 21.82, 49.00, 109.34, 123.37, 124.61, 129.65, 129.98,

133.56, 140.13, 147.22, 158.93. HRMS calculated for $C_{17}H_{14}N_3O$ $[M + H]^+$, 276.1131; found, 276.1138. Analytical RP-HPLC R_t = 12.69 min; determined with HPLC method A.

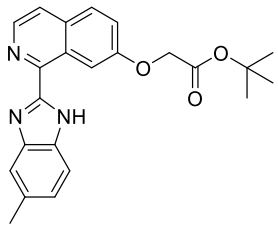

***tert*-Butyl 2-{[1-(5-methyl-1*H*-1,3-benzodiazol-2-yl)isoquinolin-7-yl]oxy}acetate (2.47)**

According to the procedure described for **2.28**, a mixture of **2.46** (45 mg, 0.16 mmol), K_2CO_3 (68 mg, 0.49 mmol) and *tert*-butyl bromoacetate (0.025 mL, 0.17 mmol) were reacted to give **2.47** (42 mg, 0.11 mmol, 66%) as an off-white solid. ^{1}H NMR (400 MHz, $CDCl_3$) δ 1.52 (s, 9H, C(C**H**$_3$)$_3$), 2.52 (s, 3H, CH_3), 4.88 (s, 2H, CH_2), 7.09 – 7.21 (m, 1H, ArH benzimidazole), 7.28 – 7.45 (m, 1H, ArH benzimidazole), 7.52 (dd, 1H, *J* = 2.6, 9.0 Hz, ArH isoquinoline), 7.66 (d, 1H, *J* = 5.4 Hz, ArH isoquinoline), 7.70 – 7.86 (m, 2H, ArH isoquinoline and ArH benzimidazole), 8.46 (d, 1H, *J* = 5.4 Hz, ArH isoquinoline), 9.67 – 9.75 (m, 1H, ArH isoquinoline), 10.78 (br s, 1H, NH). ^{13}C NMR (101 MHz, $CDCl_3$) δ 22.05, 28.27, 65.77, 82.72, 107.06, 110.63*, 110.98*, 120.20*, 120.42*, 122.20, 124.08, 124.19*, 125.81*, 127.92, 128.68, 133.47, 134.34, 140.03, 143.24, 145.19, 151.39, 157.82, 167.83 (*designates carbons linked to broadened benzimidazole protons, as determined by gHSQC, gHMBC experiment). HRMS calculated for $C_{23}H_{23}N_3NaO_3$ $[M + Na]^+$, 412.1632; found, 412.1602.

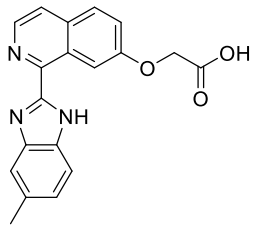

2-{[1-(5-Methyl-1*H*-1,3-benzodiazol-2-yl)isoquinolin-7-yl]oxy}acetic acid (2.48)

According to the procedure described for **2.30**, a mixture of **2.47** (350 mg, 0.90 mmol) and TFA gave **2.48** (179 mg) as a yellow solid. This compound was used as such for next reaction without further purification.

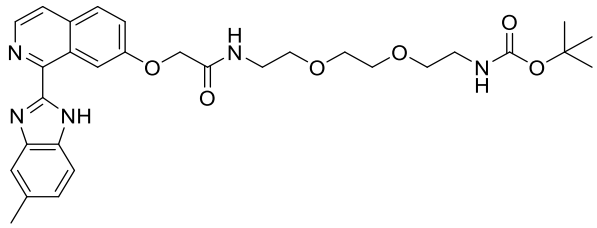

***tert*-Butyl *N*-(2-{2-[2-(2-{[1-(5-methyl-1*H*-1,3-benzodiazol-2-yl)isoquinolin-7-yl]-oxy}acetamido)-ethoxy]ethoxy}ethyl)carbamate (2.49)**

According to the procedure described for **2.32**, a mixture of **2.48** (20 mg, 0.06 mmol), **2.12** (45 mg, 0.18 mmol), HATU (24 mg, 0.06 mmol), DIPEA (20 µL, 0.12 mmol) gave a residue that was purified by silica gel column chromatography (50% EtOAc/hexane to 3% MeOH/EtOAc) to give **2.49** (14 mg, 0.02 mmol, 43%) as a colourless solid. ^{1}H NMR (400 MHz, $CDCl_3$) δ 1.42 (s, 9H, C(C**H**$_3$)$_3$)), 2.50 (s, 3H, CH_3), 3.27 (q, 2H, *J* = 5.5 Hz, m, 2H, C**H**$_2$NH), 3.41 – 3.67 (m, 10H, 5 × CH_2), 4.85 (s, 2H, OCH_2CO), 5.04 (m, 1H, *J* = 6.7 Hz, NH), 7.14 (dd, 1H, *J* = 1.5, 8.3 Hz, ArH benzimidazole), 7.19 (br s, 1H, NH), 7.36 – 7.56 (m, 2H, ArH isoquinoline, ArH benzimidazole), 7.65 (d, 2H, *J* = 5.5 Hz, ArH isoquinoline, ArH benzimidazole), 7.80 (d, 1H, *J* = 9.0 Hz, ArH isoquinoline), 8.46 (d, 1H, *J* = 5.4 Hz, ArH isoquinoline), 9.73 (s, 1H, ArH isoquinoline). ^{13}C NMR (101 MHz, $CDCl_3$) δ 21.91, 28.53, 39.06, 40.41, 67.71, 69.94, 70.21, 70.30, 70.32, 79.46, 108.44, 122.14, 123.32, 125.20, 127.78, 128.89, 133.55, 140.06, 145.21, 150.80, 156.11, 157.05, 168.02. HRMS calculated for $C_{30}H_{38}N_5O_6$ $[M + H]^+$, 564.2817; found, 564.2769. Analytical RP-HPLC R_t = 16.66 min; determined with HPLC method A.

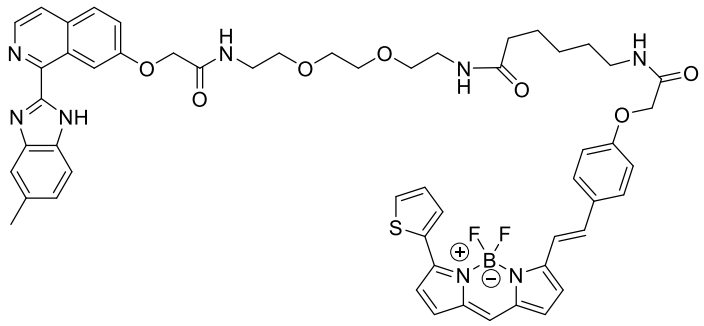

[12-(2-{4-[({5-[(2-{2-[2-(2-{[1-(5-Methyl-1*H*-1,3-benzodiazol-2-yl)isoquinolin-7-yl]oxy}acetamido)ethoxy]ethoxy}ethyl)carbamoyl]pentyl}carbamoyl)methoxy]phenyl}ethenyl)-4-(thiophen-2-yl)-2-(λ²-fluoranidyl)-1λ⁴-aza-3λ⁴-aza-2λ¹-boratricyclo[7.3.0.0³,⁷]dodeca-3,5,7,9,11-pentaene-2,2,2-triium-1-id-2-yl]-λ²-fluoranide (2.50)

According to the procedure for **2.36**, **2.49** (7 mg, 0.01 mmol) was treated with TFA to give *N*-{2-[2-(2-aminoethoxy)ethoxy]ethyl}-2-{[1-(5-methyl-1*H*-1,3-benzodiazol-2-

yl)isoquinolin-7-yl]oxy}trifluoroacetate salt in assumed quantitative yield as a yellow solid. The trifluoroacetate salt was purified using semi-preparative RP-HPLC. This purified trifluoroacetate salt (5.5 mg, 9.52 µmol) on reaction with BOPIPY630/650-SE (1.2 mg, 1.9 µmol) provided **2.50** (0.9 mg, 0.89 µmol, 49%) as a dark blue solid. HRMS calculated for $C_{54}H_{55}BF_2N_8NaO_7S$ $[M + Na]^+$, 1031.3877; found, 1031.3969. Analytical RP-HPLC R_t = 21.68 min; determined with HPLC method A.

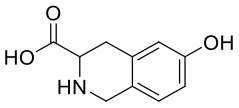

6-Hydroxy-1,2,3,4-tetrahydroisoquinoline-3-carboxylic acid (2.52)

The compound was synthesised according to a previously reported literature synthesis of **2.52**.[189] To a solution of commercially available (+/-)-*m*-tyrosine **2.51** (4.0 g, 22.07 mmol) in aqueous HCl (50.0 mL, 0.05 M), was added aqueous formaldehyde solution (5.0 mL, 37% w/w) and the mixture was stirred at 90 °C for 1 h. The reaction mixture was cooled to rt, filtered, resulting solid was washed with water, acetone and dried in an oven (90 °C) to give **2.52** (2.1 g, 10.88 mmol, 48%) as a colourless solid. ^{1}H NMR (400 MHz, $D_2O^{\#}$) δ 2.73 (dd, 1H, *J* = 11.0, 16.4 Hz, C**H***HCHNH), 2.92 (dd, 1H, *J* = 4.5, 16.5 Hz, CH**H***CHNH), 3.38 (dd, 1H, *J* = 4.5, 11.0 Hz, C**H**NH), 3.73 – 3.9 (m, 2H, NHC**H₂***), 6.40 – 6.51 (m, 2H, ArH), 6.87 (d, 1H, *J* = 8.3 Hz, ArH) (* designates diastereotopic protons). ^{13}C NMR (101 MHz, $D_2O^{\#}$) δ 32.03, 45.96, 58.01, 117.30, 118.14, 120.55, 127.30, 135.26, 164.38, 181.23. $^{\#}$Due to the insolubility of **2.52** in MeOD-d_4, DMSO-d_6 and D_2O, NMR spectra were obtained by dissolving 31 mg of **2.52** in a solution of basified D_2O (20 mg KOH in 0.8 mL D_2O). HRMS calculated for $C_{10}H_{10}NO_3$ $[M – H]^-$, 192.0651; found, 192.0666.

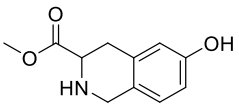

Methyl 6-hydroxy-1,2,3,4-tetrahydroisoquinoline-3-carboxylate (2.53)

To a solution of **2.52** (2.0 g, 10.35 mmol) in MeOH (50 mL) was added H_2SO_4 (1.0 mL, 96% *w*/*w*) and the reaction refluxed for 12 h. The reaction mixture was cooled to rt, neutralised with $NaHCO_3$ solution and extracted with EtOAc. The EtOAc layer was washed with brine solution, dried over $MgSO_4.H_2O$ and the solvent removed under reduced pressure to give **2.53** (2.05 g, 9.90 mmol, 96%) as an off-white solid. ^{1}H NMR

(400 MHz, $CDCl_3$) δ 2.80 – 3.03 (m, 2H, NHCHC**H₂***), 3.68 – 3.74 (m, 1H, NHC**H**), 3.76 (s, 3H, OCH_3), 3.93 – 4.10 (m, 2H, NHC**H₂***), 4.68 (br m, 2H, OH, NH), 6.48 (d, 1H, *J* = 2.6 Hz, ArH), 6.60 (dd, 1H, *J* = 2.6, 8.3 Hz, ArH), 6.85 (d, 1H, *J* = 8.3 Hz, ArH). * designates diastereotopic protons. ^{13}C NMR (101 MHz, $CDCl_3$) δ 31.48, 46.66, 52.45, 55.73, 114.30, 115.62, 125.78, 127.36, 134.12, 154.91, 173.44. HRMS calculated for $C_{11}H_{14}NO_3$ $[M + H]^+$, 208.0968; found, 208.0950. The synthesis of methyl ester **2.53** from **2.52** has previously been reported[182, 190-193] however none of these reports include spectroscopic data for **2.53**.

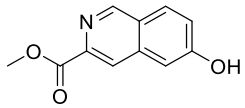

Methyl 6-hydroxyisoquinoline-3-carboxylate (2.54)

Following the procedure described for **2.24**, a mixture of **2.53** (1.2 g, 5.79 mmol) and DDQ (2.63 g, 11.58 mmol) gave **2.54** (0.6g, 2.95 mmol, 52%) as an off-white solid. ^1H NMR (400 MHz, MeOD-d_4) δ 3.99 (s, 3H, OC**H₃**), 7.23 (d, *J* = 2.3 Hz, 1H, ArH), 7.34 (dd, *J* = 8.9, 2.4 Hz, 1H, ArH), 8.01 (d, *J* = 8.9 Hz, 1H, ArH), 8.37 (s, 1H, ArH), 9.04 (s, 1H, ArH). ^{13}C NMR (101 MHz, MeOD-d_4) δ 53.01, 109.88, 123.57, 123.97, 126.30, 131.11, 139.25, 141.89, 152.66, 162.04, 167.28. HRMS calculated for $C_{11}H_9NNaO_3$ $[M + Na]^+$, 226.0475; found, 226.0462. The synthesis of **2.54** from **2.53** has previously been reported[182] but without spectroscopic data of **2.54**.

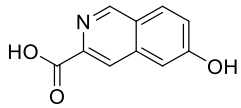

6-Hydroxyisoquinoline-3-carboxylic acid (2.55)

Following the procedure described for **2.25**, a mixture of **2.54** (0.6 g, 2.95 mmol) and LiOH (0.212 g, 8.86 mmol) gave **2.55** (0.5 g, 2.64 mmol, 90%) as yellow solid. ^1H NMR (400 MHz, DMSO-d_6) δ 7.55 – 7.63 (m, 2H, ArH), 8.39 (d, 1H, *J* = 8.7 Hz, ArH), 8.66 (s, 1H, ArH), 9.46 (s, 1H, ArH), 11.79 (br s, 1H, CO_2H). ^{13}C NMR (101 MHz, DMSO-d_6) δ 109.88, 122.88, 123.65, 123.92, 132.49, 135.02, 139.40, 148.32, 163.39, 163.77. HRMS calculated for $C_{10}H_8NO_3$ $[M + H]^+$, 190.0499; found, 190.0512.

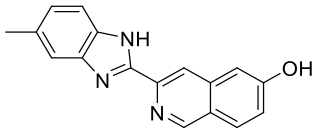

3-(6-Methyl-1*H*-1,3-benzodiazol-2-yl)isoquinolin-6-ol (2.56)

Following the procedure described for **2.26**, a mixture of **2.55** (0.2 g, 1.05 mmol) and 3,4-diaminotoluene (0.13 g, 1.05 mmol) gave **2.56** (75 mg, 0.27 mmol, 26%) as an off-white solid. ^{1}H NMR (400 MHz, MeOD-d_4) δ 2.49 (s, 3H, CH_3), 7.12 (d, 1H, *J* = 8.4 Hz, ArH isoquinoline or ArH benzimidazole), 7.20 – 7.30 (m, 2H, ArH isoquinoline and ArH benzimidazole), 7.44 (s, 1H, ArH benzimidazole), 7.54 (s, 1H, ArH benzimidazole), 7.98 (d, 1H, *J* = 8.8 Hz, ArH isoquinoline), 8.43 (s, 1H, ArH isoquinoline), 9.15 (s, 1H, ArH isoquinoline). ^{13}C NMR (101 MHz, MeOD-d_4) δ 21.78, 109.11, 118.02, 122.20, 125.57, 131.01, 139.78, 143.17, 152.99, 161.65. HRMS calculated for $C_{17}H_{14}N_3O$ $[M + H]^+$, 276.1131; found, 276.1114. Analytical RP-HPLC R_t = 13.83 min; determined with HPLC method A.

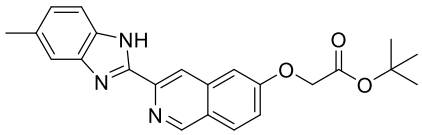

***tert*-Butyl 2-{[3-(5-methyl-1*H*-1,3-benzodiazol-2-yl)isoquinolin-6-yl]oxy}acetate (2.57)**

Following the procedure described for **2.28**, a mixture of **2.56** (18 mg, 0.06 mmol), K_2CO_3 (25 mg, 0.18 mmol) and *tert*-butyl bromoacetate (20 µL, 0.13 mmol) gave **2.57** (24 mg, 0.06 mmol, 94%) as an off-white solid. ^{1}H NMR (500 MHz, $CDCl_3$) δ 1.53 (s, 9H, C(C**H**$_3$)$_3$), 2.50 (s, 3H, CH_3), 4.68 (s, 2H, CH_2), 7.07 (d, 1H, *J* = 2.5 Hz, ArH isoquinoline or ArH benzimidazole), 7.09 – 7.16 (m, 1H, ArH isoquinoline or ArH benzimidazole), 7.34 (dd, 1H, *J* = 2.5, 8.9 Hz, ArH isoquinoline), 7.40 – 7.82 (s, 2H, ArH benzimidazole), 7.91 (d, 1H, *J* = 8.9 Hz, ArH isoquinoline), 8.68 (s, 1H, ArH isoquinoline), 9.10 (s, 1H, ArH isoquinoline), 10.74 (br s, 1H, NH). ^{13}C NMR (126 MHz, $CDCl_3$) δ 21.92, 28.25, 65.75, 83.14, 106.05, 107.48, 117.69, 121.32, 125.23, 129.84, 138.22, 142.54, 151.42, 159.93, 167.31. HRMS calculated for $C_{23}H_{24}N_3O_3$ $[M + H]^+$, 390.1812; found, 390.1798.

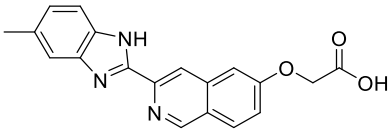

2-{[3-(5-Methyl-1*H*-1,3-benzodiazol-2-yl)isoquinolin-6-yl]oxy}acetic acid (2.58)

Following the procedure described for **2.30**, a mixture of **2.57** (40 mg, 0.10 mmol) and TFA gave **2.58** (70 mg) as a yellow solid. ^{1}H NMR (500 MHz, DMSO-d_6) δ 2.43 (s, 3H, C**H**$_3$), 4.91 (s, 2H, C**H**$_2$), 7.06 (d, 1H, *J* = 8.2 Hz, ArH isoquinoline or ArH benzimidazole), 7.32 – 7.45 (m, 2H, ArH isoquinoline and/or ArH benzimidazole), 7.46 – 7.55 (m, 2H, ArH isoquinoline and/or ArH benzimidazole), 8.15 (d, 1H, *J* = 8.9 Hz, ArH isoquinoline), 8.66 (s, 1H, ArH isoquinoline), 9.33 (s, 1H, ArH isoquinoline). HRMS calculated for $C_{19}H_{14}N_3O_3$ $[M - H]^-$, 332.1041; found, 332.1064.

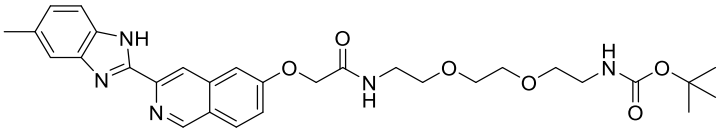

***tert*-Butyl *N*-(2-{2-[2-(2-{[3-(5-methyl-1*H*-1,3-benzodiazol-2-yl)isoquinolin-6-yl] oxy}acetamido)-ethoxy]ethoxy}ethyl)carbamate (2.59)**

According to the procedure described for **2.32**, a mixture of **2.58** (17 mg, 0.05 mmol), **2.12** (38 mg, 0.15 mmol), HATU (20 mg, 0.05 mmol) and DIPEA (20 µL, 0.11 mmol) gave a residue that was purified by silica gel column chromatography (50% EtOAc/hexane to 10% MeOH/EtOAc) to give **2.59** (11 mg, 0.02 mmol, 39%) as an off-white solid. ^{1}H NMR (400 MHz, $CDCl_3$) δ 1.42 (s, 9H, C(C**H**$_3$)$_3$), 2.50 (s, 3H, C**H**$_3$), 3.23 – 3.36 (m, 2H, CONHC**H**$_2$ or C**H**$_2$NHBoc), 3.47 – 3.65 (m, 10H, 5 × C**H**$_2$), 4.66 (s, 2H, OC**H**$_2$), 5.04 (br s, 1H, NH), 7.05 (s, 1H, NH), 7.10 – 7.15 (m, 1H, ArH benzimidazole or ArH isoquinoline), 7.17 (d, 1H, *J* = 2.4, 2.5 Hz, ArH benzimidazole or ArH isoquinoline), 7.31 (dd, 1H, *J* = 2.4, 8.9 Hz, ArH isoquinoline), 7.37 – 7.49 (s, 1H, ArH benzimidazole), 7.50 – 7.70 (br s, 1H, ArH benzimidazole), 7.94 (d, 1H, *J* = 9.0 Hz, ArH isoquinoline), 8.69 (s, 1H, ArH isoquinoline), 9.12 (s, 1H, ArH isoquinoline). ^{13}C NMR (101 MHz, $CDCl_3$) δ 21.91, 28.55, 39.09, 40.46, 67.44, 69.83, 70.35, 70.41, 79.51, 107.07, 118.46, 118.48, 120.82, 125.28, 125.48, 130.05, 133.97, 138.00, 150.33, 151.61, 156.14, 159.10, 167.43. HRMS calculated for $C_{30}H_{38}N_5O_6$ $[M + H]^+$, 564.2817; found, 564.2784. Analytical RP-HPLC R_t = 16.81 min; determined with HPLC method A.

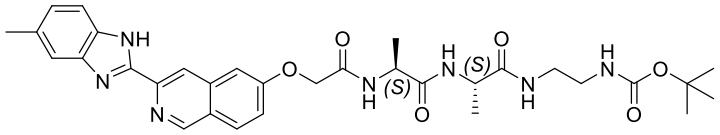

***tert*-Butyl *N*-{2-[(2*S*)-2-[(2*S*)-2-(2-{[3-(5-methyl-*1H*-1,3-benzodiazol-2-yl)isoquinolin-6-yl]oxy}acetamido)propanamido]propanamido]ethyl}carbamate (2.60)**

According to the procedure described for **2.32**, a mixture of **2.58** (20 mg, 0.06 mmol), **2.18** (54 mg,), HATU (24 mg, 0.06 mmol) and DIPEA (20 µL, 0.12 mmol) gave a residue that was purified by silica gel column chromatography (50% EtOAc/hexane to 12% MeOH/EtOAc) to give **2.60** (16 mg, 0.02 mmol, 37%) as an off-white solid ^{1}H NMR (500 MHz, DMSO-d_6) δ 1.19 (d, 3H, J = 7.1 Hz, CH_3 Alanine), 1.29 (d, 3H, J = 7.1 Hz, CH_3 Alanine), 1.35 (s, 9H, C(C**H**$_3$)$_3$), 2.44 (s, 3H, C**H**$_3$, benzimidazole), 2.91 – 2.99 (m, 2H, CH_2), 3.00 – 3.13 (m, 2H, CH_2), 4.18 – 4.26 (m, 1H, CH), 4.36 – 4.44 (m, 1H, CH), 4.72 – 4.82 (m, 2H, OCH_2), 6.74 (t, 1H, J = 5.8 Hz, NH), 7.05 – 7.09 (m, 1H, ArH benzimidazole), 7.42 (s, 1H, ArH benzimidazole), 7.45 (dd, 1H, J = 2.4, 8.9 Hz, ArH isoquinoline), 7.49 – 7.55 (m, 2H, ArH benzimidazole or ArH isoquinoline), 7.86 (t, 1H, J = 5.7 Hz, NH), 8.11 (d, 1H, J = 7.5 Hz, NH), 8.17 (d, 1H, J = 9.0 Hz, ArH isoquinoline), 8.36 (d, 1H, J = 7.4 Hz, NH), 8.67 (s, 1H, ArH isoquinoline), 9.34 (s, 1H, ArH isoquinoline). ^{13}C NMR (126 MHz, DMSO-d_6) δ 18.19, 18.21, 21.37, 28.21, 38.73, 39.52*, 48.09, 48.32, 66.85, 77.65, 106.67, 117.29, 120.94, 124.07, 124.49, 129.79, 137.57, 142.44, 150.73, 151.60, 155.58, 159.53, 166.84, 171.52, 172.11 (*underneath DMSO-d_6 peaks, identified through gHSQC experiment). HRMS calculated for $C_{32}H_{40}N_7O_6$ $[M + H]^+$, 618.3035; found, 618.3073.

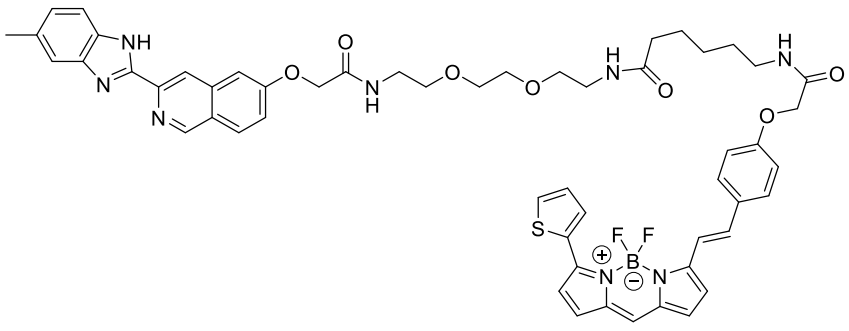

[12-(2-{4-[({5-[(2-{2-[2-(2-{[3-(5-Methyl-1*H*-1,3-Benzodiazol-2-yl)isoquinolin-6-yl]oxy}acetamido)ethoxy]ethoxy}ethyl)carbamoyl]pentyl}carbamoyl)methoxy]phenyl}ethenyl)-4-(thiophen-2-yl)-2-(λ²-fluoranidyl)-1λ⁴-aza-3λ⁴-aza-2λ¹-

boratricyclo[7.3.0.0³,⁷]dodeca-3,5,7,9,11-pentaene-2,2,2-triium-1-id-2-yl]-λ²-fluoranide (2.61)

According to the procedure for **2.36**, **2.59** (5.0 mg, 0.01 mmol) was treated with TFA to give *N*-{2-[2-(2-aminoethoxy)ethoxy]ethyl}-2-{[3-(5-methyl-1*H*-1,3-benzodiazol-2-yl)isoquinolin-6-yl]oxy}acetamide trifluoroacetate salt in assumed quantitative yield as a yellow solid. The trifluoroacetate salt was purified using semi-preparative RP-HPLC. This purified trifluoroacetate salt (5.3 mg, 9.17 µmol) on reaction with BOPIPY630/650-SE (1.7 mg, 2.52 µmol) provided **2.61** (2.2 mg, 2.18 µmol, 86%) as a dark blue solid. HRMS calculated for $C_{54}H_{55}BF_2N_8NaO_7S$ $[M + Na]^+$, 1031.3877; found, 1031.3849. Analytical RP-HPLC R_t = 20.96 min; determined with HPLC method A.

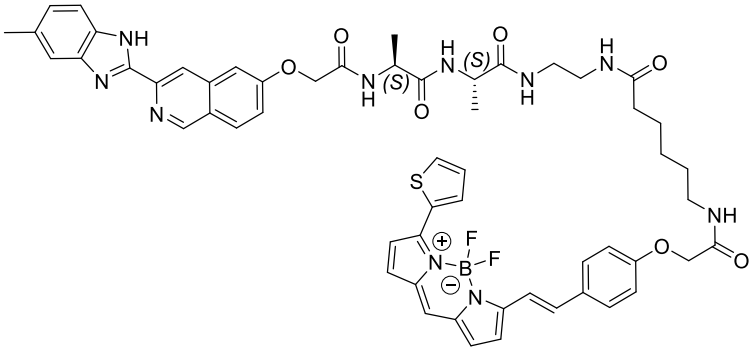

(12-{2-[4-({[5-({2-[(2*S*)-2-[(2*S*)-2-(2-{[3-(5-Methyl-1*H*-1,3-Benzodiazol-2-yl)isoquinolin-6-yl]oxy}acetamido)propanamido]propanamido]ethyl}carbamoyl) pentyl]carbamoyl}methoxy)phenyl]ethenyl}-4-(thiophen-2-yl)-2-(λ²-fluoranidyl)-1λ⁴-aza-3λ⁴-aza-2λ¹-boratricyclo[7.3.0.0³,⁷]dodeca-3,5,7,9,11-pentaene-2,2,2-triium-1-id-2-yl)-λ²-fluoranide (2.62)

According to the procedure for **2.36**, **2.60** (9.0 mg, 0.01 mmol) was treated with TFA to give (2*S*)-*N*-[(*1S*)-1-[(2-aminoethyl)carbamoyl]ethyl]-2-(2-{[3-(5-methyl-1H-1,3-benzodiazol-2-yl)isoquinolin-6-yl]oxy}acetamido)propanamide trifluoroacetate salt in assumed quantitative yield as a yellow solid. The trifluoroacetate salt was purified using semi-preparative RP-HPLC. This trifluoroacetate salt (9.2 mg, 14.56 µmol) on reaction with BOPIPY630/650-SE (1.7 mg, 2.52 µmol) provided **2.62** (1.9 mg, 1.83 µmol, 73%) as a dark blue solid. HRMS calculated for $C_{56}H_{57}BF_2N_{10}NaO_7S$ $[M + Na]^+$, 1085.4095; found, 1085.4166. Analytical RP-HPLC R_t = 20.51 min; determined with HPLC method A.

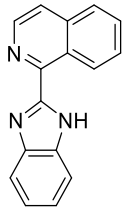

1-(1*H*-Benzimidazol-2-yl)isoquinoline (2.6)

Following the procedure described for **2.26**, a mixture of A mixture of commercially available **2.63** (0.5 g, 2.88 mmol) and *o*-phenylenediamine (0.31 g, 2.88 mmol) gave **2.6** (0.27 g, 1.10 mmol, 38%) as an off-white solid.

^{1}H NMR (400 MHz, Methanol-d_4) δ 7.28 – 7.40 (m, 2H, ArH benzimidazole), 7.65 (s, 1H, ArH benzimidazole), 7.75 – 7.87 (m, 3H, ArH benzimidazole and ArH isoquinoline), 7.90 (d, 1H, J = 5.9 Hz, ArH isoquinoline), 7.97 – 8.05 (m, 1H, ArH isoquinoline), 8.64 (d, 1H, J = 5.6 Hz, ArH isoquinoline), 9.45 – 9.54 (m, 1H, ArH isoquinoline). ^{13}C NMR (101 MHz, Methanol-d_4) δ 123.62, 127.91, 128.25, 128.71, 129.59, 131.88, 138.67, 142.83, 149.04, 152.34. HRMS calculated for $C_{16}H_{12}N_3$ $[M + H]^+$, 246.1026; found, 246.1029. Analytical RP-HPLC R_t = 12.93 min; determined with HPLC method A.

NMR of this compound was also carried out in DMSO-d_6 to compare with literature reported data of this compound in DMSO-d_6. ^{1}H NMR spectroscopy data in DMSO-d_6 was consistent with previous literature report (^{13}C NMR data not reported in literature).[76] ^{1}H NMR (400 MHz, DMSO-d_6) δ 7.22 – 7.36 (m, 2H, ArH benzimidazole), 7.59 – 7.66 (m, 1H, ArH benzimidazole), 7.80 – 7.91 (m, 3H, ArH benzimidazole and ArH benzimidazole), 7.96 – 8.03 (m, 1H, ArH isoquinoline), 8.03 – 8.13 (m, 1H, ArH isoquinoline), 8.70 (d, 1H, J = 5.5, ArH isoquinoline), 10.09 – 10.13 (m, 1H, ArH isoquinoline), 13.22 (s, 1H, NH). ^{13}C NMR (101 MHz, DMSO-d_6) δ 112.05, 119.72, 121.94, 122.34, 123.63, 125.95, 127.21, 127.82, 128.61, 130.61, 134.02, 136.77, 141.64, 144.07, 146.64, 151.17.

Excitation and emission spectra of fluorescent compounds

These experiments were all carried out by members of the Stephen Hill's research group at the University of Nottingham. The excitation and emission spectra for each fluorescent compound (10 μM in methanol) were measured in Griener Bio-One white 96 well flat bottom plates using a BMG LabTech CLARIOstar read type 'top optic' (software version 5.20 RS; firmware version 1.20) and analysed using BMG MARS (software version 3.10 RS). Alexa Flour 633 presets were used. Excitation wavelength 540 – 640 nm (1.0 stepwidth), excitation bandwidth 10 nm, emission wavelength 668 nm, emission bandwidth 16 nm, gain 1500, measured 0.2 sec. And excitation wavelength 592 nm excitation bandwidth 16 nm, emission wavelength 620 – 700 nm (0.2 stepwidth), emission bandwidth 10 nm, gain 1500, measured 0.2 sec.

Excitation and emission maxima data for fluorescent compounds

Fluorescent compound	Excitation (max) (nm)	Emission (max) (nm)
2.36	624	641
2.37	624	641
2.38	624	641
2.39	624	641
2.50	624	642
2.61	624	642
2.62	624	641

7.3 Experimental procedure and data for compounds as described in chapter 3

7.3.1 Chemical studies

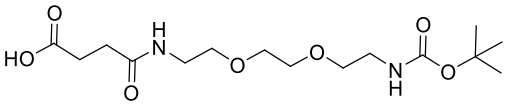

3-({2-[2-(2-{[(*tert*-Butoxy)carbonyl]amino}ethoxy)ethoxy]ethyl}carbamoyl)-propanoic acid (3.13)

This compound was prepared according to a previously reported synthesis of **3.13**.[86] To a solution of **2.12** (0.8 g, 3.22 mmol, synthesis described in section 2.2.1, chapter 2) in $CHCl_3$ (20.0 mL) was added succinic anhydride (0.32 g, 3.22 mmol) at 0 °C. The reaction was warmed to rt and stirred for 12 h. The reaction solvent was removed under reduced pressure and the residue was purified by silica gel column chromatography (eluting with 20% MeOH/EtOAc) to provide **3.13** (0.73 g, 2.09 mmol, 65%) as a clear oil. ^{1}H NMR (400 MHz, $CDCl_3$) δ 1.42 (s, 9H, C(C**H$_3$**)$_3$), 2.44 – 2.53 (m, 2H, CH_2), 2.61 – 2.70 (m, 2H, CH_2), 3.24 – 3.34 (m, 2H, CH_2), 3.43 (q, 2H, *J* = 5.1 Hz, CH_2), 3.53 (q, 4H, *J* = 5.1 Hz, 2 × **CH$_2$**), 3.60 (s, 4H, 2 × **CH$_2$**), 5.17 (br s, 1H, NH), 6.78 (br s, 1H, NH), 7.44 (br s, 1H, CO_2H). HRMS calculated for $C_{15}H_{28}N_2NaO_7$ $[M + Na]^+$, 371.1789; found, 371.1759.

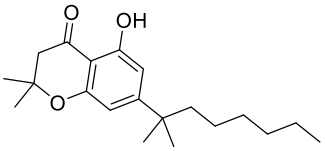

5-Hydroxy-2,2-dimethyl-7-(2-methyloctan-2-yl)-3,4-dihydro-2*H*-1-benzopyran-4-one (3.15)

This compound was prepared according to a previously reported synthesis of **3.15**.[234] To a suspension of phosphorous pentoxide (0.27 g, 1.90 mmol) in methanesulfonic acid (8.3 mL, 126.93 mmol) under N_2 atmosphere was added commercially available 5-(2-methyloctan-2-yl)benzene-1,3-diol **3.14** (0.3 g, 1.27 mmol) and 3,3-dimethylacrylic acid (0.2 g, 1.90 mmol). The reaction mixture was stirred at 70 °C under N_2 atmosphere for 12 h. Subsequently, the reaction mixture was cooled down, poured into a mixture of ice/water and extracted with DCM. The resulting organic layer was then dried over $MgSO_4.H_2O$, concentrated under reduced pressure and purified by column

chromatography (eluting with 1 to 5% EtOAc/hexane) to give **3.15** (0.28 g, 0.88 mmol, 69%) as pale-yellow oil. ^{1}H NMR (400 MHz, $CDCl_3$) δ 0.77 – 0.88 (m, 3H, $CH_2C\mathbf{H_3}$ dimethylheptyl chain), 0.98 – 1.10 (m, 2H, CH_2), 1.15 – 1.21 (m, 6H, 3 × $\mathbf{CH_2}$), 1.22 (s, 6H, $C(C\mathbf{H_3})_2$ dimethylheptyl chain), 1.46 (s, 6H, $OC(C\mathbf{H_3})_2$ pyran ring), 1.49 – 1.57 (m, 2H, CH_2), 2.70 (s, 2H, CH_2CO), 6.36 (d, 1H, *J* = 1.6 Hz, ArH), 6.44 (d, 1H, *J* = 1.7 Hz, ArH), 11.53 (s, 1H, OH). ^{13}C NMR (101 MHz, $CDCl_3$) δ 14.18, 22.75, 24.70, 26.84, 28.56, 30.03, 31.83, 38.87, 44.14, 48.20, 78.81, 105.39, 105.87, 106.72, 159.66, 161.40, 162.66, 197.55. HRMS calculated for $C_{20}H_{30}NaO_3$, 341.2087; found, 341.2064.

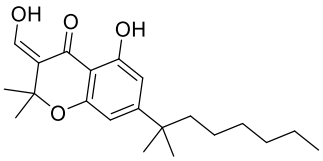

5-Hydroxy-3-(hydroxymethylidene)-2,2-dimethyl-7-(2-methyloctan-2-yl)-3,4-dihydro-2*H*-1 benzopyran-4-one (3.16)

Compound **3.16** was prepared according to a literature procedure except using conventional heating instead of the reported microwave irradiation.[137] A solution of **3.15** (0.5 g, 1.57 mmol) in THF (6.0 mL) was added to a suspension of NaH (0.37 g, 15.70 mmol) in THF (5.0 mL) at 0 °C under N_2 atmosphere. Upon addition of NaH, the reaction mixture turned green, which was then stirred at 45 °C for 15 min, followed by addition of ethyl formate (1.51 mL, 18.84 mmol). The reaction mixture was then heated at 65 °C. The colour of the reaction mixture changed to orange and rapid evolution of gas was observed. The reaction mixture was cooled to rt and stirred for 20 min or until the evolution of gas subsided. Now, the reaction mixture was again heated to 65 °C and stirred for 6 h. The reaction mixture was acidified to pH 3-5 using aqueous 1M HCl and extracted with DCM. The combined organic layer was washed with brine, dried over $MgSO_4.H_2O$, the solvent removed by evaporation under reduced pressure and purified by column chromatography (eluting with 1 to 5% EtOAc/hexane) to give **3.16** (0.382 g, 1.10 mmol, 70%) as pale yellow oil. ^{1}H NMR (400 MHz, $CDCl_3$) δ 0.80 – 0.88 (m, 3H, $CH_2C\mathbf{H_3}$ dimethylheptyl chain), 1.00 – 1.09 (m, 2H, CH_2), 1.14 – 1.21 (m, 6H, 3 × $\mathbf{CH_2}$), 1.22 (s, 6H, $C(C\mathbf{H_3})_2$ dimethylheptyl chain), 1.50 – 1.56 (m, 2H, CH_2), 1.58 (s, 6H, $OC(C\mathbf{H_3})_2$ pyran ring), 6.35 (d, 1H, *J* = 1.6 Hz, ArH), 6.47 (d, 1H, *J* = 1.6 Hz, ArH), 7.34 (d, 1H, *J* = 11.6 Hz, C**H**OH), 11.28 (s, 1H, OH), 13.48 (d, 1H, *J* = 11.7 Hz, CHO**H**). ^{13}C NMR (101 MHz, $CDCl_3$) δ 14.18, 22.74, 24.69, 28.33, 28.52, 30.02, 31.82, 38.87, 44.15, 78.37,

104.96, 106.30, 107.50, 114.46, 158.80, 161.60, 161.73, 162.75, 189.52. HRMS calculated for $C_{21}H_{31}O_4$ $[M + H]^+$, 347.2217; found, 347.2197.

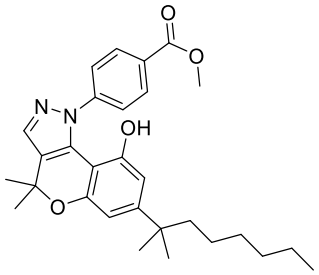

Methyl 4-[9-hydroxy-4,4-dimethyl-7-(2-methyloctan-2-yl)-1*H*,4*H*-chromeno[4,3-c]pyrazol-1-yl]benzoate (3.18)

To a solution of **3.16** (0.3 g, 0.86 mmol) in MeOH (30 mL) was added commercially available 4-hydrazinobenzoic acid (0.14 g, 0.95 mmol) followed by addition of two drops of concentrated H_2SO_4 (98% solution). The reaction mixture was stirred at 75 °C for 8 h. The reaction solvent was removed by evaporation under reduced pressure and the residue was neutralised with saturated $NaHCO_3$ solution. The solution was extracted with EtOAc, the combined organic layer was washed with water, brine solution, dried over $MgSO_4.H_2O$, and the solvent removed by evaporation under reduced pressure. The residue was purified by silica gel column chromatography (eluting with 20 to 30% EtOAc/hexane) to provide **3.18** (0.25 g, 0.52 mmol, 61%) as a foamy orange solid. ^{1}H NMR (400 MHz, $CDCl_3$) δ 0.83 (t, 3H, *J* = 6.9 Hz, $CH_2C\mathbf{H_3}$ dimethylheptyl chain), 0.96 – 1.09 (m, 2H, CH_2), 1.17 (s, 6H, $C(C\mathbf{H_3})_2$ dimethylheptyl chain), 1.12 – 1.28 (m, 6H, 3 × $\mathbf{CH_2}$), 1.43 – 1.52 (m, 2H, CH_2), 1.61 (s, 6H, $OC(C\mathbf{H_3})_2$ of pyran ring), 3.84 (s, 3H, OCH_3), 6.29 (d, 1H, *J* = 1.7 Hz, ArH phenol), 6.63 (d, 1H, *J* = 1.7 Hz, ArH phenol), 6.76 (br s, 1H, OH), 7.44 (d, 2H, *J* = 8.6 Hz, ArH methyl benzoate), 7.45 (s, 1H, ArH pyrazole), 7.95 (d, 2H, *J* = 8.6 Hz, ArH methyl benzoate). ^{13}C NMR (101 MHz, $CDCl_3$) δ 14.18, 22.70, 24.67, 27.32, 28.66, 29.99, 31.83, 37.94, 44.44, 52.38, 76.97, 102.44, 107.96, 108.63, 123.79, 125.19, 128.10, 130.01, 133.31, 134.90, 146.59, 150.73, 153.53, 154.21, 167.03. HRMS calculated for $C_{29}H_{36}N_2NaO_4$ $[M + Na]^+$, 499.2567; found, 499.2554. Analytical RP-HPLC Rt = 24.24 min; determined with HPLC method B.

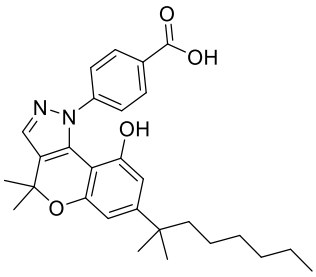

4-[9-Hydroxy-4,4-dimethyl-7-(2-methyloctan-2-yl)-1*H*,4*H*-chromeno[4,3-c]pyrazol-1-yl]benzoic acid (3.19)

To a solution of **3.18** (0.25 g, 0.52 mmol) in THF (3.0 mL) was added a solution of LiOH (40 mg, 1.57 mmol) in water (3.0 mL) and the reaction stirred for 12 h. The reaction solvent was removed by evaporation under reduced pressure and residue acidified to pH 2.0-3.0 with aqueous 3M HCl. The resulting precipitate was washed with water (pH 5.0) and air dried to give **3.19** (0.24 g, 0.52 mmol, yield quantitative) as light pink solid. ^{1}H NMR (400 MHz, MeOD-d_4) δ 0.82 – 0.90 (m, 3H, $CH_2C\mathbf{H_3}$ dimethylheptyl chain), 1.03 – 1.15 (m, 2H, CH_2), 1.18 – 1.29 (m, 12H, $C(C\mathbf{H_3})_2$ dimethylheptyl chain and 3 × $C\mathbf{H_2}$), 1.52 – 1.58 (m, 2H, CH_2), 1.59 (s, 6H, $OC(C\mathbf{H_3})_2$ pyran ring), 6.35 (d, 1H, *J* = 1.7 Hz, ArH phenol), 6.54 (d, 1H, *J* = 1.8 Hz, ArH phenol), 7.44 (d, 2H, *J* = 8.8 Hz, ArH benzoic acid), 7.63 (s, 1H, ArH pyrazole), 8.06 (d, 2H, *J* = 8.8 Hz, ArH benzoic acid). ^{13}C NMR (101 MHz, MeOD-d_4) δ 14.39, 23.60, 25.71, 27.45, 29.24, 30.98, 32.83, 38.74, 45.35, 77.76, 103.28, 108.33, 108.48, 124.95, 126.10, 131.01, 135.01, 135.81, 147.79, 153.38, 154.40, 155.54, 169.63. HRMS calculated for $C_{28}H_{35}N_2O_4$ $[M + H]^+$, 463.2591; found, 463.2552. Analytical RP-HPLC Rt = 22.21 min; determined with HPLC method B.

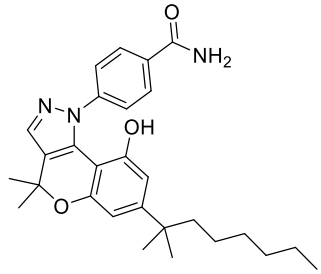

4-[9-Hydroxy-4,4-dimethyl-7-(2-methyloctan-2-yl)-1*H*,4*H*-chromeno[4,3-c]pyrazol-1-yl]benzamide (3.20)

A solution of DIPEA (0.3 mL, 1.73 mmol) in DMF (2.0 mL) was added to a mixture of **3.19** (100 mg, 0.21 mmol), NH_4Cl (56 mg, 1.08 mmol) and HBTU (82 mg, 0.21 mmol) under N_2 atmosphere and stirred for 12 h. The reaction solvent was removed under reduced pressure and the residue was partitioned between EtOAc and water (pH 2.0). The

organic layer was separated, washed with water, brine, dried over $MgSO_4.H_2O$, concentrated under reduced pressure and residue purified by column chromatography (eluting with 5% EtOAc/hexane to 1% MeOH/EtOAc) to give **3.20** (81 mg, 0.17 mmol, 81%) as pale orange solid. ^{1}H NMR (400 MHz, $CDCl_3$) δ 0.82 (t, 3H, *J* = 6.9 Hz, $CH_2C\mathbf{H_3}$ dimethylheptyl chain), 1.04 (s, 2H, CH_2), 1.12 – 1.26 (m, 12H, $C(C\mathbf{H_3})_2$ dimethylheptyl chain and 3 × CH_2), 1.45 – 1.54 (m, 2H), 1.61 (s, 6H, $OC(C\mathbf{H_3})_2$ pyran ring), 5.85 (m, $CONH_2$), 6.38 (d, 1H, *J* = 1.7 Hz, ArH phenol), 6.62 (d, 1H, *J* = 1.6 Hz, ArH phenol), 6.72 (br s, OH), 7.40 (d, 2H, *J* = 8.4 Hz, ArH benzamide), 7.54 (s, 1H, ArH pyrazole), 7.77 (d, 2H, *J* = 8.5 Hz, ArH benzamide). ^{13}C NMR (101 MHz, $CDCl_3$) δ 14.22, 22.74, 24.73, 27.32, 28.70, 30.02, 31.86, 38.05, 44.44, 77.36, 102.07, 108.15, 108.50, 124.06, 125.13, 128.08, 131.02, 134.06, 134.42, 145.56, 151.27, 154.20, 154.39, 169.77. HRMS calculated for $C_{28}H_{35}N_3NaO_3$ $[M + Na]^+$, 484.2571; found, 484.2537.

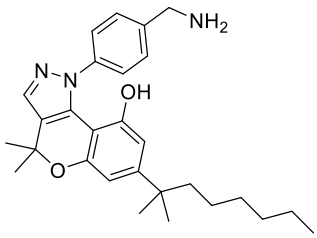

1-[4-(Aminomethyl)phenyl]-4,4-dimethyl-7-(2-methyloctan-2-yl)-1*H*,4*H*-chromeno[4,3-c]pyrazol-9-ol (3.21)

A solution of **3.20** (0.12 g, 0.27 mmol) in THF (6.0 mL) was added to a suspension of $LiAlH_4$ (51 mg, 1.34 mmol) in THF (3.0 mL) at 0 °C under N_2 atmosphere. The reaction was stirred for 2 h at rt and then for 12 h at 70 °C. The reaction was quenched by adding water (3 mL), a solution of 15% NaOH in water (1.0 mL) and then water (5.0 mL) at 0 °C and the reaction mixture was stirred for 30 min. The resulting suspension was filtered through celite and the filtrate was concentrated under reduced pressure and the residue was partitioned between EtOAc and water. The organic layer was separated, dried over $MgSO_4.H_2O$ and solvent removed by evaporation under reduced pressure to give **3.21** (113 mg) as a reddish oil. It was used as such in next reaction without further purification. HRMS calculated for $C_{28}H_{38}N_3O_2$ $[M + H]^+$, 448.2959; found, 448.2919.

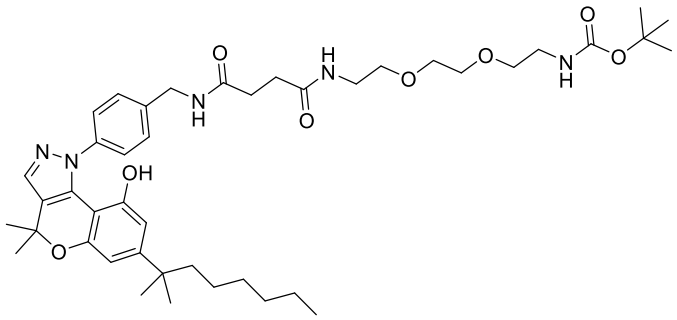

***tert*-Butyl *N*-{2-[2-(2-{3-[({4-[9-Hydroxy-4,4-dimethyl-7-(2-methyloctan-2-yl)-1*H*,4*H*-chromeno[4,3c]pyrazol-1-yl]phenyl}methyl)carbamoyl]propanamido}ethoxy)ethoxy]ethyl}carbamate (3.22)**

A solution of **3.13** (50 mg, 0.14 mmol), HBTU (53 mg, 0.14 mmol), DIPEA (0.1 mL, 0.43 mmol) in DMF (4.0 mL) under N_2 atmosphere was stirred for 10 min. A solution of benzylamine **3.21** (69 mg, 0.14 mmol) in DMF (1.0 mL) was then added and the reaction stirred for 5 h. The reaction solvent was removed under reduced pressure. The residue was partitioned between EtOAc and H_2O. The organic layer was then washed with saturated NH_4Cl solution, saturated $NaHCO_3$ solution, water, brine solution, dried over $MgSO_4.H_2O$ and concentrated under reduced pressure. The residue was further purified by silica gel column chromatography (eluting with 50% EtOAc/hexane to 7% MeOH/EtOAc) to provide **3.22** (38 mg, 0.05 mmol, 34%) as yellowish-orange solid. ^{1}H NMR (400 MHz, $CDCl_3$) δ 0.83 (t, 3H, *J* = 6.9 Hz, $CH_2C\mathbf{H_3}$ dimethylheptyl chain), 0.98 – 1.08 (m, 2H, CH_2), 1.11 – 1.28 (m, 12H, $C(C\mathbf{H_3})_2$ dimethylheptyl chain and 3 × $\mathbf{CH_2}$), 1.42 (s, 9H, $C(C\mathbf{H_3})_3$), 1.45 – 1.53 (m, 2H, CH_2), 1.60 (s, 6H, $OC(C\mathbf{H_3})_2$ pyran ring), 2.42 – 2.55 (m, 4H, $COC\mathbf{H_2}C\mathbf{H_2}CO$), 3.20 (q, 2H, *J* = 5.4 Hz, CH_2), 3.38 (q, 2H, *J* = 5.1 Hz, CH_2), 3.47 – 3.54 (m, 4H, 2 × $\mathbf{CH_2}$), 3.55 – 3.63 (m, 4H, 2 × $\mathbf{CH_2}$), 4.39 (d, 2H, *J* = 5.9 Hz, CH_2 benzylacylamide), 5.32 (br s, 1H, NH), 6.36 – 6.43 (m, 1H, ArH phenol), 6.58 (d, 1H, *J* = 1.7 Hz, ArH phenol), 6.79 (br s, 1H, NH), 7.00 (br s, 1H, NH), 7.22 (d, 2H, *J* = 8.1 Hz, ArH benzylacetamide), 7.34 (d, 2H, *J* = 8.3 Hz, ArH benzylacetamide), 7.48 (s, 1H, ArH pyrazole), 7.98 (br s, 1H, OH). ^{13}C NMR (101 MHz, $CDCl_3$) δ 14.05, 22.58, 24.56, 27.27, 28.42, 28.56, 29.68, 29.89, 31.56, 31.71, 37.74, 39.41, 40.32, 43.19, 44.34, 69.47, 70.17, 79.51, 92.79, 102.46, 107.76, 107.82, 124.08, 124.39, 127.51, 133.03, 134.11, 136.87, 142.24, 151.41, 152.81, 153.91, 172.32. HRMS calculated for $C_{43}H_{63}N_5NaO_8$ $[M + Na]^+$, 800.4569; found, 800.4494. Analytical RP-HPLC Rt = 26.17 min; determined with HPLC method B.

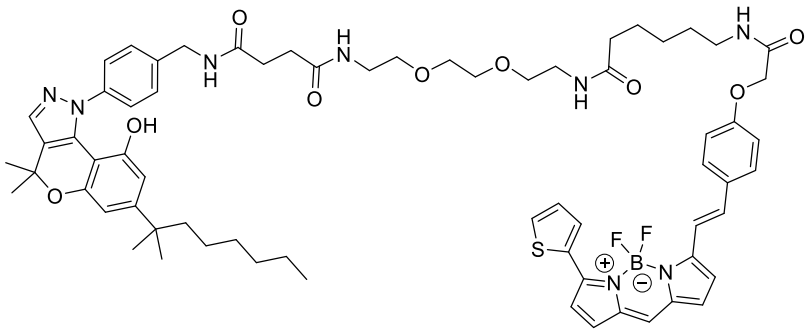

{2-Fluoro-4-[(*E*)-2-[4-({[5-({2-[2-(2-{3-[({4-[9-Hydroxy-4,4-dimethyl-7-(2-methyloctan-2-yl)-1*H*,4*H*-chromeno[4,3-c]pyrazol-1-l]phenyl}methyl)carbamoyl] propanamido} ethoxy)ethoxy]ethyl}carbamoyl)pentyl]carbamoyl}methoxy) phenyl]ethenyl]-12-(thiophen-2-yl)-1λ^4,3-diaza-2-boratricyclo[7.3.0.0^{3,7}]dodeca-1(12),4,6,8,10-pentaen-2-ium-2-yl}-lλ^2-fluoranide (**3.23**)

To a solution of **3.22** (4 mg, 5.14 μmol) in DCM (2.0 mL) at 0 °C was added TFA (0.5 mL). The reaction mixture was stirred for 2 h, reaction solvent and TFA was removed by evaporation under reduced pressure to provide the amine *N*-{2-[2-(2-aminoethoxy)ethoxy]ethyl}-*N*'-({4-[9-hydroxy-4,4-dimethyl-7-(2-methyloctan-2-yl)-1*H*,4*H*-chromeno[4,3-c]pyrazol-1-yl]phenyl}methyl)butanediamide in assumed quantitative yield as the trifluoroacetate salt. This amino TFA salt was purified using semi-preparative RP-HPLC. To a solution of this purified amino TFA salt (3.61 mg, 4.56 μmol) in DMF (200 μL) was added a solution of DIPEA (1.0 μL, 6.05 μmol) in DMF (100 μL), followed by addition of solution of BOPIPY-630/650-SE (1.0 mg, 1.51 μmol) in DMF (600 μL) and reaction stirred in the dark for 12 h. The reaction solvents were removed under reduced pressure and residue purified by semi-preparative RP-HPLC, freeze-dried to give **3.23** (1.92 mg, 1.57 μmol, yield quantitative) as a dark blue solid. HRMS calculated for $C_{67}H_{81}BF_2N_8NaO_9S$ $[M + Na]^+$, 1245.5806; found, 1245.5740. Analytical RP-HPLC Rt = 24.54 min; determined with HPLC method B.

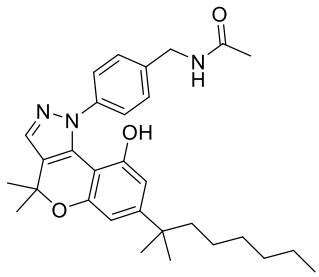

***N*-({4-[9-Hydroxy-4,4-dimethyl-7-(2-methyloctan-2-yl)-1*H*,4*H*-chromeno[4,3-c]pyrazol-1 yl]phenyl}methyl)acetamide (3.25)**

To a solution of **3.21** (33 mg, 0.07 mmol) in DCM (3.0 mL) under N_2 atmosphere was added solution of Ac_2O (20 µL, 0.20 mmol) in DCM (1.0 mL), followed by addition of Et_3N (50 µL, 0.34 mmol) and reaction mixture was stirred for 12 h. At this point, MS of crude reaction mixture indicated the formation of mixture of **3.24** and **3.25**. The reaction solvent was removed by evaporation under reduced pressure, the residue partitioned between EtOAc and water, the EtOAc layer was washed with brine, dried over $MgSO_4.H_2O$ and purified by column chromatography (eluting with 5% EtOAc/hexane to 100% EtOAc) to give 21 mg of reddish solid containing **3.24** and **3.25** in a ratio of 3:1 (determined by ^{1}H NMR spectroscopy). A solution of NaOH (5 mg, 0.12 mmol) in water (0.5 mL) was added to solution of this reddish solid (10.0 mg) in MeOH (3.0 mL) and stirred for 3h. The solvent removed by evaporation under reduced pressure and the residue partitioned between EtOAc and saturated NH_4Cl solution. The organic layer was separated, washed with water, brine, dried over $MgSO_4.H_2O$ and solvent removed by evaporation under reduced pressure to give **3.25** (7 mg, 0.01 mmol, 42% over two steps from **3.21**) as dark orange solid. ^{1}H NMR (400 MHz, $CDCl_3$) δ 0.83 (t, 3H, *J* = 6.8 Hz, $CH_2C\mathbf{H_3}$ dimethylheptyl chain), 1.01 – 1.11 (m, 2H, CH_2), 1.13 – 1.30 (m, 12H, $C(C\mathbf{H_3})_2$ dimethylheptyl chain and 3 × $\mathbf{CH_2}$), 1.47 – 1.55 (m, 2H, CH_2), 1.61 (s, 6H, $OC(C\mathbf{H_3})_2$ pyran ring), 1.96 (s, 3H, $NHCOC\mathbf{H_3}$), 4.31 (d, 2H, *J* = 5.8 Hz, $C\mathbf{H_2}NH$), 6.22 (t, 1H, *J* = 5.8 Hz, NH), 6.36 (d, 1H, *J* = 1.7 Hz, ArH phenol), 6.63 (d, 1H, *J* = 1.6 Hz, ArH phenol), 7.21 (d, 2H, *J* = 8.1 Hz, ArH benzylacetamide), 7.37 (d, 2H, *J* = 8.1 Hz, ArH benzylacetamide), 7.49 (s, 1H, ArH pyrazole). ^{13}C NMR (101 MHz, $CDCl_3$) δ 14.22, 22.74, 23.28, 24.72, 27.42, 28.74, 30.05, 31.88, 37.95, 43.41, 44.48, 77.36, 102.67, 108.29, 108.56, 124.49, 124.72, 127.76, 133.12, 134.42, 137.01, 142.09, 150.90, 153.26, 154.08, 170.93. HRMS calculated for $C_{30}H_{40}N_3O_3$ $[M + H]^+$, 490.3064; found 490.3051. Analytical RP-HPLC Rt = 21.86 min; determined with HPLC method B.

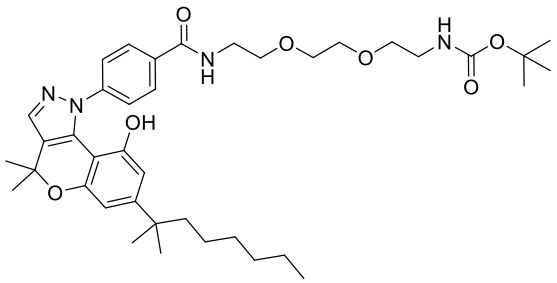

***tert*-Butyl *N*-(2-{2-[2-({4-[9-hydroxy-4,4-dimethyl-7- (2-methyloctan-2-yl)-1*H*,4*H*-chromeno[4,3 c]pyrazol-1-yl]phenyl}formamido)ethoxy]ethoxy}ethyl)carbamate (3.26)**

Carboxylic acid **3.19** (26 mg, 0.05 mmol), **2.12** (28 mg, 0.11 mmol), HATU (22 mg, 0.05 mmol) and DIPEA (30 µL, 0.16 mmol) were reacted according to the procedure described for the preparation of **3.22** and the crude residue purified by silica gel column chromatography (eluting with 50% EtOAc/hexane to 4% MeOH/EtOAc) to provide **3.26** (22 mg, 0.03 mmol, 60%) as an orange solid. ^{1}H NMR (400 MHz, $CDCl_3$) δ 0.76 – 0.90 (m, 3H, $CH_2C\mathbf{H_3}$ dimethylheptyl chain), 1.01 – 1.12 (m, 2H, CH_2), 1.13 – 1.29 (m, 6H, 3 × $\mathbf{CH_2}$), 1.23 (s, 6H, $C(C\mathbf{H_3})_2$ dimethylheptyl chain), 1.39 (s, 9H, $C(C\mathbf{H_3})_3$), 1.48 – 1.56 (m, 2H, CH_2), 1.61 (s, 6H, $OC(C\mathbf{H_3})_2$ pyran ring), 3.01 (q, 2H, *J* = 5.1 Hz, CH_2), 3.51 (t, 2H, *J* = 5.1 Hz, CH_2), 3.58 – 3.82 (m, 8H, 3 × $C\mathbf{H_2}$), 5.22 (t, 1H, *J* = 5.3 Hz, NH), 6.46 – 6.56 (m, 1H, ArH phenol), 6.60 (d, 1H, *J* = 1.7 Hz, ArH phenol), 7.18 (t, 1H, *J* = 5.4 Hz, NH), 7.48 (d, 2H, *J* = 8.4 Hz, ArH benzamide), 7.52 (s, 1H, ArH pyrazole), 7.71 (d, 2H, *J* = 8.2 Hz, ArH benzamide), 8.22 (s, 1H, OH). ^{13}C NMR (101 MHz, $CDCl_3$) δ 14.21, 22.75, 24.74, 27.38, 28.52, 28.75, 30.09, 31.90, 37.96, 39.95, 40.53, 44.62, 69.57, 69.84, 70.28, 76.99, 77.36, 80.41, 102.52, 107.87, 123.68, 125.00, 127.27, 132.13, 133.29, 134.86, 145.95, 151.58, 153.16, 154.08, 156.80, 167.56. HRMS calculated for $C_{39}H_{56}N_4NaO_7$ $[M + Na]^+$, 715.4041; found, 715.4016. Analytical RP-HPLC Rt = 23.62 min; determined with HPLC method B.

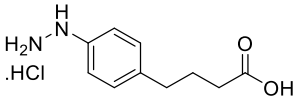

4-(4-Hydrazinylphenyl)butanoic acid hydrochloride (3.28)

This compound was prepared by following a procedure adapted from literature.[235-236] A suspension of commercially available 4-(4-aminophenyl)butanoic acid **3.27** (0.5 g, 2.79 mmol) and aqueous HCl (37% w/w, 5 mL) was heated at 120 °C for 10 min to give a clear solution. This solution was cooled to -5 °C to give a brownish crystalline solid, to

which was added a solution of $NaNO_2$ (0.21 g, 3.07 mmol) in water (3 mL) and stirred at -5 °C for 20 min. This solution was then added to a solution of $SnCl_2.2H_2O$ (1.89 g, 8.37 mmol) in water (2 mL) at -20 °C and stirred for 40 min at -20 °C. A greyish precipitate formed which was filtered, washed with cold water, diethyl ether and dried at room temperature to give **3.28** (0.32 g, 1.38 mmol, 50%) as colourless crystalline solid. ^{1}H NMR (400 MHz, MeOD-d_4) δ 1.83 – 1.91 (m, 2H, $CH_2C\mathbf{H_2}CH_2CO$), 2.28 (t, 2H, *J* = 7.4 Hz, $CH_2CH_2C\mathbf{H_2}CO$), 2.55 – 2.66 (m, 2H, $C\mathbf{H_2}CH_2CH_2CO$), 6.93 (d, 2H, *J* = 8.5 Hz, ArH), 7.19 (d, 2H, *J* = 8.5 Hz, ArH). ^{13}C NMR (101 MHz, MeOD-d_4) δ 27.95, 34.08, 35.25, 116.52, 116.49, 130.54, 137.95, 137.79, 144.28, 177.28. HRMS calculated for $C_{10}H_{15}N_2O_2$ $[M + H]^+$, 195.1128; found, 195.1140.

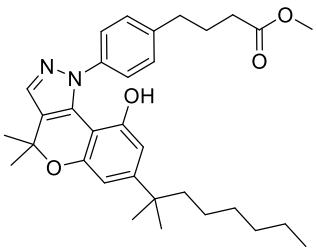

Methyl 4-{4-[9-hydroxy-4,4-dimethyl-7-(2-methyloctan-2-yl)-1*H*,4*H*-chromeno[4,3-c]pyrazol-1-yl]phenyl}butanoate (3.29)

This compound was prepared following the procedure described for **3.18**, using compound **3.16** (0.2 g, 0.58 mmol) and **3.28** (0.15 g, 0.63 mmol). The residue was purified by silica gel column chromatography (eluting with 10 to 50% EtOAc/hexane) to provide **3.29** (0.13 g, 0.25 mmol, 43%) as a yellowish orange oil. ^{1}H NMR (400 MHz, $CDCl_3$) δ 0.77 – 0.89 (m, 3H, $CH_2C\mathbf{H_3}$ dimethylheptyl chain), 0.97 – 1.12 (m, 2H, CH_2), 1.14 – 1.27 (m, 12H, $C(C\mathbf{H_3})_2$ dimethylheptyl chain and 3 × $C\mathbf{H_2}$), 1.47 – 1.55 (m, 2H, CH_2), 1.61 (s, 6H, $OC(C\mathbf{H_3})_2$ pyran ring), 1.93 – 2.09 (m, 2H, $CH_2C\mathbf{H_2}CH_2CO$), 2.35 (t, 2H, *J* = 7.2 Hz, $CH_2CH_2C\mathbf{H_2}CO$), 2.71 (t, 2H, *J* = 7.3 Hz, $C\mathbf{H_2}CH_2CH_2CO$), 3.63 (s, 3H, OCH_3), 5.05 (br s, 1H, OH), 6.30 (d, 1H, *J* = 1.8 Hz, ArH phenol), 6.65 (d, 1H, *J* = 1.8 Hz, ArH phenol), 7.22 (d, 2H, *J* = 8.3 Hz, ArH phenylbutanoate), 7.36 (d, 2H, *J* = 8.3 Hz, ArH phenylbutanoate), 7.50 (s, 1H, ArH pyrazole). ^{13}C NMR (101 MHz, $CDCl_3$) δ 14.22, 22.74, 24.71, 26.32, 27.46, 28.72, 30.03, 31.87, 33.57, 35.03, 37.93, 44.45, 51.85, 76.93, 102.84, 108.66, 109.09, 124.53, 124.67, 129.25, 132.89, 134.41, 140.25, 141.15, 150.13, 153.17, 154.02, 174.38. HRMS calculated for $C_{32}H_{43}N_2O_4$ $[M + H]^+$, 519.3217; found, 519.3198. Analytical RP-HPLC Rt = 24.34 min; determined with HPLC method B.

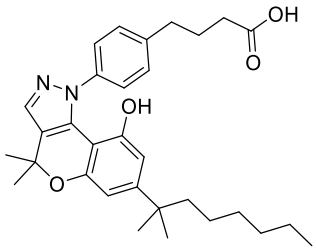

4-{4-[9-Hydroxy-4,4-dimethyl-7-(2-methyloctan-2-yl)-1*H*,4*H*-chromeno[4,3-c]pyrazol-1-yl]phenyl}butanoic acid (3.30)

According to procedure described for the preparation of **3.19**, **3.29** (0.12 g, 0.23 mmol) and LiOH (17 mg, 0.69 mmol) were reacted to give **3.30** (0.1 g, 0.21 mmol, 91%) as a yellow solid. ^{1}H NMR (400 MHz, MeOD-d_4) δ 0.81 – 0.90 (m, 3H, $CH_2C\mathbf{H_3}$ dimethylheptyl chain), 1.02 – 1.14 (m, 2H, CH_2), 1.17 – 1.31 (m, 12H, $C(C\mathbf{H_3})_2$ dimethylheptyl chain and 3 × $C\mathbf{H_2}$), 1.51 – 1.57 (m, 2H, CH_2), 1.59 (s, 6H, $OC(C\mathbf{H_3})_2$ pyran ring), 1.95 (p, 2H, *J* = 7.3 Hz, $CH_2C\mathbf{H_2}CH_2CO$), 2.33 (t, 2H, *J* = 7.4 Hz, 7.4, $CH_2CH_2C\mathbf{H_2}CO$), 2.66 – 2.75 (m, 2H, $C\mathbf{H_2}CH_2CH_2CO$), 6.33 (d, 1H, *J* = 1.2 Hz, ArH phenol), 6.52 (d, 1H, *J* = 1.1 Hz, ArH phenol), 7.20 – 7.27 (m, 4H, ArH phenylbutanoic acid), 7.53 – 7.57 (m, 1H, ArH pyrazole). ^{13}C NMR (101 MHz, MeOD-d_4) δ 14.40, 23.61, 25.71, 27.51, 27.99, 29.25, 30.99, 32.84, 34.55, 35.77, 38.69, 45.36, 77.69, 103.40, 108.29, 108.34, 125.33, 125.42, 129.43, 134.81, 134.90, 142.26, 142.47, 153.56, 154.07, 155.54, 177.74. HRMS calculated for $C_{31}H_{40}N_2NaO_4$ $[M + Na]^+$, 527.2880; found, 527.2890.

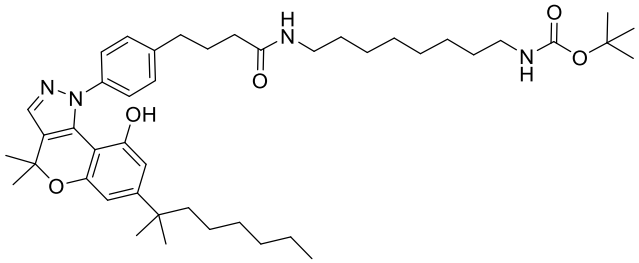

***tert*-Butyl *N*-[8-(4-{4-[9-hydroxy-4,4-dimethyl-7-(2-methyloctan-2-yl)-1*H*,4*H*-chromeno[4,3-c]pyrazol-1-yl]phenyl}butanamido)octyl]carbamate (3.31)**

This compound was prepared by following procedure described for the preparation of **3.22**, using **3.30** (25 mg, 0.05 mmol), **2.10** (30 mg, 0.08 mmol, synthesis described in section 2.2.1, chapter 2), HBTU (24 mg, 0.05 mmol) and DIPEA (50 µL, 0.15 mmol). The residue was purified by silica gel column chromatography (eluting with 70% EtOAc/hexane to 2% MeOH/EtOAc) to provide **3.31** (26 mg, 0.03 mmol, 72%) as a pale oil. ^{1}H NMR (400 MHz, $CDCl_3$) δ 0.83 (t, 3H, *J* = 6.8 Hz, $CH_2C\mathbf{H_3}$ dimethylheptyl chain),

0.99 – 1.11 (m, 2H, CH_2), 1.12 – 1.22 (m, 12H, C(C**H**$_3$)$_2$ dimethylheptyl chain and 3 × C**H**$_2$), 1.23 – 1.32 (m, 8H, 4 × C**H**$_2$), 1.36 – 1.47 (m, 13H, C(C**H**$_3$)$_3$ and 2 × C**H**$_2$), 1.48 – 1.54 (m, 2H, CH_2), 1.60 (s, 6H, OC(C**H**$_3$)$_2$ pyran ring), 1.86 – 1.98 (m, 2H, CH_2C**H**$_2$$CH_2$CO), 2.10 (t, 2H, *J* = 7.2 Hz, CH_2CH_2C**H**$_2$CO), 2.64 (t, 2H, *J* = 7.1 Hz, C**H**$_2$$CH_2CH_2$CO), 3.03 (q, 2H, *J* = 6.7 Hz, C**H**$_2$NH), 3.15 (q, 2H, *J* = 6.6 Hz, C**H**$_2$NH), 4.59 (br s, 1H, NH), 5.89 (t, 1H, *J* = 5.8 Hz, NH), 6.39 (d, 1H, *J* = 1.6 Hz, ArH phenol), 6.59 (d, 1H, *J* = 1.6 Hz, ArH phenol), 7.13 (d, 2H, *J* = 8.1 Hz, ArH phenylbutanamide), 7.19 (s, 1H, OH), 7.31 (d, 2H, *J* = 8.1 Hz, ArH phenylbutanamide), 7.47 (s, 1H, ArH pyrazole). ^{13}C NMR (101 MHz, $CDCl_3$) δ 14.04, 22.56, 23.48, 24.54, 26.55, 26.71, 26.93, 27.29, 28.40, 28.54, 29.01, 29.02, 29.39, 29.88, 31.70, 34.72, 35.50, 37.72, 39.52, 40.49, 41.97, 44.32, 76.63, 102.56, 107.98, 108.15, 124.20, 128.56, 133.12, 133.91, 140.36, 140.79, 151.19, 152.75, 153.82, 173.22. HRMS calculated for $C_{44}H_{66}N_4NaO_5$ $[M + Na]^+$, 753.4925; found, 753.4863. Analytical RP-HPLC Rt = 26.25 min; determined with HPLC method B.

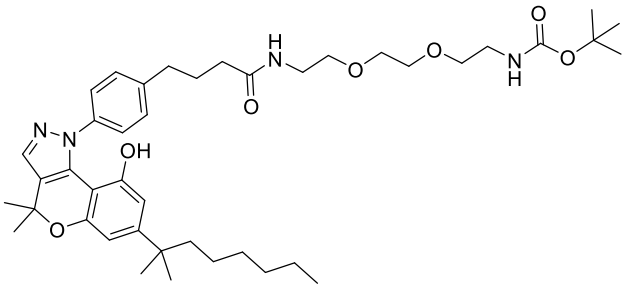

***tert*-Butyl *N*-(2-{2-[2-(4-{4-[9-hydroxy-4,4-dimethyl-7-(2-methyloctan-2-yl)-1*H*,4*H*-chromeno[4,3c]pyrazol-1-yl]phenyl}butanamido)ethoxy]ethoxy}ethyl)carbamate (3.32)**

This compound was prepared by following procedure described for the preparation of **3.22**, using **3.30** (25 mg, 0.05 mmol), **2.12** (22 mg, 0.08 mmol), HBTU (24 mg, 0.05 mmol) and DIPEA (50 µL, 0.15 mmol). Purification was done by silica gel column chromatography (eluting with 50% EtOAc/hexane to 3% MeOH/EtOAc) to provide **3.32** (19 mg, 0.02 mmol, 53%) as pale oily liquid. ^{1}H NMR (400 MHz, $CDCl_3$) δ 0.83 (t, 3H, *J* = 6.8 Hz, CH_2C**H**$_3$ dimethylheptyl chain), 1.00 – 1.11 (m, 2H, CH_2), 1.14 – 1.27 (m, 12H, 2 × C(C**H**$_3$)$_2$ dimethylheptyl chain and 3 × C**H**$_2$), 1.43 (s, 9H, C(C**H**$_3$)$_3$), 1.48 – 1.55 (m, 2H, CH_2), 1.61 (s, 6H, OC(C**H**$_3$)$_2$ pyran ring), 1.93 – 2.05 (m, 2H, CH_2C**H**$_2$$CH_2$CO), 2.21 (t, 2H, *J* = 7.2 Hz, CH_2CH_2C**H**$_2$CO), 2.69 (t, 2H, *J* = 7.1 Hz, C**H**$_2$$CH_2CH_2$CO), 3.15 (q, 2H, *J* = 5.3 Hz, CH_2), 3.41 (q, 2H, *J* = 5.3 Hz, CH_2), 3.50 (t, 2H, *J* = 5.2 Hz, CH_2),

3.56 (t, 2H, J = 5.0 Hz, CH_2), 3.61 (s, 4H, 2 × CH_2), 5.16 (br s, 1H, NH), 6.13 (br s, 1H, NH), 6.38 (s, 1H, ArH phenol), 6.59 (d, 1H, J = 1.6 Hz, ArH phenol), 7.11 (br s, 1H, OH), 7.17 (d, 2H, J = 8.0 Hz, ArH phenylbutanamide), 7.33 (d, 2H, J = 8.0 Hz, ArH phenylbutanamide), 7.48 (s, 1H, ArH pyrazole). ^{13}C NMR (101 MHz, $CDCl_3$) δ 14.22, 22.74, 24.71, 27.19, 27.48, 28.56, 28.73, 30.06, 31.88, 34.94, 35.95, 37.89, 39.43, 40.46, 44.51, 69.75, 70.09, 70.27, 70.36, 76.88, 80.02, 102.80, 108.17, 124.24, 128.72, 133.11, 134.13, 140.34, 141.14, 151.24, 152.84, 154.02, 156.45, 173.22. HRMS calculated for $C_{42}H_{63}N_4O_7$ $[M + H]^+$, 735.4691; found, 735.4675. Analytical RP-HPLC Rt = 23.80 min; determined with HPLC method B.

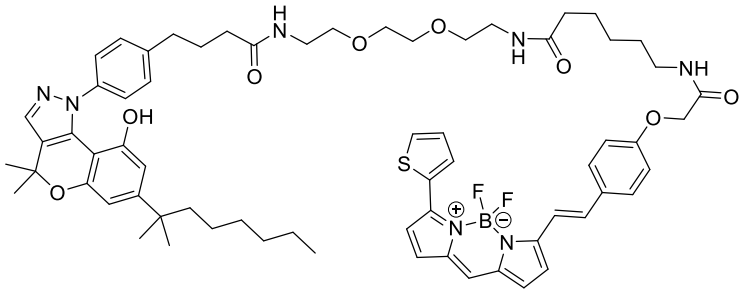

[12-(2-{4-[({5-[(2-{2-[2-(4-{4-[9-Hydroxy-4,4-dimethyl-7-(2-methyloctan-2-yl)-1*H*,4*H*-chromeno[4,3-c]pyrazol-1-yl]phenyl}butanamido)ethoxy]ethoxy} ethyl)carbamoyl]pentyl}carbamoyl)methoxy]phenyl}ethenl)-2-(- λ^2-fluoranidyl) -4-(thiophen-2-yl)-1λ^4-aza-3λ^4-aza-2λ^1-boratricyclo[7.3.0.0^{3,7}]dodeca-3,5,7,9,11-pentaene-2,2,2-triium-1-id-2-yl]-λ^2-fluoranide (**3.33**)

Following the procedure described for **3.23**, **3.32** (4.8 mg, 6.53 μmol) was reacted with TFA to give *N*-{2-[2-(2-aminoethoxy)ethoxy]ethyl}-4-{4-[9-hydroxy-4,4-dimethyl-7-(2-ethyloctan-2-yl)-1*H*,4*H*-chromeno[4,3-c]pyrazol-1-yl]phenyl}butanamide trifluoroacetate in assumed quantitative yield as yellow solid. This amino TFA salt was purified using semi-preparative RP-HPLC. This purified trifluoroacetate salt (4.1 mg, 5.47 μmol) on reaction with BODIPY-630/650-SE (1.0 mg, 1.51 μmol) gave **3.33** (1.57 mg, 1.33 μmol, 88%) as a dark blue solid. HRMS calculated for $C_{66}H_{80}BF_2N_7NaO_8S$ $[M + Na]^+$, 1202.5747; found, 1202.5687. Analytical RP-HPLC Rt = 25.32 min; determined with HPLC method B.

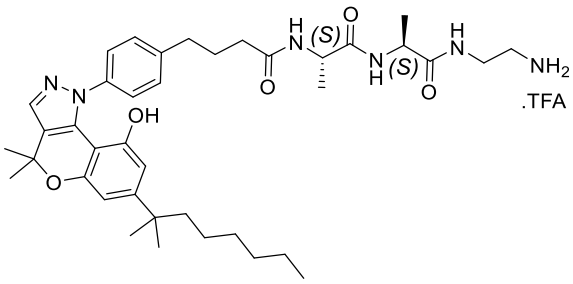

***N*-[(1*S*)-1-{[(1*S*)-1-[(2-Aminoethyl)carbamoyl]ethyl]carbamoyl}ethyl]-4-{4-[9-hydroxy-4,4-dimethyl-7-(2-methyloctan-2-yl)-1*H*,4*H*-chromeno[4,3-c]pyrazol-1-yl]phenyl}butanamide (3.38)**

Fmoc solid-phase synthesis was used for the preparation of **3.38**. 1,2-Diaminoethane trityl resin (0.70 mg, 0.083 mmol, mmols calculated on the basis of substitution (1.18 mmol/g) provided by vendor) was swelled in DMF overnight and then reacted with a solution of Fmoc-Ala-OH (0.13 g, 0.41 mmol), HBTU (0.16 g, 0.41 mmol) and DIPEA (0.14 mL, 0.83 mmol) in DMF (0.9 mL) and mixture shaken for 1 h. The resin was drained under low vacuum and then treated again with same quantities of Fmoc-Ala-OH, HBTU and DIPEA as described previously. The resin was washed with DMF and drained. The resin was capped by treating with a solution of Ac_2O (500 µL) and DIPEA (500 µL) in DMF (1 mL) for 20 min. The amount of Fmoc-Ala bound to the resin **3.35** determined by a Fmoc loading test (described below) was 0.78 mmol/g. The Fmoc was cleaved by treating the resin **3.35** with 20% *v*/*v* piperidine/DMF solution for 20 min, followed by washing the Fmoc deprotected **3.35** with DMF and drying under low vacuum. Reaction of the next Fmoc-Ala-OH (0.09 g, 0.31 mmol) with the Fmoc deprotected **3.35** using HBTU (0.12 g, 0.31 mmol), DIPEA (0.11 mL, 0.61 mmol) and DMF (0.6 mL) gave **3.36**, followed by Fmoc deprotection (carried out as described previously in this paragraph). Carboxylic acid **3.30** (15 mg, 0.03 mmol), HATU (12 mg, 0.03 mmol), DIPEA (0.01 mL, 0.09 mmol) and DMF (2.0 mL) were mixed and then reacted with the Fmoc deprotected **3.36** for 4 h. The resin (**3.37**) was drained, washed successively with DMF, DCM, dried under low vacuum and transferred to a round bottom flask. A solution of 5% TFA in DCM v/v was added to the round bottom flask containing **3.37** and resulting suspension was stirred for 2 h. The suspension was filtered and the filtrate was concentrated under reduced pressure to give 28 mg of light yellow solid, 20 mg of which was purified by semi-preparative RP-HPLC to give **3.38** trifluoroacetate salt (9 mg, 0.01 mmol) as a colourless solid. ^{1}H NMR (400 MHz, MeOD-d_4) δ 0.82 – 0.90 (m, 3H, $CH_2C\mathbf{H_3}$ dimethylheptyl chain), 1.06 – 1.13 (m, 2H, CH_2), 1.17 – 1.26 (m, 12H, $C(C\mathbf{H_3})_2$ dimethylheptyl chain and 3 × $C\mathbf{H_2}$), 1.35 (s,

3H, CH_3 alanine), 1.37 (s, 3H, CH_3 alanine), 1.51 – 1.56 (m, 2H, CH_2), 1.58 (s, 6H, 2 × OC(C**H**$_3$)$_2$ pyran ring), 1.96 (p, 2H, *J* = 7.6 Hz, CH_2), 2.28 – 2.36 (m, 2H, CH_2), 2.64 – 2.75 (m, 4H, 2 × C**H**$_2$), 3.17 – 3.29 (m, 2H, CH_2), 4.20 – 4.33 (m, 2H, C**H** Ala), 6.32 (d, 1H, *J* = 0.9 Hz, ArH phenol), 6.50 (d, 1H, *J* = 0.9 Hz, ArH phenol), 7.19 – 7.27 (m, 4H, ArH 4-phenylbutanamide), 7.55 (s, 1H, ArH pyrazole). ^{13}C NMR (101 MHz, MeOD-d_4) δ 14.41, 17.65, 17.88, 23.62, 25.73, 27.50, 28.55, 29.25, 29.27, 31.01, 32.85, 35.90, 36.08, 38.68, 41.85, 43.17, 45.39, 50.71, 51.01, 77.66, 103.50, 108.09, 108.50, 125.26, 125.40, 129.43, 134.82, 134.98, 142.17, 142.50, 154.01, 155.54, 175.24, 175.26, 176.30. HRMS calculated for $C_{39}H_{57}N_6O_5$ $[M + H]^+$, 689.4385; found, 689.4363.

Fmoc loading test

A piperidine/DMF solution (20% *v*/*v*, 1.0 mL) was added to 7.87 mg of Fmoc-alanine bound resin and shaken for 1 h. A portion of this solution (100 µL) was diluted to 10 mL with DMF and the absorbance was measured at 301 nm (after baseline correction with piperidine/DMF solution (20% *v*/*v*))

$$\text{Fmoc-alanine bound to the resin (mmol/g)} = \frac{100 \times absorbance}{7.8 \times weight\ of\ resin\ (mg)}$$

$$= \frac{100 \times 0.48}{7.8 \times 7.87} = 0.78\ mmol/g$$

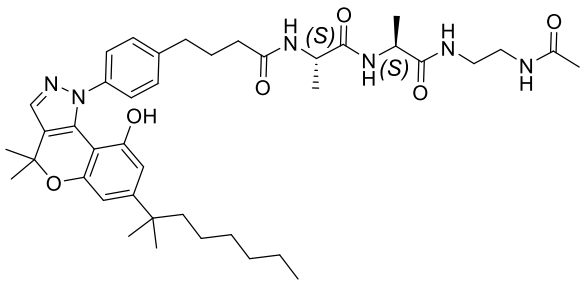

***N*-[(1*S*)-1-{[(1*S*)-1-[(2-Acetamidoethyl)carbamoyl]ethyl]carbamoyl}ethyl]-4-{4-[9-hydroxy-4,4-dimethyl-7-(2-methyloctan-2-yl)-1*H*,4*H*-chromeno[4,3-c]pyrazol-1-yl]phenyl}butanamide (3.39)**

To a solution of **3.38** (2.0 mg, 3.0 µmol) and Ac_2O (0.3 µL, 3.0 µmol) in $CHCl_3$ (3.0 mL) was added Et_3N (1.2 µL, 9 µmol) and the reaction stirred 2 h. The reaction solvent was removed by evaporation under reduced pressure and the residue purified by semi-preparative RP-HPLC to give **3.39** (2 mg, 2.73 µmol, 94%) as a colourless solid. HRMS calculated for $C_{41}H_{58}N_6NaO_6$ $[M + Na]^+$, 753.4315; found, 753.4278. Analytical RP-HPLC Rt = 21.27 min; determined with HPLC method B.

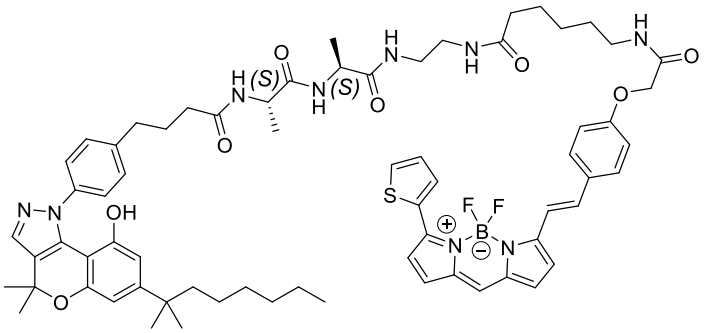

(12-{2-[4-({[5-({2-[(2*S*)-2-[(2*S*)-2-(4-{4-[9-Hydroxy-4,4-dimethyl-7-(2-methyloctan-2-yl)-1*H*,4*H*-chromeno[4,3-c]pyrazol-1-yl]phenyl}butanamido)propanamido] propanamido]ethyl}carbamoyl)pentyl]carbamoyl}methoxy)phenyl]ethenyl}-2-(-λ^2-fluoranidyl)-4-(thiophen-2-yl)-1λ^4-aza-3λ^4-aza-2λ^1-boratricyclo[7.3.0.0^{3,7}]dodeca-3,5,7,9,11-pentaene-2,2,2-triium-1-id-2-yl)-λ^2-fluoranide (**3.40**)

Following the procedure described for **3.23**, **3.38** (3.1 mg, 5.28 μmol) was reacted with BODIPY-630/650-SE (1.0 mg, 1.51 μmol) to give **3.40** (0.92 mg, 0.74 μmol, 49%) as a dark blue solid. HRMS calculated for $C_{68}H_{82}BF_2N_9NaO_8S$ $[M + Na]^+$, 1256.5965; found, 1256.5860. Analytical RP-HPLC Rt = 24.57 min; determined with HPLC method B.

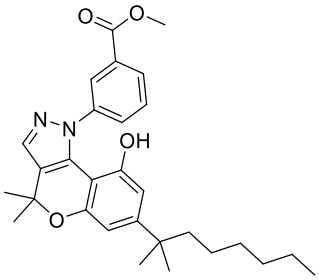

Methyl 3-[9-hydroxy-4,4-dimethyl-7-(2-methyloctan-2-yl)-1*H*,4*H*-chromeno[4,3-c]pyrazol-1-yl]benzoate (3.41)

This compound was prepared by following the procedure described for **3.18**, using **3.16** (100 mg, 0.29 mmol) and commercially available 3-hydrazinobenzoic acid hydrochloride (60 mg, 0.31 mmol). The crude compound was purified by silica gel column chromatography (eluting with 5% EtOAc/hexane to 15% EtOAc/hexane) to provide **3.41** (70 mg, 0.14 mmol, 49%) as an orange solid. ^{1}H NMR (400 MHz, $CDCl_3$) δ 0.83 (t, 3H, *J* = 6.9 Hz, $CH_2C\mathbf{H_3}$ dimethylheptyl chain), 1.00 – 1.09 (m, 2H, CH_2), 1.11 – 1.29 (m, 12H, $C(C\mathbf{H_3})_2$ dimethylheptyl chain and 3 × $C\mathbf{H_2}$), 1.45 – 1.53 (m, 2H, CH_2), 1.62 (s, 6H, $OC(C\mathbf{H_3})_2$ pyran ring), 3.80 (s, 3H, OCH_3), 6.07 (s, 1H, OH), 6.28 (d, 1H, *J* = 1.7 Hz, ArH phenol), 6.64 (d, 1H, *J* = 1.6 Hz, ArH phenol), 7.37 (t, 1H, *J* = 7.9 Hz, ArH methyl benzoate), 7.46 (s, 1H, ArH pyrazole), 7.52 – 7.58 (m, 1H, ArH methyl benzoate), 7.86

(dt, 1H, *J* = 1.3 Hz, 7.8 Hz, ArH methyl benzoate), 8.07 (t, 1H, *J* = 1.9 Hz, ArH methyl benzoate). ^{13}C NMR (101 MHz, $CDCl_3$) δ 14.20, 22.74, 24.69, 27.44, 28.69, 30.04, 31.86, 37.92, 44.45, 52.37, 76.96, 102.46, 108.00, 108.82, 124.83, 125.39, 128.29, 128.53, 128.82, 130.44, 133.11, 134.67, 143.05, 150.45, 153.37, 154.18, 166.87. HRMS calculated for $C_{29}H_{36}N_2NaO_4$ $[M + Na]^+$, 499.2567; found, 499.2556. Analytical RP-HPLC Rt = 23.92 min; determined with HPLC method B.

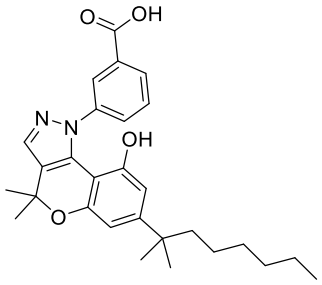

3-[9-Hydroxy-4,4-dimethyl-7-(2-methyloctan-2-yl)-1*H*,4*H*-chromeno[4,3-c]pyrazol-1-yl]benzoic acid (3.42)

According to the procedure described for **3.19**, **3.41** (0.14 g, 0.29 mmol) was reacted with LiOH (21 mg, 0.88 mmol) to give **3.42** (0.13 g, 0.27 mmol, 93%) as a yellow solid. ^{1}H NMR (400 MHz, MeOD-d_4) δ 0.82 – 0.89 (m, 3H, $CH_2C\mathbf{H_3}$ dimethylheptyl chain), 1.04 – 1.14 (m, 2H, CH_2), 1.18 – 1.28 (m, 12H, $C(C\mathbf{H_3})_2$ dimethylheptyl chain and 3 × $C\mathbf{H_2}$), 1.51 – 1.58 (m, 2H, CH_2), 1.60 (s, 6H, $OC(C\mathbf{H_3})_2$ pyran ring), 6.33 (d, 1H, *J* = 1.8 Hz, ArH phenol), 6.53 (d, 1H, *J* = 1.8 Hz, ArH phenol), 7.45 – 7.54 (m, 2H, ArH benzoic acid), 7.60 (s, 1H, ArH pyrazole), 7.97 – 8.04 (m, 2H, ArH benzoic acid). ^{13}C NMR (101 MHz, MeOD-d_4) δ 14.39, 23.62, 25.70, 27.52, 29.23, 31.01, 32.83, 38.71, 45.34, 77.70, 103.22, 108.30, 108.44, 125.72, 126.52, 129.34, 129.37, 133.69, 135.02, 135.41, 144.56, 153.42, 154.28, 155.53, 169.99. HRMS calculated for $C_{28}H_{35}N_2O_4$ $[M + H]^+$, 463.2591; found, 463.2557.

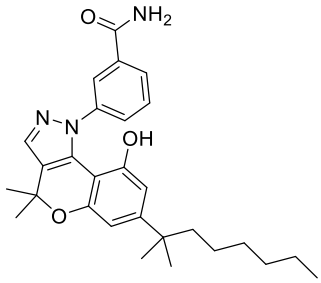

3-[9-Hydroxy-4,4-dimethyl-7-(2-methyloctan-2-yl)-1*H*,4*H*-chromeno[4,3-c]pyrazol-1-yl]benzamide (3.43)

This compound was prepared by following the procedure used for the preparation of **3.20**, using **3.42** (95 mg, 0.20 mmol), DIPEA (0.3 mL, 1.64 mmol), NH_4Cl (55 mg, 1.02 mmol) and HBTU (78 mg, 0.20 mmol). Purification was done by silica gel column chromatography (eluting with 50% EtOAc/hexane to 80% EtOAc/hexane) to provide **3.43** (72 mg, 0.15 mmol, 78%) as a colourless solid. ^{1}H NMR (400 MHz, $CDCl_3$) δ 0.82 (t, 3H, *J* = 6.7 Hz, $CH_2C\mathbf{H_3}$ dimethylheptyl chain), 0.99 – 1.10 (m, 2H, CH_2), 1.10 – 1.30 (m, 12H, $C(C\mathbf{H_3})_2$ dimethylheptyl chain and 3 × $C\mathbf{H_2}$), 1.42 – 1.53 (m, 2H, CH_2), 1.61 (s, 6H, 2 × $OC(C\mathbf{H_3})_2$ pyran ring), 6.13 (br s, 1H, NH), 6.38 (d, 1H, *J* = 1.7 Hz, ArH phenol), 6.59 (br s, 1H, NH), 6.62 (d, 1H, *J* = 1.6 Hz, ArH phenol), 7.18 (t, 1H, *J* = 7.9 Hz, ArH benzamide), 7.35 (d, 1H, *J* = 8.1 Hz, ArH benzamide), 7.43 (s, 1H, ArH pyrazole), 7.57 (d, 1H, *J* = 7.7 Hz, ArH benzamide), 7.73 (s, 1H, ArH benzamide), 8.11 (br s, 1H, OH). ^{13}C NMR (101 MHz, $CDCl_3$) δ 14.21, 22.74, 24.73, 27.42, 28.68, 30.04, 31.87, 37.98, 44.43, 76.80, 102.45, 108.34, 108.48, 122.79, 124.77, 126.32, 127.89, 128.65, 133.56, 134.51, 142.96, 151.17, 153.78, 154.24, 170.05. HRMS calculated for $C_{28}H_{35}N_3NaO_3$ [M + Na]$^+$, 484.2571; found, 484.2558.

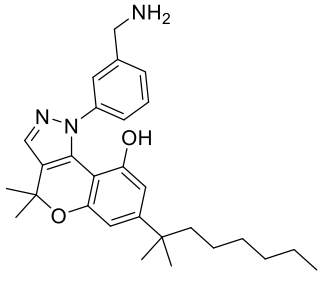

1-[3-(Aminomethyl)phenyl]-4,4-dimethyl-7-(2-methyloctan-2-yl)-1*H*,4*H*-chromeno[4,3-c]pyrazol-9-ol (3.44)

According to the procedure for **3.21**, using **3.43** (0.11 g, 0.23 mmol) and $LiAlH_4$ (44 mg, 1.16 mmol) gave **3.44** (105 mg) as a reddish oil, which was used without further purification in the next reaction.

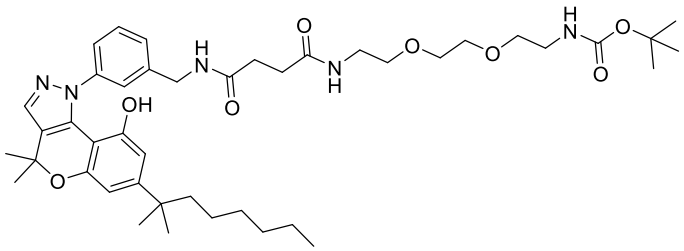

***tert*-Butyl *N*-{2-[2-(2-{3-[({3-[9-hydroxy-4,4-dimethyl-7-(2-methyloctan-2-yl)-1*H*,4*H*-chromeno[4,3 c]pyrazol-1-yl]phenyl}methyl)carbamoyl]propanamido} ethoxy)ethoxy]ethyl}carbamate (3.45)**

According to the procedure described for **3.22**, **3.44** (71 mg) was reacted with **3.13** (55 mg, 0.16 mmol), HBTU (60 mg, 0.16 mmol) and DIPEA (0.1 mL, 0.47 mmol). Purification of the crude compound by silica gel column chromatography (eluting with 50% EtOAc/hexane to 7% MeOH/EtOAc) gave **3.45** (44 mg, 0.06 mmol, 37%) as a reddish solid. ^{1}H NMR (400 MHz, $CDCl_3$) δ 0.76 – 0.91 (m, 3H, $CH_2C\mathbf{H_3}$ dimethylheptyl chain), 0.98 – 1.13 (m, 2H, CH_2), 1.14 – 1.28 (m, 12H, $C(C\mathbf{H_3})_2$ dimethylheptyl chain and 3 × $C\mathbf{H_2}$), 1.43 (s, 9H, $C(C\mathbf{H_3})_3$), 1.49 – 1.56 (m, 2H, CH_2), 1.61 (s, 6H, $OC(C\mathbf{H_3})_2$ pyran ring), 2.38 – 2.48 (m, 2H, CH_2), 2.48 – 2.58 (m, 2H, CH_2), 3.14 – 3.24 (m, 2H, CH_2), 3.28 (q, 2H, *J* = 5.4 Hz, CH_2), 3.42 (t, 2H, *J* = 5.0 Hz, CH_2), 3.47 – 3.69 (m, 6H, 3 × $C\mathbf{H_2}$), 4.28 (d, 2H, *J* = 5.8 Hz, $NHC\mathbf{H_2}$ benzylacetamide), 5.19 (br s, 1H, NH), 6.47 (br s, 1H, NH), 6.49 – 6.55 (m, 1H, ArH phenol), 6.61 (d, 1H, *J* = 1.7 Hz, ArH phenol), 6.65 (br s, 1H, NH), 7.16 – 7.24 (m, 2H, ArH benzylacetamide), 7.30 (t, 1H, *J* = 7.7 Hz, ArH benzylacetamide), 7.43 – 7.50 (m, 1H, ArH benzylacetamide), 7.48 (s, 1H, ArH pyrazole), 8.12 (br s, 1H, OH). ^{13}C NMR (101 MHz, $CDCl_3$) δ 14.21. 22.75, 24.81, 27.41, 28.57, 28.77, 30.10, 31.93, 32.02, 37.94, 39.62, 40.49, 43.65, 44.64, 69.37, 70.42, 77.05*, 79.63*, 102.82, 107.75, 108.04, 122.69, 123.84, 124.62, 126.80, 128.81, 133.00, 134.34, 138.36, 143.32, 151.70, 153.04, 154.22, 171.96, 172.84, (* denoted carbon observed with gHMBC correlation). HRMS calculated for $C_{43}H_{63}N_5NaO_8$ $[M + Na]^+$, 800.4569; found, 800.4544. Analytical RP-HPLC Rt = 22.22 min; determined with HPLC method B.

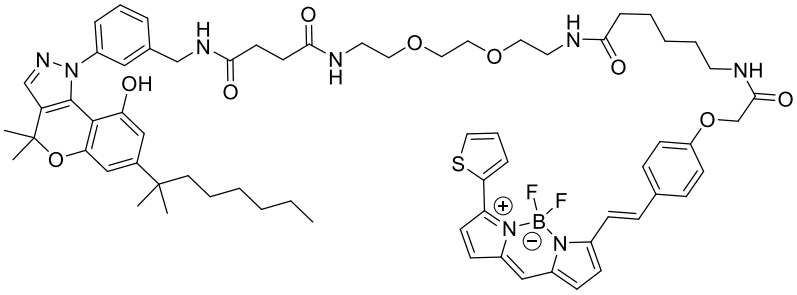

(12-{2-[4-({[5-({2-[2-(2-{3-[({3-[9-Hydroxy-4,4-dimethyl-7-(2-methyloctan-2-yl)-1*H*,4*H* chromeno[4,3-c]pyrazol-1-yl]phenyl}methyl)carbamoyl]propanamido} ethoxy)ethoxy] ethyl}carbamoyl)pentyl]carbamoyl}methoxy)phenyl]ethenyl}-2-(-λ²-fluoranidyl)-4-(thiophen-2-yl)-1λ⁴-aza-3λ⁴-aza-2λ¹-boratricyclo [7.3.0.0^{3,7}] dodeca-3,5,7,9,11-pentaene-2,2,2-triium-1-id-2-yl)-λ²-fluoranide (3.46)

Following the procedure described for **3.23**, **3.45** (4.0 mg, 5.14 µmol) was reacted with TFA to give *N*-{2-[2-(2-aminoethoxy)ethoxy]ethyl}-*N*'-({3-[9-hydroxy-4,4-dimethyl-7-(2-methyloctan-2-yl)-1*H*,4*H*-chromeno[4,3-c]pyrazol-1-yl]phenyl}methyl)butanediamide trifluoroacetate in assumed quantitative yield as yellow solid. This amino TFA salt was purified using semi-preparative RP-HPLC. This purified trifluoroacetate salt (4.5 mg, 5.68 µmol) on reaction with BODIPY-630/650-SE (1.0 mg, 1.51 µmol) gave **3.46** (0.25 mg, 0.20 µmol, 14%) as a dark blue solid. HRMS calculated for $C_{67}H_{81}BF_2N_8NaO_9S$ $[M + Na]^+$, 1245.5806; found, 1245.5739. Analytical RP-HPLC Rt = 24.47 min; determined with HPLC method B.

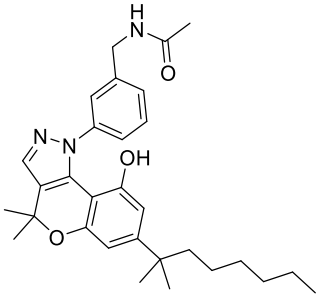

***N*-({3-[9-Hydroxy-4,4-dimethyl-7-(2-methyloctan-2-yl)-1*H*,4*H*-chromeno[4,3-c]pyrazol-1 yl]phenyl}methyl)acetamide (3.47)**

According to procedure described for **3.25**, **3.44** (30 mg, 0.07 mmol) was reacted with Ac_2O (10 µL, 0.10 mmol) and Et_3N (50 µL, 0.34 mmol). Analysis of the reaction mixture by MS indicated formation of a mixture of monoacetylated-**3.44** and diacetylated-**3.44**. The reaction solvent was removed under reduced pressure, the residue dissolved in MeOH (3.0 mL) and treated with a solution of NaOH (5.0 mg) in water (0.5 mL) at 0 °C

and stirred for 3 h. The reaction solvent was removed under reduced pressure, the residue partitioned between EtOAc and saturated NH_4Cl solution. The organic layer was separated, washed with saturated $NaHCO_3$ solution, water, brine, dried over $MgSO_4.H_2O$, and solvent removed by evaporation under reduced pressure to give **3.47** (12.0 mg, 0.02 mmol, 36% over two steps from **3.44**) as a light pink solid. ^{1}H NMR (400 MHz, MeOD-d_4) δ 0.81 – 0.90 (m, 3H, $CH_2C\mathbf{H_3}$ dimethylheptyl chain), 1.03 – 1.15 (m, 2H, CH_2), 1.16 – 1.32 (m, 12H, $C(C\mathbf{H_3})_2$ dimethylheptyl chain and 3 × $C\mathbf{H_2}$), 1.46 – 1.57 (m, 2H, CH_2), 1.59 (s, 6H, $OC(C\mathbf{H_3})_2$ pyran ring), 1.95 (s, 3H, $NHCOC\mathbf{H_3}$), 4.38 (s, 2H, $C\mathbf{H_2}NH$), 6.32 (d, 1H, *J* = 1.8 Hz, ArH phenol), 6.53 (d, 1H, *J* = 1.8 Hz, ArH phenol), 7.20 – 7.25 (m, 1H, ArH benzylacetamide), 7.25 – 7.30 (m, 2H, ArH benzylacetamide), 7.33 – 7.39 (m, 1H, ArH benzylacetamide), 7.58 (s, 1H, ArH pyrazole). ^{13}C NMR (101 MHz, MeOD-d_4) δ 14.39, 22.61, 23.62, 25.74, 27.50, 29.23, 31.02, 32.87, 38.71, 43.77, 45.38, 77.70, 103.43, 108.34, 108.45, 124.16, 124.31, 125.63, 127.35, 129.50, 134.89, 135.08, 140.56, 144.60, 153.46, 154.17, 155.57, 173.11. HRMS calculated for $C_{30}H_{39}N_3NaO_3$ $[M + Na]^+$, 512.2884; found, 512.2873. Analytical RP-HPLC Rt = 22.08 min; determined with HPLC method B.

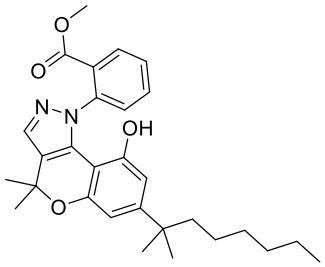

Methyl 2-[9-hydroxy-4,4-dimethyl-7-(2-methyloctan-2-yl)-1*H*,4*H*-chromeno[4,3-c]pyrazol-1-yl]benzoate (3.48)

According to the procedure for **3.18**, **3.16** (0.3 g, 0.86 mmol) was reacted with commercially available 2-hydrazinobenzoic acid (0.18 g, 0.95 mmol). Purification was done by silica gel column chromatography (eluting with 5% EtOAc/hexane to 30% EtOAc/hexane) to provide **3.48** (0.17 g, 0.35 mmol, 41%) as a yellow solid. ^{1}H NMR (400 MHz, $CDCl_3$) δ 0.83 (t, 3H, *J* = 6.9 Hz, $CH_2C\mathbf{H_3}$ dimethylheptyl chain), 0.95 – 1.08 (m, 2H, CH_2), 1.11 – 1.28 (m, 12H, $C(C\mathbf{H_3})_2$ dimethylheptyl chain and 3 × $C\mathbf{H_2}$), 1.42 – 1.52 (m, 2H, CH_2), 1.64 (s, 6H, $OC(C\mathbf{H_3})_2$ pyran ring), 3.57 (s, 3H, OCH_3), 5.71 (br s, 1H, OH), 6.22 (d, 1H, *J* = 1.7 Hz, ArH phenol), 6.60 (d, 1H, *J* = 1.7 Hz, ArH phenol), 7.35 (dd, 1H, *J* = 1.2 Hz, 7.9 Hz, ArH methyl benzoate), 7.42 (td, 1H, *J* = 1.3 Hz, 7.6 Hz, ArH methyl benzoate), 7.48 (s, 1H, ArH pyrazole), 7.52 (td, 1H, *J* = 1.6 Hz, 7.7 HZ, 7.7

Hz, ArH methyl benzoate), 7.82 (dd, 1H, *J* = 1.6 Hz, 7.7 Hz, ArH methyl benzoate). ^{13}C NMR (101 MHz, $CDCl_3$) δ 14.05, 22.58, 24.53, 27.43, 28.54, 29.88, 31.71, 37.76, 44.31, 52.44, 76.72, 102.25, 108.07, 108.48, 123.59, 127.84, 127.98, 128.17, 130.09, 132.23, 134.23, 134.30, 141.66, 150.32, 153.15, 153.78, 167.17. HRMS calculated for $C_{29}H_{36}N_2NaO_4$ $[M + Na]^+$, 499.2567; found, 499.2528. Analytical RP-HPLC Rt = 22.75 min; determined with HPLC method B.

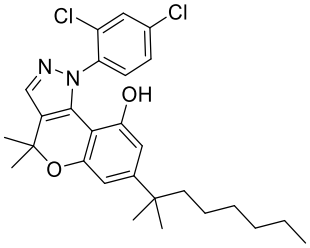

1-(2,4-Dichlorophenyl)-4,4-dimethyl-7-(2-methyloctan-2-yl)-1*H*,4*H*-chromeno[4,3-c]pyrazol-9-ol (3.4)

Following procedure described for **3.18**, **3.16** (22 mg, 0.06 mmol) was reacted with commercially available 2,4-dichlorophenylhydrazine hydrochloride (54 mg, 0.25 mmol). Purification of crude compound was carried out by silica gel column chromatography (eluting with 20 to 30% EtOAc/hexane) to provide **3.4** (21 mg, 0.04 mmol, 72%) as a reddish orange oil. The synthesis of **3.4** was previously reported with microwave irradiation.[137] ^{1}H NMR (400 MHz, $CDCl_3$) δ 0.83 (t, 3H, *J* = 7.0 Hz, $CH_2C\mathbf{H_3}$ dimethylheptyl chain), 0.92 – 1.07 (m, 2H, CH_2), 1.10 – 1.30 (m, 12H, $C(C\mathbf{H_3})_2$ dimethylheptyl chain and 3 × $C\mathbf{H_2}$), 1.42 – 1.51 (m, 2H, CH_2), 1.64 (s, 3H, $OC(C\mathbf{H_3}CH_3)$ pyran ring), 1.65 (s, 3H, $OC(CH_3C\mathbf{H_3})$ pyran ring), 6.14 (d, 1H, *J* = 1.7 Hz, ArH phenol), 6.58 (d, 1H, *J* = 1.6 Hz, ArH phenol), 7.21 – 7.25 (m, 1H, 8.5 Hz, ArH 2,4-dichlorobenzene), 7.27 – 7.31 (m, 1H, ArH 2,4-dichlorobenzene), 7.42 (d, 1H, *J* = 2.2 Hz, ArH 2,4-dichlorobenzene), 7.50 (s, 1H, ArH pyrazole). ^{13}C NMR (101 MHz, $CDCl_3$) δ 14.21, 22.72, 24.67, 27.73, 27.76, 28.61, 28.67, 30.01, 31.86, 37.90, 44.45, 76.70, 102.25, 107.30, 108.69, 123.18, 127.08, 129.39, 129.49, 132.68, 134.28, 134.61, 139.79, 150.76, 153.43, 154.05. HRMS calculated for $C_{27}H_{33}Cl_2N_2O_2$ $[M + H]^+$, 487.1914; found, 487.1894. Analytical RP-HPLC Rt = 24.94 min; determined with HPLC method B.

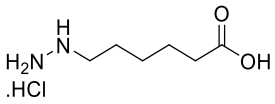

6-Hydrazinylhexanoic acid hydrochloride (3.50)

To a solution of hydrazine monohydrochloride (1.76 g, 25.63 mmol) was added NaOH (1.43 g, 35.89 mmol) and commercially available 6-bromohexanoic acid **3.49** (1.0 g, 5.13 mmol) in dioxane (15 mL), water (15 mL) and the reaction mixture stirred at 90 °C for 20 h. The reaction solvents were removed by evaporation under reduced pressure. The residue was dissolved in water, which was removed from the resulting solution by evaporation under reduced pressure. This process of co-distillation of the residual reaction mixture with water was repeated five times. Next, the residue was acidified (pH 2 - 3) with 6M aqueous HCl and diluted with water to give a 30 mL solution, which was then extracted with 100 mL mixture of EtOH:EtOAc (25% *v*/*v*). The aqueous layer was extracted once more with 50 mL EtOAc. The organic layers were combined, washed with water (30 mL) and the solvent removed under reduced pressure to give **3.50** (0.57 g) as a yellow semisolid, which was used in next reaction without further purification. HRMS calculated for $C_6H_{15}N_2O_2$ $[M + H]^+$, 147.1128; found, 147.1118.

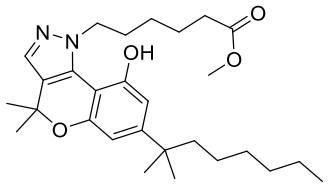

Methyl 6-[9-hydroxy-4,4-dimethyl-7-(2-methyloctan-2-yl)-1*H*,4*H*-chromeno[4,3-c]pyrazol-1-yl]hexanoate (3.51)

According to the procedure for **3.18**, **3.16** (0.16 g, 0.46 mmol) was reacted with **3.50** (0.25 g, 1.38 mmol). Purification was done by silica gel column chromatography (eluting with 10 to 30% EtOAc/hexane) to provide **3.51** (91 mg, 0.19 mmol, 42%) as a pale oil. ^{1}H NMR (500 MHz, $CDCl_3$) δ 0.82 (t, 3H, *J* = 7.0 Hz, $CH_2C\mathbf{H_3}$ dimethylheptyl chain), 1.01 – 1.12 (m, 2H, CH_2), 1.13 – 1.24 (m, 12H, $C(C\mathbf{H_3})_2$ dimethylheptyl chain and 3 × $C\mathbf{H_2}$), 1.25 – 1.32 (m, 2H, CH_2), 1.49 – 1.54 (m, 2H, CH_2), 1.56 (s, 6H, $OC(C\mathbf{H_3})_2$ pyran ring), 1.58 – 1.64 (m, 2H, CH_2), 1.81 – 1.93 (m, 2H, CH_2), 2.21 (t, 2H, *J* = 7.59 Hz, CH_2), 3.62 (s, 3H, OCH_3), 4.57 – 4.68 (m, 2H, pyrazole-CH_2), 6.52 (d, 1H, *J* = 1.8 Hz, ArH phenol), 6.59 (d, 1H, *J* = 1.8 Hz, ArH phenol), 7.34 (s, 1H, ArH pyrazole), 8.82 (s, 1H, OH). ^{13}C NMR (126 MHz, $CDCl_3$) δ 14.18, 22.74, 24.49, 24.73, 26.04, 27.40, 28.75, 29.82, 30.07,

31.87, 33.77, 37.83, 44.49, 51.75, 52.96, 76.32, 103.05, 107.68, 108.51, 123.18, 131.97, 132.91, 151.32, 152.76, 154.28, 175.03. HRMS calculated for $C_{28}H_{43}N_2O_4$ $[M + H]^+$, 471.3217; found, 471.3187. Analytical RP-HPLC Rt = 23.31 min; determined with HPLC method B.

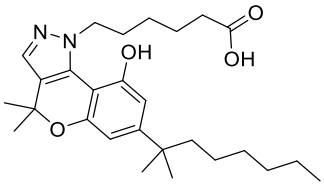

6-[9-Hydroxy-4,4-dimethyl-7-(2-methyloctan-2-yl)-1*H*,4*H*-chromeno[4,3-c]pyrazol-1-yl]hexanoic acid (3.52)

According to the procedure for **3.19**, reaction of **3.51** (67 mg, 0.14 mmol) with LiOH (17 mg, 0.71 mmol) gave **3.52** (0.05 g, 0.11 mmol, 81%) as a pale yellow solid. ^{1}H NMR (400 MHz, MeOD-d_4) δ 0.79 – 0.89 (m, 3H, $CH_2C\mathbf{H_3}$ dimethylheptyl chain), 1.03 – 1.14 (m, 2H, CH_2), 1.17 – 1.33 (m, 14H, $C(C\mathbf{H_3})_2$ dimethylheptyl chain and 4 × $C\mathbf{H_2}$), 1.52 – 1.62 (m, 10H, $OC(C\mathbf{H_3})_2$ pyran ring and 2 × $C\mathbf{H_2}$), 1.80 (p, 2H, J = 7.5 Hz, CH_2), 2.21 (t, 2H, J = 7.4 Hz, CH_2), 4.66 (t, 2H, J = 7.4 Hz, pyrazole-CH_2), 6.54 (d, 1H, J = 1.8 Hz, ArH phenol), 6.58 (d, 1H, J = 1.8 Hz, ArH phenol), 7.61 (s, 1H, ArH pyrazole). ^{13}C NMR (101 MHz, MeOD-d_4) δ 14.40, 23.61, 25.73, 27.08, 27.29, 29.18, 30.99, 31.06, 32.84, 34.71, 38.78, 45.34, 53.91, 76.87, 102.78, 108.46, 109.00, 124.76, 131.92, 135.95, 153.71, 155.22, 156.00, 177.35. HRMS calculated for $C_{27}H_{41}N_2O_4$ $[M + H]^+$, 457.3061; found, 457.3039.

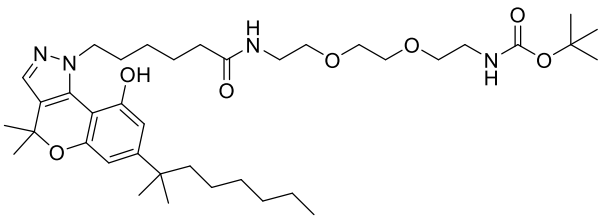

***tert*-Butyl *N*-{2-[2-(2-{6-[9-hydroxy-4,4-dimethyl-7-(2-methyloctan-2-yl)-1*H*,4*H*-chromeno[4,3-c]pyrazol-1-yl]hexanamido}ethoxy)ethoxy]ethyl}carbamate (3.53)**

According to the procedure for **3.22**, reaction of **3.52** (30 mg, 0.07 mmol), **2.12** (32 mg, 0.13 mmol), HATU (25 mg, 0.06 mmol) and DIPEA (0.04 mL, 0.19 mmol), followed by column purification (eluting with 50% EtOAc/hexane to 5% MeOH/EtOAc) provided **3.53** (18 mg, 0.02 mmol, 39%) as a yellowish-orange oil. ^{1}H NMR (400 MHz, $CDCl_3$) δ 0.83 (t, 3H, J = 6.8 Hz, $CH_2C\mathbf{H_3}$ dimethylheptyl chain), 1.03 – 1.10 (m, 2H, CH_2), 1.14

– 1.28 (m, 12H, C(C**H**$_3$)$_2$ dimethylheptyl chain and 3 × C**H**$_2$), 1.40 – 1.48 (m, 11H, pyrazole-CH$_2$CH$_2$C**H**$_2$ and C(C**H**$_3$)$_3$), 1.49 – 1.54 (m, 2H, CH$_2$), 1.56 (s, 6H, OC(C**H**$_3$)$_2$ pyran ring), 1.69 – 1.81 (m, 2H, pyrazole-CH$_2$CH$_2$CH$_2$C**H**$_2$), 1.89 – 1.97 (m, 2H, pyrazole-CH$_2$C**H**$_2$), 2.19 (t, 2H, *J* = 7.8 Hz, pyrazole-CH$_2$CH$_2$CH$_2$CH$_2$C**H**$_2$**)**, 3.27 – 3.36 (m, 2H, CH$_2$), 3.49 – 3.72 (m, 10H, 5 × C**H**$_2$), 4.48 – 4.61 (m, 2H, pyrazole-CH$_2$), 5.01 (br s, 1H, NH), 6.31 (br s, 1H, NH), 6.52 (d, 1H, *J* = 1.8 Hz, ArH phenol), 6.55 (d, 1H, *J* = 1.7 Hz, ArH phenol), 7.28 (s, 1H, ArH pyrazole), 9.40 (s, 1H, OH). ^{13}C NMR (101 MHz, CDCl$_3$) δ 14.23, 22.78, 24.78, 25.20, 27.51, 28.20, 28.55, 28.83, 30.12, 31.92, 35.71, 37.81, 39.58, 40.51, 44.55, 52.83, 69.87, 70.32, 70.49, 76.38, 103.26, 107.60, 108.13, 122.80, 132.15, 132.40, 152.41, 154.13, 175.04. HRMS calculated for $C_{38}H_{62}N_4NaO_7$ $[M + Na]^+$, 709.4511; found, 709.4529. Analytical RP-HPLC Rt = 22.93 min; determined with HPLC method B.

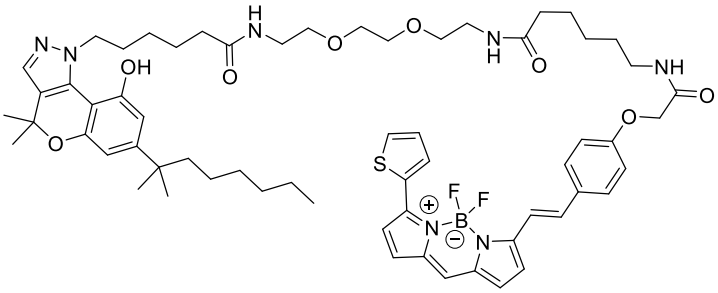

(12-{2-[4-({[5-({2-[2-(2-{6-[9-Hydroxy-4,4-dimethyl-7-(2-methyloctan-2-yl)-1*H*,4*H*-chromeno[4,3-c]pyrazol-1-yl]hexanamido}ethoxy)ethoxy]ethyl} carbamoyl)pentyl]carbamoyl}methoxy)phenyl]ethenyl}-2-(-λ^2-fluoranidyl)-4-(thiophen-2-yl)-1λ^4-aza-3λ^4-aza-2λ^1-boratricyclo[7.3.0.0^{3,7}]dodeca-3,5,7,9,11-pentaene-2,2,2-triium-1-id-2-yl)-λ^2-fluoranide (3.54)

Following the procedure described for **3.23**, **3.53** (4.1 mg, 5.97 μmol) was reacted with TFA to give *N*-{2-[2-(2-aminoethoxy)ethoxy]ethyl}-6-[9-hydroxy-4,4-dimethyl-7-(2-methyloctan-2-yl)-1*H*,4*H*-chromeno[4,3-c]pyrazol-1-yl]hexanamide trifluoroacetate in assumed quantitative yield as yellow solid. This amino TFA salt was purified using semi-preparative RP-HPLC. This purified trifluoroacetate salt (4.7 mg, 6.70, μmol) on reaction with BODIPY-630/650-SE (1.0 mg, 1.51 μmol) gave **3.54** (0.64 mg, 0.56 μmol, 37%) as dark blue solid. HRMS calculated for $C_{62}H_{80}BF_2N_7NaO_8S$ $[M + Na]^+$, 1154.5747; found, 1154.5694. Analytical RP-HPLC Rt = 24.50 min; determined with HPLC method B.

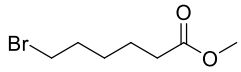

Methyl 6-bromohexanoate (3.56)

To a solution of commercially available 6-bromohexanoic acid **3.55** (1.0 g, 5.12 mmol) in MeOH (30 mL) was added two drops of conc. H_2SO_4 (98%). The reaction mixture was stirred at 70 °C for 12 h. The reaction solvent was removed under reduced pressure, the residue neutralised with saturated sodium $NaHCO_3$ solution and extracted with EtOAc. The organic layer was then washed with water, brine solution, dried over $MgSO_4.H_2O$, solvent removed by evaporation under rescued pressure to provide **3.56** (0.68 g, 3.25 mmol, 63%) as a clear liquid. NMR spectroscopy data of **3.56** was consistent with a previous literature report[237]. ^{1}H NMR (400 MHz, $CDCl_3$) δ 1.39 – 1.52 (m, 2H, CH_2), 1.58 – 1.67 (m, 2H, CH_2), 1.80 – 1.92 (m, 2H, CH_2), 2.31 (t, 2H, *J* = 7.4 Hz, CH_2), 3.39 (t, 2H, *J* = 6.8 Hz, CH_2), 3.65 (d, 3H, *J* = 1.2 Hz CH_3). ^{13}C NMR (101 MHz, $CDCl_3$) δ 24.16, 27.74, 32.48, 33.57, 33.91, 51.64, 173.97.

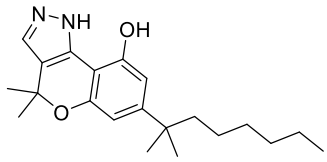

4,4-Dimethyl-7-(2-methyloctan-2-yl)-2*H*,4*H*-chromeno[4,3-c]pyrazol-9-ol (3.57)

The synthesis of **3.57** was done following the procedure described for **3.18,** using **3.16** (0.25 g, 0.74 mmol) and hydrazine monohydrochloride (76 mg, 1.11 mmol) except that H_2SO_4 was not used in the reaction. Purification of crude compound was done by silica gel column chromatography (eluting with 10 to 50% EtOAc/hexane) to provide **3.57** (0.21 g, 0.61 mmol, 83%) as a pale solid. Synthesis of **3.57** was previously reported with microwave irradiation.[137] ^{1}H NMR (400 MHz, $CDCl_3$) δ 0.83 (t, 3H, *J* = 6.9 Hz, $CH_2C\mathbf{H_3}$ dimethylheptyl chain), 1.02 – 1.12 (m, 2H, CH_2), 1.13 – 1.30 (m, 12H, $C(C\mathbf{H_3})_2$ dimethylheptyl chain and 3 × $C\mathbf{H_2}$), 1.50 – 1.58 (m, 2H, CH_2), 1.64 (s, 6H, $OC(C\mathbf{H_3})_2$ pyran ring), 6.52 (d, 1H, *J* = 1.6 Hz, ArH phenol), 6.59 (d, 1H, *J* = 1.6, ArH phenol), 7.33 (s, 1H, ArH pyrazole), 8.16 (s, 1H, NH or OH), 9.96 (s, 1H, NH or OH). ^{13}C NMR (101 MHz, $CDCl_3$) δ 14.23, 22.81, 24.79, 29.02, 29.72, 30.15, 31.92, 38.20, 44.64, 76.96, 101.12, 106.53, 106.89, 120.14, 122.57, 142.66, 153.17, 153.25, 153.42. HRMS calculated for $C_{21}H_{31}N_2O_2$ $[M + H]^+$, 343.2380; found, 343.2352

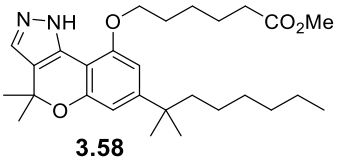

3.58

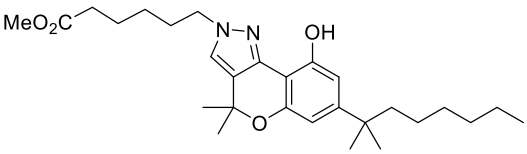

3.59

Synthesis of methyl 6-{[4,4-dimethyl-7-(2-methyloctan-2-yl)-1*H*,4*H*-chromeno[4,3-c]pyrazol-9-yl]oxy}hexanoate (3.58) and methyl 6-[9-hydroxy-4,4-dimethyl-7-(2-methyloctan-2-yl)-2*H*,4*H*-chromeno[4,3-c]pyrazol-2-yl]hexanoate (3.59)

To a solution of **3.57** (50 mg, 0.15 mmol) and **3.56** (46 mg, 0.22 mmol) in dry THF (12 mL) was added Cs_2CO_3 (81 mg, 0.25 mmol) and the reaction mixture stirred at 70 °C for 12 h under N_2 atmosphere. After the completion of the reaction, the solvent was removed under reduced pressure and the residue diluted with EtOAc/NH_4Cl solution. The organic layer was separated, washed with water, brine solution, dried over $MgSO_4.H_2O$ and concentrated under reduced pressure. Purification by silica gel column chromatography (eluting with 10 to 25% EtOAc/hexane) provided **3.59** (27 mg, yield 40%) as a pale oil and (after continued elution with 25 to 50% EtOAc/hexane) **3.58** (34 mg, 50%) as a colourless solid.

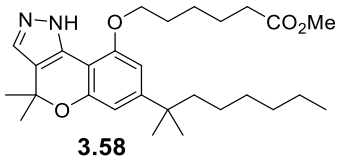

3.58

^{1}H NMR (400 MHz, $CDCl_3$) δ 0.84 (t, 3H, *J* = 6.8 Hz, $CH_2C\mathbf{H_3}$ dimethylheptyl chain), 1.00 – 1.12 (m, 2H, CH_2), 1.15 – 1.23 (m, 6H, 3 × $C\mathbf{H_2}$), 1.26 (s, 6H, $C(C\mathbf{H_3})_2$ dimethylheptyl chain), 1.49 – 1.60 (m, 4H, 2 × $C\mathbf{H_2}$), 1.63 (s, 6H, $OC(C\mathbf{H_3})_2$ pyran ring), 1.70 – 1.79 (m, 2H, CH_2), 1.87 – 2.01 (m, 2H, CH_2), 2.37 (t, 2H, *J* = 7.4 Hz, CH_2), 3.67 (s, 3H, OCH_3), 4.15 (t, 2H, *J* = 6.6 Hz, phenol-CH_2), 6.47 (d, 1H, *J* = 1.5 Hz, ArH phenol), 6.59 (d, 1H, *J* = 1.4 Hz, ArH phenol), 7.40 (s, 1H, ArH pyrazole), 8.72 (br s, 1H, OH). ^{13}C NMR (101 MHz, $CDCl_3$) δ 14.21, 22.77, 24.75, 25.84, 28.99, 29.16, 29.50, 30.09, 31.87, 33.97, 38.45, 44.58, 51.73, 68.24, 77.86, 101.23, 102.00, 108.39, 118.98, 132.57, 153.21, 153.30, 154.33, 174.11. HRMS calculated for $C_{28}H_{43}N_2O_4$ $[M + H]^+$, 471.3217; found, 471.3175. Analytical RP-HPLC Rt = 24.60 min; determined with HPLC method B.

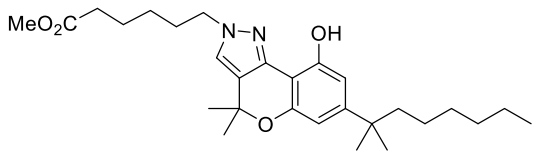

3.59

^{1}H NMR (400 MHz, $CDCl_3$) δ 0.83 (t, 3H, *J* = 6.9 Hz, CH_2CH_3 dimethylheptyl chain), 1.00 – 1.11 (m, 2H, CH_2), 1.14 – 1.22 (m, 6H, 3 × CH_2), 1.24 (s, 6H, $C(CH_3)_2$ dimethylheptyl chain), 1.30 – 1.39 (m, 2H, CH_2), 1.50 – 1.57 (m, 2H, CH_2), 1.61 (s, 6H, $OC(CH_3)_2$ pyran ring), 1.60 – 1.73 (m, 2H, CH_2), 1.83 – 1.99 (m, 2H, CH_2), 2.31 (t, 2H, *J* = 7.3 Hz, CH_2), 3.65 (s, 3H, OCH_3), 4.11 (t, 2H, *J* = 6.9 Hz, pyrazole-CH_2), 6.48 (d, 1H, *J* = 1.6 Hz, ArH phenol), 6.58 (d, 1H, *J* = 1.6 Hz, ArH phenol), 7.12 (s, 1H, ArH pyrazole), 8.30 (s, 1H, OH). ^{13}C NMR (101 MHz, $CDCl_3$) δ 14.23, 22.80, 24.45, 24.79 , 26.19, 29.04, 29.79, 30.08, 30.15, 31.92, 33.90, 38.15, 44.65, 51.68, 52.03, 76.84, 101.40, 106.50, 106.71, 120.04, 123.39, 142.45, 152.76, 152.95, 153.31, 174.03. HRMS calculated for $C_{28}H_{42}N_2NaO_4$ $[M + Na]^+$, 493.3037; found, 493.2993. Analytical RP-HPLC Rt = 26.63 min; determined with HPLC method B.

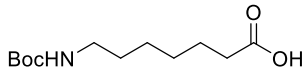

7-{[(*tert*-Butoxy)carbonyl]amino}heptanoic acid (3.61)

This compound was synthesised according to a previously reported literature synthesis of **3.61**. [221] To a solution of commercially available 7-aminoheptanoic acid **3.60** (1.0 g, 6.88 mmol), NaOH (0.27 g, 6.88 mmol) in 1,4-dioxane (20 mL) and water (10 mL) was added $(Boc)_2O$ (1.65g, 6.88 mmol) in three equal portions each after a delay of 30 min each time and the reaction stirred for 20 h. Dioxane was removed under reduced pressure, the residue was extracted once with EtOAc. The aqueous layer was acidified (pH 2-3) by addition of 1M aqueous HCl and extracted quickly three times with EtOAc. The combined organic layers were washed once with water, brine, dried over $MgSO_4.H_2O$ and solvent removed under reduced pressure to give **3.61** (1.66 g, 6.76 mmol, 98%) as a clear oil. ^{1}H NMR (400 MHz, $CDCl_3$) δ 1.20 – 1.38 (m, 4H, CH_2), 1.39 – 1.53 (m, 11H, CH_2 and $C(CH_3)_3$), 1.55 – 1.70 (m, 2H, CH_2), 2.32 (t, 2H, *J* = 7.5 Hz, CH_2), 2.94 – 3.20 (m, 2H, CH_2), 4.44 – 4.69 (m, 1H, NH), 10.07 (s, 1H, CO_2H). ^{13}C NMR (101 MHz, $CDCl_3$) δ 24.73, 26.53, 28.54, 28.82, 29.95, 34.09, 40.61, 156.18, 179.33. HRMS calculated for $C_{12}H_{23}NNaO_4$ $[M + Na]^+$, 268.1519; found, 268.1527.

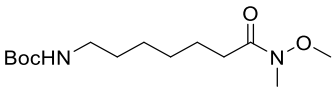

***tert*-Butyl *N*-{6-[Methoxy(methyl)carbamoyl]hexyl}carbamate (3.62)**

According to the procedure for **3.22**, **3.61** (0.5 g, 2.03 mmol) was reacted with *N*,*O*-dimethylhydroxylamine hydrochloride (0.3 g, 3.06 mmol), HBTU (1.16 g, 3.05 mmol) and DIPEA (1.1 mL, 6.11 mmol), except that THF was used as a solvent instead of DMF in the reaction. The residue was purified by silica gel column chromatography (eluting with 10 to 60% EtOAc/hexane) to provide **3.62** (0.49 g, 1.72 mmol, 85%) as a clear oil. NMR spectroscopy data of **3.62** was consistent with a previous literature report[238]. ^{1}H NMR (400 MHz, $CDCl_3$) δ 1.24 – 1.36 (m, 4H, 2 × **C**$\mathbf{H_2}$), 1.37 – 1.51 (m, 11H, CH_2 and C(C$\mathbf{H_3}$)$_3$), 1.53 – 1.68 (m, 2H, CH_2), 2.38 (t, 2H, J = 7.6 Hz, CH_2), 3.07 (q, 2H, J = 6.7 Hz, CH_2), 3.14 (s, 3H, CH_3), 3.65 (s, 3H, CH_3), 4.56 (br s, 1H, NH). ^{13}C NMR (101 MHz, $CDCl_3$) δ 24.56, 26.64, 28.51, 29.12, 29.98, 31.82, 32.25, 40.57, 61.28, 79.03, 156.07, 174.68.

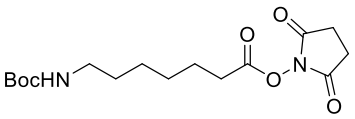

2,5-Dioxopyrrolidin-1-yl 7-{[(*tert*-butoxy)carbonyl]amino}heptanoate (3.65)

According to the procedure for **3.22**, **3.61** (0.4 g, 1.63 mmol) was reacted with *N*-hydroxysuccinimide (0.24 g, 2.12 mmol), HBTU (0.62 g, 1.63 mmol) and DIPEA (0.9 mL, 4.89 mmol). Purification was done by silica gel column chromatography (eluting with 10 to 45% EtOAc/hexane) to provide **3.65** (0.51 g, 1.47 mmol, 91%) as a clear oil. NMR spectroscopy data of **3.65** was consistent with a previous literature report[221]. ^{1}H NMR (400 MHz, $CDCl_3$) δ 1.24 – 1.58 (m, 15H, 3 × C$\mathbf{H_2}$ and C(C$\mathbf{H_3}$)$_3$), 1.68 – 1.80 (m, 2H, CH_2), 2.59 (t, 2H, J = 7.4 Hz, CH_2), 2.76 – 2.92 (m, 4H, 2 × C$\mathbf{H_2}$), 3.10 (q, 2H, J = 6.7 Hz, CH_2), 4.55 (br s, 1H, NH). ^{13}C NMR (101 MHz, $CDCl_3$) δ 24.60, 25.71, 26.34, 28.49, 28.55, 29.90, 30.97, 40.51, 79.15, 156.10, 168.71, 169.31.

7.3.2 Computational studies

Primary amino acid sequences of the CB_1R (Uniprot id – P21554) and CB_2R (Uniprot id - P34972) for the homology modelling were obtained from UniProt.[239] Alignment of target receptor amino acid sequence – (CB_2R (Uniprot id - P34972)) and template receptor's amino acid sequence –(CB_1R (Uniprot id – P21554)) amino acid sequence was carried out with a multiple sequence alignment web server T-coffee.[213] Structures of the ligands were drawn with Avogadro[216] (version 1.2) and optimised by energy minimisation using the Merck Molecular ForceField (MMFF94). The CB_2R homology model was built using Modeller[214] (version 9.19) with the CB_1R crystal structure (PDB ID: 5XRA)[113] as a template. The docking studies were carried out with GOLD[217] (version 5.5) using ChemPLP scoring method with default settings. In the docking studies, a scaffold constraint was used and the binding site for ligands was specified as a 20 Å region around the CB_1R co-crystallised ligand AM11542 (PDB ID: 5XRA). Docking poses were visualised with PyMOL (The PyMOL Molecular Graphics System, version 2.0.3 Schrödinger, LLC.).

7.3.3 Pharmacological studies

Radioligand binding assays and cAMP functional assays were carried out as described in section 7.1.2. In the radioligand binding assay, [^{3}H]-CP55,940 was used in a concentration of 2.5 nM per well for determining the CB_1R affinity and 1 nM per well for determining the CB_2R affinity of test compounds. CB_1R and CB_2R membrane preparations were used at a concentration of 7.5 μg/well and 5.0 μg/well respectively.

7.4 Experimental procedure and data for compounds as described in chapter 4

7.4.1 Chemical studies

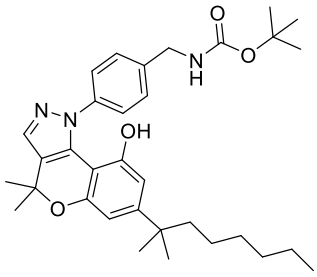

***tert*-Butyl *N*-({4-[9-hydroxy-4,4-dimethyl-7-(2-methyloctan-2-yl)-1*H*,4*H*-chromeno[4,3-c]pyrazol-1-yl]phenyl}methyl)carbamate (4.10)**

To a solution of **3.21** (44 mg, 0.09 mmol) in DCM (2.0 mL) was added $(Boc)_2O$ (25 mg, 0.11 mmol) followed by addition of Et_3N (0.02 mL, 0.15 mmol) at 0 °C; the reaction was warmed to rt and stirred for 12 h. The reaction solvent was removed under reduced pressure and the residue was partitioned between DCM/H_2O. The DCM layer was washed with NH_4Cl solution, water, dried over $MgSO_4.H_2O$, concentrated under reduced pressure, and the residue purified by silica gel column chromatography (eluting with 10 - 40% EtOAc/hexane) to give **4.10** (19 mg, 0.03 mmol, 35%) as a clear oil. ^{1}H NMR (400 MHz, $CDCl_3$) δ 0.84 (t, 3H, *J* = 6.8 Hz, $CH_2C\mathbf{H_3}$), 1.01 – 1.09 (m, 2H, CH_2), 1.13 – 1.28 (m, 12H, 3 × $C\mathbf{H_2}$ and $C(C\mathbf{H_3})_2$ dimethylheptyl chain), 1.45 (s, 9H, $C(C\mathbf{H_3})_3$), 1.48 – 1.55 (m, 2H, CH_2), 1.61 (s, 6H, $OC(C\mathbf{H_3})_2$ pyran ring), 4.17 (d, 2H, *J* = 5.5 Hz, $C\mathbf{H_2}$NH), 4.87 – 4.97 (m, 1H, NH), 6.05 (s, 1H, OH), 6.33 – 6.38 (m, 1H, ArH phenol), 6.64 (d, 1H, *J* = 1.5 Hz, ArH phenol), 7.23 – 7.29 (m, 2H, ArH phenol), 7.39 – 7.46 (m, 2H, ArH phenol), 7.51 (s, 1H, ArH pyrazole). ^{13}C NMR (101 MHz, $CDCl_3$) δ 14.21, 22.73, 24.71, 27.42, 27.69, 28.56, 28.72, 30.04, 31.87, 37.95, 44.44, 44.51, 102.75, 108.29, 108.81, 124.44, 124.86, 127.97, 132.89, 134.59, 141.87, 150.56, 153.19, 154.07, 156.37. HRMS calculated for $C_{33}H_{45}N_3NaO_4$ $[M + Na]^+$, 570.3302; found, 570.3268.

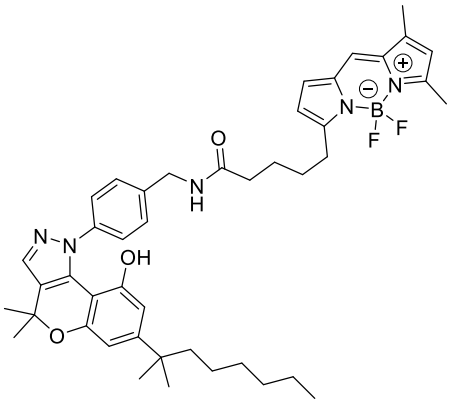

2,2-Difluoro-4-{4-[({4-[9-hydroxy-4,4-dimethyl-7-(2-methyloctan-2-yl)-1*H*,4*H*-chromeno[4,3-c]pyrazol-1-yl]phenyl}methyl)carbamoyl]butyl}-10,12-dimethyl-1λ^5,3-diaza-2-boratricyclo[7.3.0.0^{3,7}]dodeca-1(12),4,6,8,10-pentaen-1-ylium-2-uide (4.05)

To a solution of **4.10** (3 mg, 5.47 μmol) in DCM (2.0 mL) at 0 °C was added TFA (0.5 mL). The reaction mixture was warmed to rt and stirred for 2 h, volatiles were removed under reduced pressure to provide 1-[4-(aminomethyl)phenyl]-4,4-dimethyl-7-(2-methyloctan-2-yl)-1*H*,4*H*-chromeno[4,3-c]pyrazol-9-ol trifluoroacetate in assumed quantitative yield as yellow solid. This amino TFA salt was purified using semi-preparative RP-HPLC. To a solution of this purified trifluoroacetate salt (2.9 mg, 5.16 μmol) in DMF (200 μL) was added a solution of DIPEA (1.8 μL, 10.3 μmol) in DMF (100 μL), followed by addition of a solution of BOPIPY-FL-SE (1.1 mg, 2.71 μmol) in DMF (600 μL) and the reaction was stirred in dark for 12 h. The reaction solvents were removed under reduced pressure and the residue purified by semi-preparative RP-HPLC and freeze dried to give **4.05** (3.71 mg, 4.95 μmol, quantitative) as an orange solid. HRMS calculated for $C_{44}H_{54}BF_2N_5NaO_3$ $[M + Na]^+$, 772.4188; found, 772.4211. Analytical RP-HPLC Rt = 23.87 min; determined with HPLC method B.

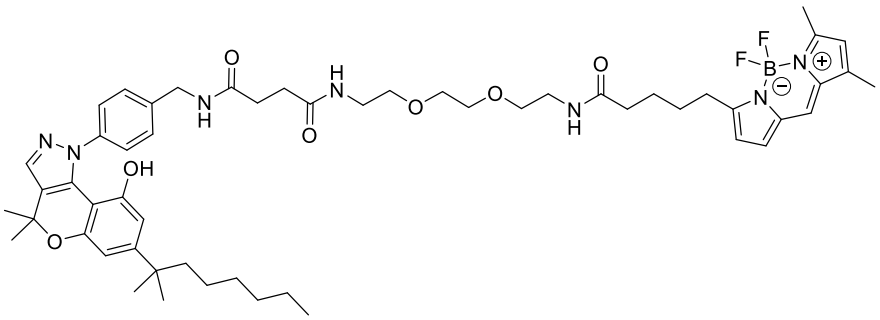

2,2-Difluoro-4-[4-({2-[2-(2-{3-[({4-[9-hydroxy-4,4-dimethyl-7-(2-methyloctan-2-yl)-1*H*,4*H*-chromeno[4,3-c]pyrazol-1-yl]phenyl}methyl)carbamoyl]propanamido}-

ethoxy)ethoxy]ethyl}carbamoyl)butyl]-10,12-dimethyl-1λ^5,3-diaza-2-boratricyclo[7.3.0.0^{3,7}]dodeca-1(12),4,6,8,10-pentaen-1-ylium-2-uide (4.01)

Following the procedure described for **4.05**, **3.22** (5.0 mg, 6.42 μmol) was reacted with TFA (0.5 mL) to give *N*-{2-[2-(2-aminoethoxy)ethoxy]ethyl}-*N*'-({4-[9-hydroxy-4,4-dimethyl-7-(2-methyloctan-2-yl)-1*H*,4*H*-chromeno[4,3-c]pyrazol-1-yl]phenyl}methyl)-butanediamide trifluoroacetate in assumed quantitative yield as yellow solid. This amino TFA salt was purified using semi-preparative RP-HPLC. Reaction of this purified trifluoroacetate salt (4.7 mg, 5.93 μmol) with BODIPY-FL-SE (1.0 mg, 2.39 μmol) gave **4.01** (2.98 mg, 3.04 μmol, quantitative) as an orange solid. HRMS calculated for $C_{54}H_{72}BF_2N_7NaO_7$ $[M + Na]^+$, 1002.5456; found, 1002.5502. Analytical RP-HPLC Rt = 22.82 min; determined with HPLC method B.

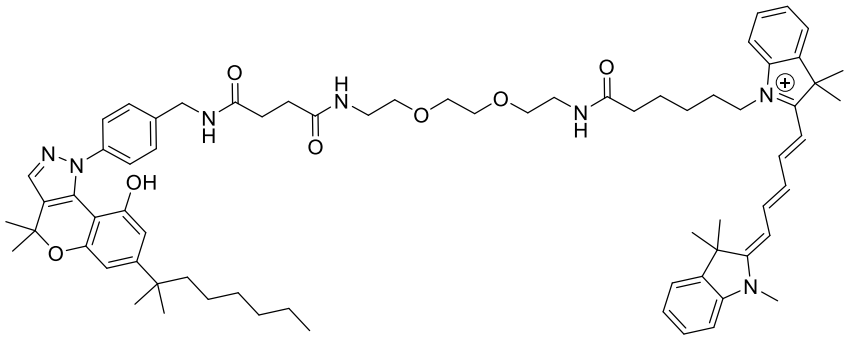

1-[5-({2-[2-(2-{3-[({4-[9-Hydroxy-4,4-dimethyl-7-(2-methyloctan-2-yl)-1*H*,4*H*-chromeno[4,3-c]pyrazol-1-yl]phenyl}methyl)carbamoyl]propanamido}ethoxy)ethoxy]ethyl}carbamoyl)pentyl]-3,3-dimethyl-2-[(*1E*,*3E*)-5-[(*2E*)-1,3,3-trimethyl -2,3-dihydro-1*H*-indol-2-ylidene]penta-1,3-dien-1-yl]-3*H*-indol-1-ium (4.02)

Following the procedure described for **4.05**, **3.22** (4.0 mg, 5.14 μmol) was reacted with TFA (0.5 mL) to give *N*-{2-[2-(2-aminoethoxy)ethoxy]ethyl}-*N*'-({4-[9-hydroxy-4,4-dimethyl-7-(2-methyloctan-2-yl)-1*H*,4*H*-chromeno[4,3-c]pyrazol-1-yl]phenyl}methyl) butanediamide trifluoroacetate in assumed quantitative yield as yellow solid. This amino TFA salt was purified using semi-preparative RP-HPLC. Reaction of this purified trifluoroacetate salt (3.9 mg, 4.87 μmol) with Cy5-SE (1.0 mg, 1.62 μmol) gave **4.02** (2.9 mg, 2.53 μmol, quantitative) as a bright blue solid. HRMS calculated for $C_{70}H_{92}N_7O_7$ $[M]^+$, 1142.7053; found, 1142.7137. Analytical RP-HPLC Rt = 23.03 min; determined with HPLC method B.

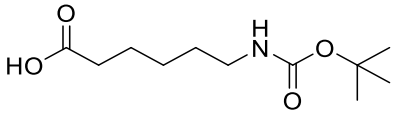

6-{[(*tert*-Butoxy)carbonyl]amino}hexanoic acid (4.12)

This compound was prepared according to a previously reported literature synthesis of **4.12**.[221] To a solution of commercially available 6-aminohexanoic acid **4.11** (1.0 g, 7.62 mmol), NaOH (0.30 g, 7.62 mmol) in 1,4-dioxane (20 mL) and water (10 mL) was added $(Boc)_2O$ (1.75g, 8.00 mmol) in three equal portions (with a delay of 30 min before addition of next portion of $(Boc)_2O$), and reaction stirred for 20 h. Dioxane was removed under reduced pressure and the residue was extracted once with EtOAc. The aqueous layer was acidified (pH 2-3) by addition of 1M aqueous HCl solution and extracted quickly three times with EtOAc. The combined EtOAc layers were washed once with water, brine, dried over $MgSO_4.H_2O$, and concentrated under reduced pressure to give **4.12** (1.26 g, 5.44 mmol, 71%) as a clear oil. ^{1}H NMR (400 MHz, $CDCl_3$) δ 1.30 – 1.40 (m, 2H, CH_2), 1.43 (s, 9H, C(C**H**$_3$)$_3$), 1.47 – 1.51 (m, 2H, CH_2), 1.58 – 1.71 (m, 2H, CH_2), 2.34 (t, 2H, *J* = 7.4 Hz, CH_2), 3.11 (d, 2H, *J* = 6.8 Hz, CH_2), 4.57 (s, 1H, NH). HRMS calculated for $C_{11}H_{20}NO_4$ $[M - H]^-$, 230.1398; found, 230.1409.

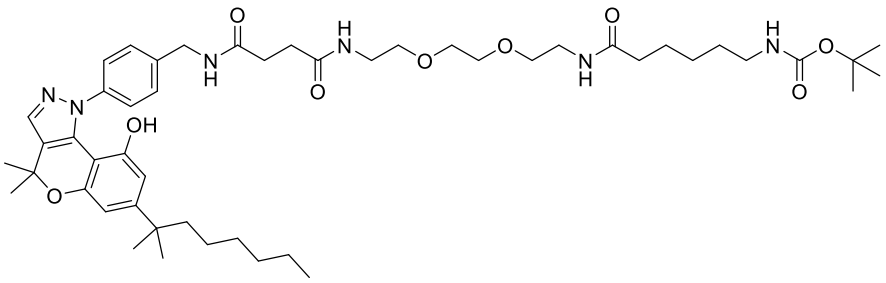

***tert*-Butyl *N*-[5-({2-[2-(2-{3-[({4-[9-hydroxy-4,4-dimethyl-7-(2-methyloctan-2-yl)-1*H*,4*H*-chromeno[4,3-c]pyrazol-1-yl]phenyl}methyl)carbamoyl]propanamido}ethoxy)ethoxy]ethyl}carbamoyl)pentyl]carbamate (4.13)**

To a solution of **3.22** (12 mg, 0.015 mmol) in DCM (3.0 mL) at 0 °C was added TFA (0.5 mL). The reaction mixture was warmed to rt, stirred for 3 h and volatiles removed under reduced pressure to give *N*-{2-[2-(2-aminoethoxy)ethoxy]ethyl}-*N*'-({4-[9-hydroxy-4,4-dimethyl-7-(2-methyloctan-2-yl)-1*H*,4*H*-chromeno[4,3-c]pyrazol-1-yl]phenyl}methyl)-butanediamide trifluoroacetate in assumed quantitative yield as a yellow solid. The solution of Boc-deprotected **3.22** trifluoroacetate salt (16 mg) in DCM (1.0 mL) was added to a solution of **4.12** (5 mg, 21.61 mmol), TFFH (6 mg, 21.61 mmol) and Et_3N (0.01 mL, 0.05 mmol) in DCM (2.0 mL) under a N_2 atmosphere and the reaction was

stirred for 12 h. The reaction solvent was removed under reduced pressure and the residue was partitioned between DCM/H_2O. The DCM layer was washed with saturated NH_4Cl solution, water, brine solution, dried over $MgSO_4.H_2O$ and concentrated under reduced pressure. The residue was purified by a short silica gel column (eluting with 40% EtOAc/hexane to 8% MeOH/EtOAc) to provide **4.13** (10 mg, 0.01 mmol, 34%) as clear liquid. ^{1}H NMR (400 MHz, $CDCl_3$) δ 0.82 (t, 3H, *J* = 6.9 Hz, $CH_2C\mathbf{H_3}$), 1.01 – 1.09 (m, 2H, CH_2), 1.12 – 1.32 (m, 14H, 4 × $C\mathbf{H_2}$ and $C(C\mathbf{H_3})_2$ dimethylheptyl chain), 1.41 (s, 9H, $C(C\mathbf{H_3})_3$), 1.47 – 1.53 (m, 2H, CH_2), 1.59 (s, 8H, $C\mathbf{H_2}$ and $OC(C\mathbf{H_3})_2$ pyran ring), 1.89 (s, 2H, CH_2), 2.08 (t, 2H, *J* = 7.5 Hz, CH_2), 2.44 – 2.60 (m, 4H, $NHCOC\mathbf{H_2}C\mathbf{H_2}CONH$), 2.95 – 3.04 (m, 2H, CH_2), 3.31 (q, 2H, *J* = 5.2 Hz, CH_2), 3.36 – 3.46 (m, 2H, CH_2), 3.48 – 3.56 (m, 4H, 2 × $C\mathbf{H_2}$), 3.59 (s, 4H, 2 × $C\mathbf{H_2}$), 4.43 (d, 2H, *J* = 5.9 Hz, CH_2), 4.79 – 4.89 (m, 1H, NH), 6.42 – 6.47 (m, 1H, ArH phenol), 6.57 (d, 1H, *J* = 1.6 Hz, ArH phenol), 6.74 – 6.82 (m, 1H, NH), 6.84 – 6.91 (m, 1H, NH), 6.95 – 7.03 (m, 1H, NH), 7.13 – 7.21 (m, 2H, ArH phenol), 7.30 – 7.38 (m, 2H, ArH phenol), 7.47 (d, 1H, *J* = 1.2 Hz, ArH pyrazole), 8.12 (br s, 1H, OH). ^{13}C NMR (101 MHz, C_3) δ 14.22, 22.75, 24.73, 25.40, 26.45, 26.45, 27.42, 28.60, 28.74, 29.73, 30.07, 31.83, 31.89, 36.26, 37.92, 39.43, 39.51, 40.46, 40.55, 43.16, 44.52, 69.69, 69.98, 70.36, 70.43, 102.57, 107.89, 116.50, 124.21, 124.60, 127.07, 134.31, 136.80, 142.52, 151.70, 152.98, 154.06, 172.67, 172.72, 174.16. HRMS calculated for $C_{49}H_{74}N_6NaO_9$ $[M + Na]^+$, 913.5409; found, 913.5382.

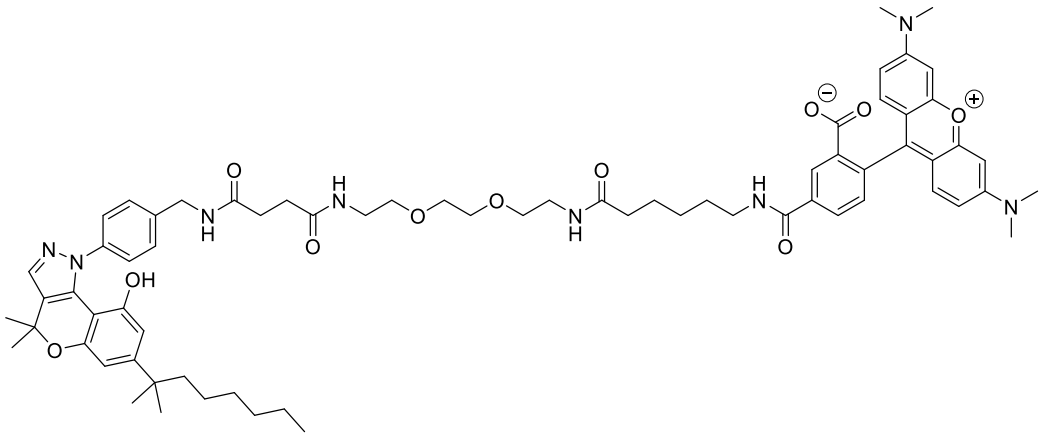

9-(2-Carboxy-4-{[5-({2-[2-(2-{3-[({4-[9-hydroxy-4,4-dimethyl-7-(2-methyloctan-2-yl)-1*H*,4*H*-chromeno[4,3-c]pyrazol-1-yl]phenyl}methyl)carbamoyl]propanamido}-ethoxy) ethoxy]ethyl}carbamoyl)pentyl]carbamoyl}phenyl)-3,6-bis(dimethyl-amino)-10λ^4-xanthen-10-ylium (4.03)

Following the procedure described for **4.05**, **4.13** (4.0 mg, 4.48 µmol) was reacted with TFA (0.5 mL) to give *N*-{2-[2-(2-aminoethoxy)ethoxy]ethyl}-*N*'-({4-[9-hydroxy-4,4-dimethyl-7-(2-methyloctan-2-yl)-1*H*,4*H*-chromeno[4,3-c]pyrazol-1-yl]phenyl}methyl)-butanediamide trifluoroacetate in assumed quantitative yield as a yellow solid. This amino TFA salt was purified using semi-preparative RP-HPLC. Reaction of this purified trifluoroacetate salt (4.3 mg, 4.75 µmol) with TAMRA-SE (1.0 mg, 1.89 µmol) gave **4.03** (3.21 mg, 2.66 µmol, quantitative) as a pink solid. HRMS calculated for $C_{69}H_{86}N_8NaO_{11}$ $[M + Na]^+$, 1225.6308; found, 1225.6288. Analytical RP-HPLC Rt = 20.06 min; determined with HPLC method B.

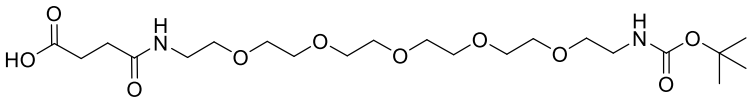

3-[(17-{[(*tert*-Butoxy)carbonyl]amino}-3,6,9,12,15-pentaoxaheptadecan-1-yl)carbamoyl] propanoic acid (4.15)

To a solution of commercially available *tert*-butyl *N*-(17-amino-3,6,9,12,15-pentaoxaheptadecan-1-yl)carbamate **4.14** (30 mg, 0.08 mmol) in $CHCl_3$ (5.0 mL) was added succinic anhydride (83 mg, 0.08 mmol) at 0 °C. The reaction was warmed to rt and stirred for 12 h. The reaction solvent was removed under reduced pressure to provide **4.15** (117 mg) as a colourless solid. This compound was used as such in the next reaction without further purification. ^{1}H NMR (400 MHz, $CDCl_3$) δ 1.43 (s, 9H, C(C**H**$_3$)$_3$), 2.47 – 2.58 (m, 2H, CH_2), 2.60 – 2.70 (m, 2H, CH_2), 3.20 – 3.35 (m, 2H, CH_2), 3.39 – 3.47 (m, 2H, CH_2), 3.48 – 3.57 (m, 4H, 2 × C**H**$_2$), 3.58 – 3.77 (m, 16H, 8 × C**H**$_2$), 5.22 (s, 1H, NH), 7.08 (s, 1H, NH). ^{13}C NMR (101 MHz, $CDCl_3$) δ 28.41, 30.47, 30.91, 39.47, 40.31, 69.58, 70.06, 70.40, 70.53, 79.27, 170.56, 172.88, 174.55. HRMS calculated for $C_{21}H_{40}N_2NaO_{10}$ $[M + Na]^+$, 503.2585; found, 503.2575.

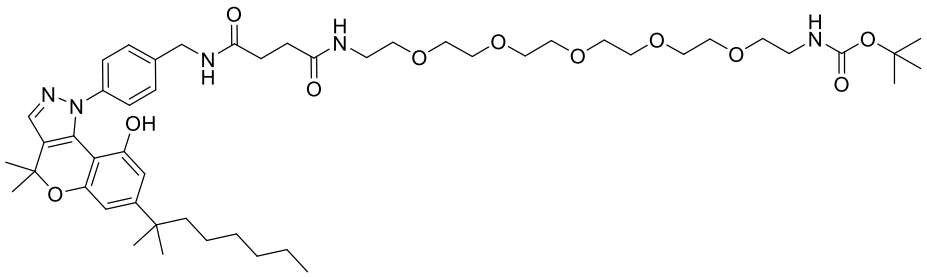

***tert*-Butyl *N*-(17-{3-[({4-[9-hydroxy-4,4-dimethyl-7-(2-methyloctan-2-yl)-1*H*,4*H*-chromeno[4,3-c]pyrazol-1-yl]phenyl}methyl)carbamoyl]propanamido}-3,6,9,12,15-pentaoxaheptadecan-1-yl)carbamate (4.16)**

To a solution of **4.10** (20 mg, 0.03 mmol) in DCM (3.0 mL) at 0 °C was added TFA (0.5 mL). The reaction mixture was warmed to rt and stirred for 2 h, volatiles were removed under reduced pressure to provide 1-[4-(aminomethyl)phenyl]-4,4-dimethyl-7-(2-methyloctan-2-yl)-1*H*,4*H*-chromeno[4,3-c]pyrazol-9-ol in assumed quantitative yield as trifluoroacetate salt. The solution of Boc-deprotected **4.10** trifluoroacetate salt (22 mg) in DCM (2.0 mL) was added to a solution of **4.15** (12 mg, 0.02 mmol), TFFH (7 mg, 0.02 mmol) and Et_3N (0.01 mL, 0.05 mmol) in DCM (2.0 mL) under a N_2 atmosphere and the reaction was stirred for 12 h. The reaction solvent was removed under reduced pressure and the residue was partitioned between DCM/H_2O. The DCM layer was washed with saturated NH_4Cl solution, water, brine solution, dried over $MgSO_4.H_2O$ and concentrated under reduced pressure. The residue was further purified by a short silica gel column (eluting with 70% EtOAc/hexane to 12% MeOH/EtOAc) to provide **4.16** as a clear oil (7 mg, 0.01 mmol, 25%). ^{1}H NMR (400 MHz, MeOD-d_4) δ 0.86 (t, 3H, J = 6.7 Hz, $CH_2C\mathbf{H_3}$), 1.04 – 1.14 (m, 2H, CH_2), 1.16 – 1.33 (m, 14H, 4 × $C\mathbf{H_2}$ and $C(C\mathbf{H_3})_2$ dimethylheptyl chain), 1.43 (s, 9H, $C(C\mathbf{H_3})_3$), 1.51 – 1.65 (m, 8H, $C\mathbf{H_2}$ and $OC(C\mathbf{H_3})_2$ pyran ring), 2.55 (t, 4H, J = 2.9 Hz, 2 × $C\mathbf{H_2}$), 3.20 (t, 2H, J = 5.6 Hz, CH_2), 3.35 (d, 2H, J = 5.4 Hz, CH_2), 3.46 – 3.54 (m, 4H, 2 × $C\mathbf{H_2}$), 3.61 (d, 14H, J = 12.6 Hz, 7 × $C\mathbf{H_2}$), 4.42 (s, 2H, CH_2), 6.29 – 6.34 (m, 1H, ArH phenol), 6.49 – 6.55 (m, 1H, ArH phenol), 7.23 – 7.38 (m, 4H, ArH phenol), 7.57 (s, 1H, ArH pyrazole). ^{13}C NMR (101 MHz, MeOD-d_4) δ 14.41, 23.62, 25.73, 27.51, 28.79, 29.26, 31.01, 32.21, 32.30, 32.85, 38.71, 40.49, 41.30, 43.67, 45.37, 70.53, 71.06, 71.27, 71.28, 71.52, 71.57, 77.74, 103.45, 108.37, 125.42, 128.34, 135.03, 139.23, 143.40, 153.46, 154.14, 155.58, 174.61, 174.66. HRMS calculated for $C_{49}H_{75}N_5NaO_{11}$ $[M + Na]^+$, 932.5355; found, 932.5318.

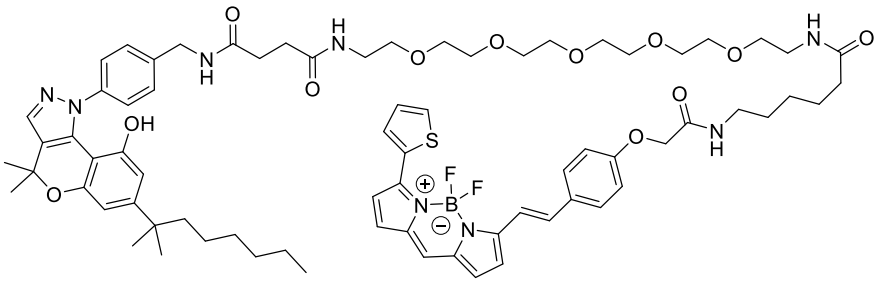

2,2-Difluoro-4-[(*E*)-2-{4-[({5-[(17-{3-[({4-[9-hydroxy-4,4-dimethyl-7-(2-methyloctan-2-yl)-1*H*,4*H*-chromeno[4,3-c]pyrazol-1-yl]phenyl}methyl)-carbamoyl]propanamido}-3,6,9,12,15-pentaoxaheptadecan-1-yl)carbamoyl]-pentyl}carbamoyl)methoxy]phenyl}ethenyl]-12-(thiophen-2-yl)-1λ^5,3-diaza-2-boratricyclo[7.3.0.0^{3,7}]dodeca-1(12),4,6,8,10-pentaen-1-ylium-2-uide (4.04)

Following the procedure described for **4.05**, **4.16** (4.5 mg, 4.94 µmol) was reacted with TFA (0.5 mL) to give *N*-(17-amino-3,6,9,12,15-pentaoxaheptadecan-1-yl)-*N*'-({4-[9-hydroxy-4,4-dimethyl-7-(2-methyloctan-2-yl)-1*H*,4*H*-chromeno[4,3-c]pyrazol-1-yl]phenyl}methyl) butanediamide trifluoroacetate in assumed quantitative yield as yellow solid. This amino TFA salt was purified using semi-preparative RP-HPLC. Reaction of this purified trifluoroacetate salt (4.2 mg, 4.54 µmol) with BODIPY-630/650-SE (1.0 mg, 1.51 µmol) gave **4.04** (3.53 mg, 2.60 µmol, quantitative) as a dark blue solid. HRMS calculated for $C_{73}H_{93}BF_2N_8NaO_{12}S$ $[M + Na]^+$, 1377.6599; found, 1377.6560. Analytical RP-HPLC Rt = 23.40 min; determined with HPLC method B.

The amino peptide linker conjugates (**4.25-4.27**) were synthesised using 1,2-diaminoethane trityl resin (0.1 g) by solid phase peptide synthesis as described for compound **3.38** in chapter 7, section 7.3.1

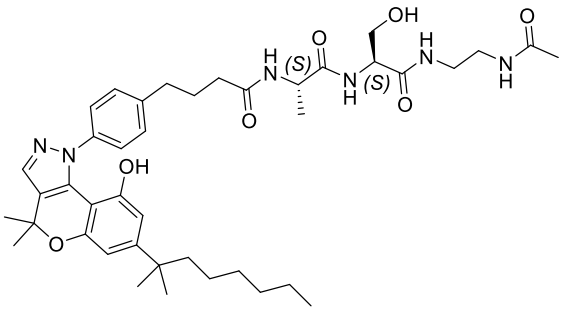

***N*-[(1*S*)-1-{[(1*S*)-1-[(2-Aminoethyl)carbamoyl]-2-hydroxyethyl]carbamoyl}ethyl]-4-{4-[9-hydroxy-4,4-dimethyl-7-(2-methyloctan-2-yl)-1*H*,4*H*-chromeno[4,3-c]pyrazol-1-yl]phenyl}butanamide (4.06)**

To a solution of **4.25** (3.0 mg, 3.6 µmol) in $CHCl_3$ (1.0 mL) was added Ac_2O (0.3 µL, 3.3 µmol), Et_3N (2.0 µL, 11 µmol) and the reaction stirred for 2 h. The reaction solvent was removed by evaporation under reduced pressure and the residue purified by semi-preparative RP-HPLC to give **4.06** (1.2 mg, 1.60 µmol, 44%) as a colourless solid. HRMS calculated for $C_{41}H_{58}N_6NaO_7$ $[M + Na]^+$, 769.4259; found, 769.4194. Analytical RP-HPLC Rt = 20.33 min; determined with HPLC method B.

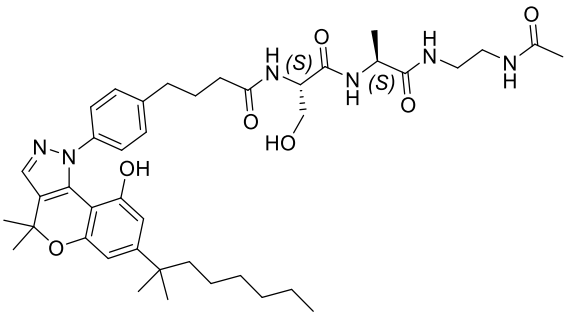

***N*-[(1*S*)-1-{[(1*S*)-1-[(2-Aminoethyl)carbamoyl]-2-hydroxyethyl]carbamoyl}ethyl]-4-{4-[9-hydroxy-4,4-dimethyl-7-(2-methyloctan-2-yl)-1*H*,4*H*-chromeno[4,3-c]pyrazol-1-yl]phenyl}butanamide (4.07)**

According to procedure described for **4.06**, **4.26** (3.0 mg, 3.6 µmol) was reacted with Ac_2O (0.3 µL, 3.3 µmol) and Et_3N (2.0 µL, 11 µmol) to give **4.07** (1.8 mg, 2.40 µmol, 67%) as a colourless solid. HRMS calculated for $C_{41}H_{58}N_6NaO_7$ $[M + Na]^+$, 769.4259; found, 769.4213. Analytical RP-HPLC Rt = 20.33 min; determined with HPLC method B.

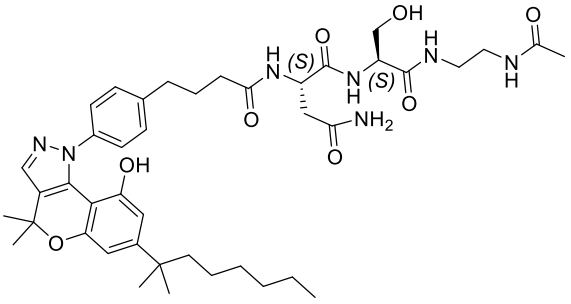

(2*S*)-*N*-[(1*S*)-1-[(2-Acetamidoethyl)carbamoyl]-2-hydroxyethyl]-2-(4-{4-[9-hydroxy-4,4-dimethyl-7-(2-methyloctan-2-yl)-1*H*,4*H*-chromeno[4,3-c]pyrazol-1-yl]phenyl}butanamido) butanediamide (4.08)

According to procedure described for **4.06**, **4.27** (4.0 mg, 4.6 µmol) was reacted with Ac_2O (0.4 µL, 0.4 µmol) and Et_3N (2.0 µL, 14 µmol) to give **4.08** (1.1 mg, 1.39 µmol, 30%) as a colourless solid. HRMS calculated for $C_{42}H_{59}N_7NaO_8$ $[M + Na]^+$, 812.4317;

found, 812.4280. Analytical RP-HPLC Rt = 18.89 min; determined with HPLC method B.

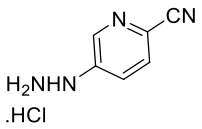

5-Hydrazinylpyridine-2-carbonitrile (4.29)

This compound was prepared by modification of a reported literature synthesis of **4.29**.[222] To a solution of commercially available 5-amino-2-cyanopyridine **4.28** (0.3 g, 2.51 mmol) in aqueous HCl (6 M, 10.0 mL) at -10 °C was added a solution of $NaNO_2$ (0.3 g, 4.35 mmol) in water (3.0 mL) and stirred for 30 min at -10 °C. To the reaction mixture was added a solution of $SnCl_2.2H_2O$ (2.84 g, 12.59 mmol) in water (10 mL) and the reaction stirred for at 0 °C for 2 h. The reaction mixture was slowly basified to pH 10.0-11.0 with aqueous KOH solution (10% *w*/*v*) and extracted with EtOAc. The EtOAc layer was washed with water, brine, dried over $MgSO_4.H_2O$ and removed by evaporation under reduced pressure to give **4.29** (0.41 g) as light brown solid. Compound **4.29** slowly degrades in to an unknown impurity and was therefore used in the next reaction without further purification. HRMS calculated for $C_6H_6N_4Na$ $[M + Na]^+$, 157.0485; found, 157.0474.

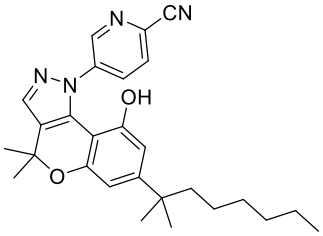

5-[9-Hydroxy-4,4-dimethyl-7-(2-methyloctan-2-yl)-1*H*,4*H*-chromeno[4,3-c]pyrazol-1-yl]pyridine-2-carbonitrile (4.30)

To a solution of **3.16** (0.15 g, 0.43 mmol) in MeOH (20 mL) was added **4.29** (0.17 g, 1.02 mmol), followed by addition of two drops of conc. H_2SO_4 (98%) and the reaction stirred at 70 °C for 2 h. The reaction solvents was removed under reduced pressure, the residue neutralised with saturated $NaHCO_3$ solution and extracted with EtOAc. The EtOAc layer was then separated, washed with water, brine solution, dried over $MgSO_4.H_2O$, concentrated under reduced pressure and the residue purified by silica gel column chromatography (eluting with 10 – 25% EtOAc/hexane) to give **4.30** (0.16 g, 0.37 mmol,

86%) as a light yellow oil. ^{1}H NMR (400 MHz, $CDCl_3$) δ 0.82 (t, 3H, *J* = 6.9 Hz, CH_2**CH_3**), 0.96 – 1.09 (m, 2H, CH_2), 1.11 – 1.29 (m, 12H, 3 × C**H_2** and C(C**H_3**)**$_2$** dimethylheptyl chain), 1.42 – 1.52 (m, 2H, CH_2), 1.62 (s, 6H, OC(C**H_3**)**$_2$** pyran ring), 6.26 (d, 1H, *J* = 1.6 Hz, ArH phenol), 6.63 (d, 1H, *J* = 1.6 Hz, ArH phenol), 6.95 (s, 1H, OH), 7.61 (s, 1H, ArH pyrazole), 7.82 (d, 1H, *J* = 8.3 Hz, ArH pyridine), 7.99 – 8.07 (m, 1H, ArH pyridine), 8.66 (d, 1H, *J* = 2.9 Hz, ArH pyridine). ^{13}C NMR (101 MHz, $CDCl_3$) δ 14.20, 22.73, 24.68, 27.33, 28.64, 29.99, 31.82, 38.02, 44.35, 101.77, 107.70, 109.13, 116.84, 125.99, 128.83, 130.02, 131.25, 133.62, 136.79, 142.04, 146.44, 150.03, 154.33, 154.35. HRMS calculated for $C_{27}H_{32}N_4NaO_2$ $[M + Na]^+$, 467.2417; found, 467.2377.

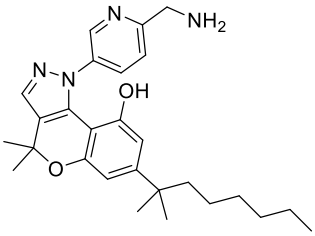

1-[6-(Aminomethyl)pyridin-3-yl]-4,4-dimethyl-7-(2-methyloctan-2-yl)-1*H*,4*H*-chromeno[4,3-c]pyrazol-9-ol (4.31)

A solution of **4.30** (0.13 g, 0.30 mmol) in THF (10.0 mL) was added to a solution of $LiAlH_4$ in THF (0.6 mL, 1M) at 0 °C under N_2 atmosphere. The reaction was warmed to rt and stirred for 2 h. The reaction was quenched by adding water (3 mL), a solution of 15% NaOH in water (1.0 mL) at 0 °C and the mixture stirred at rt for 10 min. The mixture was partitioned between EtOAc and water. The EtOAc layer was separated, dried over $MgSO_4.H_2O$ and concentrated under reduced pressure to give amine **4.31** (117 mg) as a yellowish solid. This compound was used as such in the next reaction without further purification. HRMS calculated for $C_{27}H_{37}N_4O_2$ $[M + H]^+$, 449.2911; found, 449.2906.

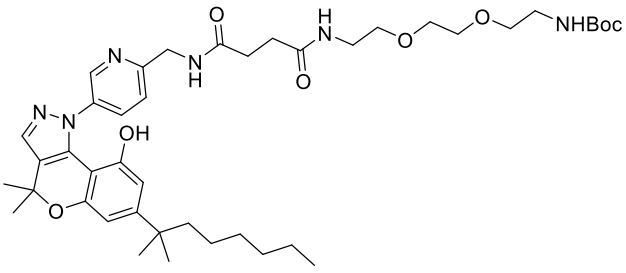

***tert*-Butyl *N*-{2-[2-(2-{3-[({5-[9-hydroxy-4,4-dimethyl-7-(2-methyloctan-2-yl)-1*H*,4*H*-chromeno[4,3-c]pyrazol-1-yl]pyridin-2-yl}methyl)carbamoyl]-propanamido} ethoxy)ethoxy]ethyl}carbamate (4.09)**

To a solution of **3.13** (18 mg, 0.05 mmol), HBTU (19 mg, 0.05 mmol) in DMF (1.0 mL) was added DIPEA (0.03 mL, 0.15 mmol) under N_2 atmosphere and the reaction was stirred for 10 min. A solution of amine **4.31** (23 mg) in DMF (1.0 mL) was added to the reaction mixture and reaction stirred for 12 h. The reaction solvent was removed under reduced pressure and the residue was partitioned between EtOAc/H_2O. The EtOAc layer was washed with saturated NH_4Cl solution, water, brine solution, dried over $MgSO_4.H_2O$ and concentrated under reduced pressure. The residue was purified by silica gel column chromatography (eluting with 30% EtOAc/hexane to 5% MeOH/EtOAc) to provide **4.09** (18 mg, 0.02 mmol, 46%) as a yellow oil. ^{1}H NMR (400 MHz, MeOD-d_4) δ 0.86 (t, 3H, J = 6.8 Hz, $CH_2C\mathbf{H_3}$), 1.03 – 1.13 (m, 2H, CH_2), 1.15 – 1.33 (m, 12H, 3 × $C\mathbf{H_2}$ and $C(C\mathbf{H_3})_2$ dimethylheptyl chain), 1.35 – 1.49 (m, 9H, $C(C\mathbf{H_3})_3$), 1.49 – 1.66 (m, 8H, CH_2 and $OC(C\mathbf{H_3})_2$ pyran ring), 2.51 – 2.66 (m, 4H, 2 × $C\mathbf{H_2}$), 3.17 – 3.25 (m, 2H, CH_2), 3.35 (t, 2H, J = 5.5 Hz, CH_2), 3.45 – 3.56 (m, 4H, 2 × $C\mathbf{H_2}$), 3.56 – 3.64 (m, 4H, 2 × $C\mathbf{H_2}$), 4.53 (s, 2H, CH_2) 6.30 – 6.38 (m, 1H, ArH phenol), 6.51 – 6.56 (m, 1H, ArH phenol), 7.44 – 7.53 (m, 1H, ArH phenol), 7.66 (s, 1H, ArH pyrazole), 7.76 – 7.82 (m, 1H, ArH pyridine), 8.42 (d, 1H, J = 2.4 Hz, ArH pyridine). ^{13}C NMR (101 MHz, MeOD-d_4) δ 14.40, 23.64, 25.74, 27.51, 28.77, 29.24, 31.04, 32.03, 32.14, 32.23, 32.86, 38.75, 40.43, 41.22, 45.23, 45.36, 70.59, 71.08, 71.29, 77.75, 102.98, 108.29, 108.62, 122.15, 125.93, 133.89, 135.31, 136.30, 140.09, 145.35, 153.13, 154.54, 155.61, 157.86, 174.68, 174.99. HRMS calculated for $C_{42}H_{62}N_6NaO_8$ $[M + Na]^+$, 801.4521; found, 801.4568. Analytical RP-HPLC Rt = 20.53 min; determined with HPLC method B.

7.4.2 Pharmacological studies

Radioligand binding assays and cAMP functional assays were carried out as described in section 7.1.2. In the radioligand binding assay, [^{3}H]-CP55,940 was used in a concentration of 0.75 nM per well for determining the CB_1R affinity and 0.5 nM per well for determining the CB_2R affinity of test compounds. Both CB_1R and CB_2R membrane preparations were used in the concentration of 3.0 μg per well.

7.5 Experimental procedure and data for compounds as described in chapter 5

7.5.1 Chemical studies

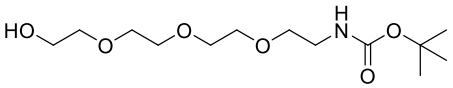

***tert*-Butyl *N*-(2-{2-[2-(2-hydroxyethoxy)ethoxy]ethoxy}ethyl)carbamate (5.11)**

This compound was prepared according to a previously reported synthesis of **5.11**.[240] To a solution of commercially available 2-{2-[2-(2-aminoethoxy)ethoxy]ethoxy}ethan-1-ol **5.10** (0.4 g, 2.07 mmol) in EtOH (5.0 mL) was added a solution of $(Boc)_2O$ (0.5 g, 2.27 mmol) in EtOH (3.0 mL) at 0 °C. The reaction was warmed to rt and stirred for 12 h. The solvent was evaporated under reduced pressure to give **5.11** (0.61 g) as a yellow oil, which was used in the next reaction without further purification. ^{1}H NMR (400 MHz, $CDCl_3$) δ 1.40 (s, 9H, C(C**H**$_3$)$_3$), 3.26 (q, 2H, *J* = 6.9 Hz, CH_2), 3.42 – 3.52 (m, 2H, CH_2), 3.54 – 3.79 (m, 13H, OH and 6 × C**H**$_2$), 5.60 (br s, 1H, NH). ^{13}C NMR (101 MHz, $CDCl_3$) δ 27.45, 28.49, 40.43, 61.66, 70.13, 70.30, 70.49, 70.66, 72.69, 78.99, 85.22, 146.78, 156.25. HRMS calculated for $C_{13}H_{27}NNaO_6$ $[M + Na]^+$, 316.1731; found, 316.1735.

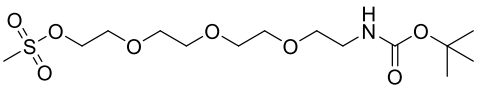

***tert*-Butyl *N*-[2-(2-{2-[2-(methanesulfonyloxy)ethoxy]ethoxy}ethoxy)ethyl] carbamate (5.12)**

To a solution of **5.11** (0.61 g, 2.08 mmol) in DCM (5.0 mL) was added Et_3N (0.44 mL, 3.12 mmol) and $MeSO_2Cl$ (0.21 mL, 2.70 mmol) under N_2 atmosphere at 0 °C and the reaction mixture warmed to rt and stirred for 12 h. The reaction solvent was removed under reduced pressure and the residue was partitioned between EtOAc and water. The EtOAc layer was dried over $MgSO_4.H_2O$, concentrated under reduced pressure and the residue was purified by silica gel column chromatography (eluting with 30% EtOAc/hexane to 70% EtOAc/hexane) to give **5.12** (0.73 g, 1.98 mmol, 96% over two steps from **5.10**) as a clear oil. ^{1}H NMR (400 MHz, $CDCl_3$) δ 1.42 (s, 9H, C(C**H**$_3$)$_3$), 3.05 (s, 3H, C**H**$_3$), 3.29 (q, 2H, *J* = 5.4 Hz, CH_2), 3.51 (t, 2H, *J* = 5.1 Hz, CH_2), 3.55 – 3.70 (m, 8H, 4 × C**H**$_2$), 3.71 – 3.80 (m, 2H, CH_2), 4.30 – 4.41 (m, 2H, CH_2), 4.99 (s, 1H, NH). ^{13}C NMR (101 MHz, $CDCl_3$) δ 28.50, 37.76, 40.42, 69.11, 69.32, 70.29, 70.60, 70.73,

79.28, 156.04. HRMS calculated for $C_{14}H_{29}NNaO_8S$ [M + Na]$^+$, 394.1506; found, 394.1473.

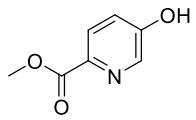

Methyl 5-hydroxypyridine-2-carboxylate (5.14)

To a solution of commercially available 5-hydroxypyridine-2-carboxylic acid **5.13** (1.0 g, 7.19 mmol) in MeOH (3.0 mL) was added dropwise $SOCl_2$ (1.0 mL) at 0 °C. The reaction mixture was stirred at 75 °C for 12 h. The solvent was removed under reduced pressure and the residue was evaporated to give **5.14** (1.2 g) as an off-white solid, which was used as such in the next reaction without further purification. ^{1}H NMR (400 MHz, MeOD-d_4) δ 4.05 – 4.10 (m, 3H, CH_3), 8.00 – 8.12 (m, 1H, ArH), 8.37 – 8.50 (m, 2H, ArH). HRMS calculated for $C_7H_7NNaO_3$ [M + Na]$^+$, 176.0318; found, 176.0306.

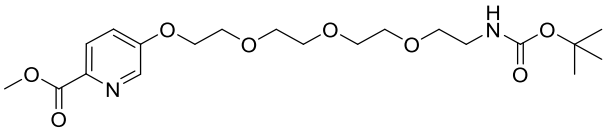

Ethyl 5-(2-{2-[2-(2-{[(*tert*-butoxy)carbonyl]amino}ethoxy)ethoxy]ethoxy}ethoxy) pyridine-2-carboxylate (5.15)

A mixture of **5.14** (0.27 g, 1.76 mmol) and K_2CO_3 (0.48 g, 3.52 mmol) in dry DMF (2.0 mL) was stirred at rt under N_2 atmosphere for 10 min, followed by addition of a solution of **5.12** (0.59 g, 1.58 mmol) in DMF (1.0 mL). The reaction mixture was stirred at 60 °C for 7 h. The reaction solvent was removed under reduced pressure and the residue was partitioned between EtOAc/water. The EtOAc layer was washed with water, brine solution, dried over $MgSO_4.H_2O$, concentrated under reduced pressure and the residue purified by silica gel column chromatography (eluting with 30% EtOAc/hexane to 2% MeOH/EtOAc) to provide **5.15** (0.44 g, 1.02 mmol, 64% over two steps from **5.14**) as yellow oil. ^{1}H NMR (400 MHz, $CDCl_3$) δ 1.42 (s, 9H, C(C**H**$_3$)$_3$), 3.30 (q, 2H, *J* = 5.3 Hz, CH_2), 3.52 (t, 2H, *J* = 5.2 Hz, CH_2), 3.56 – 3.67 (m, 4H, 2 × C**H**$_2$), 3.63 – 3.70 (m, 2H, CH_2), 3.70 – 3.78 (m, 2H, CH_2), 3.86 – 3.93 (m, 2H, CH_2), 3.97 (s, 3H, CH_3), 4.20 – 4.27 (m, 2H, CH_2), 4.99 (s, 1H, NH), 7.28 (dd, 1H, *J* = 8.7 Hz, ArH), 8.09 (d, 1H, *J* = 8.7 Hz, ArH), 8.41 (d, 1H, *J* = 2.8 Hz, ArH). ^{13}C NMR (101 MHz, $CDCl_3$) δ 28.55, 40.45, 52.79, 68.22, 69.56, 70.34, 70.36, 70.72, 70.76, 71.08, 79.31, 120.60, 126.60, 138.72, 140.46,

156.08, 157.68, 165.55. HRMS calculated for $C_{20}H_{32}N_2NaO_8$ $[M + Na]^+$, 451.2051; found, 451.2017.

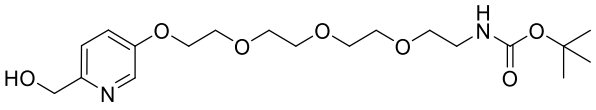

***tert*-Butyl *N*-(2-{2-[2-(2-{[6-(hydroxymethyl)pyridin-3-yl]oxy}ethoxy)ethoxy] ethoxy} ethyl) carbamate (5.16)**

To a solution of **5.15** (0.33 g, 0.78 mmol) in THF (10.0 mL) at 0 °C was added a solution of $LiAlH_4$ (1.2 mL of a 1M solution in THF) under N_2 atmosphere. The reaction was warmed to rt and stirred for 1 h. The reaction was quenched by adding water (3 mL), a solution of 15% NaOH in water (1.0 mL) and then water (3.0 mL) at 0 °C and the reaction mixture stirred for 30 min. The resulting suspension was filtered through celite, the filtrate was concentrated under reduced pressure and the residue was partitioned between EtOAc and water. The EtOAc layer was dried over $MgSO_4.H_2O$ and solvent removed under reduced pressure to give **5.16** (0.3 g) as an orange oil, which was used as such in the next reaction without further purification. HRMS calculated for $C_{19}H_{32}N_2NaO_7$ $[M + Na]^+$, 423.2102; found, 423.2088.

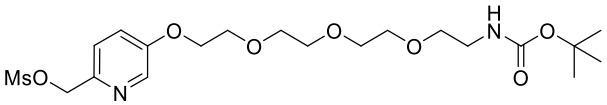

***tert*-Butyl *N*-[2-(2-{2-[2-({6-[(methanesulfonyloxy)methyl]pyridin-3-yl}oxy)ethoxy] ethoxy}ethoxy)ethyl]carbamate (5.17)**

According to the procedure described for the synthesis of **5.12**, reaction of **5.16** (0.25 g, 0.61 mmol) with $MeSO_2Cl$ (0.06 mL, 0.80 mmol) gave **5.17** (0.3 g) as a red liquid, which was used as such in the next reaction without further purification.

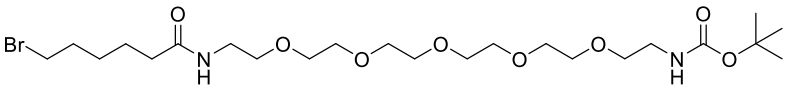

***tert*-Butyl *N*-[17-(6-bromohexanamido)-3,6,9,12,15-pentaoxaheptadecan-1-yl]carbamate (5.18)**

To a solution of commercially available 6-bromohexanoic acid **3.49** (15 mg, 0.07 mmol) in DCM (2.0 mL) was added TFFH (20 mg, 0.07 mmol), Et_3N (0.02 mL, 0.09 mmol) under N_2 atmosphere and the reaction stirred at 0 °C for 5 min. A solution of commercially

available *tert*-butyl *N*-(17-amino-3,6,9,12,15-pentaoxaheptadecan-1-yl)carbamate **4.16** (29 mg, 0.07 mmol) in DCM (1.0 mL) was added to the reaction mixture and reaction stirred at rt for 5 h. The reaction mixture was concentrated under reduced pressure. The residue was partitioned between DCM and H_2O. The DCM layer was washed with water, saturated $NaHCO_3$ solution, brine solution, dried over $MgSO_4.H_2O$ and the solvent removed under reduced pressure to provide **5.18** (36 mg, 0.06 mmol, 84%) as a clear oil, which was used as such in the next reaction without further purification. ^{1}H NMR (400 MHz, $CDCl_3$) δ 1.33 – 1.52 (m, 11H, C(C**H₃**)**₃** and CH_2), 1.59 – 1.72 (m, 2H, CH_2), 1.80 – 1.91 (m, 2H, CH_2), 2.18 (t, 2H, *J* = 7.5 Hz, CH_2), 2.99 (s, 1H, NH), 3.24 – 3.32 (m, 2H, CH_2), 3.36 – 3.46 (m, 4H, 2 × C**H₂**), 3.48 – 3.56 (m, 4H, 2 × C**H₂**), 3.56 – 3.69 (m, 16H, 8 × C**H₂**), 6.43 (br s, 1H, NH). ^{13}C NMR (101 MHz, $CDCl_3$) δ 24.87, 27.88, 28.52, 32.57, 33.79, 36.33, 39.27, 70.02, 70.25, 70.35, 70.59, 70.65, 156.15, 173.02. HRMS calculated for $C_{23}H_{45}BrN_2NaO_8$ $[M + Na]^+$, 579.2251; found, 579.2248.

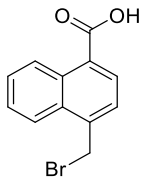

4-(Bromomethyl)naphthalene-1-carboxylic acid (5.20)

This compound was prepared according to according to a previously reported synthesis of **5.20**.[229] A mixture of commercially available 4-methylnaphthalene-1-carboxylic acid **5.19** (0.5 g, 2.68 mmol), NBS (0.52 g, 2.95 mmol) and AIBN (0.4 mL, 12% *w*/*v* solution in acetone) in CCl_4 (20.0 mL) was stirred at 80 °C for 4 h. The reaction solvent was removed under reduced pressure, the residue was partitioned between EtOAc and 15% *w*/*v* aqueous solution of citric acid. The EtOAc layer was dried over $MgSO_4.H_2O$ to give **5.20** (0.91 g) as a colourless solid, which was used as such in next reaction without further purification. ^{1}H NMR (400 MHz, MeOD-d_4) δ 5.07 (s, 2H, CH_2), 7.61 – 7.69 (m, 3H, ArH), 8.08 – 8.12 (m, 1H, ArH), 8.24 – 8.29 (m, 1H, ArH), 8.92 – 8.97 (m, 1H, ArH). HRMS calculated for $C_{12}H_8BrO_2$ $[M - H]^-$, 262.9713; found, 262.9695.

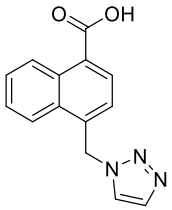

4-[(1*H*-1,2,3-Triazol-1-yl)methyl]naphthalene-1-carboxylic acid (5.21)

This compound was prepared according to according to a previously reported synthesis of **5.21**.[230] To a solution of **5.20** (0.5 g, 0.1.88 mmol) in DMF (7.0 mL) was added 1,2,3-triazoline (0.4 g, 5.66 mmol) under a N_2 atmosphere and the reaction was stirred at 50 °C for 12 h. The reaction solvent was removed under reduced pressure and the residue was acidified to pH 2.0-3.0 with aq. 1M HCl. The resulting precipitate was washed with water and air-dried to give **5.21** (0.34 g, 1.34 mmol, 91% over two steps from 4-methylnaphthalene-1-carboxylic acid) as an off-white solid. ^{1}H NMR (400 MHz, DMSO-d_6) δ 6.20 (s, 2H, CH_2), 7.29 (d, 1H, J = 7.5 Hz, ArH naphthalene), 7.60 – 7.74 (m, 2H, ArH naphthalene), 7.77 (d, 1H, J = 1.0 Hz, ArH triazoline), 8.09 (d, 1H, J = 7.4 Hz, ArH naphthalene), 8.20 (d, 1H, J = 1.0 Hz, ArH triazoline), 8.23 – 8.31 (m, 1H, ArH naphthalene), 8.81 – 8.91 (m, 1H, ArH naphthalene), 13.29 (s, 1H, COOH). HRMS calculated for $C_{14}H_{11}N_3NaO_2$ $[M + Na]^+$, 276.0743; found, 276.0728.

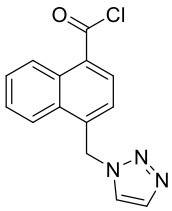

4-[(1*H*-1,2,3-Triazol-1-yl)methyl]naphthalene-1-carbonyl chloride (5.22)

A solution of **5.21** (0.32 g, 1.24 mmol) in $SOCl_2$ (10.0 mL) was stirred at 80 °C for 12 h with a water condenser and a $CaCl_2$ guard tube. $SOCl_2$ was removed under reduced pressure and the residue was co-evaporated with $CHCl_3$ to give **5.22** (0.34 g) as a yellow solid, which was used in the next reaction without further purification.

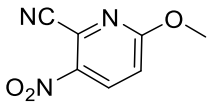

6-Methoxy-3-nitropyridine-2-carbonitrile (5.23)

To a solution of commercially available 6-chloro-3-nitropyridine-2-carbonitrile **5.9** (4.0 g, 21.79 mmol) in dry THF (15.0 mL) at 0 °C was added dropwise a solution of NaOMe (5.0 mL, 20% *w*/*v* solution in MeOH) in dry MeOH (4.0 mL) over 30 min under N_2 atmosphere. The reaction mixture was stirred at rt for 6 h. The reaction solvent was removed under reduced pressure and the residue was partitioned between EtOAc, water. The EtOAc layer was washed with saturated solution of NH_4Cl, brine, dried over $MgSO_4.H_2O$, concentrated under reduced pressure, and the residue purified by silica gel column chromatography (eluting with 10% EtOAc/hexane to 30% EtOAc/hexane) to provide **5.23** (2.41 g, 13.45 mmol, 62%) as a colourless solid. Continued elution (with 30% EtOAc/hexane) provided side product **5.25** (1.52 g, 7.19 mmol, 33%, spectral data reported later). **5.23** ^{1}H NMR (400 MHz, $CDCl_3$) δ 4.09 (s, 3H, CH_3), 7.11 (d, 1H, *J* = 9.2 Hz, ArH), 8.45 (d, 1H, *J* = 9.2 Hz, ArH). **5.23** ^{13}C NMR (101 MHz, $CDCl_3$) δ 55.89, 114.09, 116.10, 126.84, 135.58, 141.79, 166.37. HRMS calculated for **5.23** $C_7H_5N_3NaO_3$ $[M + Na]^+$, 202.0223; found, 202.0207.

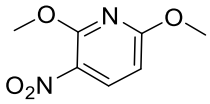

2,6-Dimethoxy-3-nitropyridine (5.24) - <u>side product</u> formed during synthesis of 5.23

To a solution of commercially available 6-chloro-3-nitropyridine-2-carbonitrile **5.9** (0.5 g, 2.72 mmol) in dry MeOH (3.0 mL) at 0 °C was added a solution of NaOMe (1.9 mL, 20% *w*/*v* solution in MeOH) under N_2 atmosphere. The reaction mixture was stirred at rt for 6 h. The reaction solvent was removed under reduced pressure and the residue was partitioned between EtOAc, water. The EtOAc layer was washed with saturated solution of NH_4Cl, brine, dried over $MgSO_4.H_2O$, concentrated under reduced pressure, and the residue purified by silica gel column chromatography (eluting with 10% EtOAc/hexane to 20% EtOAc/hexane) to provide **5.24** (0.48 g, 2.59 mmol, 95%) as a light yellow solid. ^{1}H NMR (400 MHz, $CDCl_3$) δ 4.00 (s, 3H, CH_3), 4.10 (s, 3H, CH_3), 6.35 (d, 1H, *J* = 8.8 Hz, ArH), 8.31 (d, 1H, *J* = 8.8 Hz, ArH). ^{13}C NMR (101 MHz, $CDCl_3$) δ 54.73, 54.85, 102.85, 138.80, 157.57, 165.56. HRMS calculated for $C_7H_8N_2NaO_4$ $[M + Na]^+$, 207.0376; found, 207.0372.

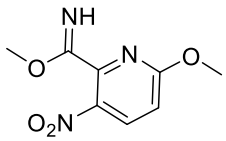

Methyl 6-methoxy-3-nitropyridine-2-carboximidate (5.25) - <u>optimised</u> procedure

To a solution of commercially available 6-chloro-3-nitropyridine-2-carbonitrile **5.9** (48 mg, 0.26 mmol) in dry MeOH (2.0 mL) at 0 °C was added dropwise a solution of NaOMe (0.06 mL, 20% *w*/*v* solution in MeOH) in dry MeOH (1.0 mL) over 5 min under N_2 atmosphere and the reaction stirred for 10 min. Another solution of NaOMe (0.06 mL, 20% *w*/*v* solution in MeOH) in dry MeOH (1.0 mL) was added to the reaction mixture. The reaction was stirred for 6 h at rt. The reaction solvent was removed under reduced pressure, the residue was neutralised with aqueous 0.5M HCl solution and extracted with EtOAc. The EtOAc layer was dried over $MgSO_4.H_2O$, concentrated under reduced pressure to provide **5.25** (52 mg, 0.24 mmol, 94%) as a yellow oil. ^{1}H NMR (400 MHz, $CDCl_3$) δ 3.89 (s, 3H, CH_3), 4.03 (s, 3H, CH_3), 6.87 (d, 1H, *J* = 8.9 Hz, ArH), 8.06 (d, 1H, *J* = 8.9 Hz, ArH). ^{13}C NMR (101 MHz, $CDCl_3$) δ 54.27, 55.03, 113.07, 135.30, 164.99, 165.78. HRMS calculated for $C_8H_{10}N_3O_4$ $[M + H]^+$, 212.0666; found, 212.0657.

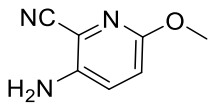

3-Amino-6-methoxypyridine-2-carbonitrile (5.26)

To a solution of **5.23** (2.3 g, 12.84 mmol) in MeOH (15.0 mL) at 0°C was added $SnCl_2.2H_2O$ (17.4 g, 77.03 mmol) and the reaction stirred at rt for 6 h. The reaction solvent was removed under reduced pressure; the residue was partitioned between EtOAc and aqueous 2M KOH solution. The EtOAc layer was concentrated under reduced pressure and the residue was purified by silica gel column chromatography (eluting with 30% EtOAc/hexane to 50% EtOAc/hexane) to provide **5.26** (1.15 g, 7.71 mmol, 62%) as a pale yellow solid. ^{1}H NMR (400 MHz, $CDCl_3$) δ 3.85 (s, 3H, CH_3), 5.62 – 5.66 (m, 2H, NH_2), 6.76 (d, 1H, *J* = 8.8 Hz, ArH), 7.03 (d, 1H, *J* = 8.8 Hz, ArH). ^{13}C NMR (101 MHz, $CDCl_3$) δ 53.22, 117.27, 123.74, 130.70, 141.43, 154.34, 170.57. MS calculated for $C_7H_8N_3O$ $[M + H]^+$, 150.0; found, 150.7.

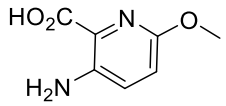

3-Amino-6-methoxypyridine-2-carboxylic acid (5.8)

To a solution of **5.26** (1.1 g, 7.37 mmol) in MeOH (30.0 mL) was added a solution of KOH (5.0 g, 89.12 mmol) in water (20.0 mL) and the reaction was stirred at 80 °C for 12 h. The reaction solvent was removed by evaporation under reduced pressure, the residue acidified to pH 2.0-3.0 with aqueous 6M HCl and extracted with a solvent mixture of MeOH:EtOAc (20% *v*/*v*). The combined organic layers were washed with water, brine, dried over $MgSO_4.H_2O$ to give a brown solid, which after recrystallisation from MeOH gave **5.8** (0.73 g, 4.34 mmol, 59%) as a pale yellow solid. ^{1}H NMR (400 MHz, MeOD-d_4) δ 3.92 (s, 3H, CH_3), 6.97 (d, 1H, J = 9.0 Hz, ArH), 7.37 (d, 1H, J = 9.0 Hz, ArH). ^{13}C NMR (101 MHz, MeOD-d_4) δ 54.52, 119.70, 121.18, 133.13, 143.80, 156.17, 169.21. HRMS calculated for $C_7H_9N_2O_3$ $[M + H]^+$, 169.0608; found, 169.0597.

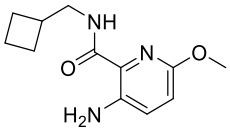

3-Amino-*N*-(cyclobutylmethyl)-6-methoxypyridine-2-carboxamide (5.27)

A solution of **5.8** (0.34 g, 2.03 mmol), HATU (0.85 g, 2.23 mmol), DIPEA (1.1 mL, 6.08 mmol) in DMF (4.0 mL) under a N_2 atmosphere was stirred for 10 min. A solution of 1-cyclobutylmethanamine hydrochloride (0.27 g, 2.23 mmol) in DMF (1.0 mL) was then added and the reaction stirred for 5 h. The reaction solvent was removed under reduced pressure. The residue was partitioned between EtOAc and H_2O. The organic layer was then washed with saturated NH_4Cl solution, saturated $NaHCO_3$ solution, water, brine solution, dried over $MgSO_4.H_2O$ and concentrated under reduced pressure. The residue was further purified by silica gel column chromatography (eluting with 20% EtOAc/hexane to 30% EtOAc/hexane) to provide **5.27** (0.33 g, 1.39 mmol, 68%) as an orange solid. ^{1}H NMR (400 MHz, $CDCl_3$) δ 1.69 – 1.87 (m, 2H, CH_2 cyclobutane), 1.84 – 1.97 (m, 2H, CH_2 cyclobutane), 2.02 – 2.14 (m, 2H, CH_2 cyclobutane), 2.49 – 2.65 (m, 1H, $NHCH_2CH$), 3.38 – 3.46 (m, 2H, $NHCH_2$), 3.83 (s, 3H, CH_3), 5.48 – 5.78 (m, 2H, NH_2), 6.71 (d, 1H, J = 8.8 Hz, ArH), 7.02 (d, 1H, J = 8.8 Hz, ArH), 7.84 (br s, 1H, NH). ^{13}C NMR (101 MHz, $CDCl_3$) δ 18.44, 25.72, 35.40, 43.98, 53.13, 116.31, 124.67, 130.80, 140.80, 154.27, 167.76. HRMS calculated for $C_{12}H_{17}N_3NaO_2$ $[M + Na]^+$, 258.1213; found, 258.1195.

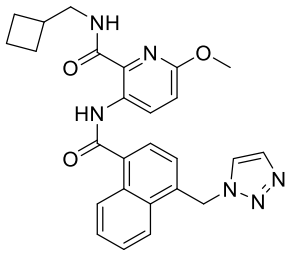

***N*-(Cyclobutylmethyl)-6-methoxy-3-{4-[(1*H*-1,2,3-triazol-1-yl)methyl]naphthalene-1-amido}pyridine-2-carboxamide (5.3)**

Compound **5.3** was prepared by following a literature procedure reported for the synthesis of analogous pyridyl-2-carboxamides.[223] To a solution of **5.22** (0.34 g, 1.24 mmol) in $CHCl_3$ (10.0 mL) was added a solution of **5.27** (0.19 g, 0.83 mmol), DIPEA (0.45 mL, 2.47 mmol) in $CHCl_3$ (3.0 mL) at 0°C under N_2 atmosphere. The reaction mixture was stirred at 80 °C for 4 h. The solvent was removed under reduced pressure and the residue was dissolved in EtOAc. The EtOAc solution was washed with saturated $NaHCO_3$ solution, water, brine, dried over $MgSO_4.H_2O$, concentrated under reduced pressure and purified by silica gel column chromatography (50% EtOAc/hexane to 70% EtOAc) to provide **5.3** (0.35 g, 0.75 mmol, 92%) as a colourless solid.

This compound was also prepared using **5.31** (0.26 g, 0.64 mmol), 1-cyclobutylmethanamine hydrochloride (0.08 g, 0.71 mmol), HATU (0.27 g, 0.71 mmol), and DIPEA (0.4 mL, 1.93 mmol) according to the procedure described for the synthesis of **5.27**, to give **5.3** (0.26 g, 0.55 mmol, 86%) as a colourless solid.

^{1}H NMR (400 MHz, $CDCl_3$) δ 1.67 – 1.82 (m, 2H, CH_2 cyclobutane), 1.83 – 1.97 (m, 2H, CH_2 cyclobutane), 2.03 – 2.14 (m, 2H, CH_2 cyclobutane), 2.52 – 2.64 (m, 1H, 26), 3.37 – 3.44 (m, 2H, NHC**H$_2$**), 3.94 (s, 3H, OCH_3), 6.05 (s, 2H, CH_2 triazoline), 7.02 (d, 1H, *J* = 9.1 Hz, ArH pyridine), 7.38 (d, 1H, *J* = 1.0 Hz, ArH triazoline), 7.42 (d, 1H, *J* = 7.3 Hz, ArH naphthalene), 7.51 – 7.66 (m, 2H, ArH naphthalene), 7.67 (d, 1H, *J* = 1.0 Hz, ArH triazoline), 7.84 (d, 1H, *J* = 7.3 Hz, ArH naphthalene), 7.95 – 8.02 (m, 1H, ArH naphthalene), 8.13 – 8.21 (m, 1H, NH), 8.51 – 8.60 (m, 1H, ArH naphthalene), 9.32 (d, 1H, *J* = 9.1 Hz, ArH pyridine), 12.64 (s, 1H, NH). ^{13}C NMR (101 MHz, $CDCl_3$) δ 18.43, 25.70, 35.06, 44.32, 52.27, 53.58, 115.89, 123.20, 123.61, 124.97, 126.80, 126.88, 127.71, 127.95, 129.77, 131.03, 131.70, 132.97, 133.25, 133.29, 134.41, 136.38, 157.86, 167.11, 167.74. HRMS calculated for $C_{26}H_{26}N_6NaO_3$ $[M + Na]^+$, 493.1959; found, 493.1911. Analytical RP-HPLC Rt = 18.72 min; determined with HPLC method B.

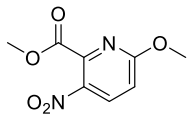

Methyl 6-methoxy-3-nitropyridine-2-carboxylate (5.28)

To a cooled (0 °C) solution of 6-chloro-3-nitropyridine-2-carbonitrile **5.9** (0.2 g, 1.09 mmol) in MeOH (10.0 mL) was added dropwise a solution of NaOMe (0.2 mL, 20% *w*/*v* solution in MeOH) in methanol (4.0 mL) under N_2 atmosphere. The reaction mixture was stirred at 0 °C for 15 min, followed by addition of another solution of NaOMe (0.3 mL, 20% *w*/*v* solution in MeOH) in methanol (4.0 mL). The reaction mixture was stirred at rt for 6 h, followed by dropwise addition of a solution of H_2SO_4 (0.5 mL, 96% *w*/*w*) in water (4.0 mL). The reaction was stirred for 2 h. The solvent was removed under reduced pressure and the residue neutralised with saturated $NaHCO_3$ solution, extracted with EtOAc. The EtOAc layer was washed with brine, dried over $MgSO_4.H_2O$, concentrated and the residue purified by silica gel chromatography (10 to 30% EtOAc/hexane) to provide **5.28** (0.16 g, 0.76 mmol, 70% over two steps from 6-methoxy-3-nitropyridine-2-carbonitrile) as yellow oil. ^{1}H NMR (400 MHz, $CDCl_3$) δ 4.01 (s, 3H, CO_2CH_3), 4.06 (s, 3H, 9, OCH_3), 6.90 (d, 1H, *J* = 9.1 Hz, ArH), 8.33 (d, 1H, *J* = 9.2 Hz, ArH). ^{13}C NMR (101 MHz, $CDCl_3$) δ 53.48, 55.28, 112.80, 135.03, 136.72, 146.44, 164.95, 166.27. HRMS calculated for $C_8H_8N_2NaO_5$ $[M + Na]^+$, 235.0325; found, 235.0333.

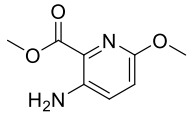

Methyl 3-amino-6-methoxypyridine-2-carboxylate (5.29)

According to the procedure described for **5.26**, **5.28** (0.14 g, 0.66 mmol) was reacted with $SnCl_2.2H_2O$ (1.5 g, 6.60 mmol). The crude compound was purified by silica gel chromatography (10% EtOAc/hexane to 30% EtOAc/hexane) to provide **5.29** (0.09 g, 0.47 mmol, 72%) as pale yellow solid. ^{1}H NMR (400 MHz, $CDCl_3$) δ 3.91 (s, 3H, CO_2CH_3), 3.92 (s, 3H, OCH_3), 5.44 (s, 2H, NH_2), 6.80 (d, 1H, *J* = 8.9 Hz, ArH), 7.04 (d, 1H, *J* = 8.9 Hz, ArH). ^{13}C NMR (101 MHz, $CDCl_3$) δ 52.23, 53.41, 118.11, 122.41, 130.17, 142.88, 155.12, 168.13. HRMS calculated for $C_8H_{10}N_2NaO_3$ $[M + Na]^+$, 205.0584; found, 205.0588.

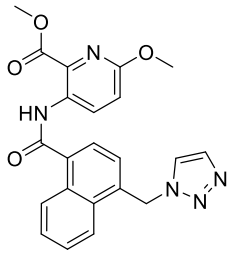

Methyl 6-methoxy-3-{4-[(1*H*-1,2,3-triazol-1-yl)methyl]naphthalene-1-amido}pyridine-2-carboxylate (5.30)

According to the procedure described for **5.3**, **5.29** (71 mg, 0.39 mmol) was reacted with **5.22** (182 mg, 0.67 mmol) and DIPEA (0.2 mL, 1.17 mmol). The crude compound was purified by silica gel chromatography (50% EtOAc/hexane to 100% EtOAc/hexane) to provide **5.30** (112 mg, 0.27 mmol, 69%) as a colourless solid. ^{1}H NMR (400 MHz, $CDCl_3$) δ 3.94 (s, 3H, CO_2CH_3), 3.99 (s, 3H, OCH_3), 6.06 (s, 2H, CH_2), 7.08 (d, 1H, *J* = 9.2 Hz, ArH pyridine), 7.39 – 7.43 (m, 2H, ArH naphthalene and triazoline), 7.56 – 7.64 (m, 2H, ArH naphthalene), 7.68 (s, 1H, ArH triazoline), 7.82 (d, 1H, *J* = 7.3 Hz, ArH naphthalene), 7.99 – 8.06 (m, 1H, ArH naphthalene), 8.48 – 8.57 (m, 1H, ArH naphthalene), 9.26 (d, 1H, *J* = 9.2 Hz, ArH pyridine), 11.42 (s, 1H, NH). ^{13}C NMR (101 MHz, $CDCl_3$) δ 52.13, 53.11, 53.82, 117.00, 123.22, 123.65, 124.89, 126.50, 126.63, 127.85, 128.05, 128.84, 130.88, 131.62, 132.66, 133.42, 134.40, 135.97, 158.75, 167.49, 168.23. HRMS calculated for $C_{22}H_{19}N_5NaO_4$ $[M + Na]^+$, 440.1329; found, 440.1295.

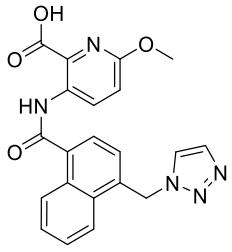

6-Methoxy-3-({4-[(1*H*-1,2,3-triazol-1-yl)methyl]naphthalene-1-carbonyl}amino) pyridine-2-carboxylic acid (5.31)

To a solution of compound **5.30** (378 mg, 0.91 mmol) in THF (7 mL) was added a solution of KOH (254 mg, 4.53 mmol) in water (5.0 mL) at 0°C. The reaction mixture was stirred at rt for 12 h. The solvent was removed under reduced pressure and the residue was acidified (pH 2.0-3.0) with aqueous 2.0 M HCl solution resulting in the appearance of a colourless precipitate which was collected by filtration and washed with water. The precipitate was air dried to give **5.31** (317 mg, 0.78 mmol, 87%) as a colourless solid. ^{1}H NMR (400 MHz, DMSO-d_6) δ 3.92 (s, 3H, OCH_3), 6.20 (s, 2H, CH_2), 7.18 (d, 1H, *J* =

9.0 Hz, ArH pyridine), 7.41 (d, 1H, *J* = 7.4 Hz, ArH naphthalene), 7.62 – 7.73 (m, 2H, ArH naphthalene), 7.77 (s, 1H, ArH triazoline), 7.85 (d, 1H, *J* = 7.3 Hz, ArH naphthalene), 8.23 (s, 1H, ArH triazoline), 8.29 (d, 1H, *J* = 7.9 Hz, ArH naphthalene), 8.40 (d, 1H, *J* = 8.6 Hz, ArH naphthalene), 8.66 (d, 1H, *J* = 8.9 Hz, ArH pyridine), 11.16 (s, 1H, NH), 13.36 (s, 1H, CO_2H). ^{13}C NMR (101 MHz, DMSO-d_6) δ 50.49, 53.58, 115.29, 123.75, 125.05, 125.35, 125.84, 126.02, 127.25, 129.92, 130.77, 131.11, 133.56, 133.81, 134.47, 134.76, 134.79, 158.57, 166.77, 167.69. HRMS calculated for $C_{21}H_{17}N_5NaO_4$ $[M + Na]^+$, 426.1173; found, 426.1197.

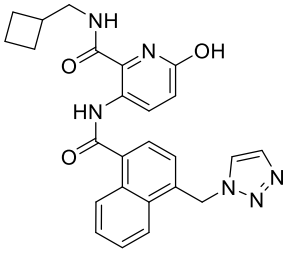

***N*-(cyclobutylmethyl)-6-hydroxy-3-{4-[(1*H*-1,2,3-triazol-1-yl)methyl]naphthalene-1-amido}pyridine-2-carboxamide (5.32)**

This compound was prepared according to previously published synthesis of **5.32**.[223] A mixture of **5.3** (0.33 g, 0.69 mmol) and pyridine hydrochloride (0.80 g, 6.97 mmol) was heated at 180 °C for 5 h. Water was slowly added to the hot reaction mixture (to prevent formation of solid cake), and diluted reaction mixture neutralised with $NaHCO_3$ solution, extracted with EtOAc. The EtOAc layer was washed with water, brine, dried over $MgSO_4.H_2O$ and purified by silica gel column chromatography (eluting with 50 to 70% EtOAc/hexane) to give **5.32** (0.162 g, 0.35 mmol, 51%) as a colourless solid. ^1H NMR (400 MHz, $CDCl_3$) δ 1.55 – 1.71 (m, 2H, CH_2 cyclobutane), 1.72 – 1.88 (m, 2H, CH_2 cyclobutane), 1.91 – 2.06 (m, 2H, CH_2 cyclobutane), 2.37 – 2.54 (m, 1H, $NHCH_2C\mathbf{H}$), 3.31 (t, 2H, *J* = 6.6 Hz, $NHC\mathbf{H}_2$), 6.05 (s, 2H, CH_2 triazoline), 6.98 (d, 1H, *J* = 9.1 Hz, ArH pyridine), 7.33 – 7.40 (m, 1H, ArH naphthalene), 7.44 (s, 1H, ArH triazoline), 7.51 – 7.62 (m, 2H, ArH naphthalene), 7.71 (s, 1H, ArH triazoline), 7.83 (d, 1H, *J* = 7.3 Hz, ArH naphthalene), 7.91 – 7.99 (m, 1H, ArH naphthalene), 8.30 – 8.44 (m, 1H, NH), 8.55 (d, 1H, *J* = 8.3 Hz, ArH naphthalene), 9.22 – 9.34 (m, 1H, ArH pyridine), 9.51 – 9.94 (m, 1H, OH), 12.60 (s, 1H, NH). ^{13}C NMR (101 MHz, $CDCl_3$) δ 18.31, 25.73, 25.86, 34.90, 44.54, 52.27, 115.07, 122.93, 124.05, 124.90, 126.70, 126.74, 127.71, 127.94, 129.67, 130.89, 131.46, 132.18, 132.60, 133.80, 134.04, 136.30, 157.43, 166.62, 167.55. HRMS calculated for $C_{25}H_{24}N_6NaO_3$ $[M + Na]^+$, 479.1802; found, 479.1811.

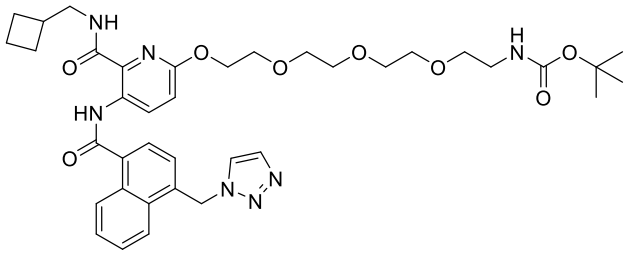

***tert*-Butyl *N*-[2-(2-{2-[2-({6-[(cyclobutylmethyl)carbamoyl]-5-{4-[(1*H*-1,2,3-triazol-1-yl)methyl]naphthalene-1-amido}pyridin-2-yl}oxy)ethoxy]ethoxy}ethoxy)ethyl] carbamate (5.33)**

To a solution of **5.32** (25 mg, 0.05 mmol) in DMF (2.0 mL) was added **5.12** (31 mg, 0.08 mmol), NaI (25 mg, 0.16 mmol), Ag_2CO_3 (76 mg, 0.27 mmol) and the reaction mixture stirred at 90 °C for 3 h. The reaction mixture was filtered to remove inorganic salts, the filtrate was evaporated under reduced pressure and the residue dissolved in EtOAc. The EtOAc solution was washed with water, brine, dried over $MgSO_4.H_2O$ and concentrated under reduced pressure. The residue was purified by silica gel column chromatography (eluting with solvent mixture of 80% EtOAc, 10% THF and 10% hexane (solvent combination identified by TLC for the optimal separation of **5.33** and **5.12**)) to give **5.33** (10 mg, 0.01 mmol, 25%) as a clear oil. ^{1}H NMR (400 MHz, $CDCl_3$) δ 1.44 (s, 9H, C(C**H**$_3$)$_3$), 1.67 – 1.80 (m, 2H, CH_2 cyclobutane), 1.83 – 1.99 (m, 2H, CH_2 cyclobutane), 2.03 – 2.15 (m, 2H, CH_2 cyclobutane), 2.50 – 2.64 (m, 1H, NHCH$_2$C**H**), 3.21 – 3.37 (m, 2H, CH_2), 3.37 – 3.46 (m, 2H, NHC**H**$_2$), 3.48 – 3.58 (m, 2H, CH_2), 3.59 – 3.81 (m, 8H, 4 × C**H**$_2$), 3.86 – 3.97 (m, 2H, CH_2), 4.39 – 4.50 (m, 2H, CH_2), 5.01 (br s, 1H, NH), 6.06 (s, 2H, CH_2 triazoline), 7.06 (d, 1H, *J* = 9.2 Hz, ArH pyridine), 7.38 (s, 1H, ArH triazoline), 7.43 (d, 1H, *J* = 7.3 Hz, ArH naphthalene), 7.53 – 7.64 (m, 2H, ArH naphthalene), 7.68 (s, 1H, ArH triazoline), 7.85 (d, 1H, *J* = 7.2 Hz, ArH naphthalene), 7.96 – 8.03 (m, 1H, ArH naphthalene), 8.11 (t, 1H, *J* = 5.9 Hz, NH), 8.51 – 8.58 (m, 1H, ArH naphthalene), 9.33 (d, 1H, *J* = 9.2 Hz, ArH pyridine), 12.64 (s, 1H, NH). ^{13}C NMR (101 MHz, $CDCl_3$) δ 18.43, 25.74, 28.57, 35.08, 44.35, 52.27, 65.62, 69.63, 70.39, 70.75, 70.80, 71.02, 116.22, 123.21, 123.60, 124.97, 126.80, 126.89, 127.72, 127.96, 129.68, 131.03, 131.70, 132.97, 133.28, 133.41, 134.41, 136.37, 157.31, 167.08, 167.74. HRMS calculated for $C_{38}H_{49}N_7NaO_8$ $[M + Na]^+$, 754.3535; found, 754.3482. Analytical RP-HPLC Rt = 18.96 min; determined with HPLC method B.

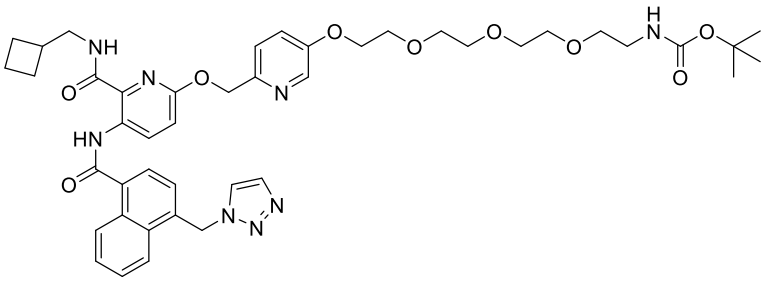

***tert*-Butyl *N*-[2-(2-{2-[2-({6-[({6-[(cyclobutylmethyl)carbamoyl]-5-{4-[(1*H*-1,2,3-triazol-1-yl)methyl]naphthalene-1-amido}pyridin-2-yl}oxy)methyl]pyridin-3-yl}oxy)ethoxy]ethoxy}ethoxy)ethyl]carbamate (5.34)**

Hydroxy pyridine **5.32** (20 mg, 0.04 mmol), **5.17** (23 mg), NaI (19 mg, 0.13 mmol), and Ag_2CO_3 (60 mg, 0.22 mmol) were reacted according to the procedure described for the preparation of **5.33** and the crude residue was purified by silica gel column chromatography (eluting with 30% EtOAc/hexane to 100% EtOAc) to provide **5.34** (24 mg, 0.03 mmol, 64%) as red liquid. ^{1}H NMR (400 MHz, $CDCl_3$) δ 1.42 (s, 9H, C(C**H**$_3$)$_3$), 1.67 – 1.81 (m, 2H, CH_2 cyclobutane), 1.83 – 1.98 (m, 2H, CH_2 cyclobutane), 2.01 – 2.14 (m, 2H, CH_2 cyclobutane), 2.50 – 2.63 (m, 1H, NHCH$_2$C**H**), 3.23 – 3.33 (m, 2H, CH_2), 3.34 – 3.42 (m, 2H, NHC**H**$_2$), 3.52 (t, 2H, *J* = 5.1 Hz, CH_2), 3.57 – 3.78 (m, 8H, 4 × C**H**$_2$), 3.83 – 3.92 (m, 2H, CH_2), 4.12 – 4.23 (m, 2H, CH_2), 5.02 (br s, 1H, NH), 5.40 (s, 2H, CH_2 short pyridyl linker), 6.04 (s, 2H, CH_2 triazoline), 7.10 (d, 1H, *J* = 9.1 Hz, ArH pyridine), 7.20 – 7.25 (m, 1H, ArH short pyridyl linker), 7.33 – 7.46 (m, 3H, ArH short pyridyl linker, ArH naphthalene, ArH triazoline), 7.51 – 7.64 (m, 2H, ArH naphthalene), 7.67 (s, 1H, ArH triazoline), 7.82 (d, 1H, *J* = 7.3 Hz, ArH naphthalene), 7.96 – 8.04 (m, 1H, ArH naphthalene), 8.21 – 8.35 (m, 2H, NH and ArH short pyridyl linker), 8.47 – 8.58 (m, 1H, ArH naphthalene), 9.32 (d, 1H, *J* = 9.1 Hz, ArH pyridine), 12.61 (s, 1H, NH). ^{13}C NMR (101 MHz, $CDCl_3$) δ 18.42, 25.81, 28.54, 35.08, 44.50, 52.23, 68.06, 68.93, 69.70, 70.35, 70.71, 70.75, 71.02, 115.84, 122.05, 122.46, 123.17, 123.60, 124.94, 126.75, 126.85, 127.67, 127.91, 129.82, 130.98, 131.65, 132.94, 133.27, 133.32, 134.37, 136.30, 137.44, 149.48, 154.56, 156.09, 156.70, 167.06, 167.70. HRMS calculated for $C_{44}H_{54}N_8NaO_9$ $[M + Na]^+$, 861.3906; found, 861.3876. Analytical RP-HPLC Rt = 17.89 min; determined with HPLC method B.

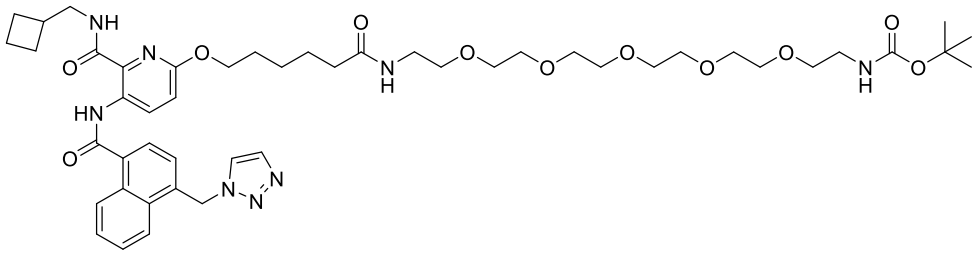

***tert*-Butyl *N*-{17-[6-({6-[(cyclobutylmethyl)carbamoyl]-5-{4-[(1*H*-1,2,3-triazol-1-yl) methyl] naphthalene-1-amido}pyridin-2-yl}oxy)hexanamido]-3,6,9,12,15-pentaoxaheptadecan-1-yl}carbamate (5.35)**

Hydroxy pyridine **5.32** (18 mg, 0.04 mmol), **5.18** (21 mg, 0.04 mmol), NaI (19 mg, 0.13 mmol), and Ag_2CO_3 (60 mg, 0.22 mmol) were reacted according to the procedure described for the preparation of **5.33** and the crude residue was purified by silica gel column chromatography (eluting with 50% EtOAc/hexane to 6% MeOH/EtOAc) to provide **5.35** (21 mg, 0.02 mmol, 56%) as clear, oily liquid. ^{1}H NMR (400 MHz, $CDCl_3$) δ 1.43 (s, 9H, C(C**H**$_3$)$_3$), 1.48 – 1.59 (m, 2H, CH_2), 1.67 – 1.78 (m, 4H, CH_2), 1.79 – 1.98 (m, 4H, 2 × C**H**$_2$), 2.02 – 2.13 (m, 2H, CH_2), 2.23 (t, 2H, *J* = 7.5 Hz, CH_2), 2.50 – 2.64 (m, 1H, NHCH$_2$C**H**), 3.19 – 3.35 (m, 2H, CH_2), 3.36 – 3.42 (m, 2H, NHC**H**$_2$ cyclobutane), 3.43 – 3.48 (m, 4H, 2 × C**H**$_2$), 3.49 – 3.58 (m, 4H, 2 × C**H**$_2$), 3.58 – 3.74 (m, 14H, 7 × C**H**$_2$), 4.25 (t, 2H, *J* = 6.4 Hz, CH_2), 5.08 (br s, 1H, NH), 6.05 (s, 2H, CH_2 triazoline), 6.22 (br s, 1H, NH), 6.99 (d, 1H, *J* = 9.2 Hz, ArH pyridine), 7.38 (s, 1H, ArH triazoline), 7.43 (d, 1H, *J* = 7.3 Hz, ArH naphthalene), 7.52 – 7.63 (m, 2H, ArH naphthalene), 7.68 (s, 1H, ArH triazoline), 7.84 (d, 1H, *J* = 7.2 Hz, ArH naphthalene), 7.95 – 8.03 (m, 1H, ArH naphthalene), 8.13 (t, 1H, *J* = 5.8 Hz, NH), 8.50 – 8.59 (m, 1H, ArH naphthalene), 9.30 (d, 1H, *J* = 9.2 Hz, ArH pyridine), 12.63 (s, 1H, NH). ^{13}C NMR (101 MHz, $CDCl_3$) δ 18.41, 25.52, 25.69, 26.00, 28.56, 28.82, 35.05, 36.56, 39.29, 44.29, 52.26, 66.11, 70.08, 70.33, 70.38, 70.64, 70.66, 70.68, 70.69, 70.72, 115.97, 123.18, 124.94, 126.78, 126.87, 127.67, 127.92, 129.78, 131.01, 131.67, 132.92, 133.09, 133.16, 136.39, 156.13, 157.65, 167.12, 167.68, 172.98. HRMS calculated for $C_{48}H_{68}N_8NaO_{11}$ $[M + Na]^+$, 955.4900; found, 955.4918. Analytical RP-HPLC Rt = 19.03 min; determined with HPLC method B.

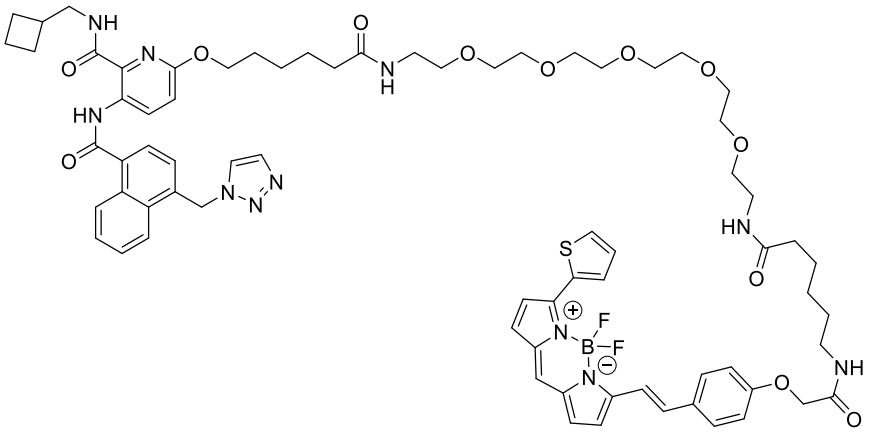

4-[(*E*)-2-[4-({[5-({17-[6-({6-[(Cyclobutylmethyl)carbamoyl]-5-{4-[(1*H*-1,2,3-triazol-1-yl)methyl]naphthalene-1-amido}pyridin-2-yl}oxy)hexanamido]-3,6,9,12,15-pentaoxaheptadecan-1-yl}carbamoyl)pentyl]carbamoyl}methoxy)phenyl]ethenyl]-2,2-difluoro-12-(thiophen-2-yl)-1λ^5-aza-3λ^4-aza-2λ^4-boratricyclo[7.3.0.0^{3,7}]dodeca-1(12),4,6,8,10-pentaen-1-ylium-3-ide (5.36)

To a solution of **5.35** (3 mg, 3.21 μmol) in DCM (2.0 mL) at 0 °C was added TFA (0.5 mL). The reaction mixture was stirred for 2 h, the solvent and TFA were removed by evaporation under reduced pressure to provide the amine 6-({5-[(17-amino-3,6,9,12,15-pentaoxaheptadecan-1-yl)carbamoyl]pentyl}oxy)-*N*-(cyclobutylmethyl)-3-{4-[(1*H*-1,2,3-triazol-1-yl)methyl]naphthalene-1-amido}pyridine-2-carboxamide trifluoroacetate in assumed quantitative yield as yellow solid. This trifluoroacetate salt was purified using semi-preparative RP-HPLC. To a solution of this purified trifluoroacetate salt (3.61 mg, 3.81 μmol) in DMF (100 μL) was added a solution of DIPEA (1.0 μL, 6.05 μmol) in DMF (100 μL), followed by addition of solution of BOPIPY630/650-SE (1.0 mg, 1.51 μmol) in DMF (800 μL) and the reaction stirred in the dark for 12 h. The reaction solvents were removed under reduced pressure and the residue was purified by semi-preparative RP-HPLC to give **5.36** (1.21 mg, 0.87 μmol, 58%) as a dark blue solid. HRMS calculated for $C_{72}H_{86}BF_2N_{11}NaO_{12}S$ $[M + Na]^+$, 1400.6143; found, 1400.6126. Analytical RP-HPLC Rt = 21.25 min; determined with HPLC method B.

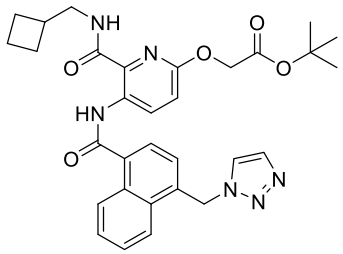

***tert*-Butyl 2-({6-[(cyclobutylmethyl)carbamoyl]-5-{4-[(1*H*-1,2,3-triazol-1-yl)methyl]naphthalene-1-amido}pyridin-2-yl}oxy)acetate (5.37)**

Hydroxy pyridine **5.32** (87 mg, 0.19 mmol), *tert*-butyl bromoacetate (112 mg, 0.57 mmol), and Ag_2CO_3 (263 mg, 0.95 mmol) were reacted according to the procedure described for the preparation of **5.33** except that NaI was not added. The crude residue was purified by silica gel column chromatography (eluting with 50% EtOAc/hexane to 70% EtOAc/Hexane) to provide **5.37** (102 mg, 0.18 mmol, 94%) as colourless solid. ^{1}H NMR (400 MHz, $CDCl_3$) δ 1.41 (s, 9H, C(C**H**$_3$)$_3$), 1.68 – 1.83 (m, 2H, CH_2 cyclobutane), 1.84 – 2.00 (m, 2H, CH_2 cyclobutane), 2.04 – 2.20 (m, 2H, CH_2 cyclobutane), 2.50 – 2.65 (m, 1H, NHCH$_2$C**H**), 3.31 – 3.50 (m, 2H, NHC**H**$_2$), 4.67 (s, 2H, CH_2CO), 6.06 (s, 2H, CH_2 triazoline), 7.14 (d, 1H, *J* = 9.1 Hz, ArH pyridine), 7.36 – 7.40 (m, 1H, ArH triazoline), 7.43 (d, 1H, *J* = 7.3 Hz, ArH naphthalene), 7.53 – 7.65 (m, 2H, ArH naphthalene), 7.65 – 7.72 (m, 1H, ArH triazoline), 7.85 (d, 1H, *J* = 7.3 Hz, ArH naphthalene), 7.92 – 8.07 (m, 2H, NH and ArH naphthalene), 8.50 – 8.61 (m, 1H, ArH naphthalene), 9.40 (d, 1H, *J* = 9.2 Hz, ArH pyridine), 12.67 (s, 1H, NH). ^{13}C NMR (101 MHz, $CDCl_3$) δ 18.39, 25.83, 28.11, 35.02, 44.63, 52.25, 64.77, 76.84, 77.16, 77.48, 82.43, 115.78, 123.21, 123.62, 124.99, 126.77, 126.84, 127.74, 127.97, 129.36, 131.01, 131.69, 133.06, 133.64, 133.95, 134.41, 136.24, 156.19, 166.91, 167.78, 168.67. HRMS calculated for $C_{31}H_{34}N_6NaO_5$ $[M + Na]^+$, 593.2483; found, 593.2474. Analytical RP-HPLC Rt = 19.87 min; determined with HPLC method B.

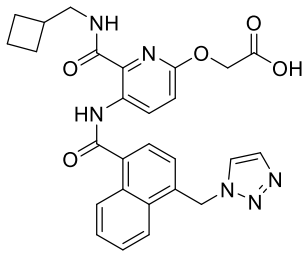

2-({6-[(Cyclobutylmethyl)carbamoyl]-5-{4-[(1*H*-1,2,3-triazol-1-yl)methyl] naphthalene-1-amido}pyridin-2-yl}oxy)acetic acid (5.38)

To a solution of **5.37** (39 mg, 0.07 mmol) in DCM (2 mL) at 0 °C was added TFA (2 mL, 26.13 mmol) and the mixture was stirred for 5 h. DCM and TFA were removed under reduced pressure and the residue was co-evaporated with $CHCl_3$ to provide **5.38** (33 mg, 0.06 mmol, 95%) as a colourless solid. ^{1}H NMR (400 MHz, $CDCl_3$) δ 1.61 – 1.75 (m, 2H, CH_2 cyclobutane), 1.77 – 1.92 (m, 2H, CH_2 cyclobutane), 1.98 – 2.11 (m, 2H, CH_2 cyclobutane), 2.49 – 2.62 (m, 1H, $NHCH_2C\mathbf{H}$), 3.25 – 3.38 (m, 2H, $NHC\mathbf{H_2}$), 4.83 (s, 2H, CH_2CO), 6.07 (s, 2H, CH_2 triazoline), 7.17 (d, 1H, *J* = 9.2 Hz, ArH pyridine), 7.41 (d, 1H, *J* = 7.3 Hz, ArH naphthalene), 7.45 (s, 1H, ArH triazoline), 7.56 – 7.65 (m, 2H, ArH naphthalene), 7.78 (s, 1H, ArH triazoline), 7.84 (d, 1H, *J* = 7.2 Hz, ArH naphthalene), 7.91 (t, 1H, *J* = 5.9 Hz, NH), 7.94 – 8.00 (m, 1H, ArH naphthalene), 8.49 – 8.58 (m, 1H, ArH naphthalene), 9.41 (d, 1H, *J* = 9.2 Hz, ArH pyridine), 12.67 (s, 1H, NH). ^{13}C NMR (101 MHz, $CDCl_3$) δ 18.40, 25.71, 34.82, 44.63, 52.60, 63.37, 115.91, 123.01, 124.17, 125.05, 126.80, 126.98, 127.91, 128.18, 129.48, 131.00, 131.58, 132.50, 133.60, 133.93, 134.17, 136.31, 155.87, 166.79, 167.85, 172.43. HRMS calculated for $C_{27}H_{26}N_6NaO_5$ [M + Na]$^+$, 537.1857; found, 537.1857.

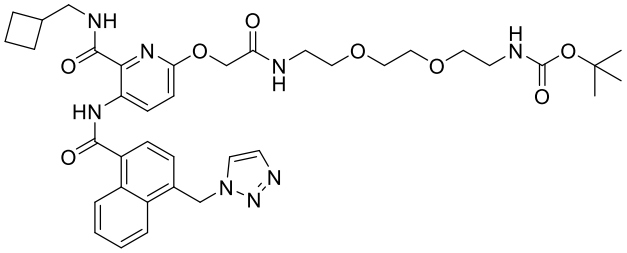

***tert*-Butyl *N*-[2-(2-{2-[2-({6-[(cyclobutylmethyl)carbamoyl]-5-{4-[(1*H*-1,2,3-triazol-1-yl)methyl]naphthalene-1-amido}pyridin-2-yl}oxy)acetamido]-ethoxy}ethoxy)ethyl]carbamate (5.39)**

A solution of **5.38** (22 mg, 0.04 mmol), HBTU (16 mg, 0.04 mmol), DIPEA (22 μL, 0.13 mmol) in DMF (1.0 mL) under N_2 atmosphere was stirred for 5 min. A solution of **2.12** (13 mg, 0.05 mmol) in DMF (1.0 mL) was then added and the reaction stirred for 12 h. The reaction solvent was removed under reduced pressure. The residue was dissolved in water and EtOAc was added. The EtOAc layer was then washed with saturated $NaHCO_3$ solution, water, brine solution, dried over $MgSO_4.H_2O$ and concentrated under reduced pressure. The residue was purified by silica gel column chromatography (eluting with 30% EtOAc/hexane to 5% MeOH/EtOAc) to provide **5.39** (19 mg, 0.02 mmol, 59%) as a colourless solid. ^{1}H NMR (400 MHz, $CDCl_3$) δ 1.44 (s, 9H, $C(C\mathbf{H_3})_3$), 1.67 – 1.80 (m, 2H, CH_2 cyclobutane), 1.83 – 1.99 (m, 2H, CH_2 cyclobutane), 2.02 – 2.16 (m, 2H, CH_2

cyclobutane), 2.51 – 2.67 (m, 1H, NHCH$_2$C**H**), 3.18 – 3.35 (m, 2H, CH$_2$), 3.36 – 3.42 (m, 2H, NHC**H$_2$** cyclobutane), 3.44 – 3.65 (m, 10H, 5 × C**H$_2$**), 4.74 (s, 2H, OCH$_2$CO), 5.01 (br s, 1H, NH), 6.06 (s, 2H, CH$_2$ triazoline), 6.77 (br s, 1H, NH), 7.13 (d, 1H, *J* = 9.1 Hz, ArH pyridine), 7.39 (d, 1H, *J* = 0.9 Hz, ArH triazoline), 7.43 (d, 1H, *J* = 7.3 Hz, ArH naphthalene), 7.54 – 7.63 (m, 2H, ArH naphthalene), 7.68 (d, 1H, *J* = 0.9 Hz, ArH triazoline), 7.84 (d, 1H, *J* = 7.3 Hz, ArH naphthalene), 7.97 – 8.03 (m, 1H, ArH naphthalene), 8.03 – 8.15 (m, 1H, NH), 8.49 – 8.60 (m, 1H, ArH naphthalene), 9.41 (d, 1H, *J* = 9.1 Hz, ArH pyridine), 12.70 (s, 1H, NH). ^{13}C NMR (101 MHz, CDCl$_3$) δ 18.39, 25.79, 28.55, 34.94, 39.04, 40.42, 44.68, 52.23, 66.24, 69.80, 70.18, 70.33, 70.40, 115.57, 123.23, 123.65, 125.02, 126.67, 126.80, 127.76, 127.98, 129.82, 130.98, 131.68, 133.16, 133.71, 134.17, 134.41, 136.06, 155.54, 156.09, 166.80, 167.83, 168.86. HRMS calculated for $C_{38}H_{48}N_8NaO_8$ [M + Na]$^+$, 767.3487; found, 767.3485. Analytical RP-HPLC Rt = 17.69 min; determined with HPLC method B.

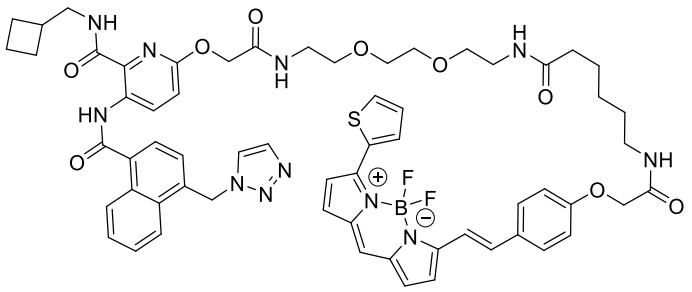

4-[(*E*)-2-[4-({[2-(2-{2-[2-({6-[(Cyclobutylmethyl)carbamoyl]-5-{4-[(1*H*-1,2,3-triazol-1-yl)methyl]naphthalene-1-amido}pyridin-2-yl}oxy)acetamido]ethoxy} ethoxy)ethyl] carbamoyl}methoxy)phenyl]ethenyl]-2,2-difluoro-12- (thiophen-2-yl)-1λ^5,3-diaza-2-boratricyclo[7.3.0.0^{3,7}]dodeca-1(12),4,6,8,10-pentaen-1-ylium-2-uide (5.40)

Following the procedure described for **5.36**, **5.39** (3.0 mg, 4.02 μmol) was reacted with TFA (0.5 mL) to give 6-[({2-[2-(2-aminoethoxy)ethoxy]ethyl}carbamoyl)methoxy]-*N*-(cyclobutylmethyl)-3-{4-[(1*H*-1,2,3-triazol-1-yl)methyl]naphthalene-1-amido}pyridine-2-carboxamide trifluoroacetate in assumed quantitative yield as a yellow solid. This trifluoroacetate salt was purified using semi-preparative RP-HPLC. Reaction of this purified trifluoroacetate salt (3.1 mg, 4.08 μmol) with BODIPY-630/650-SE (1.0 mg, 1.51 μmol) gave **5.40** (1.76 mg, 1.47 μmol, 98%) as a dark blue solid. HRMS calculated for $C_{62}H_{66}BF_2N_{11}NaO_9S$ [M + Na]$^+$, 1212.4729; found, 1212.4701. Analytical RP-HPLC Rt = 20.09 min; determined with HPLC method B.

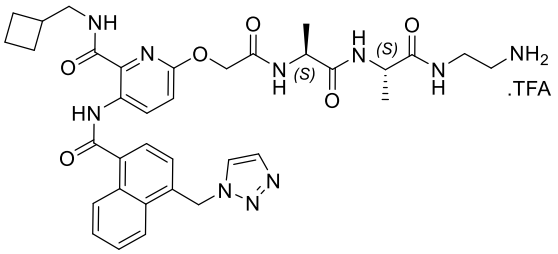

6-({[(*1S*)-1-{[(*1S*)-1-[(2-Aminoethyl)carbamoyl]ethyl]carbamoyl}ethyl]carbamoyl}methoxy)-*N*-(cyclobutylmethyl)-3-{4-[(1*H*-1,2,3-triazol-1-yl)methyl]naphthalene-1-amido}pyridine-2-carboxamide trifluoroacetate (5.44)

According to the Fmoc solid phase peptide synthesis described for the preparation of **3.38** in chapter 7, section 7.3.1, reaction of **5.38** (70 mg, 0.13 mmol) and Fmoc deprotected resin-bound **5.42** (143 mg) and then purification of the crude compound by RP-HPLC gave **5.44** (20 mg, 0.02 mmol) as a colourless solid. ^{1}H NMR (400 MHz, DMSO-d_6) δ 1.14 – 1.28 (m, 6H, 2 × C**H**$_3$ alanines), 1.61 – 1.73 (m, 2H, CH_2 cyclobutane), 1.75 – 1.84 (m, 2H, CH_2 cyclobutane), 1.87 – 2.00 (m, 2H, CH_2 cyclobutane), 2.54 (s, 1H, NHCH$_2$C**H**), 2.79 – 2.87 (m, 2H, 2 × N**H**), 3.23 – 3.32 (m, 6H, 3 × C**H**$_2$), 4.14 – 4.24 (m, 1H, C**H**CONH), 4.30 – 4.40 (m, 1H, C**H**CONH), 4.78 – 5.00 (m, 2H, OCH$_2$CO), 6.21 (s, 2H, CH_2 triazoline), 7.28 (d, 1H, *J* = 9.1 Hz, ArH pyridine), 7.38 (d, 1H, *J* = 7.4 Hz, ArH naphthalene), 7.63 – 7.72 (m, 2H, ArH naphthalene), 7.74 (m, 2H, NH_2), 7.78 (d, 1H, *J* = 1.0 Hz, ArH triazoline), 7.85 (d, 1H, *J* = 7.3 Hz, ArH naphthalene), 8.00 (t, 1H, *J* = 5.7 Hz, NH), 8.26 (d, 1H, *J* = 1.0 Hz, ArH triazoline), 8.28 – 8.33 (m, 1H, ArH naphthalene), 8.36 – 8.43 (m, 1H, ArH naphthalene), 8.69 – 8.78 (m, 1H, NH), 9.18 (d, 1H, *J* = 9.1 Hz, ArH pyridine), 12.63 (s, 1H, NH). HRMS calculated for $C_{35}H_{43}N_{10}O_6$ $[M + H]^+$, 699.3362; found, 699.3393.

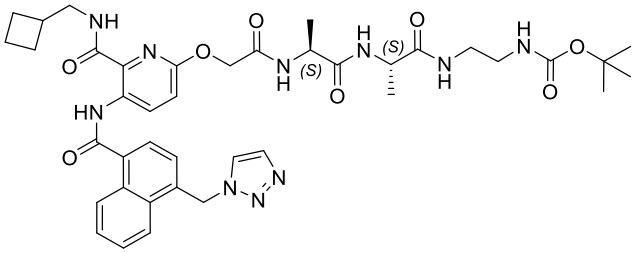

***N*-(Cyclobutylmethyl)-6-({[(1*S*)-1-{[(1*S*)-1-[(2-acetamidoethyl)carbamoyl]ethyl]carbamoyl}ethyl]carbamoyl}methoxy)-3-{4-[(1*H*-1,2,3-triazol-1-yl)methyl]naphthalene-1-amido}pyridine-2-carboxamide (5.45)**

To a solution of **5.44** (16 mg, 0.02 mmol) in DMF (2.0 mL) was added $(Boc)_2O$ (5 mg, 0.02 mmol), followed by addition of Et_3N (4.1 µL, 0.03 mmol), and the reaction was

stirred for 12 h. The solvent was removed under reduced pressure and a portion of the obtained residue (6.0 mg from total 28 mg crude residue) was purified by semi-preparative RP-HPLC to give **5.45** (1.3 mg, 1.62 µmol, 38%) as a colourless solid. HRMS calculated for $C_{40}H_{50}N_{10}NaO_8$ $[M + Na]^+$, 821.3705; found, 821.3716. Analytical RP-HPLC Rt = 17.22 min; determined with HPLC method B.

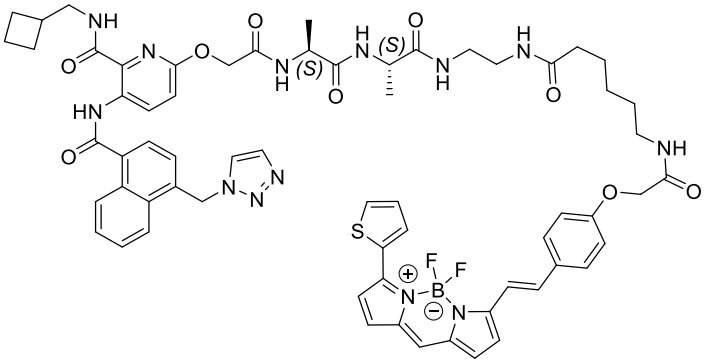

4-[(*E*)-2-[4-({[5-({2-[(2*S*)-2-[(2*S*)-2-[2-({6-[(Cyclobutylmethyl)carbamoyl]-5-{4-[(1*H*-1,2,3-triazol-1-yl)methyl]naphthalene-1-amido}pyridin-2-yl}oxy)acetamido] propanamido]propanamido]ethyl}carbamoyl)pentyl]carbamoyl}methoxy) phenyl]ethenyl]-2,2-difluoro-12-(thiophen-2-yl)-1λ^5-aza-3λ^4-aza-2λ^4-boratricyclo [7.3.0.0^{3,7}]dodeca-1(12),4,6,8,10-pentaen-1-ylium-3-ide (5.46)

Following the procedure described for **5.36**, **5.44** (3.7 mg, 4.55 µmol) was reacted with BODIPY-630/650-SE (1.0 mg, 1.51 µmol) to give **5.46** (0.24 mg, 0.19 µmol, 13%) as a dark blue solid. HRMS calculated for $C_{64}H_{68}BF_2N_{13}NaO_9S$ $[M + Na]^+$, 1266.4947; found, 1266.4891. Analytical RP-HPLC Rt = 19.63 min; determined with HPLC method B. The low yield of the reaction was due to the poor solubility of **5.46** in DMSO-water solution, which made purification by semi-preparative RP-HPLC challenging.

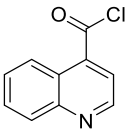

Quinoline-4-carbonyl chloride (5.48)

According to the procedure described for the preparation of **5.22**, commercially available quinoline-4-carboxylic acid **5.47** (0.2 g, 1.07 mmol) was reacted with $SOCl_2$ (5.0 mL) to give **5.48** (0.2 g) as a yellow solid, which was used as such in the following reaction.

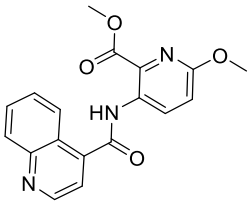

Methyl 6-methoxy-3-[(quinoline-4-carbonyl)amino]pyridine-2-carboxylate (5.49)

To a solution of **5.48** (0.2 g, 1.07 mmol) in $CHCl_3$ (7.0 mL) was added a solution of **5.29** (0.13 g, 0.71 mmol) and DIPEA (0.4 mL, 2.14 mmol) in $CHCl_3$ (3.0 mL) at 0°C under N_2 atmosphere. The reaction mixture was warmed to rt and stirred for 7 h. The solvent was removed under reduced pressure and the residue was dissolved in EtOAc. The EtOAc layer was washed with saturated $NaHCO_3$ solution, water, brine, dried over $MgSO_4.H_2O$, concentrated under reduced pressure and the residue purified by silica gel chromatography (50% EtOAc/hexane to 100% EtOAc) to provide **5.49** (0.19 g, 0.58 mmol, 82%) as a colourless solid. ^{1}H NMR (400 MHz, $CDCl_3$) δ 3.96 (s, 3H, CO_2CH_3), 4.00 (s, 3H, OCH_3), 7.09 (d, 1H, *J* = 9.2 Hz, ArH pyridine), 7.62 – 7.67 (m, 1H, ArH quinoline), 7.69 (d, 1H, *J* = 4.3 Hz, ArH quinoline), 7.76 – 7.84 (m, 1H, ArH quinoline), 8.19 (d, 1H, *J* = 8.5 Hz, ArH quinoline), 8.44 (d, 1H, *J* = 8.2 Hz, ArH quinoline), 9.07 (d, 1H, *J* = 4.3 Hz, ArH quinoline), 9.25 (d, 1H, *J* = 9.2 Hz, ArH pyridine), 11.56 (s, 1H, NH). ^{13}C NMR (101 MHz, $CDCl_3$) δ 53.23, 53.88, 117.09, 118.69, 124.60, 125.48, 128.05, 129.07, 130.18, 130.27, 132.65, 134.05, 141.36, 149.17, 150.16, 159.00, 165.88, 168.29. HRMS calculated for $C_{18}H_{15}N_3NaO_4$ $[M + Na]^+$, 360.0955; found, 360.0928.

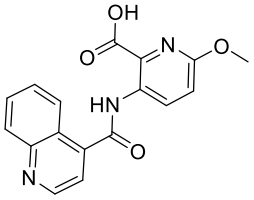

6-Methoxy-3-[(quinoline-4-carbonyl)amino]pyridine-2-carboxylic acid (5.50)

According to the procedure for **5.31**, a solution of **5.49** (0.19 g, 0.57 mmol) and KOH (0.16 g, 2.84 mmol) gave **5.50** (0.18 g, 0.57 mmol, quantitative) as yellow solid. ^{1}H NMR (400 MHz, DMSO-d_6) δ 3.92 (s, 3H, OCH_3), 7.18 (d, 1H, *J* = 8.9 Hz, ArH pyridine), 7.67 – 7.76 (m, 1H, ArH quinoline), 7.80 (d, 1H, *J* = 4.3 Hz, ArH quinoline), 7.83 – 7.92 (m, 1H, ArH quinoline), 8.14 (d, 1H, *J* = 8.3 Hz, ArH quinoline), 8.35 (d, 1H, *J* = 8.2 Hz, ArH quinoline), 8.49 (d, 1H, *J* = 8.9 Hz, ArH pyridine), 9.08 (d, 1H, *J* = 4.3 Hz, ArH quinoline), 11.19 (s, 1H, NH). ^{13}C NMR (101 MHz, DMSO-d_6) δ 53.67, 115.04, 119.16, 123.93, 125.50, 127.76, 129.33, 129.82, 130.24, 135.49, 135.75, 141.40, 147.94, 150.34,

159.18, 165.21, 167.44. HRMS calculated for $C_{17}H_{12}N_3O_4$ [M - H]$^-$, 322.0833; found, 322.0822.

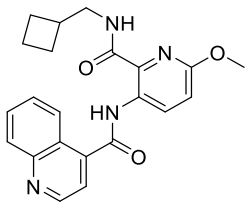

***N*-{2-[(Cyclobutylmethyl)carbamoyl]-6-methoxypyridin-3-yl}squinoline-4-carboxamide (5.6)**

According to the procedure described for **5.27**, **5.50** (0.17 g, 0.53 mmol) was reacted with 1-cyclobutylmethanamine hydrochloride (0.07 g, 0.58 mmol), HATU (0.2 g, 0.53 mmol) and DIPEA (0.3 mL, 1.58 mmol). Purification of the crude compound by silica gel column chromatography (eluting with 10% EtOAc/hexane to 60% EtOAc/hexane) gave **5.6** (0.19 g, 0.49 mmol, 93%) as a colourless solid. ^{1}H NMR (400 MHz, $CDCl_3$) δ 1.69 – 1.80 (m, 2H, CH_2 cyclobutane), 1.82 – 2.00 (m, 2H, CH_2 cyclobutane), 2.03 – 2.19 (m, 2H, CH_2 cyclobutane), 2.48 – 2.65 (m, 1H, NHCH_2C**H**), 3.38 – 3.45 (m, 2H, NHC**H$_2$**), 3.94 (s, 3H, OCH_3), 7.03 (d, 1H, *J* = 9.1 Hz, ArH pyridine), 7.58 – 7.65 (m, 1H, ArH quinoline), 7.70 (d, 1H, *J* = 4.4 Hz, ArH quinoline), 7.74 – 7.81 (m, 1H, ArH quinoline), 8.10 – 8.22 (m, 2H, NH and ArH quinoline), 8.47 (d, 1H, *J* = 9.3 Hz, ArH quinoline), 9.04 (d, 1H, *J* = 4.3 Hz, ArH quinoline), 9.29 (d, 1H, *J* = 9.1 Hz, ArH pyridine), 12.82 (s, 1H, NH). ^{13}C NMR (101 MHz, $CDCl_3$) δ 18.41, 25.68, 35.03, 44.33, 53.59, 115.91, 118.78, 124.74, 125.63, 127.81, 129.92, 130.05, 132.92, 133.16, 141.56, 149.12, 150.26, 158.03, 166.01, 167.03. HRMS calculated for $C_{22}H_{22}N_4NaO_3$ [M + Na]$^+$, 413.1584; found, 413.1558. Analytical RP-HPLC Rt = 17.07 min; determined with HPLC method B.

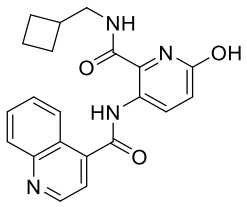

***N*-{2-[(Cyclobutylmethyl)carbamoyl]-6-hydroxypyridin-3-yl}quinoline-4-carboxamide (5.51)**

According to the procedure described for **5.32**, **5.6** (0.18 g, 0.47 mmol) was reacted with pyridine hydrochloride (1.09 g, 9.47 mmol). Purification of the crude compound by silica

gel column chromatography (eluting with 30% EtOAc/hexane to 70% EtOAc/hexane) gave **5.51** (0.11 g, 0.29 mmol, 63%) as a yellow solid. ^{1}H NMR (400 MHz, DMSO-d_6) δ 1.61 – 1.73 (m, 2H, CH_2 cyclobutane), 1.75 – 1.86 (m, 2H, CH_2 cyclobutane), 1.90 – 2.02 (m, 2H, CH_2 cyclobutane), 3.24 – 3.31 (m, 3H, NHC**H**$_2$ and NHCH$_2$C**H**), 7.03 (d, 1H, *J* = 8.9 Hz, ArH pyridine), 7.66 – 7.75 (m, 1H, ArH quinoline), 7.80 (d, 1H, *J* = 4.3 Hz, ArH quinoline), 7.84 – 7.92 (m, 1H, ArH quinoline), 8.14 (d, 1H, *J* = 8.4 Hz, ArH quinoline), 8.30 – 8.38 (m, 1H, 9, ArH quinoline), 8.66 (t, 1H, *J* = 5.6 Hz, NH), 9.01 (d, 1H, *J* = 7.1 Hz, ArH pyridine), 9.09 (d, 1H, *J* = 4.3 Hz, ArH quinoline), 11.12 (s, 1H, OH), 12.63 (s, 1H, NH). ^{13}C NMR (101 MHz, DMSO-d_6) δ 17.73, 25.11, 34.40, 43.73, 118.84, 123.71, 125.29, 127.76, 129.54, 130.13, 131.46, 141.16, 148.21, 150.55, 164.66. HRMS calculated for $C_{21}H_{19}N_4O_3$ [M - H]$^-$, 375.1463; found, 375.1472.

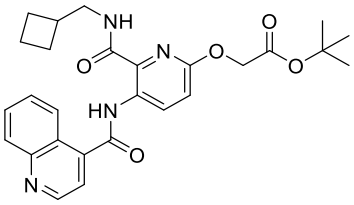

***tert*-Butyl 2-({6-[(cyclobutylmethyl)carbamoyl]-5-(quinoline-4-amido)pyridin-2-yl}oxy) acetate (5.52)**

According to the procedure described for **5.33**, **5.51** (32 mg, 0.08 mmol) was reacted with *tert*-butyl bromoacetate (25 mg, 0.13 mmol), NaI (38 mg, 0.25 mmol), and Ag_2CO_3 (117 mg, 0.42 mmol). Purification of the crude compound by silica gel column chromatography (eluting with 20% EtOAc/hexane to 30% EtOAc/hexane) gave **5.52** (39 mg, 0.08 mmol, 94%) as a clear oil. ^{1}H NMR (400 MHz, $CDCl_3$) δ 1.41 (s, 9H, C(C**H**$_3$)$_3$), 1.68 – 1.82 (m, 2H, CH_2 cyclobutane), 1.84 – 2.00 (m, 2H, CH_2 cyclobutane), 2.03 – 2.18 (m, 2H, CH_2 cyclobutane), 2.51 – 2.63 (m, 1H, *J* = 7.6 Hz, NHCH$_2$C**H**), 3.36 – 3.46 (m, 2H, *J* = 7.3 Hz, NHC**H**$_2$), 4.67 (s, 2H, OCH$_2$CO), 7.14 (d, 1H, *J* = 9.1 Hz, ArH pyridine), 7.58 – 7.67 (m, 1H, ArH quinoline), 7.70 (d, 1H, *J* = 4.4 Hz, ArH quinoline), 7.73 – 7.81 (m, 1H, ArH quinoline), 7.96 (t, 1H, *J* = 6.0 Hz, NH), 8.13 – 8.20 (m, 1H, ArH quinoline), 8.43 – 8.50 (m, 1H, ArH quinoline), 9.04 (d, 1H, *J* = 4.3 Hz, ArH quinoline), 9.37 (d, 1H, *J* = 9.1 Hz, ArH pyridine), 12.85 (s, 1H, NH). ^{13}C NMR (101 MHz, $CDCl_3$) δ 18.38, 25.82, 28.10, 35.01, 44.64, 64.78, 76.84, 77.16, 77.48, 82.45, 115.82, 118.79, 124.72, 125.61, 127.87, 129.56, 130.09, 130.10, 133.60, 141.46, 149.14, 150.27, 156.41, 166.10, 166.85, 168.60. HRMS calculated for $C_{27}H_{30}N_4NaO_5$ [M + Na]$^+$, 513.2108; found, 513.2081.

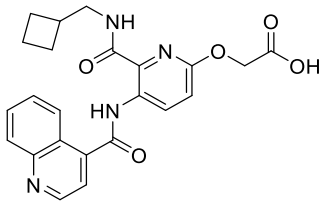

2-({6-[(Cyclobutylmethyl)carbamoyl]-5-(quinoline-4-amido)pyridin-2-yl}oxy)acetic acid (5.53)

According to the procedure for **5.38**, a solution of **5.52** (21 mg, 0.04 mmol) and TFA (2.0 mL, 17.54 mmol) gave **5.53** (27 mg) as a yellow solid. Compound **5.53** was used as such for next reaction without further purification. HRMS calculated for $C_{23}H_{21}N_4O_5$ $[M - H]^-$, 433.1517; found, 433.1498.

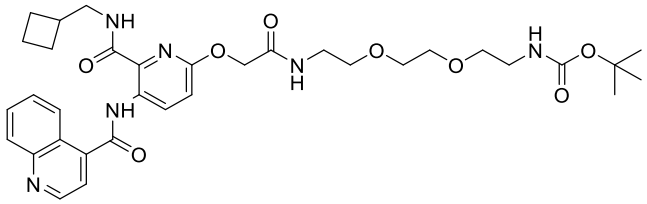

***tert*-Butyl *N*-[2-(2-{2-[2-({6-[(cyclobutylmethyl)carbamoyl]-5-(quinoline-4-amido)pyridin-2-yl}oxy)acetamido]ethoxy}ethoxy)ethyl]carbamate (5.54)**

According to the procedure described for **5.27**, **5.53** (22 mg, 0.05 mmol) was reacted with **2.12** (18 mg, 0.07 mmol), HBTU (19 mg, 0.05 mmol) and DIPEA (30 µL, 0.15 mmol). Purification of the crude compound by silica gel column chromatography (eluting with 50% EtOAc/hexane to 5% MeOH/EtOAc) gave **5.54** (21 mg, 0.03 mmol, 62%) as a colourless solid. ^{1}H NMR (400 MHz, $CDCl_3$) δ 1.44 (s, 9H, C(C**H**$_3$)$_3$), 1.69 – 1.81 (m, 2H, CH_2 cyclobutane), 1.85 – 1.97 (m, 2H, CH_2 cyclobutane), 2.06 – 2.15 (m, 2H, CH_2 cyclobutane), 2.54 – 2.65 (m, 1H, NHCH$_2$C**H**), 3.25 – 3.36 (m, 2H, CH_2), 3.38 – 3.45 (m, 2H, NHC**H**$_2$, cyclobutane), 3.47 – 3.65 (m, 10H, 5 × C**H**$_2$), 4.75 (s, 2H, OCH$_2$CO), 5.00 (br s, 1H, NH), 6.76 (br s, 1H, NH), 7.14 (d, 1H, *J* = 9.1 Hz, ArH pyridine), 7.60 – 7.67 (m, 1H, ArH quinoline), 7.71 (d, 1H, *J* = 4.4 Hz, ArH quinoline), 7.75 – 7.83 (m, 1H, ArH quinoline), 8.02 – 8.12 (m, 1H, NH), 8.18 (d, 1H, *J* = 8.5 Hz, ArH quinoline), 8.46 (d, 1H, *J* = 8.5 Hz, ArH quinoline), 9.05 (d, 1H, *J* = 4.4 Hz, ArH quinoline), 9.38 (d, 1H, *J* = 9.1 Hz, ArH pyridine), 12.89 (s, 1H, NH). ^{13}C NMR (101 MHz, $CDCl_3$) δ 18.40, 25.81, 28.56, 34.95, 44.72, 66.29, 69.83, 70.21, 70.42, 115.64, 118.84, 124.74, 125.56, 127.97, 130.03, 130.22, 133.73, 141.45, 149.04, 150.23, 166.14, 166.77. HRMS calculated for $C_{34}H_{44}N_6NaO_8$ $[M + Na]^+$, 687.3113; found, 687.3124. Analytical RP-HPLC Rt = 16.38 min; determined with HPLC method B.

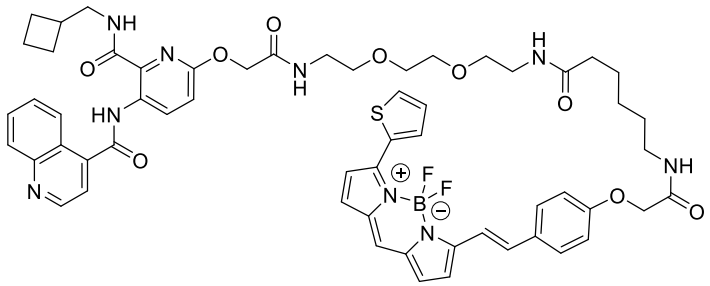

4-[(*E*)-2-(4-{[(5-{[2-(2-{2-[2-({6-[(Cyclobutylmethyl)carbamoyl]-5-(quinoline-4-amido)pyridin-2-yl}oxy)acetamido]ethoxy}ethoxy)ethyl]carbamoyl}pentyl)carbamoyl]methoxy}phenyl)ethenyl]-2,2-difluoro-12-(thiophen-2-yl)-1λ^5-aza-3λ^4-aza-2λ^4-boratricyclo[7.3.0.0^{3,7}]dodeca-1(12),4,6,8,10-pentaen-1-ylium-3-ide (5.55)

Following the procedure described for **5.36**, **5.54** (3.0 mg, 4.51 µmol) was reacted with TFA (0.5 mL) to give *N*-{6-[({2-[2-(2-aminoethoxy)ethoxy]ethyl}carbamoyl)methoxy]-2-[(cyclobutylmethyl) carbamoyl]pyridin-3-yl}quinoline-4-carboxamide trifluoroacetate salt in assumed quantitative yield as yellow solid. This trifluoroacetate salt was purified using semi-preparative RP-HPLC. Reaction of this purified trifluoroacetate salt (3.1 mg, 4.56 µmol) with BODIPY-630/650-SE (1.0 mg, 1.51 µmol) gave **5.55** (1.89 mg, 1.70 µmol, quantitative) as a dark blue solid. HRMS calculated for $C_{58}H_{62}BF_2N_9NaO_9S$ $[M + Na]^+$, 1132.4354; found, 1132.4330. Analytical RP-HPLC Rt = 19.37 min; determined with HPLC method B.

7.5.2 Computational studies

Docking studies were carried out using GOLD[217] (version 5.5; ChemPLP scoring method, default settings) using crystal structure of CB_1R (PDB ID: 5XRA) published by Hua *et al.*[113]. The ligand **5.3** was drawn with MarvinSketch[225224224224] (version 16.10). The lowest energy conformation of **5.3** (was obtained from a conformational search carried out with MarvinSketch (using Merck Molecular ForceField – MMFF94 with default settings (optimization limit strict, maximum number of conformers 10) and option "return only the lowest conformation found" selected), shown in Figure 5.1, chapter 5) was used for docking studies with and without restricting the bonds from rotation. The Cambridge Structural Database (CSD[173]; version 5.38 November 2016 + 2 updates) was searched using ConQuest (version 1.19) for three-dimensional structures of compounds similar to 5.3 using substructure queries shown in chapter 5, Figure 5.2. The binding site in the receptor was defined as the 15 Å region around the CB_1R co-crystallised ligand AM11542 (PDB ID: 5XRA) in the docking studies. Docking poses were visualised with PyMOL (The PyMOL Molecular Graphics System, version 2.0.3 Schrödinger, LLC.).

7.5.3 Pharmacological studies

Radioligand binding assays and cAMP functional assays were carried out as described in section 7.1.2. In the radioligand binding assay, [^{3}H]-CP55,940 was used in a concentration of 0.75 nM per well for determining the CB_1R affinity and 0.5 nM per well for determining the CB_2R affinity of test compounds. Both CB_1R and CB_2R membrane preparations were used at a concentration of 3.0 μg per well.

Appendix

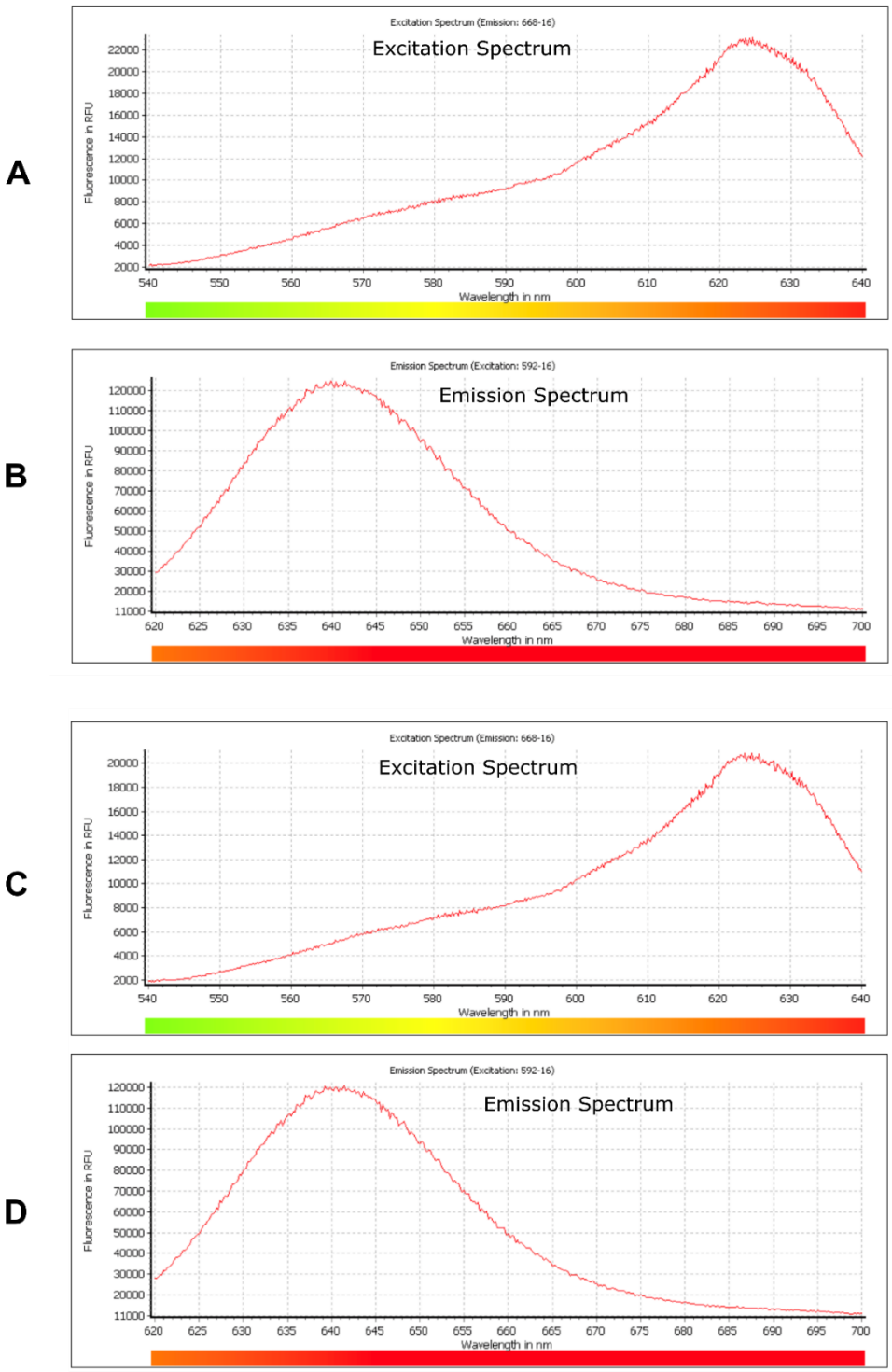

Figure A.1 Representative excitation and emission spectra: Panel (A-B) – Fluorescent ligand **2.38** (chapter 2, section 2.2.2) and Panel (C-D) – **2.37** (chapter 2, section 2.2.2). Data is generated by members of the Professor Stephen Hill's group at the University of Nottingham.

NMR spectra of (benzimidazolyl)isoquinolinol 2.26

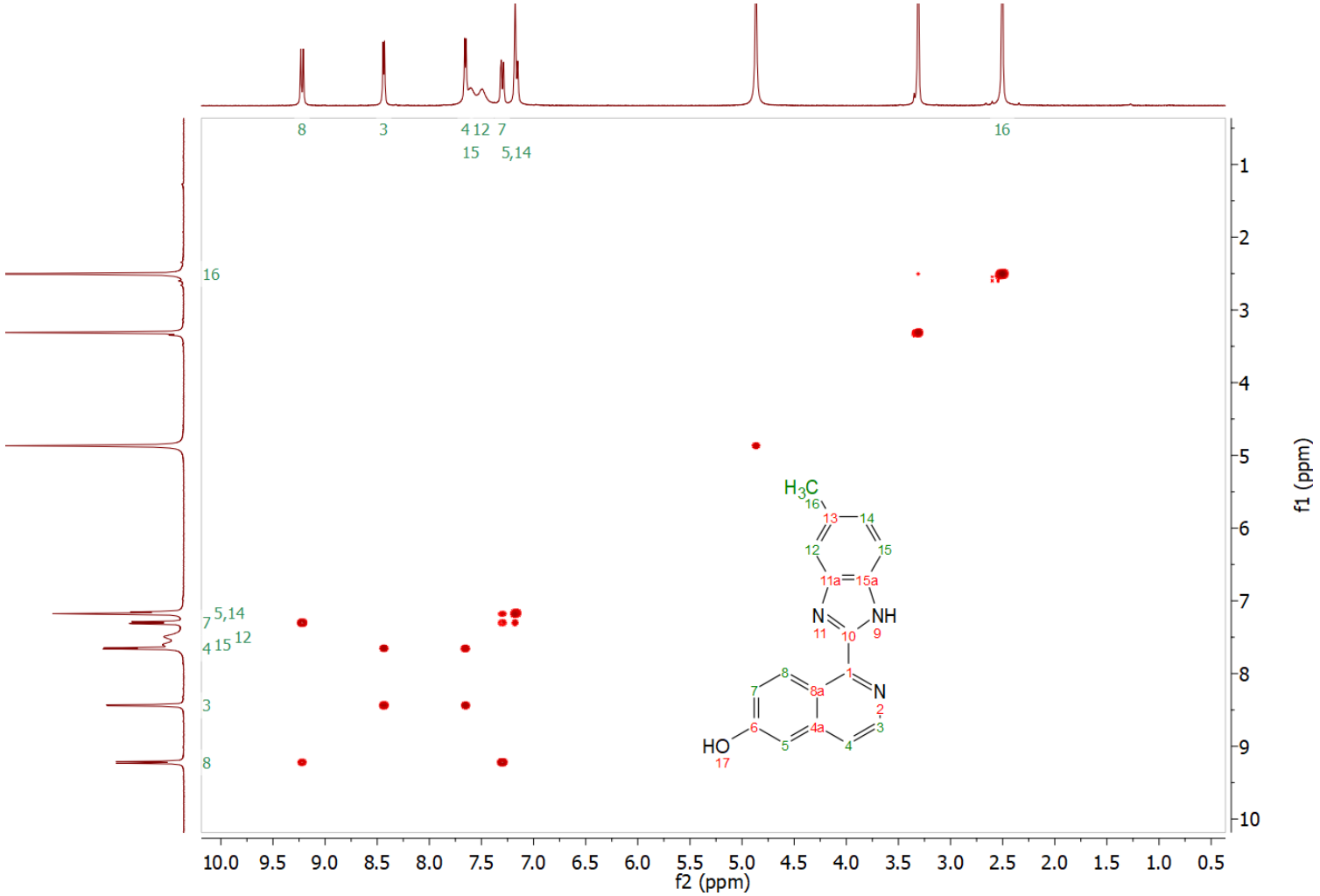

Figure A.2 gCOSY spectrum of **2.26** in MeOD-d_4 at 25 °C.

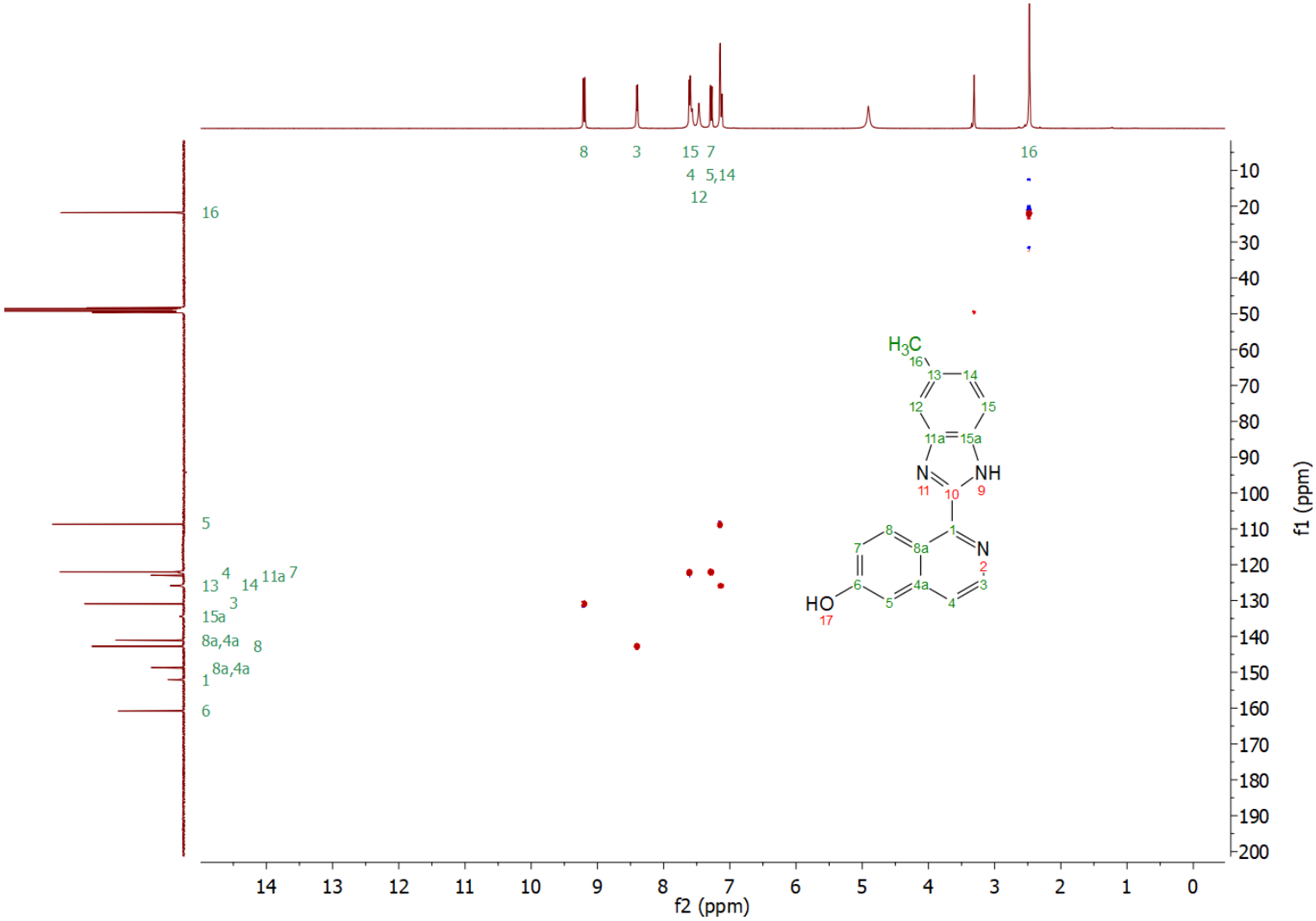

Figure A.3 gHSQC spectrum of **2.26** in MeOD-d_4 at 25 °C.

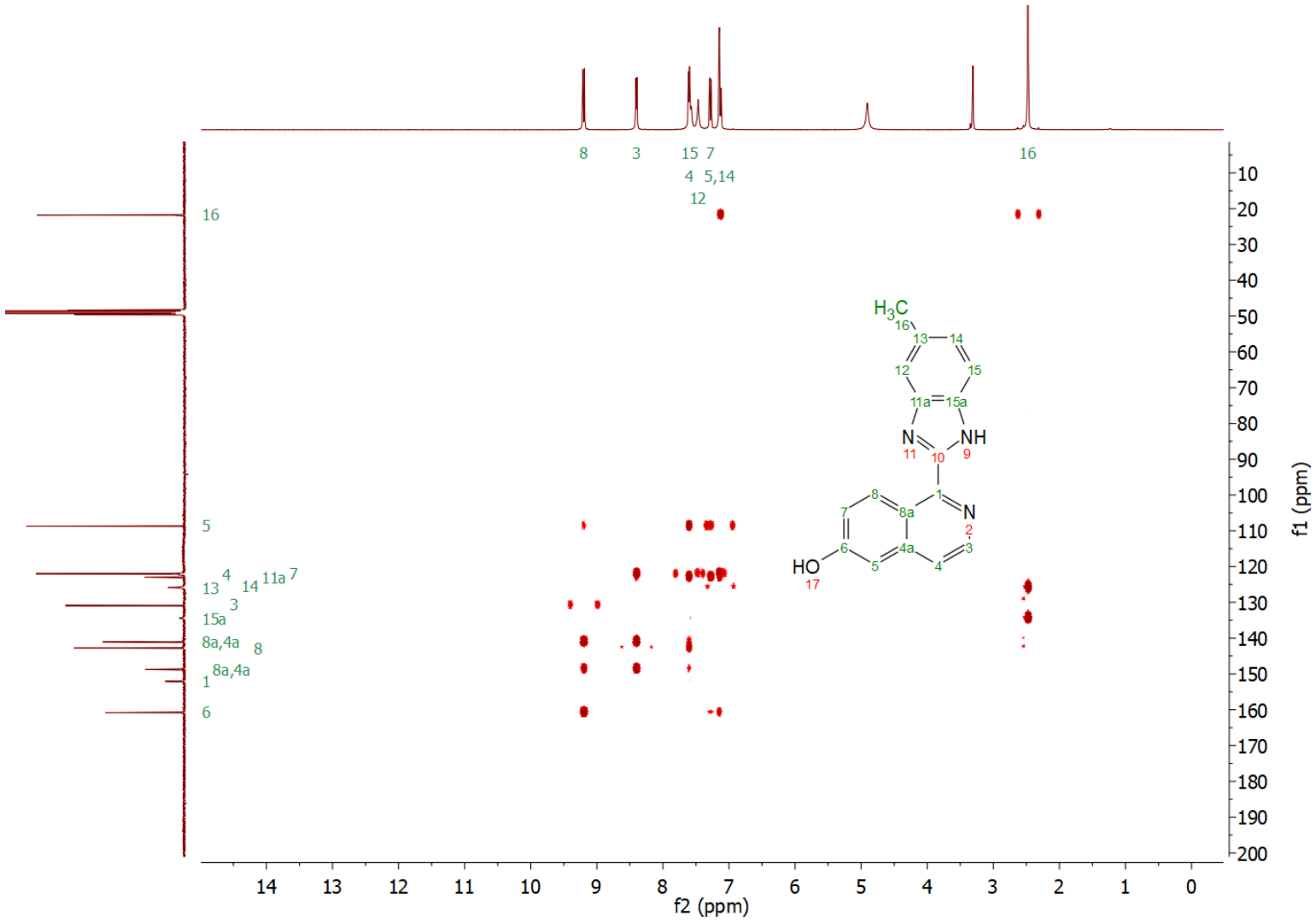

Figure A.4 gHMBC spectrum of **2.26** in MeOD-d_4 at 25 °C.

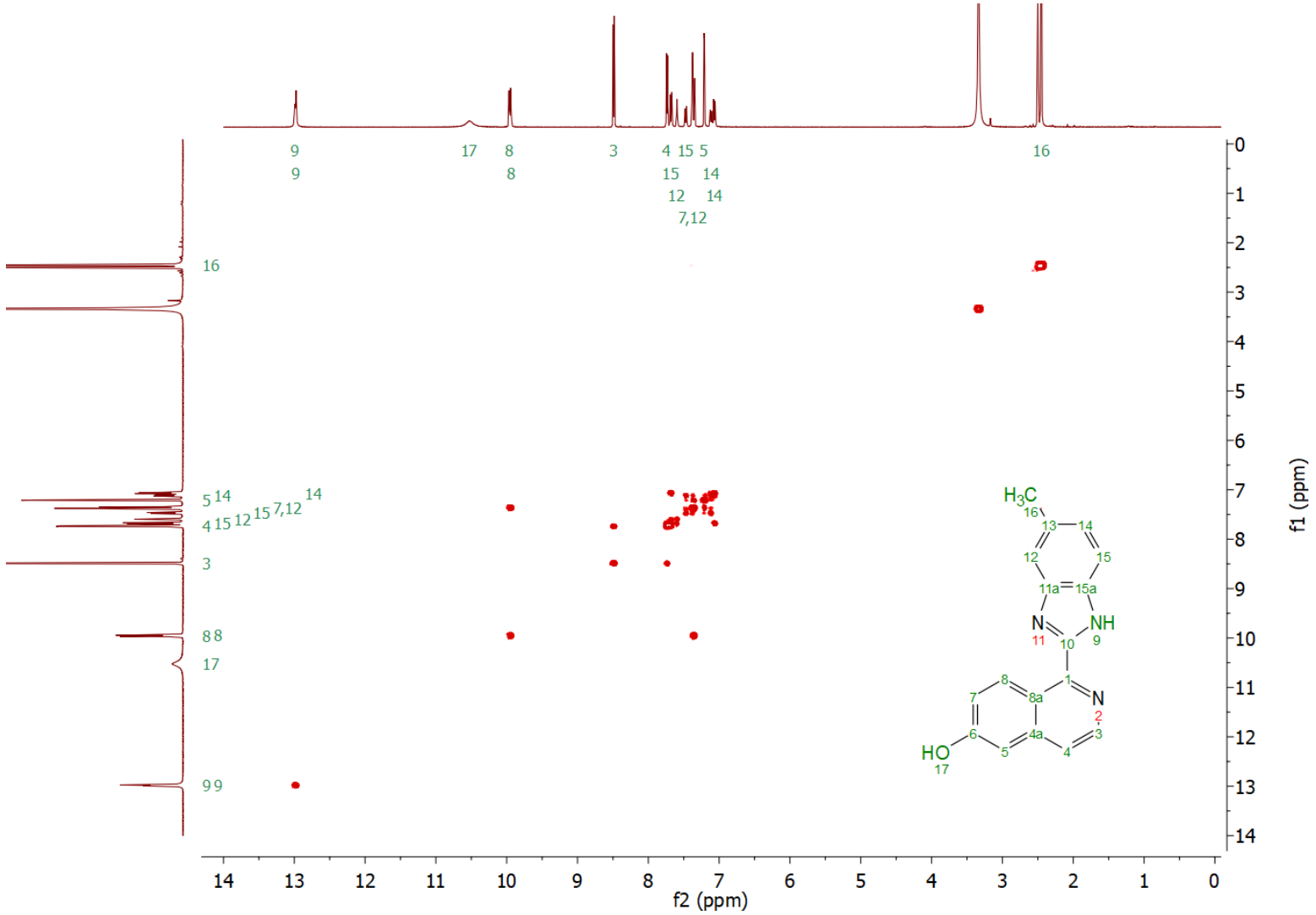

Figure A.5 gCOSY spectrum of **2.26** in DMSO-d_6 at 25 °C.

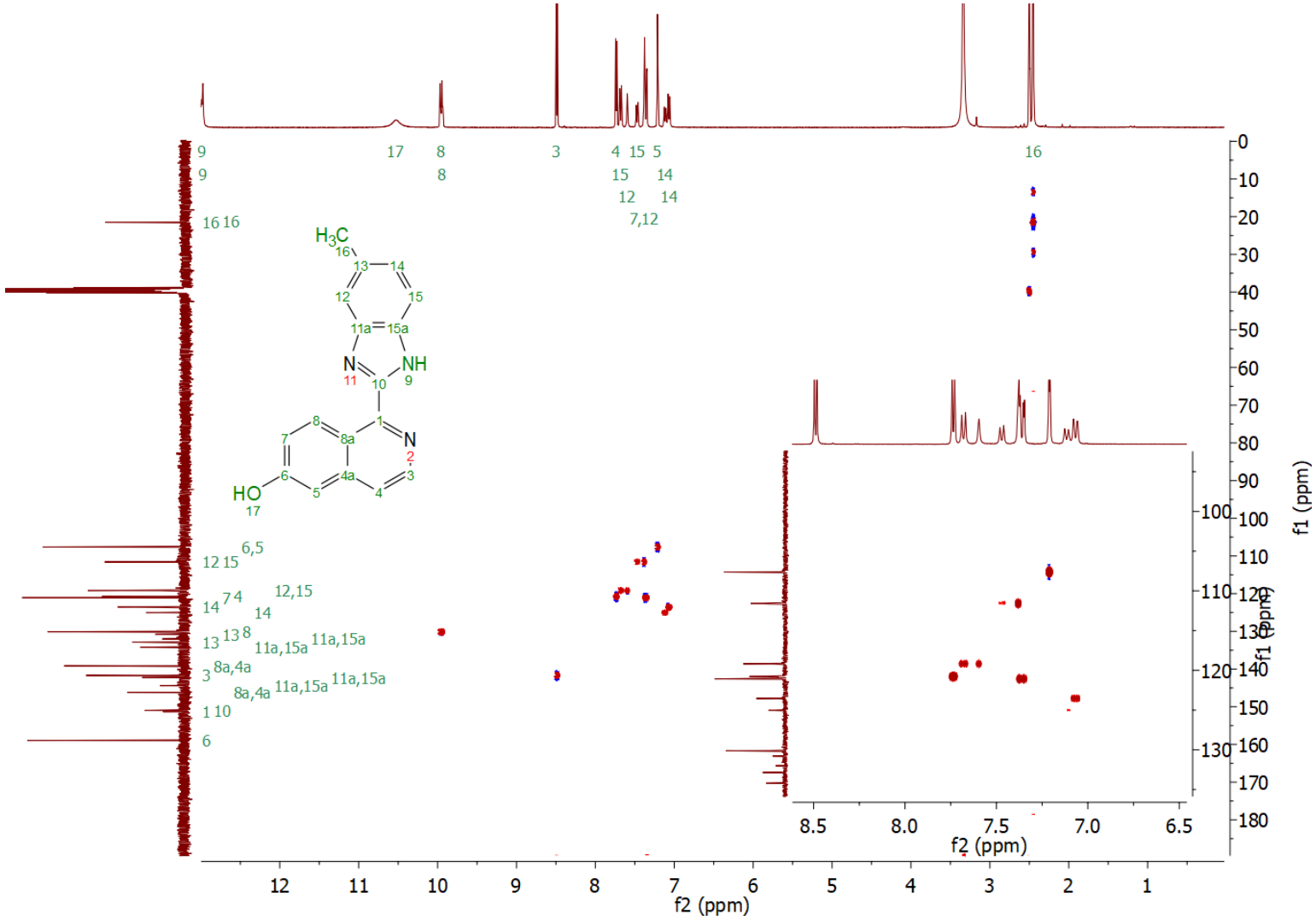

Figure A.6 gHSQC spectrum (inset shows aromatic region) of **2.26** in DMSO-d_6 at 25 °C.

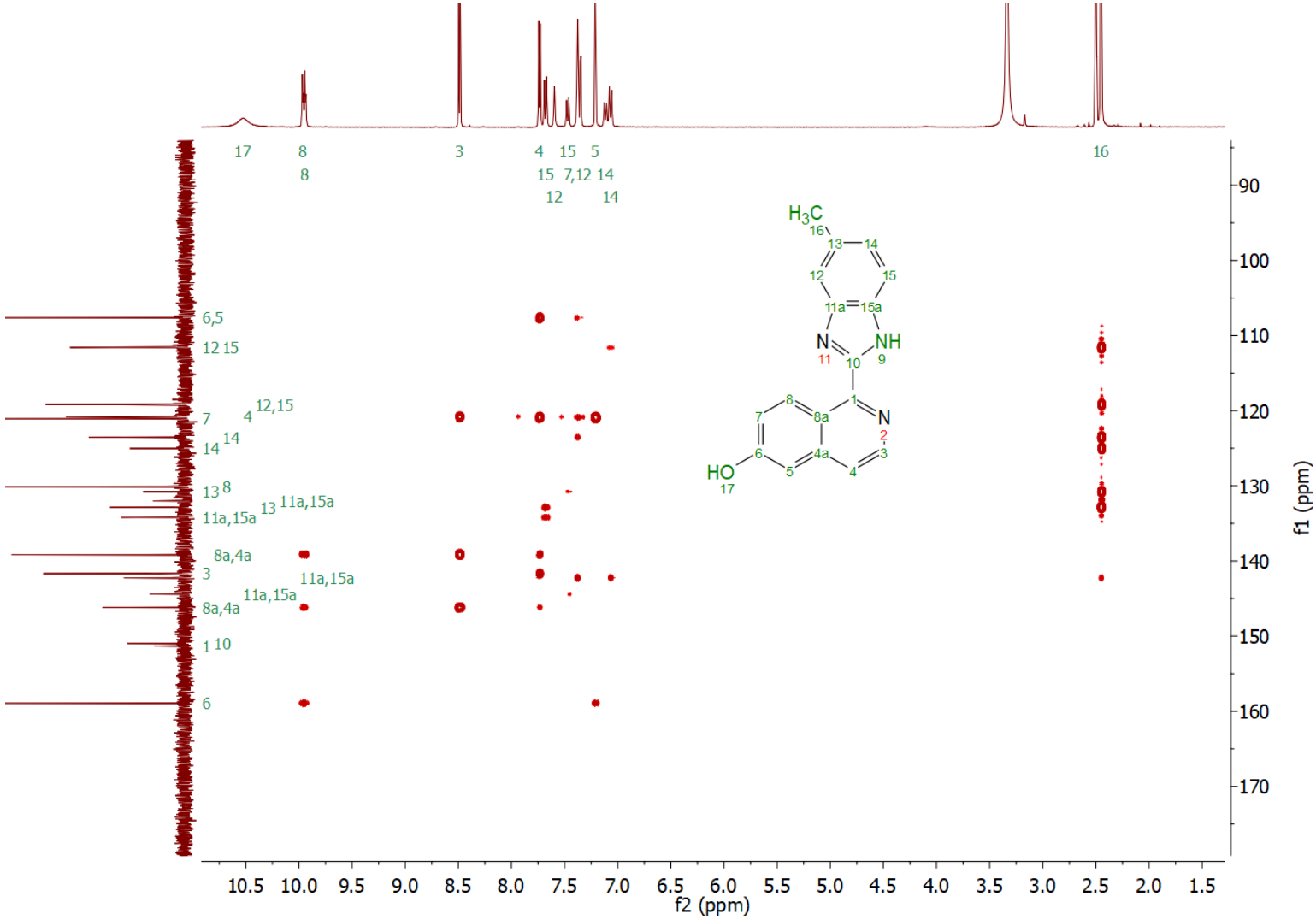

Figure A.7 gHMBC spectrum of **2.26** in DMSO-d_6 at 25 °C.

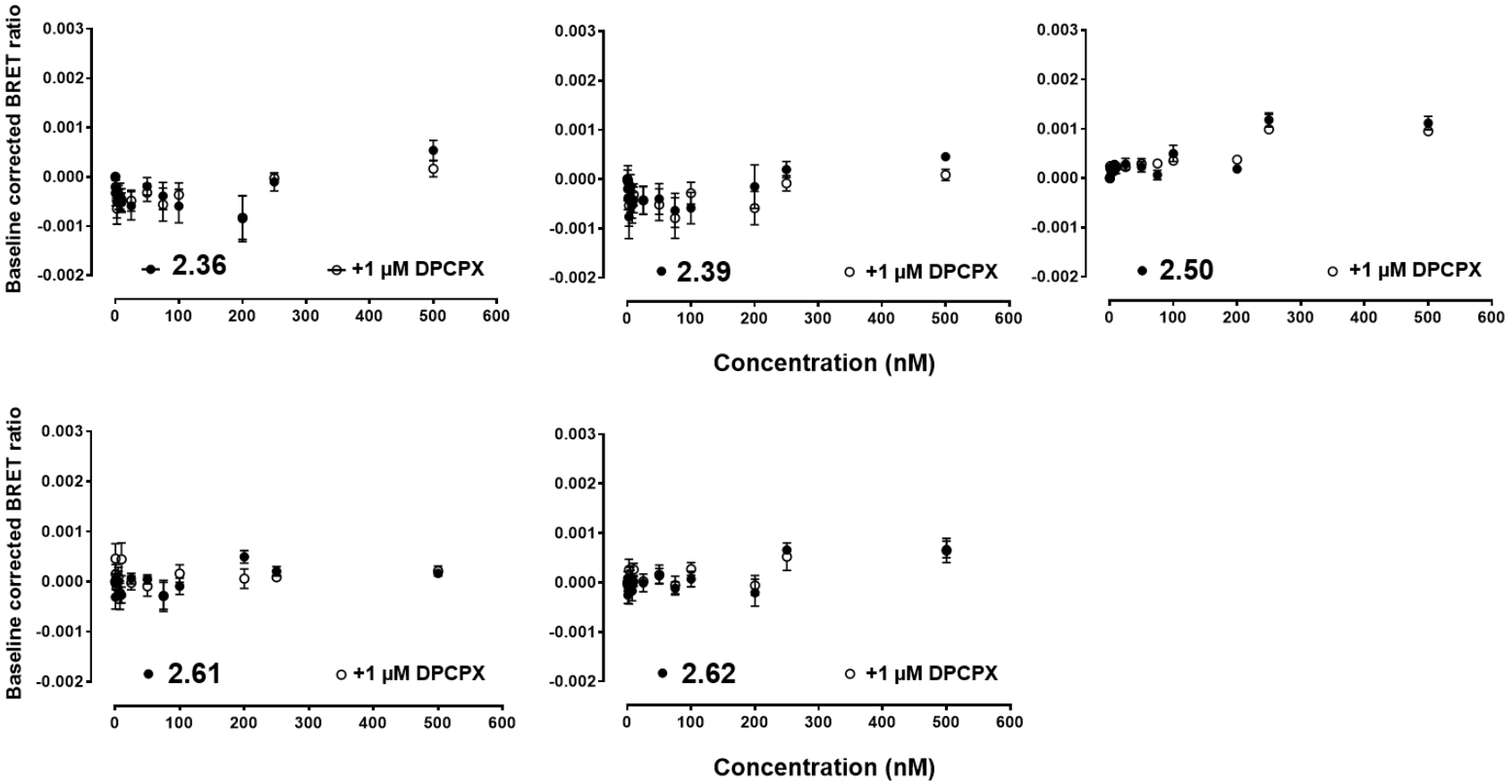

Figure A.8 HEK-293 cells stably transfected with *N*-terminally NLuc-labelled hA_1AR were treated with increasing concentrations of fluorescent ligand and the BRET ratio measured after direct addition of the NLuc substrate furimazine (10µM).[90] Non-specific binding was assessed in the absence and presence of 1µM DPCPX. Pooled raw BRET ratio's were baseline corrected (minus vehicle + furimazine BRET ratios) with data expressed as fold increase in BRET ratios over basal. Data represents five - seven independent experiments (in triplicate) and is expressed as mean ± SEM. Data is generated by members of the Professor Stephen Hill's group at the University of Nottingham.

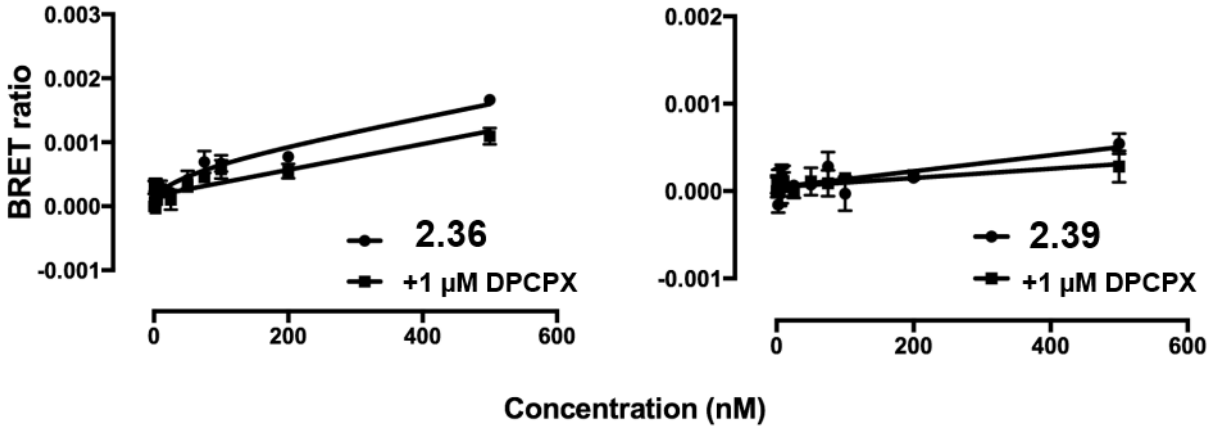

Figure A.9 HEK-293 cells stably transfected with *N*-terminally NLuc-labelled hA_3AR were treated with increasing concentrations of fluorescent ligand and the BRET ratio measured after direct addition of the NLuc substrate furimazine (10µM).[90] Non-specific binding was assessed in the absence and presence of 1µM MRS1220. Pooled raw BRET ratio's were baseline corrected (minus vehicle + furimazine BRET ratios) with data expressed as fold increase in BRET ratios over basal. Data represents five - seven independent experiments (in triplicate) and is expressed as mean ± SEM. Data generated by members of the Professor Stephen Hill's group at the University of Nottingham.

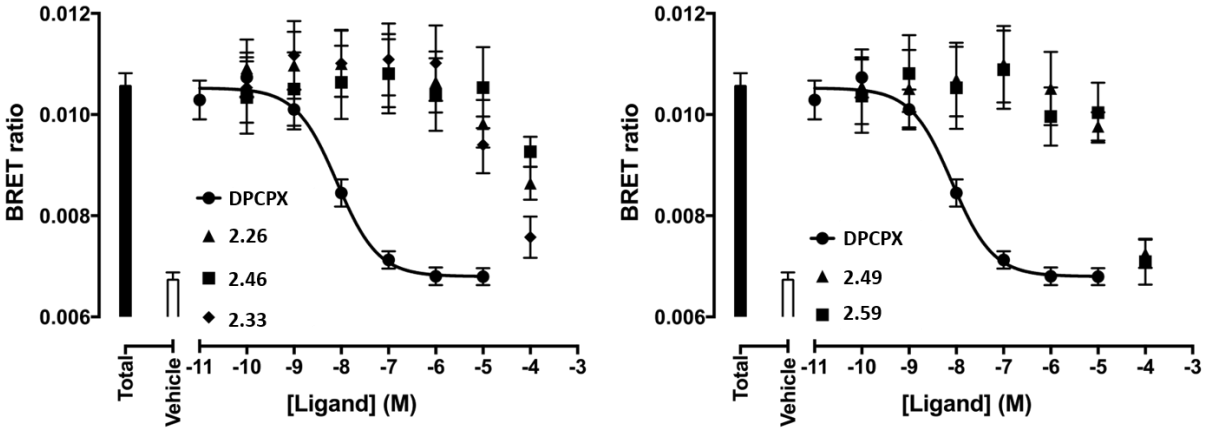

Figure A.10 HEK-293 cells stably expressing *N*-terminal NLuc tagged hA_1AR were co-incubated with a fixed concentration of CA200645 (25nM) and increasing concentrations of unlabelled ligand (1h at 37°C). The A_1AR selective antagonist DPCPX was included as a positive control. Total CA200645 binding and vehicle are shown by the black and white bars respectively. Data was pooled from five independent experiments and is expressed as mean ± SEM. Data generated by members of the Professor Stephen Hill's group at the University of Nottingham.

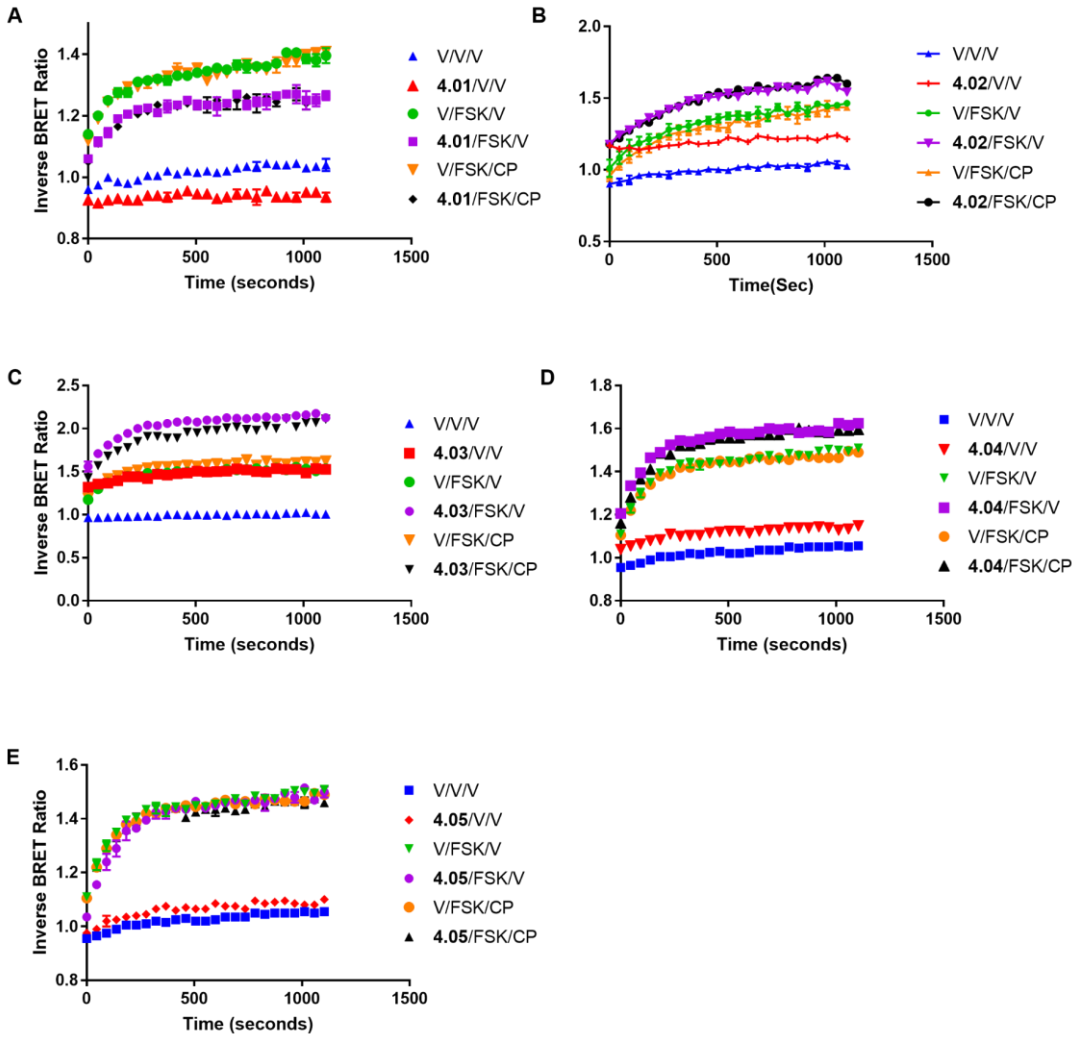

Figure A.11 cAMP BRET assay screen of fluorescent ligands (at 10 μM) – **4.01** panel A, **4.02** panel B, **4.03** panel C, **4.04** panel D, and **4.05** panel E at WT HEK-293 cells. Data is representative of a single experiment carried in duplicate and is expressed as mean ± SEM. CP (CP55,940), FSK (Forskolin), V (Vehicle).

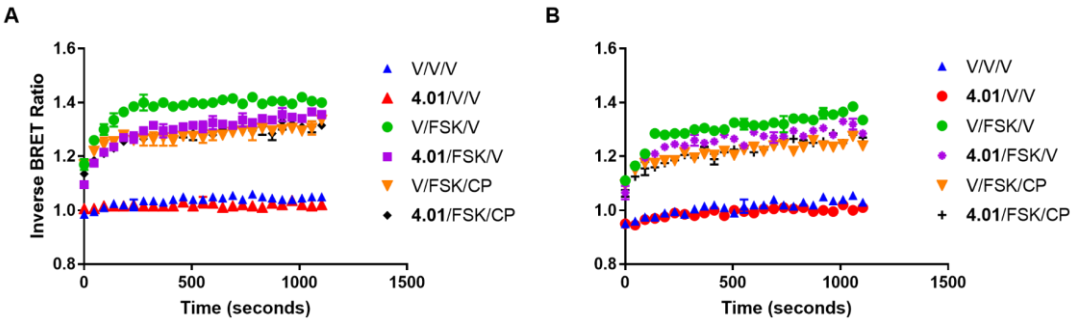

Figure A.12 cAMP BRET assay screen of fluorescent ligands **4.01** (3 μM) panel A and (1 μM) panel B at HEK-293 cells stably expressing hCB_2R. Data is representative of a single experiment carried in duplicate and is expressed as mean ± SEM. CP (CP55,940), FSK (Forskolin), V (vehicle).

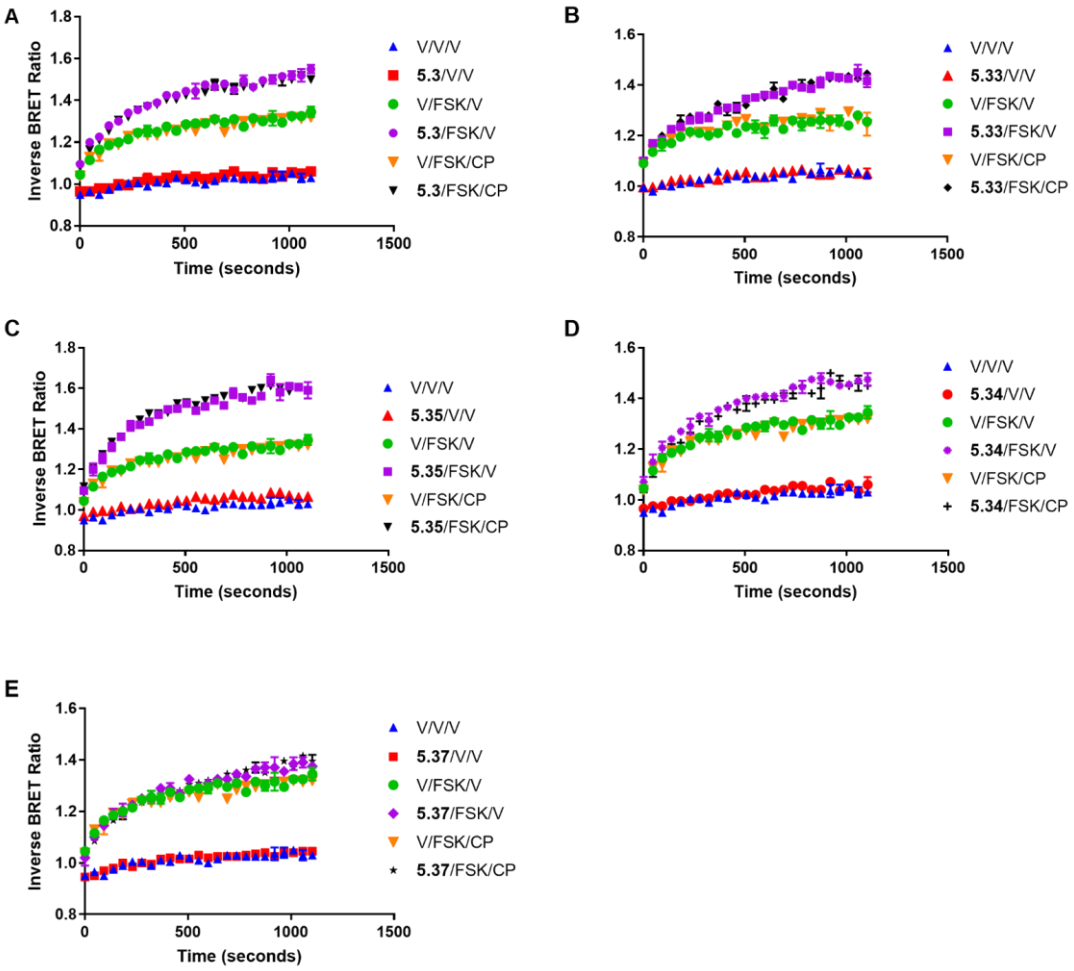

Figure A.13 cAMP BRET assay screen of **5.3** (10 μM) panel A, **5.33** (10 μM) panel B, **5.35** (10 μM) panel C, **5.34** (10 μM) panel D, and **5.37** (10 μM) panel E at WT HEK-293 cells. Data is representative of a single experiment carried in duplicate and is expressed as mean ± SEM. CP (CP55,940), FSK (Forskolin), V (vehicle).

References

1. Hauser, A. S.; Attwood, M. M.; Rask-Andersen, M.; Schiöth, H. B.; Gloriam, D. E., Trends in GPCR drug discovery: new agents, targets and indications. *Nat. Rev. Drug Discov* **2017,** *16*, 829-842.
2. Brian, K., The Structural Basis of G-Protein-Coupled Receptor Signaling (Nobel Lecture). *Angew. Chem. Int. Ed.* **2013,** *52* (25), 6380-6388.
3. Pándy-Szekeres, G.; Munk, C.; Tsonkov, T. M.; Mordalski, S.; Harpsøe, K.; Hauser, A. S.; Bojarski, A. J.; Gloriam, D. E., GPCRdb in 2018: adding GPCR structure models and ligands. *Nucleic Acids Res.* **2018,** *46* (D1), D440-D446.
4. Kobilka, B. K., G protein coupled receptor structure and activation. *Biochim. Biophys. Acta* **2007,** *1768* (4), 794-807.
5. Poms, M.; Ansorge, P.; Martinez-Gil, L.; Jurt, S.; Gottstein, D.; Fracchiolla, K. E.; Cohen, L. S.; Güntert, P.; Mingarro, I.; Naider, F., NMR Investigation of Structures of G-protein Coupled Receptor Folding Intermediates. *J. Biol. Chem.* **2016,** *291* (53), 27170-27186.
6. Liang, Y.-L.; Khoshouei, M.; Radjainia, M.; Zhang, Y.; Glukhova, A.; Tarrasch, J.; Thal, D. M.; Furness, S. G. B.; Christopoulos, G.; Coudrat, T.; Danev, R.; Baumeister, W.; Miller, L. J.; Christopoulos, A.; Kobilka, B. K.; Wootten, D.; Skiniotis, G.; Sexton, P. M., Phase-plate cryo-EM structure of a class B GPCR–G-protein complex. *Nature* **2017,** *546*, 118-123.
7. Liang, Y.-L.; Khoshouei, M.; Glukhova, A.; Furness, S. G. B.; Zhao, P.; Clydesdale, L.; Koole, C.; Truong, T. T.; Thal, D. M.; Lei, S.; Radjainia, M.; Danev, R.; Baumeister, W.; Wang, M.-W.; Miller, L. J.; Christopoulos, A.; Sexton, P. M.; Wootten, D., Phase-plate cryo-EM structure of a biased agonist-bound human GLP-1 receptor–Gs complex. *Nature* **2018,** *555*, 121-125.
8. Draper-Joyce, C. J.; Khoshouei, M.; Thal, D. M.; Liang, Y.-L.; Nguyen, A. T. N.; Furness, S. G. B.; Venugopal, H.; Baltos, J.-A.; Plitzko, J. M.; Danev, R.; Baumeister, W.; May, L. T.; Wootten, D.; Sexton, P. M.; Glukhova, A.; Christopoulos, A., Structure of the adenosine-bound human adenosine A1 receptor–Gi complex. *Nature* **2018,** *558*, 559-563.
9. Hanlon, C. D.; Andrew, D. J., Outside-in signaling – a brief review of GPCR signaling with a focus on the *Drosophila* GPCR family. *J. Cell Sci.* **2015,** *128* (19), 3533-3542.
10. Hilger, D.; Masureel, M.; Kobilka, B. K., Structure and dynamics of GPCR signaling complexes. *Nat. Struct. Mol. Biol.* **2018,** *25* (1), 4-12.
11. Rasmussen, S. G. F.; Choi, H.-J.; Fung, J. J.; Pardon, E.; Casarosa, P.; Chae, P. S.; DeVree, B. T.; Rosenbaum, D. M.; Thian, F. S.; Kobilka, T. S.; Schnapp, A.; Konetzki, I.; Sunahara, R. K.; Gellman, S. H.; Pautsch, A.; Steyaert, J.; Weis, W. I.; Kobilka, B. K., Structure of a nanobody-stabilized active state of the β2 adrenoceptor. *Nature* **2011,** *469*, 175-181.
12. Ranjan, R.; Dwivedi, H.; Baidya, M.; Kumar, M.; Shukla, A. K., Novel Structural Insights into GPCR–β-Arrestin Interaction and Signaling. *Trends Cell Biol.* **2017,** *27* (11), 851-862.
13. DeWire, S. M.; Ahn, S.; Lefkowitz, R. J.; Shenoy, S. K., β-Arrestins and Cell Signaling. *Annu. Rev. Physiol.* **2007,** *69* (1), 483-510.
14. Reiter, E.; Ayoub, M. A.; Pellissier, L. P.; Landomiel, F.; Musnier, A.; Tréfier, A.; Gandia, J.; De Pascali, F.; Tahir, S.; Yvinec, R.; Bruneau, G.; Poupon, A.;

Crépieux, P., β-arrestin signalling and bias in hormone-responsive GPCRs. *Mol. Cell. Endocrinol.* **2017,** *449*, 28-41.
15. Shenoy, S. K.; Lefkowitz, R. J., β-arrestin-mediated receptor trafficking and signal transduction. *Trends Pharmacol. Sci.* **2011,** *32* (9), 521-533.
16. Kenakin, T.; Christopoulos, A., Signalling bias in new drug discovery: detection, quantification and therapeutic impact. *Nat. Rev. Drug Discov* **2012,** *12*, 205-216.
17. Manglik, A.; Lin, H.; Aryal, D. K.; McCorvy, J. D.; Dengler, D.; Corder, G.; Levit, A.; Kling, R. C.; Bernat, V.; Hübner, H.; Huang, X.-P.; Sassano, M. F.; Giguère, P. M.; Löber, S.; Da, D.; Scherrer, G.; Kobilka, B. K.; Gmeiner, P.; Roth, B. L.; Shoichet, B. K., Structure-based discovery of opioid analgesics with reduced side effects. *Nature* **2016,** *537*, 185.
18. Rob, H.; Alex, D.; Alex, C.; Katy, S.; William, D.; Stephen, H.; Chris, B.; Eamonn, K.; Graeme, H., The novel μ-opioid receptor agonist PZM21 depresses respiration and induces tolerance to antinociception. *Br. J. Pharmacol* **2018,** *175* (13), 2653-2661.
19. Irannejad, R.; Tomshine, J. C.; Tomshine, J. R.; Chevalier, M.; Mahoney, J. P.; Steyaert, J.; Rasmussen, S. G. F.; Sunahara, R. K.; El-Samad, H.; Huang, B.; von Zastrow, M., Conformational biosensors reveal GPCR signalling from endosomes. *Nature* **2013,** *495*, 534-540.
20. Irannejad, R.; Pessino, V.; Mika, D.; Huang, B.; Wedegaertner, P. B.; Conti, M.; von Zastrow, M., Functional selectivity of GPCR-directed drug action through location bias. *Nat. Chem. Biol.* **2017,** *13*, 799-807.
21. Gomes, I.; Ayoub, M. A.; Fujita, W.; Jaeger, W. C.; Pfleger, K. D. G.; Devi, L. A., G Protein–Coupled Receptor Heteromers. *Annu. Rev. Pharmacool. Toxicol.* **2016,** *56* (1), 403-425.
22. Foster, D. J.; Conn, P. J., Allosteric modulation of GPCRs: new insights and potential utility for treatment of schizophrenia and other CNS disorders. *Neuron* **2017,** *94* (3), 431-446.
23. Lewis, J. A.; Lebois, E. P.; Lindsley, C. W., Allosteric modulation of kinases and GPCRs: design principles and structural diversity. *Curr. Opin. Chem. Biol.* **2008,** *12* (3), 269-280.
24. Vernall, Andrea J.; Hill, Stephen J.; Kellam, B., The evolving small-molecule fluorescent-conjugate toolbox for Class A GPCRs. *Br. J. Pharmacol* **2014,** *171* (5), 1073-1084.
25. Cooper, A.; Singh, S.; Hook, S.; Tyndall, J. D. A.; Vernall, A. J., Chemical Tools for Studying Lipid-Binding Class A G Protein–Coupled Receptors. *Pharmacol. Rev.* **2017,** *69* (3), 316-353.
26. Ceccarini, J.; De Hert, M.; Van Winkel, R.; Peuskens, J.; Bormans, G.; Kranaster, L.; Enning, F.; Koethe, D.; Leweke, F. M.; Van Laere, K., Increased ventral striatal CB1 receptor binding is related to negative symptoms in drug-free patients with schizophrenia. *NeuroImage* **2013,** *79*, 304-312.
27. Ceccarini, J.; Ahmad, R.; Van de Vliet, L.; Casteels, C.; Vandenbulcke, M.; Vandenberghe, W.; Van Laere, K., CB1R PET in premanifest and manifest Huntington's disease is related to disease onset and disease burden. *J. Nucl. Med.* **2016,** *57* (supplement 2), 20-20.
28. Ahmad, R.; Goffin, K.; Van den Stock, J.; De Winter, F.-L.; Cleeren, E.; Bormans, G.; Tournoy, J.; Persoons, P.; Van Laere, K.; Vandenbulcke, M., In vivo type 1 cannabinoid receptor availability in Alzheimer's disease. *Eur. Neuropsychopharmacol.* **2014,** *24* (2), 242-250.

29. Flanagan, C. A., Chapter 10 - GPCR-radioligand binding assays. In *Methods Cell Biol.*, K. Shukla, A., Ed. Academic Press: 2016; Vol. 132, pp 191-215.
30. Klotz, K. N.; Hessling, J.; Hegler, J.; Owman, C.; Kull, B.; Fredholm, B. B.; Lohse, M. J., Comparative pharmacology of human adenosine receptor subtypes – characterization of stably transfected receptors in CHO cells. *Naunyn-Schmiedeberg's Arch. Pharmacol.* **1997,** *357* (1), 1-9.
31. Bouaboula, M.; Bourrié, B.; Rinaldi-Carmona, M.; Shire, D.; Le Fur, G.; Casellas, P., Stimulation of cannabinoid receptor CB1 induces krox-24 expression in human astrocytoma cells. *J. Biol. Chem.* **1995,** *270* (23), 13973-13980.
32. Felder, C. C.; Joyce, K. E.; Briley, E. M.; Mansouri, J.; Mackie, K.; Blond, O.; Lai, Y.; Ma, A. L.; Mitchell, R. L., Comparison of the pharmacology and signal transduction of the human cannabinoid CB1 and CB2 receptors. *Mol. Pharmacol.* **1995,** *48* (3), 443-450.
33. Fichna, J.; Bawa, M.; Thakur, G. A.; Tichkule, R.; Makriyannis, A.; McCafferty, D.-M.; Sharkey, K. A.; Storr, M., Cannabinoids alleviate experimentally induced intestinal inflammation by acting at central and peripheral receptors. *PLoS One* **2014,** *9* (10), e109115.
34. Soethoudt, M.; Stolze, S. C.; Westphal, M. V.; van Stralen, L.; Martella, A.; van Rooden, E. J.; Guba, W.; Varga, Z. V.; Deng, H.; van Kasteren, S. I.; Grether, U.; Ijzerman, A. P.; Pacher, P.; Carreira, E. M.; Overkleeft, H. S.; Ioan-Facsinay, A.; Heitman, L. H.; van der Stelt, M., Selective Photoaffinity Probe That Enables Assessment of Cannabinoid CB2 Receptor Expression and Ligand Engagement in Human Cells. *J. Am. Chem. Soc.* **2018,** *140* (19), 6067-6075.
35. Glukhova, A.; Thal, D. M.; Nguyen, A. T.; Vecchio, E. A.; Jörg, M.; Scammells, P. J.; May, L. T.; Sexton, P. M.; Christopoulos, A., Structure of the Adenosine A1 Receptor Reveals the Basis for Subtype Selectivity. *Cell* **2017,** *168* (5), 867-877.e13.
36. Arun, K. H. S.; Kaul, C. L.; Ramarao, P., Green fluorescent proteins in receptor research: An emerging tool for drug discovery. *J. Pharmacol. Toxicol. Methods* **2005,** *51* (1), 1-23.
37. Böhme, I.; Beck-Sickinger, A. G., Illuminating the life of GPCRs. *Cell Commun Signal.* **2009,** *7* (1), 16.
38. Ciruela, F.; Vilardaga, J.-P.; Fernández-Dueñas, V., Lighting up multiprotein complexes: lessons from GPCR oligomerization. *Trends Biotechnol.* **2010,** *28* (8), 407-415.
39. Marchalant, Y.; Brownjohn, P. W.; Bonnet, A.; Kleffmann, T.; Ashton, J. C., Validating Antibodies to the Cannabinoid CB2 Receptor: Antibody Sensitivity Is Not Evidence of Antibody Specificity. *J. Histochem. Cytochem.* **2014,** *62* (6), 395-404.
40. Grimsey, N. L.; Goodfellow, C. E.; Scotter, E. L.; Dowie, M. J.; Glass, M.; Graham, E. S., Specific detection of CB1 receptors; cannabinoid CB1 receptor antibodies are not all created equal! *J. Neurosci. Methods* **2008,** *171* (1), 78-86.
41. M., M. Y.; H., D. M.; Luis, V.; Marya, S.; Marco, K.; L., H. T.; Pasko, R., Antibodies to cannabinoid type 1 receptor co-react with stomatin-like protein 2 in mouse brain mitochondria. *Eur. J. Neurosci.* **2013,** *38* (3), 2341-2348.
42. Ciruela, F.; Jacobson, K. A.; Fernández-Dueñas, V., Portraying G Protein-Coupled Receptors with Fluorescent Ligands. *ACS Chem. Biol.* **2014,** *9* (9), 1918-1928.
43. Vernall, A. J.; Stoddart, L. A.; Briddon, S. J.; Ng, H. W.; Laughton, C. A.; Doughty, S. W.; Hill, S. J.; Kellam, B., Conversion of a non-selective adenosine

receptor antagonist into A 3-selective high affinity fluorescent probes using peptide-based linkers. *Org. Biomol. Chem.* **2013,** *11* (34), 5673-5682.
44. Stoddart, L. A.; Kilpatrick, L. E.; Briddon, S. J.; Hill, S. J., Probing the pharmacology of G protein-coupled receptors with fluorescent ligands. *Neuropharmacology* **2015,** *98*, 48-57.
45. Stoddart, L. A.; White, C. W.; Nguyen, K.; Hill, S. J.; Pfleger, K. D. G., Fluorescence- and bioluminescence-based approaches to study GPCR ligand binding. *Br. J. Pharmacol* **2016,** *173* (20), 3028-3037.
46. Petrov, R. R.; Ferrini, M. E.; Jaffar, Z.; Thompson, C. M.; Roberts, K.; Diaz, P., Design and evaluation of a novel fluorescent CB2 ligand as probe for receptor visualization in immune cells. *Bioorg. Med. Chem. Lett.* **2011,** *21* (19), 5859-5862.
47. Martín-Fontecha, M.; Angelina, A.; Rückert, B.; Rueda-Zubiaurre, A.; Martín-Cruz, L.; van de Veen, W.; Akdis, M.; Ortega-Gutiérrez, S.; López-Rodríguez, M. L.; Akdis, C. A.; Palomares, O., A Fluorescent Probe to Unravel Functional Features of Cannabinoid Receptor CB1 in Human Blood and Tonsil Immune System Cells. *Bioconjugate Chem.* **2018,** *29* (2), 382-389.
48. Bruno, A.; Lembo, F.; Novellino, E.; Stornaiuolo, M.; Marinelli, L., Beyond radio-displacement techniques for Identification of CB_1 Ligands: The First Application of a Fluorescence-quenching Assay. *Sci. Rep.* **2014,** *4*.
49. Sexton, M.; Woodruff, G.; Horne, E. A.; Lin, Y. H.; Muccioli, G. G.; Bai, M.; Stern, E.; Bornhop, D. J.; Stella, N., NIR-mbc94, a fluorescent ligand that binds to endogenous CB_2 receptors and is amenable to high-throughput screening. *Chem. Biol.* **2011,** *18* (5), 563-568.
50. Fredholm, B. B.; Ijzerman, A. P.; Jacobson, K. A.; Linden, J.; Müller, C. E., International Union of Basic and Clinical Pharmacology. LXXXI. Nomenclature and Classification of Adenosine Receptors—An Update. *Pharmacol. Rev.* **2011,** *63* (1), 1-34.
51. Jacobson, K. A., Introduction to Adenosine Receptors as Therapeutic Targets. In *Adenosine Receptors in Health and Disease*, Wilson, C. N.; Mustafa, S. J., Eds. Springer Berlin Heidelberg: Berlin, Heidelberg, 2009; pp 1-24.
52. Sattin, A.; Rall, T. W., The Effect of Adenosine and Adenine Nucleotides on the Cyclic Adenosine 3',5'-Phosphate Content of Guinea Pig Cerebral Cortex Slices. *Mol. Pharmacol.* **1970,** *6* (1), 13-23.
53. Fredholm, B. B.; Ijzerman, A. P.; Jacobson, K. A.; Klotz, K.-N.; Linden, J., International Union of Pharmacology. XXV. Nomenclature and Classification of Adenosine Receptors. *Pharmacol. Rev.* **2001,** *53* (4), 527-552.
54. Sheth, S.; Brito, R.; Mukherjea, D.; Rybak, L. P.; Ramkumar, V., Adenosine receptors: expression, function and regulation. *Int. J. Mol. Sci.* **2014,** *15* (2), 2024-2052.
55. Chen, J.-F.; Eltzschig, H. K.; Fredholm, B. B., Adenosine receptors as drug targets — what are the challenges? *Nat. Rev. Drug Discov* **2013,** *12*, 265-286.
56. Ghimire, G.; Hage, F. G.; Heo, J.; Iskandrian, A. E., Regadenoson: A focused update. *J. Nucl. Cardiol* **2012**, 284-288.
57. Jacobson, M. A., Molecular biology of adenosine receptors. In *Adenosine and adenine nucleotides: from molecular biology to integrative physiology*, Springer: 1995; pp 5-13.
58. Dinh, W.; Albrecht-Küpper, B.; Gheorghiade, M.; Voors, A. A.; van der Laan, M.; Sabbah, H. N., Partial Adenosine A1 Agonist in Heart Failure. In *Heart Fail.*,

Bauersachs, J.; Butler, J.; Sandner, P., Eds. Springer International Publishing: Cham, 2017; pp 177-203.
59. Giorgi, I.; Nieri, P., Adenosine A1 modulators: a patent update (2008 to present). *Expert Opin. Ther. Patents* **2013,** *23* (9), 1109-1121.
60. Varani, K.; Vincenzi, F.; Merighi, S.; Gessi, S.; Borea, P. A., Biochemical and Pharmacological Role of A1 Adenosine Receptors and Their Modulation as Novel Therapeutic Strategy. In *Protein Reviews: Volume 19*, Atassi, M. Z., Ed. Springer Singapore: Singapore, 2017; pp 193-232.
61. Meibom, D.; Albrecht-Küpper, B.; Diedrichs, N.; Hübsch, W.; Kast, R.; Krämer, T.; Krenz, U.; Lerchen, H. G.; Mittendorf, J.; Nell, P. G., Neladenoson Bialanate Hydrochloride: A Prodrug of a Partial Adenosine A1 Receptor Agonist for the Chronic Treatment of Heart Diseases. *ChemMedChem* **2017,** *12* (10), 728-737.
62. Massie, B. M.; O'connor, C. M.; Metra, M.; Ponikowski, P.; Teerlink, J. R.; Cotter, G.; Weatherley, B. D.; Cleland, J. G.; Givertz, M. M.; Voors, A., Rolofylline, an adenosine A1− receptor antagonist, in acute heart failure. *New Engl. J. Med.* **2010,** *363* (15), 1419-1428.
63. Cheng, R. K. Y.; Segala, E.; Robertson, N.; Deflorian, F.; Doré, A. S.; Errey, J. C.; Fiez-Vandal, C.; Marshall, F. H.; Cooke, R. M., Structures of Human A1 and A2A Adenosine Receptors with Xanthines Reveal Determinants of Selectivity. *Structure* **2017,** *25* (8), 1275-1285.e4.
64. Segala, E.; Guo, D.; Cheng, R. K. Y.; Bortolato, A.; Deflorian, F.; Doré, A. S.; Errey, J. C.; Heitman, L. H.; Ijzerman, A. P.; Marshall, F. H.; Cooke, R. M., Controlling the Dissociation of Ligands from the Adenosine A2A Receptor through Modulation of Salt Bridge Strength. *J. Med. Chem.* **2016,** *59* (13), 6470-6479.
65. Jacobson, K. A.; Müller, C. E., Medicinal chemistry of adenosine, P2Y and P2X receptors. *Neuropharmacology* **2016,** *104*, 31-49.
66. Müller, C. E.; Jacobson, K. A., Recent developments in adenosine receptor ligands and their potential as novel drugs. *Biochim. Biophys. Acta* **2011,** *1808* (5), 1290-1308.
67. Jacobson, K. A.; IJzerman, A. P.; Linden, J., 1, 3-dialkylxanthine derivatives having high potency as antagonists at human A2B adenosine receptors. *Drug Dev. Res.* **1999,** *47* (1), 45-53.
68. Borrmann, T.; Hinz, S.; Bertarelli, D. C. G.; Li, W.; Florin, N. C.; Scheiff, A. B.; Müller, C. E., 1-Alkyl-8-(piperazine-1-sulfonyl)phenylxanthines: Development and Characterization of Adenosine A2B Receptor Antagonists and a New Radioligand with Subnanomolar Affinity and Subtype Specificity. *J. Med. Chem.* **2009,** *52* (13), 3994-4006.
69. Abo-Salem, O. M.; Hayallah, A. M.; Bilkei-Gorzo, A.; Filipek, B.; Zimmer, A.; Müller, C. E., Antinociceptive effects of novel A2B adenosine receptor antagonists. *J. Pharmacol. Exp. Ther.* **2004,** *308* (1), 358-366.
70. Pfister, J. R.; Belardinelli, L.; Lee, G.; Lum, R. T.; Milner, P.; Stanley, W. C.; Linden, J.; Baker, S. P.; Schreiner, G., Synthesis and Biological Evaluation of the Enantiomers of the Potent and Selective A1-Adenosine Antagonist 1,3-Dipropyl-8-[2-(5,6-epoxynorbonyl)]- xanthine. *J. Med. Chem.* **1997,** *40* (12), 1773-1778.
71. Kiesman, W. F.; Zhao, J.; Conlon, P. R.; Petter, R. C.; Jin, X.; Smits, G.; Lutterodt, F.; Sullivan, G. W.; Linden, J., Norbornyllactone-substituted xanthines as adenosine A1 receptor antagonists. *Bioorg. Med. Chem.* **2006,** *14* (11), 3654-3661.

72. Kiesman, W. F.; Zhao, J.; Conlon, P. R.; Dowling, J. E.; Petter, R. C.; Lutterodt, F.; Jin, X.; Smits, G.; Fure, M.; Jayaraj, A., Potent and orally bioavailable 8-bicyclo [2.2. 2] octylxanthines as adenosine A1 receptor antagonists. *J. Med. Chem.* **2006,** *49* (24), 7119-7131.
73. J Szentmiklosi, A.; Cseppento, A.; Gesztelyi, R.; Zsuga, J.; Kortvely, A.; Harmati, G.; P Nanasi, P., Xanthine derivatives in the heart: blessed or cursed? *Curr. Med. Chem.* **2011,** *18* (24), 3695-3706.
74. Chang, L. C.; Brussee, J.; IJzerman, A. P., Non-Xanthine Antagonists for the Adenosine A1 Receptor. *Chem. Biodivers.* **2004,** *1* (11), 1591-1626.
75. Kalk, P.; Eggert, B.; Relle, K.; Godes, M.; Heiden, S.; Sharkovska, Y.; Fischer, Y.; Ziegler, D.; Bielenberg, G. W.; Hocher, B., The adenosine A1 receptor antagonist SLV320 reduces myocardial fibrosis in rats with 5/6 nephrectomy without affecting blood pressure. *Br. J. Pharmacol* **2007,** *151* (7), 1025-1032.
76. Cosimelli, B.; Taliani, S.; Greco, G.; Novellino, E.; Sala, A.; Severi, E.; Da Settimo, F.; La Motta, C.; Pugliesi, I.; Antonioli, L.; Fornai, M.; Colucci, R.; Blandizzi, C.; Daniele, S.; Trincavelli, M. L.; Martini, C., Derivatives of Benzimidazol-2-ylquinoline and Benzimidazol-2-ylisoquinoline as Selective A(1) Adenosine Receptor Antagonists with Stimulant Activity on Human Colon Motility. *ChemMedChem* **2011,** *6* (10), 1909-1918.
77. Müller, C. E., A1-Adenosine receptor antagonists. *Expert Opin. Ther. Patents* **1997,** *7* (5), 419-440.
78. Louvel, J.; Guo, D.; Soethoudt, M.; Mocking, T. A. M.; Lenselink, E. B.; Mulder-Krieger, T.; Heitman, L. H.; Ijzerman, A. P., Structure-kinetics relationships of Capadenoson derivatives as adenosine A1 receptor agonists. *Eur. J. Med. Chem.* **2015,** *101*, 681-691.
79. Rosentreter, U.; Krämer, T.; Shimada, M.; Hübsch, W.; Diedrichs, N.; Krahn, T.; Henninger, K.; Stasch, J. P.; Wischnat, R., Substituierte 2-thio-3,5-dicyano-4-phenyl-6-aminopyridine und ihre verwendung. WO2003053441 A1. Bayer Healthcare Ag assignee. 2003.
80. Baltos, J.-A.; Vecchio, E. A.; Harris, M. A.; Qin, C. X.; Ritchie, R. H.; Christopoulos, A.; White, P. J.; May, L. T., Capadenoson, a clinically trialed partial adenosine A1 receptor agonist, can stimulate adenosine A2B receptor biased agonism. *Biochem. Pharmacol.* **2017,** *135*, 79-89.
81. Jacobson, K. A.; Ukena, D.; Padgett, W.; Kirk, K. L.; Daly, J. W., Molecular probes for extracellular adenosine receptors. *Biochem. Pharmacol.* **1987,** *36* (10), 1697-1707.
82. Kecskés, M.; Kumar, T. S.; Yoo, L.; Gao, Z.-G.; Jacobson, K. A., Novel Alexa Fluor-488 labeled antagonist of the A2A adenosine receptor: Application to a fluorescence polarization-based receptor binding assay. *Biochem. Pharmacol.* **2010,** *80* (4), 506-511.
83. Briddon, S. J.; Middleton, R. J.; Cordeaux, Y.; Flavin, F. M.; Weinstein, J. A.; George, M. W.; Kellam, B.; Hill, S. J., Quantitative analysis of the formation and diffusion of A_1-adenosine receptor-antagonist complexes in single living cells. *Proc. Natl. Acad. Sci. U. S. A.* **2004,** *101* (13), 4673-4678.
84. Kozma, E.; Kumar, T. S.; Federico, S.; Phan, K.; Balasubramanian, R.; Gao, Z.-G.; Paoletta, S.; Moro, S.; Spalluto, G.; Jacobson, K. A., Novel fluorescent antagonist as a molecular probe in A3 adenosine receptor binding assays using flow cytometry. *Biochem. Pharmacol.* **2012,** *83* (11), 1552-1561.
85. Fernández-Dueñas, V.; Taura, J. J.; Cottet, M.; Gómez-Soler, M.; López-Cano, M.; Ledent, C.; Watanabe, M.; Trinquet, E.; Pin, J.-P.; Luján, R.; Durroux, T.;

Ciruela, F., Untangling dopamine-adenosine receptor-receptor assembly in experimental parkinsonism in rats. *Dis. Model. Mech.* **2015,** *8* (1), 57-63.
86. Vernall, A. J.; Stoddart, L. A.; Briddon, S. J.; Hill, S. J.; Kellam, B., Highly potent and selective fluorescent antagonists of the human adenosine A_3 receptor based on the 1,2,4-triazolo[4,3-a]quinoxalin-1-one scaffold. *J. Med. Chem.* **2012,** *55* (4), 1771-1782.
87. Kozma, E.; Suresh Jayasekara, P.; Squarcialupi, L.; Paoletta, S.; Moro, S.; Federico, S.; Spalluto, G.; Jacobson, K. A., Fluorescent ligands for adenosine receptors. *Bioorg. Med. Chem. Lett.* **2013,** *23* (1), 26-36.
88. Köse, M.; Gollos, S.; Karcz, T.; Fiene, A.; Heisig, F.; Behrenswerth, A.; Kieć-Kononowicz, K.; Namasivayam, V.; Müller, C. E., Fluorescent-Labeled Selective Adenosine A2B Receptor Antagonist Enables Competition Binding Assay by Flow Cytometry. *J. Med. Chem.* **2018**, 4301-4316.
89. G, B. J.; Richard, M.; Luke, A.; T, M. L.; J, B. S.; Barrie, K.; J, H. S., Influence of fluorophore and linker composition on the pharmacology of fluorescent adenosine A1 receptor ligands. *Br. J. Pharmacol* **2010,** *159* (4), 772-786.
90. Stoddart, L. A.; Johnstone, E. K. M.; Wheal, A. J.; Goulding, J.; Robers, M. B.; Machleidt, T.; Wood, K. V.; Hill, S. J.; Pfleger, K. D. G., Application of BRET to monitor ligand binding to GPCRs. *Nat Meth* **2015,** *12* (7), 661-663.
91. Brand, F.; Klutz, A. M.; Jacobson, K. A.; Fredholm, B. B.; Schulte, G., Adenosine A2A receptor dynamics studied with the novel fluorescent agonist Alexa488-APEC. *Eur. J. Pharmacol.* **2008,** *590* (1), 36-42.
92. Stoddart, Leigh A.; Vernall, Andrea J.; Denman, Jessica L.; Briddon, Stephen J.; Kellam, B.; Hill, Stephen J., Fragment Screening at Adenosine-A3 Receptors in Living Cells Using a Fluorescence-Based Binding Assay. *Chem. Biol.* **2012,** *19* (9), 1105-1115.
93. Kumar, T. S.; Mishra, S.; Deflorian, F.; Yoo, L. S.; Phan, K.; Kecskés, M.; Szabo, A.; Shinkre, B.; Gao, Z.-G.; Trenkle, W.; Jacobson, K. A., Molecular probes for the A2A adenosine receptor based on a pyrazolo[4,3-e][1,2,4]triazolo[1,5-c]pyrimidin-5-amine scaffold. *Bioorg. Med. Chem. Lett.* **2011,** *21* (9), 2740-2745.
94. Macchia, M.; Salvetti, F.; Barontini, S.; Calvani, F.; Gesi, M.; Hamdan, M.; Lucacchini, A.; Pellegrini, A.; Soldani, P.; Martini, C., Fluorescent probes for adenosine receptors: Synthesis and biology of N-6-dansylaminoalkyl-substituted NECA derivatives. *Bioorg. Med. Chem. Lett.* **1998,** *8* (22), 3223-3228.
95. Macchia, M.; Salvetti, F.; Bertini, S.; Di Bussolo, V.; Gattuso, L.; Gesi, M.; Hamdan, M.; Klotz, K. N.; Laragione, T.; Lucacchini, A.; Minutolo, F.; Nencetti, S.; Papi, C.; Tuscano, D.; Martini, C., 7-nitrobenzofurazan (NBD) derivatives of 5 '-N-ethylearboxamidoadenosine (NECA) as new fluorescent probes for human A(3) adenosine receptors. *Bioorg. Med. Chem. Lett.* **2001,** *11* (23), 3023-3026.
96. Macchia, M.; Bertini, S.; Di Bussolo, V.; Manera, C.; Martini, C.; Minutolo, F.; Mori, C.; Saccomanni, G.; Tuscano, D.; Luigi Ferrarini, P., 4-[6-(Dansylamino)hexylamino]-7-methyl-2-phenyl-1,8-naphthyridine as a new potential fluorescent probe for studying A1-adenosine receptor. *Il Farmaco* **2002,** *57* (10), 783-786.
97. Middleton, R. J.; Briddon, S. J.; Cordeaux, Y.; Yates, A. S.; Dale, C. L.; George, M. W.; Baker, J. G.; Hill, S. J.; Kellam, B., New Fluorescent Adenosine A1-Receptor Agonists That Allow Quantification of Ligand−Receptor Interactions in Microdomains of Single Living Cells. *J. Med. Chem.* **2007,** *50* (4), 782-793.

98. Dale, C. L.; Hill, S. J.; Kellam, B., New potent, short-linker BODIPY-630/650[trade mark sign] labelled fluorescent adenosine receptor agonists. *MedChemComm* **2012,** *3* (3), 333-338.
99. Pacher, P.; Bátkai, S.; Kunos, G., The endocannabinoid system as an emerging target of pharmacotherapy. *Pharmacol. Rev.* **2006,** *58* (3), 389-462.
100. Katona, I.; Freund, T. F., Multiple functions of endocannabinoid signaling in the brain. *Annu. Rev. Neurosci.* **2012,** *35*, 529-558.
101. Devane, W. A.; Dysarz, F. A.; Johnson, M. R.; Melvin, L. S.; Howlett, A. C., Determination and characterization of a cannabinoid receptor in rat-brain. *Mol. Pharmacol.* **1988,** *34* (5), 605-613.
102. Matsuda, L. A.; Lolait, S. J.; Brownstein, M. J.; Young, A. C.; Bonner, T. I., Structure of a cannabinoid receptor and functional expression of the cloned cDNA. *Nature* **1990,** *346* (6284), 561-564.
103. Herkenham, M.; Lynn, A. B.; Little, M. D.; Johnson, M. R.; Melvin, L. S.; De Costa, B. R.; Rice, K. C., Cannabinoid receptor localization in brain. *Proc. Natl. Acad. Sci. U. S. A.* **1990,** *87* (5), 1932-1936.
104. Glass, M.; Dragunow, M.; Faull, R. L. M., Cannabinoid receptors in the human brain: A detailed anatomical and quantitative autoradiographic study in the fetal, neonatal and adult human brain. *Neuroscience* **1997,** *77* (2), 299-318.
105. Engeli, S.; Böhnke, J.; Feldpausch, M.; Gorzelniak, K.; Janke, J.; Bátkai, S.; Pacher, P.; Harvey-White, J.; Luft, F. C.; Sharma, A. M.; Jordan, J., Activation of the Peripheral Endocannabinoid System in Human Obesity. *Diabetes* **2005,** *54* (10), 2838-2843.
106. Bosier, B.; Muccioli, G. G.; Hermans, E.; Lambert, D. M., Functionally selective cannabinoid receptor signalling: Therapeutic implications and opportunities. *Biochem. Pharmacol.* **2010,** *80* (1), 1-12.
107. Pertwee, R. G.; Howlett, A. C.; Abood, M. E.; Alexander, S. P. H.; Di Marzo, V.; Elphick, M. R.; Greasley, P. J.; Hansen, H. S.; Kunos, G.; Mackie, K.; Mechoulam, R.; Ross, R. A., International Union of Basic and Clinical Pharmacology. LXXIX. Cannabinoid Receptors and Their Ligands: Beyond CB1 and CB2. *Pharmacol. Rev.* **2010,** *62* (4), 588-631.
108. Nogueras-Ortiz, C.; Yudowski, G. A., The Multiple Waves of Cannabinoid 1 Receptor Signaling. *Mol. Pharmacol.* **2016,** *90* (5), 620-626.
109. Nguyen, P. T.; Schmid, C. L.; Raehal, K. M.; Selley, D. E.; Bohn, L. M.; Sim-Selley, L. J., β-Arrestin2 Regulates Cannabinoid CB1 Receptor Signaling and Adaptation in a Central Nervous System Region–Dependent Manner. *Biol. Psychiatry* **2012,** *71* (8), 714-724.
110. Pacher, P.; Kunos, G., Modulating the endocannabinoid system in human health and disease–successes and failures. *The FEBS journal* **2013,** *280* (9), 1918-1943.
111. Shao, Z.; Yin, J.; Chapman, K.; Grzemska, M.; Clark, L.; Wang, J.; Rosenbaum, D. M., High-resolution crystal structure of the human CB1 cannabinoid receptor. *Nature* **2016,** *540* (7634), 602-606.
112. Hua, T.; Vemuri, K.; Pu, M.; Qu, L.; Han, G. W.; Wu, Y.; Zhao, S.; Shui, W.; Li, S.; Korde, A., Crystal structure of the human cannabinoid receptor CB 1. *Cell* **2016,** *167* (3), 750-762. e14.
113. Hua, T.; Vemuri, K.; Nikas, S. P.; Laprairie, R. B.; Wu, Y.; Qu, L.; Pu, M.; Korde, A.; Jiang, S.; Ho, J.-H.; Han, G. W.; Ding, K.; Li, X.; Liu, H.; Hanson, M. A.; Zhao, S.; Bohn, L. M.; Makriyannis, A.; Stevens, R. C.; Liu, Z.-J., Crystal structures of agonist-bound human cannabinoid receptor CB1. *Nature* **2017,** *547*, 468-471.

114. Rasmussen, S. G. F.; DeVree, B. T.; Zou, Y.; Kruse, A. C.; Chung, K. Y.; Kobilka, T. S.; Thian, F. S.; Chae, P. S.; Pardon, E.; Calinski, D.; Mathiesen, J. M.; Shah, S. T. A.; Lyons, J. A.; Caffrey, M.; Gellman, S. H.; Steyaert, J.; Skiniotis, G.; Weis, W. I.; Sunahara, R. K.; Kobilka, B. K., Crystal structure of the β2 adrenergic receptor–Gs protein complex. *Nature* **2011,** *477*, 549-557.
115. Galiègue, S.; Mary, S.; Marchand, J.; Dussossoy, D.; Carrière, D.; Carayon, P.; Bouaboula, M.; Shire, D.; Fur, G.; Casellas, P., Expression of central and peripheral cannabinoid receptors in human immune tissues and leukocyte subpopulations. *The FEBS Journal* **1995,** *232* (1), 54-61.
116. Savonenko, A. V.; Melnikova, T.; Wang, Y.; Ravert, H.; Gao, Y.; Koppel, J.; Lee, D.; Pletnikova, O.; Cho, E.; Sayyida, N., Cannabinoid CB2 receptors in a mouse model of Aβ amyloidosis: Immunohistochemical analysis and suitability as a PET biomarker of neuroinflammation. *PLoS One* **2015,** *10* (6), e0129618.
117. Dhopeshwarkar, A.; Mackie, K., CB2 Cannabinoid receptors as a therapeutic target—what does the future hold? *Mol. Pharmacol.* **2014,** *86* (4), 430-437.
118. Nogueras-Ortiz, C.; Roman-Vendrell, C.; Mateo-Semidey, G. E.; Liao, Y.-H.; Kendall, D. A.; Yudowski, G. A.; Luo, K., Retromer stops beta-arrestin 1–mediated signaling from internalized cannabinoid 2 receptors. *Mol. Biol. Cell* **2017,** *28* (24), 3554-3561.
119. Soethoudt, M.; Grether, U.; Fingerle, J.; Grim, T. W.; Fezza, F.; de Petrocellis, L.; Ullmer, C.; Rothenhäusler, B.; Perret, C.; van Gils, N.; Finlay, D.; MacDonald, C.; Chicca, A.; Gens, M. D.; Stuart, J.; de Vries, H.; Mastrangelo, N.; Xia, L.; Alachouzos, G.; Baggelaar, M. P.; Martella, A.; Mock, E. D.; Deng, H.; Heitman, L. H.; Connor, M.; Di Marzo, V.; Gertsch, J.; Lichtman, A. H.; Maccarrone, M.; Pacher, P.; Glass, M.; van der Stelt, M., Cannabinoid CB2 receptor ligand profiling reveals biased signalling and off-target activity. *Nat Commun.* **2017,** *8*, 1-14.
120. Onaivi, E. S.; Ishiguro, H.; Liu, Q.-R., Chapter 18 - Future perspectives: Cannabinoid CB2 receptor ligands and their therapeutic potential in mental diseases A2 - Fattore, Liana. In *Cannabinoids in Neurologic and Mental Disease*, Academic Press: San Diego, 2015; pp 425-444.
121. Han, S.; Thatte, J.; Buzard, D. J.; Jones, R. M., Therapeutic Utility of Cannabinoid Receptor Type 2 (CB2) Selective Agonists. *J. Med. Chem.* **2013,** *56* (21), 8224-8256.
122. Maccarrone, M., The Endocannabinoid System and its Manifold Central Actions. In *Handbook of Neurochemistry and Molecular Neurobiology: Neural Lipids*, Lajtha, A.; Tettamanti, G.; Goracci, G., Eds. Springer US: Boston, MA, 2010; pp 385-405.
123. Ganesh, A. T.; Spyros, P. N.; Alexandros, M., CB1 Cannabinoid Receptor Ligands. *Mini-Rev. Med. Chem.* **2005,** *5* (7), 631-640.
124. Aghazadeh Tabrizi, M.; Baraldi, P. G.; Borea, P. A.; Varani, K., Medicinal Chemistry, Pharmacology, and Potential Therapeutic Benefits of Cannabinoid CB2 Receptor Agonists. *Chem. Rev.* **2016,** *116* (2), 519-560.
125. Balas, L.; Cascio, M. G.; Marzo, V. D.; Durand, T., Synthesis of a potential photoactivatable anandamide analog. *Bioorg. Med. Chem. Lett.* **2006,** *16* (14), 3765-3768.
126. Wang, J.; Ueda, N., Biology of endocannabinoid synthesis system. *Prostaglandins Other Lipid Mediat.* **2009,** *89* (3), 112-119.
127. Ueda, N.; Tsuboi, K.; Uyama, T., Chapter 8 - Metabolic Enzymes for Endocannabinoids and Endocannabinoid-Like Mediators A2 - Marzo, Vincenzo

Di. In *The Endocannabinoidome*, Wang, J., Ed. Academic Press: Boston, 2015; pp 111-135.
128. Kerbrat, A.; Ferré, J.-C.; Fillatre, P.; Ronzière, T.; Vannier, S.; Carsin-Nicol, B.; Lavoué, S.; Vérin, M.; Gauvrit, J.-Y.; Le Tulzo, Y.; Edan, G., Acute Neurologic Disorder from an Inhibitor of Fatty Acid Amide Hydrolase. *New Engl. J. Med.* **2016,** *375* (18), 1717-1725.
129. van Esbroeck, A. C. M.; Janssen, A. P. A.; Cognetta, A. B.; Ogasawara, D.; Shpak, G.; van der Kroeg, M.; Kantae, V.; Baggelaar, M. P.; de Vrij, F. M. S.; Deng, H.; Allarà, M.; Fezza, F.; Lin, Z.; van der Wel, T.; Soethoudt, M.; Mock, E. D.; den Dulk, H.; Baak, I. L.; Florea, B. I.; Hendriks, G.; De Petrocellis, L.; Overkleeft, H. S.; Hankemeier, T.; De Zeeuw, C. I.; Di Marzo, V.; Maccarrone, M.; Cravatt, B. F.; Kushner, S. A.; van der Stelt, M., Activity-based protein profiling reveals off-target proteins of the FAAH inhibitor BIA 10-2474. *Science* **2017,** *356* (6342), 1084-1087.
130. Showalter, V. M.; Compton, D. R.; Martin, B. R.; Abood, M. E., Evaluation of binding in a transfected cell line expressing a peripheral cannabinoid receptor (CB2): identification of cannabinoid receptor subtype selective ligands. *J. Pharmacol. Exp. Ther.* **1996,** *278* (3), 989-999.
131. Gaoni, Y.; Mechoulam, R., Isolation, structure, and partial synthesis of an active constituent of hashish. *J. Am. Chem. Soc.* **1964,** *86* (8), 1646-1647.
132. Bow, E. W.; Rimoldi, J. M., The Structure–Function Relationships of Classical Cannabinoids: CB1/CB2 Modulation. *Perspect. Medicin. Chem.* **2016,** *8*, 17-39.
133. G, P. R.; Michael, G. T.; A, S. L.; A, R. R.; Kenneth, B. W.; Bijali, S.; K, R. R.; R, M. B., O-1057, a potent water-soluble cannabinoid receptor agonist with antinociceptive properties. *Br. J. Pharmacol* **2000,** *129* (8), 1577-1584.
134. Pertwee, R. G.; Ross, R. A.; Craib, S. J.; Thomas, A., (−)-Cannabidiol antagonizes cannabinoid receptor agonists and noradrenaline in the mouse vas deferens. *Eur. J. Pharmacol.* **2002,** *456* (1), 99-106.
135. A, T.; L, B. G.; M, P. A.; K, R. R.; A, R. R.; G, P. R., Cannabidiol displays unexpectedly high potency as an antagonist of CB1 and CB2 receptor agonists in vitro. *Br. J. Pharmacol* **2007,** *150* (5), 613-623.
136. Morales, P.; Reggio, P. H.; Jagerovic, N., An Overview on Medicinal Chemistry of Synthetic and Natural Derivatives of Cannabidiol. *Front. Pharmacol.* **2017,** *8* (422), 1-18.
137. Cumella, J.; Hernandez-Folgado, L.; Giron, R.; Sanchez, E.; Morales, P.; Hurst, D. P.; Gomez-Canas, M.; Gomez-Ruiz, M.; Pinto, D.; Goya, P.; Reggio, P. H.; Martin, M. I.; Fernandez-Ruiz, J.; Silva, A. M. S.; Jagerovic, N., Chromenopyrazoles: Non-psychoactive and Selective CB1 Cannabinoid Agonists with Peripheral Antinociceptive Properties. *ChemMedChem* **2012,** *7* (3), 452-463.
138. Rhee, M. H.; Vogel, Z.; Barg, J.; Bayewitch, M.; Levy, R.; Hanuš, L.; Breuer, A.; Mechoulam, R., Cannabinol derivatives: Binding to cannabinoid receptors and inhibition of adenylylcyclase. *J. Med. Chem.* **1997,** *40* (20), 3228-3233.
139. Jose, C.; Laura, H. F.; Rocio, G.; Eva, S.; Paula, M.; P., H. D.; Maria, G. C.; Maria, G. R.; A., P. D. C. G.; Pilar, G.; H., R. P.; Isabel, M. M.; Javier, F. R.; S., S. A. M.; Nadine, J., Chromenopyrazoles: Non-psychoactive and Selective CB1 Cannabinoid Agonists with Peripheral Antinociceptive Properties. *ChemMedChem* **2012,** *7* (3), 452-463.
140. Ford, B. M.; Franks, L. N.; Tai, S.; Fantegrossi, W. E.; Stahl, E. L.; Berquist, M. D.; Cabanlong, C. V.; Wilson, C. D.; Penthala, N. R.; Crooks, P. A.; Prather, P.

L., Characterization of structurally novel G protein biased CB1 agonists: Implications for drug development. *Pharmacol. Res.* **2017,** *125*, 161-177.
141. Pertwee, R. G., Pharmacology of cannabinoid receptor ligands. *Curr. Med. Chem.* **1999,** *6*, 635-664.
142. Lange, J. H. M.; van Stuivenberg, H. H.; Veerman, W.; Wals, H. C.; Stork, B.; Coolen, H. K. A. C.; McCreary, A. C.; Adolfs, T. J. P.; Kruse, C. G., Novel 3,4-diarylpyrazolines as potent cannabinoid CB1 receptor antagonists with lower lipophilicity. *Bioorg. Med. Chem. Lett.* **2005,** *15* (21), 4794-4798.
143. Rinaldi-Carmona, M.; Barth, F.; Millan, J.; Derocq, J.-M.; Casellas, P.; Congy, C.; Oustric, D.; Sarran, M.; Bouaboula, M.; Calandra, B.; Portier, M.; Shire, D.; Brelière, J.-C.; Fur, G. L., SR 144528, the First Potent and Selective Antagonist of the CB2 Cannabinoid Receptor. *J. Pharmacol. Exp. Ther.* **1998,** *284* (2), 644-650.
144. Niehaus, J. L.; Liu, Y.; Wallis, K. T.; Egertová, M.; Bhartur, S. G.; Mukhopadhyay, S.; Shi, S.; He, H.; Selley, D. E.; Howlett, A. C., CB_1 cannabinoid receptor activity is modulated by the cannabinoid receptor interacting protein CRIP 1a. *Mol. Pharmacol.* **2007,** *72* (6), 1557-1566.
145. Pagé, D.; Yang, H.; Brown, W.; Walpole, C.; Fleurent, M.; Fyfe, M.; Gaudreault, F.; St-Onge, S., New 1,2,3,4-tetrahydropyrrolo[3,4-b]indole derivatives as selective CB2 receptor agonists. *Bioorg. Med. Chem. Lett.* **2007,** *17* (22), 6183-6187.
146. Song, Z. H.; Bonner, T. I., A lysine residue of the cannabinoid receptor is critical for receptor recognition by several agonists but not WIN55212-2. *Mol. Pharmacol.* **1996,** *49* (5), 891-896.
147. Slipetz, D. M.; O'Neill, G. P.; Favreau, L.; Dufresne, C.; Gallant, M.; Gareau, Y.; Guay, D.; Labelle, M.; Metters, K. M., Activation of the human peripheral cannabinoid receptor results in inhibition of adenylyl cyclase. *Mol. Pharmacol.* **1995,** *48* (2), 352-361.
148. Banister, S. D.; Moir, M.; Stuart, J.; Kevin, R. C.; Wood, K. E.; Longworth, M.; Wilkinson, S. M.; Beinat, C.; Buchanan, A. S.; Glass, M.; Connor, M.; McGregor, I. S.; Kassiou, M., Pharmacology of Indole and Indazole Synthetic Cannabinoid Designer Drugs AB-FUBINACA, ADB-FUBINACA, AB-PINACA, ADB-PINACA, 5F-AB-PINACA, 5F-ADB-PINACA, ADBICA, and 5F-ADBICA. *ACS Chem. Neurosci.* **2015,** *6* (9), 1546-1559.
149. Fan, H.; Ravert, H. T.; Holt, D. P.; Dannals, R. F.; Horti, A. G., Synthesis of 1-(2,4-dichlorophenyl)-4-cyano-5-(4-[^{11}C]methoxyphenyl)-*N*-(piperidin-1-yl)-1*H*-pyrazole-3-carboxamide ([^{11}C]JHU75528) and 1-(2-bromophenyl)-4-cyano-5-(4-[^{11}C]methoxyphenyl)-*N*-(piperidin-1-yl)-1*H*-pyrazole-3-carboxamide ([^{11}C]JHU75575) as potential radioligands for PET imaging of cerebral cannabinoid receptor. *J. Labelled Compd. Radiopharm.* **2006,** *49* (12), 1021-1036.
150. Burns, H. D.; Van Laere, K.; Sanabria-Bohorquez, S.; Hamill, T. G.; Bormans, G.; Eng, W. S.; Gibson, R.; Ryan, C.; Connolly, B.; Patel, S.; Krause, S.; Vanko, A.; Van Hecken, A.; Dupont, P.; De Lepeleire, I.; Rothenberg, P.; Stoch, S. A.; Cote, J.; Hagmann, W. K.; Jewell, J. P.; Lin, L. S.; Liu, P.; Goulet, M. T.; Gottesdiener, K.; Wagner, J. A.; de Hoon, J.; Mortelmans, L.; Fong, T. M.; Hargreaves, R. J., [^{18}F]MK-9470, a positron emission tomography (PET) tracer for *in vivo* human PET brain imaging of the cannabinoid-1 receptor. *Proc. Natl. Acad. Sci. U.S.A.* **2007,** *104* (23), 9800-9805.

151. Evens, N.; Muccioli, G. G.; Houbrechts, N.; Lambert, D. M.; Verbruggen, A. M.; Van Laere, K.; Bormans, G. M., Synthesis and biological evaluation of carbon-11-and fluorine-18-labeled 2-oxoquinoline derivatives for type 2 cannabinoid receptor positron emission tomography imaging. *Nucl. Med. Biol.* **2009,** *36* (4), 455-465.
152. Forrest, I. S.; Green, D. E.; Rose, S. D.; Skinner, G. C.; Torres, D. M., Fluorescent-labeled cannabinoids. *Res. Commun. Chem. Pathol. Pharmacol.* **1971,** *2* (6), 787-792.
153. Koga, D.; Santa, T.; Hagiwara, K.; Imai, K.; Takizawa, H.; Nagano, T.; Hirobe, M.; Ogawa, M.; Sato, T.; Inoue, K., High-performance liquid chromatography and fluorometric detection of arachidonylethanolamide (anandamide) and its analogues, derivatized with 4-(*N*-chloroformylmethyl-*N*-methyl) amino-7-*N*, *N*-dimethylaminosulphonyl-2, 1, 3-benzoxadiazole (DBD-COCl). *Biomed. Chromatogr.* **1995,** *9* (1), 56-57.
154. Yates, A. S.; Doughty, S. W.; Kendall, D. A.; Kellam, B., Chemical modification of the naphthoyl 3-position of JWH-015: In search of a fluorescent probe to the cannabinoid CB_2 receptor. *Bioorg. Med. Chem. Lett.* **2005,** *15* (16), 3758-3762.
155. Cooper, A. G.; MacDonald, C.; Glass, M.; Hook, S.; Tyndall, J. D. A.; Vernall, A. J., Alkyl indole-based cannabinoid type 2 receptor tools: Exploration of linker and fluorophore attachment. *Eur. J. Med. Chem.* **2018,** *145*, 770-789.
156. Daly, C. J.; Ross, R. A.; Whyte, J.; Henstridge, C. M.; Irving, A. J.; McGrath, J. C., Fluorescent ligand binding reveals heterogeneous distribution of adrenoceptors and 'cannabinoid-like' receptors in small arteries. *Br. J. Pharmacol.* **2010,** *159* (4), 787-796.
157. Martín-Couce, L.; Martín-Fontecha, M.; Capolicchio, S.; López-Rodríguez, M. L.; Ortega-Gutiérrez, S., Development of Endocannabinoid-Based Chemical Probes for the Study of Cannabinoid Receptors. *J. Med. Chem.* **2011,** *54* (14), 5265-5269.
158. Martin-Couce, L.; Martin-Fontecha, M.; Palomares, O.; Mestre, L.; Cordomi, A.; Hernangomez, M.; Palma, S.; Pardo, L.; Guaza, C.; Lopez-Rodriguez, M. L.; Ortega-Gutierrez, S., Chemical Probes for the Recognition of Cannabinoid Receptors in Native Systems. *Angew. Chem. Int. Ed.* **2012,** *51* (28), 6896-6899.
159. Martin-Fontecha, M.; Eiwegger, T.; Jartti, T.; Rueda-Zubiaurre, A.; Tiringer, K.; Stepanow, J.; Puhakka, T.; Ruckert, B.; Ortega-Gutierrez, S.; Lopez-Rodriguez, M. L.; Akdis, M.; Akdis, C. A.; Palomares, O., The expression of cannabinoid receptor 1 is significantly increased in atopic patients. *J. Allergy Clin. Immunol.* **2014,** *133* (3), 926-929.
160. Bai, M.; Sexton, M.; Stella, N.; Bornhop, D. J., MBC94, a conjugable ligand for cannabinoid CB2 receptor imaging. *Bioconjugate Chem.* **2008,** *19* (5), 988-992.
161. Zhang, S.; Shao, P.; Bai, M., In vivo type 2 cannabinoid receptor-targeted tumor optical imaging using a near infrared fluorescent probe. *Bioconjugate Chem.* **2013,** *24* (11), 1907-1916.
162. Zhang, S.; Shao, P.; Ling, X.; Yang, L.; Hou, W.; Thorne, S. H.; Beaino, W.; Anderson, C. J.; Ding, Y.; Bai, M., In vivo inflammation imaging using a CB_2R-targeted near infrared fluorescent probe. *Am. J. Nucl. Med. Mol. Imaging* **2015,** *5* (3), 246-58.
163. Wu, Z.; Shao, P.; Zhang, S.; Ling, X.; Bai, M., Molecular imaging of human tumor cells that naturally overexpress type 2 cannabinoid receptors using a quinolone-based near-infrared fluorescent probe. *J. Biomed. Opt.* **2014,** *19* (7), 76016.

164. Ling, X.; Zhang, S.; Shao, P.; Li, W.; Yang, L.; Ding, Y.; Xu, C.; Stella, N.; Bai, M., A novel near-infrared fluorescence imaging probe that preferentially binds to cannabinoid receptors CB_2R over CB_1R. *Biomaterials* **2015,** *57*, 169-178.
165. Zhang, S.; Jia, N.; Shao, P.; Tong, Q.; Xie, X. Q.; Bai, M., Target-selective phototherapy using a ligand-based photosensitizer for Type 2 cannabinoid receptor. *Chem. Biol.* **2014,** *21* (3), 338-344.
166. Bornhop, D. J.; Bai, M.; Stella, N.; Stern, E. Cannabinoid receptor targeted agent. US Patent 8,367,714 B2. Vanderbilt University, University of Washington assignee. US8367714 B2, 2013.
167. Singh, S.; Cooper, S.; Glenn, J. R.; Beresford, J.; Percival, L. R.; Tyndall, J. D. A.; Hill, S. J.; Kilpatrick, L. E.; Vernall, A. J., Synthesis of novel (benzimidazolyl)isoquinolinols and evaluation as adenosine A1 receptor tools. *RSC Advances* **2018,** *8* (29), 16362-16369.
168. Howlett, A. C.; Barth, F.; Bonner, T. I.; Cabral, G.; Casellas, P.; Devane, W. A.; Felder, C. C.; Herkenham, M.; Mackie, K.; Martin, B. R.; Mechoulam, R.; Pertwee, R. G., International Union of Pharmacology. XXVII. Classification of cannabinoid receptors. *Pharmacol. Rev.* **2002,** *54* (2), 161-202.
169. Cawston, E. E.; Redmond, W. J.; Breen, C. M.; Grimsey, N. L.; Connor, M.; Glass, M., Real-time characterization of cannabinoid receptor 1 (CB1) allosteric modulators reveals novel mechanism of action. *Br. J. Pharmacol* **2013,** *170* (4), 893-907.
170. Jiang, L. I.; Collins, J.; Davis, R.; Lin, K.-M.; DeCamp, D.; Roach, T.; Hsueh, R.; Rebres, R. A.; Ross, E. M.; Taussig, R.; Fraser, I.; Sternweis, P. C., Use of a cAMP BRET Sensor to Characterize a Novel Regulation of cAMP by the Sphingosine 1-Phosphate/G13 Pathway. *J. Biol. Chem.* **2007,** *282* (14), 10576-10584.
171. Müller, C. E.; Jacobson, K. A., Xanthines as Adenosine Receptor Antagonists. In *Methylxanthines*, Fredholm, B. B., Ed. Springer Berlin Heidelberg: Berlin, Heidelberg, 2011; pp 151-199.
172. Novellino, E.; Cosimelli, B.; Ehlardo, M.; Greco, G.; Iadanza, M.; Lavecchia, A.; Rimoli, M. G.; Sala, A.; Da Settimo, A.; Primofiore, G.; Da Settimo, F.; Taliani, S.; La Motta, C.; Klotz, K.-N.; Tuscano, D.; Trincavelli, M. L.; Martini, C., 2-(Benzimidazol-2-yl)quinoxalines: A Novel Class of Selective Antagonists at Human A1 and A3 Adenosine Receptors Designed by 3D Database Searching. *J. Med. Chem.* **2005,** *48* (26), 8253-8260.
173. Allen, F. H.; Bellard, S.; Brice, M.; Cartwright, B. A.; Doubleday, A.; Higgs, H.; Hummelink, T.; Hummelink-Peters, B.; Kennard, O.; Motherwell, W., The Cambridge Crystallographic Data Centre: computer-based search, retrieval, analysis and display of information. *Acta Crystallogr. B Struct. Cryst. Cryst. Chem.* **1979,** *35* (10), 2331-2339.
174. Gao, Z.-G.; Van Muijlwijk-Koezen, J. E.; Chen, A.; Müller, C. E.; Ijzerman, A. P.; Jacobson, K. A., Allosteric Modulation of A3 Adenosine Receptors by a Series of 3-(2-Pyridinyl)isoquinoline Derivatives. *Mol. Pharmacol.* **2001,** *60* (5), 1057-1063.
175. Heitman, L. H.; Göblyös, A.; Zweemer, A. M.; Bakker, R.; Mulder-Krieger, T.; van Veldhoven, J. P. D.; de Vries, H.; Brussee, J.; Ijzerman, A. P., A Series of 2,4-Disubstituted Quinolines as a New Class of Allosteric Enhancers of the Adenosine A3 Receptor. *J. Med. Chem.* **2009,** *52* (4), 926-931.
176. Ma, Z.; Du, L.; Li, M., Toward Fluorescent Probes for G-Protein-Coupled Receptors (GPCRs). *J. Med. Chem.* **2014,** *57* (20), 8187-8203.

177. Cinelli, M. A.; Cordero, B.; Dexheimer, T. S.; Pommier, Y.; Cushman, M., Synthesis and biological evaluation of 14-(aminoalkyl-aminomethyl)aromathecins as topoisomerase I inhibitors: Investigating the hypothesis of shared structure-activity relationships. *Bioorg. Med. Chem.* **2009,** *17* (20), 7145-7155.
178. Song, H. Y.; Ngai, M. H.; Song, Z. Y.; MacAry, P. A.; Hobley, J.; Lear, M. J., Practical synthesis of maleimides and coumarin-linked probes for protein and antibody labelling via reduction of native disulfides. *Org. Biomol. Chem.* **2009,** *7* (17), 3400-3406.
179. Li, J. J.; Tino, J. A. Preparation of tetrahydroisoquinoline analogs for therapeutic use in stimulating endogenous production or release of growth hormone. Bristol-Myers Squibb Co., USA assignee. WO2001085695A1, 2001.
180. Maillard, M. C.; Brookfield, F. A.; Courtney, S. M.; Eustache, F. M.; Gemkow, M. J.; Handel, R. K.; Johnson, L. C.; Johnson, P. D.; Kerry, M. A.; Krieger, F.; Meniconi, M.; Muñoz-Sanjuán, I.; Palfrey, J. J.; Park, H.; Schaertl, S.; Taylor, M. G.; Weddell, D.; Dominguez, C., Exploiting differences in caspase-2 and -3 S2 subsites for selectivity: Structure-based design, solid-phase synthesis and in vitro activity of novel substrate-based caspase-2 inhibitors. *Biorg. Med. Chem.* **2011,** *19* (19), 5833-5851.
181. Ma, D.; Wu, W.; Yang, G.; Li, J.; Li, J.; Ye, Q., Tetrahydroisoquinoline based sulfonamide hydroxamates as potent matrix metalloproteinase inhibitors. *Bioorg. Med. Chem. Lett.* **2004,** *14* (1), 47-50.
182. Abeywardane, A.; Brunette, S. R.; Burke, M. J.; Kirrane, T. M., Jr.; Man, C. C.; Marshall, D. R.; Padyana, A. K.; Razavi, H.; Sibley, R.; Smith Keenan, L. L.; Snow, R. J.; Sorcek, R. J.; Takahashi, H.; Taylor, S. J.; Turner, M. R.; Young, E. R. R.; Zhang, Q.; Zhang, Y.; Zindell, R. M. Pyrazole derivatives which inhibit leukotriene production and their preparation. Boehringer Ingelheim International GmbH, Germany assignee. WO2014014874A1, 2014.
183. Ishiguro, S.; Kawaguchi, N.; Nakakoshi, M.; Shimada, S.; Seya, M.; Nomoto, M.; Okue, M.; Tomizuka, H. Preparation of isoquinoline derivatives as protease inhibitors. Snow Brand Milk Prod Co Ltd, Japan assignee. JP07304744A, 1995.
184. Chen, S.; Li, Y.; Ni, P.; Yang, B.; Huang, H.; Deng, G.-J., One-Pot Cascade Synthesis of Substituted Carbazoles from Indoles, Ketones, and Alkenes Using Oxygen as the Oxidant. *J. Org. Chem.* **2017,** *82* (6), 2935-2942.
185. Shamim, T.; Gupta, M.; Paul, S., The oxidative aromatization of Hantzsch 1,4-dihydropyridines by molecular oxygen using surface functionalized silica supported cobalt catalysts. *J. Mol. Catal. A: Chem.* **2009,** *302* (1), 15-19.
186. Dong, J.; Shi, X.-X.; Yan, J.-J.; Xing, J.; Zhang, Q.; Xiao, S., Efficient and Practical One-Pot Conversions of N-Tosyltetrahydroisoquinolines into Isoquinolines and of N-Tosyltetrahydro-β-carbolines into β-Carbolines through Tandem β-Elimination and Aromatization. *Eur. J. Org. Chem.* **2010,** (36), 6987-6992.
187. Tsang, A. S.-K.; Jensen, P.; Hook, J. M.; Hashmi, A. S. K.; Todd, M. H., An oxidative carbon–carbon bond-forming reaction proceeds via an isolable iminium ion. *Pure Appl. Chem.* **2011,** *83* (3), 655-665.
188. Höck, S.; Marti, R.; Riedl, R.; Simeunovic, M., Thermal cleavage of the Fmoc protection group. *CHIMIA International Journal for Chemistry* **2010,** *64* (3), 200-202.
189. Ornstein, P. L.; Arnold, M. B.; Augenstein, N. K.; Paschal, J. W., Syntheses of 6-oxodecahydroisoquinoline-3-carboxylates. Useful intermediates for the

preparation of conformationally defined excitatory amino acid antagonists. *J. Org. Chem.* **1991,** *56* (14), 4388-4392.
190. Mjalli, A. M.; Jones, D.; Gohimmukkula, D. R.; Huang, G.; Zhu, J.; Rao, M.; Andrews, R. C.; Ren, T. Benzazole derivatives and their preparation, compositions, and methods of use as β-secretase inhibitors. Transtech Pharma, Inc., USA assignee. WO2006099379A2, 2006.
191. Seiwert, S.; Beigelman, L.; Buckman, B.; Serebryany, V.; Stoycheva, A. D. Preparation of proline tripeptides and analogs as inhibitors of hepatitis C virus replication for treating hepatitis C infection and liver fibrosis. InterMune, Inc., USA assignee. WO2010045266A1, 2010.
192. Karanewsky, D. S.; Fotsing, J.; Tachdjian, C.; Arellano, M. Identification of human T2R receptors that respond to bitter compounds that elicit the bitter taste in compositions, and the use thereof in assays to identify compounds that inhibit (block) bitter taste in compositions and use thereof. Senomyx, Inc., USA assignee. WO2011106114A1, 2011.
193. Calderwood, E. F.; Duffey, M.; Gould, A. E.; Greenspan, P. D.; Kulkarni, B.; Lamarche, M. J.; Rowland, R. S.; Tregay, M.; Vos, T. J. Preparation of nitrogen-containing heteroaryl-substituted aryl bicycles as kinase inhibitors for the treatment of cancer. Millennium Pharmaceuticals, Inc., USA assignee. WO2007067444A1, 2007.
194. Sridharan, V.; Saravanan, S.; Muthusubramanian, S.; Sivasubramanian, S., NMR investigation of hydrogen bonding and 1,3-tautomerism in 2-(2-hydroxy-5-substituted-aryl) benzimidazoles. *Magn. Reson. Chem.* **2005,** *43* (7), 551-556.
195. Saito, H.; Tanaka, Y.; Nagata, S., The Hydrogen bond studied by Nitrogen-14 Nuclear Magnetic Resonance .IV. Nitrogen-14 chemical Shifts of Five-membered and Six-membered N-Heterocycles Determined by Heteronuclear Magnetic Double Resonance with the Aid of Two- and Three-bond N-H Spin Couplings. *J. Am. Chem. Soc.* **1973,** *95* (2), 324-328.
196. Lee, I. S. H.; Jeoung, E. H.; Lee, C. K., Synthesis and tautomerism of 2-aryl- and 2-heteroaryl derivatives of benzimidazole. *J. Heterocycl. Chem.* **1996,** *33* (6), 1711-1716.
197. Claramunt, R. M.; Lopez, C.; Alkorta, I.; Elguero, J.; Yang, R.; Schulman, S., The tautomerism of Omeprazole in solution: a H-1 and C-13 NMR study. *Magn. Reson. Chem.* **2004,** *42* (8), 712-714.
198. Benassi, R.; Lazzeret.P; Schenett.L; Taddei, F.; Vivarell.P, NMR study of tautomerism in substituted 2-chlorobenzimidazoles. *Tetrahedron Lett.* **1971,** (35), 3299-3300.
199. Papadopoulos, E. P.; Hollstein, U., Carbon–13 NMR Studies of Tautomerism in Some 2-Substituted Imidazoles and Benzimidazoles. *Org. Magn. Resonance* **1982,** *19* (4), 188-191.
200. England, C. G.; Ehlerding, E. B.; Cai, W., NanoLuc: A Small Luciferase Is Brightening Up the Field of Bioluminescence. *Bioconjugate Chem.* **2016,** *27* (5), 1175-1187.
201. Franck, B.; Blaschke, G.; Schlingloff, G., Oxidative condensations of quaternary phenolic bases. *Angelo. Chem.* **1963,** *75* (20), 957-965.
202. Chiodini, L.; Di Ciommo, M.; Merlini, L., Synthesis of some N-heteroaromatic analogues of cannabinoids. *J. Heterocyclic Chem.* **1981,** *18* (1), 23-25.
203. Press, J. B.; Birnberg, G. H., Heterocyclic-fused benzopyrans as cannabinoid analogues. *J. Heterocyclic Chem.* **1985,** *22* (2), 561-564.

204. Jagerovic, N.; Hernandez-Folgado, L.; Alkorta, I.; Goya, P.; Navarro, M.; Serrano, A.; Rodriguez de Fonseca, F.; Dannert, M. T.; Alsasua, A.; Suardiaz, M.; Pascual, D.; Martín, M. I., Discovery of 5-(4-Chlorophenyl)-1-(2,4-dichlorophenyl)-3-hexyl-1H-1,2,4-triazole, a Novel in Vivo Cannabinoid Antagonist Containing a 1,2,4-Triazole Motif. *J. Med. Chem.* **2004,** *47* (11), 2939-2942.
205. Morales, P.; Gómez-Cañas, M.; Navarro, G.; Hurst, D. P.; Carrillo-Salinas, F. J.; Lagartera, L.; Pazos, R.; Goya, P.; Reggio, P. H.; Guaza, C.; Franco, R.; Fernández-Ruiz, J.; Jagerovic, N., Chromenopyrazole, a Versatile Cannabinoid Scaffold with in Vivo Activity in a Model of Multiple Sclerosis. *J. Med. Chem.* **2016,** *59* (14), 6753-6771.
206. Morales, P.; Vara, D.; Goméz-Cañas, M.; Zúñiga, M. C.; Olea-Azar, C.; Goya, P.; Fernández-Ruiz, J.; Díaz-Laviada, I.; Jagerovic, N., Synthetic cannabinoid quinones: Preparation, in vitro antiproliferative effects and in vivo prostate antitumor activity. *Eur. J. Med. Chem.* **2013,** *70*, 111-119.
207. Morales, P.; Blasco-Benito, S.; Andradas, C.; Gómez-Cañas, M.; Flores, J. M.; Goya, P.; Fernández-Ruiz, J.; Sánchez, C.; Jagerovic, N., Selective, Nontoxic CB2 Cannabinoid o-Quinone with in Vivo Activity against Triple-Negative Breast Cancer. *J. Med. Chem.* **2015,** *58* (5), 2256-2264.
208. Morales, P.; Whyte, L. S.; Chicharro, R.; Gómez-Cañas, M.; Pazos, M. R.; Goya, P.; Irving, A. J.; Fernández-Ruiz, J.; Ross, R. A.; Jagerovic, N., Identification of Novel GPR55 Modulators Using Cell-Impedance-Based Label-Free Technology. *J. Med. Chem.* **2016,** *59* (5), 1840-1853.
209. McLamore, W. M., Preparation of Some Alkylbenzoquinones. *J. Am. Chem. Soc.* **1951,** *73* (5), 2221-2225.
210. Chen, X.; She, J.; Shang, Z.-C.; Wu, J.; Zhang, P., Room-temperature synthesis of pyrazoles, diazepines, β-enaminones, and β-enamino esters using silica-supported sulfuric acid as a reusable catalyst under solvent-free conditions. *Synth. Commun.* **2009,** *39* (6), 947-957.
211. Rynearson, K. D.; Buckle, R. N.; Barnes, K. D.; Herr, R. J.; Mayhew, N. J.; Paquette, W. D.; Sakwa, S. A.; Nguyen, P. D.; Johnson, G.; Tanzi, R. E.; Wagner, S. L., Design and synthesis of aminothiazole modulators of the gamma-secretase enzyme. *Bioorg. Med. Chem. Lett.* **2016,** *26* (16), 3928-3937.
212. Grimsey, N. L.; Goodfellow, C. E.; Dragunow, M.; Glass, M., Cannabinoid receptor 2 undergoes Rab5-mediated internalization and recycles via a Rab11-dependent pathway. *Biochim. Biophys. Acta* **2011,** *1813* (8), 1554-1560.
213. Di Tommaso, P.; Moretti, S.; Xenarios, I.; Orobitg, M.; Montanyola, A.; Chang, J.-M.; Taly, J.-F.; Notredame, C., T-Coffee: a web server for the multiple sequence alignment of protein and RNA sequences using structural information and homology extension. *Nucleic Acids Res.* **2011,** *39* (Web Server issue), W13-W17.
214. Eswar, N.; Webb, B.; Marti-Renom, M. A.; Madhusudhan, M. S.; Eramian, D.; Shen, M.-y.; Pieper, U.; Sali, A., Comparative Protein Structure Modeling Using Modeller. *Current protocols in bioinformatics / editoral board, Andreas D. Baxevanis ... [et al.]* **2006,** *0 5*, Unit-5.6.
215. Shen, M.-y.; Sali, A., Statistical potential for assessment and prediction of protein structures. *Protein Science : A Publication of the Protein Society* **2006,** *15* (11), 2507-2524.

216. Hanwell, M. D.; Curtis, D. E.; Lonie, D. C.; Vandermeersch, T.; Zurek, E.; Hutchison, G. R., Avogadro: an advanced semantic chemical editor, visualization, and analysis platform. *J. Cheminform.* **2012,** *4* (1), 17.
217. Jones, G.; Willett, P.; Glen, R. C.; Leach, A. R.; Taylor, R., Development and validation of a genetic algorithm for flexible docking. *J. Mol. Biol.* **1997,** *267* (3), 727-748.
218. Rhee, M.-H., Functional role of serine residues of transmembrane dopamin VII in signal transduction of CB2 cannabinoid receptor. *J. Vet. Sci. 3* (3), 185-191.
219. Hurst, D. P.; Grossfield, A.; Lynch, D. L.; Feller, S.; Romo, T. D.; Gawrisch, K.; Pitman, M. C.; Reggio, P. H., A lipid pathway for ligand binding is necessary for a cannabinoid G protein-coupled receptor. *J. Biol. Chem.* **2010,** *285* (23), 17954-17964.
220. Jakowiecki, J.; Filipek, S., Hydrophobic Ligand Entry and Exit Pathways of the CB1 Cannabinoid Receptor. *J. Chem. Inf. Model.* **2016,** *56* (12), 2457-2466.
221. Gavande, N.; Kim, H.-L.; Doddareddy, M. R.; Johnston, G. A. R.; Chebib, M.; Hanrahan, J. R., Design, Synthesis, and Pharmacological Evaluation of Fluorescent and Biotinylated Antagonists of ρ1 GABAC Receptors. *ACS Med. Chem. Lett.* **2013,** *4* (4), 402-407.
222. Fleck, R. W.; Guo, X.; Lo, H. Y.; Man, C. C. Substituted pyrazole compounds useful as soluble epoxide hydrolase inhibitors and their preparation and pharmaceutical compositions. Boehringer Ingelheim International G.m.b.H., Germany; Boehringer Ingelheim Pharma G.m.b.H. & Co. K.-G. assignee. WO2007067836A2, 2007.
223. Plowright, A. T.; Nilsson, K.; Antonsson, M.; Amin, K.; Broddefalk, J.; Jensen, J. r.; Lehmann, A.; Jin, S.; St-Onge, S.; Tomaszewski, M. J., Discovery of agonists of cannabinoid receptor 1 with restricted central nervous system penetration aimed for treatment of gastroesophageal reflux disease. *J. Med. Chem.* **2012,** *56* (1), 220-240.
224. Amin, K.; Broddefalk, J.; Chen, Y.; Desfosses, H.; Liu, Z.; Milburn, C.; Nilsson, K.; Tremblay, M.; Walpole, C.; Wei, Z.-Y.; Yang, H. Preparation of pyridine carboxamides as CB1 receptor ligands. AstraZeneca AB, Swed. assignee. WO2007061360A2, 2007.
225. MarvinSketch was used for the conformational search (version 16.10.3.0), 2016, ChemAxon (http://www.chemaxon.com).
226. Light, M. E.; Quesada, R.; Gale, P. A., CCDC 1475756: Experimental Crystal Structure Determination. *CSD Communication* **2016**, DOI: 10.5517/ccdc.csd.cc1ljn1t.
227. Ouahrouch, A.; Taourirte, M.; Lazrek, H. B.; Engels, J. W.; Bolte, M., Crystal structure of 2-benzamido-N-(2,2-diethoxyethyl)benzamide. *Acta Cryst. E* **2015,** *71* (3), o214-o215.
228. Baravkar, S. B.; Roy, A.; Gawade, R. L.; Puranik, V. G.; Sanjayan, G. J., Nucleophilic Ring-Opening of Benzoxazinones by DBU: Some Observations. *Synth. Commun.* **2014,** *44* (20), 2955-2960.
229. Goergens, U.; Yoneta, Y.; Murata, T.; Mihara, J.; Domon, K.; Shimojo, E.; Shibuya, K.; Ichihara, T. Arylpyrrolines and related compounds as insecticides and their preparation. Bayer Cropscience AG, Germany assignee. WO2009097992A1, 2009.
230. Cheng, Y.-X.; Tomaszewski, M.; Yang, H. Preparation of isoindole derivatives useful for treating pain, gastrointestinal diseases and cancer. AstraZeneca AB, Swed assignee. WO2007139464A1, 2007.

231. Guo, Z.-X.; Cammidge, A. N.; McKillop, A.; Horwell, D. C., N-vs O-Alkylation in 2 (1H)-quinolinone derivatives. *Tetrahedron Lett.* **1999,** *40* (38), 6999-7002.
232. Liu, Y.; Xu, Y.; Jung, S. H.; Chae, J., A facile and green protocol for nucleophilic substitution reactions of sulfonate esters by recyclable ionic liquids [bmim][X]. *Synlett* **2012,** *23* (18), 2692-2698.
233. M., M. J.; Christa, M.; Michelle, Y.; S., G. P.; P., F. D.; Michelle, G., Affinity and Efficacy Studies of Tetrahydrocannabinolic Acid A at Cannabinoid Receptor Types One and Two. *Cannabis and Cannabinoid Research* **2017,** *2* (1), 87-95.
234. Morales, P.; Azofra, L. M.; Cumella, J.; Hernandez-Folgado, L.; Roldan, M.; Alkorta, I.; Jagerovic, N., Preparation of 2,2-dimethylchroman-4-ones from 5-alkyl-substituted resorcinols: microwave-assisted synthesis and theoretical calculations. *ARKIVOC (Gainesville, FL, U. S.)* **2014,** (2), 319-332, 14 pp.
235. Brodfuehrer, P. R.; Chen, B. C.; Sattelberg Sr, T. R.; Smith, P. R.; Reddy, J. P.; Stark, D. R.; Quinlan, S. L.; Gregory Reid, J.; Thottathil, J. K.; Wang, S., An Efficient Fischer Indole Synthesis of Avitriptan, a Potent 5-HT1D Receptor Agonist. *J. Org. Chem.* **1997,** *62* (26), 9192-9202.
236. Ahlström, M. M.; Ridderström, M.; Zamora, I.; Luthman, K., CYP2C9 structure-metabolism relationships: Optimizing the metabolic stability of COX-2 inhibitors. *J. Med. Chem.* **2007,** *50* (18), 4444-4452.
237. Edem, P. E.; Czorny, S.; Valliant, J. F., Synthesis and Evaluation of Radioiodinated Acyloxymethyl Ketones as Activity-Based Probes for Cathepsin B. *J. Med. Chem.* **2014,** *57* (22), 9564-9577.
238. Segretti, M. C. F.; Vallerini, G. P.; Brochier, C.; Langley, B.; Wang, L.; Hancock, W. W.; Kozikowski, A. P., Thiol-Based Potent and Selective HDAC6 Inhibitors Promote Tubulin Acetylation and T-Regulatory Cell Suppressive Function. *ACS Med. Chem. Lett.* **2015,** *6* (11), 1156-1161.
239. The UniProt Consortium, UniProt: the universal protein knowledgebase. *Nucleic Acids Res.* **2017,** *45* (D1), D158-D169.
240. Yang, K. S.; Budin, G.; Tassa, C.; Kister, O.; Weissleder, R., Bioorthogonal Approach to Identify Unsuspected Drug Targets in Live Cells. *Angew. Chem., Int. Ed.* **2013,** *52* (40), 10593-10597.